Minnesota River Invasive Carp Prevention Workplan: Minnesota DNR

Report compiled by:
Phillip H. Larson[1], Patrick Belmont[2], Water Resources Center[3]

[1]Earth Science Programs, AGES Laboratory, Geography - Minnesota State University, Mankato
Phillip.larson@mnsu.edu
[2]Watershed Sciences - Utah State University
Patrick.belmont@usu.edu
[3]Water Resources Center – Minnesota State University, Mankato
https://cset.mnsu.edu/wrc/

Data Storage:

All data related to the tasks conducted within this study can be accessed here:
https://geo.mnsu.edu/geo/DNR-InvasiveCarp/
Username: landforms
Password: rocks

Each task will contain a dedicated folder with data collected during the work on that task. This data will be available on this server, barring any Minnesota State University IT related issues, for three years following submission of this report. Please download the data at your convenience.

Background:

Invasive carp are a concern for the Minnesota Department of Natural Resources (MN DNR) and citizens of the state of Minnesota for biological, recreational, and economical reasons. The MN DNR fisheries division recently completed a GIS analysis depicting areas most accessible to invasive carp via their natural swimming ability. As expected, the Mississippi River watershed up to St. Anthony Falls and the Minnesota River watershed are the most vulnerable to Invasive carp expansion via swimming pathways. In addition to being accessible, the Minnesota River appears to have the habitat requirements to support Invasive carp populations. Preventing the establishment of the Invasive carp species is the ideal strategy. One of the tools in the prevention toolkit is establishing barriers to fish movement.

Problem Statement:

The Minnesota River watershed is the largest susceptible watershed in Minnesota to establishment of Invasive carp via natural migration pathways, making it a high priority for management actions to reduce the impact and upstream migration of Invasive carp. Establishment of Invasive carp in Minnesota would also increase the potential risk

to lakes in the region and bordering watersheds. A barrier system deterring or preventing fish movement is being considered as a tool for preventing establishment of Invasive carp. Deciding whether to apply this tool is complicated by questions of effectiveness, impacts to native aquatic communities, costs, impacts of Invasive carps on native aquatic communities, hydraulic impacts, recreational values, economic values, effectiveness of Invasive carp control strategies, and the advancement of alternative technology/concept solutions. A feasible barrier must maintain effectiveness thresholds during high water events and barrier efficiency is tied to both hydrologic and geomorphologic characteristics of the river. Little data exists regarding the geomorphologic and hydrologic characteristics of the main stem of the Minnesota River. The expected benefits of a barrier system on the Minnesota River necessitate a thorough analysis to begin to determine feasibility.

Project Definition:
A comprehensive analysis to determine the best solution to Invasive carp migration would require a large amount of resources which are not available at this time. However, an initial collection and analysis of hydrologic and geomorphic data is vital as a first step in this comprehensive analysis. As expected, there are many potential starting points for determining the feasibility of a barrier solution based on interpretation of current knowledge, philosophies, strategic thinking, stakeholder views, and budget. Thus, this phase of the project will focus on a geomorphologic and hydrologic analysis to produce data that will aid the appropriate bodies in identifying possible barrier locations on the Minnesota River. Despite current opinions, both positive and negative, the MN DNR has not limited the choice of barrier technologies that may be considered. This is largely due to a lack of data that would aid in decision making. In addition to providing information deemed useful for evaluating the feasibility and effectiveness of installing barriers within the Minnesota River system, this proposed analysis will attempt to determine possible hydrologic connectivity with the Red River watershed to help determine the possibility of the Minnesota River serving as a conduit for potential invasion of Invasive carp into the Red River and Lake Winnipeg watershed.

Minnesota River:
- 335 mile-long river with low gradient, ~0.74 ft/mile
- 16,770 square mile watershed
- Known to be a net-depositional system with a significant fraction of the high sediment loads contributed from tributaries being deposited within the mainstem Minnesota River Valley
- Relatively unconfined valley where flood waters spread out over broad area
- Significant increases in flow and overbank flooding observed over the past three decades
- Diverse aquatic community with many species migrating significant distances both within the mainstem and in tributaries in order to complete their life cycle
- Watershed has nutrient levels and habitat types such as connected backwater lakes that appear suitable for Invasive carp
- Land use is primarily agricultural and many human-built structures (roads, levees, bridges, wing-dams, etc.) exist along the main stem river and tributaries

Objectives
1) Provide data that will support the appropriate entities to identify the most suitable sites on the Minnesota River for potential barrier systems and assess the feasibility at these sites.
2) Collect data that may allow for the identification of potential connections of the Minnesota River watershed with the Red River watershed.

Focus
The project will focus on the main stem of the Minnesota River and the Minnesota/Red River watershed boundary.

Phase 1: GIS Floodplain Analysis
Task 1: Floodplain Mapping - GIS floodplain analysis depicting, 100-year, 500-year, and largest observed flood events

      To determine areas within the Minnesota River valley that would be potential locations of fish barriers, the analysis of the floodplain morphology and flooding events from the Minnesota-Mississippi River confluence to Lake Traverse in Western Minnesota needs to be completed.

      An initial analysis of the width of floodplain inundated as a function of water elevation above bank can be done using only the LiDAR (Light Detection and Ranging) data. This analysis is completed using an open-source plug-in for ArcMap developed by Patrick Belmont and Barr Engineering (for details, see Belmont, 2011). Basic input data to run the tool simply includes river stage-duration data (real or synthetic) at multiple cross sections and a high resolution DEM. For the purposes of this work, we will use synthetic stage-duration data that floods the landscape at regular intervals above the geomorphic bank (every 0.25 m). The tool interpolates a three-dimensional water surface (TIN) between cross sections for each stage included in the input stage-duration spreadsheet, converts the TIN to a grid, and subtracts the elevation of the DEM to generate a water depth grid. This analysis does NOT involve any hydraulic calculations, but is instead a quick and easy approach for mapping out reaches of the river that with relatively wide versus narrow floodplains. This will help focus future aspects of the study.

      To determine the actual floodplain inundated during the, 100-year, 500-year, and highest recorded flood event, several additional pieces of information are needed. First and foremost, the 100 and 500 year flood events must be determined. Given the amount of uncertainty that is inherent in such predictions, we will conduct a series of flood frequency analyses, using the standard Log Pearson III approach, Extreme Value Distribution approach, as well as more recently developed approaches to account for potential non-stationary hydrologic conditions (e.g., Gilroy and McCuen, 2012). Once the range of reasonable estimates for the 100 and 500 year floods have been generated,

hydraulic calculations are needed to accurately predict river stage as a function of discharge. We will conduct these hydraulic calculations using standard practices and the US Army Corps of Engineers HEC-RAS software. The model will be calibrated using a set of measurements from surveys with an Acoustic Doppler Current Profiler (ADCP) and will be validated/verified using a second set of ADCP measurements plus measurements from USGS gaging stations.

Initial estimates could be completed using generic cross sections of the channel, estimated from regional hydraulic geometry relationships. However, robust hydraulic calculations require measured channel cross sections, presumably extracted from the bathymetry map generated as part of this project.

Utilizing other data such as measured historic meander migration rates over the past 25 years will help determine locations within the Minnesota River valley that may experience "cut-offs" or are susceptible to dynamic channel form change. These changes in channel morphology, during flooding events, can provide alternative avenues for Invasive carp migration and must be taken into consideration if a barrier is constructed.

RESULTS: *Inundation Mapping*
Testing a Semi-Automated Geospatial Methodology for Floodplain Inundation Mapping: Case Study of the Minnesota River Valley
Author(s): Carson A. Smith[1], Phillip Larson[1], Patrick Belmont[2]
[1]Earth Science Programs/AGES Laboratory - Minnesota State University, Mankato
[2]Watershed Sciences - Utah State University

Corresponding Author:
Carson A. Smith – Email: carson.smith@amecfw.com, carson.smith@woodplc.com;
Phone: 9529562007

GIS Data Available (links require username/password: landforms/rock):
FEMA flood maps: https://geo.mnsu.edu/geo/DNR-InvasiveCarp/Carson-Inundation/Carson'sAPP/Carson's%20Flood%20Mapping/Cleaned_Output/
New flood maps produced in this study:
5-year: https://geo.mnsu.edu/geo/DNR-InvasiveCarp/Carson-Inundation/Carson'sAPP/Carson's%20Flood%20Mapping/Cleaned_Output/RI_5yr/
10-year: https://geo.mnsu.edu/geo/DNR-InvasiveCarp/Carson-Inundation/Carson'sAPP/Carson's%20Flood%20Mapping/Cleaned_Output/RI_10yr/
25-year: https://geo.mnsu.edu/geo/DNR-InvasiveCarp/Carson-Inundation/Carson'sAPP/Carson's%20Flood%20Mapping/Cleaned_Output/RI_25yr/
50-year: https://geo.mnsu.edu/geo/DNR-InvasiveCarp/Carson-Inundation/Carson'sAPP/Carson's%20Flood%20Mapping/Cleaned_Output/RI_50yr/
100-year: https://geo.mnsu.edu/geo/DNR-InvasiveCarp/Carson-Inundation/Carson'sAPP/Carson's%20Flood%20Mapping/Cleaned_Output/RI_100yr/
FloodScript: https://geo.mnsu.edu/geo/DNR-InvasiveCarp/Carson-Inundation/Carson'sAPP/Carson's%20Flood%20Mapping/Flood_Script/

GageData: https://geo.mnsu.edu/geo/DNR-InvasiveCarp/Carson-Inundation/Carson'sAPP/Carson's%20Flood%20Mapping/Gage%20Data/

1. Introduction

Floods occur when a river's discharge exceeds its bankfull capacity (Castro and Jackson 2001) and commonly occur along active fluvial channels as part of the natural hydro-geomorphic flow regime. When floods take place, flows spill into a river's floodplain - a relatively flat topographic feature adjacent to a river channel formed solely or in combination from lateral accretion, vertical accretion, or braid channel accretion (Mertes 1997; Nanson and Croke 1992; Castro and Jackson 2001; Tockner and Stanford 2002). The physical characteristics of a floodplain and its flood regime will impact its hydrologic connectivity laterally, longitudinally, vertically, and temporally (Amoros and Bornette 2002). Hydrologic connectivity within a floodplain will vary depending on the spatial distribution of landforms (oxbow lakes/riverine lakes, floodplain ponds and marshes, side arms, backwaters, cut-offs etc.) created by fluvial processes acting within the floodplain (Galat et al. 1997; Amoros and Bornette 2002). Flood inundation mapping is a method used to better understand how a floodplain becomes hydrologically connected as river flood waters rise. Understanding the relationship between flooding and floodplain connectivity is crucial for analyzing the possible hydrologic avenues in which invasive fish species, such as Eurasian carp, can utilize to migrate and naturalize in the Minnesota River Basin (Figure 1.1).
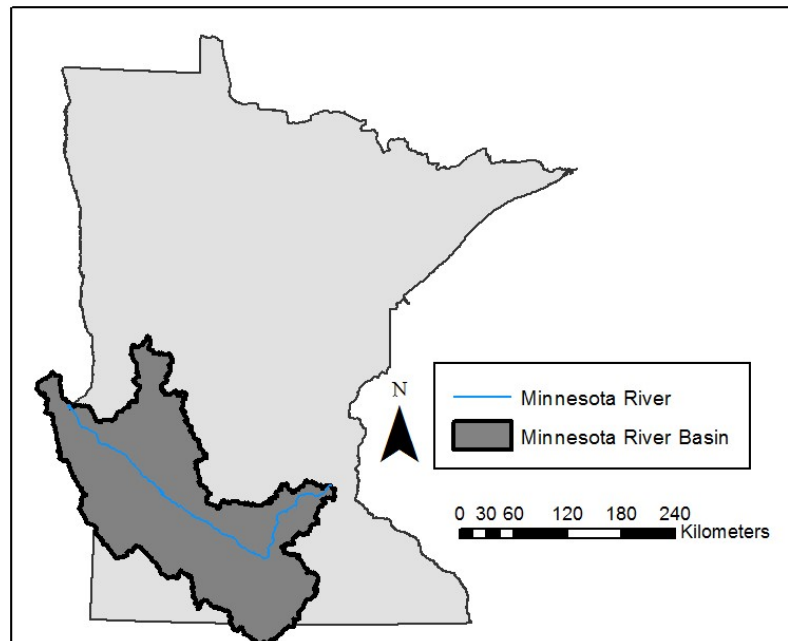
Figure 1.1. This map shows the extent of the 44,000 km^2 Minnesota River Basin

1.1. Overview of Standard Methodology for Flood Inundation Mapping:

Typically, flood inundation mapping begins with the calculation of a design flow (i.e. hypothetical flow used for planning) through either hydrologic or statistical models. Hydrologic models estimate flows through precipitation/runoff analysis while statistical models estimate flows through flood frequency analysis (Merwade et al. 2008). Cross-sections are then constructed in locations that capture topographic variations and possible flow obstructions in the floodplain from data collected in the field or from topographic maps/digital topography (FEMA 2011). The most accurate cross-sections will include detailed channel geometries from field surveyed river bathymetry (National Research Council 2009). Surface water elevations are estimated from a hydraulic model that input flows calculated from hydrologic/statistical models, cross-sections, floodplain structure data, and other hydraulic parameters such as Manning's Roughness Coefficients. The surface water elevations are geo-referenced to a Digital Terrain Model (DTM) where the DTM is then subtracted from the water surface to show flood depth and extent (Merwade et al. 2008). As this suggests, mapping flood inundation in this way is extremely laborious and resource (both financial and in terms of time) intensive. Large budgets and extensive temporal frameworks are necessary to complete this sort of methodology on large rivers.

1.2 Flood Inundation Mapping in the United States (A Broader Relevance):

In order reduce the impact of flooding on private and public structures in the United States, the National Flood Insurance Program (NFIP) was created from the passage of the 1968 Housing and Urban Development Act and encouraged communities to implement floodplain management regulations as well as provide flood insurance to property owners (Browne and Hoyt 2000; FEMA 2016). This eventually led to the development of The Flood Disaster Act of 1973, which directed local governments to map the spatial extent of the 100-year floodplain in areas of land development (Altenstadter and Clark 1974; Baker 1975). The Federal Emergency Management Agency (FEMA) is responsible for producing and maintaining Flood Insurance Rate Maps (FIRMs) to accomplish this agenda. From 2003 to 2008 the federal government spend approximately $1 billion to improve/update the nations flood maps and convert them into digital Flood Insurance Rate Maps (dFIRMs).

1.2.1. FEMA's Process of Constructing Flood Maps:

The process for creating flood maps involves three main phases (National Research Council, 2009). The first phase is carried out by both FEMA and state/local officials in which local needs are identified and flood risks are assessed. The type of flood study that is carried out is determined by the available resources and the identified risks/needs of the local community.

FEMA distinguishes between four types of approaches used to create flood inundation maps: Detailed, Limited/Detailed, Approximate and Redelineation studies (National Research Council, 2009). Detailed studies provide the most information about flood hazards such as flow estimates, floodway data tables, and flood elevation profiles and require extensive field work to determine dimensions of structures in the floodplain

such as bridges, flood walls, and culverts etc.   Limited/Detailed flood studies provide flood elevations and profile information but not flow estimates. Floodplain structures are incorporated into the models but their dimensions and elevations are not ground-truthed in the field. Approximate flood studies do not provide details of the flood hazard and only produce a rough outline of the floodplain. The accuracy of approximate studies are usually insufficient to meet regulatory standards. Redelineation studies simply digitize flood boundaries from existing flood elevation information onto the most recent topographic map/digital elevation map.

The second phase is when the map project begins and the agreed upon flood study type is conducted. This entails a period of data collection, modeling, map creation, and a quality control assessment (National Research Council 2009). This phase is the longest part of the process and can take from one to two years to complete. The third phase includes an appeal period where the floor is opened up for local community input/concerns and an adoption period where the map is finalized and adopted by the local community.

1.3. FEMAs Progress in the Minnesota River Valley:

There are currently nine counties along the Minnesota River that contain unmodernized dFIRMs and seven counties that contain modernized dFIRMs (Figure 1.2). The modernized sections of the Minnesota River contain effective map dates ranging from 2006 – 2016 while the unmodernized sections of the river contain effective map dates ranging from 1976 – 2000. The dates of effective map panels can be searched on FEMA's website (FEMA 2016).
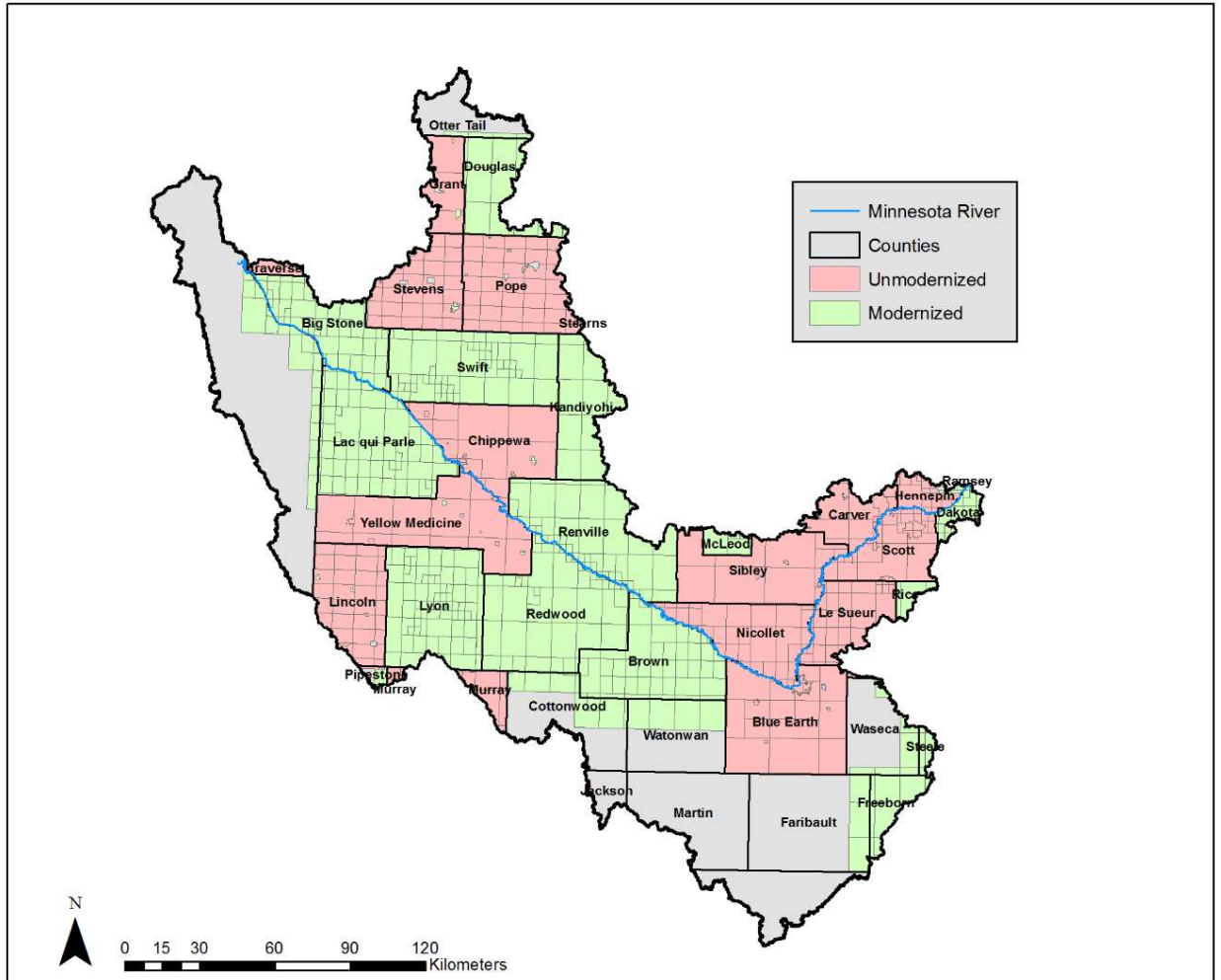
Figure 1.2. This map shows counties in the Minnesota River Basin that are modernized (Green) and those that are unmodernized or in the processes of modernization (Red).

1.3.1. Issues Using FEMA dFIRMs for Basin Wide Flood Analysis and Backwater Connectivity

Depending on the type of study, flood mapping can be costly and time consuming. The cost of flood studies typically ranges from $900 per river mile for approximate studies to $13,500 per river mile for detailed studies (National Research Council 2009). Flood maps are not updated on a regular schedule despite constant changes occurring within the floodplain. This is largely because flood studies are conducted county by county and can take up to three years or more to complete (National Research Council 2009), which can result in outdated river sections. There is no requirement that streamline used in a particular county study matches across county boarders. This results in gaps or overlaps in flood layers between counties (Figure 1.3). Adding to this inconsistency, methods may vary by each county depending on the contractor hired to conduct the study. Also, because the flood studies were conducted at different times, the resolution of the base terrain/digital elevation map used to calculate flood depths vary greatly. This results in flood maps showing certain floodplain features

as inundated when they should not have been (Figure 1.4) and disconnected flood levels when examining reaches along the reach of the river.
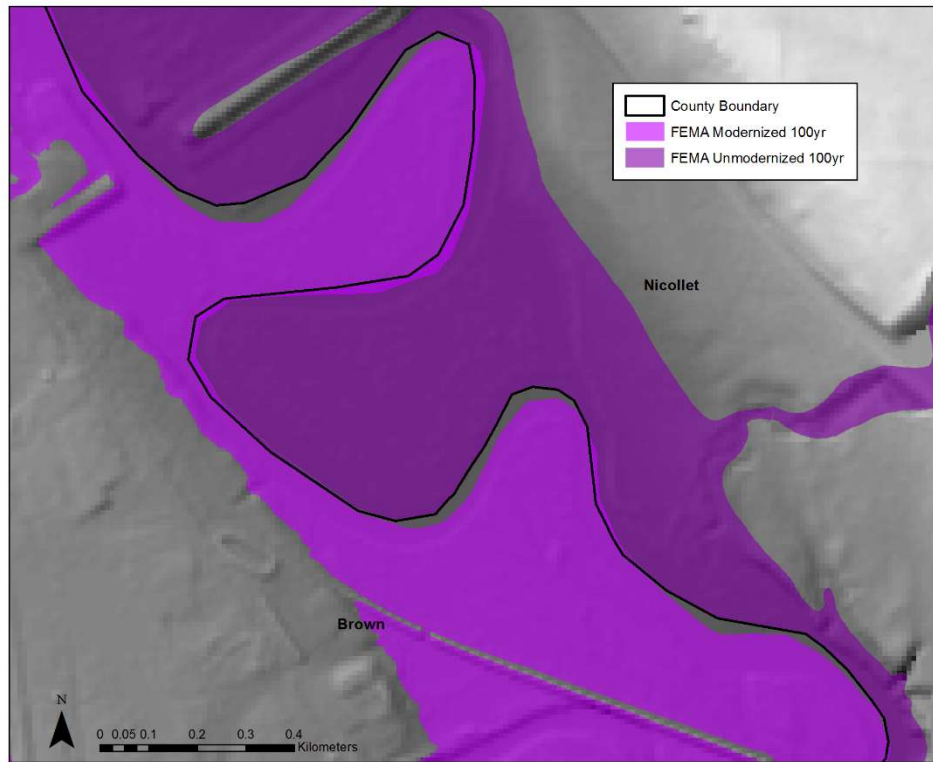
Figure 1.3. This map shows a common discrepancy between different county FEMA dFIRM layers.
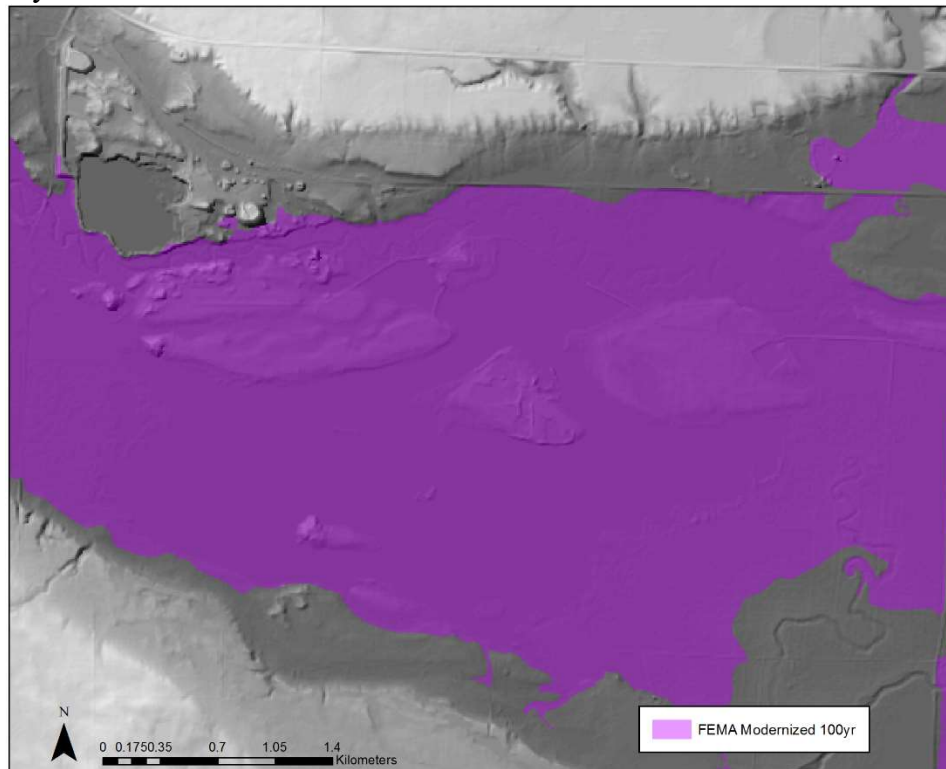
Figure 1.4. This map shows features within a floodplain that are shown to be inundated by FEMA's dFIRM 100-year flood layer that should not be. Note some of the higher topography within the floodplain. This is much higher than the 100-year flood level, but is, for some unknown reason, incorporated as inundated.

Certain geospatial tools such as the Floodplain Mapper Toolbox (FMT) have shown applicability for creating large-scale flood maps without some of these aforementioned issues in FEMA maps (NCED 2016). The FMT was developed to extend the functionality of a larger toolset called the Barr-NCED Floodplain Mapper (Belmont et al. 2009). The user of the FMT is first required to create cross-sections on in order to identify the geomorphic top of channel bank, which is ultimately used to estimate the elevation of bankfull discharge. Following this, the user interpolates a flood surface elevation from the base elevation of bankfull discharge. Flood elevation values used to generate the flood surfaces are determined by raising the flood surface for each cross-section by a uniform user defined amount (i.e. elevation) above the bankfull level. While this is an efficient way to create large-scale (i.e. more "zoomed in") flood maps, it is not optimal for creating flood maps on a smaller, basin wide scale because of varying topography and hydrology. It is difficult to connect entire river reaches using this tool to create uniform estimation of flood inundation throughout a river valley.

In what follows is a description of a methodological approach developed and tested on the Minnesota River valley of south-central Minnesota, USA. This method attempts to address the difficulties discovered in the methodologies used previously by government agencies and in the scholarly literature. We describe these issues above. This new tool is designed to estimate continuous flood inundation levels throughout the entirety of the Minnesota River valley. We qualitatively test this model against the FEMA maps for the Minnesota River valley to verify the effectiveness of this new tool. This section of the report will include a tutorial for future users on how to conduct this analysis for themselves and have a detailed discussion regarding the associated uncertainties and assumptions inherent in this analysis. If questions arise, please contact the corresponding author listed.

2. A Semi-Automated Geospatial Approach to Inundation Mapping

The method designed for this study utilizes flood stage data from Minnesota River stream gages that are maintained by the United States Geological Survey (USGS) and the National Weather Service (NWS), as well as a 10-meter Light Detection and Ranging (LiDAR) derived Digital Terrain Model (DTM), (USGS 2016; US Department of Commerce 2016). The workflow for this method was partially automated using the scripting/programming language Python 2.7, as well as ESRI ArcGIS 10.3.

2.1. Preliminary Workflow

2.1.1. Manual Procedures
A number of prerequisite manual procedures were required for input into the automated part of the workflow (Figure 2.1). This included calculating recurrence

intervals (RI) of stage heights obtained from nine gages (Table 1) along the Minnesota River and the digitization of cross-sections at each gage location perpendicular to the slope of the floodplain (Figure 2.1.1). The RI were calculated at each gage for the largest flood on record for each year of recorded data using the Weibull plotting-position formula (Hjalimarsom and Thomas, 1992; Makkonen, 2005):

$$\text{eq: } RI = (n+1)/m$$

where n is the number of years on record while the variable m is the ranked order of flood magnitude with 1 being of the largest magnitude. Stage heights corresponding to an RI were input into the attribute table of the cross-sections in ArcMap 10.3. The cross-section shapefile was then used as input for the automated construction of flood surface elevations.

Given the difficulty we experienced in trying to conduct this analysis using prior methods (discussed previously) like those originally proposed and the uncertainty present in the changing hydrologic regime of the Minnesota River basin, we utilized this traditional RI calculation within this newly developed tool and strongly suggest this only be used as an estimation. The limited temporal framework of this work and the need for a tool to create a uniform, continuous estimation of flood inundation throughout the river valley required we prioritized development of this new tool and we used a very traditional RI calculation to test the tool against the FEMA maps. We did not have time to test multiple RI calculations or thoroughly field check the cross-sections utilized. That said, any method to calculate RI could be substituted into this tool and used for future estimations. The corresponding author could assist in this, if needed.
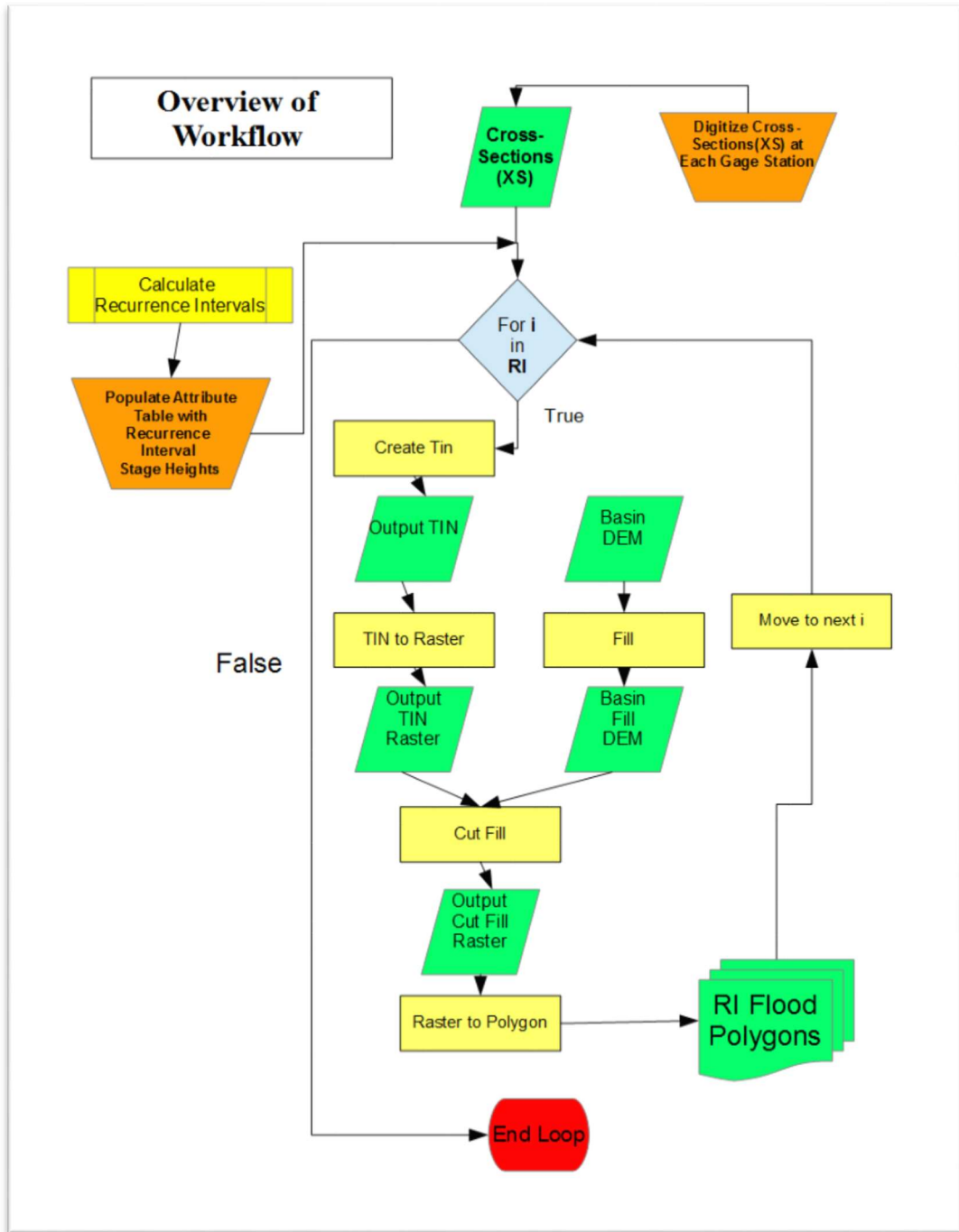
Figure 2.1. This flowchart is an overview of the initial workflow for creating flood surfaces. Orange trapezoids represent manual process. Yellow rectangles with an extra set of lines represent processes that contain multiple steps where the yellow rectangles without the extra set of lines represent a single process. Green parallelograms represent an output layer from a process.
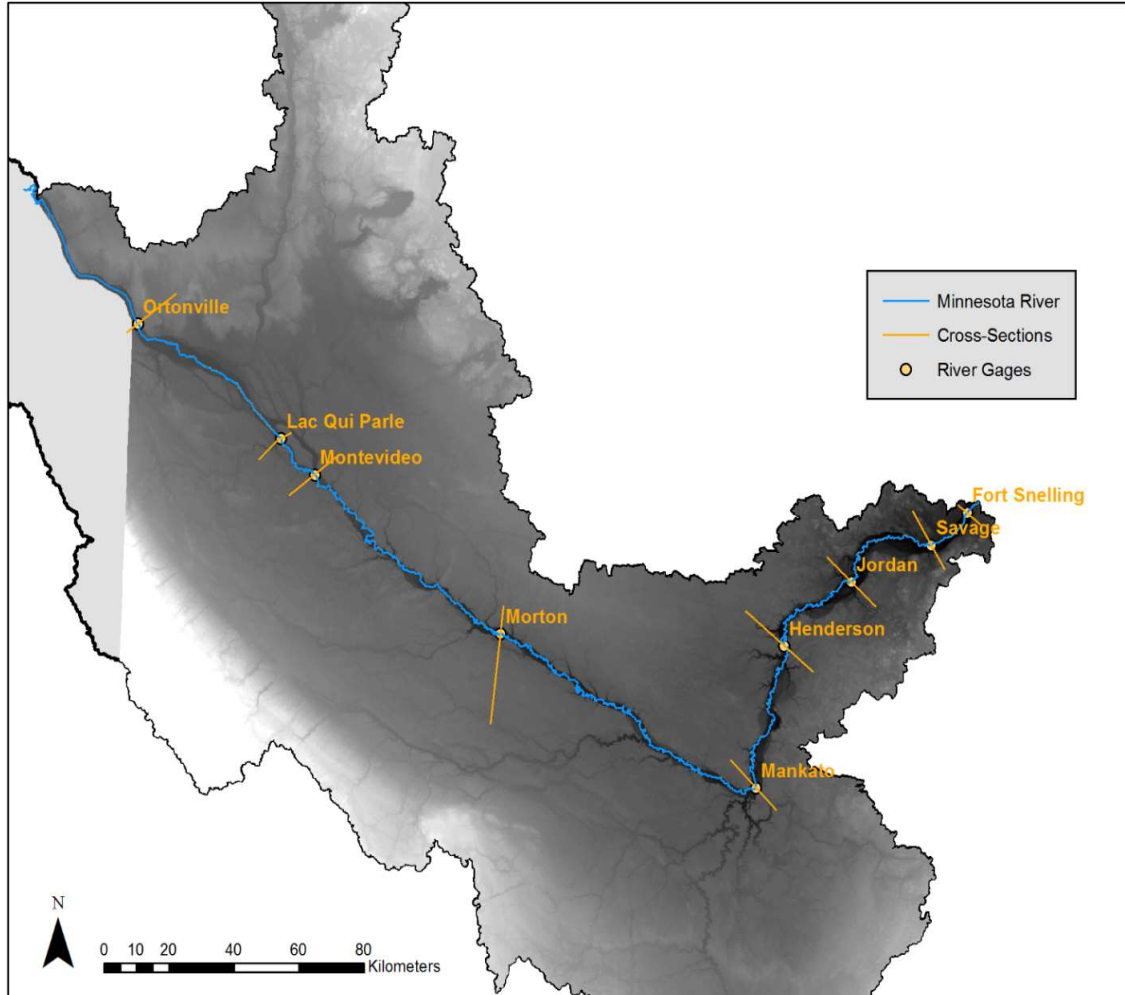
Figure 2.1.1. This figure shows the locations of the river gages along the Minnesota River and the cross-sections used to create the flood surfaces in the initial workflow.

2.1.2. Automation Procedures for Stage Heights of Each RI

The automation of flood surface elevations was written in Python 2.7 and relied on the use of the ArcPy module. The basic steps of this script can be viewed in Figure 2.1. A Triangulated Irregular Network (TIN) was created from the digitized cross-sections for an elevation of a particular RI and was converted into a raster. Then, a Cut-Fill procedure was used to subtract the flood elevation raster from the basin digital terrain model (DTM). The resulting raster was converted to a polygon and selected by location to a Minnesota River shapefile in order to obtain parts of the flood polygon that could be considered hydrologically connected. This process was repeated in a loop until flood polygons were created for all stage heights associated with 5, 10, 25, 50, and 100 year RIs. Data variability and availability from gaging station to gaging station, with a max record of less than 100 years, resulted in no 500 year analysis being conducted. We did not feel confident in the high level of uncertainty in such a calculation both due to limited data availability and the changing hydrologic nature of the Minnesota River valley.

13

2.1.3. Observed Limitations of Preliminary Workflow:

The limitations of the preliminary workflow were apparent in the results.   The linear interpolation of elevation values between cross-sections were vulnerable to underestimation and overestimation with respect to the elevation values of the basin DTM.   Underestimation was more pronounced in the 5yr flood elevation surface (Figure 2.1.2) and overestimation was more pronounced in the 100yr flood elevation surface (Figure 2.1.3). By itself, overestimated flood surfaces are harder to find. The FEMA 100-year floodplain shapefile can be used for comparison when looking for areas of overestimation in a flood surface (Figure 2.1.4). The underlying reason for over and underestimation in the flood surface is due to variability in the floodplains topography and slope. In order to account for the flood surfaces to portray variability in topography and slope, new procedures were added to the workflow.
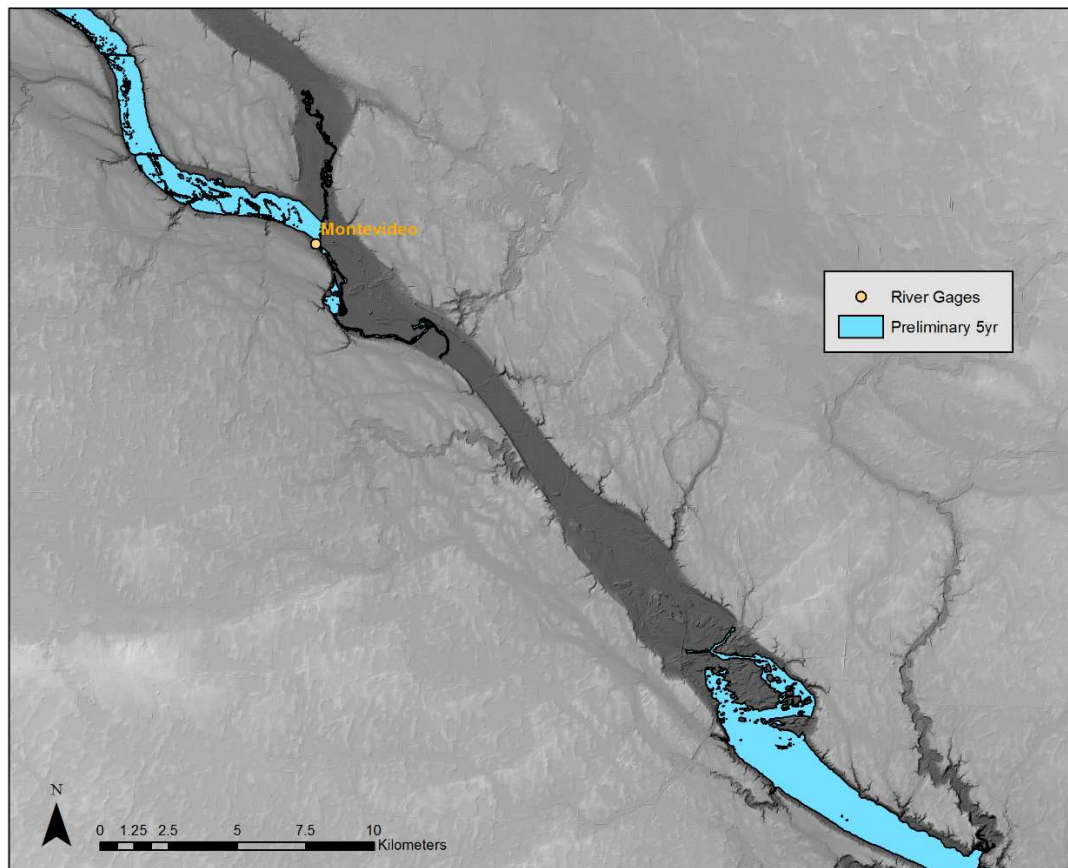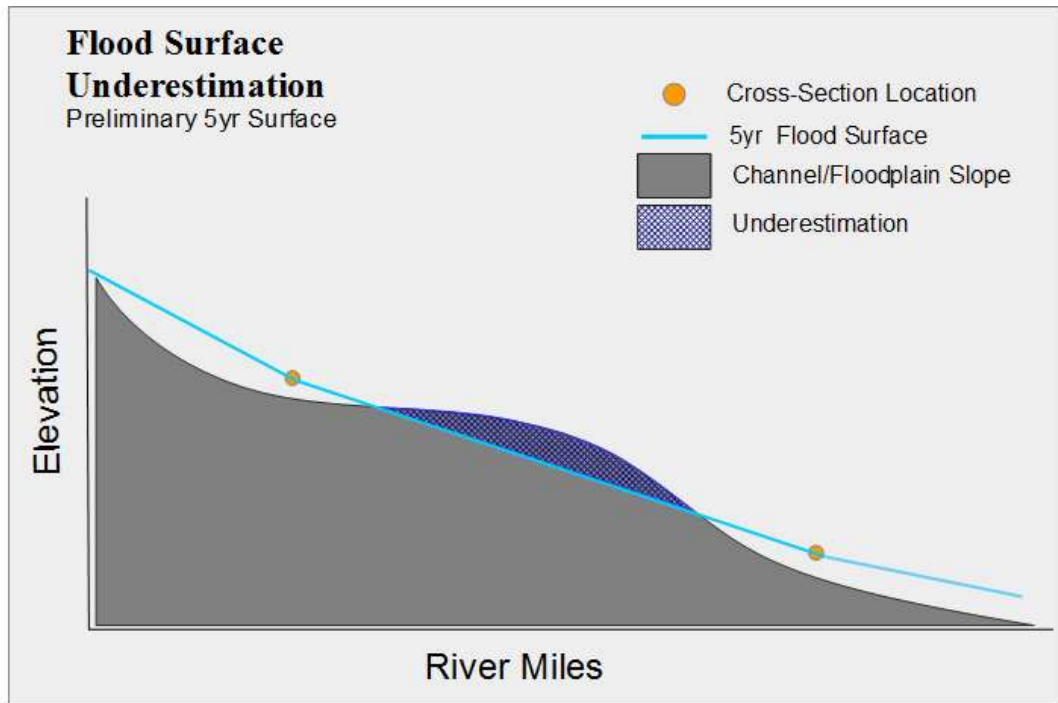
Figure 2.1.2. The top map shows where a section of the 5-year flood surface is interpolated below the elevations of the floodplain in the DTM between Mankato and Montevideo. The bottom picture is a simplified profile interpretation of what is happening in the top map.
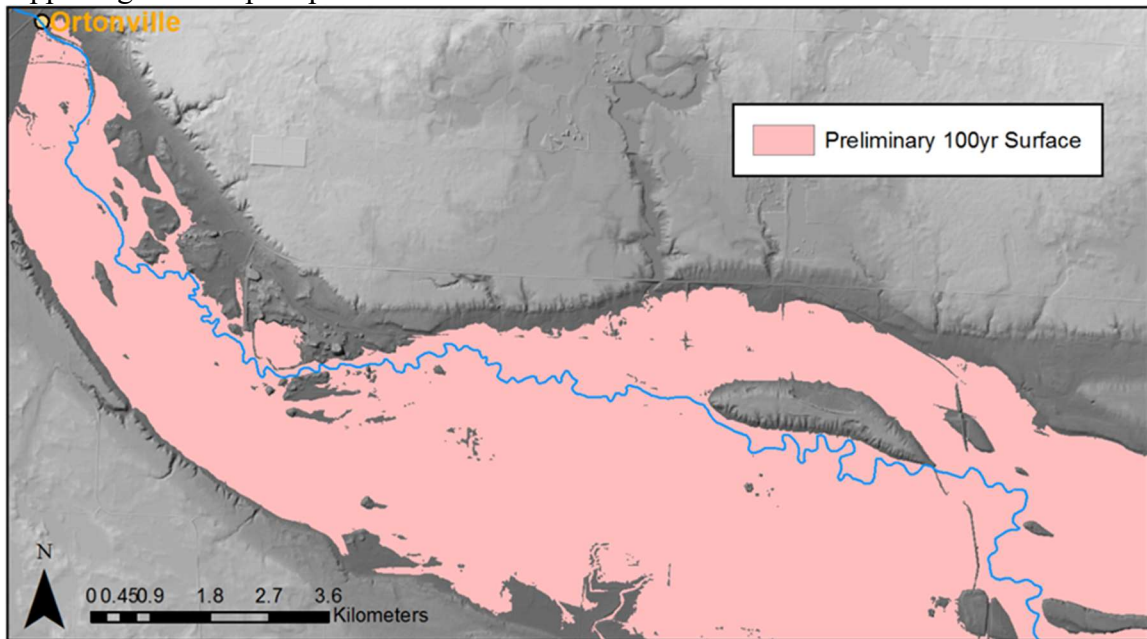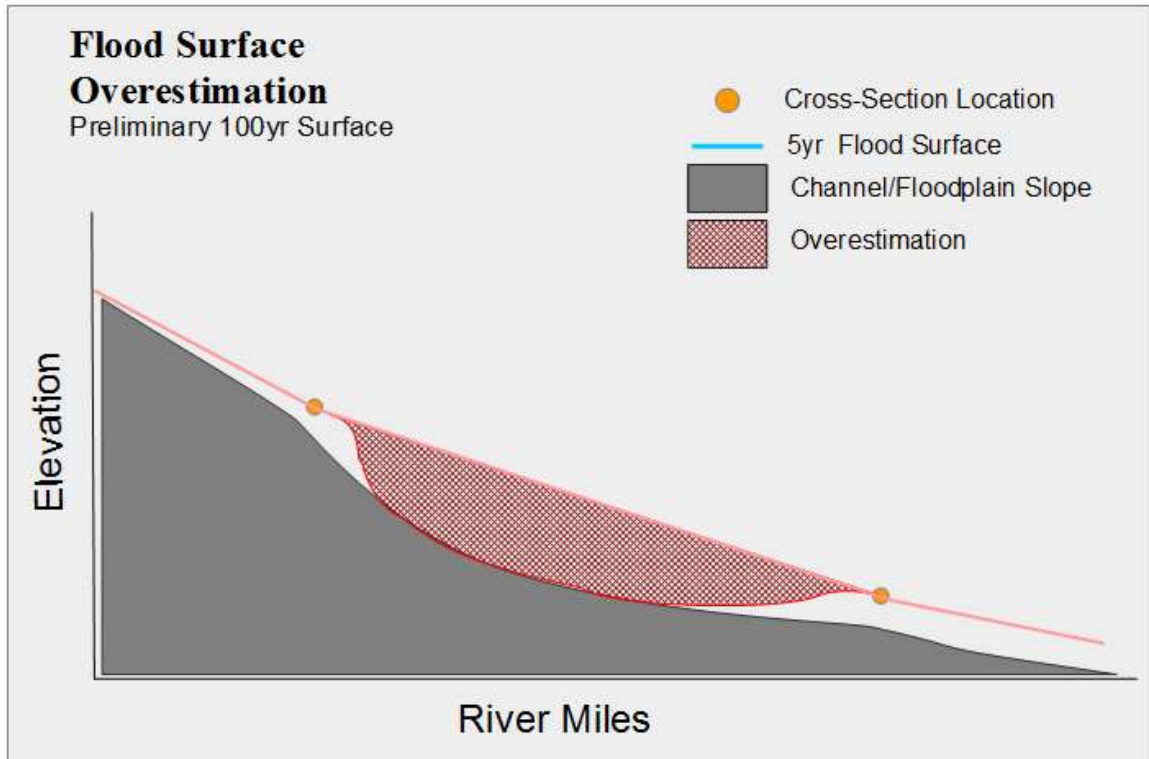
Figure 2.1.3. The top map shows where a section of the 100-year flood surface is overestimated with regards to elevations of the floodplain in the DTM. The bottom picture is a simplified profile interpretation of what is happening in the top map.
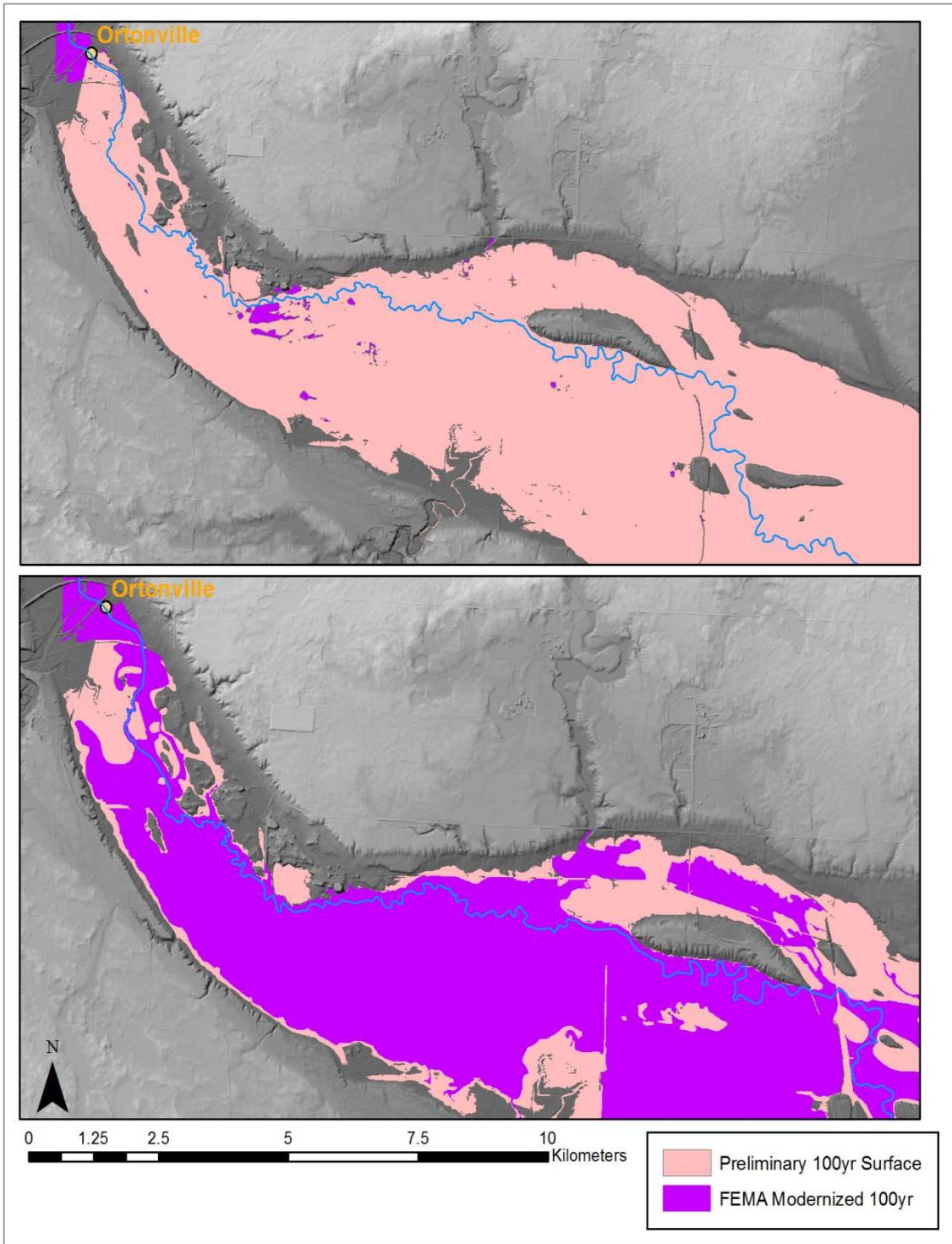
Figure 2.1.4. This figure shows a comparison between the preliminary 100-year flood surface and FEMAs 100-year flood surface. The top map shows the FEMA layer overlaid by the preliminary layer. The bottom map shows the FEMA layer overlaying the preliminary layer.

2.2. Adjusted Workflow

New manual procedures were added in order to systematically create more cross-sections. A collection of automated procedures was added in order to ensure that the flood surface outputs were influenced by the underlying topography. An overview of the adjusted workflow can be viewed in Figure 2.2.
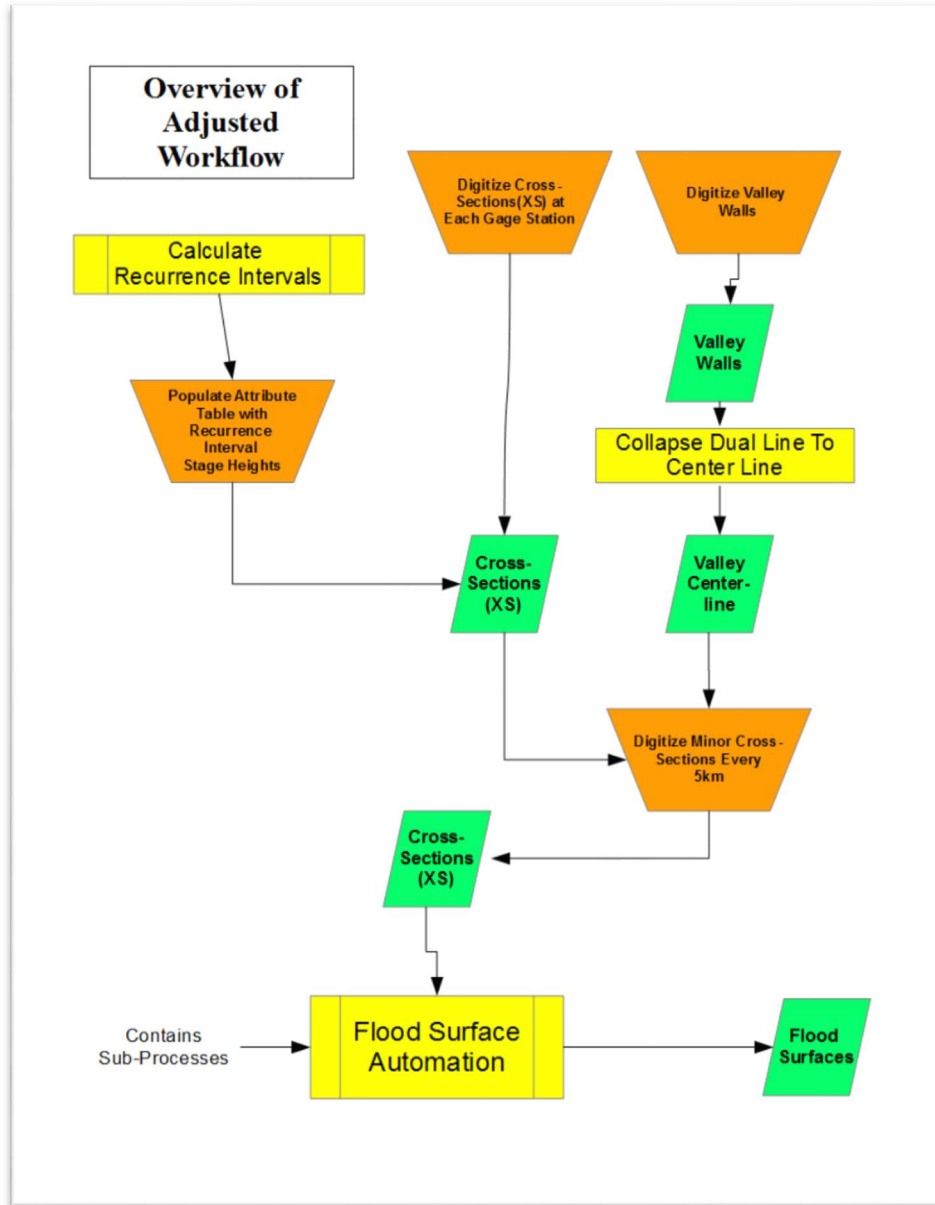
Figure 2.2. This flowchart is an overview of the adjusted workflow of creating flood surfaces. Orange trapezoids represent manual process. Yellow rectangles with an extra set of lines represent processes that contain multiple steps where the yellow rectangles without the extra set of lines represent a single process. Green parallelograms represent an output layer from a process.

2.2.1. Manual Procedures

In order to capture the variability of floodplain topography and slope, more cross-sections needed to be digitized from Ortonville to Mankato. From this point forward, cross-sections that are associated with a river gage will be referred to as major cross-sections. Cross-sections digitized between the major cross-sections will be referred to as Minor or Intermediate cross-sections. Minor cross-sections were digitized at equal 5 kilometer intervals while intermediate cross-sections were digitized at distinct breaks in the slope due either to natural knickpoints or anthropogenic flow control structures. These new cross-sections allows the interpolated flood surface to adjust to variable floodplain topography.

To create the minor cross-sections at equidistant intervals, the Minnesota River valley walls were digitized excluding upper terraces that did not reflect the slope direction of the contemporary floodplain. Using ArcMap's 'Collapse Dual Lines to Centerline' tool a Valley Centerline shapefile was created. Minor cross-sections were then digitized approximately every 5 kilometers along the Valley Centerline shapefile (Figure 2.2.1). Intermediate cross-sections were digitized immediately upstream and downstream from flood control structures that result in an abrupt change in elevation (Figure 2.2.2). This is to enforce an abrupt elevation change when interpolating a flood surface using elevation data stored in the cross-sections.

A base stream elevation represented in the DTM was assigned to every cross-section at the point of intersection. The LiDAR derived DEMs from MnGeo have been 'hydro-flattened' which results in consistent water surface below a bankfull discharge. Base elevations were added to each cross-section for later use as a reference point in the automated section of the workflow.
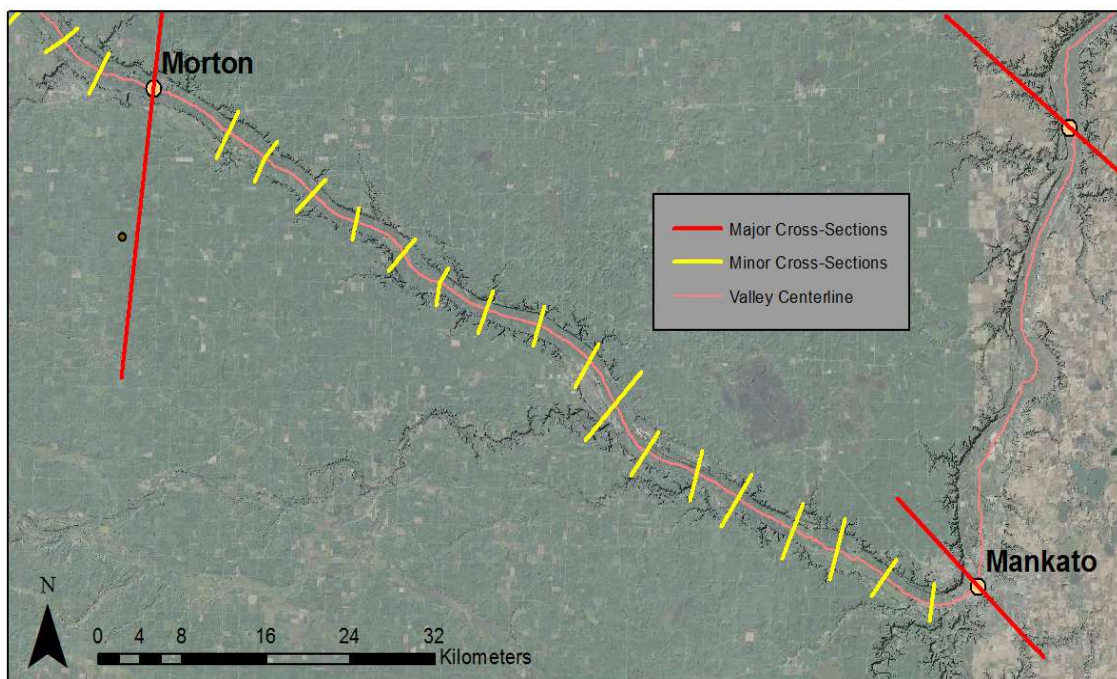
Figure 2.2.1. Minor cross-sections were digitized approximately every 5 kilometers along a valley centerline.
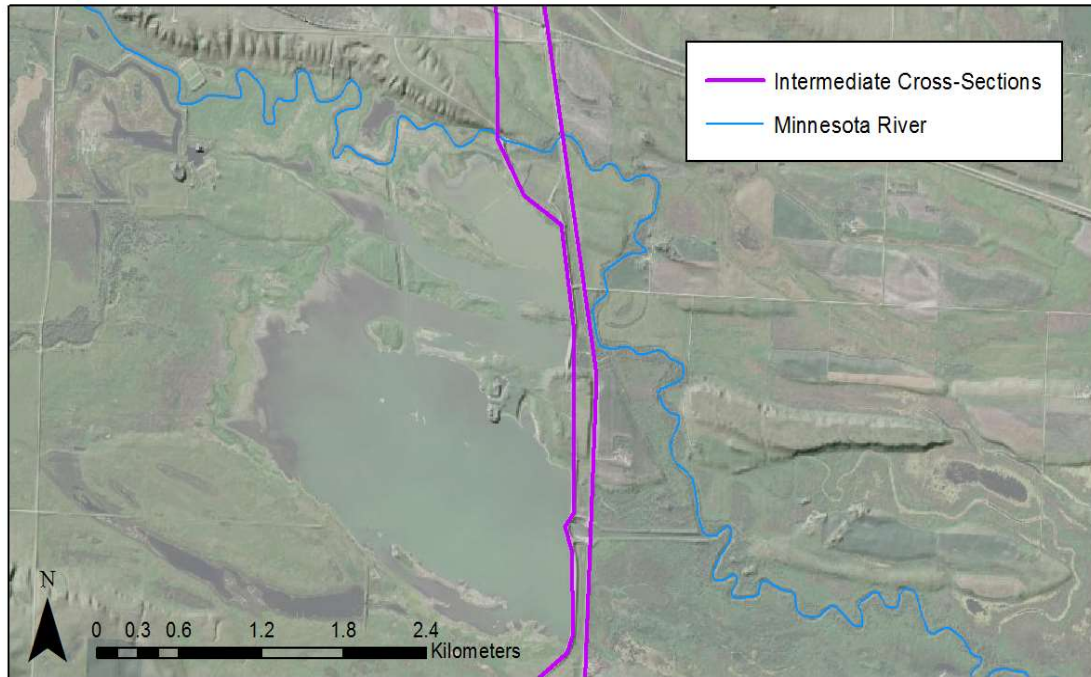
Figure 2.2.2. Intermediate cross-sections are digitized immediately upstream and downstream from flow control structures.

2.2.2. Automated Procedures

Once the new cross-sections were complete, they were input into the flood surface automation process consisting of seven steps (Figure 2.2.2.1.). Each step consists of its own sub-processes that will be explained in detail (2.2.2a. – 2.2.2i.). Note that the workflow described in Figure 2.1. is the seventh step in this automated procedure.
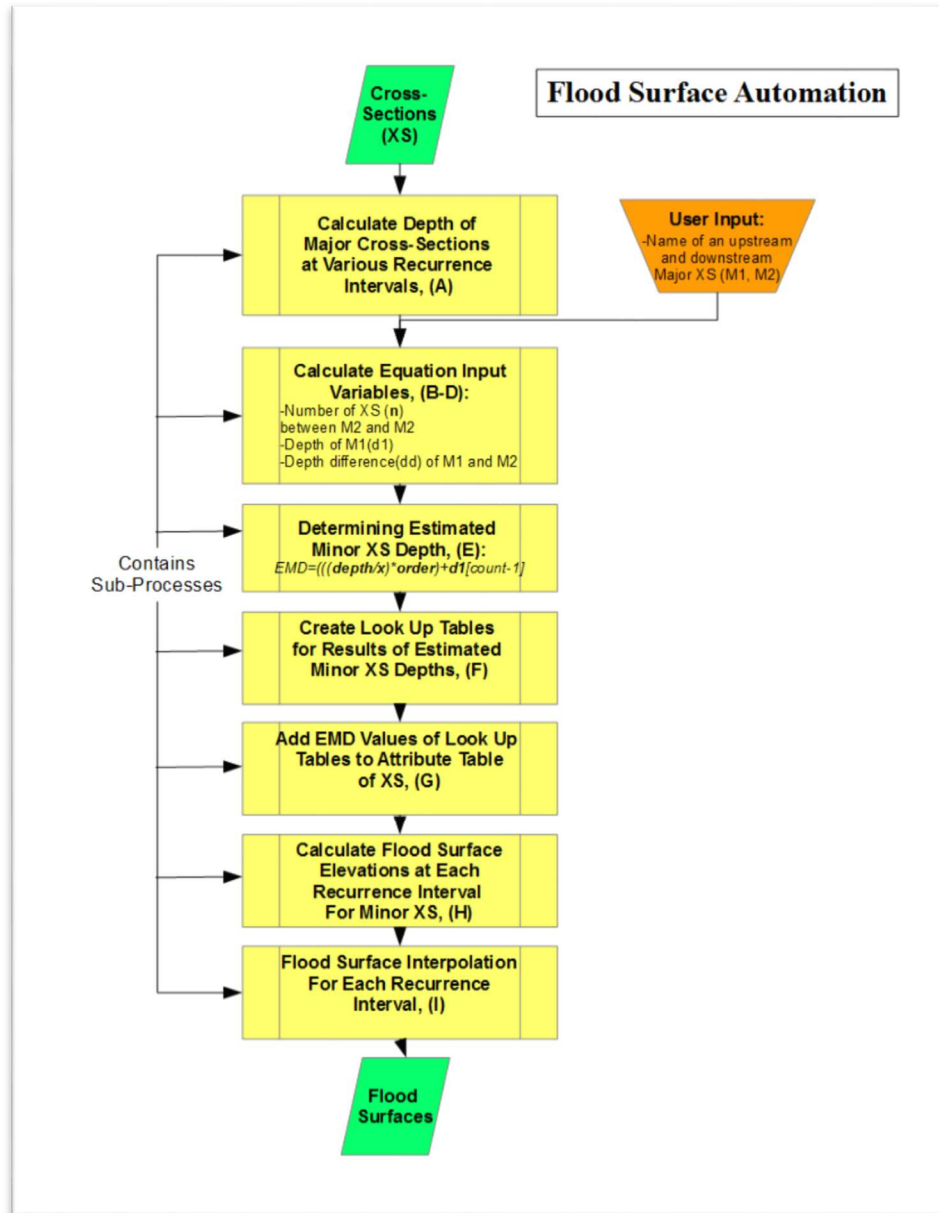
Figure 2.2.2.1. This figure shows the seven processes that make up the 'Flood Surface Automation' process in Figure 2.

Step 1: Calculate Depth of Major Cross-Sections at Various Recurrence Intervals (A)

The first step is to calculate the differences (depths) at each major cross-section between the elevation of each recurrence interval and the corresponding base stream elevation (Figure 2.2.2a.). This was accomplished by creating a 'nested loop', or in other words a loop inside a loop. The outside loop iterates through each field in the cross-section attribute table that corresponds with a recurrence interval while the inside loop iterates through each row. Note that each row with the attribute table corresponds to an individual cross-section. With each iteration of the inside loop depth was calculated by subtracting base stream elevation from the elevation of a recurrence interval. A

conditional statement followed to ensure that any field lacking an elevation for a recurrence interval (i.e. all minor and intermediate cross-sections) received a depth of zero as opposed to a negative number. After all major cross-sections received depth values, the attribute table was updated and used as input for Step 2.
Step 2: Calculate Equation Input Variables (B-D)

Given the names of two major cross-sections, Step 2 creates variables that will be used as input for an equation that will calculate depth values for the minor and intermediate cross-sections. (Figure 2.2.2b. – Figure 2.2.2d.). The same nested loop structure used in Step 1 is implemented in Step 2. First (Figure 2.2.2b.), two lists containing depth values and two lists containing the downstream order for the selected major cross-sections are stored as variables. Second (Figure 2.2.2c.), minor and intermediate cross-sections were appended to a list if their downstream order fell in between the downstream order of the selected major cross-sections. In addition, the number of interlaying minor and intermediate cross-sections (n) was stored as a variable. Third (Figure 2.2.2d.), four variables are finalized for the equation in Step 3 which are: 1). The number of minor and intermediate cross-sections (n), 2). The relative downstream order of the minor and intermediate cross-sections (DO), 3). The depth list variable of the major cross-section that is furthest upstream (D1), and 4). The depth difference list variable calculated from both major cross-sections. The relative downstream order is calculated using the index values of the actual downstream order list. The depth difference variable is simply calculated by subtracting the downstream depth value by the upstream depth value.

Step 3: Determine Estimated Minor/Intermediate Cross-Section Depths (E)

In Step 3 (Figure 2.2.2e.), the Estimated Minor/Intermediate Depth (EMD) is calculated in the inner loop of a 'nested loop' at each recurrence interval for each cross-section that resides between two selected major cross-sections. The purposed formula for calculating EMD is:

$$\text{eq. EMD} = (((\text{depth}/\ x) * \text{order}) + d1[\text{count -1}])$$

where depth refers to a DD list value, x refers to the number of minor/intermediate cross-sections plus one (n+1), order refers to a relative DO list value and d1 refers to the depth of the upstream major cross-section. Essentially, this is a stepwise calculation where a depth value is output for each recurrence interval starting with the furthest upstream minor/intermediate cross-section and working its way to the next downstream cross-section. To ensure that flood surface elevations don't increase when a reservoir is reached, the script checks the base DEM value from the upstream cross-section. If the values did not change, the EMD value for the current cross-section will not increase. The results are then appended in the correct downstream order to a list variable titled EMD and are grouped by recurrence interval. This list is then organized in Step 4.

Step 4: Create Look Up Tables for Results of Estimated Minor Cross-Section Depths (F)

In Step 4 (Figure 2.2.2f.), the EMD list created in Step 3 is broken up into five separate lists each containing values corresponding to a recurrence interval (5-year, 10-year, 25-year, 50-year, 100-year). In order for this process to be automated, the number of minor/intermediate cross-sections (n) is used to correctly break apart the EMD list. For example, let's say that n = 8. The resulting length of the EMD list, assuming five recurrence intervals, would be 40. Because the list values are first ordered by recurrence interval and second by relative downstream order, n can be used to break up the according to its index value. The five resulting lists are then combined with the actual downstream order list (DO) to create five dictionaries of keys and values where the keys contain downstream orders and the values contain the depths. This was necessary in order reference the calculated depth values to the correct cross-section in Step 5.

Step 5: Add EMD Values of Look Up Tables to Attribute Table of Cross-Section (G)

In Step 5 (Figure 2.2.2G.), estimated depth values are added to each minor/intermediate cross-section in the shapefiles attribute table.   A conditional statement was placed inside of a nested loop that checked if the downstream order in the attribute table was equal to keys in all five dictionaries. If it was, depth values were added. If it wasn't, it would move on to the next recurrence interval until all cross-sections and recurrence intervals where checked.

Step 6: Calculate Flood Surface Elevations at Each RI for Minor Cross-Sections (H)

In Step 6 (Figure 2.2.2H.), flood surface elevations are calculated for each minor/ intermediate cross-section and recurrence interval by simply adding the base stream elevation to the estimated depth calculated in the prior five steps.

Step 7: Flood Surface Interpolation for Each RI(I)
Step 7 (Figure 2.2.2I.) is the final step in creating flood surfaces at each recurrence interval and contains the same workflow as the whole automated process in the preliminary methodology.
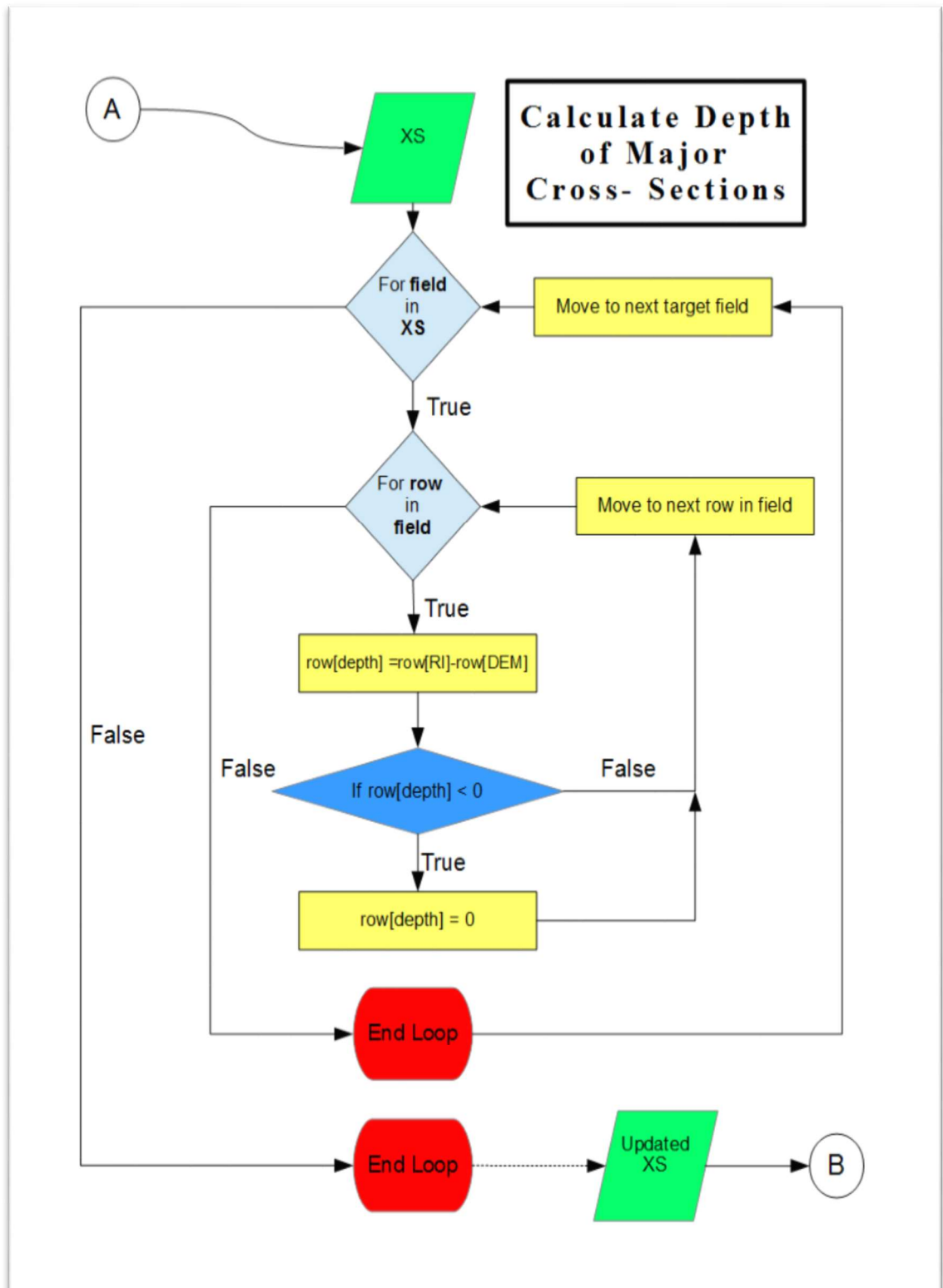
Figure 2.2.2.A. This figure shows the workflow for Step 1 in the automated process.
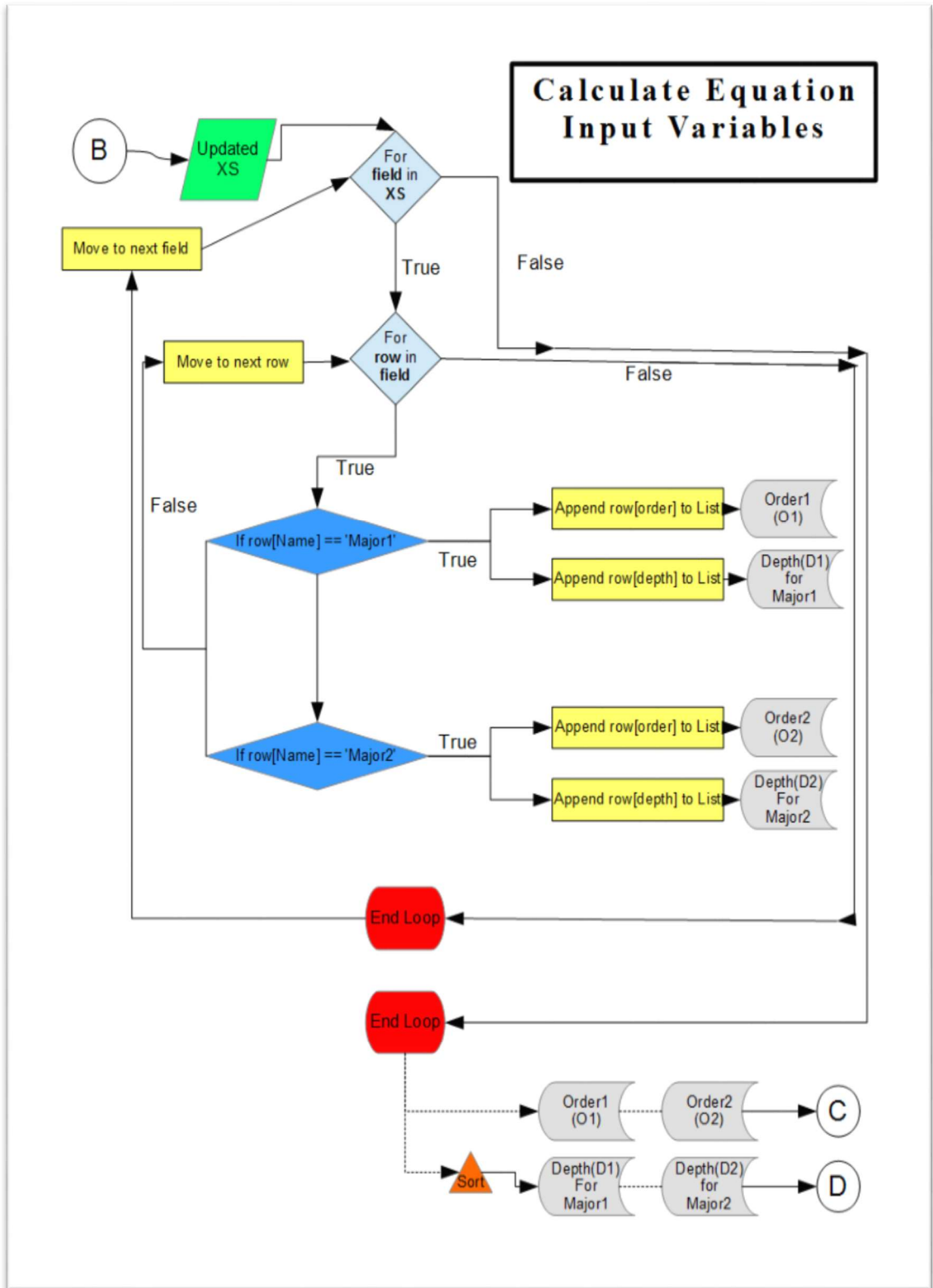
Figure 2.2.2.B. This figure shows the workflow for Step 2b in the automated process.
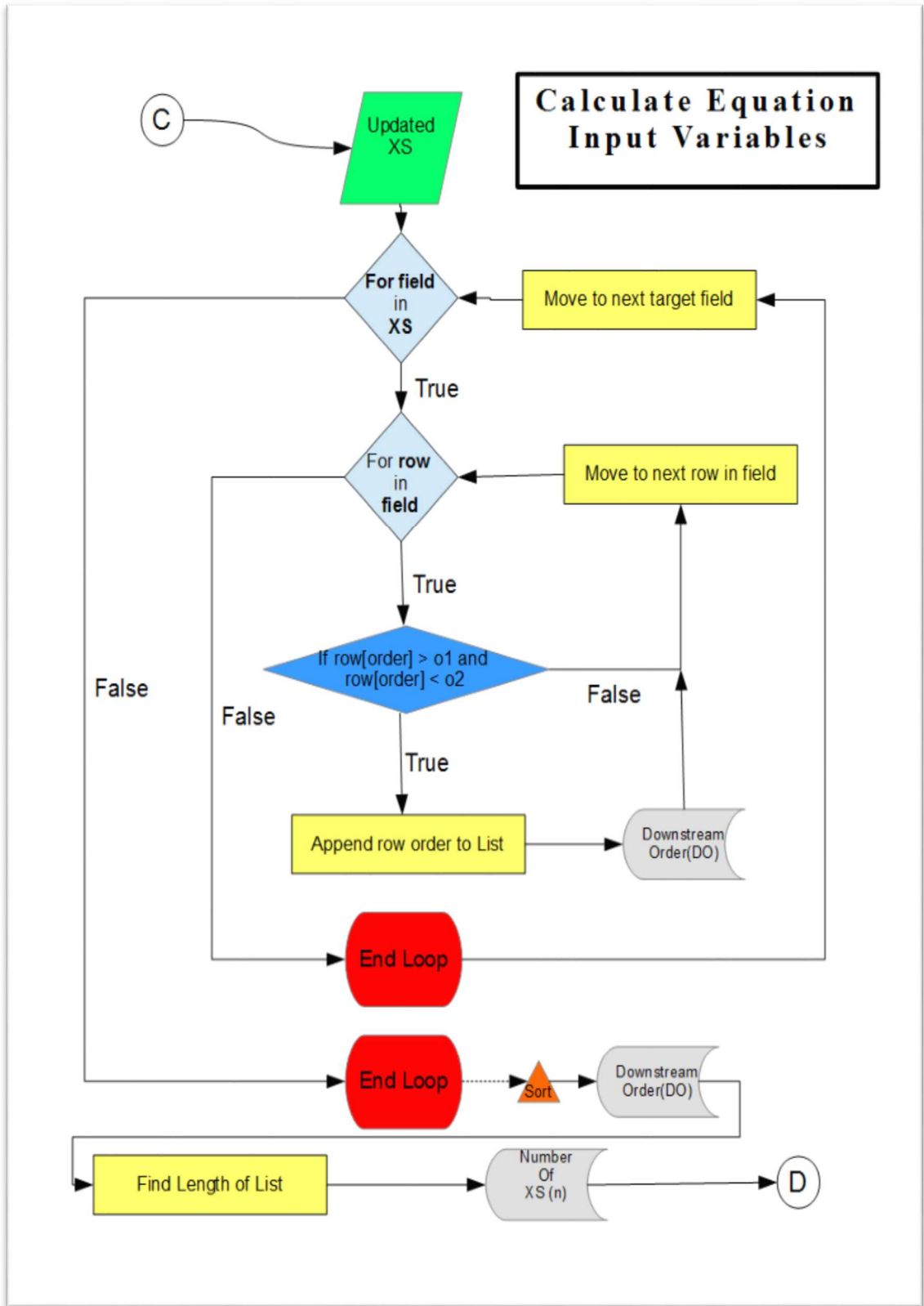
Figure 2.2.2.C. This figure shows the workflow for Step 2c in the automated process.
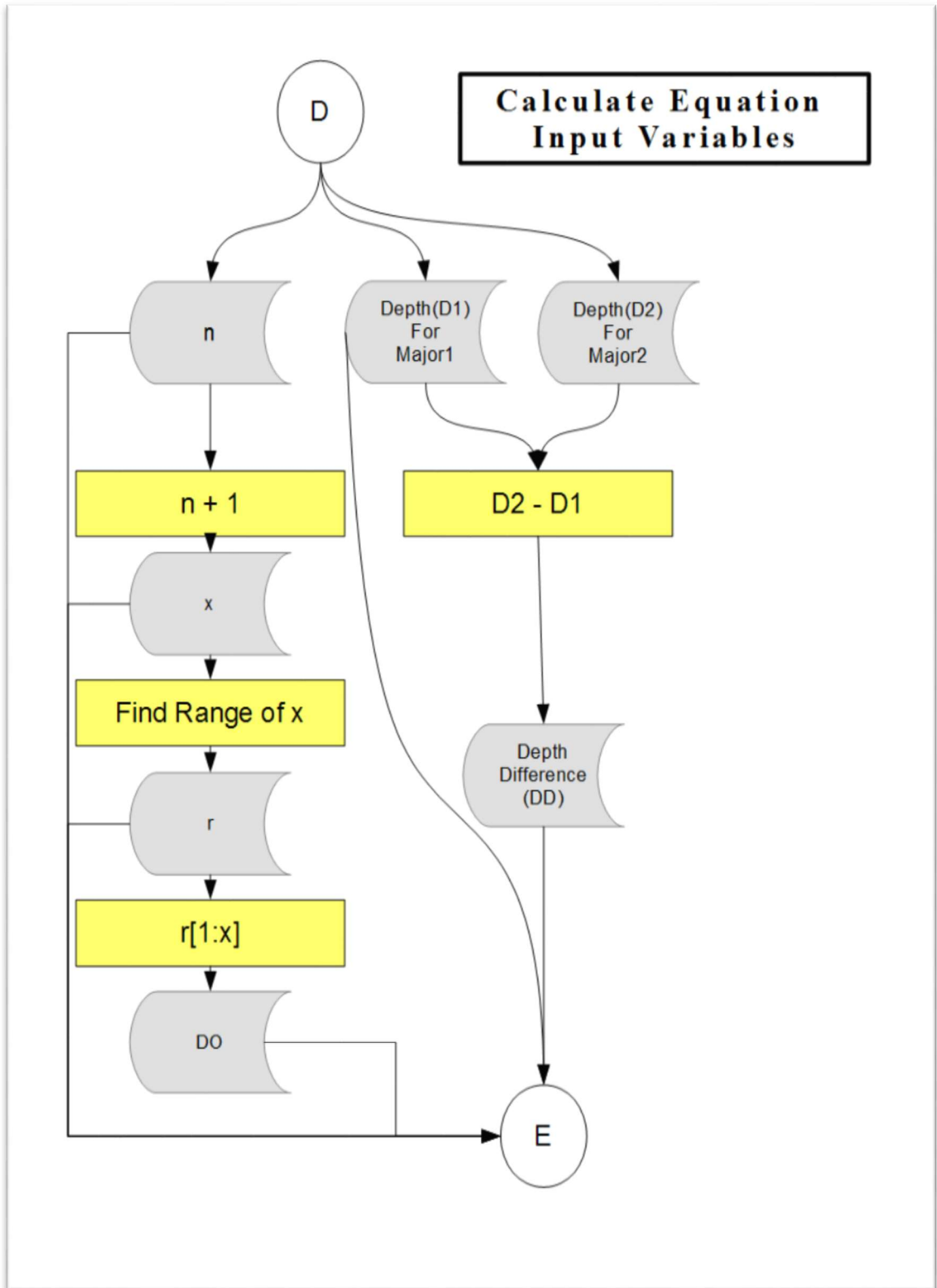
Figure 2.2.2.D. This figure shows the workflow for Step 2d in the automated process.
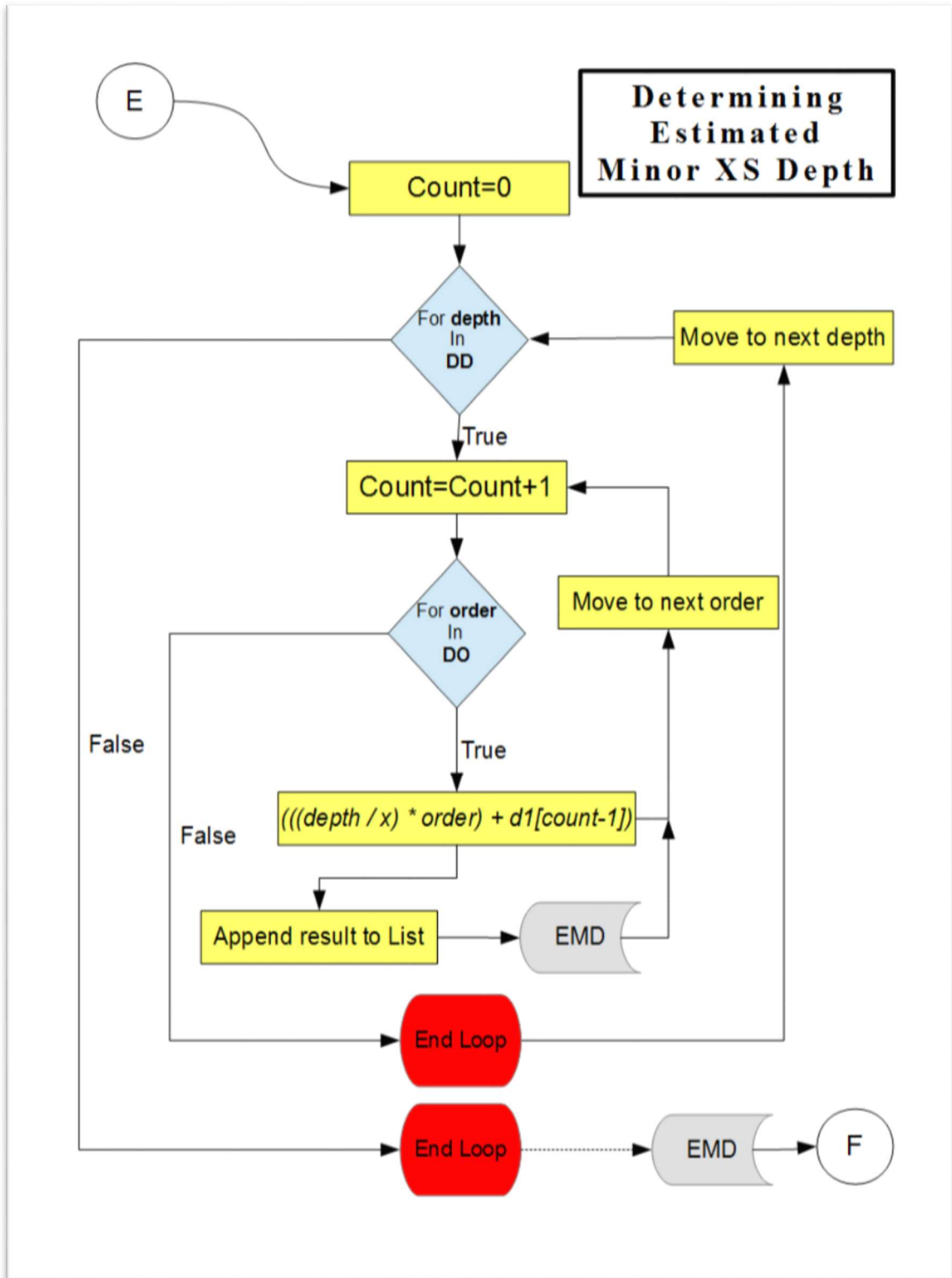
Figure 2.2.2.E. This figure shows the workflow for Step 4 in the automated process.
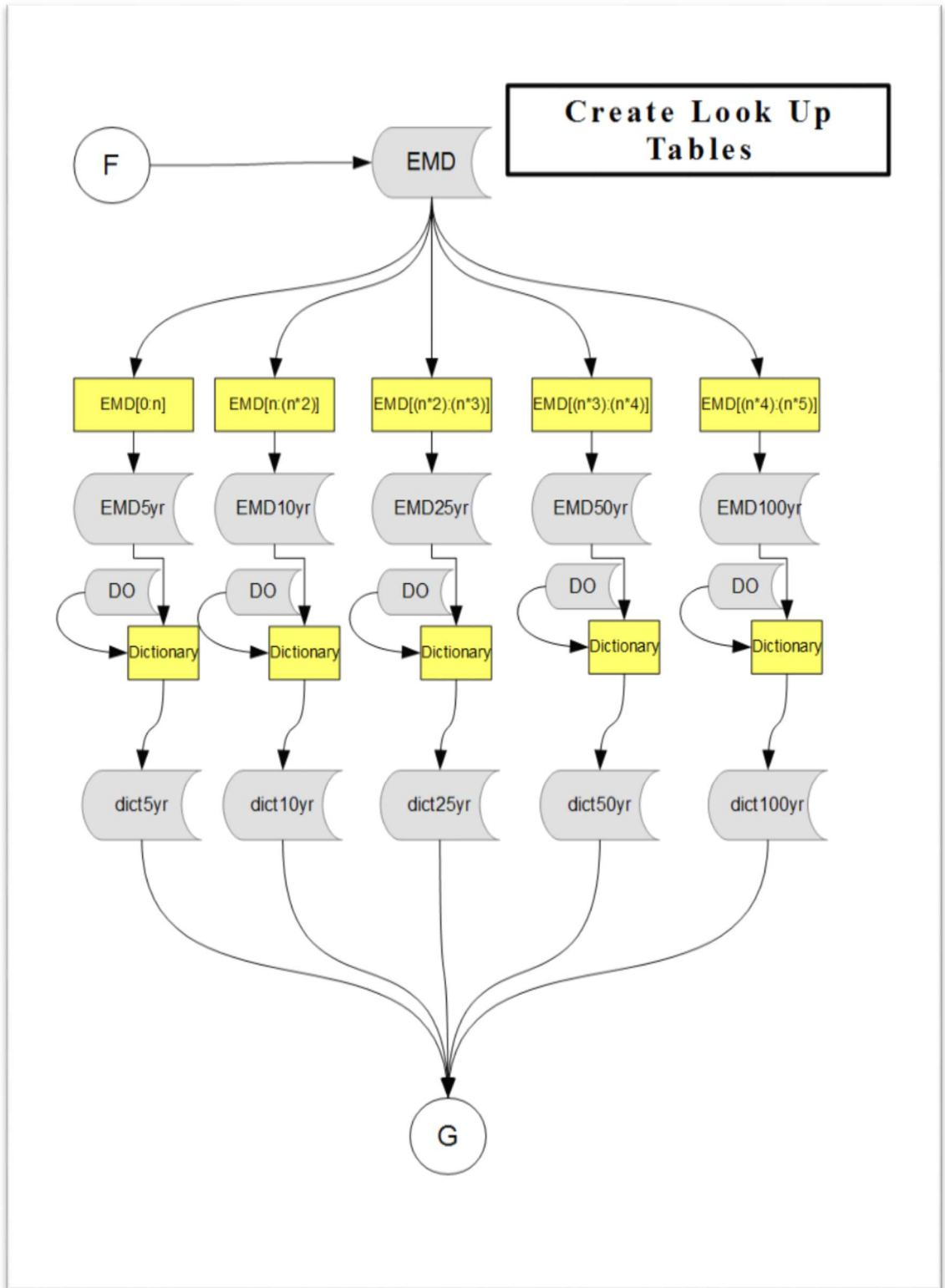
Figure 2.2.2.F. This figure shows the workflow for Step 5 in the automated process
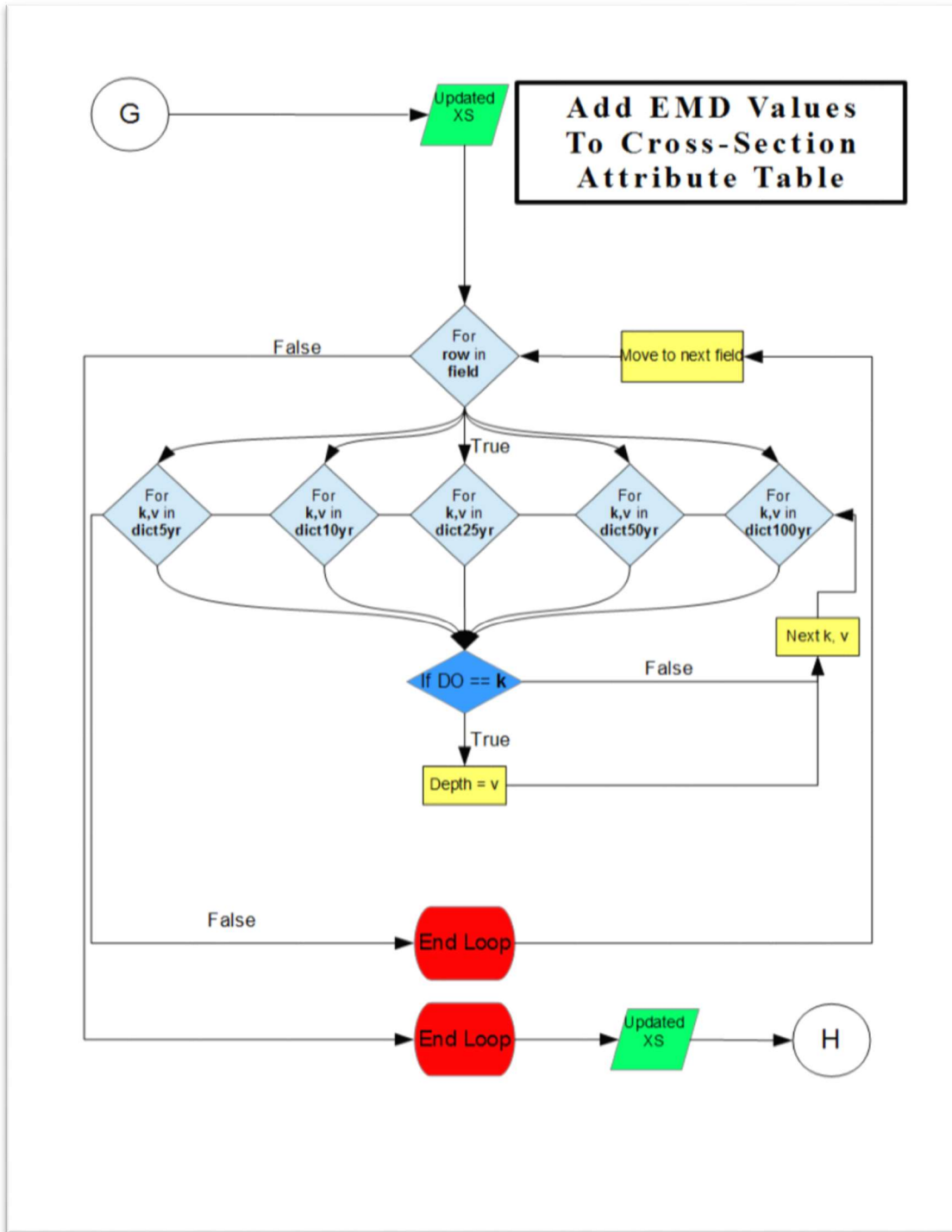
Figure 2.2.2.G. This figure shows the workflow for Step 5 in the automated process.
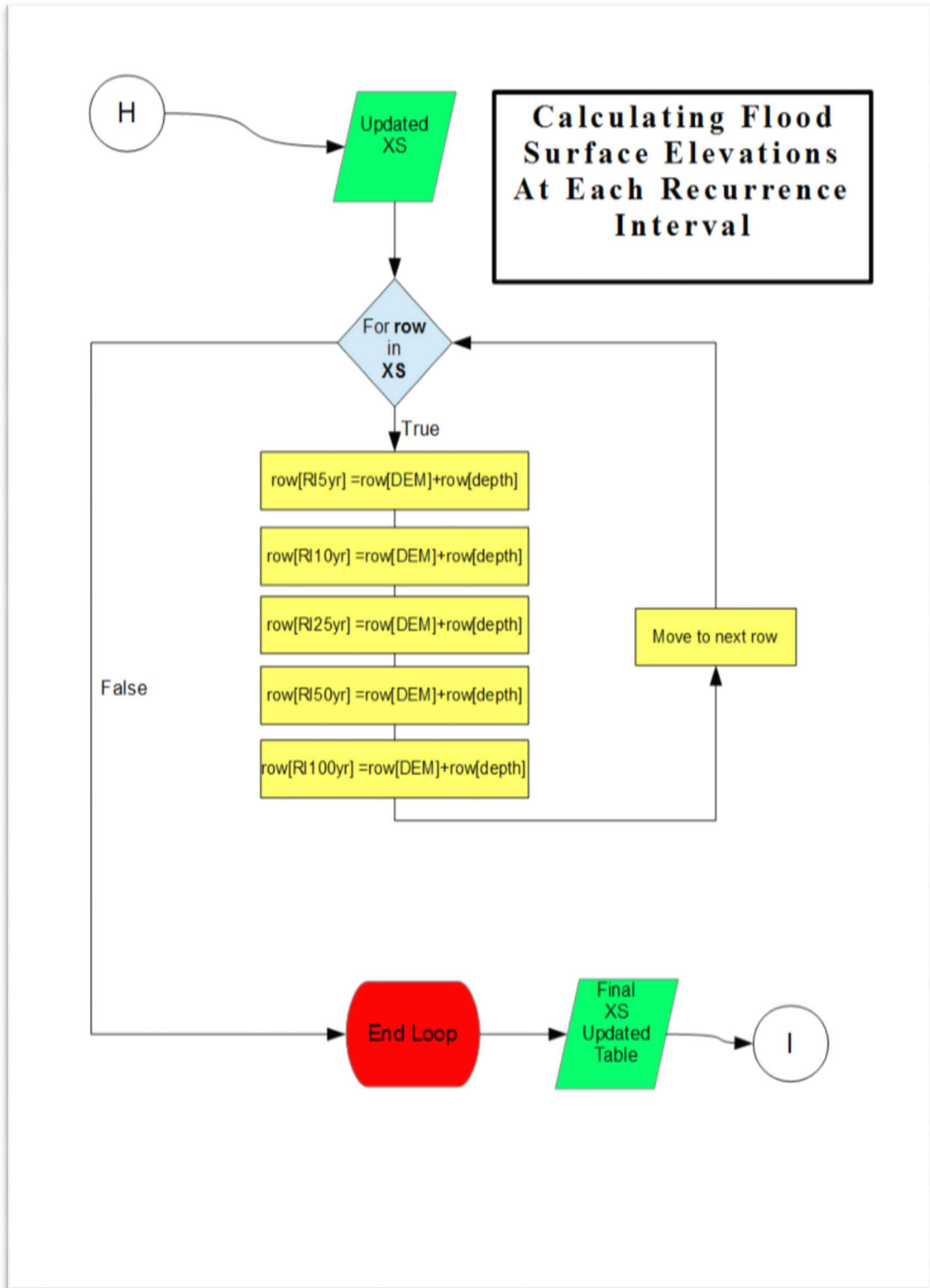
Figure 2.2.2.H. This figure shows the workflow for Step 5 in the automated process.
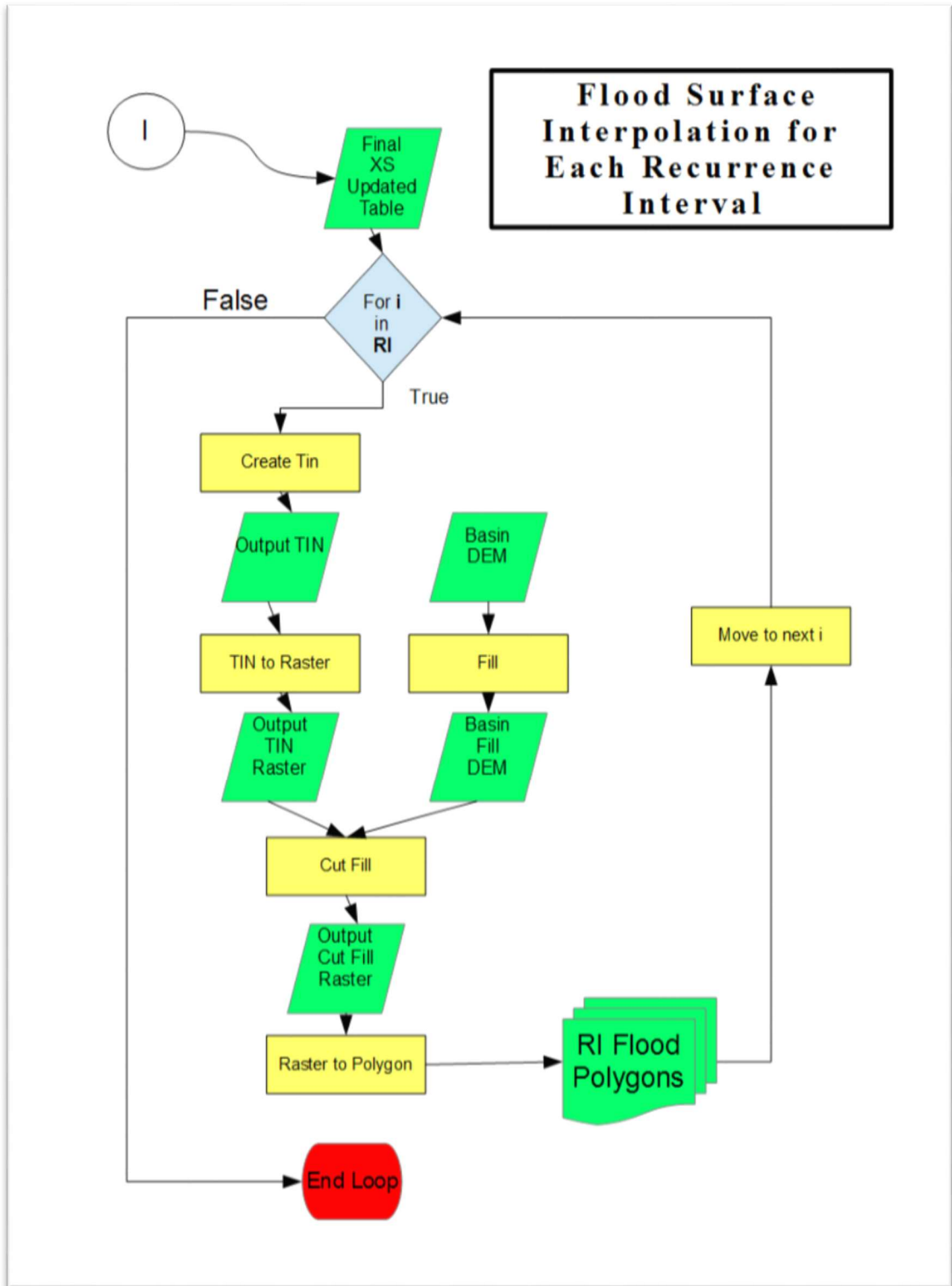
Figure 2.2.2.I. This figure shows the workflow for Step 5 in the automated process.

2.2.3. Final Cleanup

Due to the nature of the 10 meter DTM, the elevation of flood-protection walls only around a meter in width tended to contain inconsistent elevations. This would essential create a gap in the flood wall allowing breach to occur and floods to be mapped behind the flood-protection wall when it should not have been. Most of the flood levees on the Minnesota River are at least designed to handle the 100-year flood. Sitting at an elevation of 938 feet, Montevideo's flood levee system is designed to handle the 100-year flood plus three feet (City of Montevideo 2011). The calculated flood height for the 100-year flood in Montevideo was 933 feet yet the flood output showed the city to be inundated. In order to remove areas that incorrectly show inundation the 'Erase' tool was used in ArcMap 10.3 (Figure 2.2.3.). This cleanup process was completed for all of the levees shown in Table 2.
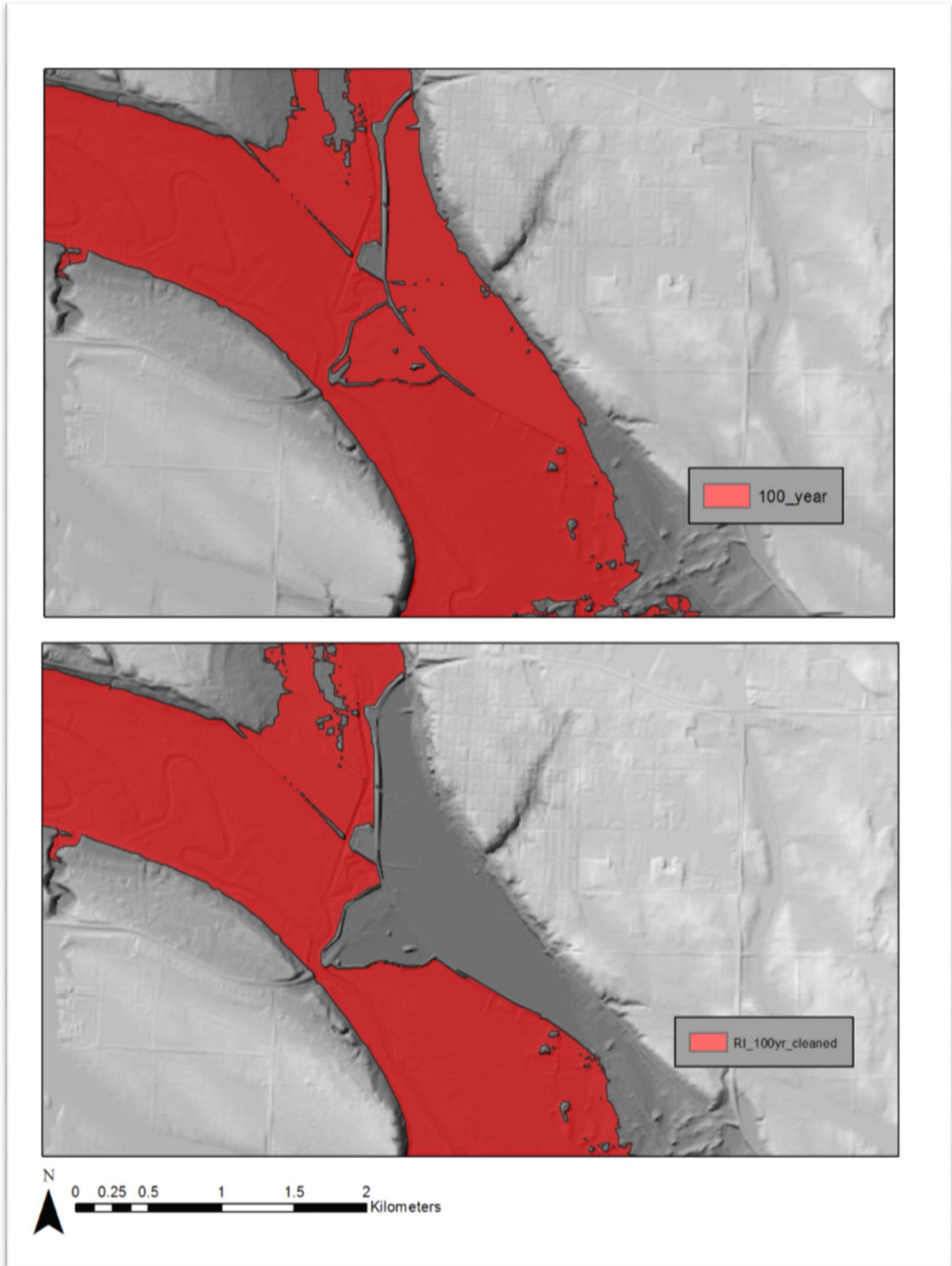
Figure 2.2.3. This figure shows the direct output from the model on top and the post clean 100-year flood polygon on bottom for the city of Montevideo.

3. Discussion/Conclusion

The details of logic behind and design of the partially automated process of mapping floodplain inundation at stage height recurrence intervals representing the 5-year, 10-year, 25-year, 50-year, and 100-year flood are presented here. These methods provide an efficient way to establish the basic probability of inundation extent at any part in the floodplain throughout the entire river reach. In the lower reach of the Minnesota River valley downstream of Mankato, results show that the floodplain becomes almost completely inundated with hydrologically connected water marking little difference between the extents of the 5-year and 100-year flood. In the upper reach of the Minnesota River valley upstream of Mankato, results show that the floodplain is generally less hydrologically connected and also marks greater differences between the extents at each recurrence interval.

The results of the adjusted method proved to be successful in reducing errors associated with overestimating and underestimating flood surfaces as described. All areas that were underestimated in the results of the preliminary method were corrected in the adjusted method (Figure 3.1.). In addition, all areas that were overestimated in the results of the preliminary method were corrected in the adjusted method (Figure 3.2.). The results of the adjusted method more closely match the calculated 100-year flood surface that FEMA created compared to the results from the preliminary method (Figure 3.3.). Throughout the entire valley, the 100-year flood surface created in the adjusted method closely match the 100-year flood surface created by FEMA (Figure 3.4.). The basic premise of this method should be able to be applied to any river, anywhere, and utilized with different methods of RI calculation, provided that the stream or river has gages and a sufficient number of years recorded to be confident in the statistical calculation of RI.

3.1. Limitations/Assumptions

Further validation is required in order to address uncertainties in the 10-meter DEMs capability to accurately extract elevation values of structures in the floodplain that are narrower than 10 meters. In order to better assess hydrologic connectivity in the floodplain at various stage recurrence intervals, the use of a higher spatial resolution 1-meter DEM is desired if enough computing power and memory are available. At this time and with the temporal and fiscal limitations present, we were only able to utilize the 10-meter. Also, it is important to note that the automated model is not a hydraulic model, but attempts to simulate inundation based on the assumption that flood depths increase moving downstream. The rate at which depth is increased is based on the spacing of cross-sections and not necessarily the location in which a tributary stream enters the main stem.

Depending on the hardware in the computer, the script for automating flood surfaces may take up to 45 minutes or longer. However, if the computer contains a large solid state hard drive and adequate processor, the script can be run in as little as 5 minutes because multiprocessing functionality was coded in as an option.
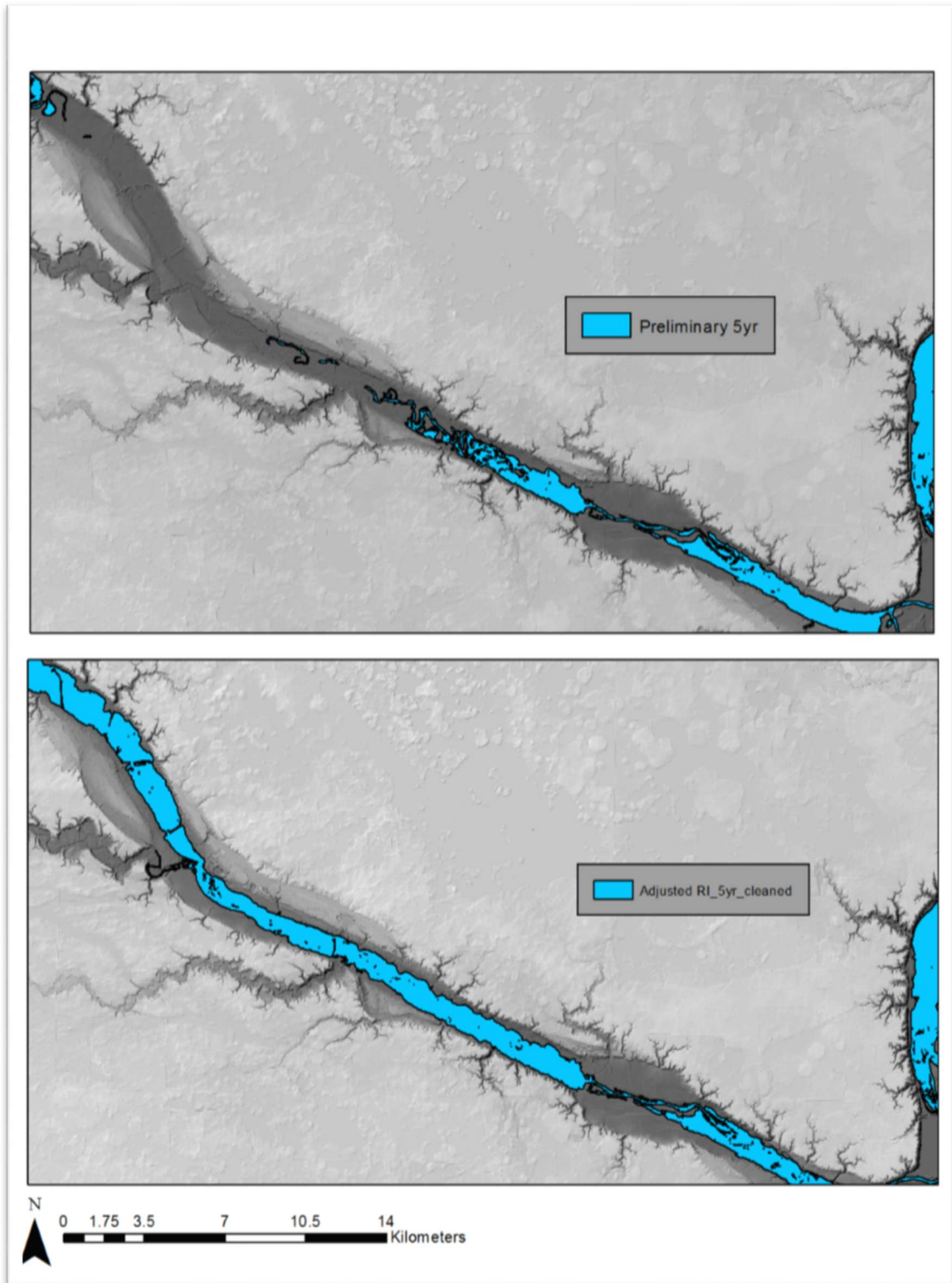
Figure 3.1. This figure compares the results from the preliminary method (top) to the adjusted method (below) in the reach between Montevideo, MN and Mankato, MN.
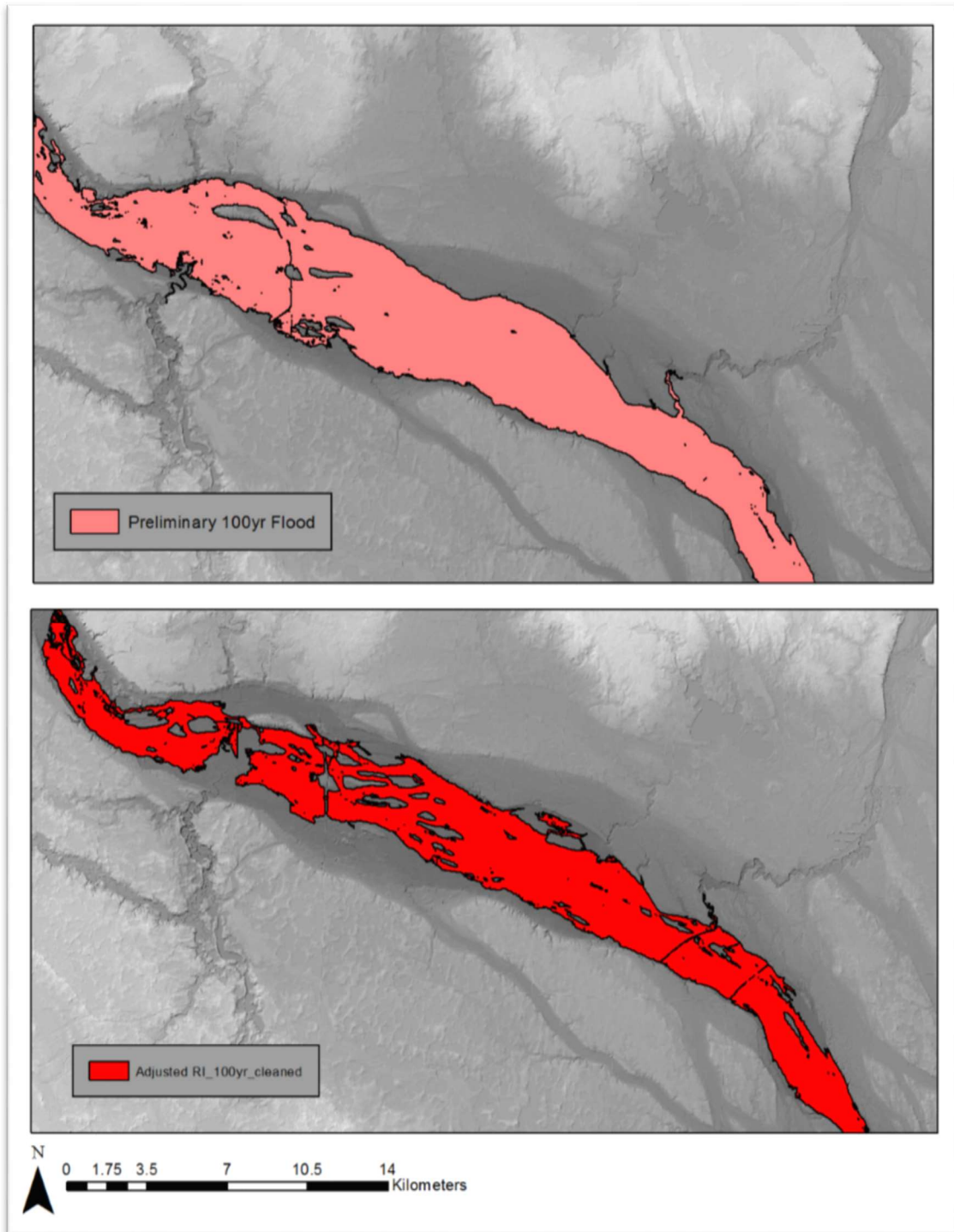
Figure 3.2. This figure compares the results from the preliminary method (top) to the adjusted method (below) in the reach near Ortonville, MN.
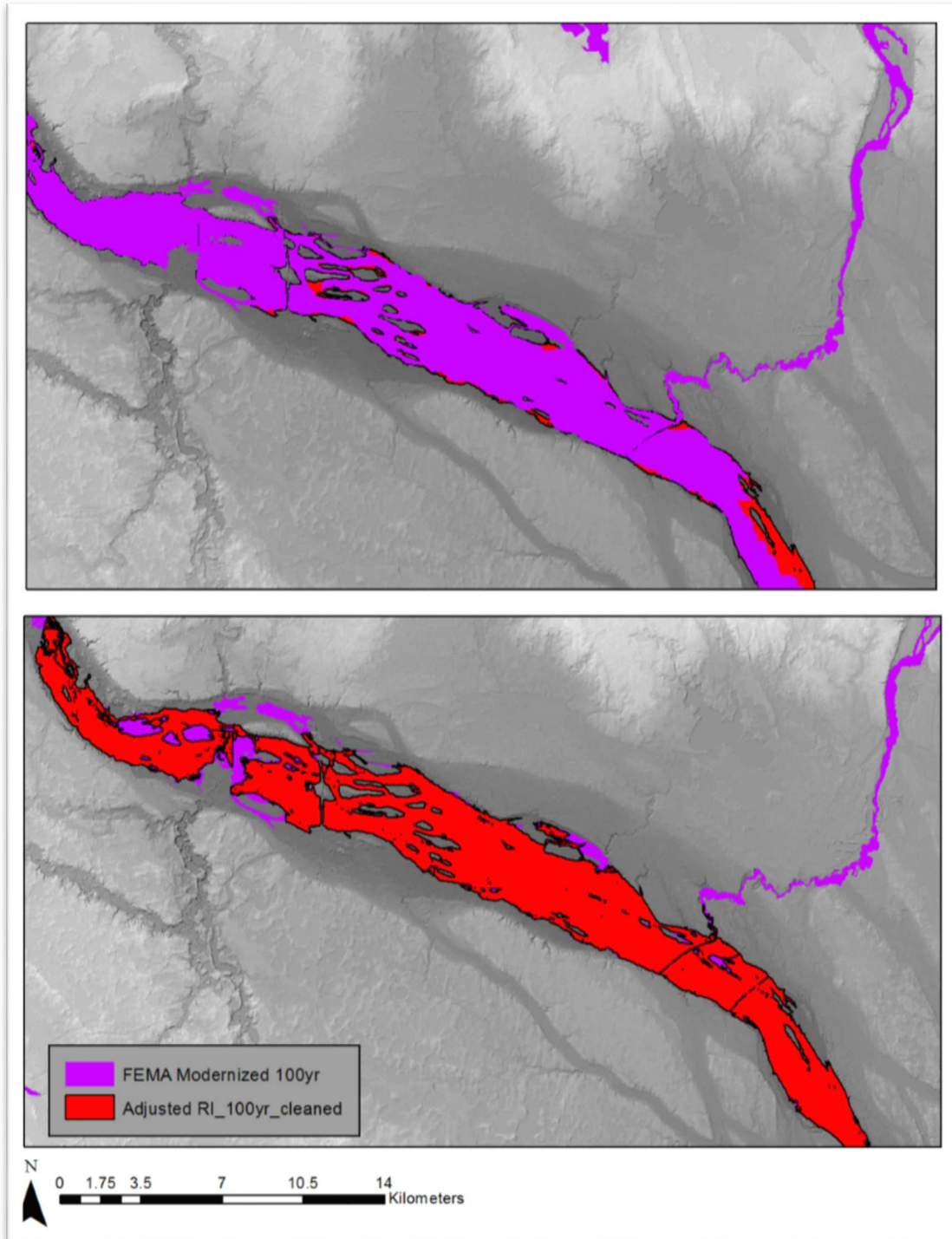
Figure 3.3. This figure shows a comparison between the FEMA 100-year floodplain and the Adjusted 100-year floodplain created in this method. The above map shows the FEMA layer on top while the below map shows the FEMA layer on bottom.
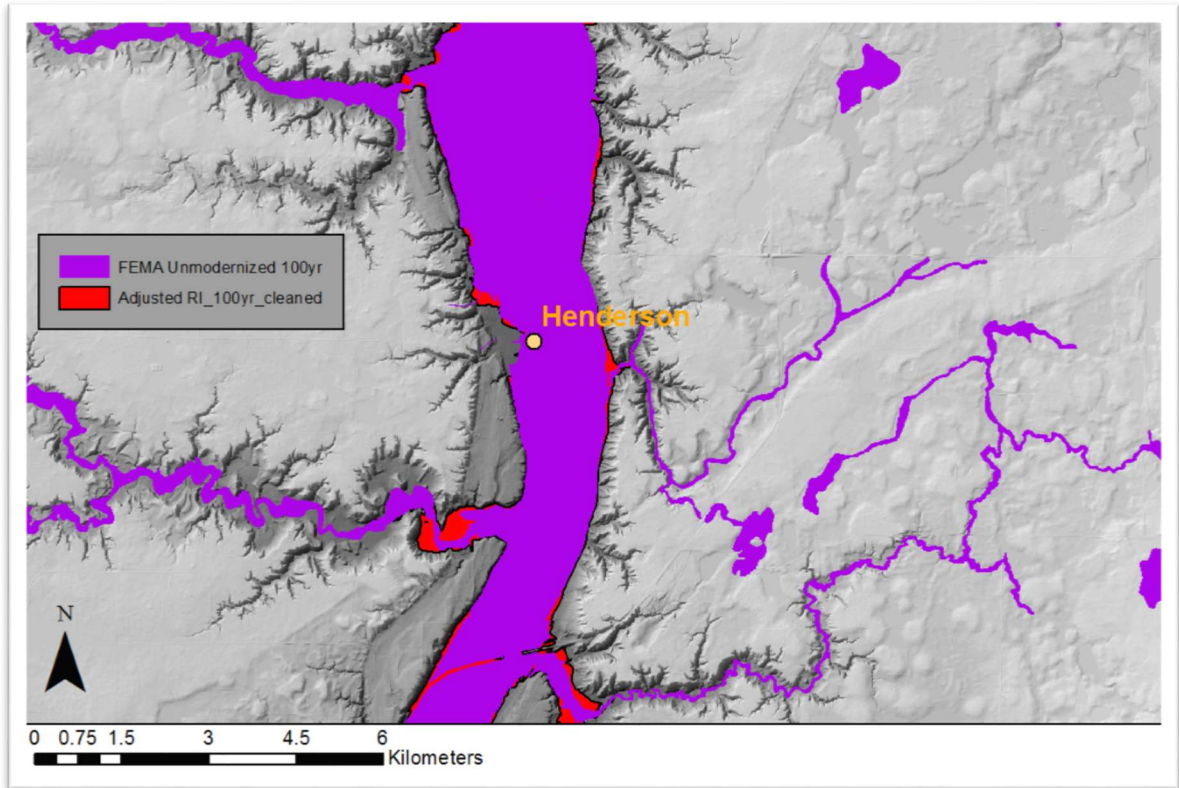
Figure 3.4. The Figure shows a comparison between the FEMA 100-year floodplain and the Adjusted 100-year floodplain near Henderson, MN. Note that the FEMA 100-year layer is unmodernized, meaning that it was created in a study prior to the year 2000. Also notice that the FEMA layer is shifted slightly north and doesn't quite match up with the location of Henderson's flood levee.

River Gauge	DEM River Elevation(ft)	5 Yr RI(ft)	10 Yr RI(ft)	25 Yr RI(ft)	50 Yr RI(ft)	100 Yr RI(ft)	Years on Record
Ortonville	966	966.62	967.7	969.22	969.26	969.4	77
Lac Qui Parle	934	935.89	936.8	938.8	940	940.1	68
Montevideo	919	924.8	926.38	929	931	933	106
Morton	822	832.5	832.7	834	835	840	15
Mankato	760	768.12	772.47	775.25	777	778	112
Henderson	725	738.3	739.5	742	744	747	32
Jordan	695	715.9	721.81	723.5	723.65	725	78
Savage	687	711.6	714.6	717	720	724	46

Fort Snelling	687	706.7	709.76	711.5	720	723	9

Table 1: This table contains the stage height of five different recurrence intervals along with the number of years that stream data was recorded by each gauge. It also includes the elevation of the Minnesota River at each gauge station for the basin DEM.

City	Elevation of Flood Control Structure	Design Flood Protection	Sources
Montevideo	938 feet	100-year flood + 3 feet	City of Montevideo, 2011
Granite Falls	912 feet	100-year flood + 3 feet	USACE, 2016
New Ulm	814 feet	100-year flood + 2 feet	USACE, 2016
Mankato	778.14-780.14 feet	100-year flood	USACE, 2016
Henderson	745 feet to 743 feet	170-year + 3 feet	USACE, 2016
Chaska	728.5 feet	100-year	USACE, 2016
Carver	726.5 feet	100-year	Mason, 2011

Table 2: This table shows the elevations of flood levees along the Minnesota River along with the magnitude of flood that they are designed to protect against

4. References

Amoros, C. and Bornette, G., 2002. Connectivity and biocomplexity in waterbodies of riverine floodplains. Freshwater Biology, 47(4):761-776.

Belmont, P., 2011. Floodplain width adjustments in response to rapid base level fall and knickpoint migration. Geomorphology, 128(1-2), pp.92-102.

Belmont, P., Shostal, C., Anderson, T. and Wong, M., 2009. Barr-NCED Mapper Channel-Floodplain Sediment Exchange Modeling.

Browne, M.J. and Hoyt, R.E., 2000. The demand for flood insurance: empirical evidence. Journal of risk and uncertainty, 20(3): 291-306.

Castro, J. M. and Jackson, P. L., 2001. Bankfull Discharge Recurrence Intervals and Regional Hydraulic Geometry Relationships: Patterns in the Pacific Northwest, USA. JAWRA Journal of the American Water Resources Association, 37: 1249–1262. doi:10.1111/j.1752-1688.2001.tb03636.x

FEMA. 2016. FEMA Flood Map Service Center: FEMA.gov, Retrieved July 27, 2016, from http://msc.fema.gov/portal

FEMA. 2011. Guidelines and Standards for Flood Risk Analysis and Mapping. Appendix K: Format and Standards for Flood Insurance Rate Maps.

Hjalimarsom, H.W. and Thomas, B.E., 1992. New look at regional flood-frequency relations for arid lands. Journal of Hydraulic Engineering, 118(6): 868-886.

Galat, D.L., Kubisiak, J.F., Hooker, J.B. and Sowa, L.M., 1997. Geomorphology, distribution and connectivity of lower Missouri River floodplain waterbodies scoured by the flood of 1993. Verhandlungen-Internationale Vereinigung für theoretische und angewandte Limnologie, 26:869-878.

Makkonen, L., 2005, January. A new approach to estimating return periods of extreme events. In IABSE Symposium Report (Vol. 90, No. 3, pp. 75-82). International Association for Bridge and Structural Engineering.

Mason, N. 2011. Council Orders Carver Levee Raised. Retrieved November 20, 2016, from http://www.swnewsmedia.com/chaska_herald/news/council-orders-carver-levee_raised/article_6fa0c221-d8f9-5d1c-943e-501aaa3fc673.html

Mertes, L.A., 1997. Documentation and significance of the perirheic zone on inundated floodplains. Water Resources Research, 33(7):1749-1762.

Merwade, V., Olivera, F., Arabi, M. and Edleman, S., 2008. Uncertainty in flood inundation mapping: current issues and future directions. Journal of Hydrologic Engineering, 13(7): 608-620.

MnGeo. 2014. LiDAR Elevation, Minnesota River Basin, Southwest Minnesota, 2010. Retrieved August 12, 2016, from http://www.mngeo.state.mn.us/chouse/metadata/lidarswmn2010.html

National Research Council. 2009. Mapping the zone: improving flood map accuracy. Committee on FEMA Flood Maps, National Research Council, National Academies Press, Washington, DC.

Nanson, G.C. and Croke, J.C., 1992. A genetic classification of floodplains. Geomorphology, 4(6): 459-486.

NCED. 2016. Research Resources | National Center for Earth-Surface Dynamics 2. Retrieved August 12, 2016, from http://www.nced.umn.edu/community/research/resources

Tockner, K. and Stanford, J.A., 2002. Riverine flood plains: present state and future trends. Environmental conservation, 29(03):308-330.

USACE. 2016.US Army Corps of Engineers - National Levee Database. Retrieved November 23, 2016, from http://nld.usace.army.mil/egis/f?p=471:1:0::NO

US Department of Commerce, N. 2016. NOAA - National Weather Service - Water. Retrieved July 29, 2016 from, Water.weather.gov. Available at: http://water.weather.gov/ahps/

USGS. 2016. USGS Surface-Water Data for Minnesota. Retrieved July 29, 2016 from, http://waterdata.usgs.gov/mn/nwis/sw

5. Flood Inundation Tutorial

Required External Python Dependencies:
Click
dotmap
multiprocess
Required Programs:
Python 2.7x

ArcGIS 10.x
Required Input For Script:
Cross-Section Shapefile
River Centerline Shapefile
Surface DEM
Control Points
Steps Start Here
Make sure environment path variables are pointing to ArcGIS10.x
Open 'System properties' in 'Computer'
Click 'Advanced system settings'

Click the 'Environment Variables' button
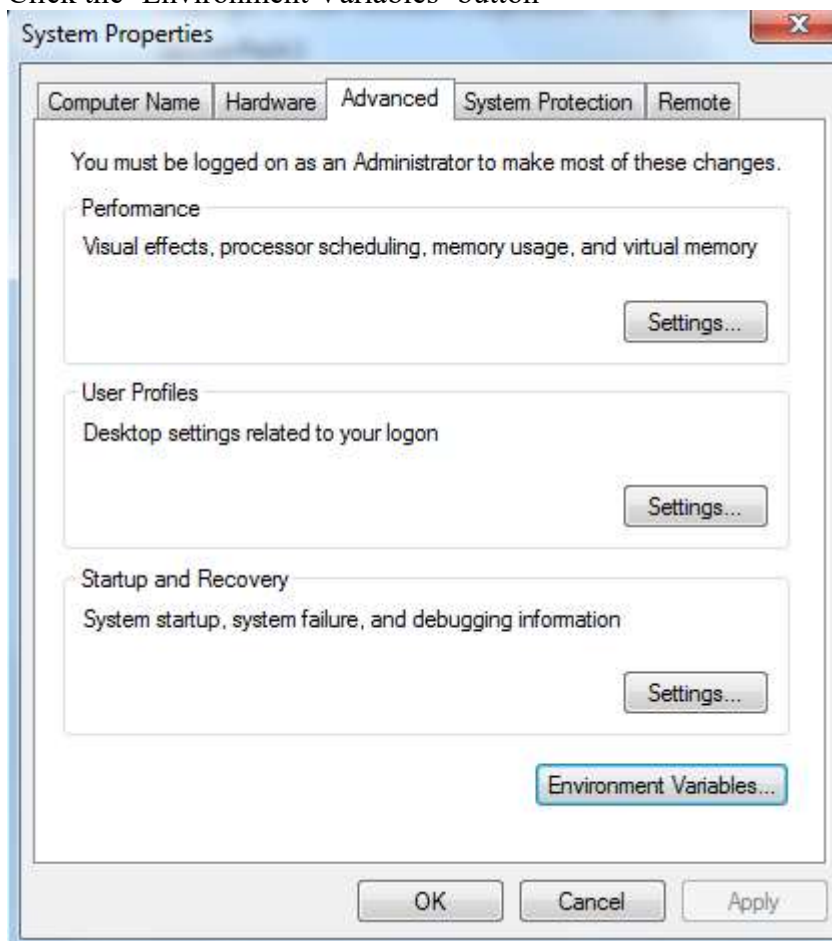
In the 'System variables' list, click the row that contains 'Path' under the 'Variable' column and the click the 'Edit' Button.
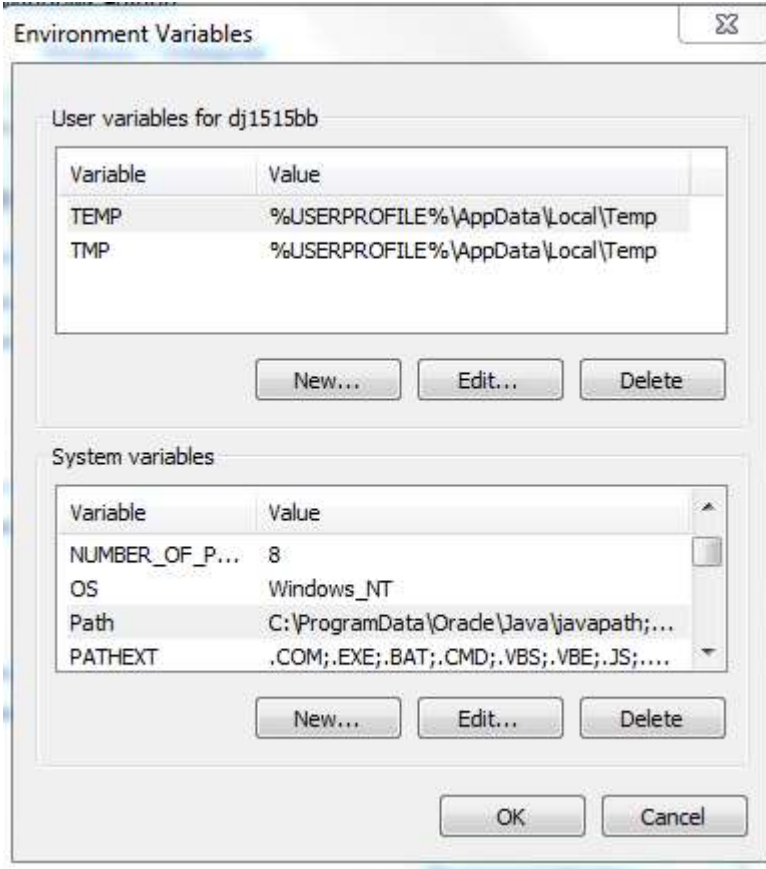
Copy the file paths located in the 'Value' column and paste them to a text document. This ensures that a copy of the system path variables will remain if the path variables get mixed up.

At the end of the list add the following paths:

;C:\Python27\ArcGIS10.3\
;C:\Python27\ArcGIS10.3\Lib
;C:\Python27\ArcGIS10.3\Lib\site-packages
;C:\Python27\ArcGIS10.3\DLLs
;C:\Python27\ArcGIS10.3\libs
;C:\Python27\ArcGIS10.3\Scripts

Click 'OK' to finish

Install pip by going to https://pip.pypa.io/en/stable/installing/

Installing with get-pip.py

To install pip, securely download get-pip.py. [2]

Right click 'get-pip.py' and save link as 'get-pip.py' in this folder 'C:/Python27/ArcGIS10.3'
First open 'PowerShell'.
Click on the Start Menu and type in "powershell" and then open PowerShell.
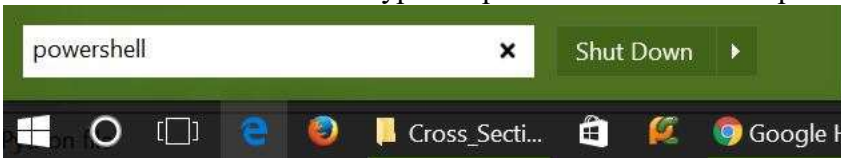
In the PowerShell terminal type: get-pip.py

```
PS C:\> get-pip.py
```

Once pip is finished downloading type the following commands into the PowerShell Terminal to install the script dependencies

```
PS C:\> pip install click
PS C:\> pip install dotmap
PS C:\> easy_install multiprocess
```

some code in the __init__.py file needs to be changed in order to handle some errors
Go to C:\Python27\ArcGIS10.3\Lib\site-packages\multiprocess
In the multiprocess folder open __init__.py (Right click and edit with IDLE)
In line 84 change 'import _multiprocess as _multiprocessing' to:

```
try:
    import _multiprocess as _multiprocessing
except ImportError:
    import _multiprocessing
```

Save and exit all windows except for the PowerShell window.

Steps

Verify that your modules have been installed. In PowerShell type 'python' and click enter:
Type the following:

```
>>> import click
>>> import dotmap
>>> import multiprocess
```

If no errors show up, the modules have been installed.
Type 'Ctrl Z' to exit the python

```
>>> import click
>>> import dotmap
>>> import multiprocess
>>>
PS C:\>
```

In PowerShell navigate to the folder where the 'startflood' script is located. Type "cd (folder name)" to move up a directory or type "cd .." to move down a directory. Type "ls" to list all files and folders within a directory. For example:

```
PS C:\Users\Carson\Desktop> cd flood
PS C:\Users\Carson\Desktop\flood>
```

Create an empty output folder anywhere that is desired. The path to this output folder will be used in step 6d.

Once in the desired folder, type the following command to run the script:
Note that the user will need to specify file paths to their data.

```
PS C:\Users\Carson\Desktop\flood> python startflood.py c
```

When prompted:
Enter the filepath of the Basin DEM then hit enter.
Enter the filepath of the River Centerline Shapefile then hit enter.
Enter the filepath of the cross-sections Shapefile then hit enter.
Enter the filepath of the output folder then hit enter.
Enter the filepath of a scratch geodatabase then hit enter.
Enter 'N' to enable multiprocessing (WARNING: Will utilize up to 100% of all CPU) or False to run script using only 1 CPU core, then hit enter.

```
PS C:\Users\dj1515bb\Desktop\For DNR\Flood_Script> python startflood.py c
Basin DEM [C:\Users\dj1515bb\Desktop\For DNR\Flood_Script\Input\input\basin_fill.tif]:
Centerline shapefile [C:\Users\dj1515bb\Desktop\For DNR\Flood_Script\Input\input\centerline.shp]:
Cross sections shapefile [C:\Users\dj1515bb\Desktop\For DNR\Flood_Script\Input\input\cross_sections.shp]:
Control Points [C:\Users\dj1515bb\Desktop\For DNR\Flood_Script\Input\input\control points.shp]:
Output folder [C:\Users\dj1515bb\Desktop\Test_Output]:
Scratch GDB [C:\Users\dj1515bb\Desktop\For DNR\Flood_Script\TEMP.gdb]:
Enable Multiprocessing? [y/N]:
```

*Note that while specifying path, brackets ([]) should not be used.

Notes
It is recommended that multiprocessing is disabled if the script outputs are written to a HDD hard drive. If it is enabled, a HDD hard drive will likely become a bottle neck for the CPU and decrease overall performance. It is however recommended that multiprocessing is enabled if script outputs are written to a SSD hard drive because of increased read and write rates.

RESULTS: Planform Change and Lateral Stream Migration
Planform Channel Change of the Lower Minnesota River (1937-2013)

Author(s): Devon Libby[1], Phillip Larson[1], Patrick Belmont[2]
[1]Earth Science Programs/AGES Laboratory - Minnesota State University, Mankato
[2]Watershed Sciences - Utah State University

Corresponding Author:
Devon Libby – Email: dj_libby@hotmail.com; Phone: 5073823227

1. Introduction

In attempting to understand change within the fluvial system, temporal and spatial scales of analysis must be established (Schumm and Lichty 1965; Schumm 1977; Lawler 1993; Grabowski, Surian, and Gurnell 2014). In the case of temporal scale, Trimble and Cooke (1991) state "the recent past sets the stage for contemporary processes, which may not be fully intelligible without an appreciation of the past." Thus, in order to understand the contemporary fluvial system, it is crucial to assess historical change within the system (Winterbottom 2000; Rhoads 2003), particularly when trying to understand channel planform dynamics (Hickin and Nanson 1984; Jones 1994; Hooke 1995;Gurnell 1997; Winterbottom 2000; Urban and Rhoads 2003; Gurnell, Downward, and Hughes, McDowell, and Marcus 2006; Block 2014).

In addition to establishing a temporal framework of study, an appropriate spatial scale needs to be considered for the research. In fluvial systems, this can range anywhere from drainage pattern networks to an individual grain of sediment. Schumm (1985) states that reach scale analysis is of most interest to geomorphologists who are concerned with what the pattern of the river reveals about its history and behavior. Since this is the primary purpose of the research in this thesis, most of the focus in this chapter is at the reach scale; however, it should be noted that both larger and smaller scale elements and processes need to be given credence to make reach-scale interactions fully intelligible.

The purpose of the research in this chapter is take the error and uncertainty analysis conduct within Libby (2018) and apply it to the planform measurements calculated in a GIS. These measurements on the Minnesota River will then aid in filling the gap of knowledge that currently exists on the main stem Minnesota River. Since discharge and sediment have significantly increased from various anthropogenic activities, primarily linked to land use and climate change, the following research

questions will be explored: 1) Have the channel migration rates remained stable over the past 76 years of aerial photographic record (1937-2013), or are increases or decreases observed? 2) If the latter, do these increases and decreases show any spatial or temporal patterns? 3) Does channel width fluctuate over this similar time frame? 4) If so, are there spatial or temporal patterns related to this change? 5) How have human modification to the river (e.g. bridges, flood control structures, etc.) effected planform channel change in the upstream and downstream directions? 6) In relation to the invasive carp problem, are there controlled reaches of the Minnesota River that exhibit very little change and could potentially be suitable for invasive carp barriers?

Specifically, these research questions will be applied on the last 160 km (100 mi) of the Minnesota River, extending from the Blue Earth/Minnesota River confluence down the Minnesota/Mississippi River confluence (Figure 1). This stretch of river is of interest for stopping the advancement of invasive carp along with being the end of the primary transfer corridor adjusting to increasing discharge and sediment yields from the MRB before entering the Mississippi (Engstrom, Almendinger, and Wolin 2009; Belmont et al. 2011; Kelly et al. 2017).
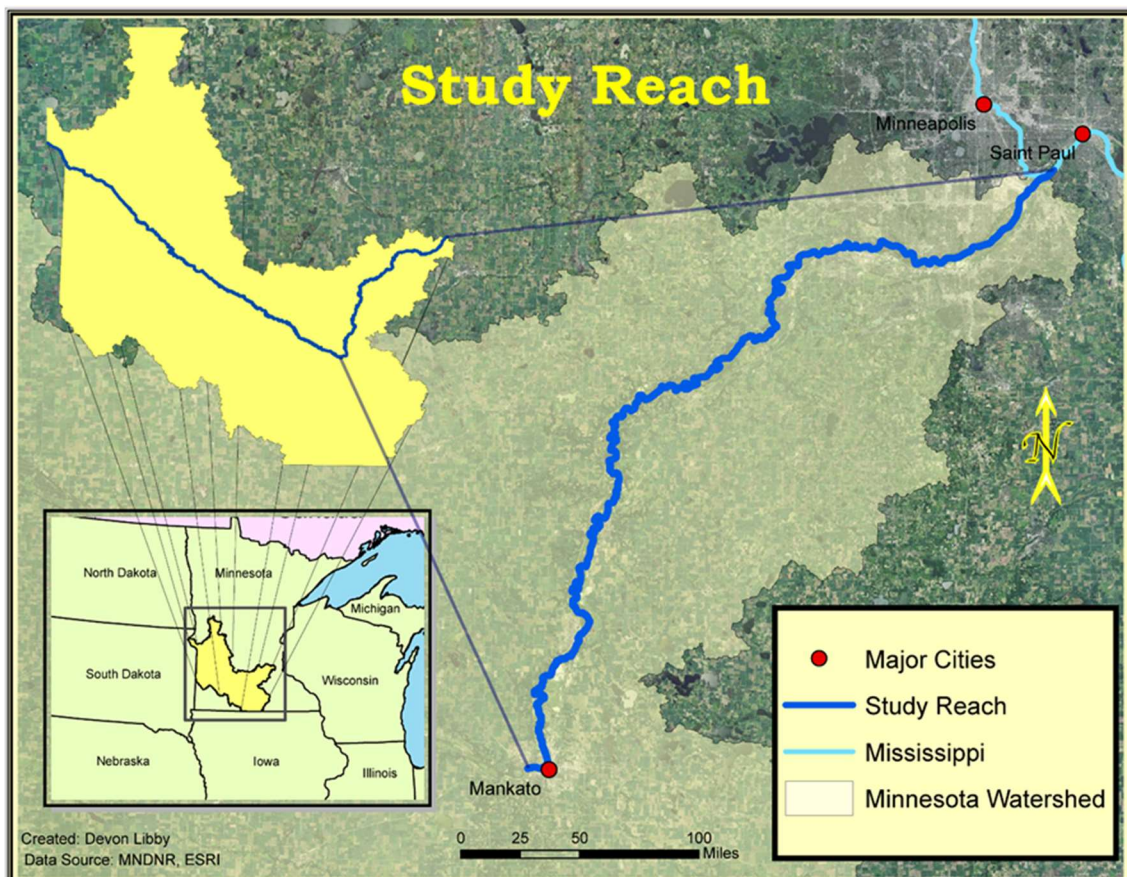
Figure 1. The study reach for this research is the 160 km (100 mi) of the Minnesota River beginning in Mankato and ending with the confluence with the Mississippi River.

1.1. Study Area

The Minnesota River Basin (MRB) is a dynamic, transient landscape because of ongoing landscape-scale adjustment due to the retreat of continental glacial ice that covered much of the landscape ~12,000 14,000 years BP (Clayton and Moran 1982; Fenton et al. 1983; Teller, Leverington, and Mann 2002). The Des Moines Lobe of the Laurentide Ice Sheet flowed over much of the MRB leaving behind a thick package of glacial and glacio-fluvial sediments (Hallberg and Kemmis 1986; Patterson 1997; Patterson and Wright 1998;). As climate warmed at the end of the last glacial maximum (~11,000 years BP; Ojakangas and Matcsh 1982) meltwater pooled in pro-glacial lakes in many ice-marginal locations. One such proglacial lake, Lake Agassiz (Upham 1896; Teller, Leverington, and Mann 2002; Fisher 2003), was formed in the northwestern Minnesota, eastern North Dakota, and extended into Canada nearly to the Hudson Bay and was damned behind the Big Stone Moraine of west central Minnesota (Thorleifson 1996; Fisher 2004). Eventually, Lake Agassiz breached its basin through several spillways including the Gulf of Mexico, Arctic Ocean, North Atlantic Ocean, and Hudson Bay (Thorleifson 1996; Teller, Leverington, and Mann 2002). The initial breach of meltwater occurred in west central Minnesota as Lake Agassiz meltwater either overtopped (i.e. spillover) or flowed through (as a result of moraine dam failure) the Big Stone Moraine sometime before (Wright Jr, Lease, and Johnson 1998; Teller, Leverington, and Mann 2002; Lepper et al. 2007). This breaching event carved the present-day Minnesota River Valley which is nearly 8km (5 mi) wide in certain areas (Upham 1896; Thorleifson 1996; Teller, Leverington, and Mann 2002; Fisher 2003, 2004; Lepper et al. 2007).   Following recession of the flood waters, the Minnesota River Valley became the new base level for tributary streams flowing into the valley. As a result, the tributaries of the modern Minnesota River are still responding to this abrupt, 40 (mouth) 300 (downstream) meter, base level change (Clayton Moran 1982; Moran 1982; Ojakangas and Matcsh 1982; Gran et al. 2009; Gran, Belmont, Day, Jennings, et al. 2011). This, in turn, has resulted in a landscape prone to high sediment yields as these tributaries incise through the landscape (Fisher 2004; Belmont et al. 2011; Gran, Belmont, Day, Finnegan, et al. 2011; Libby, 2018).

However, this geologically-young system and its evolution has experienced further perturbation through anthropogenic alteration of land cover and hydrology following European settlement (Engstrom, Almendinger, and Wolin 2009; Belmont et al. 2011; Schottler et al. 2014). The MRB was historically a landscape dominated by wetlands (Musser, Kudelka, and Moore 2009), which are vital for water and sediment retention in the uplands of this landscape (Mitsch and Gosselink 2000). However, starting in the early 1900's the landscape began to be drained to more effectively cultivate the landscape (Lenhart et al. 2011). Currently, 78% of the MRB is row crop agriculture largely occupied by corn and soybean fields (Musser, Kudelka, and Moore 2009; Belmont et al. 2011).

In addition, artificial forms of surface and subsurface drainage have dramatically altered hydrology and erosional processes in the MRB (Kelley and Nater 2000; Kelley et al. 2006; Engstrom, Almendinger, and Wolin 2009; Mulla and Sekely 2009; Schottler 2012; Schottler et al. 2014). One of the most prevalent forms of drainage is subsurface

tiling. Tiling is a network of tubes with small perforations below the soil surface used to capture and pipe infiltrating water off the landscape (Schottler 2012; Foufoula-Georgiou et al. 2015). This system of drainage changes flow patterns, rainfall-runoff timing, and landscape storage driving new hydrologic regimes (Foufoula-Georgiou et al. 2015). The hydrology of the region is further impacted by shifting climatic conditions. In Minnesota an increase in mean annual precipitation, number of days receiving precipitation, and amount of intense rainfall events per year cause increased frequency and magnitude of peak discharges throughout the region's fluvial systems (Novotny and Stefan 2007; Gran, Belmont, Day, Jennings, et al. 2011; Yuan and Mitchell 2014; Kelly et al. 2017).

Ultimately, anthropogenic perturbations (e.g. climate, land use, and modification of hydrology) have resulted in more erosive rivers (Schottler et al. 2014). Lake Pepin, a naturally dammed lake located just downstream of the confluences of the Minnesota and Mississippi River, has received a ten-fold increase (85,000 mg/year prior to 1830's to as high as 850,000 mg/year between 1950-2008) in sediment since European settlement (Engstrom, Almendinger, and Wolin 2009; Belmont et al. 2011). Significantly, the Minnesota River plays a primary role in this ongoing sediment accumulation as 90% of the sediment comes from the Minnesota River which only contributes 38% of the discharge to lake (Kelley and Nater 2000; Kelley et al. 2006; Belmont et al. 2011). Prior to this period, sediment contributions remained static to the lake for nearly 10,000 years (Kelley et al. 2006; Engstrom, Almendinger, and Wolin 2009; Blumentritt, Engstrom, and Balogh 2013; Belmont and Foufoula-Georgiou 2017).

Of this increase in sediment loads, near-channel sources have shown to be major contributors in the MRB especially from the tall bluffs below the knick-zones on Minnesota River tributaries (Belmont et al. 2011; Schottler et al. 2014; Belmont and Foufoula-Georgiou 2017). In the 1950's a large portion of the sediment load shifted to field sources which was combatted with various conservation efforts and tillage practices reducing this sediment source, yet the sediment rates did not decline (Belmont and Foufoula-Georgiou 2017). This is explained from the shift going back to near channel sources due to the altered hydrology from the prevalence of various forms of artificial drainage, and increased precipitation events (Novotny and Stefan 2007; Foufoula-Georgiou et al. 2015; Belmont and Foufoula-Georgiou 2017; Kelly et al. 2017).

1.1.2. Significance of the Study Area

Rivers are naturally dynamic features but will quickly change morphological characteristics because of anthropogenic and climatic forces acting within or on a watershed (Schumm 1977; VanLooy and Martin 2005). Channel morphology change or stability is the result of prevailing hydrological conditions of which runoff and sediment yield are the most influential (Knox 1977). Given the drastic hydrologic change and sediment load increase over the past century and a half within the MRB (Engstrom, Almendinger, and Wolin 2009; Foufoula-Georgiou et al. 2015; Groten, Ellison, and Hendrickson 2016; Kelly et al. 2017), further study of channel change is necessary to better understand how the river is responding through time in the context of both landscape and ecological management.

1.1.2.1. Fluvial Geomorphology and River Management

Several equations predicting channel behavior from Schumm (1969) were discussed in Libby (2018), but notably an increase in discharge, which is observed in the modern Minnesota River, can be exemplified using the following equation.

$$eq. Q^+ \cong \frac{w^+ \ d^+ \ (w/d)^+ \ \lambda^+}{s^-}$$

where discharge (Q), channel width (w), depth (d), width-depth ratio (w/d), meander wave length (λ), channel slope (s), and sinuosity (S). Plus signs (+) indicate an increase while negative signs (-) indicate a decrease in that variable. Using these general relationships, it is likely that given what we know about the ongoing change in the MRB, we can expect to see an increase in channel width (Lauer et al. 2017), width depth ratio, and channel wavelength, and a decrease in sinuosity. Increased sediment loads (Engstrom, Almendinger, and Wolin 2009; Belmont et al. 2011; Groten, Ellison, and Hendrickson 2016) and subsequent turbidity impairment (Belmont and Foufoula-Georgiou 2017) have plagued the Minnesota River and much of the Upper Mississippi River Basin (UMRB) resulting in unhealthy ecosystems (Foufoula-Georgiou et al. 2015) and increasing sand deposition/aggradation in the farthest downstream portions of the Lower Minnesota River (Jennings 2016). Recently, Groten, Ellison, and Hendrickson (2016) have shown that sediment yield from Mankato to Jordan increases by two and half times. However downstream of Jordan, a significant decrease is seen revealing a sediment sink. The erosional processes of channel migration and channel width change are contributing to these sediment dynamics as near channel sources. Therefore, quantification of channel planform change on the Minnesota River will aid in spatially identifying areas of acute concern (i.e. greatest near-channel sediment contributions).

This increase in sedimentation in certain reaches of the fluvial system has led to the need to dredge parts of the Minnesota River for it to remain navigable for barges. This is also true for Lake Pepin and the Mississippi, which has seen a ten-fold increase in sediment post-European settlement (USACE 2007; Engstrom, Almendinger, and Wolin 2009; Belmont et al. 2011). The Minnesota River's portion of the inland barge navigation network is important with several of the world's largest grain marketing companies operating terminals to provide to both domestic and foreign markets. These terminals serve as the most cost-effective distribution routes for areas of the upper Midwest. The estimated 4 million tons of product moving annually on the Minnesota River saves an estimated $50,000,000 in costs opposed to using other transportation routes (e.g. Great Lakes, rail, etc.). In the event that the Minnesota River is no longer navigable, these are costs that would be passed on to the producer (i.e. the farmer) in the form of lower prices offered by the grain companies (USACE 2007). The USACE admits that projecting future dredging maintenance on the Minnesota River is difficult with the many unknowns and variables effecting channel maintenance (USACE 2007), prompting the need for a better understanding of the planform channel adjustments of the river.

A better understanding of migration and width adjustment extends beyond dredging to all existing and future infrastructure in the Minnesota River Valley. This region is heavily occupied with many cities abutting the river and personal residences near the river which are susceptible to the erosional forces of the river (Johannesson and Parker 1985). Therefore, if geomorphic trends in the river planform change are seen, informed decisions can also be made to protect current structures and guide how to better engineer future structures to handle any anticipated trending changes (Kondolf, Piégay, and Landon 2002). The benefits of this knowledge are of monetary value but also are of safety concern to protect human life.

With all that is known about the issues facing the MRB, little is known on how the primary drainage of the MRB, the Minnesota River, has adjusted in response to these changes. Therefore, this research aims to fill an essential gap by revealing historic temporal and spatial trends of planform channel change on the lower Minnesota River (Figure 1), in a period dominated by anthropogenic modification of the fluvial system. Specifically, the lower Minnesota is of interest since the last 15 river miles are currently being actively dredged (USACE 2007). A large majority of this sediment comes from the Le Sueur River which contributes 24-30% of the total suspended solid load despite the watershed occupying only 7% of the MRB. This load enters the Minnesota River via the Blue Earth River in Mankato which marks the beginning of the study area (Figure 1).

1.1.2.2. Ecological/Biological Management

In addition to helping understand ongoing change in the fluvial system, assessment of channel change can aid in ecological and biological management practices within the riparian corridor (Bunn and Arthington 2002; Foufoula-Georgiou et al. 2015). In the case of the Minnesota River, feasibility of an instream barrier, to hinder the upstream advancement of invasive carp, is not well understood. Planform channel change analysis is essential to this assessment. Not only does a stretch of the river need to be stable in terms of migration and width to place a barrier, but it also needs to be in a location where it will not be cut-off from the main channel during a flood. In addition, if channel form change occurs (i.e. lateral migration, translation sinuosity, width, pattern change, etc.), a barrier could be rendered ineffective as the river is no longer the same as what the barrier was designed for. Without this understanding, an uninformed decision of placement could lead to millions of tax payer dollars being wasted if a barrier was compromised in any of the aforementioned ways.

In terms of instream barriers, the lower Minnesota River is a preferred location since urban development in the river valley has created several stretches of river that are already controlled (e.g. Mankato's Flood Walls). It is also of concern to block the advancement of invasive carp from travelling any farther upstream than necessary to avoid threatening other basins like the Red River Basin.

2. Methods

To conduct planform channel change analysis of the lower Minnesota River, we apply a method of measuring channel migration, width, and sinuosity using GIS analysis to assess channel change dynamics through historical time. This analysis incorporates both image registration and bankline digitization error (Libby, 2018) which will collectively be referred to as total spatial error.

Total spatial error considers both the registration and digitizing error present in a GIS-based methodology. Block (2014) offers an exemplary approach to quantifying the total spatial error margin for GIS planform studies based on data derived from DOQs and georectified aerial photographs. The total spatial error for channels digitized based of DOQs is as follows:

$$\text{eq. Total Spatial Error} = \sqrt{(average\ RMSE\ of\ the\ DOQ)^2 + (digitization\ error)^2}$$

The total spatial error for channels digitized based on georeferenced imagery need to not only account the RMSE of the aerial photograph but also the RMSE of the DOQ (source error) used to derive the GCPs during the image registration process. This formula is as follows:

$$\text{eq. Total Spatial Error} = $$
$$\sqrt{(average\ RMSE\ of\ the\ DOQ + average\ RMSE\ of\ the\ aerial\ photograph)^2 + (digitization\ error)^2}$$

Lea and Legleiter (2016) use this same premise in their methods, but instead of using RMSE, they use the error vectors from the GCPs displacement discussed in Chapter 2 of Libby (2018) to assess the spatial variable error (SVE) in image registration. The SVE is then compared to the x and y coordinates of the migration line end points to see if the measurement exceeds the error in that location. This process is done in the second MATLAB script covered in this chapter. As with any research focus, there are shifts that take place in hopes of advancement, and in channel planform studies as well as other remotely conducted studies, geospatial error is becoming an independent subject matter. SVE is the new standard for how error should be viewed and calculated in future channel migration studies.

2.2.1. Channel Migration

The banklines and centerlines that were created in Chapter 2 of Libby 2018 served as the inputs for measuring channel planform change in this report. Lateral channel movement, channel width change, and sinuosity/channel length were calculated throughout the 1937-2013 temporal scale of this analysis. To accomplish calculating channel migration four main steps were followed:

1) The National Center for Earth-Surface Dynamics (NCED) Planform Statistics Toolbox was used to create trajectory files measuring lateral channel movement along with a file storing width measurements. From this point forward, the term "trajectory" will be used to define lateral channel migration measurements.

2) The newly created data from the prior step was entered into a custom, created ArcMap tool in order to update and correct measurements as well as add required fields (x and y coordinates, paired ID's) so it can be seamlessly integrated into MATLAB

3) The output data from step 2 and the previously created error analysis in Chapter 2 is entered into Lea and Legleiter's (2016) "ChannelChangSignf" MATLAB script (

Appendix D) in order to determine which measurements are statistically significant (exceed the amount of error).

4) The tabular output data from step 3 was entered into another custom created ArcMap tool to automate the process of tying the tabular data to the spatial data along with updating fields.

2.2.1.1. National Center for Earth Surface Dynamics Planform Statistics Toolbox

Lateral channel movement was calculated using the NCED Planform Statistics toolbox (Lauer 2006). The time intervals analyzed were 1937-1951, 1951-1964, 1964-1980, 1980-1991, and 1991-2013. These intervals were selected based on the availability of imagery and based on a similar temporal scale (~10-20 years). The following steps were used to calculate lateral channel movement for the intervals of interest. This detailed step by step process will allow any future studies to exactly replicate the methods of this study.

Step 1: Add two centerlines for a given interval into ArcMap.

Step 2: Select the "Lateral Measurement" from the NCED toolbox which prompts the user to select the "to" (later date) and "from" (earlier date) centerlines from each time interval.

Step 3: After the lines are selected, a dialog box opens prompting "Y" to be entered if apex lines are to be considered. Apex lines are user generated lines within ArcMap that can be used to aid the program in correctly identifying lateral migration for bends in the river that are translated (see **Error! Reference source not found.** in Libby 2018) downstream (Lauer 2006).   Based on the suggestion of other researchers, this was left empty in this study indicating no apex lines should be considered, but could be investigated further for future studies.

Step 4: The program creates trajectory graphic lines which provide a visual in ArcMap from which lateral migration are derived. It should be noted that these lines are just graphics and not a shapefile. When this process is complete a window will open directing the user to select a location on the computer for a new polygon shapefile to be created and stored along with a file name.

Step 5: After the file is named and stored, another dialog box opens prompting the user to select a lateral offset distance from the centerline for the new polygon shapefile dimensions.

Step 6: This polygon shapefile is then created and stores the lateral migration measurements within its attribute table. This step is intended to be the terminal point for the tool, however the following steps are needed for editing errors (Figure 2) and for the future MATLAB script to be compatible with the shapefiles.
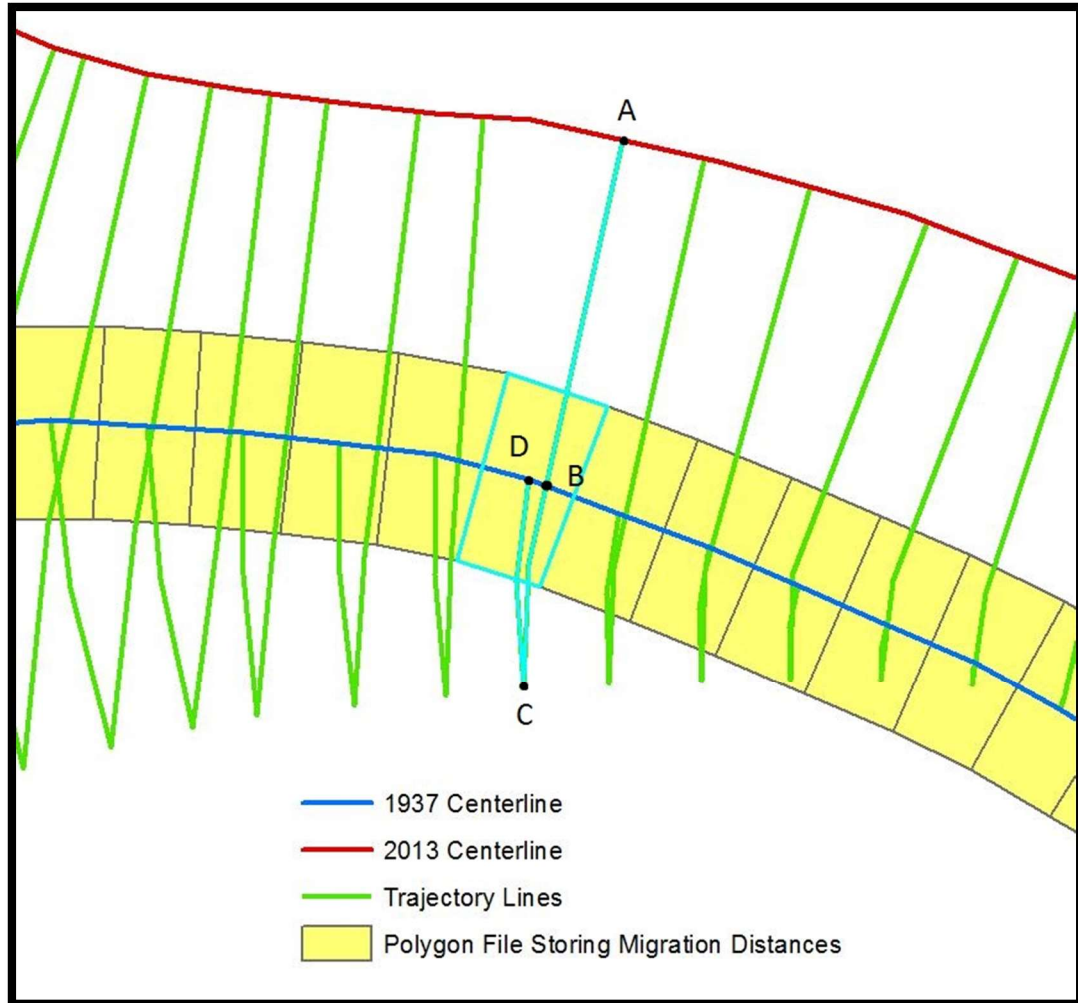
Figure 2. This figure shows inaccurate migration measurements made from the "Lateral Migration" tool. The polygon file (yellow rectangles) are what the tool uses to store the migration information based on the trajectory line graphics (green lines). The measurement from point A to point B is 36.6 meters and would an accurate measurement for lateral channel movement. However, the highlighted polygon indicates a migration distance of 79.7 meters which is the measurement of the entire highlighted trajectory line (point A-B-C-D). For this reason, it is imperative to save on edit the trajectory graphics to recalculate correct measurements.

Step 7: The graphics files discussed in step 4 need to be saved as a shapefile. This can be accomplished by right-clicking the layer and selecting "Convert Feature to Graphic". By doing this, spatial data is created for the trajectory lines (lateral migration lines) which can be manipulated by editing and recalculating measurements if needed.

Step 8: Once "Convert Feature to Graphic" is selected, a dialog box appears where the shapefile name and storage location is selected by the user. Note a check box for "Automatically delete graphics after conversion" must be selected to avoid ArcMap from crashing.

Step 9: The newly created trajectory line shapefile is added to ArcMap, and three lines running the longitudinal length of the river need to be selected and deleted in an editing session so only the lateral migration trajectory lines remain.

Step 10: Finally, all trajectory lines need to be inspected and edited to catch any errors made by the tool. This is most commonly seen where cut-offs occur (Figure). In this study, the lines were first edited by students from an upper-division fluvial geomorphology class and then inspected and further edited by myself.

This methodology for running the NCED "Lateral Migration" tool and creating the trajectory lines is summarized in Figure 1 with images showing the step by step processes of the tool.
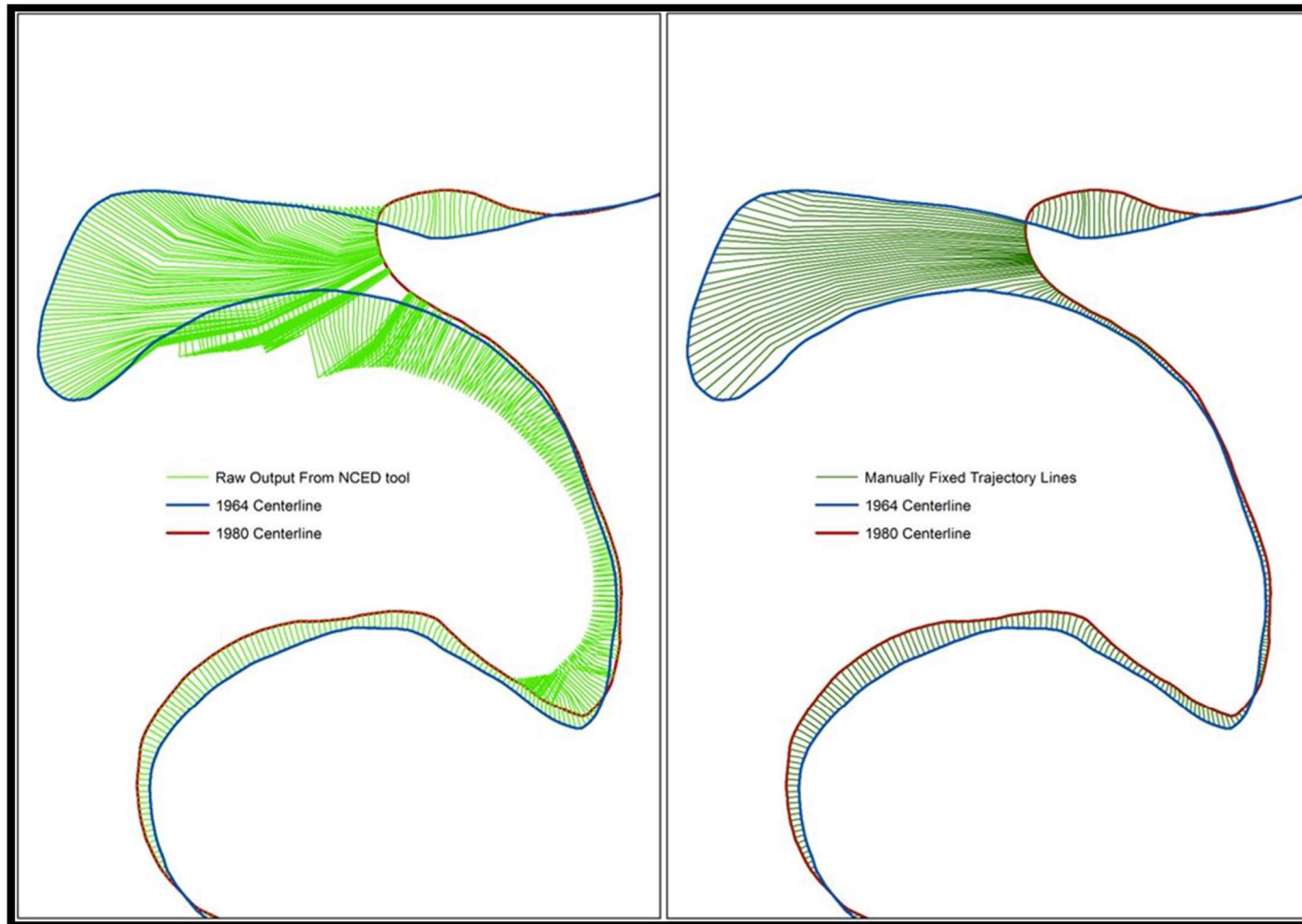
Figure 3. The first image (left) shows the raw trajectory lines from the NCED "Migration Tool." These lines clearly create false measurements much larger than what they should be by extending outside the 1964 centerline and then back in to connect to the 1980 centerline. In these cases, it was often easiest to delete the lines and manually digitize a more natural trajectory between the two centerline (right).
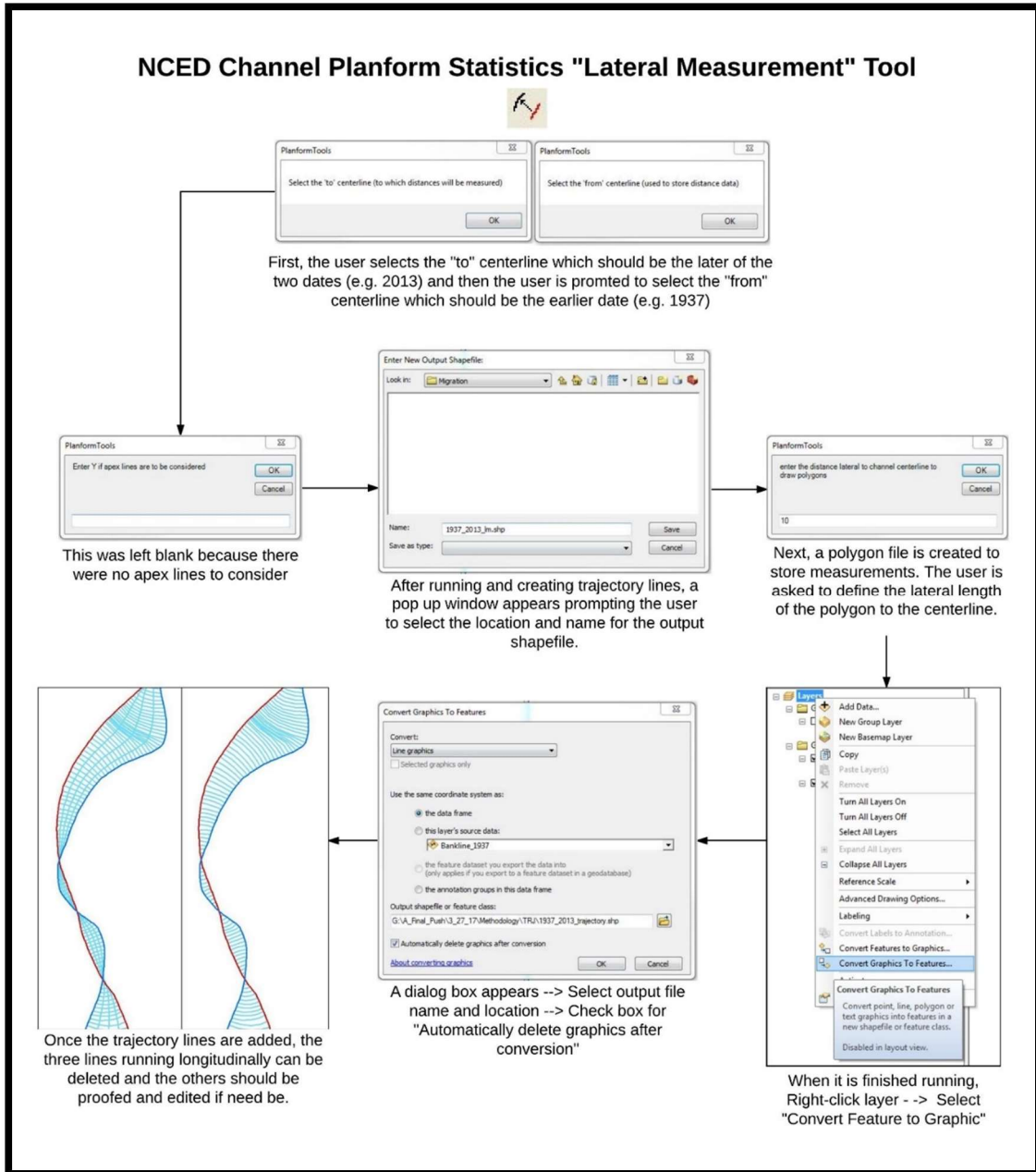
Figure 1. The NCED Channel Planform Statistics "Lateral Measurement" tool has various steps required to successfully complete the process beginning to end. The figure above shows the work flow with visuals and descriptors.

2.2.1.2. Pre MATLAB Processing

Once all trajectory lines were edited to accurately display the lateral migration of the river for each interval, a model (Figure 2) was created to set the structure for writing a python script (

Appendix E) to automate the process to prepare the data so it could be entered into the "ChannelChangeSignif" MATLAB script from Lea and Legleiter (2016). This script was written and turned into a custom ArcGIS tool (Figure 3;

Appendix E) making the automation capabilities accessible to those with no programing knowledge. The script/ArcGIS tool will be referred to as "Pre MATLAB Processing" script or tool from here on out. It is important to realize these two things are doing the exact same thing. The tool simply creates a Graphical User Interface (GUI) so the "Pre MATLAB Processing" script can be run without any code ever being seen by the user.

The "Pre MATLAB Processing" script (Figure 3;

Appendix E) accomplished two main goals:

1) It gave every trajectory line a correct measurement identifying downstream-left channel migration as positive and downstream-right channel migration as negative. This was necessary because the measurements provided with the initial NCED "Migration Tool" had inaccurate (errored) lines (Figure 2 and Figure) resulting in false measurements.

2) It gave every trajectory line XY coordinates on each end of the line and all coordinate pairs were exported as an .xls file with a common ID field linking each pair to its respective trajectory line. This file was necessary for the "ChannelChangeSignif" MATLAB script (Lea and Legleiter, 2016) to determine if the distance between the coordinate pair exceeds the error present in that location, thereby evaluating whether measurement exceeds the error in that given location or not.

The "Pre MATLAB Processing" ArcGIS tool is simplistic in that it only requires the user to set a location for storing created files, input the edited trajectory polyline shapefile, and input the centerline for the earlier year of the interval considered (Figure 3). A detailed explanation for the tool and every selection was also added in the "Show Help" portion of the tool to make it user friendly. Although the tool requires only three inputs, a series of processes run within the script and all the intermediate files are stored in a temporary folder that the script then deletes at the end in order to minimize unnecessary clutter. The "Pre MATLAB Processing" script with detailed explanation can be seen in

Appendix E.
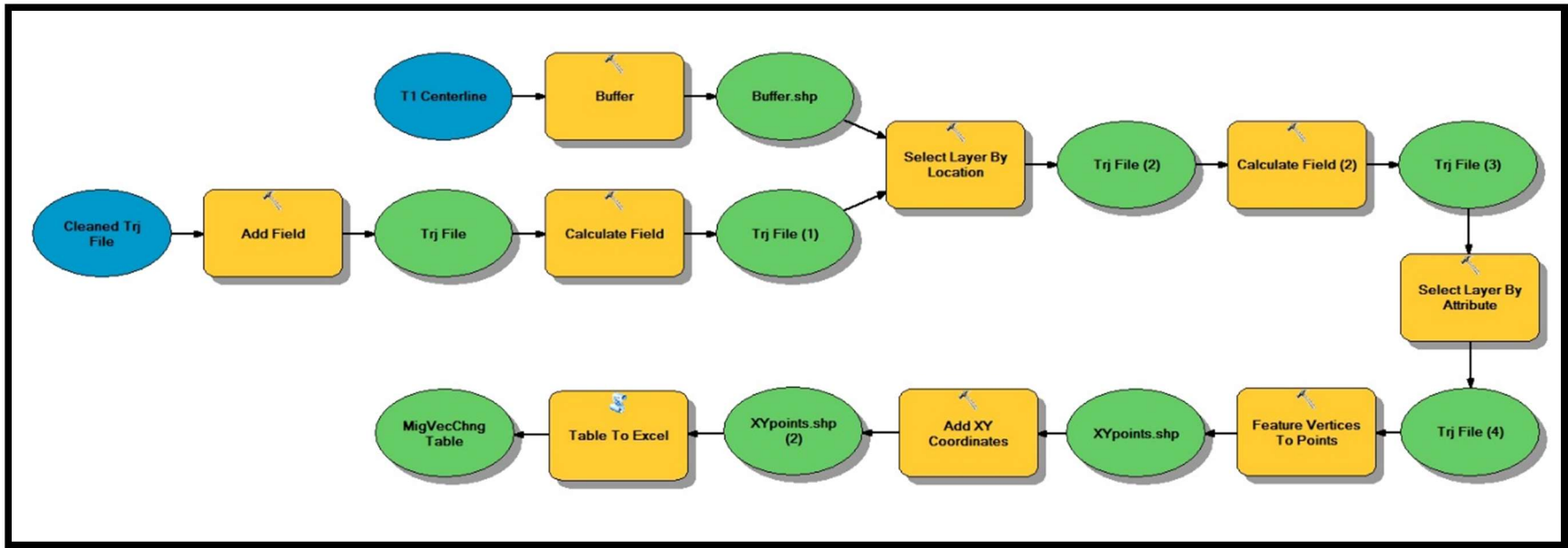
Figure 2. This model takes the edited trajectory lines and calculates the length of each line (lateral migration) and assigns negative values to migration occurring in the downstream-right direction. Each individual line is then given an XY coordinate on each end which the MATLAB script then uses to determine with the distance between the pair of points exceeds the error present in that location. The script (

Appendix E) written from this model is much more robust and fully details all the processes in the comments. This model served for a framework to initially conceptualize the main workflow of the tool.
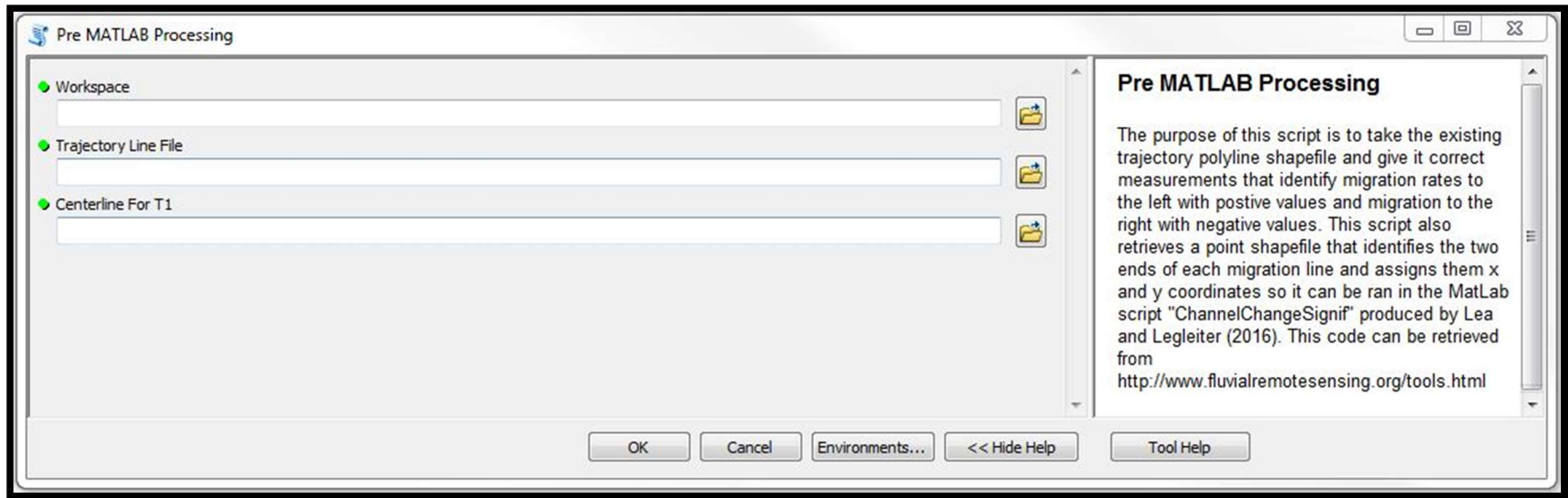
Figure 3. The Graphical User Interface (GUI) for the Pre MATLAB Processing tool has three user required inputs along with tool help descriptors defining the overall function of the tool and each input. The input and descriptors are as follows: 1) Workspace - Enter the workspace that contains the trajectory polyline file and centerline for time 1. This will be the folder where the output files will be written as well. 2) Trajectory Line File - Select the trajectory polyline file for the interval of interest. 3) Centerline for T1 - Select the polyline file for the river centerline for time 1 (the earlier of the two years in the interval).

2.2.1.3 MATLAB "ChannelChangeSignif"

The data stored in the .xls file from "Pre MATLAB Processing" script along with the error analysis output (RegErrorResults.mat) from the "QuantifyinRegistrationError" script in Chapter 2 of Libby 2018 were used at inputs into Lea and Legleiter's (2016) "ChannelChangeSignif" MATLAB script (

Appendix D). This script evaluates the lateral migration distances to the total spatial error (registration error and digitizing error) to determine is the measurements exceed the error and are significant or if they do not and are insignificant. The modifications and user supplied inputs for the "ChannelChangeSignif" script are as follows:

The easting and northing were both changed to zero since UTM coordinates were used in the "QuantifyingRegistrationError" script and no adjustments were needed. The easting and northing serve to match the coordinates from the error analysis GCPs to the trajectory line coordinates if necessary, but since the GCPs used in Chapter 2 of Libby (2018) already were input in the same coordinate system that the trajectory lines (UTM), no adjustment was needed.

Digitizing error was input to correctly match the results from the digitizing error assessment (**Error! Reference source not found.** in Libby 2018). For every interval, the average digitizing error for each year of the interval was averaged and input into the script. For instance, if year 1 had an average digitizing error of 2.00 and year 2 had an average digitizing error of 2.50, the interval average would be 2.25 and serve as the input digitizing error. The inputs used were:

<div align="center">

1937-1951 = 1.620 meters
1951-1964 = 1.330 meters
1964-1980 = 1.275 meters
1980-1991 = 1.730 meters
1991-2013 = 1.885 meters
1937-2013 = 1.715 meters

</div>

As directed in Lea and Legleiter's instructions a new variable was created in MATLAB and named "MigVecChng." This variable is n x 5 matrix (n being the number of migration measurements from the study and 5 being the columns a-e below) was populated using the information created in the XLS file from the "Pre MATLAB Processing" tool. The information input is as follows:

<div align="center">

Column 1 = ID
Column 2 = Pair ID
Column 3 = Migration Distances
Column 4 = X Coordinate
Column 5 = Y Coordinate

</div>

This transposed the variables into column-vector format so the script could run. A section of the script calculates significant and insignificant migration based off RMSE. This portion of the script had to be manually changed to the time frame specific averaged RMSE value. This section of the script also has two different equations to choose from depending on whether the periods in a given interval were warped to separate base images or if the base image itself was used as one of the periods in the interval considered.

Custom lines of script were added to further automate the processes by automatically creating the .csv file that original script required to be manually created through copy and pasting matrices out of MATLAB into Excel. The added script and comments are as follows:

% Devon Libby's additions to simplify and automate the process of creating a
% csv file containing the information of significant and nonsignificant
% migration.

% Creating the header names in an array
ColumnNames = {'FID','Sig_SVE','Sig_RMSE','Sig90'}
% Creating the ID field which will serve as the foreign key in
% to join the significant/insignificant table with the migration
% measurement table in ArcMap. This is accomplished by selecting every
% other entry from column two in the MigVecChng variable and moving it
% into a standalone matrix
ID = MigVecChng(1:2:end,2:2);
% This concatenates the ID field, SVE, RMSE, and 90th percentile
% significant/insignificant tables into one.
sigList_All = [ID sigList_SVE sigList_RMSE sigList_90];
% This function was downloaded from
% https://www.mathworks.com/matlabcentral/fileexchange/29933-csv-with-column-headers
% (credit: Keith Brady) and allows a csv file to be written from the newly
% concatenated list and given the header from "ColumnNames".
csvwrite_with_headers('MATLABoutput.csv',sigList_All,ColumnNames)

Once the script has completed running, all files that reside in the folder are prepared for processing through the "Post MATLAB Processing" tool. A script function "csvwrite_with_headers" written by Keith Brady was used and his script for the function can be seen in Appendix F.

It should be noted that when the "ChannelChangeSignif" script was first executed, an error occurred in the "scatteredInterpolant" command within the script. The error message specified "Input data point values must be specified in column-vector format." In order to fix this two lines were added to the code immediately before the "scatteredInteroplant" command

<div align="center">Xresid = Xresid';</div>

<div align="center">Yresid = Yresid';</div>

This transposed (flipped the columns and rows) the data and fixed the error. For more information see

Appendix D.

2.2.1.4. Post MATLAB Processing

After the tabular data stored in the .csv was created in MATLAB to discern between statistically significant and insignificant data, it had to be brought back into ArcMap, joined to the trajectory line shapefile, and given new downstream measurements. The new downstream measurements were necessary since the shapefile was manually edited negating the usefulness of the original downstream measurements from the Planform Toolbox. This was accomplished by creating another model (Figure 4) to set the conceptual framework for the necessary processes. A script (

Appendix G) was then written in order to create another custom ArcMap tool (Figure 5) that seamlessly integrated the output .csv of the "ChannelChangeSignif" MATLAB script with the already existing files created from prior tools. The custom script/tool to accomplish this was named "Post MATLAB Processing" and will be referred to as such moving forward. The ArcGIS tool requires the user to:

Set the workspace
Input the trajectory polyline shapefile
Input the newly created .csv that was created and properly formatted in the
"ChannelChangeSignif" MATLAB script
Enter the number of years separating the two periods in the interval being considered.
This is done so a new field can be populated with an annual migration.
Set the coordinate priority from which measures will be accumulated for linear
referencing i.e. calculating new downstream measurements. For this stretch of river,
LOWER_LEFT was selected since that is where the direction of flow begins.
LOWER_LEFT could be thought of as south west as well.
Input the centerline for the earlier period in the time interval
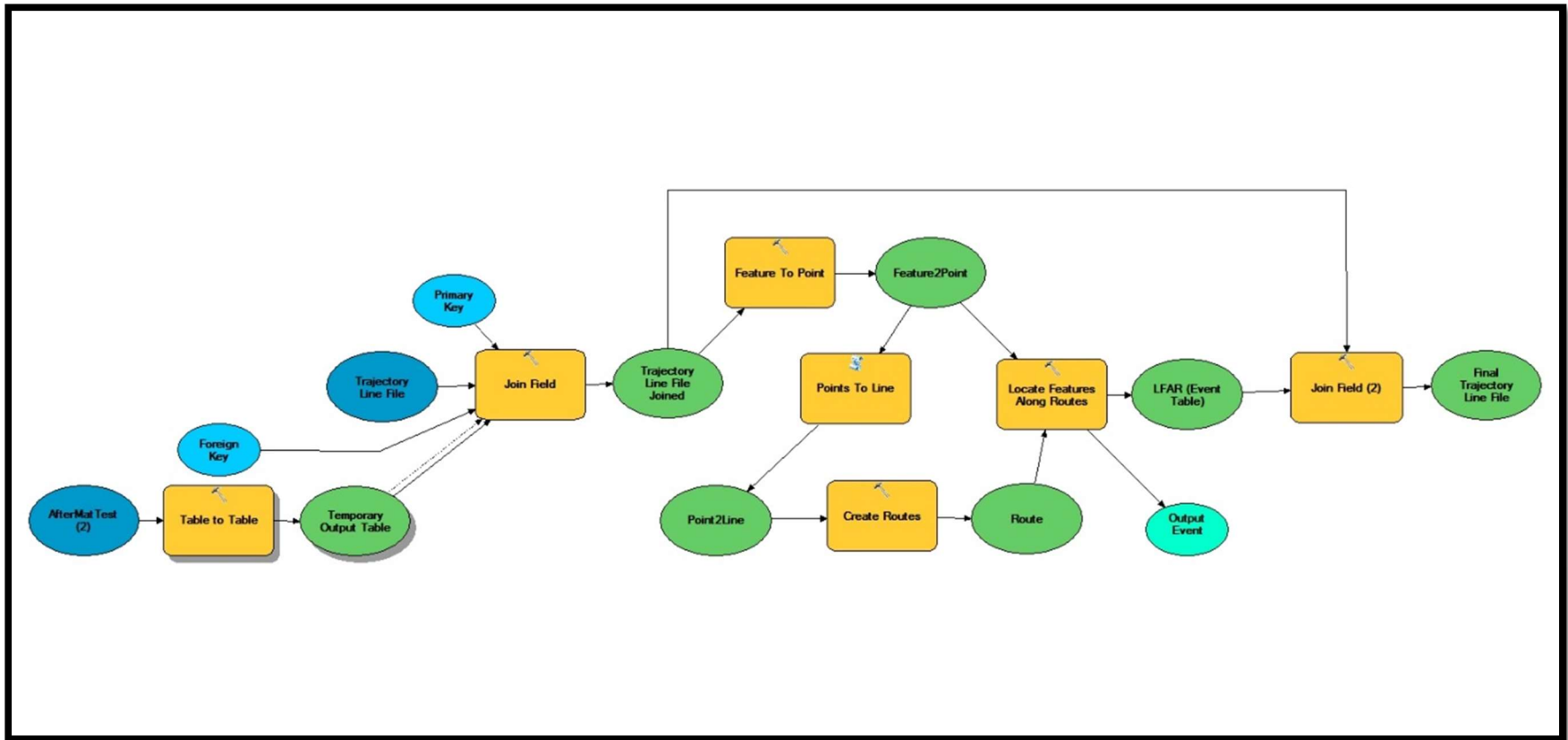
Figure 4. This model takes the newly created CSV that was output from the "ChannelChangeSignif" MATLAB script and joins the data back to the trajectory line shapefile. Once this is completed the tool recalculates downstream measurements through a series of tools and then joins the new up to date measurements to the trajectory line file. The script (Appendix 3D) written from this model is much more robust and fully details all the processes in the comments. This model served for a framework to initially conceptualize the main workflow of the tool.
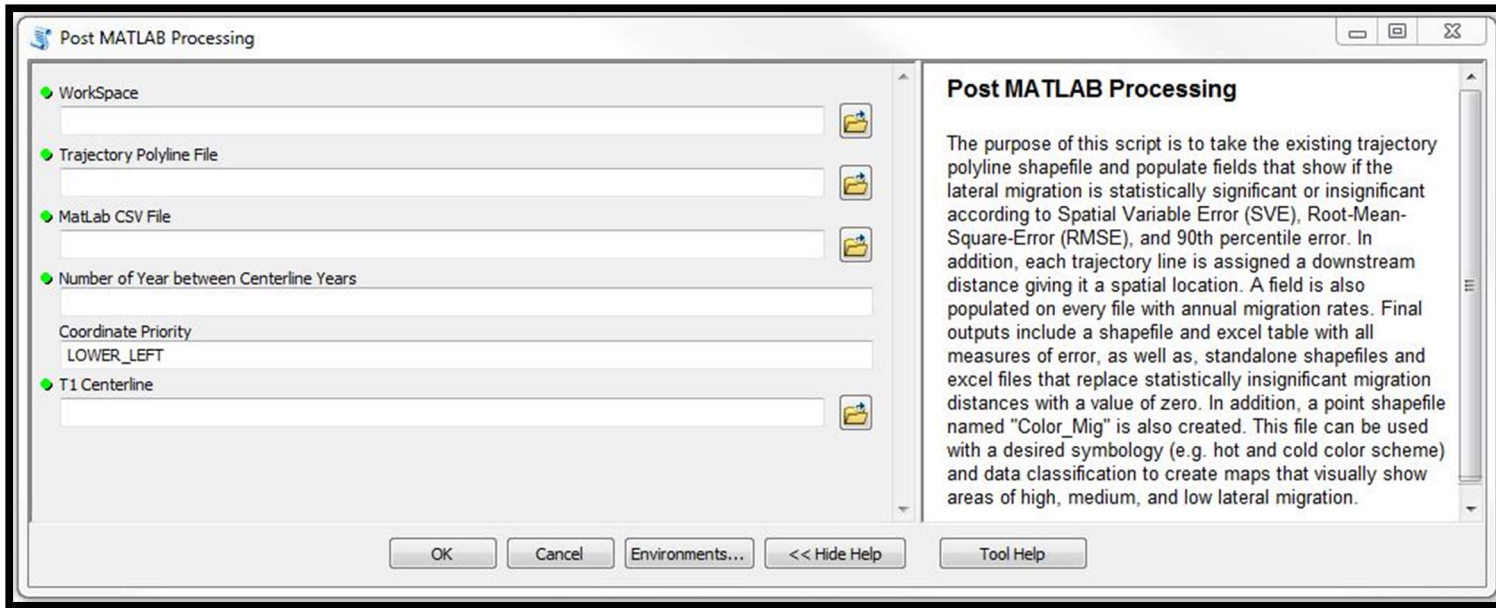
Figure 5. The GUI for the Post MATLAB Processing tool has six user required inputs along with tool help descriptors defining the overall function of the tool and each input. The input and descriptors are as follows: 1) Workspace - Set the workspace to the folder containing the appropriate trajectory polyline file and CSV file containing significant and insignificant measurements that are used as the next two inputs 2) Trajectory Polyline File - Select the appropriate trajectory polyline file. 3) MatLab CSV File - Select the appropriate CSV file containing significant and insignificant measurements. Note: this CSV file must contain only four columns with headings "FID", "SVE", "RMSE", "Ninety" respectively. If these aren't spelled and capitalized correctly the script will fail to run. 4) Number of Years between Centerline Years - Enter the number of years (interval) between the two centerlines. Example: Time 1 centerline is 1937 and Time 2 centerline is 1951. The number entered would be 14. 5) Coordinate Priority - The position from which measures will be accumulated for each output route during the linear referencing process. Options include: UPPER_LEFT —Measures will be accumulated from the point closest to the minimum bounding rectangle's upper left corner. This is the default. LOWER_LEFT —Measures will be accumulated from the point closest to the minimum bounding rectangle's lower left corner. UPPER_RIGHT —Measures will be accumulated from the point closest to the minimum bounding rectangle's upper right corner. LOWER_RIGHT —Measures will be accumulated from the point closest to the minimum bounding rectangle's lower right corner. 6) T1 Centerline - Select a polyline shapefile for the earlier of the two time periods for the interval considered.

The "ChannelChangeSignif" MATLAB script calculates significant and insignificant measures based on three metrics (SVE, RMSE, 90th percentile – for more information on these see

Appendix D). The "Post MATLAB Processing" script was written to create unique shapefiles and Excel tables for each of metrics (Figure 6). In creation of the files, an update cursor uses fields which denotes insignificant measurements as 0's significant measurements as 1's to then update the total migration and annual migration fields. If a measurement is insignificant (denoted by 0) the cursor changes the total migration and annual migration fields to 0 since they do not exceed the error present. The trajectory shapefile used to parse (separate) this data into individual files is also updated but stores all the information for the three metrics along with all migration measurements regardless of whether they are significant or insignificant. This preserves all of the original data and can always be referred back to by the user. An Excel table is also created from the newly updated shapefile as well. Another output is a point shapefile named "Color_Mig". This file can be used in combination with a desired symbology (e.g. hot and cold color scheme) and data classification to create maps visually displaying the amount of channel mobility. All intermediate files created in this script are stored in a temporary folder which are automatically deleted at the end of the script to avoid unnecessary clutter.

Input Files

MATLABoutput.txt.xml	XML Document
MATLABoutput.csv	Text File
1937_1951_trajectory.shp	Shapefile
1937.shp	Shapefile

Output Files

MATLABoutput.txt.xml	XML Document
MATLABoutput.csv	Text File
SVE.shp	Shapefile
RMSE.shp	Shapefile
Ninety.shp	Shapefile
Color_Mig.shp	Shapefile
1937_1951_trajectory.shp	Shapefile
1937.shp	Shapefile
Excel_Table_SVE.xls	Excel File
Excel_Table_RMSE.xls	Excel File
Excel_Table_Ninety.xls	Excel File
Excel_Table_All.xls	Excel File

SVE Table

SVE

FID	Shape *	Mig_Dist	SVE	MEAS	An_Mig
1796	Polyline	0	0	0	0
1796	Polyline	0	0	9.93405	0
1796	Polyline	0	0	19.934607	0
1795	Polyline	0	0	29.925954	0
1795	Polyline	0	0	39.925058	0
1795	Polyline	0	0	49.91847	0
1795	Polyline	0	0	59.898096	0
1795	Polyline	0	0	69.886639	0
1795	Polyline	0	0	79.885355	0
1795	Polyline	0	0	89.869473	0
1795	Polyline	0	0	99.868202	0
1795	Polyline	0	0	109.86762	0
1795	Polyline	0	0	119.850908	0
1794	Polyline	4.74	1	129.835078	0.34
1794	Polyline	5.97	1	139.832382	0.43
1794	Polyline	7.05	1	149.866404	0.5
1794	Polyline	7.79	1	159.875888	0.56
1794	Polyline	7.88	1	169.940797	0.56
1794	Polyline	8.62	1	180.039414	0.62
1794	Polyline	9.37	1	190.082259	0.67

1937_1951_trajectory

FID	Shape	Mig_Dist	SVE	RMSE	Ninety	MEAS	An_Mig
1796	Polyline	-1.59	0	0	0	0	-0.11
1796	Polyline	-0.53	0	0	0	9.93405	-0.04
1796	Polyline	-0.92	0	0	0	19.934607	-0.07
1795	Polyline	-1.01	0	0	0	29.925954	-0.07
1795	Polyline	-1.41	0	0	0	39.925058	-0.1
1795	Polyline	-1.5	0	0	0	49.91847	-0.11
1795	Polyline	-0.76	0	0	0	59.898096	-0.05
1795	Polyline	-0.17	0	0	0	69.886639	-0.01
1795	Polyline	-0.07	0	0	0	79.885355	0
1795	Polyline	0.84	0	0	0	89.869473	0.06
1795	Polyline	1.4	0	0	0	99.868202	0.1
1795	Polyline	2.29	0	1	0	109.86762	0.16
1795	Polyline	3.51	0	1	0	119.850908	0.25
1794	Polyline	4.74	1	1	0	129.835078	0.34
1794	Polyline	5.97	1	1	0	139.832382	0.43
1794	Polyline	7.05	1	1	0	149.866404	0.5
1794	Polyline	7.79	1	1	0	159.875888	0.56
1794	Polyline	7.88	1	1	0	169.940797	0.56

All Data Table

Figure 6. Only three files are required as inputs into the "Post MATLAB Processing" tool. The output files created from the tool include: 1) the input trajectory shapefile with new fields showing statistically significant and insignificant measurement denoted by 1's and 0's respectively along with downstream measurements and annual migration. 2) Three new polyline shapefiles (SVE, RMSE, Ninety) that show only the fields pertinent to the specific error metric and reduce insignificant measurements to 0's in the total migration and annual migration fields. 3) Excel tables for all the shapefiles in order to increase efficiency for data analysis. 4) A point shapefile named "Color_Mig" that can be used in combination with a desired symbology (e.g. hot and cold color scheme) and data classification to create maps that visually represent channel mobility.

Once all the data was run through the tool, it was manually inspected. A minor problem was noticed when "Sort Ascending" was applied to the measurement field in ArcMAP. In a couple of the intervals a handful of trajectory lines were reporting a downstream measurement of "0". Upon closer inspection, it was discovered that these trajectory lines lacked measurements because they were not connected to the T1 centerline (earlier time period centerline) which the tool used to create a route in order to assign measurements to the trajectory line (Figure 7). This issue could have been handled in multiple ways, but it was decided that the intervals affected by this problem would be corrected by fixing the trajectory lines and rerunning the data through the "Post MATLAB Tool." This was done to ensure the highest degree of accuracy with the data. Another alternative would be to manually type in the downstream measurements by using the "Identify Route Locations" tool within ArcMap. However, the main issue with this approach is that every excel table (4 total) and shapefile (5 total) would have to be opened and edited which could introduce user error along with being a time consuming and tedious process.
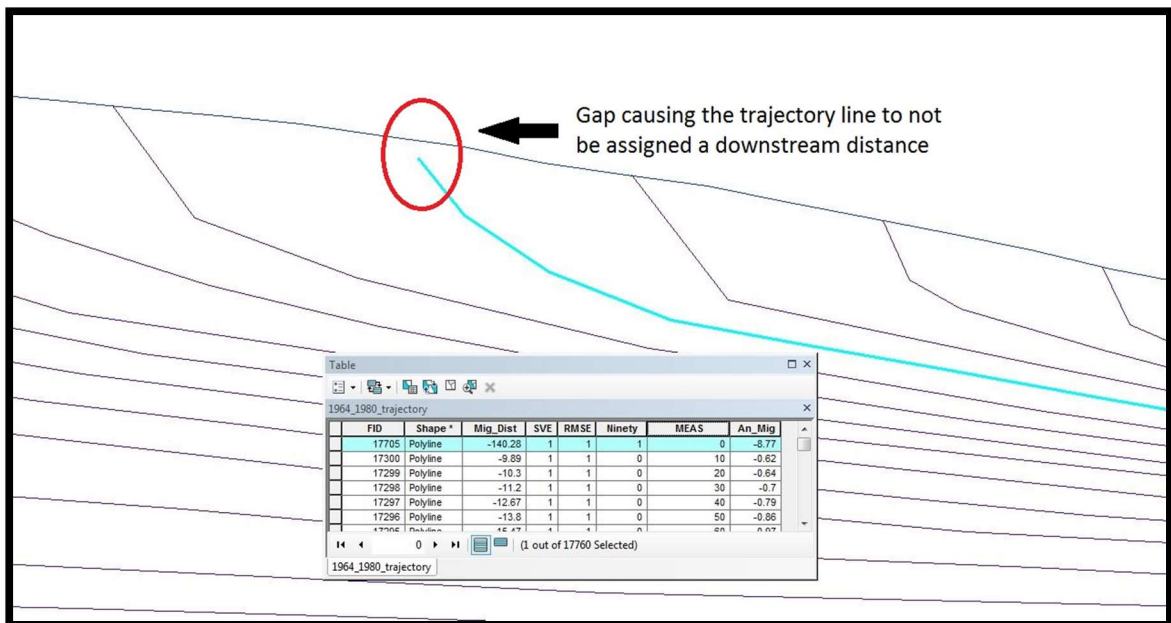
Figure 7. The trajectory was not connected to the T1 centerline. Since this centerline was converted to a route to assign downstream distances to the individual trajectory lines, the gap caused it to be passed over.

2.2.1.5 Cutoff vs Non-Cutoff Datasets

The definition used in this study for a "cutoff" needs to be explained since cutoffs were not included as channel migration in the reach analysis. These measurements were not included because a cutoff is not eroding and reworking sediment between the old channel and new channel. However, there were instances in this study where an old channel was rapidly abandoned but reworked or fully eroded all the land between the old channel and new channel. In these instances, the measurements were considered as "non-cutoff migration" since erosion and subsequent sediment reworking occurred over the

area between the old and new channel (Figure 8). The channel migration data also becomes heavily weighted by cutoff measurements when they are included alongside non cutoff migration measurements. In some cases on the Minnesota River, a cutoffs old channel location to new channel location is over thousand meters away. Although the primary focus moving forward is on channel migration without cutoff measurements, the presence of cutoffs within reaches will be discussed since they do show spatial and temporal trends that can be used to interpret the results. Cutoffs are also important to note since they are directly tied to reductions in stream sinuosity.
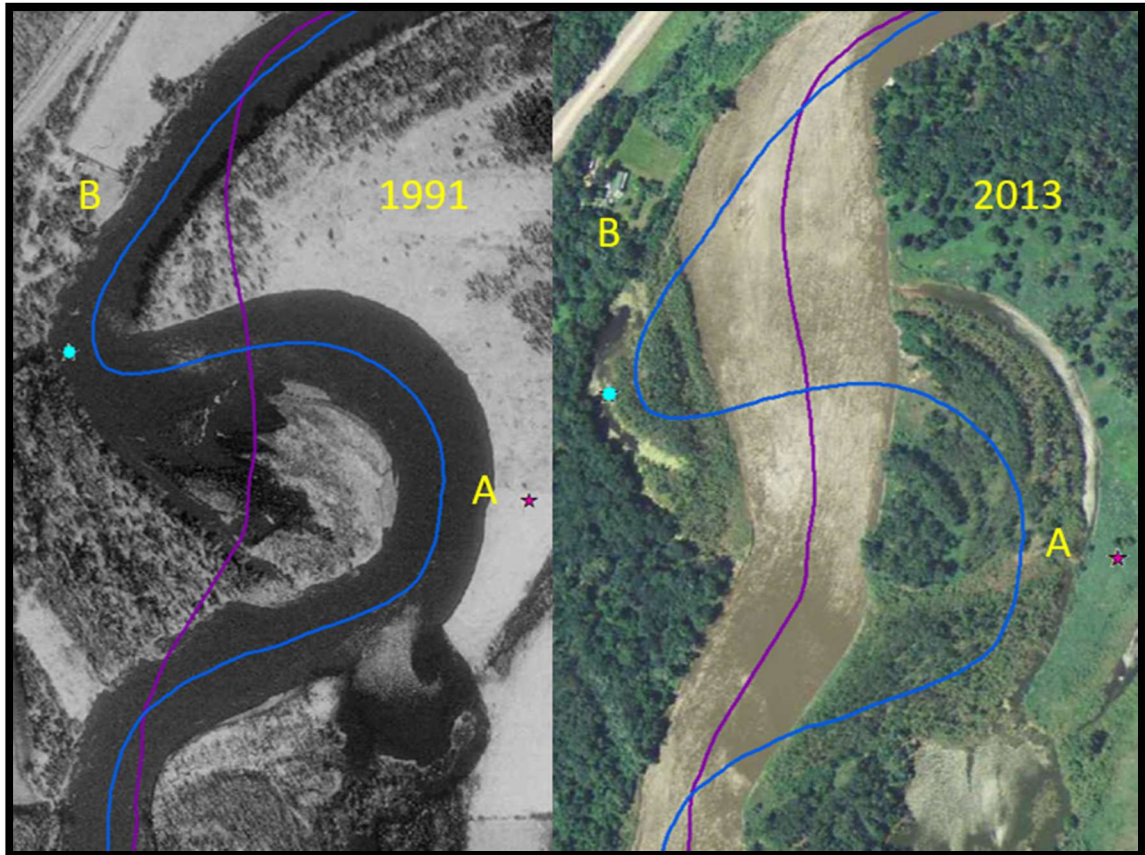
Figure 8. This figure displays the difference in cutoffs that were not considered in migration measurements (A) and "cutoffs" that were considered as migration. In cutoff A, there is clearly uneroded land that was left behind when the cutoff occurred, whereas, cutoff B eroded all the land when establishing the new channel route. The blue dot shows where an oxbow lake if forming which would cause some to call this a cutoff, but it is not in this study.

2.2.2 Width Change and Sinuosity/Stream Length

Width measurements were calculated and stored in a text file when the centerlines were created in the NCED "Centerline Interpolation" tool (see section 2.2.4 in Libby 2018; **Error! Reference source not found.**.). In order to make these files usable in ArcMap, the text files were converted to dBASE (.dbf) tables using the "Table to dBase"

tool. This process is necessary so ArcMap can handle the large amount of entries contained in the file opposed to just trying to bring the text files into ArcMap. The dBase contains the xy coodinates for the left and right side of each measurement so the "XY to Line" tool was then used to create a shapefile of the width measurements. One shortcoming of this tool is that it does not transfer all the attributes contained in the original dBASE table so it is necessary to use the ID field (optional to transfer in the "XY to Line" tool) to join the newly created shapefile back to the dBASE table in order to access width measurements and downstream distances. This can be done many ways but in order to permanently join the necessary fields the "Join Field" data management tool was used. Another option would be to create a new width measurement field using the "Calculate Geometry" function within ArcMap to populate it.

Sinuosity is simply the relationship between channel length divided by valley length. To calculate these measurements, the geometry of the centerlines was calculated in ArcMap to get channel lengths then a separate shapefile was created and digitized for the valley length. These measurements were then joined to a single table and the field calculator was used to populate a new field storing the sinuosity measurements alongside the channel lengths.

2.2.3. River Reach and Pinch Point Analysis

Once all the calculations and analysis were complete, the data was broken down into river reaches based on geomorphic breaks (Figure 9) for longitudinal spatial analysis. These reaches were defined based on geomorphic characteristics of the channel (sinuosity, meander wavelength, depositional features, etc.) and river valley width as well as any influencing anthropogenic features (urban areas, bridges, flood control structures, etc.). For detail on the how the geomorphic breaks were determined see

Appendix H. This was accomplished by adding a new "River_Reach" field to the shapefile of interest (e.g. 1937-1951 migration shapefile) and overlaying a polyline shapefile with 16 segments matching the spatial extent of each break. Another way to accomplish this is by creating a polygon shapefile for the geomorphic breaks and using a "select by location" to then edit and populate fields to the respective geomorphic break.

A secondary, river reach break system (Figure 10) was used for displaying the shapefile named "Color_Mig" that visually displays channel mobility using intuitive color schemes to represent the data (discussed in section 2.2.1.4). These river reaches were based solely on providing an appropriate extent to best qualitatively display the data and were not used for any further analysis.

Since the placement of invasive carp barriers are primary consideration of this research, several "pinch points" or areas where structures are presently controlling the stream were selected and planform change was analyzed. First, Mankato's reach of river controlled by a flood control structure is looked at followed by four bridges. These pinch points were analyzed to see if any discernable trends could be seen in the evolution of upstream vs downstream morphology over the years of record.
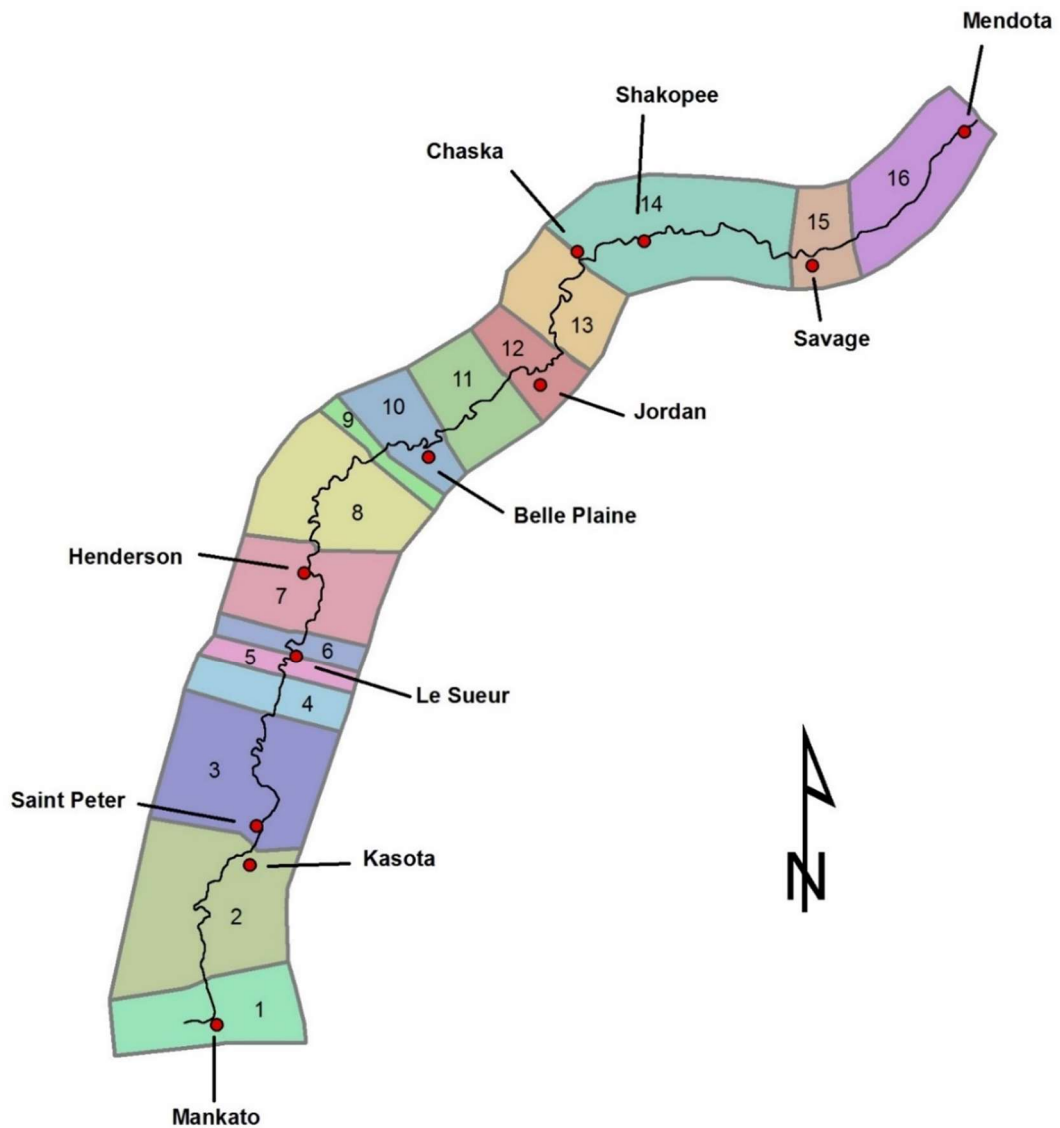
Figure 9. Displayed are the 16 geomorphic breaks that the study area was broken down into.

River Reach Break Down
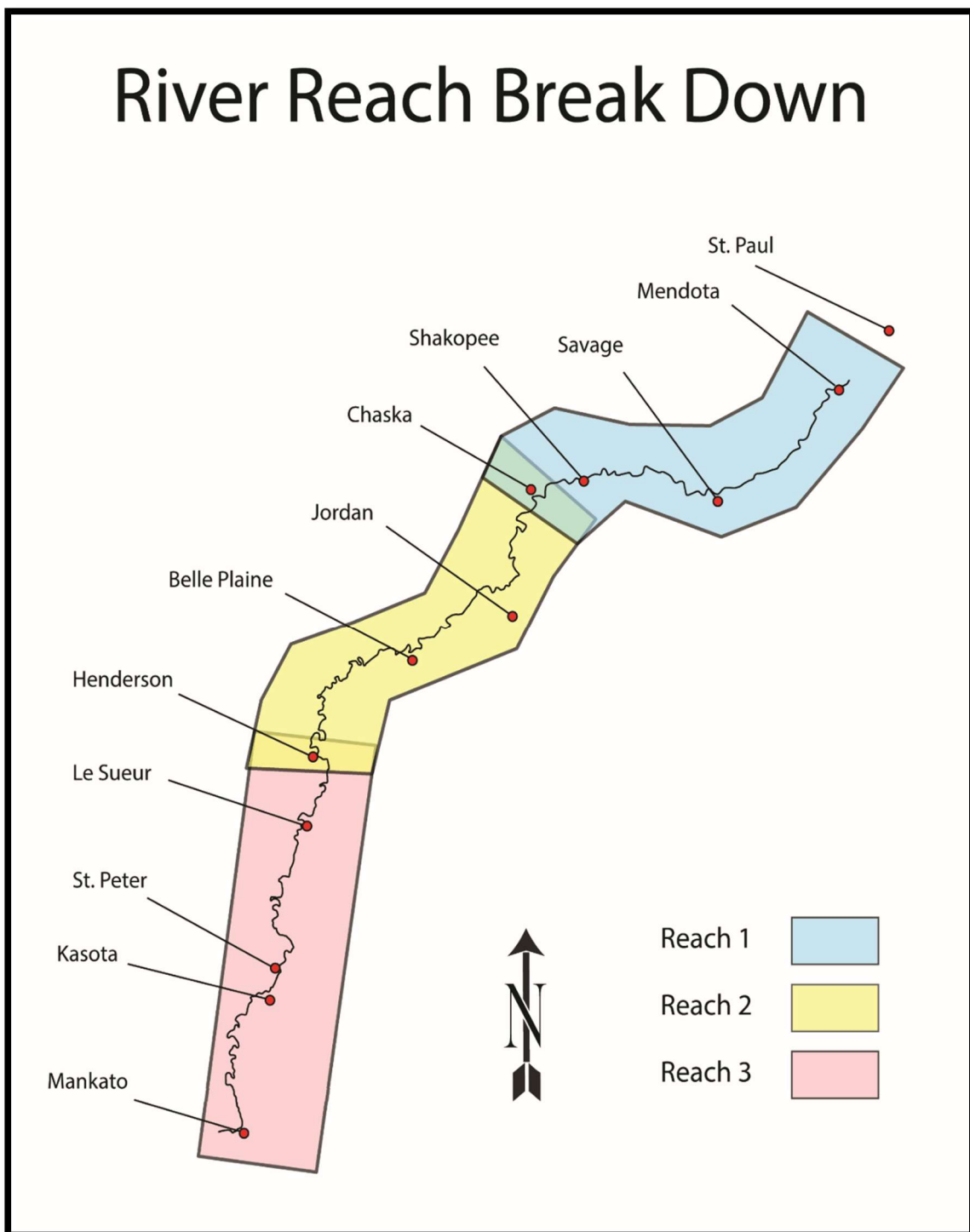
Figure 10. These are the three break points used to offer a spatial extent appropriate for viewing the "Color Migration" maps which are an output of the "Post MATLAB Processing" tool.

3. Results

3.1. Channel Migration

Channel migration can be analyzed at various scales. This section will first look at the study area as whole to see large scale spatial and temporal longitudinal trends exist. Attention will then be given to color migration maps which are also viewed at a larger scale but offer a unique view of the data by maintaining the spatial characteristics of the river. These maps are especially powerful in conveying migration to viewers without a scientific or mathematic background since graphical views of data are not necessarily intuitive to all viewers. Finally, a smaller scale focus will be given through reach analysis. Schumm (1985) states that reach scale analysis is of most interest to geomorphologists who are concerned with what the pattern of the river reveals about its history and behavior. Reach analysis also offers a higher resolution revealing if larger scale patterns are distributed over many reaches, or if acute activity or stability is seen within larger trends.

3.1.1. Large Scale Data Analysis

When viewing the data for channel migration for the lower Minnesota River at a large scale (Figure 11, Figure 12) the first ~115-120 river kilometers (Mankato to a little past Jordan) are historically more actively migrating than the downstream ~40-60 kilometers (measurements vary due to changing stream length for a given interval). Sixteen of the nineteen cutoffs of the entire temporal scale of the study appear in the upstream 90 kilometers (Figure 11). Although the next 25-30 kilometers are still active without cutoffs, a break is seen after this point where the channel migration decreases (Figure 11, Figure 12). Viewing the data at this scale shows broad patterns that are primarily spatial.

Appendix I displays every interval's annual channel migration in a standalone graph.
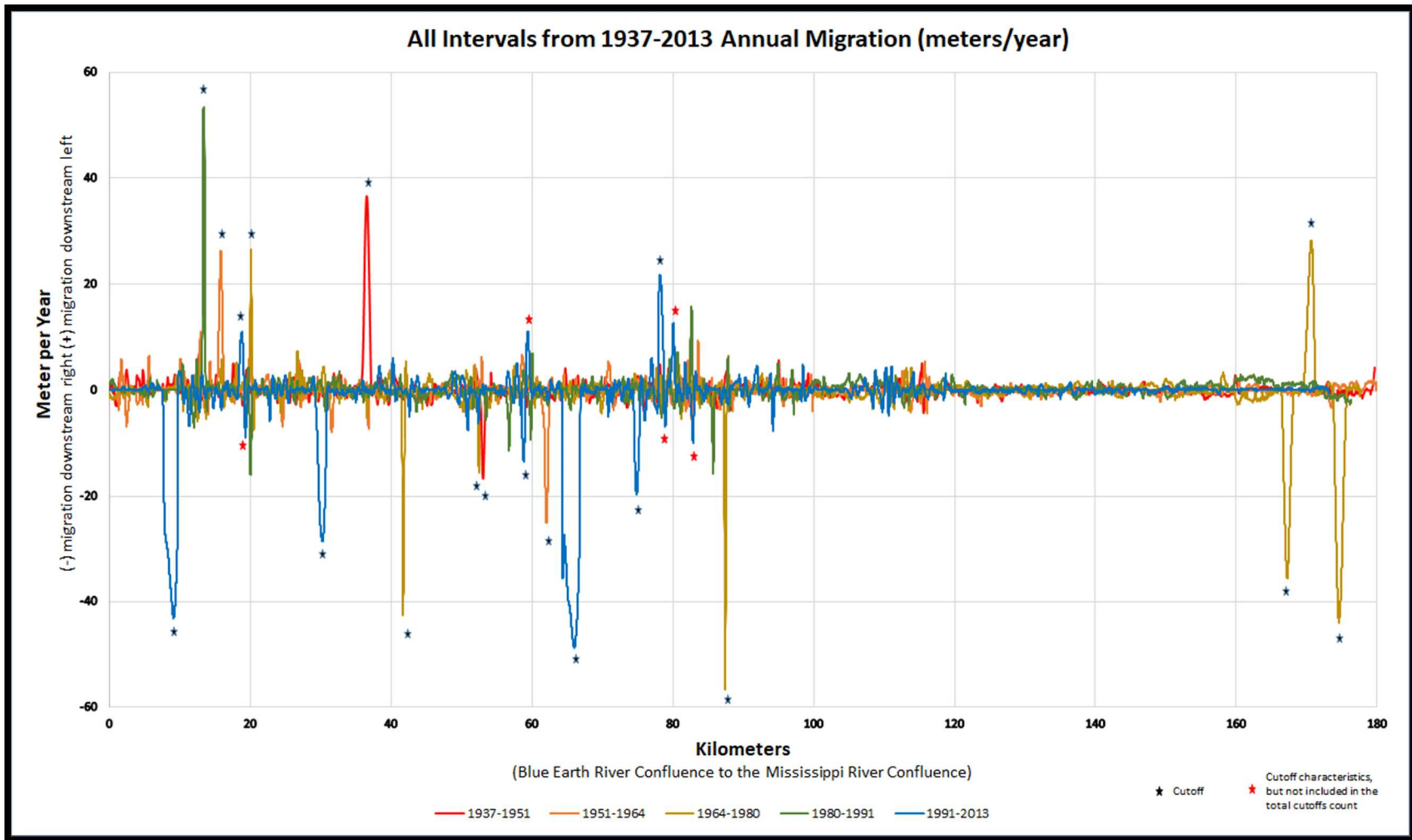
Figure 11. Graphical results for annual migration for all intervals related to downstream distance from the Blue Earth River confluence to the Mississippi River confluence with cutoff measurements included. These cutoffs are denoted on the graph with stars.
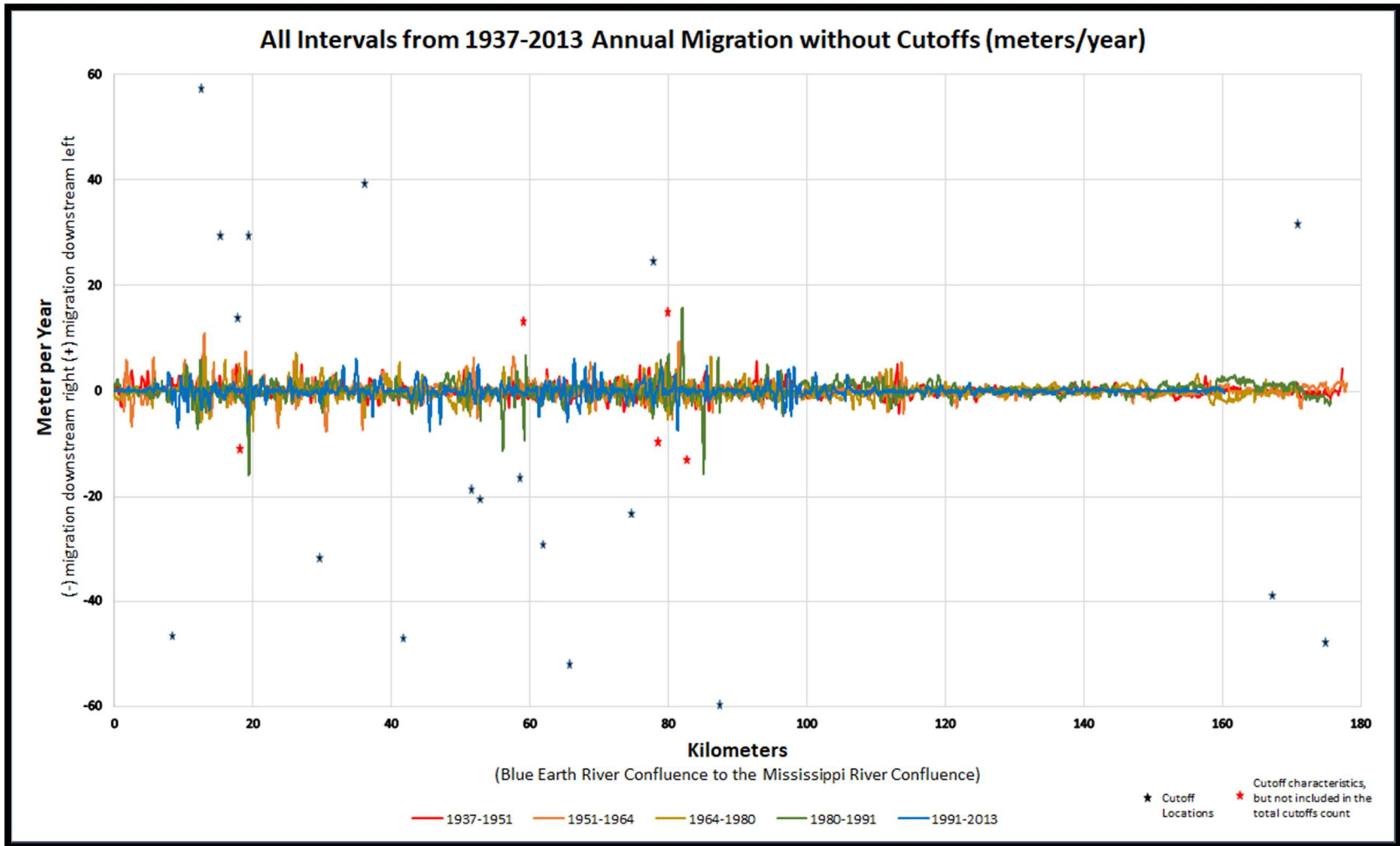
Figure 12. Graphical results for annual migration for all intervals related to downstream distance from the Blue Earth River confluence to the Mississippi River confluence with cutoffs measurements removed, however cutoff locations are denoted on the graph with stars.

3.1.1.2. Color Migration Maps (Preserving Spatial Attributes of the Data)

The results of the output "Color_Mig" shapefile produced in the Post MATLAB Script (Figure 13- Figure 15) reveal the same spatial trends as the graphical (Figure 11, Figure 12) view, however more detail is distinguishable. For instance, the first third of the study area (Figure 13) displays stretches of relative stability mixed within the more active reaches – a trend not evident in the graphical view. The area immediately downstream of the city of Henderson has also been a very active stretch of river in all the intervals considered (Figure 14). These output shapefiles demonstrate another way to display same data while maintaining spatial characteristics and applying an intuitive "hot and cold" color scheme. This view of the data shows the high degree of variability in the Minnesota River's channel migration prompting the need for more detailed reach analysis.
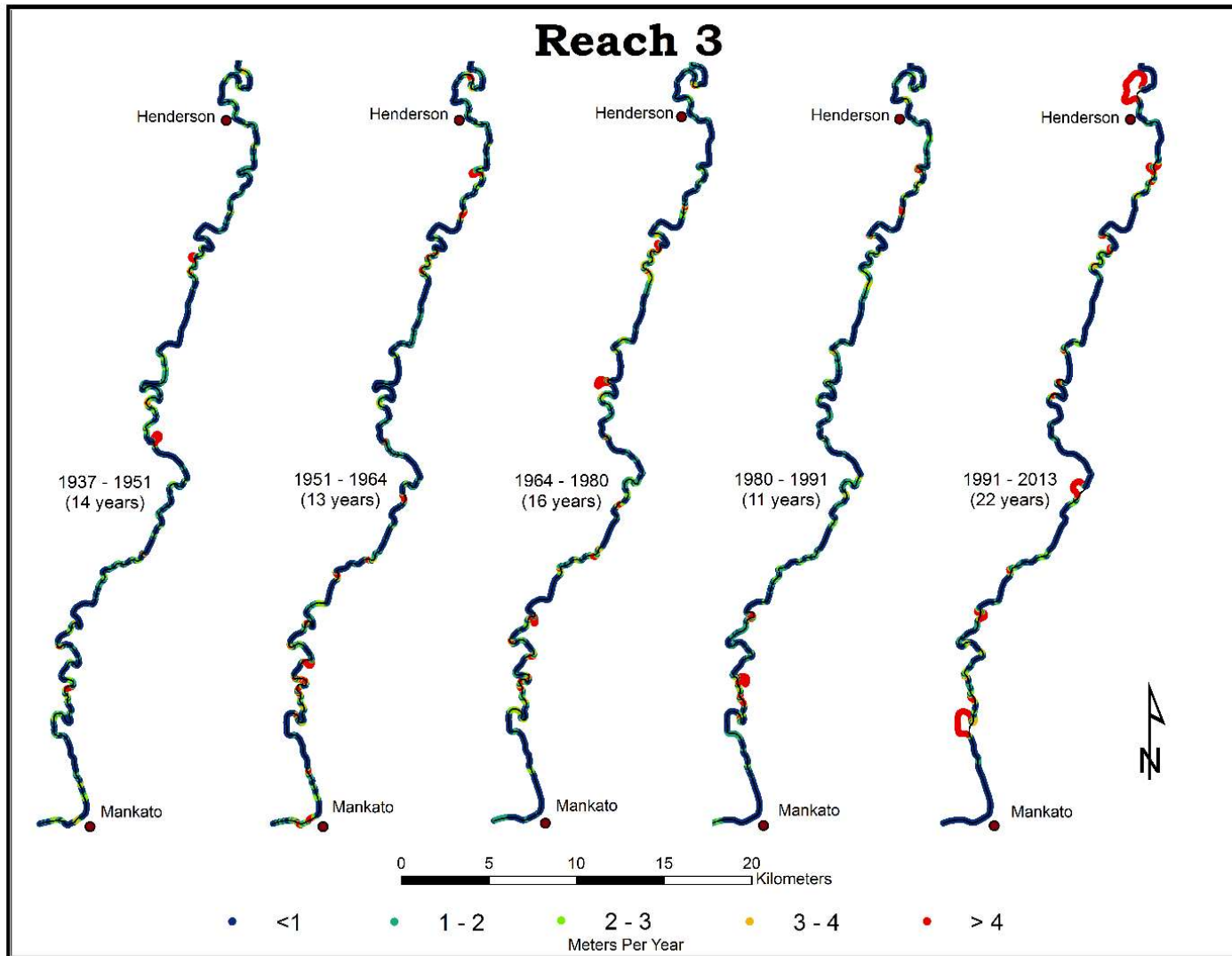
Figure 13. Displays the output for the "Color_Mig" shapefile from the Post MATLAB script in Reach 3 (Mankato to Henderson).
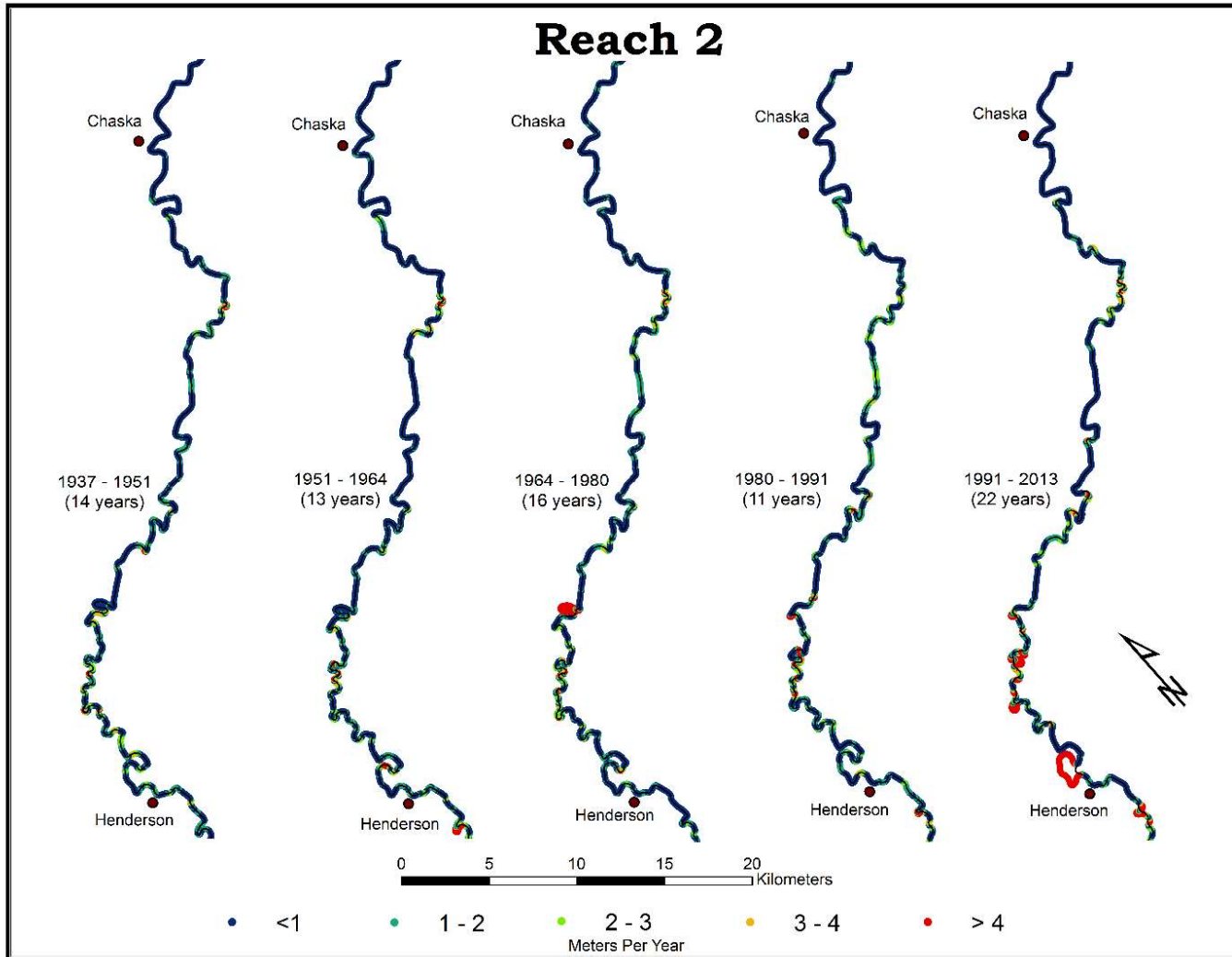
Figure 14. Displays the output for the "Color_Mig" shapefile from the Post MATLAB script in Reach 2 (Henderson to Chaska).
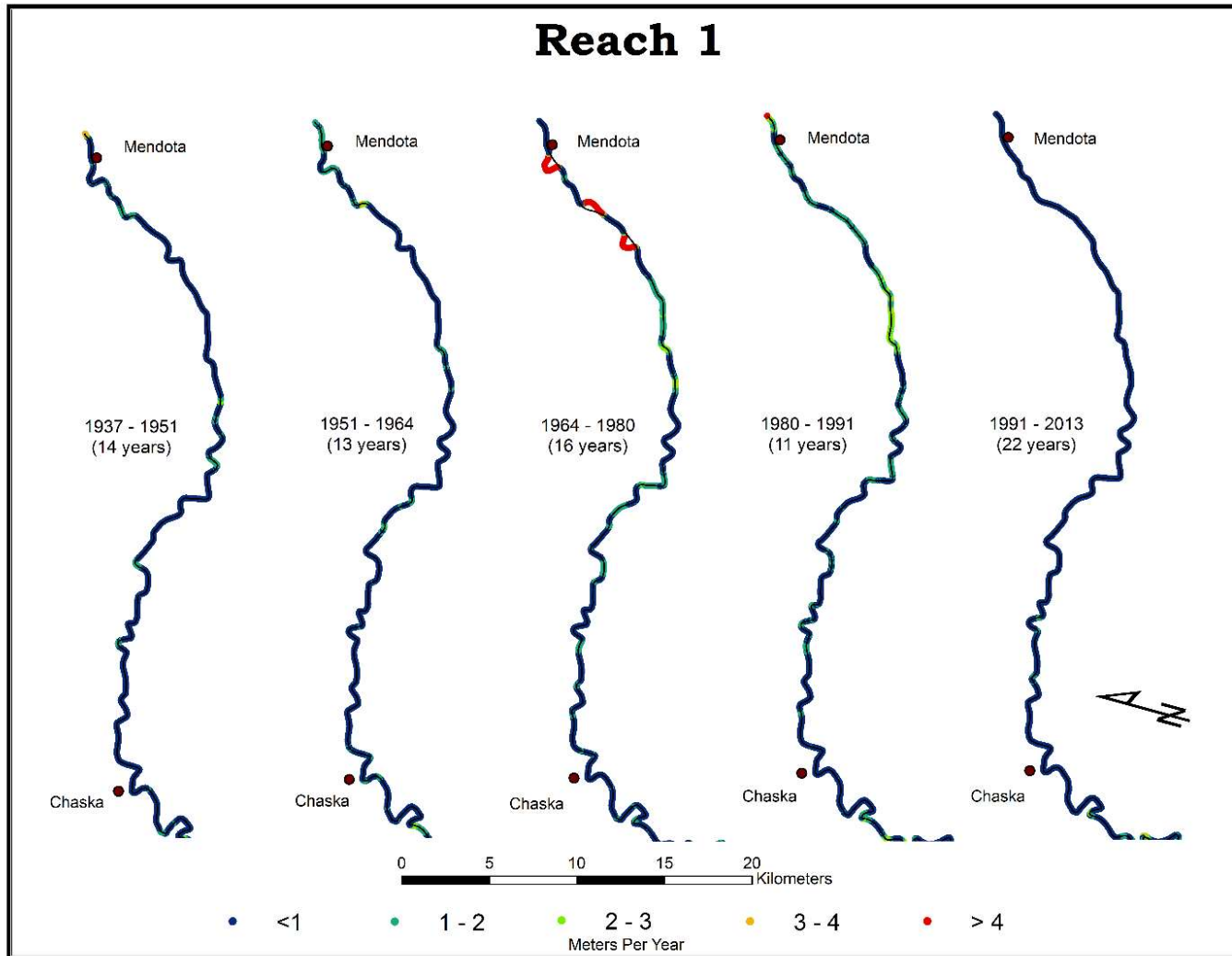
Figure 15. Displays the output for the "Color_Mig" shapefile from the Post MATLAB script in Reach 1 (Chaska to Mendota).

3.1.1.3. Geomorphic Break Reach Analysis

Geomorphic break (Figure 9) analysis revealed further temporal and spatial trends that were not intelligible in the prior forms of analysis. Considerations were given to:

- *Average annual channel migration (AACM) for each reach in each interval*
- *The overall AACM for each reach (1937-2013)*
- *The overall AACM for each interval for the whole river (Reach 1-16)*
- *The maximum annual channel migration (MACM) measurement for each reach in each interval*
- *The average MACM measurement for each reach*
- *The MACM for each interval for the whole river (Reach 1-16)*
- *Cutoff locations relation to 1-6*

Minimums values for individual reaches of a given interval were not considered since they all contain measurements of zero. Any measurement that did not exceed the error present (termed by Lea and Legleiter (2016) as statistically insignificant) was assigned the value of zero for this analysis. This was done because these measurements were almost exclusively smaller measurements, and to simply exclude them would bias the AACM measurements to appear higher than they are. Conversely, this has the potential to bias the AACM measurements to appear lower than they are, if actual migration took place, but was not enough to exceed the error in that location. The data was initially analyzed both with the insignificant measurements excluded and included as zero's. It was decided the latter analysis more accurately displayed the data.

3.1.1.3.1. Average Annual Channel Migration (AACM)

Reach 5 in the 1964-1980 interval had the highest AACM of 2.43 meters per year (m/y) (

Table **1**, Figure 16). Reach 5 also had the highest overall reach AACM rate with a reach average of 1.86 m/y (

Table **1**, Figure 17). Aside from Reach 5, Reach 2, 3, 7, 8, and 12 have been historically active reaches, all having AACM rates above the 50th percentile (median or 2nd quantile) throughout all the intervals considered (

Table **1**, Figure 17). Reach 10 has also been quite active with only one interval (1951-1964) being slightly under the 50th percentile. Reach 9 in the 1980-1991 interval had the lowest AACM of 0.11 (m/y) (

Table **1**, Figure 16). Reach 9 also had the lowest overall reach AACM rate with a reach average of 0.31 m/y (

Table **1**, Figure 17). Aside from Reach 9, Reach 6, 13, 14 and 15 have been historically inactive reaches, all having AACM rates below the 50th percentile throughout all the intervals considered (

Table **1**, Figure 16). Reach 4 and 11 have also remained inactive with the interval 1980-1991 being the exception for both.

The most recent interval of 1991-2013 interestingly marks the highest migration rates for Reach 7, 8, 10, and 12 and the lowest migration rates for Reach 1, 3, 4, 15, and 16 (

Table **1**). This interval also has three reach measurements in the 90th percentile and six measurements in the 10th percentile of all 80 AACM measurements considered (

Table **1**). This is nearly three times the amount of extreme (top and bottom 10%) values expected in a normal distribution. This is an indication that the present fluvial conditions are undergoing a change from those that historically existed. Reach 13-16 compose a little less than third of the total study area, and only contain two AACM measurements above the 50th percentile (both found in Reach 16) (

Table **1**). This indicates an overall spatial trend of decreasing channel migration on the lower Minnesota moving in the downstream direction (Figure 17) however variability is seen throughout the reaches (Figure 16, Figure 17).

Table 1. Average Annual Channel Migration

Average Annual Channel Migration by Reach and Interval (m/yr)						
Reach	1937-1951	1951-1964	1964-1980	1980-1991	1991-2013	Average
1	1.07	1.46	0.61	0.45	0.24	0.76
2	1.05	1.37	1.41	1.21	1.39	1.29
3	0.98	0.81	1.00	0.93	0.79	0.90
4	0.35	0.69	0.61	0.89	0.18	0.54
5	1.53	1.98	2.43	1.36	2.01	1.86
6	0.55	0.63	0.74	0.68	0.69	0.66
7	0.89	1.14	0.86	1.33	1.51	1.15
8	1.28	1.13	1.26	1.57	1.75	1.40
9	0.41	0.31	0.53	0.11	0.19	0.31
10	0.84	0.74	0.78	0.90	1.27	0.90
11	0.66	0.33	0.76	1.10	0.39	0.65
12	1.03	1.15	1.32	1.08	1.41	1.20
13	0.39	0.56	0.44	0.48	0.48	0.47
14	0.26	0.38	0.58	0.49	0.27	0.40
15	0.78	0.37	0.54	0.69	0.23	0.52
16	0.40	0.63	0.83	1.39	0.16	0.68
Average	0.77	0.84	0.91	0.99	0.81	0.86

10th Percentile		Quartile 1	Quartile 2	Quartile 3	90th percentile	
0.27		0.48	0.78	1.20	1.45	

< 0.27	>0.27 & <0.48	>0.48 & <0.78	>0.78 & <1.20	>1.20 & <1.45	>1.45
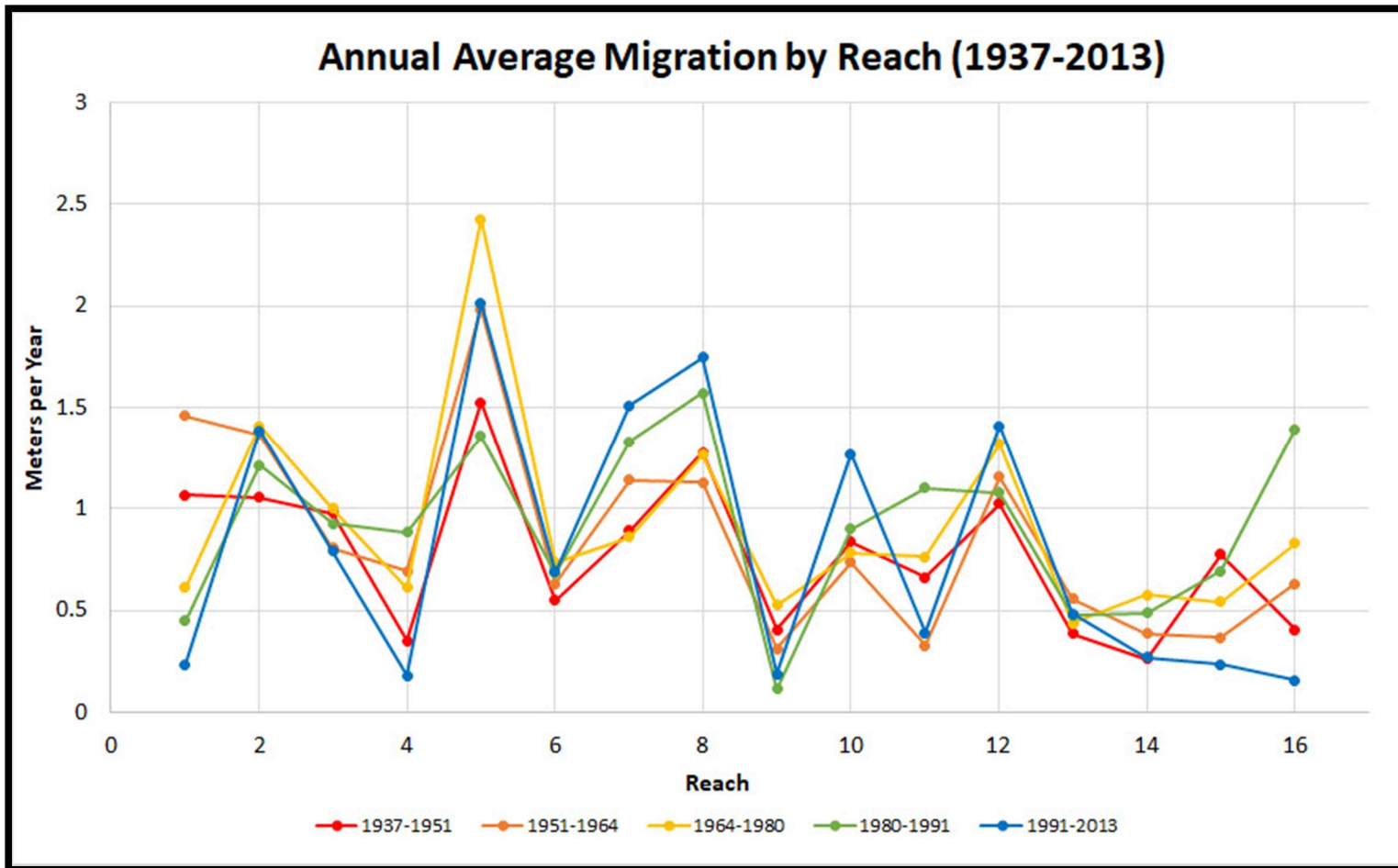
Figure 16. Graphical results for annual average migration for all intervals grouped by river reach. Reach one begins at the Blue Earth River confluence and Reach 16 ends at the Mississippi River confluence.
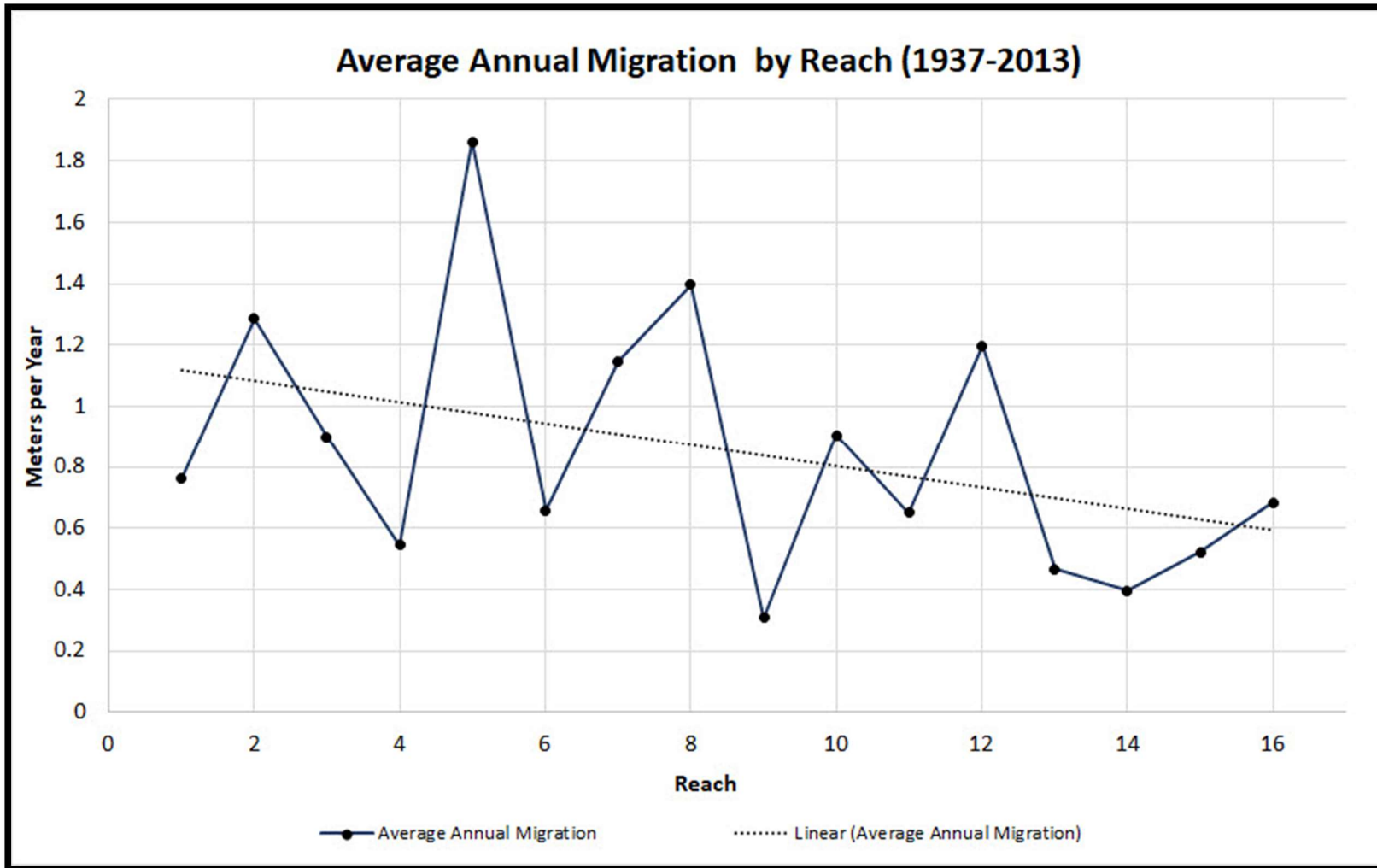
Figure 17. Graphical results showing the average migration of all years by reach. Reach 1 begins at the Blue Earth River confluence and Reach 16 ends at the Mississippi River confluence.

3.1.1.3.2. Maximum Annual Channel Migration (MACM)

Although Reach 5 had the greatest reach/interval AACM and the overall highest reach AACM, it did not rank among the highest reaches in terms of MACM (

Table **1**,

Table **2**). Reach 2 in the 1980-1991 interval had the highest MACM of any reach/interval with a measurement of 15.86 m/y or a total of 174.48 meters (Figure 18,

Table **2**). Reach 2 also had the highest average MACM of the reaches at 10.42 m/y (

Table **2**). Reach 7 and 8 also had high MACM rates with an average of 7.57 m/y and 9.95 m/y (

Table **2**). Reach 4, 9, 11, and 13-16 all averaged MACM measurements under 3 meters per year (

Table **2**). Reach 9, a reach characterized by an unusually long, straight length of channel, had lowest averaged MACM at 0.88 m/y and the lowest reach/interval measurement of 0.49 m/y in the 1991-2013 interval. Every MACM measurement in this reach fell in the 10th percentile (

Table **2**).

Reach 2, 7, and 8 contained all the 90th percentile MACM measurements revealing a strong relationship between these spatial locations over the entire temporal range of the study. In the prior section, low AACM measurements were seen in Reach 13-16 which is also the case for MACM. In these reaches, all but one MACM measurement is above the 50th percentile. Of the other nineteen measurements, eight of them are in the 25th percentile, two of which fall in the 10th percentile. This affirms another spatial/temporal trend that less channel migration is historically seen in the downstream reaches. The 1991-2013 interval show an unproportioned amount of extreme values (top and bottom 10%) relative to the other intervals much like it did in AACM. Four 10th percentile measurements and three 90th percentile measurements were recorded which is slightly under 50% of all extreme values.

Table 2. Maximum Annual Channel Migration by Reach and Inveral

Maximum Annual Channel Migration by Reach and Interval (m/yr)					
Reach	1937-1951	1951-1964	1964-1980	1980-1991	1991-2013	Total
1	3.93	6.63	2.97	2.45	1.37	3.47
2	7.13	11.01	7.49	15.86	10.63	10.42
3	4.09	7.80	5.49	4.12	7.44	5.79
4	1.13	1.55	2.72	3.58	0.67	1.93
5	4.12	6.34	4.61	3.42	7.47	5.19
6	1.49	6.42	3.20	5.58	6.08	4.55
7	4.17	6.69	4.67	11.21	11.09	7.57
8	5.34	9.40	6.6	15.75	12.64	9.95
9	0.97	0.93	1.04	0.98	0.49	0.88
10	5.69	3.83	3.27	5.10	7.46	5.07
11	1.97	1.28	2.17	3.27	4.82	2.70
12	5.12	5.53	4.25	3.28	4.59	4.55
13	2.37	3.00	1.73	3.04	3.49	2.73
14	1.60	2.20	2.17	2.04	1.60	1.92
15	2.87	2.00	3.35	1.76	0.77	2.15
16	4.31	3.27	2.63	3.04	0.78	2.81
Max	7.13	11.01	7.49	15.86	12.64	10.83

10th Percentile		Quartile 1	Quartile 2	Quartile 3	90th Percentile
1.05		2.07	3.53	5.98	9.24

< 1.05	>1.05 & <2.07	>2.07 & <3.53	>3.53 & <5.98	>5.98 & <9.24	>9.24
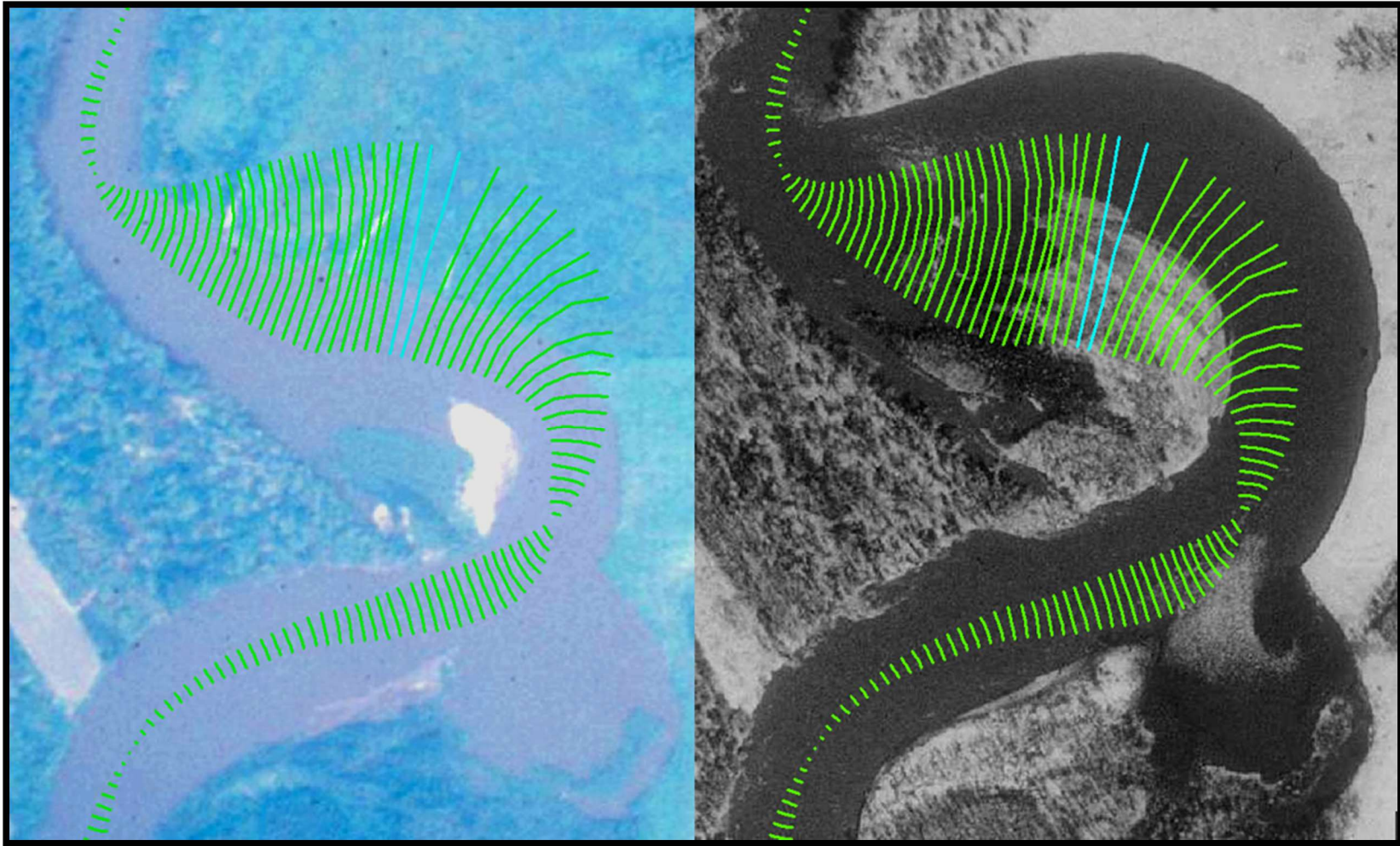
Figure 18. Reach 2 in the 1980 (left) to 1991 (right) had the the highes MACM of any reach/interval. This figure has the two measurements of 15.86 m/y (total 174.48 m) highlighted in light blue

3.1.1.3.2. Cutoff location relation to AACM and MACM

Although cutoffs measurements were removed from the reach analysis (Figure 16, Figure 17), Figure 19 displays cutoff locations with an embedded table showing the cutoffs by reach and by interval. Most cutoffs are in the upstream half of the study area (Reach 1-8) except for three cutoffs that occurred in Reach 16 in the 1964-1980 interval. Reach 2 had the most cutoffs with five total and the intervals 1964-1980 and 1991-2013 had the most cutoffs with seven a piece.

Cutoffs by Interval and Reach

Reach	1937-1951	1951-1964	1964-1980	1980-1991	1991-2013	Total
1	0	0	0	0	0	0
2	0	1	1	1	2	5
3	1	0	1	0	1	3
4	0	0	0	0	0	0
5	1	0	1	0	0	2
6	0	0	0	0	0	0
7	0	1	0	0	2	3
8	0	0	1	0	2	3
9	0	0	0	0	0	0
10	0	0	0	0	0	0
11	0	0	0	0	0	0
12	0	0	0	0	0	0
13	0	0	0	0	0	0
14	0	0	0	0	0	0
15	0	0	0	0	0	0
16	0	0	3	0	0	3
Total	2	2	7	1	7	19
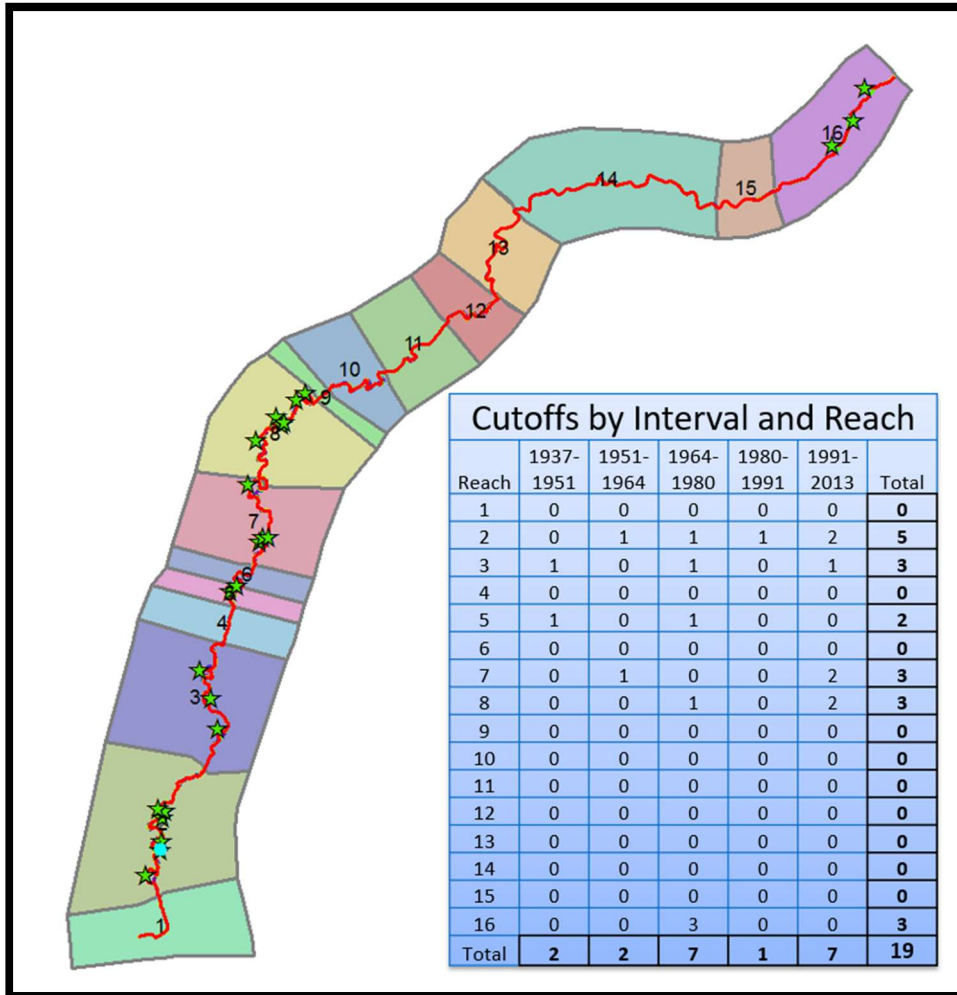
Figure 19. Stars denote cutoff locations. The embedded table shows the cutoffs by reach and by interval.

3.2. Channel Width Change

When viewing the data for channel width for the lower Minnesota River at a large scale (Figure 20) two trends were evident. Temporally, overall channel width increased from 1937-2013 (Figure 21). Spatially, the increase in channel width observed in the upstream was greatest with a gradual decrease moving in the downstream direction (Figure 21). Appendix J shows each period (1937-2013) in separate graphs. Beyond

these general trends, not much else can be seen in the data at this scale. However, reach analysis revealed more spatial and temporal trends with considerations given too:

Average channel width (ACW) for each reach in each period
The overall ACW for each reach (1937-2013)
The overall ACW for each period for the whole river (Reach 1-16)
The maximum channel width (MaxCW) measurement for each reach in each period
The MaxCW measurement for each reach
The MaxCW for each period for the whole river (Reach 1-16)
The minimum channel width (MinCW) measurement for each reach in each period
The MinCW measurement for each reach
The MinCW for each period for the whole river (Reach 1-16)
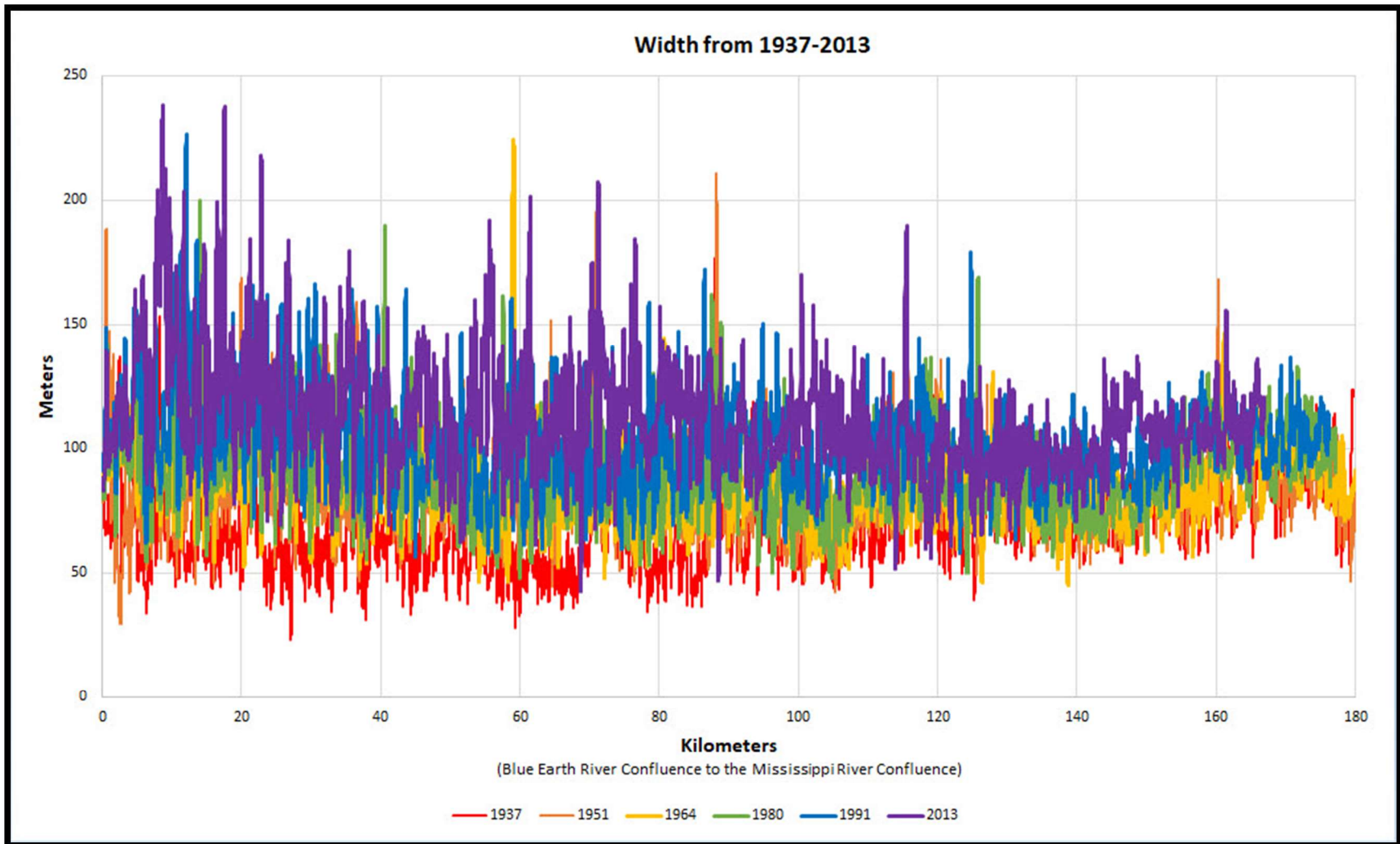
Figure 20. Graphical results for width measurements for all years related to downstream distance from the Blue Earth River confluence to the Mississippi River.
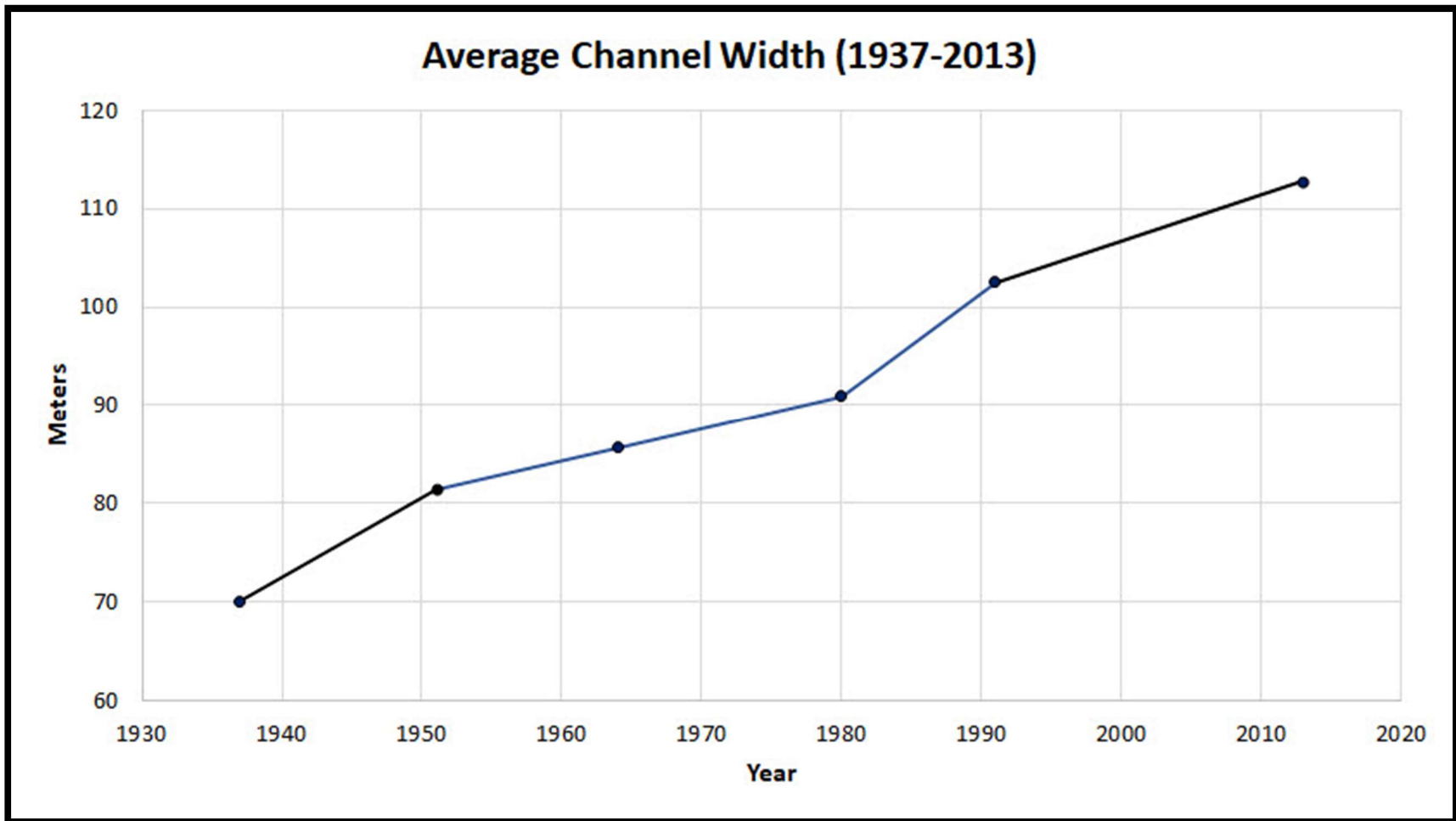
Figure 21. Graphical results for channel width change for all years. Throughout the time of record in this study a clear increase is seen.

3.2.1. Average Channel Width (ACW)

Reach 2-9 and 11 in 1937 contained all the ACW measurements below the 10th percentile with Reach 6 being the lowest at 53.94 m, while the 2013 period contained all but one (Reach 2 in 1991) of the measurements above the 90th percentile with Reach 2 being the highest at 139.05 m (

Table **3**, Figure 22). Reach 2 also had the highest overall ACW of any of the reaches at 100.19 m, and Reach 6 had the lowest overall ACW at 77.21 m (

Table **3**, Figure 22). An incremental increase in ACW of ~ 5-10 m was seen in each successive interval from 1937-2013. Reach analysis further demonstrated both the temporal increase in ACW, but also a spatial/temporal shift from channel width being greater in the downstream reaches to channel width being greater in the upstream reaches (

Table **3**, Figure 22).

Table 3. Average Channel Width by Reach and Interval

Average Channel Width by Reach and Interval (m/yr)						
Reach	1937	1951	1964	1980	1991	2013	Average
1	72.66	79.91	98.87	99.87	114.90	118.74	97.49
2	65.48	87.20	94.63	99.17	115.58	139.05	100.19
3	62.03	81.92	86.92	95.17	109.72	117.67	92.24
4	65.32	77.21	79.05	85.26	92.41	103.68	83.82
5	58.42	89.17	87.51	80.88	100.98	123.90	90.14
6	53.94	71.01	80.60	74.17	86.84	96.69	77.21
7	60.00	84.20	86.13	88.71	98.82	122.45	90.05
8	66.50	79.83	82.13	90.80	97.98	117.31	89.09
9	62.35	67.10	80.64	84.67	95.48	99.26	81.59
10	69.79	78.45	81.82	88.14	105.90	116.47	90.10
11	65.37	70.87	75.70	76.15	92.39	101.92	80.40
12	76.06	87.86	85.09	91.77	102.20	114.93	92.99
13	73.30	82.69	82.91	92.44	100.63	100.79	88.79
14	76.21	77.18	78.56	80.73	93.55	96.37	83.77
15	82.26	86.37	90.00	104.96	109.72	113.75	97.85
16	86.93	84.51	92.06	99.61	104.94	109.33	96.23
Average	70.05	81.45	85.65	90.89	102.54	112.84	89.50

10th Percentile		Quartile 1	Quartile 2		Quartile 3	90th Percentile	
66.92		78.68	87.36		99.81	114.91	

<66.92	>66.92 & <78.68	>78.68 & <87.36	>87.36 & <99.81	>99.81 & <114.91	>114.91

Figure 22. Graphical results for average channel width for all years grouped by river reach. Reach 1 begins at the Blue Earth River confluence and Reach 16 ends at the Mississippi River confluence.

3.2.2. Maximum Channel Width (MaxCW)

The greatest (>90th percentile) MaxCW measurements were relatively evenly distributed temporally (two in 1951, two in 1964, one in 1980, one in 1991, and three in 2013), yet were concentrated within Reaches 2 and 6-8. The highest recorded width measurement was 238.03 m for Reach 2 in 2013 (

Table **4**). The smallest (<10th percentile) MaxCW measurements were concentrated both temporally in the earlier time periods (four in 1937, three in 1951, one in 1964, and one in 1980) and spatially in Reaches 4-6, 9, and 11 (

Table **4**). All six of the MaxCW measurements in Reach 2 were above the median of which five were greater than the 75th percentile and three of those above the 90th percentile (

Table **4**). Whereas, all six of the MaxCW measurements in Reach 9 were below the 25th percentile of which four were in the bottom 10th percentile (

Table **4**).

Table 4. Maximum Channel Width by Reach and Interval

Maximum Channel Width by Reach and Interval (m/yr)							
Reach	1937	1951	1964	1980	1991	2013	Average
1	136.85	188.44	134.18	145.63	163.10	169.75	156.32
2	153.42	185.94	164.37	200.09	226.61	238.03	194.75
3	94.56	159.49	152.21	189.83	166.64	183.92	157.78
4	89.36	91.17	93.69	118.76	115.28	132.63	106.82
5	79.09	128.91	109.34	115.15	146.81	149.23	121.42
6	77.37	104.38	213.13	147.32	127.70	146.08	136.00
7	135.29	197.62	224.27	161.43	160.38	201.33	180.05
8	176.83	210.69	144.37	162.41	172.12	207.25	178.94
9	83.38	80.88	89.48	93.62	103.12	109.21	93.28
10	118.98	124.00	115.75	128.04	150.72	157.26	132.46
11	95.54	89.17	95.35	96.23	116.42	144.02	106.12
12	134.55	140.72	112.98	119.34	137.87	169.90	135.89
13	121.62	135.82	131.04	168.94	179.31	190.10	154.47
14	106.59	107.69	106.22	112.46	121.92	133.16	114.67
15	125.52	168.37	146.90	130.19	130.61	137.24	139.80
16	123.82	105.47	117.11	132.76	136.71	156.01	128.65
Average	176.8349	210.6944	224.2744	200.0937	226.6119	238.03	139.84

10th Percentile		Quartile 1		Quartile 2		Quartile 3	90th Percentile
93.67		113.52		134.92		162.93	192.35

<93.67	>93.67 & <113.52	>113.52 & <134.92	>134.92 & <162.93	>162.93 & <192.35	>192.35

119

3.2.2. Minimum Channel Width (MinCW)

The greatest (>90th percentile) MinCW measurements were concentrated in 1980 (one measurement), 1991 (5), and 2013 (4) and distributed among Reach 1, 5, 9, 12, 15, 16 (

Table **5**). The smallest (<10th percentile) MinCW measurements were concentrated temporally in Reach 1-8 in 1937 and Reach 1 in 1951. The lowest recorded width measurement was 23.66 m for Reach 2 in 1937 (

Table **5**). Although it is no surprise the smallest MinCW measurements are found in 1937 and 1951 and the highest MinCW measurements are found 1980, 1991, and 2013, it is interesting to see an inversion from the from the lowest falling in Reach 1-8 and the highest being concentrated downstream (Reach 9,12, 15,16) (

Table **5**).

Table 5. Minimum Channel Width by Reach and Interval

Minimum Channel Width by Reach and Interval (m/yr)							
Reach	1937	1951	1964	1980	1991	2013	Average
1	34.13	30.04	57.71	55.41	61.97	83.44	53.78
2	23.66	45.97	52.74	54.46	63.15	74.05	52.34
3	31.64	47.15	51.94	55.73	56.87	64.84	51.36
4	39.47	62.59	62.12	59.72	60.80	69.48	59.03
5	38.01	60.64	46.77	59.25	77.52	87.17	61.56
6	35.61	53.02	46.92	52.54	58.64	62.64	51.56
7	28.25	44.91	48.05	48.38	58.38	61.72	48.28
8	34.54	47.15	52.97	53.40	60.11	42.80	48.50
9	46.67	53.91	68.30	75.88	85.96	87.65	69.73
10	41.84	47.20	53.42	50.35	62.81	47.45	50.51
11	43.52	42.80	51.90	48.39	69.75	76.08	55.41
12	44.42	63.95	55.38	66.44	77.55	73.29	63.50
13	39.51	49.74	46.18	50.37	58.40	52.18	49.40
14	54.11	52.17	45.10	56.66	63.85	56.41	54.72
15	56.22	58.40	56.99	83.24	86.82	81.97	70.61
16	52.85	46.84	70.97	76.86	86.81	77.27	68.60
	23.66	30.04	45.10	48.38	56.87	42.80	56.81

10th Percentile		Quartile 1		Quartile 2		Quartile 3		90th Percentile	
39.50		47.15		55.39		63.67		77.53	

<39.50	>39.50 & <47.15	>47.15 & <55.39	> 55.39 & <63.67	>63.67 & <77.53	>77.53

3.3. Sinuosity and Channel Length

An overall decrease in sinuosity and stream length has been seen from 1937 to 2013 (Figure 23, Figure 24, Table 6). From 1937 to 1964 stream length slightly increased (< 2 kilometers) but then decreased drastically from 1964 to 2013 losing ~14 kilometers (9 kilometers from 1991 to 2013; Figure 24). However, reach analysis shows that this significant decrease in overall stream length is not occurring in all locations. Reach 5, 10, 11, and 12 are exceptions experiencing an increase in sinuosity from 1937 to 2013, and Reach 1, 4, 9, 13, 14, 15 have remained completely or almost completely static (Figure 23, Table 6). Therefore, the majority of stream length/sinuosity decrease has been concentrated in Reach 2, 3, 6, 7, 8, and 16 (Figure 23, Figure 24, Table 6)
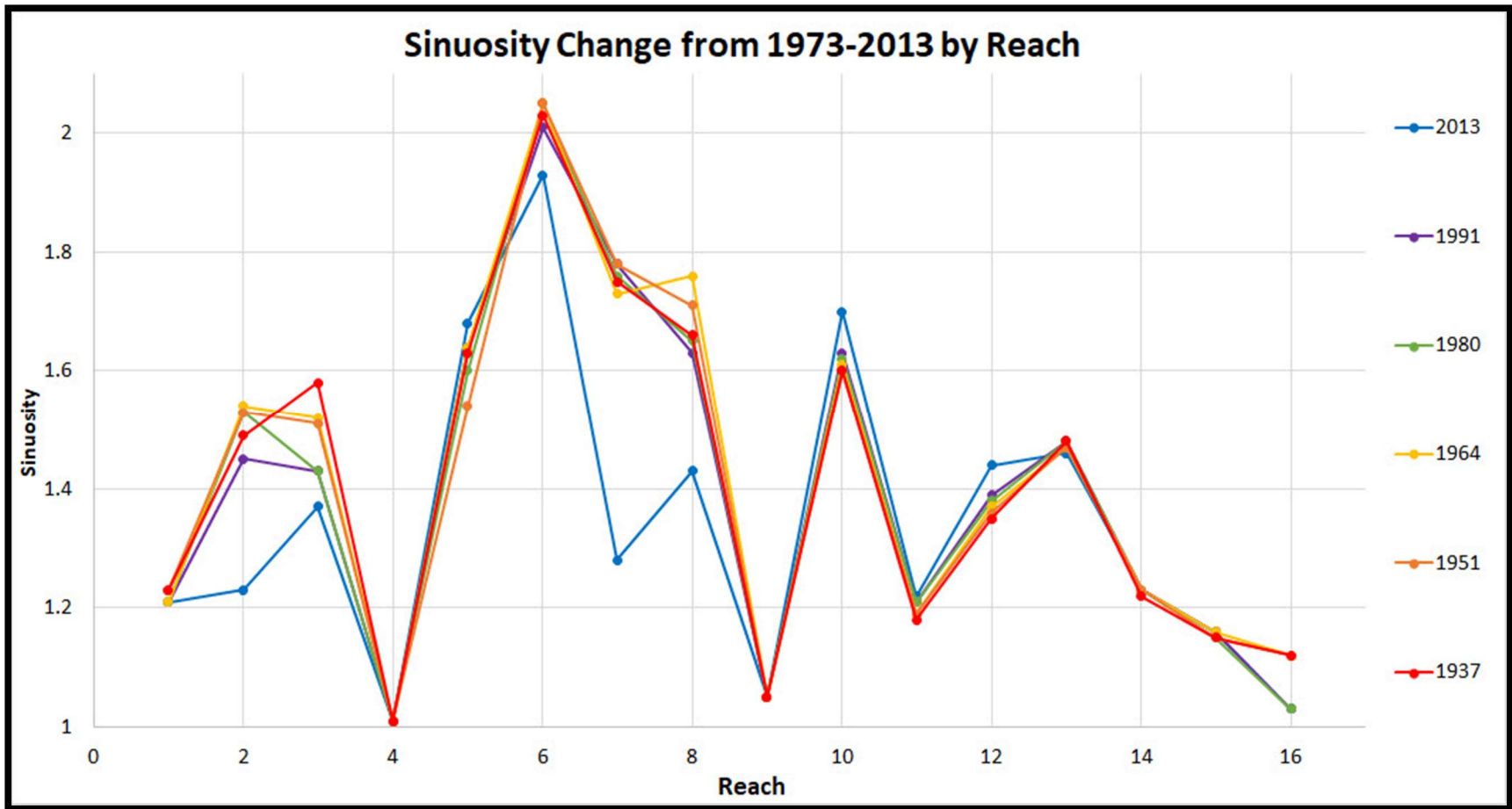
Figure 23. Sinuosity by river reach. Reach 1 begins at the Blue Earth River confluence and Reach 16 ends at the Mississippi River confluence.
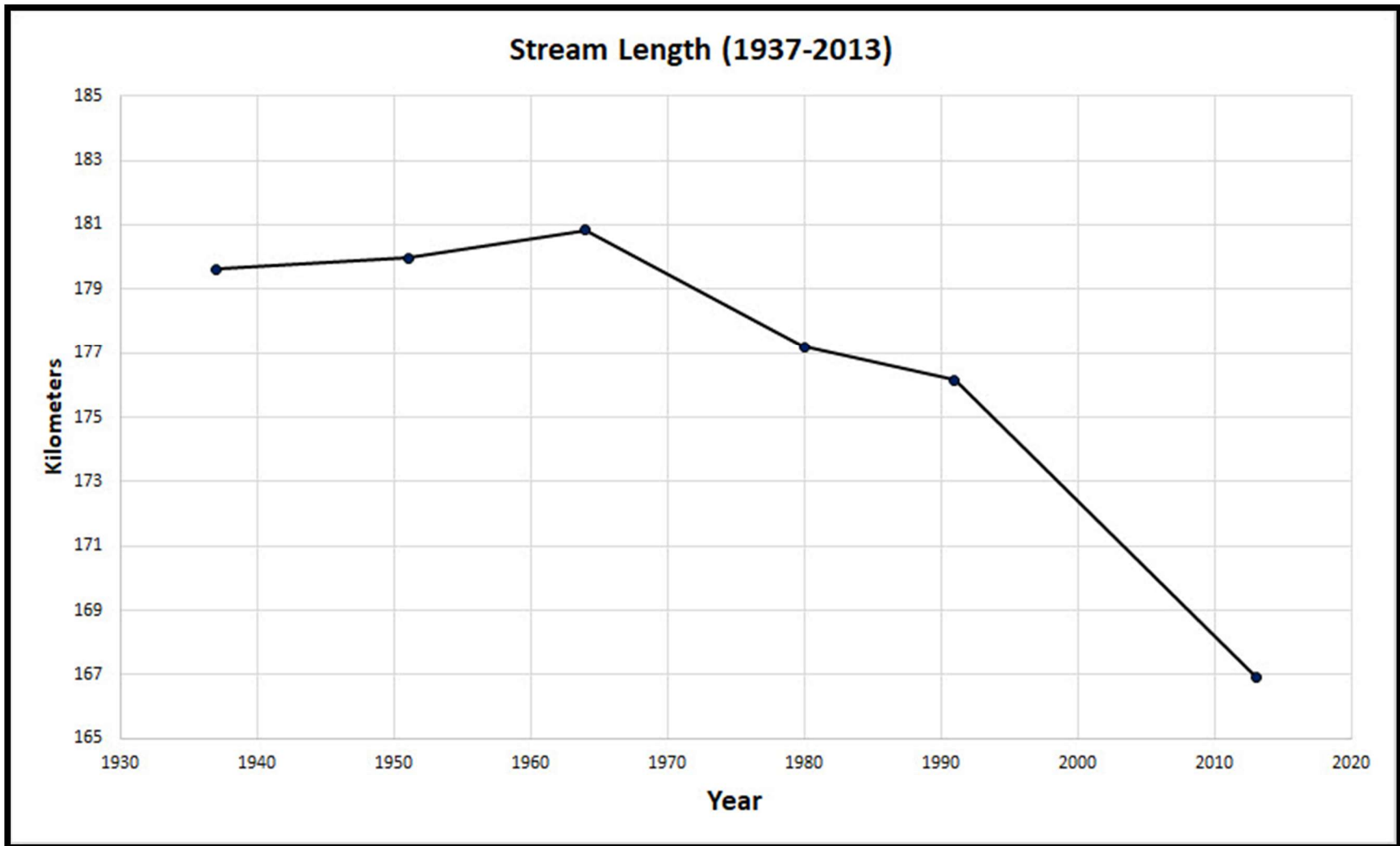
Figure 24. Stream length from 1937 to 2013. For the record of time, a significant decline in stream length has been seen.

Table 6. Sinuosity by Reach and Interval

Sinuosity by Reach and Interval (m/yr)						
Reach	1937	1951	1964	1980	1991	2013
1	1.23	1.23	1.21	1.21	1.21	1.21
2	1.49	1.53	1.54	1.53	1.45	1.23
3	1.58	1.51	1.52	1.43	1.43	1.37
4	1.01	1.01	1.01	1.01	1.01	1.01
5	1.63	1.54	1.64	1.60	1.64	1.68
6	2.03	2.05	2.05	2.05	2.01	1.93
7	1.75	1.78	1.73	1.76	1.78	1.28
8	1.66	1.71	1.76	1.65	1.63	1.43
9	1.05	1.05	1.05	1.05	1.05	1.05
10	1.60	1.60	1.61	1.62	1.63	1.70
11	1.18	1.19	1.19	1.21	1.21	1.22
12	1.35	1.36	1.37	1.38	1.39	1.44
13	1.48	1.47	1.47	1.48	1.48	1.46
14	1.22	1.23	1.23	1.23	1.23	1.23
15	1.15	1.15	1.16	1.15	1.16	1.16
16	1.12	1.12	1.12	1.03	1.03	1.03
10th Percentile		Quartile 1		Quartile 2	Quartile 3	90th Percentile
1.04		1.16		1.38	1.61	1.76
≤1.05	>1.04 & <1.16	>1.16 & <1.38	>1.38 & <1.61	>1.61 & <1.76		>1.76

3.4. Pinch Points and the Consideration of Invasive Carp Barriers

3.4.1. Mankato

Mankato's floodwall and riprap-controlled river stretch (Figure 25) has been a location of interest since it has large area of river that has been heavily engineered. The results show that since the Mankato flood walls were installed in the mid-1960's a significant decrease (~3 m/y) in channel migration occurred (Figure 26), which is uncharacteristic to other less controlled river reaches which show static or increases in migration (Figure 12). However, width did not immediately stabilize in this reach (Figure 27) and continued to rise in a manner characteristic with other river reaches (Figure 22), but recently (1991-2013) has seen its first, although minor, decrease in channel width.

Figure 25. Mankato's floodwall and riprap-controlled river stretch.
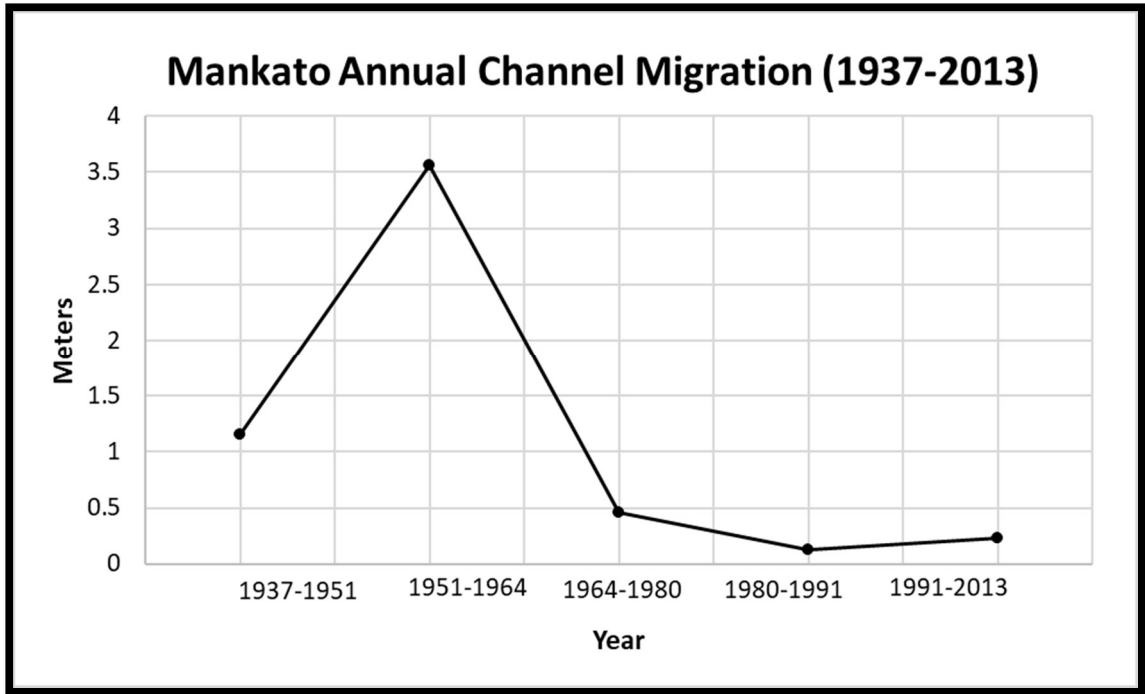
Figure 26. Average annual channel migration in Mankato's floodwall and riprap controlled river stretch.
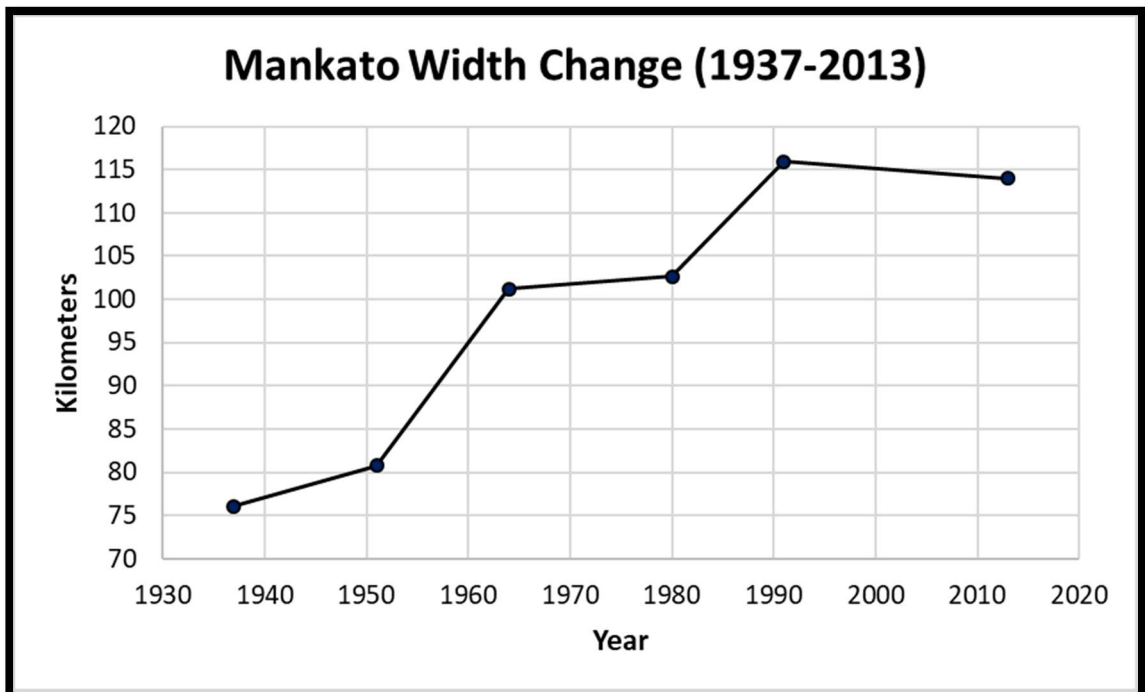
Figure 27. Width change in Mankato's floodwall and riprap-controlled river stretch.

3.4.1. Highway 14 Bridge (Mankato)

The highway 14 bridge (Figure 28) was built in 1976 which offered a location to see pre and post bridge planform characteristics. Channel migration was consistently greater downstream than upstream except for 1991-2013. It should be noted that the upstream did not change much compared to the prior interval (1980-1991), but rather the downstream became less active. Width flipped from downstream being greater to upstream being greater post-bridge occupation. The width on both sides of the bridge nearly tripled in size over the period of record (Table 7).
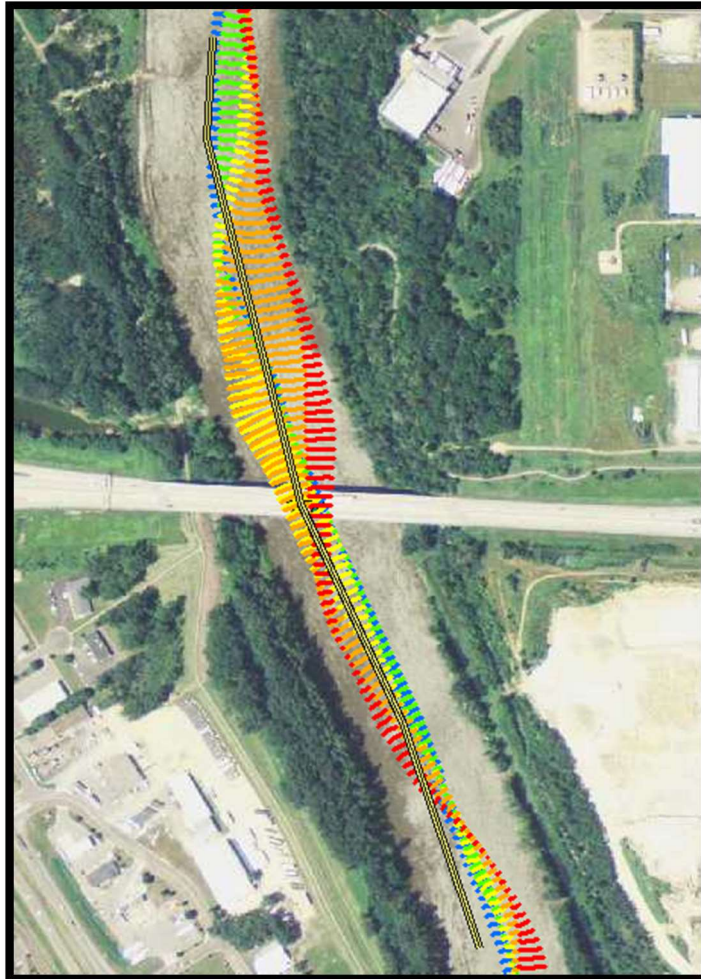
Figure 28. Highway 14 bridge on the edge of Mankato/North Mankato, MN.

Table 7. Highway 14 bridge upstream vs downstream migration and width change. The red box shows the years after the bridge was built. 1991-2013 was the only time upstream migration was greater than downstream. Width was traditionally greater downstream, but reversed after the bridge was built.

Migration (meters)	1937-1951	1951-1964	1964-1980	1980-1991	1991-2013			Average
Upstream	0.71	0.91	0.94	0.60	0.61			0.75
Downstream	0.90	3.42	1.23	1.13	0.22			1.38

Width	1937	1951	1964	1980	1991	2013	Average
Upstream	56.25	77.52	91.89	105.03	132.3	141.91	100.82
Downstream	60.99	78.73	96.99	92.99	126.14	154.43	101.71

3.4.2. Highway 22 Bridge (St. Peter)

The Highway 22 Bridge in St. Peter (Figure 29) is ~ 20 km downstream from the Highway 14 Bridge. This river crossing existed over the record of time considered in this study. The upstream portion migration has been on average five times greater than that of downstream measurements (Table 8). Interestingly, this pinch point also experienced a switch in width change being greater in the downstream to the upstream following 1964, like the Highway 14 Bridge. Therefore, this measurement indicates that Highway 14's switch in width change post-bridge construction may only be a correlation and not a cause of the structure's presence since this same switch was experienced from a bridge established over the entire time scale.
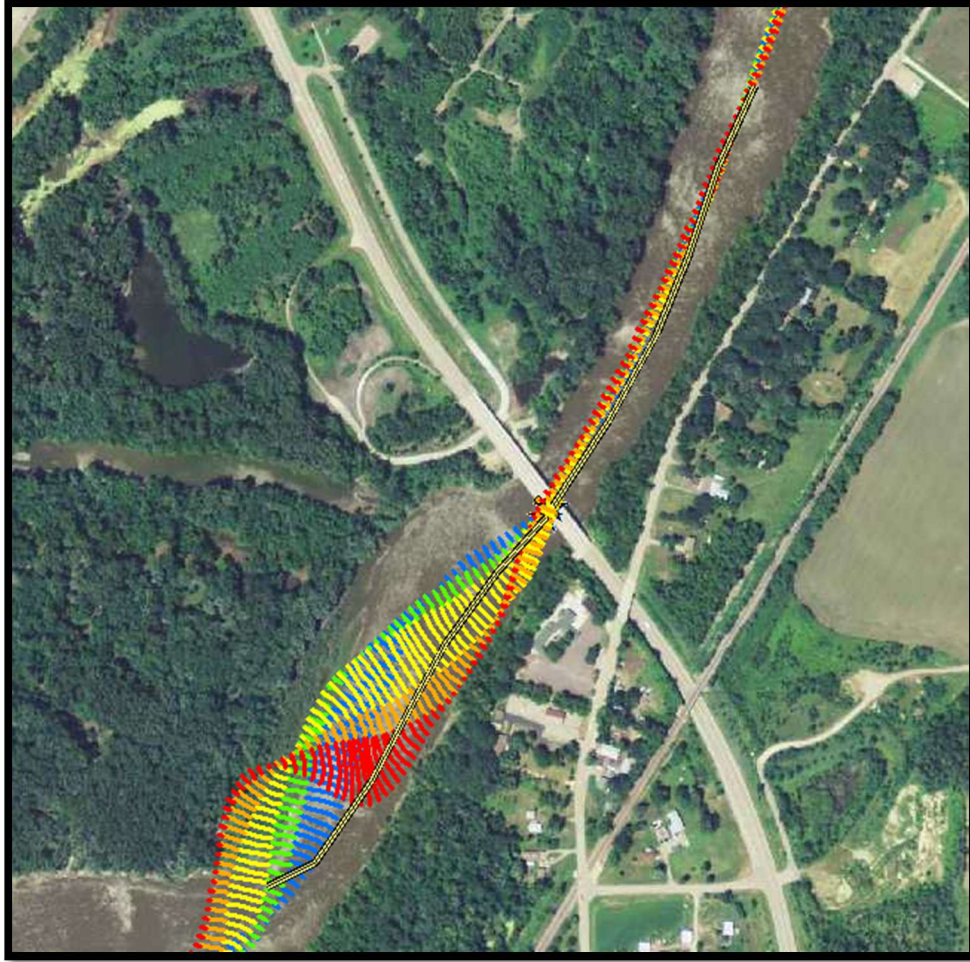
Figure 29. Highway 22 bridge on the edge of St. Peter, MN.

Table 8. Highway 22 bridge upstream vs downstream migration and width change. The red line in the migration measurements indicated the distinct break in a highly active upstream and inactive downstream. Width measurements switched from being greater downstream to upstream after the 1964 measurement.

	1937-1951	1951-1964	Migration (meters) 1964-1980	1980-1991	1991-2013			Average
Upstream	1.40	1.32	2.24	1.27	1.25			1.50
Downstream	0.44	0.31	0.46	0.24	0.08			0.31
	1937	1951	Width 1964	1980	1991	2013		Average
Upstream	40.91	84.36	85.43	107.31	122.23	119.60		93.31
Downstream	80.38	99.88	91.02	92.52	103.53	97.00		94.06

3.4.3. Highway 169 Bridge (Le Sueur)

The Highway 169 Bridge (Figure 30) near the city of Le Sueur, MN, has been fairly active in terms of migration with the most recent interval of time (1991-2013) being the least active both upstream and downstream of the bridge (

Table 9). Width change has shown unsteady trends in terms of upstream vs. downstream but overall has experienced an increase in channel width with the upstream increasing from 52.48 meters to 105.01 meters and the downstream increasing from 45.86 meters to 125.88 meters (

Table 9). However, 1964 had the greatest width of record with the upstream averaging 151.72 meters and the downstream averaging 163.75 meters (

Table 9).
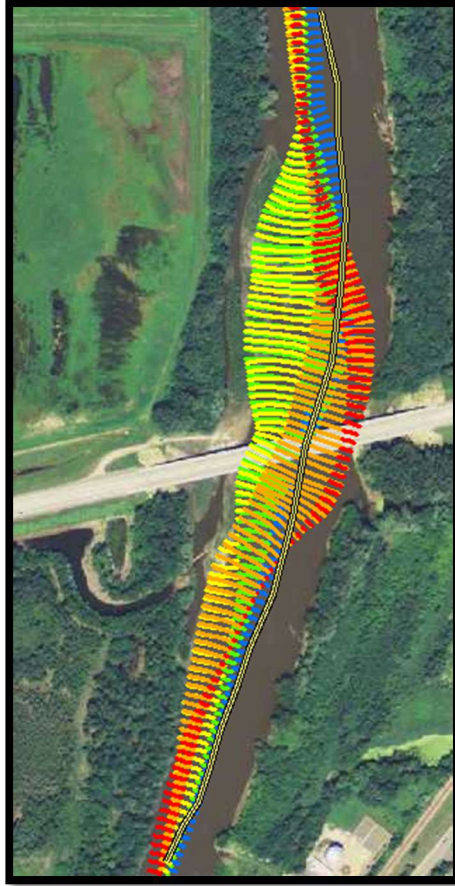
Figure 30. Highway 169 bridge on the edge of Le Sueur, MN.

Table 9. Highway 169 bridge upstream vs downstream migration and width change.

	Migration (meters)							
	1937-1951	1951-1964	1964-1980	1980-1991	1991-2013			Average
Upstream	0.68	3.16	1.65	1.36	0.40			1.45
Downstream	1.48	2.98	2.51	5.85	0.66			2.70
			Width					
	1937	1951	1964	1980	1991	2013		Average
Upstream	52.48	85.38	151.72	94.96	88.54	105.01		96.35
Downstream	45.86	83.28	163.75	95.52	81.80	125.88		99.35

3.4.4. Dan Patch Line Bridge (Savage)

The Dan Patch Line Bridge (Figure 31) offers a look at a pinch point where the Minnesota River is actively managed to maintain barge traffic (USACE 2007; Groten, Ellison, and Hendrickson 2016). This stretch has experienced relatively stable channel migration conditions with overall temporal decrease, and the most recent interval (1991-2013) marking the lowest migration rates both upstream and downstream of the bridge (Table 10). The width has been consistently greater in the downstream side of the bridge by ~5-17 meters. It should be noted that the downstream measurements are located on a meander bend (Figure 31) which likely introduce channel geometry effects on bank shear stress as well. The width has increased temporally with the upstream increasing by ~30 meters and the downstream by just under 40 meters (Table 10).

Figure 31. Dan Patch Line Bridge in Savage, MN.

Table 10. Dan Patch Line Bridge upstream vs downstream migration and width change.

	Migration (meters)							
	1937-1951	1951-1964	1964-1980	1980-1991	1991-2013			Average
Upstream	1.47	0.79	0.24	0.60	0.20			0.66
Downstream	0.92	0.53	0.48	0.95	0.19			0.61
			Width					
	1937	1951	1964	1980	1991	2013		Average
Upstream	69.39	72.85	72.01	93.16	101.92	100.29		84.94
Downstream	79.45	77.81	83.61	106.24	112.72	117.23		96.18

4. Discussion

4.1. Methodological Considerations

4.1.1. Trajectory Method vs Polygon Method

To accomplish the objectives of this research, a complete assessment of the appropriate methodologies in published literature was conducted. In that assessment a comparison between the two most commonly used methods, the Trajectory Method and the Polygon Method, was made. Consistency in quantifying channel change is important so comparative analysis among various studies can be easily made. If a uniform approach is adopted, the science of understanding planform channel adjustments will drastically improve since direct river to river comparisons can be made.

In the Polygon Method (Urban and Rhoads 2003; Giardino and Lee 2011), a series of polygons are created by two intersecting centerlines from different years. The area of each polygon is then divided by the length of the earlier year centerline to get a migration rate (Figure 32). The quotient is then divided by the number of years between the two centerlines to get an annual migration rate. The equation is as follows:

$$eq.\ Rm = \frac{A}{L}/y$$

where Rm is the migration rate, A is the area of the polygon, L is the length of the centerline length of the earlier years bordering the polygon, and y is the number of years between the channel centerlines used in the interval.

To test the Polygon Method, a model was built to automate this process in ArcMap (Figure 33). Figure 34 shows an example output of this methodology, and Figure 35 is the output from the methodology discussed previously from the NCED Planform Statistics toolbox (the method that was ultimately used in this study). Graphically, the two outputs look similar. However, upon closer analysis the polygon method underestimates the migration rates and drastically generalizes them. In this comparison, the polygon method created ~400 measurements while a 10 m interval was used with the Trajectory Method (NCED Planform) which produced ~17,500 measurements in Figure 35. The Polygon Method simply does not have enough measurements for the resolution required to do planform channel change analysis, especially on smaller reaches or pinch points like those done within this study (Figure 36). For these reasons, the polygon method is discouraged as a method of measuring channel migration. However, the framework for creating polygons (Figure 33) could be used and extended into studies focused sediment budgets and on quantifying erosion.
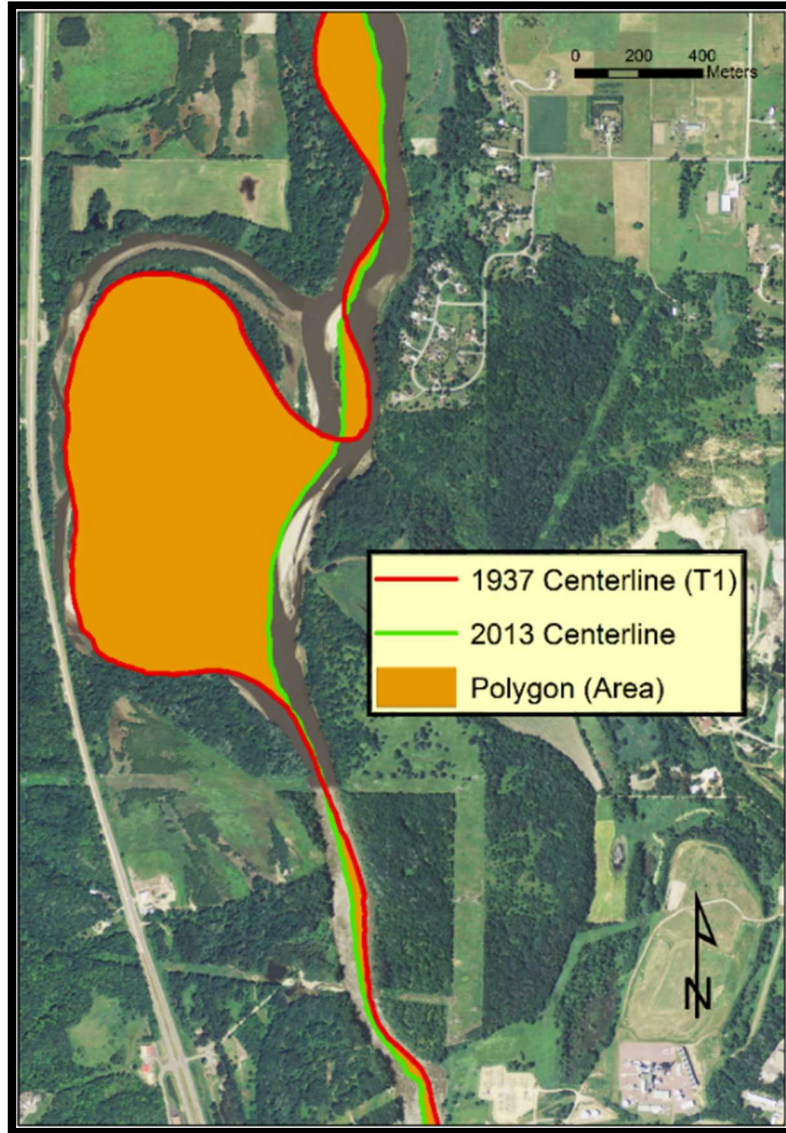
Figure 32. The required inputs to calculate migration using the Polygon Method
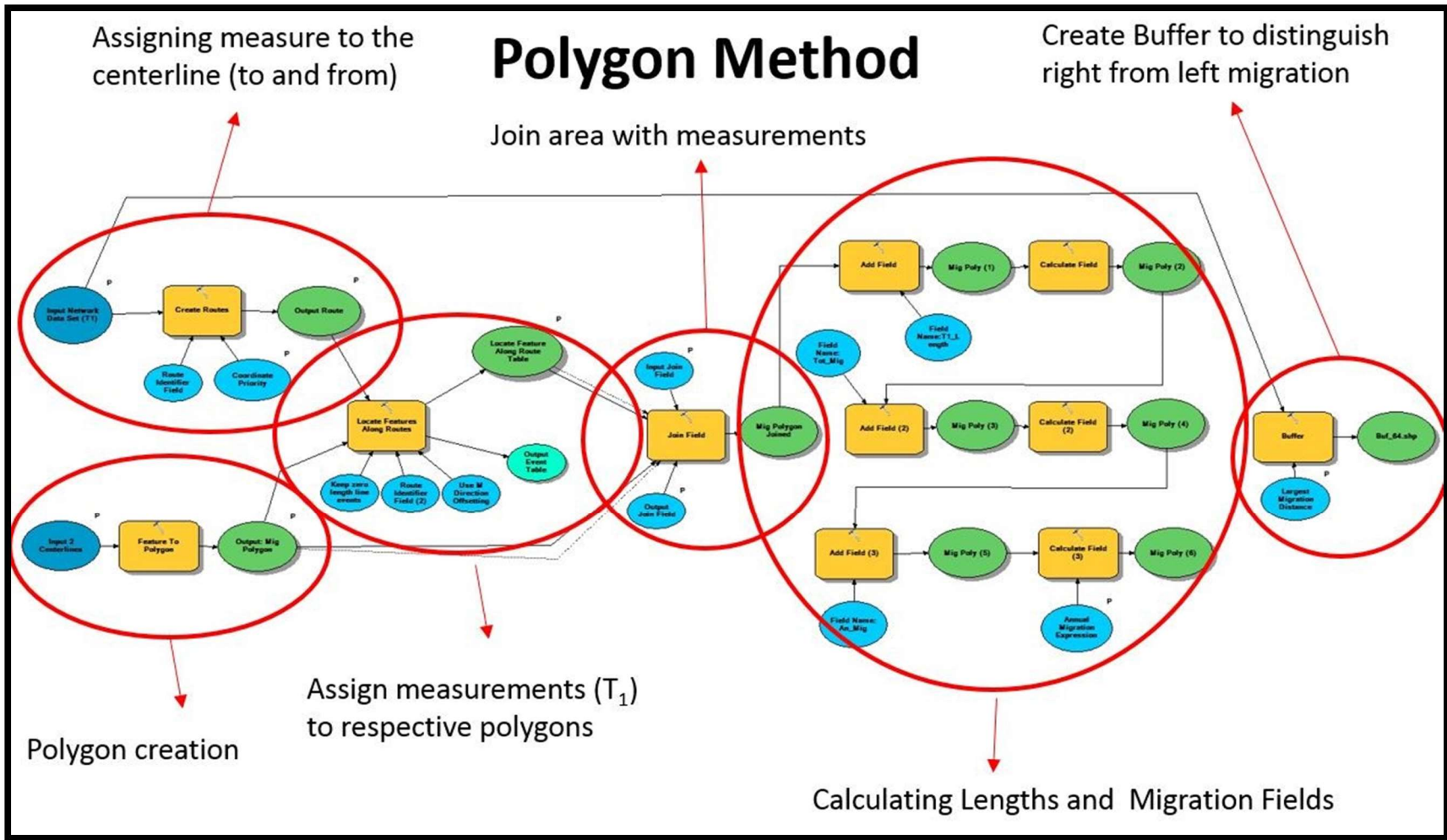
Figure 33. Polygon Method model
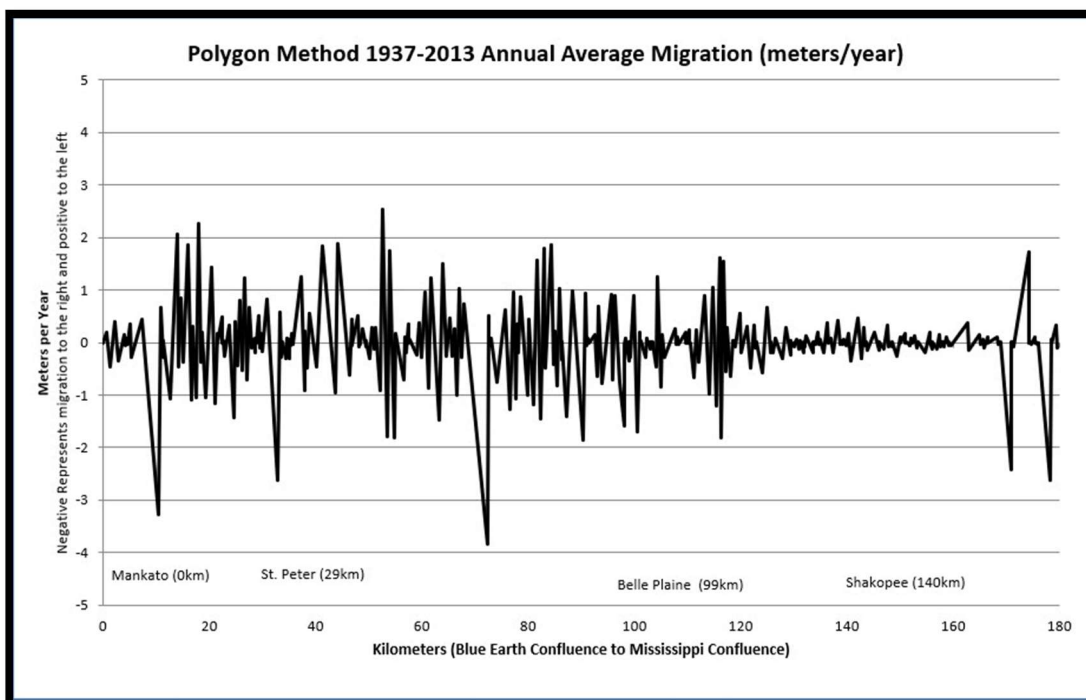
Figure 34. Output data from the Polygon Method
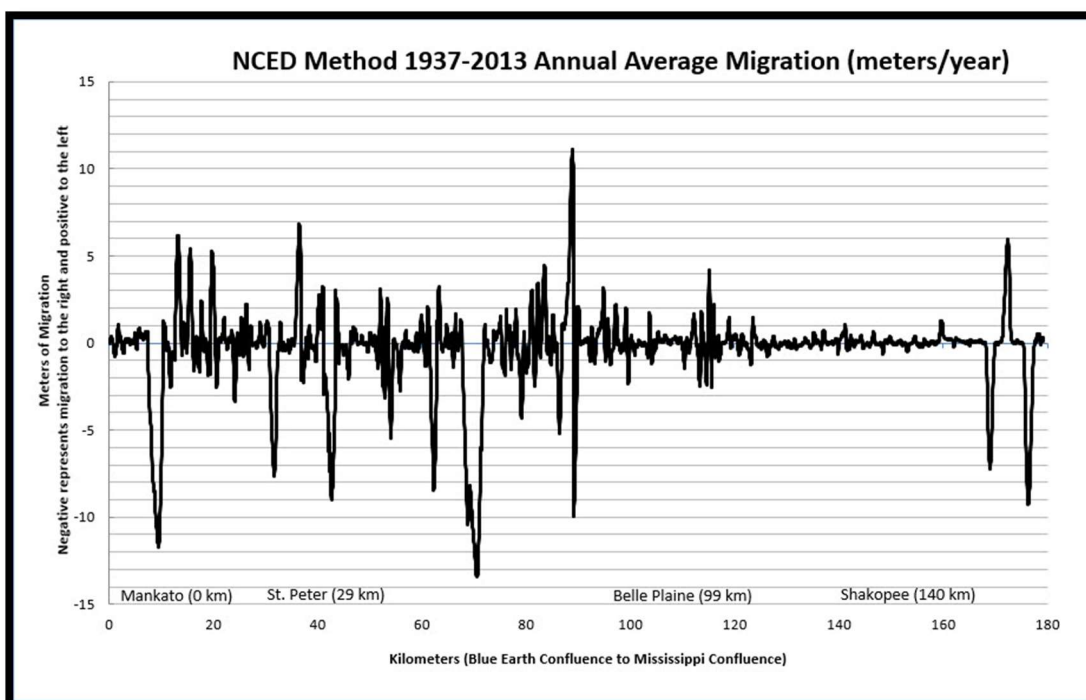
Figure 35. Output data from the NCED Planform Statistics Tools
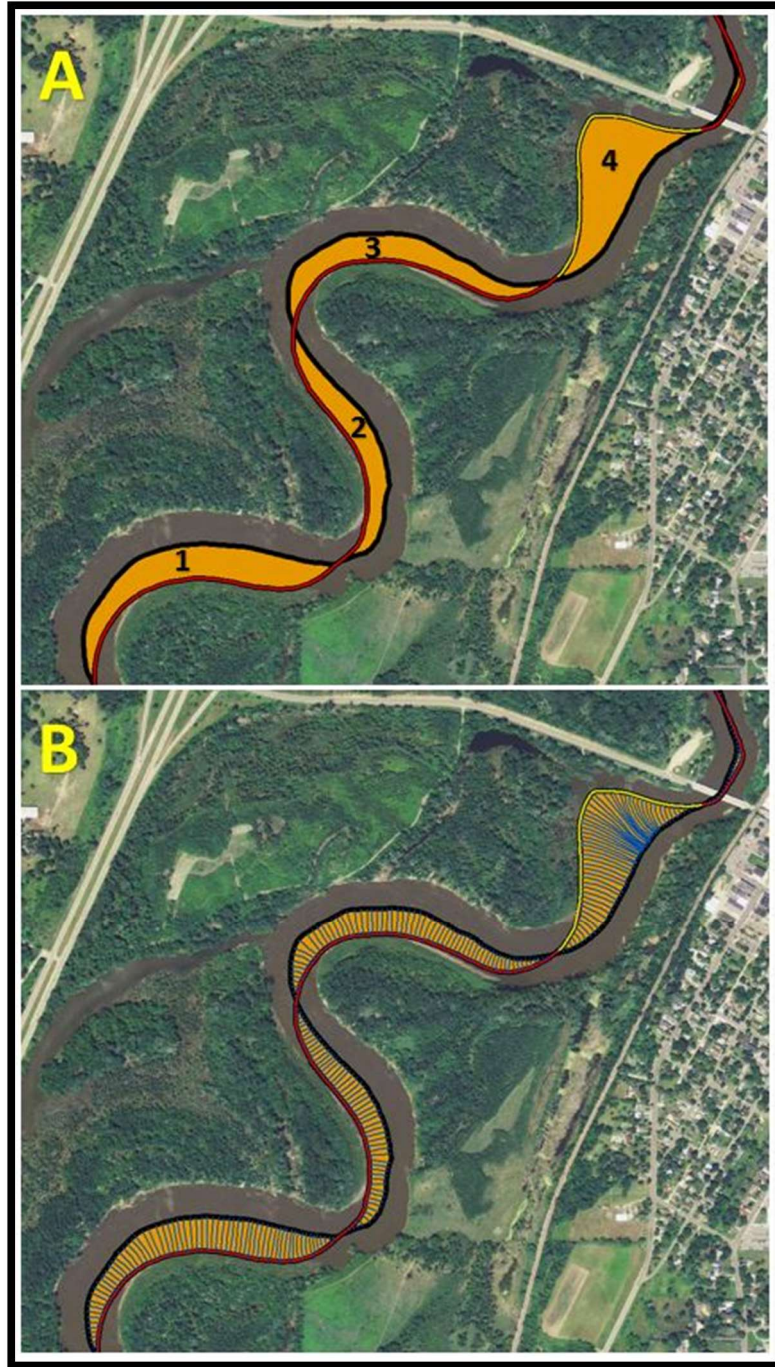
Figure 36. A) This figure displays the inputs needed in order to calculate channel migration using the polygon method. For each orange polygon (1-4), the red centerline (T1) length is used to divide the area of the polygon. Polygon has this measurement highlighted in yellow. This number is then divided by the number of years between the centerlines. In the example above, twenty-two would be used since the two input centerlines are 1991 (Red) and 2013 (Black). B) This shows an example of the trajectory lines (Blue lines) created using the planform statistics toolbox. The user defined intervals selected was ten meters therefore a new trajectory line or measurement is generated laterally between the centerlines for every 10 meters in the downstream distance.

4.1.2. Error Metrics

Lea and Legleiter's (2016) MATLAB scripts produce three error metrics: SVE, RMSE, and 90th Percentile. One of the ArcGIS tools created in this research (Figure 4 and Figure 5), specifically created separate excel and shapefile outputs (Figure 6) so a user can see study specific results for each metric. The outputs from this research were plotted spatially (Figure 37) and graphically (Figure 38) to compare differences. After comparison it is evident that the 90th percentile error metric considers measurements as statistically insignificant which are in fact real-world migration. On the other hand, RMSE likely considers too many measurements as statistically significant, since the overall RMSE measurements were so low in this study. As shown in Chapter 2 of Libby (2018), independent GCPs showed a much higher variability in error than RMSE shows. Therefore, RMSE is applying a generalized error value to an incredibly broad study area which contains localized areas that far exceed RMSE. SVE's ability to account for the spatial variability of the error makes it the most preferred error metric of the three.
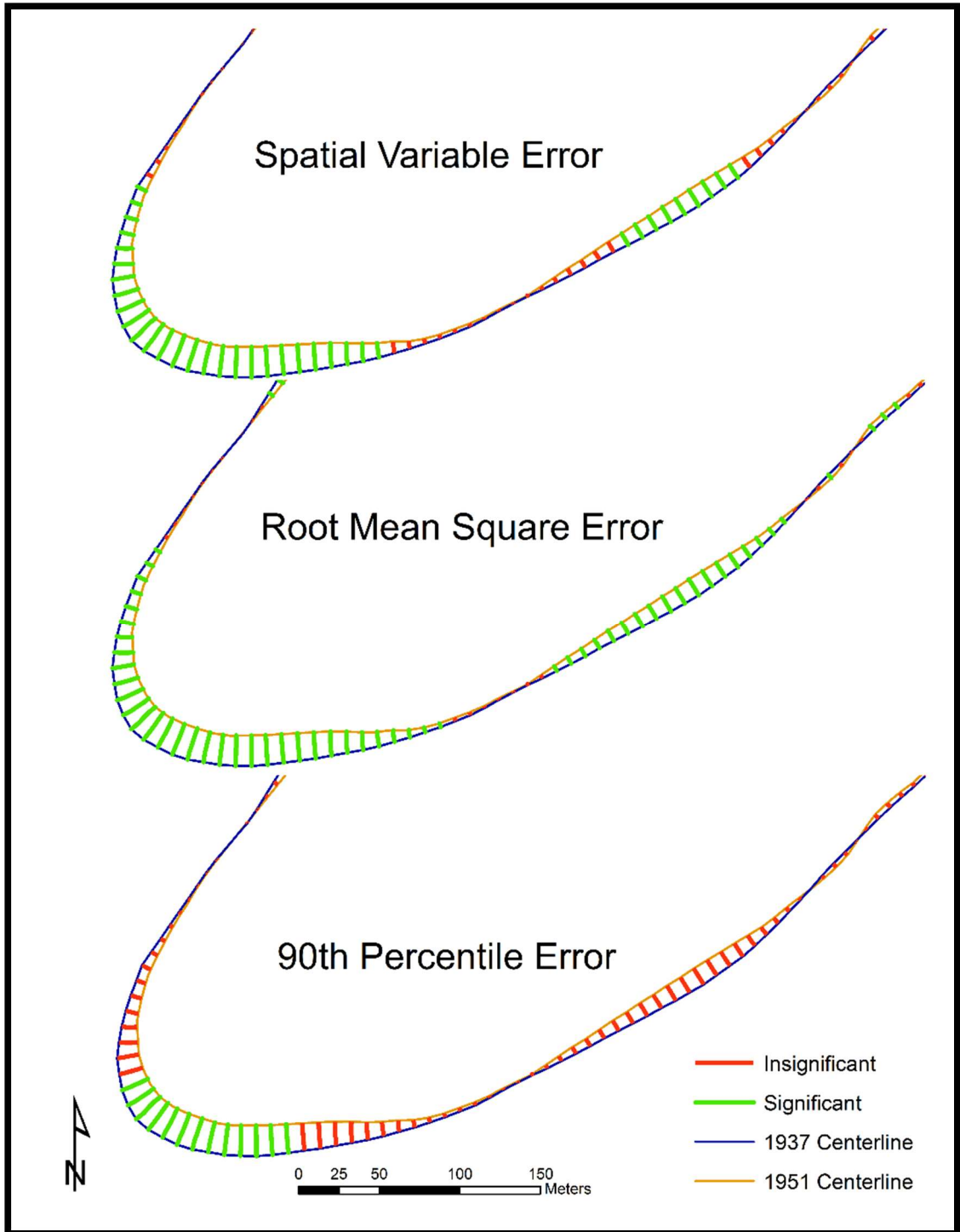
Figure 37. Spatial comparison of differing error metrics significant vs insignificant measurements.
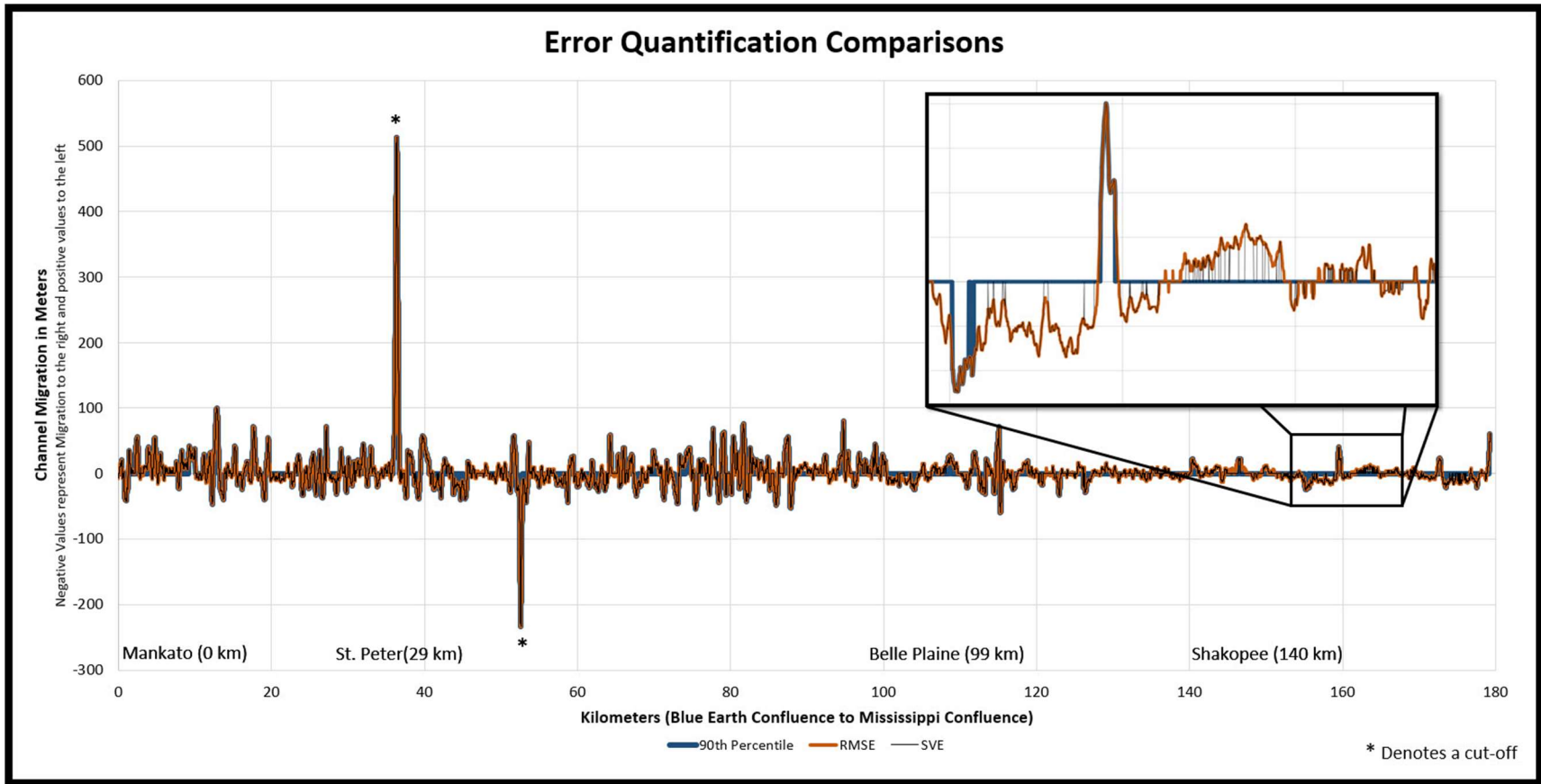
Figure 38. Graphical comparison of differing error metrics significant vs insignificant measurements.

4.1.3. Problems Overcome

The following two sections outline a few methodological problems that were overcome throughout the analysis of the research. First, an error issue running the MATLAB script "ChannelChangeSignif" will be discussed followed the considerations for handling errored trajectory lines output from the NCED Planform Statistics toolbox.

4.1.3.1. MATLAB "ChannelChangeSignif"

When running the "ChannelChangeSignif" script the scattered interpolant function raised the following exception – "The number of data point locations should equal the number of data point values." This was corrected by going back to the "ErrorQuantification" MATLAB script and tracing the root of the problem back to the original GCP text file. The issue originated from an extra blank entry at the end of the shapefiles from which they were derived creating an extra or "unequal" amount of lines in the GCP text file. Once these blank lines were deleted the data point location and data point values were equal in the matrices created in MATLAB which corrected this problem.

4.1.3.2. Errored Trajectory File Lines

The issues with errored trajectory lines which are used for measuring lateral migration (Figure 2) caused several issues throughout this research. At first, a method of using the clip function within ArcMap was formulated to automate cleaning up errored lines by using the centerlines as a bound since all migration should be contained within the two centerlines for each interval. This seemed to work well at first, however; it was unsuccessful because it would leave an extra vertex associated with the line. This gave the clipped lines three endpoints opposed to two which caused issues when trying to extract the XY coordinates to use the in the MATLAB "ChannelChangeSignf" script. Instead of the two sets of coordinates a third XY set was added for the extra vertex. For this reason, this methodology was abandoned, and all the trajectory lines were manually checked and edited.

In some cases (especially on cutoffs), hundreds of trajectory lines would be incorrect. In this case it was easiest to delete these lines all together and digitize new lines for the trajectory measurements. This, however, created a new set of problems for the "Post MATLAB Processing" script that was written for this research. Part of this scripts job was too recalculate the trajectory lines measurements and then assign new downstream distances to each line measurement since they were manually edited and had no attributes associated with them. When the new shapefiles came out of the script, it was obvious the downstream distances were far from accurate, so the script was run a single line at a time until the error was identified. When the following lines of code were run the problem became evident.

 # Feature To Point - This take the center of ever line in the trajectory file and creates a point
arcpy.FeatureToPoint_management(TrjLF, F2Point, "CENTROID")

 # Points To Line - This takes the points generated in the last tool and creates a line from them
arcpy.PointsToLine_management(F2Point, P2Line, "", "", "NO_CLOSE")

.# Create Routes - This takes the line created in the last tool and converts it to a route in order to give it measure
arcpy.CreateRoutes_lr(P2Line, "Id", Route, "LENGTH", "", "", CoorPriority, "1", "0", "NO_IGNORE", "INDEX")

 # Locate Features Along Routes - This takes the points that were created and assigns them downstream measure which will inturn give the
 # trajectory lines measure in the next step
arcpy.LocateFeaturesAlongRoutes_lr(F2Point, Route, "Id", "1 Meters", LFAR, OETP, "FIRST", "NO_DISTANCE", "ZERO", "FIELDS", "M_DIRECTON")
 # Join Field - This steps permanently joins the downstream measurements from the point file to the corresponding trajectory line
arcpy.JoinField_management(TrjLF, PKey, LFAR, "ORIG_FID", "MEAS")

The output line in the "Point to Line" function was created so measurements for downstream distances could be calculated. However, this line skipped around according to the trajectory lines object ids from which the line was derived in the prior function, "Feature to Point" (Figure 39). The trajectory lines object ids were not in order since many were manually created in the editing process to fix errored trajectory lines originally output form the NCED "Lateral Migration" tool. To overcome this problem the script was edited to the following.

 # Intersect Analysis - This creates points at the intersection of the TRJ polyline file and the T1 centerline
arcpy.Intersect_analysis([T1, TrjLF], IntPoint, "ALL", "0.1 Meters", "POINT")

 # Create Routes - This takes the line created in the last tool and converts it to a route in order to give it measure
arcpy.CreateRoutes_lr(T1, "Id", Route, "LENGTH", "", "", CoorPriority, "1", "0", "NO_IGNORE", "INDEX")

 # Locate Features Along Routes - This takes the points that were created and assigns them downstream measure which will inturn give the
 # trajectory lines measure in the next step
arcpy.LocateFeaturesAlongRoutes_lr(IntPoint, Route, "Id", "1 Meters", LFAR, OETP, "FIRST", "NO_DISTANCE", "ZERO", "FIELDS", "M_DIRECTON")

 # Wildcard is needed in order to automate selection of the foreign key since it inserts the shapefiles name and could vary among users
fid_year = arcpy.ListFields(LFAR, "FID_*_1")[0].name
 # Join Field - This steps permanently joins the downstream measurements from the point file to the corresponding trajectory line
arcpy.JoinField_management(TrjLF, PKey, LFAR, fid_year, "MEAS")

      This required the extra user inputs of a centerline from the earlier time in the interval considered and the "coordinate priority" so it the script could know the proper direction for accumulating distance. By doing this, the tool can be used on any river no matter which direction it flows.
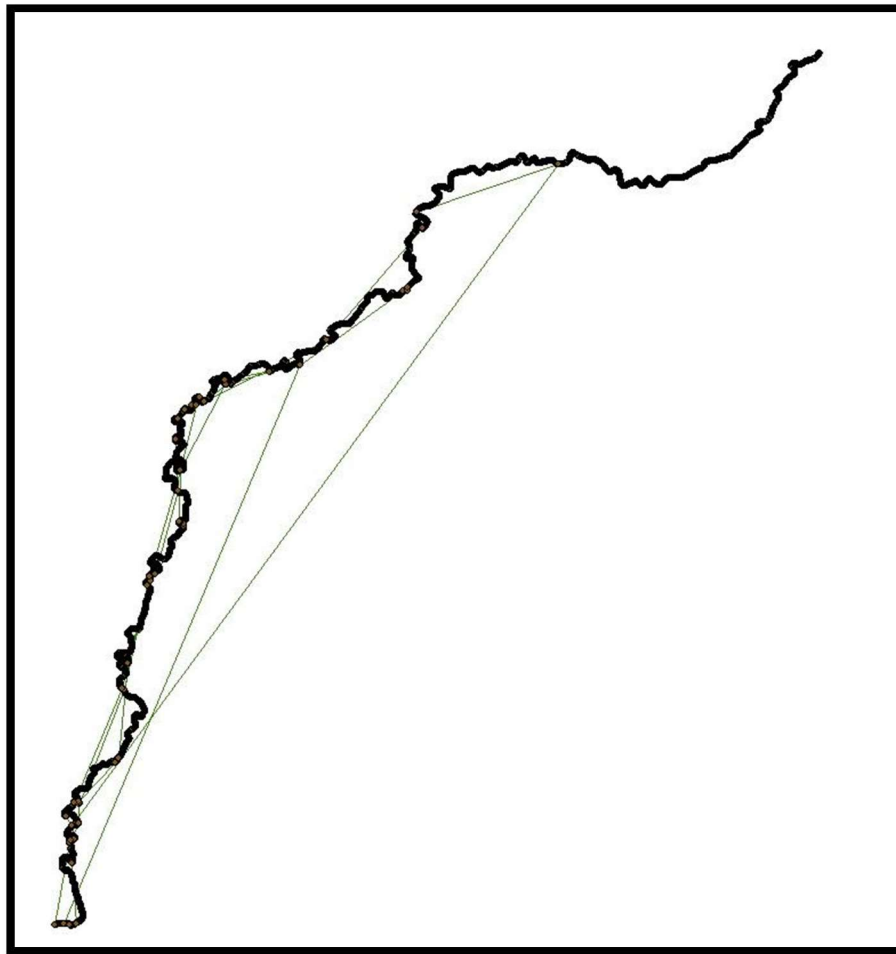
Figure 39. This shows the line created by the script from which downstream distances were being calculated. It was not immediately evident that this was the problem since this file was an intermediary file that was created and then deleted before the script terminated. The line was created according to the object id field for the points which caused a problem since many new lines were added to the original file to correct errored trajectory lines.

4.2. Planform Channel Change

As expected, the changing hydrologic and sediment regimes in the MRB has created changing planform characteristics on the Minnesota River (Lenhart et al. 2013; Lauer et al. 2017). The two most notable trends include an overall increase in channel width and decreased channel length/sinuosity. Channel migration has shown change, but not as pervasively as the other two planform characteristics. Since this study was conducted on a large stretch of river it was essential to break the data into reaches to see if the generalized trends for the entire study reach were uniform throughout, or if localized temporal and spatial differences could be observed (Figure 40 and Figure 41). Although the attention in this section will be on general spatial and temporal trends and the most and least dynamic reaches of the river,

Appendix K contains an aerial view and graphs for annual channel migration, channel width, sinuosity for every reach investigated in this study.
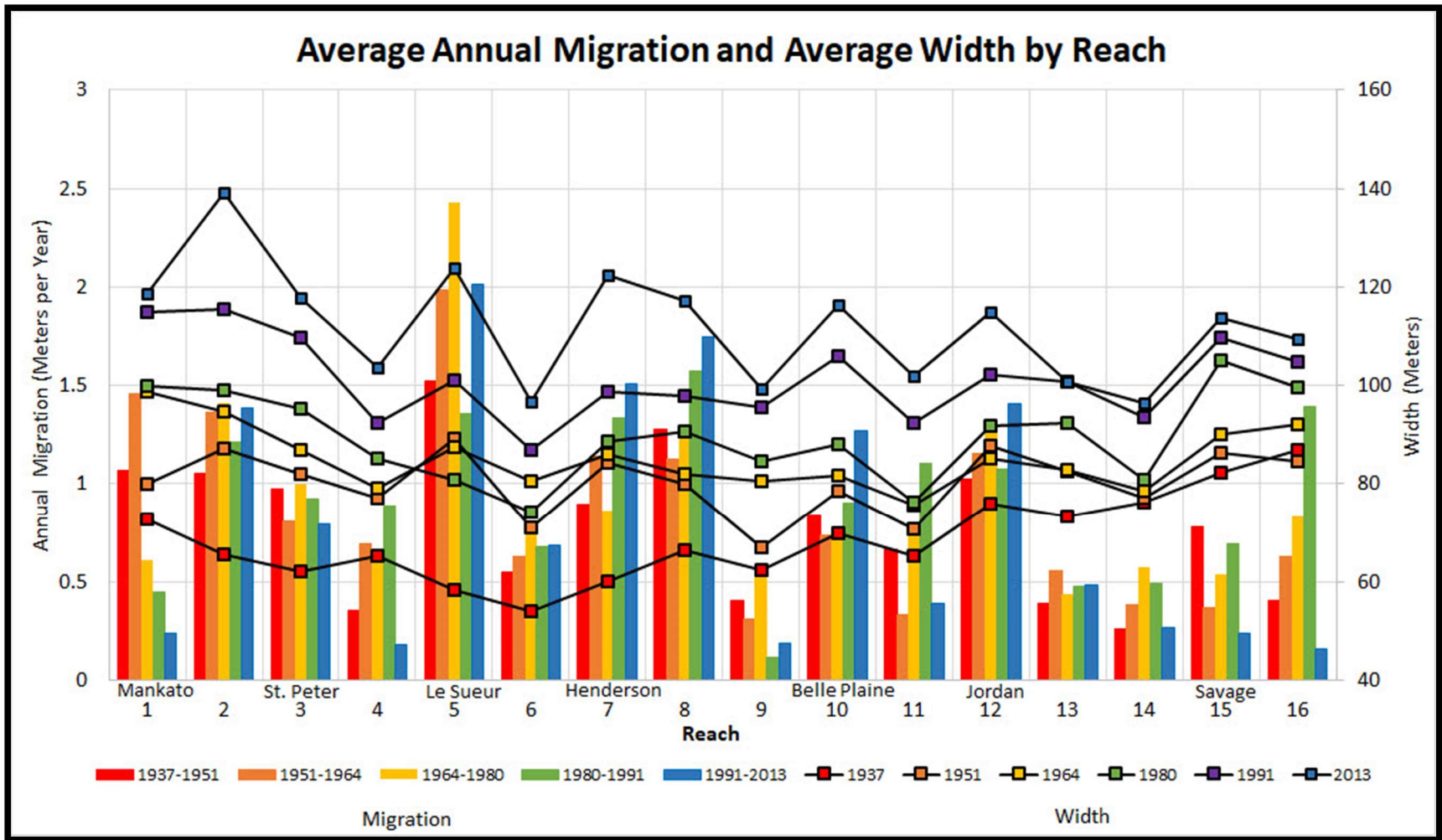
Figure 40. Annual migration and width of the lower Minnesota River channel through the delineated Reaches (Figure 9).
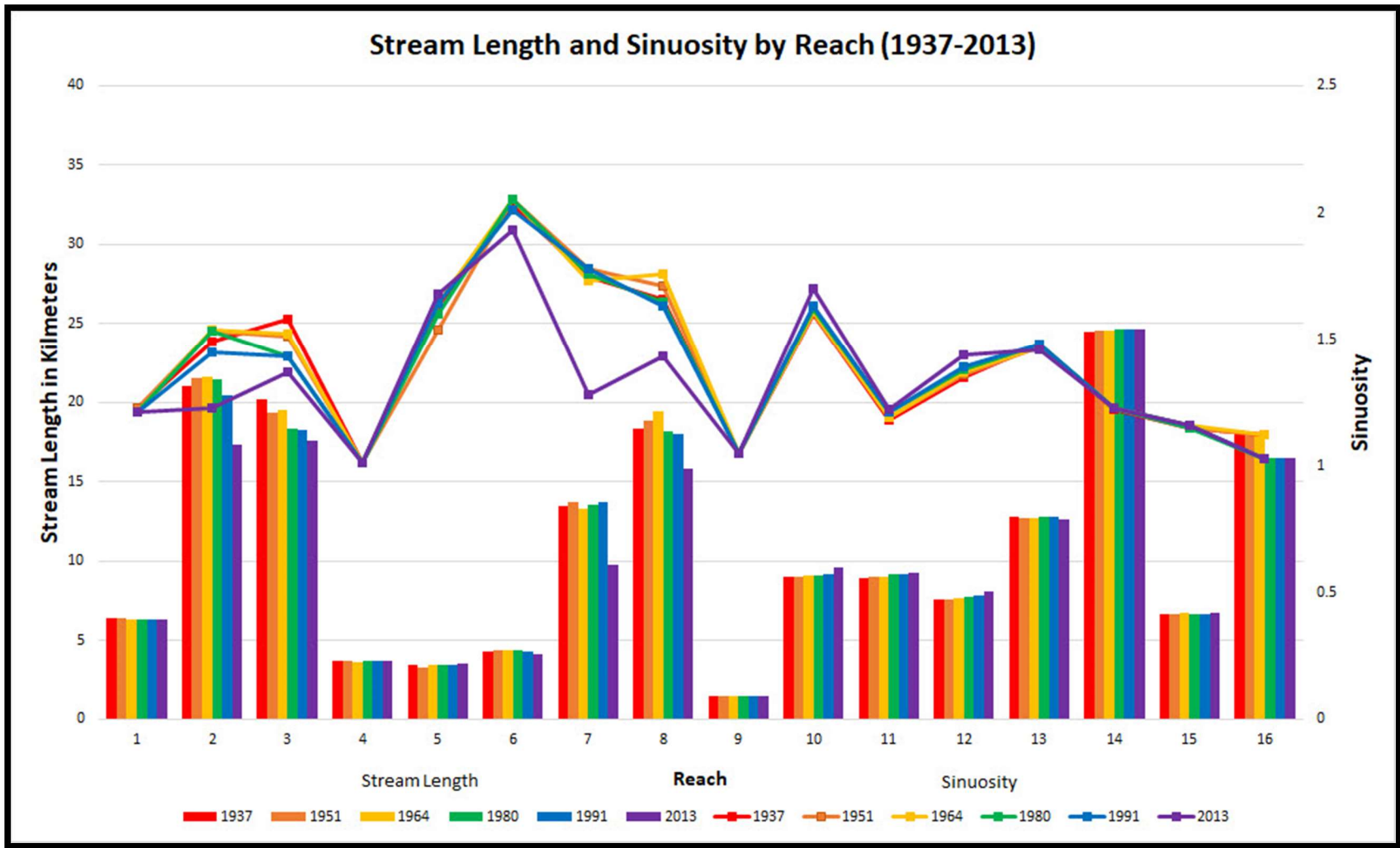
Figure 41. Stream length and sinuosity of lower Minnesota River Reaches

4.2.1. Channel Migration

Spatially, the Minnesota River has exhibited greater channel migration in the upstream reaches (1-12; Figure 9) over ~115 km between Mankato and Jordan with a marked decrease just downstream Jordan (Figure 11, Figure 12,

Table **1**,

Table **2**,
Appendix I). This spatial trend is likely seen for several reasons. Groten et al. (2016), found that the stretch of Minnesota River from Mankato to Jordan is a major sediment contributor with the USGS gauging data in Jordan displaying a sediment yield that is two and half times greater than that of Mankato. However, the stretch of the Minnesota River from Jordan to Fort Snelling reveals sediment yields significantly lower than those reaches just upstream. This suggests that the reach from Jordan to Fort Snelling is a sediment sink. In addition, and as to be expected, they also found that median bedload size decreases downstream from Mankato as well.

The downstream changes are interpreted because of a flattening stream gradient. Although the stretch of Minnesota River from Mankato to the confluence has a gentle gradient, slope significantly decreases in the most downstream reaches of the river (Figure 42). Notably, Mankato to Jordan has a slope of 0.0002 or 0.16 m/km (10 in/mi) and Jordan to Fort Snelling (near the Mississippi confluence) has a slope of 0.00006 or 0.06 m/km (3.8 in/mi) (Ellison 2015). This change in slope marks a change stream power on the Minnesota River which is why we see less channel migration in the downstream reaches as well as a sediment sink.
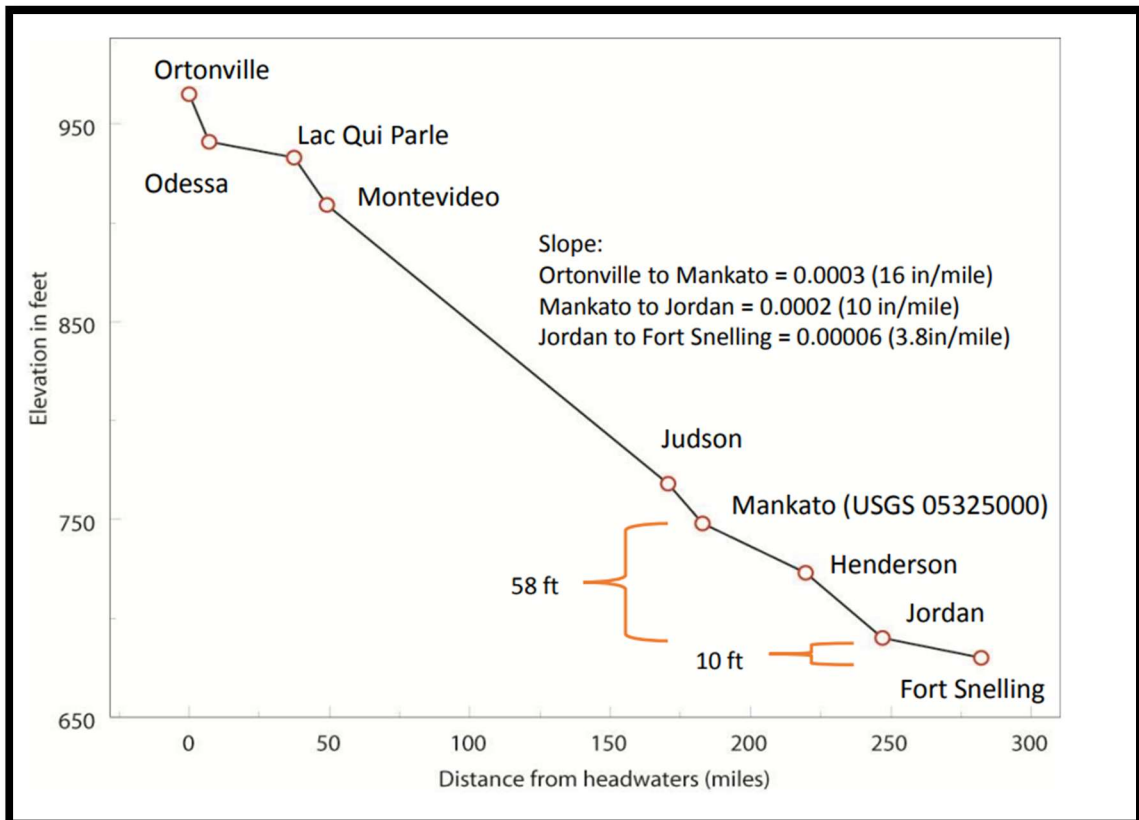
Figure 42. The Minnesota has a very low stream gradient, yet noticeable breaks are still present effecting the morphology of the river. Graphic from (Ellison 2015).

The upstream reaches have several large tributaries which contribute a great deal of sediment to the Minnesota River (Belmont et al. 2011; Gran, Belmont, Day, Jennings, et al. 2011; Groten, Ellison, and Hendrickson 2016). Among these are the Le Sueur River Watershed which has the highest sediment yield of any tributary in the MRB, contributing up to 30% of the sediment load to the Minnesota River while only occupying 7% of the MRB (Belmont et al. 2011). Groten et al. (2016) identify High Island Creek as the next highest contributor of sediment yield. This tributary enters the Minnesota River just downstream of the city of Henderson (Reach 7). Visual inspection of aerial imagery also shows several other tributaries with significant depositional features (e.g. large slumping bluffs, wide in-channel sandbars) within the tributaries themselves and large alluvial fans deposited in the Minnesota River. Among these are Seven Mile Creek, Le Sueur Creek, Rush River, and Beavens Creek, with the latter two also exhibiting large, exposed bluffs abutting the river much like the Le Sueur River.

Based on the findings of Groten et al. (2016) sediment, primarily transported in suspension, in the upstream reaches begins to fall out after Jordan, which coincides with the aforementioned reduction in slope (Figure 42). This transition falls half way through Reach 12, which is dominated by high migration rates from the channel translating downstream (Figure 43). Reach 12 marks the last reach to show any significant annual channel migration, except for Reach 16 in the 1980-1991 interval. The "Instability Concept" (Dey 2014) suggests that irregularities or perturbations in the upstream relate to modified structure in the downstream flow and sediment regime causing a river channel to meander. These upstream perturbations/irregularities include sediment deposition on the bed (Griggs 1906), velocity changes due to turbulence (Hjulström 1957), or oblique entry of flow in a channel (Friedkin 1945) all of which are seen in Reach 12 Figure 43.
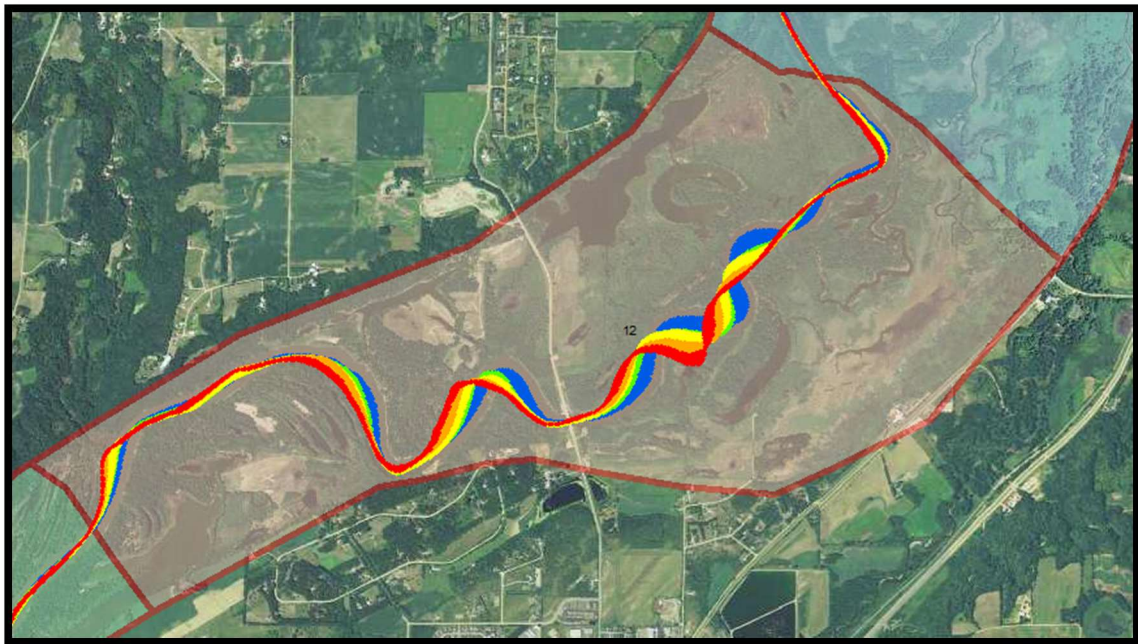
Figure 43. Reach 12 with migration displayed (Red = 1937-1951, Orange = 1951-1964, Yellow = 1964-1980, Green = 1980-1991, Blue = 1991-2013)

The highest AACM was seen in Reach 5 and the lowest AACM was seen in Reach 9, these were both short reaches and need to be viewed as such in terms of data analysis. These reaches were defined (

Appendix H) based on geomorphic characteristics of the channel (sinuosity, meander wavelength, depositional features, etc.) and river valley width as well as any influencing anthropogenic features (urban areas, bridges, flood control structures, etc.). Reach 4, 6, and 9 were significantly shorter than most of other reaches and had uncharacteristically low AACM (

Table **1**) which created breaks in the data. In hindsight, these reaches should be combined with surrounding reaches to better display the data for AACM. However, they do show the areas of highest stability on the river which was part of the objectives in this research.

Temporally, the entire study reach has seen an increasing AACM except for the most recent interval (1991-2013) which has decreased (

Table **1**). The increased AACM was expected given the higher stream flows, increased frequency of high flow events, and increased precipitation within the watershed (Novotny and Stefan 2007; Gran, Belmont, Day, Jennings, et al. 2011; Yuan and Mitchell 2014; Kelly et al. 2017). This overall increase in discharge is expected to increase the stream power of the river enabling greater amounts of channel migration/bank erosion. However, one explanation from this could be the influence of river management. Despite 1991-2013 showing a decrease in AACM, three Reaches (5, 7, and 8) are all above the 90th percentile for AACM (

Table **1**). This, however, is offset by 6 Reaches being below the 10th percentile and mostly found in urban areas. For instance, Reach 1 is Mankato's heavily engineered river stretch containing riprap, earthen levees, and cement flood walls, which has drastically reduced AACM measurements. Also Reaches 14, 15, and 16 are in the Minneapolis-St. Paul Metropolitan Area which has portions of the channel that are actively managed for barge traffic (USACE 2007, Jennings 2016). This is likely not the only reason, but can explain, in part, the observed trends in AACM.

As expected, these locations and intervals strongly correlate to the reaches and intervals experiencing the highest AACM and MACM. This reveals another form of dynamism in these reaches that not only relates to high erosional channel migration, but also to the rivers ability to change course rapidly, occupying great extents of the river valley.

4.2.2. Channel Width

Channel width has steadily increased from 1937 – 2013 (Figure 21). All reaches show an increase in channel width, but the upstream reaches increased at a higher rate than that of the downstream reaches (Figure 22). This disproportionate increase has changed the linear trend from the downstream having greater channel widths in 1937 to the upstream having greater widths by 2013 (Figure 22). This could be a result of higher channel migration in the upstream reaches enlarging the banks more rapidly than that of the lower downstream reaches.

This behavior was expected given the increase in discharge in the MRB over this period (Novotny and Stefan 2007; Yuan and Mitchell 2014; Kelly et al. 2017). Schumm (1969) associates both an increase in channel width and an increase in width/depth ratio resulting from an increase in discharge. Given the increased need for channel dredging in the lower reaches of the Minnesota River to maintain barge traffic (Groten, Ellison, and Hendrickson 2016), it can be assumed that naturally (i.e. without modification) channel depth would be decreasing, supporting an increasing width/depth ratio.

An increased width/depth ratio is generally characterized with a higher shear stress being placed on the outer bank which increases and accelerates bank erosion. Reach 2 had the highest overall ACW and the greatest ACW of any reach in 1991 and 2013 (

Table **1**). Reach 2 also had the 2nd highest overall AACM and historically high MACM, with the greatest MACM of all reach/intervals in 1991 (

Table **1**,

Table **2**). On the other hand, Reaches with low ACW (e.g. Reach 4, 6, 9,) showed low AACM (Figure 40,

Table **1**,

Table **2**).

4.2.3. Channel Sinuosity/Stream Length

The decrease in channel sinuosity and stream length observed is interpreted as a result of cutoffs occurring from 1937-2013 (Figure 19). However, the magnitude of the cutoffs is increasing resulting in an accelerated loss of sinuosity and stream length (Figure 23, Figure 24). The 1964-1980 and 1991-2013 intervals both experienced seven cutoffs (Figure 19), yet the decrease in stream length (Figure 24) was far greater in the 1991-2013 interval, especially in Reach 2, 7, and 8 (Figure 23). Figure 44shows two different cutoffs from the 1991-2013 interval, the first (Figure 44A) resulting in ~2 km of stream length lost, and the second (Figure 44B) resulting in ~3 km of stream length lost. These large cutoffs are likely due to several factors. First, they are near a major highway (HWY 169) inhibiting further migration. Second, the increase in discharge leads to more frequent floodplain inundation, increasing the likely hood for cutoffs. Notably, the cutoff in Figure 44A is in Reach 2, which had the highest amount of cutoffs of any reach (Figure 19) demonstrating the high geomorphic activity in this reach.
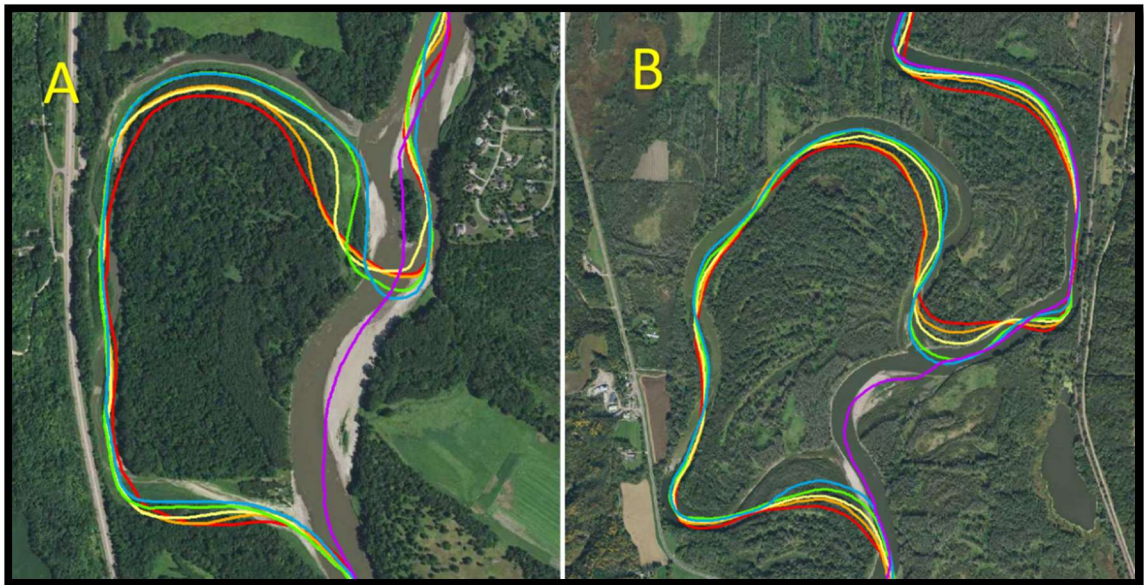
Figure 44. Displayed are two different cutoffs from the 1991-2013 interval. (A) resulted in ~2 km of stream length lost, and (B) resulting in ~3 km of stream length lost.

5. Conclusion

The Minnesota River is a highly dynamic system undergoing morphological planform channel adjustment as observed in the historical, aerial photograph record. This adjustment is likely linked to the MRB experiencing increased discharge from increased agricultural drainage practices and a changing climate resulting in more precipitation. Channel migration has been historically more active from Mankato to Jordan. Although the overall trend has revealed an increase in average annual migration (1937 to 1951 = 0.77 m/y, 1951 to 1964 = 0.84 m/y, 1964 to 1980 = 0.91 m/y, 1980 to 1991 = 0.99 m/y),

the most recent interval analyzed, 1991-2013, has shown a slight decline (0.81 m/y). However, maximum annual channel migration is increasing with the highest recorded annual measurements being in 1980-1991 (15.86 m/y) and 1991-2013 (12.64 m/y). Despite an increasing trend in AACM and MACM, several areas of the Minnesota River showed historical migration stability (Reach 6 and 9).

Channel width has nearly doubled, on average throughout the lower Minnesota River, with every channel subsection, or reach, showing an increase. Reach 2 also had the highest overall ACW of any of the reaches at 100.19 m, and Reach 6 had the lowest overall ACW at 77.21 m (

Table **3**, Figure 22). An incremental increase in ACW of ~ 5-10 m was seen in each successive interval from 1937-2013. Reach analysis further demonstrated both the temporal increase in ACW, but also a spatial/temporal shift from channel width being greater in the downstream reaches to channel width being greater in the upstream reaches (

Table **3**, Figure 22). The increase in channel width has been greater in the upstream reaches, and there has been a longitudinal shift from increasing width in the downstream direction to decreasing width (Figure 22).

Sinuosity is variable on the reach scale, but the overall trend reveals a decrease in sinuosity and, thereby, stream length. This is interpreted to be the result of recent cutoffs. The 1964-1980 and 1991-2013 intervals both experienced seven cutoffs (Figure 19), however; the decrease in stream length (Figure 24) was far greater in the 1991-2013 interval, especially in Reach 2, 7, and 8 (Figure 23) due to an increase in the magnitude of the cutoffs size.

Pinch points show a great deal of variability in planform change due to the unique features of different infrastructure. The stretch of river passing through Mankato (Figure 25) showed the greatest increase in migration stability following the floodwall and riprap-controlled being constructed in the mid-1960's leading to a decrease (~3 m/y) in channel migration (Figure 26). However, width did not immediately stabilize in this reach (Figure 27) and continued to rise in a manner characteristic with other river reaches (Figure 22), but recently (1991-2013) has seen its first, although minor, decrease in channel width.

The understanding of both spatial and temporal historic planform changes can now help aid decision makers in deciding if an area is potentially suitable for an invasive carp barrier. In addition, various lower Minnesota River Valley communities and residents can use this information to assess erosional hazards to property and infrastructure. Lastly, this information helps us better understand the historical impact of anthropogenic activities on the behavior of this fluvial system.

6. References

Aadland, L. 2015. Barrier effects on native fishes of Minnesota. Minnesota Department of Natural Resources. http://files.dnr.state.mn.us/eco/streamhab/barrier-effects.pdf (accessed May 1, 2015).

Aalto, R., J. W. Lauer, and W. E. Dietrich. 2008. Spatial and temporal dynamics of sediment accumulation and exchange along Strickland River floodplains (Papua New Guinea) over decadal-to-centennial timescales. Journal of Geophysical Research: Earth Surface 113 (F1). doi:10.1029/2006JF000627.

Amhar, F., J. Jansa, and C. Ries. 1998. The generation of true orthophotos using a 3D building model in conjunction with a conventional DTM. International Archives of Photogrammetry and Remote Sensing 32:16-22.

ArcGIS for Desktop. 2016. Fundamentals of georeferencing a raster dataset. http://desktop.arcgis.com/en/arcmap/10.3/manage-data/raster-and-images/fundamentals-for-georeferencing-a-raster-dataset.htm. (accessed January 27, 2017).

Arora, V. K., and G. J. Boer. 2001. Effects of simulated climate change on the hydrology

of major river basins. Journal of Geophysical Research: Atmospheres 106 (D4):3335-3348.

Baker, V. R. 2013. Sinuous rivers. Proceedings of the National Academy of Sciences of the United States of America 110 (21):8321-8322. doi: 10.1073/pnas.1306619110.

Belmont, P., and E. Foufoula-Georgiou. 2017. Solving water quality problems in agricultural landscapes: New approaches for these nonlinear, multiprocess, multiscale systems. Water Resources Research 53 (4):2585-2590. doi:10.1002/2017WR020839.

Belmont, P., K. B. Gran, S. P. Schottler, P. R. Wilcock, S. S. Day, C. Jennings, J. W. Lauer, E. Viparelli, J. K. Willenbring, D. R. Engstrom, and G. Parker. 2011. Large shift in source of fine sediment in the Upper Mississippi River. Environmental Science & Technology 45 (20):8804-8810. doi:10.1021/es2019109.

Black, E., C. E. Renshaw, F. J. Magilligan, J. M. Kaste, W. B. Dade, and J. D. Landis. 2010. Determining lateral migration rates of meandering rivers using fallout radionuclides. Geomorphology 123 (3-4):364-369. doi:10.1016/j.geomorph.2010.08.004

Block, D. 2014. Historical channel-planform change of the Little Colorado River near Winslow, Arizona. Scientific Investigations Report 2014-5112., US Geological Survey, Reston, Virginia.

Blumentritt, D. J., D. R. Engstrom, and S. J. Balogh. 2013. A novel repeat-coring approach to reconstruct recent sediment, phosphorus, and mercury loading from the upper Mississippi River to Lake Pepin, USA. Journal of Paleolimnology 50 (3):293-304. doi:10.1007/s10933-013-9724-8.

Booth, D. B., and C. R. Jackson. 1997. Urbanization of aquatic systems: Degradation thresholds, stormwater detection, and the limits of mitigation. JAWRA Journal of the American Water Resources Association 33 (5):1077-1090. doi:10.1111/j.1752-1688.1997.tb04126.x.

Bradley, C., and D. G. Smith. 1984. Meandering channel response to altered flow regime: Milk River, Alberta and Montana. Water Resources Research 20 (12):1913-1920. doi:10.1029/WR020i012p01913.

Brewer, P., and J. Lewin. 1998. Planform cyclicity in an unstable reach: Complex fluvial response to environmental change. Earth Surface Processes and Landforms 23 (11):989-1008.

Brezonik, P. L., K.W. Easter, L. Hatch, D. Mulla, and J. Perry. 1999. Management of diffuse pollution in agricultural watersheds: Lessons from the Minnesota River Basin. Water Science and Technology 39 (12):323-330.

Bristow, C. S., and J. L. Best. 1993. Braided rivers: perspectives and problems. Geological Society, London, Special Publications 75 (1):1-11. doi:10.1144/GSL.SP.1993.075.01.01.

Buckingham, S. E., and J. W. Whitney. 2007. GIS methodology for quantifying channel change in Las Vegas, Nevada. Journal of American Water Resources Association 43 (4):888- 898. doi:10.1111/j.1752-1688.2007.00073.x.

Bunn, S. E., and A. H. Arthington. 2002. Basic principles and ecological consequences of

altered flow regimes for aquatic biodiversity. Environmental Management 30 (4):492-507. doi:10.1007/s00267-002-2737-0.

Burkham, D. 1972. Channel changes of the Gila River in Safford valley, Arizona, 1846-1970. Geologic Survey Professtional Paper 655-G. US Geological Survey, Washington D.C.

Carlson, A. K., and B. Vondracek. 2014. Synthesis of ecology and human dimensions for predictive management of bighead and silver carp in the United States. Reviews in Fisheries Science & Aquaculture 22 (4):284-300. doi:10.1080/23308249.2014.967747.

Carlston, C. W. 1965. The relation of free meander geometry to stream discharge and its geomorphic implications. American Journal of Science 263 (10):864-885. doi:10.2475/ajs.263.10.864.

Carpenter, S. R., N. F. Caraco, D. L. Correll, R. W. Howarth, A. N. Sharpley, and V. H. Smith. 1998. Nonpoint pollution of surface waters with phosphorus and nitrogen. Ecological Applications 8 (3):559-568. doi:10.1890/1051-0761(1998)008[0559:NPOSWW]2.0.CO;2.

Carson, M. A., and M. F. Lapointe. 1983. The inherent asymmetry of river meander planform. The Journal of Geology 91 (1):41-55. doi:10.1086/628743.

Carson, M. A., and G. A. Griffiths. 1987. Bedload transport in gravel channels. Journal of Hydrology (New Zealand) 26 (1):1-151.

Chang, K. T. 2014. Introduction to geographic information systems. 7th ed. New York, NY: McGraw-Hill.

Charlton, R. 2007. Fundamentals of fluvial geomorphology. New York, NY: Routledge.

Chatley, H. 1938. Hydraulics of large rivers. J. Junior Inst. Eng 48: 401-416

Chick, J. H., and M. A. Pegg. 2001. Invasive carp in the Mississippi River Basin. Science 292 (5525):2250-2251. doi:10.1126/science.292.5525.2250.

Chrisman, N. 1982. Theory of cartographic error and its measurement in digital data bases. American Society of Photogrammetry and Remote Sensing. Falls Church, VA.

Clayton, L., and S. R. Moran. 1982. Chronology of late Wisconsinan glaciation in middle North America. Quaternary Science Reviews 1 (1):55-82. doi:10.1016/0277-3791(82)90019-1.

Comiti, F., M. Da Canal, N. Surian, L. Mao, L. Picco, and M. A. Lenzi. 2011. Channel adjustments and vegetation cover dynamics in a large gravel bed river over the last 200 years. Geomorphology 125 (1):147-159. doi:10.1016/j.geomorph.2010.09.011.

Constantine, J. A., T. Dunne, J. Ahmed, C. Legleiter, and E. D. Lazarus. 2014. Sediment supply as a driver of river meandering and floodplain evolution in the Amazon Basin. Nature Geoscience 7 (12):899-903. doi:10.1038/ngeo2282.

Crowell, M., S. P. Leatherman, and M. K. Buckley. 1991. Historical shoreline change: Error analysis and mapping accuracy. Journal of Coastal Research 7 (3):839-852.

Daniels, J. M. 2003. Floodplain aggradation and pedogenesis in a semiarid environment. Geomorphology 56 (3-4):225-242. doi:10.1016/S0169-555X(03)00153-3.

Darby, S. E., M. Rinaldi, and S. Dapporto. 2007. Coupled simulations of fluvial erosion

and mass wasting for cohesive river banks. Journal of Geophysical Research: Earth Surface 112 (F3). doi:10.1029/2006JF000722.

Davis, W. M. 1889. The rivers and valleys of Pennsylvania. National Geographic Society 1:183-252.

———. 1902. Baselevel, grade and peneplain. The Journal of Geology 10 (1):77-111.

Dawson, H. A., U. G. Reinhardt, and J. F. Savino. 2006. Use of electric or bubble barriers to limit the movement of Eurasian ruffe (Gymnocephalus cernuus). Journal of Great Lakes Research 32 (1):40-49. doi:10.3394/03801330(2006)32[40: UOEOBB]2.0.CO;2.

Day, S. S., K. B. Gran, P. Belmont, and T. Wawrzyniec. 2013a. Measuring bluff erosion part 1: Terrestrial laser scanning methods for change detection. Earth Surface Processes and Landforms 38 (10):1055-1067. doi:10.1002/esp.3353.

———. 2013b. Measuring bluff erosion part 2: Pairing aerial photographs and terrestrial laser scanning to create a watershed scale sediment budget. Earth Surface Processes and Landforms 38 (10):1068-1082. doi:10.1002/esp.3359.

DeGrandchamp, K. L., J. E. Garvey, and R. E. Colombo. 2008. Movement and habitat selection by invasive Asian carps in a large river. Transactions of the American Fisheries Society 137 (1):45-56. doi:10.1577/T06-116.1.

Dey, S. 2014. Fluvial hydrodynamics. Berlin, Heidelberg: Springer.

Dodds, W. K. 2006. Nutrients and the "dead zone": the link between nutrient ratios and dissolved oxygen in the northern Gulf of Mexico. Frontiers in Ecology and the Environment 4 (4):211-217. doi:10.1890/15409295(2006)004[0211 :NATDZT]2.0.CO;2.

Downward, S. R., A. M. Gurnell, and A. Brookes. 1994. A methodology for quantifying river channel planform change using GIS. IAHS Publications-Series of Proceedings and Reports-Intern Assoc Hydrological Sciences 224:449-456.

Dunne, T., and L. B. Leopold. 1978. Water in environmental planning. New York, NY: W.H Freeman and Company.

Dury, G. H. 1964. Principles of underfit streams. Geologic Survey Professtional Paper 452-A. US Geological Survey, Washington D.C.

Eakin, H. M. 1910. The influence of the earth's rotation upon the lateral erosion of streams. The Journal of Geology 18 (5):435-447.

Einstein, A. 1926. The cause of the formation of meanders in the Courses of Rivers and of the So-Called Baer's Law. Die Naturwissenschaften 14 (11):223-224.

Ellison, C. A. 2015. Sediment concentrations, loads, particle-size fractions, and hydroacoustics in the lower Minnesota River, 2011-2014. US Geologic Survey PowerPoint Presentation prepared in conjunction with the US Army Corps of Engineers. September 9.

Engstrom, D. R., J. E. Almendinger, and J. A. Wolin. 2009. Historical changes in sediment and phosphorus loading to the upper Mississippi River: Mass-balance reconstructions from the sediments of Lake Pepin. Journal of Paleolimnology 41 (4):563-588. doi:10.1007/s10933-008-9292-5.

Everitt, B. L. 1968. Use of the cottonwood in an investigation of the recent history of a

flood plain. American Journal of Science 266 (6):417-439. doi:10.2475/ajs.266.6.417.

Faulkner, D. J., P. H. Larson, H. M. Jol, G. L. Running, H. M. Loope, and R. J. Goble. 2016. Autogenic incision and terrace formation resulting from abrupt late-glacial base-level fall, lower Chippewa River, Wisconsin, USA. Geomorphology 266:75-95. doi:10.1016/j.geomorph.2016.04.016.

Fenton, M. M., S. Moran, J. T. Teller, and L. Clayton. 1983. Quaternary stratigraphy and history in the southern part of the Lake Agassiz basin. Special Paper 26 – Lake Agassiz, Geologic Association of Canada.

Fisher, T. G. 2003. Chronology of glacial Lake Agassiz meltwater routed to the Gulf of Mexico. Quaternary Research 59 (2):271-276. doi:10.1016/S0033-5894(03)00011-5.

———— T. G. 2004. River Warren boulders, Minnesota, USA: Catastrophic paleoflow indicators in the southern spillway of glacial Lake Agassiz. Boreas 33 (4):349- 358. doi:10.1111/j.1502-3885.2004.tb01245.x.

Florsheim, J. L., J. F. Mount, and A. Chin. 2008. Bank erosion as a desirable attribute of rivers. Bioscience 58 (6):519-529. doi:10.1641/B580608.

Forsberg, D. C. 1992. Minnesota Wetland Conservation Act of 1991: Balancing public and private interests. William Mitchell Law Review 18 (4):1021-1071.

Foufoula-Georgiou, E., Z. Takbiri, J. A. Czuba, and J. Schwenk. 2015. The change of nature and the nature of change in agricultural landscapes: Hydrologic regime shifts modulate ecological transitions. Water Resources Research 51 (8):6649-6671. doi:10.1002/2015WR017637.

Friedkin, J. F. 1945. Laboratory study of the meandering of alluvial rivers. US Army Corp of Engineers, Vicksburg, Mississippi.

Garofalo, D. 1980. The influence of wetland vegetation on tidal stream channel migration and morphology. Estuaries 3 (4):258-270. doi:10.2307/1352081.

Gay, G. R., H. H. Gay, W. H. Gay, H. A. Martinson, R. H. Meade, and J. A. Moody. 1998. Evolution of cutoffs across meander necks in Powder River, Montana, USA. Earth Surface Processes and Landforms 23 (7):651-662.

Giardino, J. R., and A. A. Lee. 2011. Rates of channel migration on the Brazos River. Contract No. 0904830898, Department of Geology & Geophysics, Texas A&M University, College Station, Texas.

Gilbert, G. K. 1877. Report on the geology of the Henry Mountains. US Geological Survery, Washington D.C.

————.. 1884. The Sufficiency of Terrestrial Rotation for the Deflection of Streams. American Journal of Science (1880-1910) 27 (162):427.

Gilroy, K. L., and R. H. McCuen. 2012. A nonstationary flood frequency analysis method to adjust for future climate change and urbanization. Journal of Hydrology 414-415:40-48. doi:10.1016/j.jhydrol.2011.10.009.

Gilvear, D., S. Winterbottom, and H. Sichingabula. 2000. Character of channel planform change and meander development: Luangwa River, Zambia. Earth Surface Processes and Landforms 25 (4):421-436. doi:10.1002/(SICI)1096-9837(200004)25:4<421::AID-ESP65>3.0.CO;2-Q.

Goudie, A. S. 2006. Global warming and fluvial geomorphology. Geomorphology 79 (3-4):384-394. doi:10.1016/j.geomorph.2006.06.023.

Grabowski, R. C., N. Surian, and A. M. Gurnell. 2014. Characterizing geomorphological change to support sustainable river restoration and management. Wiley Interdisciplinary Reviews: Water 1 (5):483-512. doi:10.1002/wat2.1037.

Graf, W. L. 2000. Locational probability for a dammed, urbanizing stream: Salt River, Arizona, USA. Environmental Management 25 (3):321-335. doi:10.1007/s002679910025.

Gran, K., P. Belmont, S. Day, C. Jennings, J. W. Lauer, E. Viparelli, P. Wilcock, and G.

Parker. 2011. An integrated sediment budget for the Le Sueur River Basin. Report wq-iw7-29o, Minnesota Polution Control Agency.

Gran, K. B., P. Belmont, S. S. Day, N. Finnegan, C. Jennings, J. W. Lauer, and P. R. Wilcock. 2011. Landscape evolution in south-central Minnesota and the role of geomorphic history on modern erosional processes. GSA Today 21 (9):7-9. doi:10.1130/G121A.1.

Gran, K. B., P. Belmont, S. S. Day, C. Jennings, A. Johnson, L. Perg, and P. R. Wilcock. 2009. Geomorphic evolution of the Le Sueur River, Minnesota, USA, and implications for current sediment loading. Geological Society of America Special Papers 451:119-130.

Gran, K. B., N. Finnegan, A. L. Johnson, P. Belmont, C. Wittkop, and T. Rittenour. 2013. Landscape evolution, valley excavation, and terrace development following abrupt postglacial base-level fall. Geological Society of America Bulletin 125 (11-12):1851-1864. doi:10.1130/B30772.1.

Griggs, R. F. 1906. The Buffalo River: An interesting meandering stream. Bulletin of the American Geographical Society 38 (3):168-177. doi:10.2307/197916.

Groten, J. T., C. A. Ellison, and J. S. Hendrickson. 2016. Suspended-sediment concentrations, bedload, particle sizes, surrogate measurements, and annual sediment loads for selected sites in the lower Minnesota River Basin, water years 2011 through 2016. Scientific Investigations Report 2016-5174, US Geological Survey. Reston, Virginia. doi: 10.3133/sir20165174.

Gurnell, A. M. 1997. Channel change on the River Dee meanders, 1946–1992, from the analysis of air photographs. River Research and Applications 13 (1):13-26. doi:10.1002/(SICI)1099-1646(199701)13:1<13::AID-RRR420>3.0.CO;2-W.

Gurnell, A. M., S. R. Downward, and R. Jones. 1994. Channel planform change on the River Dee meanders, 1876–1992. River Research and Applications 9 (4):187-204. doi:10.1002/rrr.3450090402.

Hallberg, G. R., and T. J. Kemmis. 1986. Stratigraphy and correlation of the glacial deposits of the Des Moines and James lobes and adjacent areas in North Dakota, South Dakota, Minnesota, and Iowa. Quaternary Science Reviews 5:65-68. doi:10.1016/0277-3791(86)90175-7.

Haque, C. E., and M. Q. Zaman. 1989. Coping with riverbank erosion hazard and displacement in Bangladesh: Survival strategies and adjustments. Disasters 13 (4):300-314. doi:10.1111/j.1467-7717.1989.tb00724.x.

Harvey, M. D., and C. C. Watson. 1986. Fluvial processes and morphological thresholds in incised channel restoration. JAWRA Journal of the American Water Resources Association 22 (3):359-368. doi: 10.1111/j.1752-1688.1986.tb01890.x.

He, Q., and D. E. Walling. 1996. Interpreting particle size effects in the adsorption of 137 Cs and unsupported 210 Pb by mineral soils and sediments. Journal of Environmental Radioactivity 30 (2):117-137. doi:10.1016/0265-931X(96)89275-7.

Hereford, R. 1984. Climate and ephemeral-stream processes: Twentieth-century geomorphology and alluvial stratigraphy of the Little Colorado River, Arizona. GSA Bulletin 95 (6):654-668. doi:10.1130/0016-7606(1984)95<654:CAEPTG>2.0.CO;2.

Hession, W. C., J. E. Pizzuto, T. E. Johnson, and R. J. Horwitz. 2003. Influence of bank vegetation on channel morphology in rural and urban watersheds. Geology 31 (2):147-150. doi:10.1130/0091-7613(2003)031<0147:IOBVOC>2.0.CO;2.

Hickin, E. J., and G. C. Nanson. 1984. Lateral migration rates of river bends. Journal of Hydraulic Engineering 110 (11):1557-1567. doi:10.1061/(ASCE)0733-9429(1984)110:11(1557).

Hjulström, F. 1957. A study of the meander problem. Bulletin. Institute of Hydraulics, Royal Institute of Technology. Stockholm, Sweden.

Hooke, J. 2003. River meander behaviour and instability: A framework for analysis. Transactions of the Institute of British Geographers 28 (2):238-253. doi:10.1111/1475-5661.00089.

———. 1995. River channel adjustment to meander cutoffs on the River Bollin and River Dane, northwest England. Geomorphology 14 (3):235-253. doi:10.1016/0169-555X(95)00110-Q.

———.. 2007. Spatial variability, mechanisms and propagation of change in an active meandering river. Geomorphology 84 (3-4):277-296. doi:10.1016/j.geomorph.2006.06.005.

Huang, H. Q., and G. C. Nanson. 1997. Vegetation and channel variation; a case study of four small streams in southeastern Australia. Geomorphology 18 (3-4):237-249. doi:10.1016/S0169-555X(96)00028-1.

Hughes, M. L., P. F. McDowell, and W. A. Marcus. 2006. Accuracy assessment of georectified aerial photographs: Implications for measuring lateral channel movement in a GIS. Geomorphology 74 (1-4):1-16. doi:10.1016/j.geomorph.2005.07.001.

Inglis, C. C., and G. Lacey. 1947. Meanders and their bearing on river training. Maritime and Waterways Engineering Division. The Institution of Civil Engineers Engineering Division Papers 5 (17):3-24. doi:10.1680/idivp.1947.13075.

Jennings, C. 2016. Why so much sand in the lower Minnesota River? Open Rivers Fall Edition. ISSN 2471-190X

Johannesson, H., and G. Parker. 1985. Computer simulated migration of meandering rivers in Minnesota. Project Report No. 242 Universtiy of Minnesota, St. Anthony Falls Hydraulic Laboratory., Minneapolis, MN.

Keller, E. A. 1972. Development of alluvial stream channels: A five-stage model.

Geological Society of America Bulletin 83 (5):1531-1536. doi:0.1130/0016-7606(1972)83[1531:DOASCA]2.0.CO;2.

Kelley, D. W., and E. A. Nater. 2000. Historical sediment flux from three watersheds into Lake Pepin, Minnesota, USA. Journal of Environmental Quality 29 (2):561-568. doi:10.2134/jeq2000.00472425002900020025x.

Kelley, D. W., S. A. Brachfeld, E. A. Nater, and H. E. Wright Jr. 2006. Sources of sediment in Lake Pepin on the upper Mississippi River in response to Holocene climatic changes. Journal of Paleolimnology 35 (1):193-206. doi:10.1007/s10933-005-8686-x.

Kelly, S. A., Z. Takbiri, P. Belmont, and E. Foufoula-Georgiou. 2017. Human amplified changes in precipitation–runoff patterns in large river basins of the Midwestern United States. Hydrology and Earth System Sciences 21 (10):5065-5088. doi:10.5194/hess-21-5065-2017.

Kimmerling, A., A. Buckley, P. Muehrcke, and J. Muehrcke. 2011. Map use: Reading, analysis, interpretation. Redlands, CA: Esri Press Academic.

Kleinhans, M. G. 2010. Sorting out river channel patterns. Progress in Physical Geography: Earth and Environment 34 (3):287-326. doi:10.1029/2005WR004674.

Knighton, D. 2014. Fluvial forms and processes: A new perspective. New York, NY: Routledge.

Knox, J. C. 1977. Human impacts on Wisconsin Stream Channels. Annals of the Association of American Geographers 67 (3):323-342. doi:10.1111/j.1467-8306.1977.tb01145.x.

Koel, T. M., K. S. Irons, and E. N. Ratcliff. 2000. Asian carp invasion of the upper Mississippi River System. Project Status Report 2000-05, US Department of the Interior, US Geological Survey, Upper Midwest Environmental Sciences Center, La Crosse, WI.

Kolar, C. S., D. C. Chapman, W. R. Courtenay, C. M. Housel, J. D. Williams, and D. P. Jennings. 2007. Bigheaded carps: A biological synopsis and environmental risk assessment. Bethesda, MD: American Fisheries Society

Kondolf, G. M., H. Piégay, and N. Landon. 2002. Channel response to increased and decreased bedload supply from land use change: contrasts between two catchments. Geomorphology 45 (1-2):35-51. doi:10.1016/S0169-555X(01)00188-X.

Kovacic, D. A., M. B. David, L. E. Gentry, K. M. Starks, and R. A. Cooke. 2000. Effectiveness of constructed wetlands in reducing nitrogen and phosphorus export from agricultural tile drainage. Journal of Environmental Quality 29 (4):1262-1274. doi:10.2134/jeq2000.00472425002900040033x.

Lacey, J. M. 1923. Some problems connected with the rivers and the canals in southern India. Minutes of the Proceedings of the Institution of Civil Engineers 216 (1923): 150-160. doi.org/10.1680/imotp.1923.14469.

Lane, E. W. 1955. Importance of fluvial morphology in hydraulic engineering. Proceedings (American Society of Civil Engineers) 81 (745).

Larsen, E. W., E. H. Girvetz, and A. K. Fremier. 2007. Landscape level planning in

alluvial riparian floodplain ecosystems: using geomorphic modeling to avoid conflicts between human infrastructure and habitat conservation. Landscape and Urban Planning 79 (3-4):338-346. doi:10.1016/j.landurbplan.2006.04.003.

Lauer, J. W., C. Echterling, C. Lenhart, P. Belmont, and R. Rausch. 2017. Air-photo based change in channel width in the Minnesota River basin: Modes of adjustment and implications for sediment budget. Geomorphology 297:170-184. doi:10.1016/j.geomorph.2017.09.005.

Lauer, J. W., and G. Parker. 2008. Net local removal of floodplain sediment by river meander migration. Geomorphology 96 (1-2):123-149. doi:10.1016/j.geomorph.2007.08.003.

Lauer, W. 2006. NCED Stream restoration toolbox-channel planform statistics and ArcMap project. National Center for Earth-Surface Dynamics (NCED). https://repository.nced.umn.edu/browser.php?current=author&author=35&dataset_id=15. (accessed April 5, 2018).

Lawler, D. M. 1993. The measurement of river bank erosion and lateral channel change: A review. Earth Surface Processes and Landforms 18 (9):777-821.doi:10.1002/esp.3290180905.

Lea, D. M., and C. J. Legleiter. 2016. Refining measurements of lateral channel movement from image time series by quantifying spatial variations in registration error. Geomorphology 258:11-28. doi: 10.1016/j.geomorph.2016.01.009.

Legleiter, C. J. 2014. Downstream effects of recent reservoir development on the morphodynamics of a meandering channel: Savery Creek, Wyoming, USA. River Research and Applications 31 (10):1328-1343. doi:10.1002/rra.2824.

Leliavsky, S. 1966. Introduction to Fluvial Hydraulics. New York, NY: Dover Publications

Lenhart, C., E. S. Verry, K. N. Brooks, and J. A. Magner. 2011. Adjustment of prairie pothole streams to land-use, drainage and climate changes and consequences for turbidity impairment. River Research and Applications 28 (10):1609-1619. doi:10.1002/rra.1549.

Lenhart, C. F., M. L. Titov, J. S. Ulrich, J. L. Nieber, and B. J. Suppes. 2013. The role of hydrologic alteration and riparian vegetation dynamics in channel evolution along the lower Minnesota River. Transactions of the ASABE 56 (2):549-561. doi:10.13031/2013.42686.

Leopold, L. B., and W. B. Langbein. 1966. River meanders- theory of minimum variance. Scientific American 214 (6):60-73.

Leopold, L. B., and T. Maddock Jr. 1953. The hydraulic geometry of stream channels and some physiographic implications. Professional Paper 252, US Geological Survey, Washington D.C.

Leopold, L. B., and M. G. Wolman. 1957. River channel patterns: braided, meandering, and straight. Professional Paper 282-B, US Geological Survey, Washington, D.C.
———. 1960. River meanders. Geological Society of America Bulletin 71 (6):769-793. doi:10.1130/0016-7606(1960)71[769:RM]2.0.CO;2.

Lepper, K., T. G. Fisher, I. Hajdas, and T. V. Lowell. 2007. Ages for the Big Stone

Moraine and the oldest beaches of glacial Lake Agassiz: Implications for deglaciation chronology. Geology 35 (7):667-670. doi:10.1130/G23665A.1.

Leung, Y., and J. Yan. 1998. A locational error model for spatial features. International Journal of Geographical Information Science 12 (6):607-620. doi:10.1080/136588198241699.

Libby, D. 2018. Assessing historical planform channel change in an altered watershed with quantification of error and uncertainty present in GIS/aerial photography-based analysis; case study: Minnesota River, Minnesota, USA. M.S. Thesis, Department of Geography, Minnesota State University, Mankato.

Little, W. C., C. R. Thorne, and J. B. Murphey. 1982. Mass bank failure analysis of selected Yazoo Basin streams. Transactions of the ASAE 25 (5):1321-1328. doi:10.13031/2013.33721.

Mackin, J. H. 1948. Concept of the graded river. Geological Society of America Bulletin 59 (5):463-512. doi:10.1130/0016-7606(1948)59[463:COTGR]2.0.CO;2.

Macklin, M. G., and J. Lewin. 1989. Sediment transfer and transformation of an alluvial valley floor: the River South Tyne, Northumbria, UK. Earth Surface Processes and Landforms 14 (3):233-246. doi:10.1002/esp.3290140305.

Magdalene, S. C. C. 2004. From field to stream: Rapid runoff through agricultural tile drainage systems within the Minnesota River basin. Thesis, University of Minnesota.

Matisoff, G., and P. J. Whiting. 2012. Measuring soil erosion rates using natural (7Be, 210Pb) and anthropogenic (137Cs, 239,240 Pu) radionuclides. Handbook of Environmental Isotope Geochemistry, 1:487-519. doi:10.1007/978-3-642-10637-8_25.

Matsch, C. 1983. River Warren, the southern outlet to glacial Lake Agassiz. Special Paper 26 – Lake Agassiz, Geologic Association of Canada 26:231-244.

Micheli, E. R., and J. W. Kirchner. 2002. Effects of wet meadow riparian vegetation on streambank erosion. 1. Remote sensing measurements of streambank migration and erodibility. Earth Surface Processes and Landforms 27 (6):627-639. doi:10.1002/esp.338.

Micheli, E., J. W. Kirchner, and E. W. Larsen. 2004. Quantifying the effect of riparian forest versus agricultural vegetation on river meander migration rates, Central Sacramento River, California, USA. River Research and Applications 20 (5):537-548. doi:10.1002/rra.756.

Miller, J. R. 1997. The role of fluvial geomorphic processes in the dispersal of heavy metals from mine sites. Journal of Geochemical Exploration 58 (2-3):101-118. doi:10.1016/S0375-6742(96)00073-8.

Mitsch, W. J., and J. G. Gosselink. 2000. The value of wetlands: Importance of scale and landscape setting. Ecological economics 35 (1):25-33. doi:10.1016/S0921-8009(00)00165-8.

MNDNR. 2014. DNR explains environmental DNA. http://www.dnr.state.mn.us/invasive-carp/faq.html (accessed April 14, 2015)

MnGeo. 2014. Composite image service WMS, Minnesota. http://www.mngeo.state.mn.us/chouse/metadata/composite_wms.html (accessed April, 20, 2015).

Montgomery, D. R., and J. M. Buffington. 1997. Channel-reach morphology in mountain drainage basins. Geological Society of America Bulletin 109 (5):596-611. doi:10.1130/0016-7606(1997)109<0596:CRMIMD>2.3.CO;2.

Moore, M. T., R. Kröger, M. A. Locke, R. F. Cullum, R. W. Steinriede Jr., S. Testa III, R. E. Lizotte Jr., C. T. Bryant, and C. M. Cooper. 2010. Nutrient mitigation capacity in Mississippi Delta, USA drainage ditches. Environmental Pollution 158 (1):175-184. doi:10.1016/j.envpol.2009.07.024.

Morgan, J. L., S. E. Gergel, and N. C. Coops. 2010. Aerial photography: A rapidly evolving tool for ecological management. Bioscience 60 (1):47-59. doi:10.1525/bio.2010.60.1.9.

Motta, D., J. D. Abad, E. J. Langendoen, and M. H. Garcia. 2012. A simplified 2D model for meander migration with physically-based bank evolution. Geomorphology 163-164:10-25. doi:10.1016/j.geomorph.2011.06.036.

Mount, N., and J. Louis. 2005. Estimation and propagation of error in measurements of river channel movement from aerial imagery. Earth Surface Processes and Landforms 30 (5):635-643. doi:10.1002/esp.1172.

Mount, N. J., J. Louis, R. M. Teeuw, P. M. Zukowskyj, and T. Stott. 2003. Estimation of error in bankfull width comparisons from temporally sequenced raw and corrected aerial photographs. Geomorphology 56 (1–2):65-77. doi:10.1016/S0169-555X(03)00046-1.

MPCA. 1998. Bacteria in the Minnesota River. [cited 5/2/2015. http://www.pca.state.mn.us/index.php/view-document.html?gid=9962. (accessed May 2, 2015).
———. 2002. Minnesota River Basin plan. http://www.pca.state.mn.us/index.php/view-document.html?gid=9947 (accessed May 1, 2015).
———. 2008. Nutrients: Phosphorus, nitrogen sources, impact on water quality - A general overview. http://www.pca.state.mn.us/index.php/view-document.html?gid=7939 (accessed May 2, 2015).

MRBDC. 2003. Minnesota River profile. http://mrbdc.mnsu.edu/mnbasin/fact_sheets/river_profile (accessed April, 15, 2015)
———. 2004. Minnesota River Valley formation. http://mrbdc.mnsu.edu/minnesota-river-valley-formation (accessed May 1, 2015).
———. 2011 Minnesota River Basin fast facts. http://mrbdc.mnsu.edu/minnesota-river-basin-fast-facts (accessed April 20, 2015).

Mulla, D. J., and A. C. Sekely. 2009. Historical trends affecting accumulation of sediment and phosphorus in Lake Pepin, upper Mississippi River, USA. Journal of Paleolimnology 41 (4):589-602. doi:10.1007/s10933-008-9293-4.

Musser, K., S. Kudelka, and R. Moore. 2009. Minnesota River Basin trends. Mankato, MN: Minnesota State University, Mankato, Water Resources Center.

Naden, P. S. 2010. The fine-sediment cascade. In Sediment cascades: An integrated approach, ed. T. Burt and R. Allison, 271-3-306. Oxford, UK: John Wiley & Sons.

Nanson, G. C., and E. J. Hickin. 1983. Channel migration and incision on the Beatton

River. Journal of Hydraulic Engineering 109 (3):327-337.
doi:10.1061/(ASCE)0733-9429(1983)109:3(327).

———. 1986. A statistical analysis of bank erosion and channel migration in
western Canada. Geological Society of America Bulletin 97 (4):497-504.
doi:10.1130/0016-7606(1986)97<497:ASAOBE>2.0.CO;2.

Neu, H. A. 1967. Transverse flow in a river due to earth's rotation. Journal of the
Hydraulics division 93 (5):149-166.

Nicoll, T. J., and E. J. Hickin. 2010. Planform geometry and channel migration of
confined meandering rivers on the Canadian prairies. Geomorphology 116 (1-
2):37-47. doi:10.1016/j.geomorph.2009.10.005.

NOAA. 2015. Gulf of Mexico dead zone 'above average'. http://www.noaanews.noaa.
gov/stories2015/080415-gulf-of-mexico-dead-zone-above-average.html (accessed
November, 11, 2017).

Noatch, M. R., and C. D. Suski. 2012. Non-physical barriers to deter fish movements.
Environmental Reviews 20 (1):71-82. doi:10.1139/a2012-001.

Novotny, E. V., and H. G. Stefan. 2007. Stream flow in Minnesota: Indicator of climate
change. Journal of Hydrology 334 (3-4):319-333.
doi:10.1016/j.jhydrol.2006.10.011.

O'Connor, J. E., M. A. Jones, and T. L. Haluska. 2003. Flood plain and channel dynamics
of the Quinault and Queets Rivers, Washington, USA. Geomorphology 51 (1-
3):31-59. doi: 10.1016/S0169-555X(02)00324-0.

Odgaard, A. J. 1987. Streambank erosion along two rivers in Iowa. Water resources
research 23 (7):1225-1236. doi:10.1029/WR023i007p01225.

Ojakangas, R. W., and C. L. Matcsh. 1982. Minnesota's geology. Minneapolis, MN:
University of Minnesota Press.

Onishi, Y., S. C. Jain, and J. F. Kennedy. 1976. Effects of meandering in alluvial streams.
Journal of the Hydraulics division 102 (HY7):899-917.

Osman, A. M., and C. R. Thorne. 1988. Riverbank stability analysis. I: Theory. Journal of
Hydraulic Engineering 114 (2):134-150. doi:10.1061/(ASCE)0733-
9429(1988)114:2(134).

Osterkamp, W. R., M. L. Scott, and G. T. Auble. 1998. Downstream effects of dams on
channel geometry and bottomland vegetation: Regional patterns in the Great
Plains. Wetlands 18 (4):619-633. doi:10.1007/BF03161677.

Patterson, C., and H. Wright. 1998. Contributions to Quaternary studies in Minnesota.
Report of Investigations 48 ISSN 0076-9177, Minnesota Geological Survey, St.
Paul, MN.

Patterson, C. J. 1997. Southern Laurentide ice lobes were created by ice streams: Des
Moines Lobe in Minnesota, USA. Sedimentary Geology 111 (1-4):249-261.
doi:10.1016/S0037-0738(97)00018-3.

Patton, P. C., and S. A. Schumm. 1975. Gully erosion, Northwestern Colorado: A
threshold phenomenon. Geology 3 (2):88-90. doi:10.1130/0091-
7613(1975)3<88:GENCAT>2.0.CO;2.

Pegg, M. A., and J. H. Chick. 2004. An evaluation of barriers for preventing the spread

of bighead and silver carp to the Great Lakes. Illinois Natural History Survey. http://www.iisgcp.org/research/ais/pegg.html (accessed May 1, 2015).

Pereira, W. E., and F. D. Hostettler. 1993. Nonpoint source contamination of the Mississippi River and its tributaries by herbicides. Environmental Science & Technology 27 (8):1542-1552. doi:10.1021/es00045a008.

Petrolia, D. R., and P. H. Gowda. 2006. Missing the boat: Midwest farm drainage and Gulf of Mexico hypoxia. Review of Agricultural Economics 28 (2):240-253. doi:10.1111/j.1467-9353.2006.00284.x.

Pimentel, D., L. Lach, R. Zuniga, and D. Morrison. 2000. Environmental and economic costs of nonindigenous species in the United States. Bioscience 50 (1):53-65. doi: 10.1641/0006-3568(2000)050[0053:EAECON]2.3.CO;2.

Pizzuto, J. E. 1994. Channel adjustments to changing discharges, Powder River, Montana. Geological Society of America Bulletin 106 (11):1494-1501. doi:10.1130/0016-7606(1994)106<1494:CATCDP>2.3.CO;2.

Professional Aerial Photographers Association. 2015. History of aerial photography. http://professionalaerialphotographers.com/content.aspx?page_id=22&club_id=8 08138&module_id=158950 (accessed March, 31, 2015).

Prus-Chacinski, T. M. 1954. Patterns of motion in open channel bends. Association International d'Hydrologie 3 (38):311-318.

Quraishy, M. S. 1943. River meandering and the earth's rotation. Current Science 12 (10):278-278.

Rabalais, N. N., R. E. Turner, and D. Scavia. 2002. Beyond Science into Policy: Gulf of Mexico Hypoxia and the Mississippi River: Nutrient policy development for the Mississippi River watershed reflects the accumulated scientific evidence that the increase in nitrogen loading is the primary factor in the worsening of hypoxia in the northern Gulf of Mexico. BioScience 52 (2):129-142. doi:10.1641/0006-3568(2002)052[0129:BSIPGO]2.0.CO;2.

Rasmussen, J. 2011. Regulations as a tool in Asian carp management. In Invasive Asian carps in North America. ed. D. C. Chapman and M. H. Hoff, 175-190. Bethesda, Maryland: American Fisheries Society.

Rhoades, E. L., M. A. O'Neal, and J. E. Pizzuto. 2009. Quantifying bank erosion on the South River from 1937 to 2005, and its importance in assessing Hg contamination. Applied Geography 29 (1):125-134. doi:10.1016/j.apgeog.2008.08.005.

Rhoads, B.L. 2003. Protocols for Geomorphic Characterization of Meander Bends in Illinois.

Rhoads, B. L. 2003. Protocols for geomorphic characterization of meander bends in Illinois. Prepared for Illinois Department of Natural Resources, Conservation 2000 Ecosystems Project – Embarras River 001-98, Department of Geography, University of Illinois, Urbana.

Richard, G. A., P. Y. Julien, and D. C. Baird. 2005. Statistical analysis of lateral migration of the Rio Grande, New Mexico. Geomorphology 71 (1-2):139-155. doi:10.1016/j.geomorph.2004.07.013.

Richardson, J. M., and I. C. Fuller. 2010. Quantification of channel planform change on

the lower Rangitikei River, New Zealand, 1949-2007: response to management? GeoScience ISSN 1179-4968.

Ritchie, J. C., and J. R. McHenry. 1990. Application of radioactive fallout cesium-137 for measuring soil erosion and sediment accumulation rates and patterns: A review. Journal of Environmental Quality 19 (2):215-233. doi:10.2134/jeq1990.00472425001900020006x.

Robert, A. 2014. River processes: An introduction to fluvial dynamics. New York, NY: Routledge.

Rogers, T., M. Mitchell, C. Kim, and T. Loesch. 2006. Determining orthophotograph accuracy. Geospatial Solutions 16 (3):26-29.

Rubey, W. W. 1952. Geology and mineral resources of the Hardin and Brussels Quadrangles in Illinois. Paper 201. US Geological Survery, Washington D.C.

Ruebush, B. C. 2011. In-situ tests of sound-bubble-strobe light barrier technologies to prevent the range expansions of Asian carp. Thesis, University of Illinois at Urbana-Champaign.

Sampson, S. J., J. H. Chick, and M. A. Pegg. 2009. Diet overlap among two Asian carp and three native fishes in backwater lakes on the Illinois and Mississippi rivers. Biological Invasions 11 (3):483-496. doi:10.1007/s10530-008-9265-7.

Schaffernak, F. 1950. Grundriss der Flussmorphologie und des Flussbaues: Vienna, Austria: Springer-Verlag.

Schoklitsch, A. 1937. Hydraulic structures: a text and handbook. New York, NY: The American Society of Mechanical Engineers.

Schottler, S. P., D. Engstrom, D. Blumentritt, C. Jennings, and L. Triplett. 2010. Fingerprinting sources of sediment in large agricultural river systems. Final Report to Minnesota Pollution Control Agency, St. Paul 68.

Schottler, S. P. 2012. Intensified tile drainage evaluation. Science Museum of Minnesota, Environmental and Natural Resources Trust Fund, Marine, MN.

Schottler, S. P., J. Ulrich, P. Belmont, R. Moore, J. W. Lauer, D. R. Engstrom, and J. E. Almendinger. 2014. Twentieth century agricultural drainage creates more erosive rivers. Hydrological Processes 28 (4):1951-1961. doi:10.1002/hyp.9738.

Schumm. 1969. River metamorphosis. Journal of the Hydraulics Division 95 (1):255-274.

———. 1977. The fluvial system. New York, NY: Wiley-Interscience.

———. 1979. Geomorphic thresholds: The concept and its applications. Transactions of the Institute of British Geographers 4 (4):485-515. doi:10.2307/622211.

———. 1985. Patterns of alluvial rivers. Annual Review of Earth and Planetary Sciences 13 (1):5-27. doi:10.1146/annurev.ea.13.050185.000253.

Schumm, S. A., and R. W. Lichty. 1965. Time, space, and causality in geomorphology. American Journal of Science 263 (2):110-119. doi:10.2475/ajs.263.2.110.

Severinghaus, L. L., and L. Chi. 1999. Prayer animal release in Taiwan. Biological Conservation 89 (3):301-304. doi:10.1016/S0006-3207(98)00155-4.

Shields Jr., F. D., A. Simon, and L. J. Steffen. 2000. Reservoir effects on downstream river channel migration. Environmental Conservation 27 (1):54-66.

Simon, A. 1989. A model of channel response in disturbed alluvial channels. Earth Surface Processes and Landforms 14 (1):11-26. doi:10.1002/esp.3290140103.

Simon, A., and A. J. C. Collison. 2002. Quantifying the mechanical and hydrologic effects of riparian vegetation on streambank stability. Earth Surface Processes and Landforms 27 (5):527-546. doi:10.1002/esp.325.

Simon, A., and C. R. Thorne. 1996. Channel adjustment of an unstable coarse-grained stream: opposing trends of boundary and critical shear stress, and the applicability of extremal hypotheses. Earth Surface Processes and Landforms 21 (2):155-180. doi:10.1002/(SICI)1096-9837(199602)21:2<155::AID-ESP610>3.0.CO;2-5.

Simons, D. B., and M. L. Albertson. 1960. Uniform water conveyance channels in alluvial materials. Journal of the Hydraulics division 86 (5):33-71.

Sin, S. N., H. Chua, W. Lo, and L. M. Ng. 2001. Assessment of heavy metal cations in sediments of Shing Mun River, Hong Kong. Environment International 26 (5–6):297-301. doi:0.1016/S0160-4120(01)00003-4.

Slama, C. C., C. Theurer, and S. W. Henriksen. 1980. Manual of photogrammetry. Falls Church, VA: American Society of photogrammetry.

Smakhtin, V. U. 2001. Low flow hydrology: A review. Journal of Hydrology 240 (3-4):147-186. doi:10.1016/S0022-1694(00)00340-1.

Smith, M. L. 2017. Minnesota's largest invasive carp caught in Redwood Falls. Star Tribune. http://www.startribune.com/minnesota-s-largest-invasive-carp-caught-in-redwood-falls/427263551/ (accessed April, 5 2018).

Smith, N. D., and D. G. Smith. 1984. William River: An outstanding example of channel widening and braiding caused by bed-load addition. Geology 12 (2):78-82. doi:10.1130/0091-7613(1984)12<78:WRAOEO>2.0.CO;2.

Spangler, T. 2014. $18 billion would keep Asian carp out of Great Lakes. USA Today. https://www.usatoday.com/story/news/nation/2014/01/06/asian-carp-report-great-lakes/4348241/ (accessed April 5, 2018).

Steil, M. 2007. NOAA says Dead Zone could be largest ever. MPR News. https://www.mprnews.org/story/2007/07/17/deadzonesize (accessed April, 5, 2018).

Steinberg, S. L., and S. J. Steinberg. 2015. Gis research methods: Incorporating spatial perspectives: Redlands, CA: Esri Press.

Strupczewski, W. G., V. P. Singh, and W. Feluch. 2001. Non-stationary approach to at-site flood frequency modelling I. Maximum likelihood estimation. Journal of Hydrology 248 (1-4):123-142. doi:10.1016/S0022-1694(01)00397-3.

Surian, N., and A. Cisotto. 2007. Channel adjustments, bedload transport and sediment sources in a gravel-bed river, Brenta River, Italy. Earth Surface Processes and Landforms 32 (11):1641-1656. doi:10.1002/esp.1591.

Surian, N., L. Mao, M. Giacomin, and L. Ziliani. 2009. Morphological effects of different channel-forming discharges in a gravel-bed river. Earth Surface Processes and Landforms 34 (8):1093-1107. doi:10.1002/esp.1798.

Tal, M., K. Gran, A. B. Murray, C. Paola, and D. M. Hicks. 2004. Riparian vegetation as a primary control on channel characteristics in multi-thread rivers. Riparian Vegetation and Fluvial Geomorphology 1:43-58. doi:10.1029/008WSA04.

Tal, M., and C. Paola. 2007. Dynamic single-thread channels maintained by the interaction of flow and vegetation. Geology 35 (4):347-350. doi:10.1130/G23260A.1.

Teller, J. T., D. W. Leverington, and J. D. Mann. 2002. Freshwater outbursts to the oceans from glacial Lake Agassiz and their role in climate change during the last deglaciation. Quaternary Science Reviews 21 (8-9):879-887. doi:10.1016/S0277-3791(01)00145-7.

Thorleifson, L. 1996. Review of Lake Agassiz history. Sedimentology, Geomorphology, and History of the Central Lake Agassiz Basin. Geological Association of Canada Field Trip Guidebook B 2:55-84.

Thorne, C., C. Alonso, D. Borah, S. Darby, P. Diplas, P. Julien, D. Knight, J. Pizzuto, M. Quick, and A. Simon. 1998. River width adjustment. I: Processes and mechanisms. Journal of Hydraulic Engineering 124 (9): 881-902. doi:10.1061/(ASCE)0733-9429(1998)124:9(881).

Thorne, C., J. Murphey, and W. Little. 1981. Bank stability and bank material properties in the bluffline streams of northwest Mississippi. Appendix D, Report to the Corps of Engineers, Vicksburg District under Section 32.

Thorne, C. R., A. P. G. Russell, and M. K. Alam. 1993. Planform pattern and channel evolution of the Brahmaputra River, Bangladesh. Geological Society, London, Special Publications 75 (1):257-276. doi:10.1144/GSL.SP.1993.075.01.16.

Thorne, C. R., and N. K. Tovey. 1981. Stability of composite river banks. Earth Surface Processes and Landforms 6 (5):469-484. doi:10.1002/esp.3290060507.

Tip of the Mitt Watershed Council. 2014. How to Iidentify bighead, silver, black, and grass carp. http://www.watershedcouncil.org/learn/aquatic%20invasive%20species/asian-carp/how-to-identify-bighead-and-silver-carp/ (accessed April 25, 2015)

Trimble, S. W., and R. U. Cooke. 1991. Historical sources for geomophological research in the United States. The Professional Geographer 43 (2):212-228. doi:10.1111/j.0033-0124.1991.00212.x.

U.S. Department of the Interior. 1996. National Mapping Program Technical Instructions, Part 2. Reston, Virginia.

Unwin, D. J. 1995. Geographical information systems and the problem of'error and uncertainty'. Progress in Human Geography 19 (4):549-558.

Upham, W. 1896. The glacial lake agassiz. US Geological Survey, Washington D.C.

Urban, M. A., and B. L. Rhoads. 2003. Catastrophic human-induced change in stream-channel planform and geometry in an agricultural watershed, Illinois, USA. Annals of the Association of American Geographers 93 (4):783-796. doi:10.1111/j.14678306.2003.09304001.x.

USACE. 2007. Minnesota River 9-foor channel project - Dredged material managemnt plan/environmental assessment - Minnesota River about I-35W bridge. US Army Corps of Engineers, St. Paul, MN

———. 2014. GLMRIS Report: Great Lakes and Mississippi River Interbasin Study. cited 4/15/2015. US Army Corps of Engineers.

VanLooy, J. A., and C. W. Martin. 2005. Channel and vegetation change on the Cimarron River, southwestern Kansas, 1953–2001. Annals of the Association of American Geographers 95 (4):727-739. doi:10.1111/j.1467-8306.2005.00483.x.

Vogel, R. M., C. Yaindl, and M. Walter. 2011. Nonstationarity: Flood magnification and recurrence reduction factors in the United States. Journal of the American Water Resources Association 47 (3):464-474. doi:10.1111/j.1752-1688.2011.00541.x.

Vörösmarty, C. J., M. Meybeck, B. Fekete, K. Sharma, P. Green, and J. P. M. Syvitski. 2003. Anthropogenic sediment retention: Major global impact from registered river impoundments. Global and Planetary Change 39 (1-2):169-190. doi:10.1016/S0921-8181(03)00023-7.

Wang, D., and M. Hejazi. 2011. Quantifying the relative contribution of the climate and direct human impacts on mean annual streamflow in the contiguous United States. Water Resources Research 47 (10). doi:10.1029/2010WR010283.

Wellmeyer, J. L., M. C. Slattery, and J. D. Phillips. 2005. Quantifying downstream impacts of impoundment on flow regime and channel planform, lower Trinity River, Texas. Geomorphology 69 (1-4):1-13. doi:10.1016/j.geomorph.2004.09.034.

Wickert, A. D., J. M. Martin, M. Tal, W. Kim, B. Sheets, and C. Paola. 2013. River channel lateral mobility: metrics, time scales, and controls. Journal of Geophysical Research: Earth Surface 118 (2):396-412. doi:10.1029/2012JF002386.

Williams, G. P. 1978. Bank-full discharge of rivers. Water Resources Research 14 (6):1141-1154. doi:10.1029/WR014i006p01141.

Winterbottom, S. J. 2000. Medium and short-term channel planform changes on the Rivers Tay and Tummel, Scotland. Geomorphology 34 (3-4):195-208. doi:10.1016/S0169-555X(00)00007-6.

Wishart, D., J. Warburton, and L. Bracken. 2008. Gravel extraction and planform change in a wandering gravel-bed river: The River Wear, Northern England. Geomorphology 94 (1–2):131-152. doi: 10.1016/j.geomorph.2007.05.003.

Wohl, E. 2012. Identifying and mitigating dam-induced declines in river health: Three case studies from the western United States. International Journal of Sediment Research 27 (3):271-287. doi:10.1016/S1001-6279(12)60035-3.

Wright Jr, H., K. Lease, and S. Johnson. 1998. Glacial River Warren, Lake Pepin, and the environmental history of southeastern Minnesota. In Contributions to quaternary studies in Minnesota. ed. C.J. Patterson and H.E. Wright Jr., 131-140. Minneapolis, MN: Minnesota Geological Survey Report on Investigations.

Yalin, M. S., and A. F. Da Silva. 2001. Fluvial processes.Londan, England: CRC Press.

Yang, C. T. 1971. On river meanders. Journal of Hydrology 13:231-253. doi:10.1016/0022-1694(71)90226-5.

Yao, Z., J. Xiao, W. Ta, and X. Jia. 2013. Planform channel dynamics along the Ningxia–Inner Mongolia reaches of the Yellow River from 1958 to 2008: Analysis using Landsat images and topographic maps. Environmental Earth Sciences 70 (1):97-106. doi:10.1007/s12665-012-2106-0.

Yuan, F., P. Larson, R. Mulvihill, D. Libby, J. Nelson, T. Grupa, and R. Moore. 2017.

Mapping and Analyzing Stream Network Changes in Watonwan River
Watershed, Minnesota, USA. International Journal of Geo-Information 6
(11):369. doi:10.3390/ijgi6110369.

Yuan, F., and M. Mitchell. 2014. Long-term climate change at four rural stations in
Minnesota, 1920-2010. Journal of Geography and Geology 6 (3):228.

Zanoni, L., A. Gurnell, N. Drake, and N. Surian. 2008. Island dynamics in a braided river
from analysis of historical maps and air photographs. River Research and
Applications 24 (8):1141-1159. doi:10.1002/rra.1086.

Zapata, F. 2003. The use of environmental radionuclides as tracers in soil erosion and
sedimentation investigations: recent advances and future developments. Soil and
Tillage Research 69 (1-2):3-13. doi:10.1016/S0167-1987(02)00124-1.

Appendix

Appendix A
Full registry of every collected aerial photograph used in this study sorted by year and
county.

County & Year	Photo I.D. Number	Number of GCPs Used	Total RMS Error
Blue Earth 1937	BJG-1-3**	8	0.943136
	BIP-5-92**	8	0.718186
	BIP-9-9**	8	0.661759
	BIP-9-35**	9	0.936103
Le Sueur 1937	BJG-2-25**	8	0.803199
	WF-5-338	8	0.748209
	WF-5-341	8	0.715205
	WF-5-396	8	0.915635
	WF-5-398	8	0.991539
	WF-5-345	8	0.475706
	WF-5-347	8	0.635866
	WF-5-348	10	0.978789
	WF-5-404	8	0.853785
	WF-5-406	9	0.889252
	WF-5-407	8	0.771299
	WF-5-409	8	0.923454
	WF-5-356	8	0.867018
	WF-5-354	9	0.931321
Scott 1937	BJM-3-83**	9	0.891791
	WJ-9-395	8	0.615319
	WJ-9-393	8	0.809855
	WJ-9-392	8	0.854515
	BJM-4-100**	8	0.859631

	WJ-7-326	8	0.927112
	WJ-7-305	8	0.803489
	WJ-5-255	8	0.776959
	WJ-5-227	8	0.778667
	WJ-5-217	9	0.568294
	WJ-5-219	8	0.863107
	WJ-5-221	8	0.865138
	WJ-5-223	9	0.85996
	WJ-5-178	9	0.917537
	WJ-4-172	9	0.88825
	WJ-4-123	8	0.968202
	WJ-5-268	8	0.985806
	WJ-3-78	9	0.913501
	WJ-3-73	8	0.835747
	WK-10-752	8	0.552281
Dakota 1937	WK-6-490	8	0.647758
	WK-8-650	9	0.892791
	WK-8-648	8	0.788822
	WK-5-368	8	0.959985
	WK-8-642	8	0.918655
	WN-2-146	8	0.393456
Blue Earth 1951	BIP-2G-209*	9	0.921057
	BIP-1G-144*	10	0.891252
	BIP-2G-130*	8	0.699735
	BIP-2G-160*	8	0.627338
Le Sueur 1951	WF-01H-150	9	0.6684
	WF-02H-048	9	0.994594
	WF-02H-057	8	0.971867
	WF-05H-018	8	0.782464
	WF-04H-004	8	0.775642
	WF-04H-102	8	0.951251
	WF-04H-109	8	0.708532
	WF-02H-203	8	0.823723
	WF-02H-124	9	0.668544
	WF-02H-117	8	0.735107
Scott 1951	WJ-3H-3	10	0.948917
	WJ-3H-115	8	0.96663
	WJ-3H-120	9	0.9747

	WJ-3H-122	9	0.744484
	WJ-5H-173	8	0.99068
	WJ-5H-171	8	0.708331
	WJ-4H-51	8	0.964089
	WM-4H-79	9	0.926328
	WM-5H-74	12	0.641114
	WM-2H-119	8	0.636515
	WM-2H-193	9	0.760185
	WJ-2H-191	10	0.86426
	WJ-2H-189	8	0.83109
	WJ-5H-124	8	0.376638
	WJ-5H-126	9	0.823913
	WJ-2H-183	8	0.834361
	WJ-2H-182	9	0.782781
	WJ-2H-180	10	0.961046
Dakota 1951	WK-2H-178	9	0.845294
	WK-5H-136	8	0.9113
	WK-5H-181	8	0.820057
	WK-5H-204	8	0.8903
Carver 1964	WJ-3EE-64	8	0.846215
	WJ-5EE-117	8	0.889534
	WJ-1EE-228	8	0.49325
	WJ-1EE-226	8	0.467654
	WJ-4EE-159	8	0.632615
	WJ-4EE-157	8	0.825204
	WJ-2EE-108	8	0.700044
	WJ-5EE-14	9	0.788962
	WJ-2EE-205	8	0.410915
	WJ-4EE-148	8	0.999628
Hennepin 1964	WN-1EE-8	8	0.535465
	WN-1EE-5	8	0.725886
	WN-1EE-4	8	0.459552
	WN-1EE-30	8	0.857565
	WN-1EE-26	8	0.558263
	WN-1EE-2	8	0.999143
	WN-1EE-16	8	0.245725
	WN-1EE-14	8	0.61563
	WK-4EE-69	8	0.560000
	WK-3EE-122	9	0.736709
	WJ-5EE-9	8	0.985039

	WJ-5EE-8	8	0.928404
	WJ-5EE-6	8	0.839852
Nicollet 1964	BIP-1EE-44	10	0.877704
	BIP-1EE-74	9	0.65574
	WF-4EE-91	10	0.892792
	WF-1EE-128	9	0.888442
	WF-4EE-94	8	0.805539
	WF-4EE-96	9	0.577345
	WF-2EE-27	8	0.489471
	WF-5EE-190	8	0.769535
	WF-5EE-192	10	0.918159
	WF-2EE-124	9	0.759734
	WF-5EE-48	8	0.627846
	WF-5EE-59	9	0.880104
	WF-5EE-194	8	0.934425
	WF-4EE-32	8	0.734137
	WF-1EE-5	8	0.987944
Blue Earth 1980	AS-BE-SO-14-79	8	0.817416
	AS-BE-MAN-MA-12	8	0.648751
	AS-BE-MAN-MB-7	8	0.866059
	AS-BE-MAN-MA-1	8	0.895093
	AS-BE-LIME-LM-25	8	0.994281
	AS-BE-LIME-LM-24	8	0.707572
Nicollet 1980	AS-NIC-BEL-BD-12**	8	0.82821
	AS-NIC-OSH-OW-06_E*	8	0.659469
	AS-NIC-OSH-OW-06*	8	0.533789
Le Sueur 1980	AS-LES-KAS-KA-32	9	0.595707
	AS-LES-KAS-KA-28	8	0.500884
	AS-LES-KAS-KA-15	8	0.756206
	AS-LES-KAS-KA-10	8	0.779874
	AS-LES-KAS-KA-04	9	0.559004
	AS-LES-OTT-OT-33	8	0.566047
	AS-LES-OTT-OT-27	8	0.528658
	AS-LES-OTT-OT-22	8	0.864734
	AS-LES-OTT-OT-15	8	0.530746
	AS-LES-OTT-OT-11	8	0.944928
Sibley 1980	AS-SIB-HEN-35	8	0.528763

	AS-SIB-HEN-26	8	0.875494
	AS-SIB-HEN-24	8	0.798729
	AS-SIB-HEN-13*	8	0.824433
	AS-SIB-HEN-13	8	0.978362
	AS-SIB-HEN-12	8	0.989861
	AS-SIB-JESS-35	8	0.906574
	AS-SIB-FAX-07	8	0.627286
	AS-SIB-FAX-34	8	0.666664
	AS-SIB-FAX-35	8	0.798153
	AS-SIB-FAX-36	8	0.844069
Scott 1980	AS-SCO-BLA-R26-36	8	0.77532
	AS-SCO-BLA-R26-25	8	0.960128
	AS-SCO-BLA-R26-24	8	0.889988
	AS-SCO-BLA-R26-13	8	0.951592
	AS-SCO-BLA-R25-18	8	0.927822
	AS-SCO-BLA-R25-8	8	0.933821
	AS-SCO-BLA-R25-5	8	0.537953
	AS-SCO-BLA-R25-4	8	0.572957
	AS-SCO-BLA-R25-3	8	0.927834
	AS-SCO-JACK-02	8	0.759419
	AS-SCO-SHA-T115-R23-01	9	0.848379
	AS-SCO-SHA-T115-R22-06	8	0.277945
	AS-SCO-SHA-T115-R22-05	8	0.425829
	AS-SCO-SHA-T115-R22-04	8	0.419313
	AS-SCO-SAV-06	9	0.93885
	AS-SCO-SAV-08	8	0.872587
	AS-SCO-SHA-T115-R22-01	8	0.787476
Carver 1980	AS-CAR-SANF-T114-R24-31**	8	0.979884
	AS-CAR-SANF-T114-R24-29**	8	0.887107
	AS-CAR-SANF-T114-R24-28**	8	0.763447
	AS-CAR-SANF-T114-R24-15**	8	0.767714
	AS-CAR-SANF-T114-R24-14*	8	0.475768
	AS-CAR-SANF-T114-R24-12*	8	0.63236
	AS-CAR-SANF-T114-R23-7E*	8	0.730462

	AS-CAR-SANF-T114-R23-6E*	8	0.89166
	AS-CAR-CAR-30*	8	0.702322
	AS-CAR-CAR-20*	8	0.825718
	AS-CAR-CAR-17*	8	0.749966
	AS-CAR-CHA-T115-R23-9*	8	0.802729
	AS-CAR-CHA-T115-R23-3*	8	0.891705
Hennepin 1980	AS-HEN-EP-35**	8	0.802236
	AS-HEN-EP-36**	9	0.818521
Dakota 1980	SCAN-L-10-WestHalf	8	0.985676
	SCAN-L-10-EastHalf	8	0.648762
	SCAN-L-11-WestHalf	8	0.344481
	SCAN-L-11-EastHalf	8	0.60665
	SCAN-K-12-WestHalf	8	0.796727
	SCAN-J-12-EastHalf	8	0.680568

Aerial photographs were obtained from the University of Minnesota online Aerial Index or scanned at the Borchert Library. Labeling contains type of image (aerial slide, scanned), county, township, subsection within township, and the corresponding number of the individual photos. *Not all Townships contain subsections.
*= Photo from previous year
**= Photo from following year

Appendix B
"QuantifyingRegistrationError" Script from Lea and Legleiter (2016) with modifications by Mitchell Donovan (Doctoral Candidate at Utah State University).
%% Quantifying spatial variations in image registration error
% Devin M. Lea and Carl J. Legleiter
% 'Refining measurements of lateral channel movement from image time
% series by quantifying spatial variations in registration error'
% Correspondance to: Devin Lea (dlea@uoregon.edu)
% Last modified: 11-30-15

%% NOTES:
% This script uses MATLAB functions to iteratively calculate error vectors
% (\epsilon) and the components of the error vectors (\epsilon_x and
% \epsilon_y, sometimes referred to as E_x and E_y) using leave-one-out
% cross-validation for a set of ground control point (GCP) coordinates
% supplied by the user. Eight transformation equations are available to
% the user with the cp2tform function for calculating registration errors

% between the base image coordiantes and the matching predicted image
% coordinates on the warped image. After the error residuals have been
% calculated, the script creates an interpolated surface of error values
% using one of five chosen algorithms. A separate script
% (ChannelChangeSignif.m) uses the error surfaces to compared the
% endpoints of channel migration vectors supplied by the user to determine
% if observed lateral channel migration exceeds local registration error.

% The code and its comments are written with the assumption the user is
% supplying one input image to be registered to a single base image;
% however, the script can be easily modified if more than one input image
% will be registered to the base image.

% Comments with two spaces after the % sign indicate pre-script info
% Comments with one space indicate description of what script is doing
%Comments with zero spaces indicate code that is currently commented out
%but could be used. Comments above the code should note when the code that
%is commented out is suitable to use.

%% CREDITS:
% Devin M. Lea - University of Wyoming, Department of Geography
% Now at University of Oregon, Department of Geography
% dlea@uoregon.edu
% Carl J. Legleiter - Department of Geography, University of Wyoming
% Carl.Legleiter@uwyo.edu

%% LICENSE:
% Copyright (C) 2015 Devin M. Lea and Carl J. Legleiter
%
% This program is free software: you can redistribute it and/or modify
% it under the terms of the GNU General Public License as published by
% the Free Software Foundation, either version 3 of the License, or
% any later version.
%
% This program is distributed in the hope that it will be useful,
% but WITHOUT ANY WARRANTY; without even the implied warranty of
% MERCHANTABILITY or FITNESS FOR A PARTICULAR PURPOSE. See the
% GNU General Public License for more details.
%
% For the full GNU General Public License, please see:
% <http://www.gnu.org/licenses/>.
%
% This software is made available to potential users AS IS, without any
% promise of technical support. The user is solely responsible for

% implementing the code for use in his/her own project, without
% assistance from the authors.

%% Manual inputs required from the user + possible changes
% THIS SCRIPT REQUIRES THE FOLLOWING USER INPUTS:
% 1) Base image and warp image GCP locations for each warp and base image
% pair. Locations are provided using image coordinates in a n x 2 matrix,
% where n is the number of GCPs. See the Import ground control points
% section for more details.
% ADDITIONALLY, THE USER MAY WISH TO CHANGE THE FOLLOWING:
% 1) The maximum error value displayed on the y axis for the boxplot in the
% section 'Create boxplot for visualizing error distribution'. The error is
% currently calculated as the rounded 90th percentile error value for the
% transformation method with the largest maximum error. However, this
% inherently will leave out some outlier error values that are off the
% display. The user should change this value (set by the equation
% (round(max(prctile(XYresid_all,90))))) dependent on their distribution
% of error and error visualization needs.
% 2) Error residuals used for error surface interpolation. The script is
% set up to create an interpolated surface for E_x and E_y using the
% residual error from the 2nd order polynomial transformation. If error
% from another transformation method is desired, changes need to be made to
% griddata and the caxis in the section 'Create interpolated surface of
% error values'
% 3) The user may wish to edit caxis in the section 'Create interpolated
% surface of error values' to make the positive and negative values on the
% colorbar equal in magnitude. Similarly, xlim and ylim could be edited.

%% Import ground control points
% After matching locations in an input image and base image with ground
% control points (GCPs) using appropriate software (e.g. Erdas Imagine,
% ENVI), export the GCP coordinates for the input and base images from that
% software to a text file. The coordinates will be saved as image
% coordinates. For the easiest transfer to MATLAB, open the text file in
% Microsoft Excel so that each column represents an X or Y coordinate for
% the base or warp image. In MATLAB, create two new variables in your
% workspace called 'b_GCPs' (for base image GCPs) and 'i_GCPs' (for input
% image GCPs). Copy and paste the X and Y coordinates for the input image
% from Microsoft Excel (or eqivalent program) to the variable 'i_GCPs' in
% MATLAB; do the same for the X and Y coordinates from the base image to
% paste into the variable 'b_GCPs'. When you have finished, both 'i_GCPs'
% and 'b_GCPs' variables should be n x 2 double matrices, where n is the
% number of GCPs you matched between the input and base images.

```
% NOTE: This analysis assumes you are only using two images (base and
% warp). If you have more than one input image you want to register to your
% base image, you will want to edit the variable names to avoid confusion.
% For example, in the Lea and Legleiter study for which this code was
% developed, five input images were registered to the (sixth) base image.
% To avoid confusion, the year of each input image was added to the end of
% its associated 'i_GCPs' and 'b_GCPs' variables.
% Example:
% In the Lea and Legleiter study, the base image was acquired in 2012. One
% of the input images to be registered was acquired in 1980. Thus:
% 'b_GCPs_1980' refers to GCPs placed on the 2012 base that are matched to
% GCPs placed on the 1980 input image
% 'i_GCPs_1980' refers to GCPs placed on the 1980 input image

%% Set up working directory
% Tell MATLAB where to look for any functions we might call
workDir = 'F:\Devon_Thesis\Final_ArcWork\MatLab\MatScript\1964_1980';
cd(workDir);
files = dir('*gcp.txt'); %searching for all files ending in gcp.txt, representing the image
files other than the base/reference image.
baseFile = '1964_1980gcp.txt'; %specify a name for the base file that will be loaded for
b_GCPs.
gcpData = struct; %Sets gcpData up as a structured data variable so it can store the
information efficiently.

for i = 1:length(files)

yr = files(i).name(1:4);
fprintf(yr);
fprintf('\n');

varNames = {'Id','POINT_X','POINT_Y'}; % variable names I want to keep
gcp2015table = readtable(baseFile,'ReadVariableNames',1,'Delimiter',','); %load base
GCP table
Id = gcp2015table.(varNames{1});        % store Id
POINT_X = gcp2015table.(varNames{2});   % store x coords
POINT_Y = gcp2015table.(varNames{3});   % store y coords
gcp2015table = table(Id,POINT_X,POINT_Y); % replace table by creating new table
with only these vars
gcp2015table = sortrows(gcp2015table,'Id'); % sort table at end because sorting the initial
large table is slower
```

```matlab
gcptable = readtable(files(i).name,'ReadVariableNames',1,'Delimiter',','); %load GCP
table for other images
Id = gcptable.(varNames{1});        % store Id
POINT_X = gcptable.(varNames{2});   % store x coords
POINT_Y = gcptable.(varNames{3});   % store y coords
gcptable = table(Id,POINT_X,POINT_Y); % replace table by creating new table with
only these vars
gcptable = sortrows(gcptable,'Id'); % sort table at end because sorting the initial large
table is slower

% intersect the two tables together, keeping only
% ids that appear in both tables
gcpTable = innerjoin(gcptable,gcp2015table,'key','Id');
format long % use this to stop matlab from truncating. default is "format short"
gcpTable;

%Converting table to an array so that I can work with the data.
gcpCoords = table2array(gcpTable);

gcpData(i).year = yr;
gcpData(i).b_GCPs = gcpCoords(:,4:5);
gcpData(i).i_GCPs = gcpCoords(:,2:3);

b_GCPs = gcpCoords(:,4:5);
i_GCPs = gcpCoords(:,2:3);

% If you have more than one input image to be warped as in the Lea and
% Legleiter study, note you will need to alter the following code for each
% warp and base pair for which you want to assess georegistration error.

% To make sure the GCPs coordinates are generally located correctly in
% space, use a simple scatter plot:
% Scatter plot for base image GCPs
   % figure
   % scatter(b_GCPs(:,1),b_GCPs(:,2),'b')
   % set(gca,'YDir','reverse'); axis equal; box on
   % xlabel('Image X coordinate')
   % ylabel('Image Y coordinate')
   % title('Base Image GCPs','fontsize',14)
   % % Scatter plot for input image GCPs
   % figure
   % scatter(i_GCPs(:,1),i_GCPs(:,2),'r')
   % set(gca,'YDir','reverse'); axis equal; box on
   % xlabel('Image X coordinate')
```

```
    % ylabel('Image Y coordinate')
    % title('Input Image GCPs','fontsize',14)
% NOTE: The Y-axis is called and reversed in the second command for these
% scatter plots because the origin of image coordinates is usually in the
% top left corner, as opposed to a traditional grid where the origin is
% placed at the bottom left corner (assuming x and y are positive values).

%% Leave-one-out cross-validation for geometric transformation of GCPs
% This section uses a for loop to iteratively withhold one GCP pair,
% transform map coordinates from the input image to the base image using
% the remaining n-1 GCP pairs and one of eight chosen transformation
% equations, and predict the x and y coordinate values of the withheld
% GCP on the resulting warped image by inputing the withheld base GCP
% coordinates into the fit transformation equation.

% Start loop to withhold the j'th pair of input and base GCPs per iteration
for j = 1:length(i_GCPs)
    % Get all GCP x coordinate values from input image
    Xi = i_GCPs(:,1);
    % Set j'th x coordinate equal to new variable and remove the chosen
    % coordinate from the list of all x coordinate values
    Xi_h = Xi(j);
    Xi(j) = [ ];
    % Get all GCP y coordinate values from input image
    Yi = i_GCPs(:,2);
    % Set j'th y coordinate equal to new variable and remove the chosen
    % coordinate from the list of all y coordinate values
    Yi_h = Yi(j);
    Yi(j) = [ ];
    % Combine Xi and Yi into a single matrix
    XYi = [Xi Yi];
    % Get all GCP x coordinate values from base image
    Xb = b_GCPs(:,1);
    % Set j'th x coordinate equal to new variable and remove the chosen
    % coordinate from the list of all x coordinate values
    Xb_h = Xb(j);
    Xb(j) = [ ];
    % Get all GCP y coordinate values from base image
    Yb = b_GCPs(:,2);
    % Set j'th x coordinate equal to new variable and remove the chosen
    % coordinate from the list of all x coordinate values
    Yb_h = Yb(j);
    Yb(j) = [ ];
    % Combine Xb and Yb into a single matrix
```

```
        XYb = [Xb Yb];
        % Combine the withheld points from the input and base image into two
        % matrices
        XYi_h = [Xi_h Yi_h];
        XYb_h = [Xb_h Yb_h];
        % Fit transformation equations to base image and input image GCP pairs.
        % NOTE: Values are divided (and later multiplied) by 1000 in the code
        % because large input values sometimes cause an error. This method was
        % adopted from a discussion found here:
        % http://www.mathworks.com/matlabcentral/newsreader/view_thread/30091
%       tform_sim = cp2tform((XYb/1000),(XYi/1000),'similarity');
%       tform_aff = cp2tform((XYb/1000),(XYi/1000),'affine');
%       tform_proj = cp2tform((XYb/1000),(XYi/1000),'projective');
%       tform_2poly = cp2tform((XYb/1000),(XYi/1000),'polynomial',2);
%       tform_3poly = cp2tform((XYb/1000),(XYi/1000),'polynomial',3);
%       tform_4poly = cp2tform((XYb/1000),(XYi/1000),'polynomial',4);
%       tform_pwl = cp2tform((XYb/1000),(XYi/1000),'piecewise linear');
%       tform_lwm = cp2tform((XYb/1000),(XYi/1000),'lwm');
        % Predict x and y coordinate values of withheld input image GCP using
        % transformation equations & combine coordinates into a matrix
        % 2nd Order Polynomial
        %[xm4, ym4] = [Xi_h/1000, Yi_h/1000];
        BPred = [Xi_h Yi_h];

        % Calculate residual vector distance XY (i.e., Euclidian distance, also
        % referred to as error vector /epsilon in the manuscript) and its x and
        % y components for each transformation method

        % 2nd Order Polynomial
        Xresid(j) = (Xb_h - (Xi_h));
        Yresid(j) = (Yb_h - (Yi_h));
        XYresid(j) = pdist2(XYb_h,(BPred));

    end

    % Transpose vectors containing error residuals
    gcpData(i).Xresid = Xresid';
    gcpData(i).Yresid = Yresid';
    gcpData(i).XYresid = XYresid';

    % Calculate maximum error, minimum error, and root-mean-square error for
    % the residual vector distances from each transformation method
    %maxE = max(XYresid');
    %minE = min(XYresid');
```

```matlab
XY2resid = XYresid'.^2;
RMSE = sqrt(((sum(XY2resid))/(length(XY2resid))));

% clearvars Xresid Yresid XYresid b_GCPs i_GCPs

end

%%% Plot histograms of error vectors
% Use the histograms to understand the distribution of error for each
% transformation method

hist(Xresid)
hist(Yresid)
hist(XYresid)


%%% Create boxplot for visualizing error distribution

% Create the boxplot
boxplot(XYresid,'colors','k','symbol','k*')
% The user may wish to change the maximum error displayed on the y axis;
% see Manual inputs + possible changes section for more details
axis([0.5,1.5,-0.5,(round(max(prctile(XYresid,100))))])
x1 = xlabel('Transformation Type','FontSize',15);
ylabel('GCP error (m)','FontSize',15);

%%% ANOVA test
% Tests statistical difference between means of eight transformation
% methods
%[p,table,stats] = anova1(XYresid_all);
%c = multcompare(stats);

% %%% Create interpolated surface of error values
% % Create meshgrid for calculating interpolated surface. Meshgrid size is
% % set by the minimum and maximum x and y values. A value 10% the size of
% % the range of all x and y values is added or subtracted to the meshgrid to
% % provide a buffer of space around the area of interest.
% [X,Y] = meshgrid((round(min(b_GCPs(:,1)))+0.5)-(round(range(b_GCPs(:,1))/10)):...
%     1:(round(max(b_GCPs(:,1)))+0.5)+(round(range(b_GCPs(:,1))/10)),...
%     (round(min(b_GCPs(:,2)))+0.5)-(round(range(b_GCPs(:,2))/10)):...
%     1:(round(max(b_GCPs(:,2)))+0.5)+(round(range(b_GCPs(:,2))/10)));
% % Translate values of base GCPs so they plot correctly with meshgrid
% bGCPs_trans = [(b_GCPs(:,1)-(min(b_GCPs(:,1)))+range(b_GCPs(:,1))/10) ...
%     (b_GCPs(:,2)-(min(b_GCPs(:,2)))+range(b_GCPs(:,2))/10)];
```

```
% % Use griddata to create an interpolated surface of error for E_y and E_x
% % (Vqy and Vqx, respectively) across the area defined by the convex hull of
% % the GCPs
% Vqy = griddata(b_GCPs(:,1),b_GCPs(:,2),Yresid,X,Y,'linear');
% Vqx = griddata(b_GCPs(:,1),b_GCPs(:,2),Xresid,X,Y,'linear');
%
% % Create figure to show interpolated error surface for E_y
% % NOTE: This does NOT show error and image coordinates in their true
% % location in space; the images are designed just to help the user
% % visualize areas of higher and lower error.
% figure
% kk = image(Vqy,'CDataMapping','scaled');
% % Set x and y axes limits
% xlim([0 round(range(b_GCPs(:,1))+((round(range(b_GCPs(:,1))/10))*2))])
% ylim([0 round(range(b_GCPs(:,2))+((round(range(b_GCPs(:,2))/10))*2))])
% xlabel('Image X coordinate')
% ylabel('Image Y coordinate')
% title('Interpolated \epsilon_y surface','fontsize',14)
% % Set all nan values outside the interpolated error surface to white
% set(kk,'alphadata',~isnan(Vqy))
% % Set colormap
% colormap('jet')
% % Colorbar, axes, and labeling
% h = colorbar;
% caxis([(min(Yresid)-(range(Yresid)/20)) ...
%    (max(Yresid)+(range(Yresid)/20))])
% ylabel(h, '\epsilon_y','fontsize',16)
% % Keep figure and use scatterplot to show locations of base GCPs on
% % interpolated surface
% hold on
% hh = scatter(bGCPs_trans(:,1),bGCPs_trans(:,2),50);
% set(hh,'MarkerEdgeColor','k','LineWidth',1.2)
%
% % Create figure to show interpolated error surface for E_x
% % NOTE: This does NOT show error and image coordinates in their true
% % location in space; the images are designed just to help the user
% % visualize areas of higher and lower error.
% figure
% kk = image(Vqx,'CDataMapping','scaled');
% % Set x and y axes limits
% xlim([0 round(range(b_GCPs(:,1))+((round(range(b_GCPs(:,1))/10))*2))])
% ylim([0 round(range(b_GCPs(:,2))+((round(range(b_GCPs(:,2))/10))*2))])
% xlabel('Image X coordinate')
% ylabel('Image Y coordinate')
```

```
% title('Interpolated \epsilon_x surface','fontsize',14)
% % Set all nan values outside the interpolated error surface to white
% set(kk,'alphadata',~isnan(Vqx))
% % Set colormap
% colormap('jet')
% % Colorbar, axes, and labeling
% % Colorbar axes set by min and max error values +/- 5% of range of error
% h = colorbar;
% caxis([(min(Xresid)-(range(Xresid)/20)) ...
%     (max(Xresid)+(range(Xresid)/20))])
% ylabel(h, '\epsilon_x','fontsize',16)
% % Keep figure and use scatterplot to show locations of base GCPs on
% % interpolated surface
% hold on
% hh = scatter(bGCPs_trans(:,1),bGCPs_trans(:,2),50);
% set(hh,'MarkerEdgeColor','k','LineWidth',1.2)

%% End QuantifyRegistrationError.m
% For determining statistical significance of migration vectors, use
% ChannelChangeSignif.m
% Save a .mat file of the variables generated in this script and load them
% for use with ChannelChangeSignif.m
save RegErrorResults.mat
```

Appendix C
R script written by Mitchell Donavan from Utah State University and modified Devon
Libby to fit the data used in this study

```
library("MASS") #required for 'calibrate'
#install.packages("G:/F_Drive_Arc_BU/Final_ArcWork/Error_Calc/Digitizing_Error/CS
V/Library/calibrate_1.7.2.zip")
library(calibrate) #Required for textxy that labels points.


years = c(1937,1951,1964,1980,1991,2013)

setwd("G:/F_Drive_Arc_BU/Final_ArcWork/Error_Calc/Digitizing_Error/CSV")

for (year in years){
  files = list.files(pattern= paste(year,"_*",sep=""))
  for (curr_file in files){
    for (j in (1:length(files))){
      err_data = read.csv(curr_file)
```

```r
    err_df=data.frame(matrix(NA, nrow = length(err_data[,1]), ncol = length(files)))
    colnames(err_df)=c("er_1_2","er_1_3","er_1_4",'er_2_3','er_2_4','er_3_4')

    assign(paste('err',j,sep="), abs(err_data$Mig_dist))
  }
  assign(paste('err',year,'_tot',sep="), c(err1, err2, err3, err4, err5, err6))
 }
}

#--------------------
#calculating quantiles
x = seq(from=0,to=1,by=.05)
quant.table= data.frame(matrix(NA, nrow = length(x), ncol = length(years)))
colnames(quant.table)=c('1937','1951','1964','1980','1991','2013')
quant.table$pctl= x

i=1
for (n in x){
  q1937 = round(quantile(err1937_tot,n),2)
  q1951 = round(quantile(err1951_tot,n),2)
  q1964 = round(quantile(err1964_tot,n),2)
  q1980 = round(quantile(err1980_tot,n),2)
  q1991 = round(quantile(err1991_tot,n),2)
  q2013 = round(quantile(err2013_tot,n),2)

  qtot=c(q1937,q1951,q1964,q1980,q1991,q2013)
  j=1
  for (k in qtot){
    quant.table[i,j] = k
    j=j+1
  }
  i=i+1
}

#plotting the quantile distritbutions for each year
for (j in 1:7){
  if (j==1){
    plot(x,quant.table[,j],type='l',lty=j,ylim=c(0,18),
        xlab='Quantile',ylab='Digitizing Error (m)',main='Image Digitizing Error')
  }
  else{
    par(new=T)
    plot(x,quant.table[,j],type='l',lty=j,ylim=c(0,18),xlab=",ylab=")
```

```
  }
}

grid(nx=NULL)
legend(.1,15,c('1937','1951','1964','1980','1991','2013'),lty=c(1,2,3,4,5,6))

boxplot(quant.table, main ='Digitizing Inconsistency', ylab='False Migration
(m)',xlab='Image year')
grid(nx=NULL)
dev.copy2pdf(file='G:/F_Drive_Arc_BU/Final_ArcWork/Error_Calc/Digitizing_Error/C
SV Boxplots.pdf.', width = 12, height = 8)
```

Appendix D
"ChannelChangeSignif" MATLAB script created by Lea and Legleiter (2016) with
additional lines of code added by Devon Libby.

```
%%  Assess statistical significance of lateral channel change
%  Devin M. Lea and Carl J. Legleiter
%  'Refining measurements of lateral channel movement from image time
%  series by quantifying spatial variations in registration error'
%  Correspondance to: Devin Lea (dlea@uoregon.edu)
%  Last modified: 11-30-15

%%  NOTES:
%  This script is used to assess the statistical significance of lateral
%  migration vectors. After interpolated surfaces are generated using
%  QuantifyRegistrationError.m, this script uses the endpoint verticies of
%  lateral migration vectors to create an error ellipse around the vertex
%  on the time 1 channel centerline and determines if the vertex on the
%  time 2 channel cenerline is inside or outside the error ellipse polygon.
%  If the vertex in time 2 is outside the error ellipse, the migration is
%  statistically significant, while if the vertex in time 2 is contained in
%  the error ellipse polygon the migration distance does not exceed the
%  error threshold and the change is not statistically significant.

%  The code and its comments are written with the assumption the user is
%  supplying one set of migration vectors from the registration of one
%  input image to a base image; however, comments describe where the script
%  can be modified if more than one set of migration vectors are being
%  assessed for significant channel change.
```

%% Manual inputs required from the user + possible changes

% THIS SCRIPT REQUIRES THE FOLLOWING USER INPUTS:
% 1) Variables calculated in QuantifyRegistrationError.m. Load them here if
% needed.
load RegErrorResults.mat
% 2) Migration vector distances, endpoint coordinates, and ID numbers for
% each endpoint coordinate and for each migration vector. See TestData
% Excel file for an example and 'Calculate statistical significance of

% migration vectors' section of this script for more details.
% 3) Real world coordinates from the top left corner of your base image.
% This is needed to convert the GCP coordinates in 'b_GCPs' from image
% coordinates to real world coordinates. This study assumes you will use
% UTM coordinates. In ArcGIS you can find the real world coordinate
% information about the top, left, right, and bottom pixel columns or rows
% by right-clicking your raster base image in the table of contents and
% selecting Properties -> Source. Find the values and set the coordinate
% for the x direction (i.e., easting for UTM) equal to the easting variable
% in this section. Similarly, set the coordinate for the y direction (i.e.,
% northing for UTM) equal to the northing variable.
easting = 0;
northing = 0;
% 4) Digitizing error. This is the estimated error associated with the
% user's channel bankline digitizing. The Lea and Legleiter study assumed
% this error was 2 meters based on precidence (set by Micheli and Kirchner,
% 2002; see reference in Lea and Legleiter) and based on image resolution
% of the images used in Lea and Legleiter. However, this variable will
% change based on the user and image resolution and should be changed
% accordingly in this section before error and statistical significance of
% change is assessed.
digError = 1.62;
% ADDITIONALLY, THE USER MAY WISH TO CHANGE THE FOLLOWING:
% 1) The type of interpolation calculated for scatteredInterpolant in the
% section 'Calculate statistical significance of migration vectors'. See
% MATLAB help on scatteredInterpolant for more information of the types of
% interpolation available.
% 2) If more than one pair of images are being analyzed for statistically
% significant change, the user might need to use different equations. The
% locations where these changes would be made is noted throughout the
% script.

%% Generating lateral migration vectors in ArcGIS
% In this section, real-world coordinates from the endpoints of lateral
% channel migration vectors (x_m1, y_m1; x_m2, y_m2 from Fig. 3) are pasted
% into a matrix called MigVecChng. This matrix also will contain a specific
% ID for each migration vector, a pair ID linking the two coordinates that
% define the migration vector, and the calculated migration vector
% distance. All of these variables making up the matrix are created and
% calculated in ArcGIS using the Planform Statistics Tools developed by Wes
% Lauer (currently at Seattle University). These tools are available for
% download at the National Center for Earth-Surface Dynamics website
% through the University of Minnesota at this webpage:
% http://www.nced.umn.edu/content/stream-restoration-toolbox

% The following section provides a detailed description of the steps that
% must be completed before the code at the end of the section can be run to
% calculate significant and not significant migration vectors.

% Visit the NCED website noted above, open the Planform Statistics tab, and
% download the ArcMap addin called PlanformTools2.0.esriAddIn to your
% working folder. You can also download other useful files, such as the
% powerpoint file named PlanformStatisticsTools_v2.0 for ArcGIS 10, which
% shows how all addin tools can be used.
% Launch ArcMap and from the main menu select Customize -> Add-In Manager
% to verify Planform Tools have installed successfully. Click on the
% Customize button and then New to set up a new toolbar from which you can
% access the tools. Give the toolbar a name like Planform Stats and click
% OK; a new, empty toolbar should be added to your ArcMap window. Place the
% tools on the toolbar by going to Commands tab of the Customize dialog and
% look under Add-In Controls, where you should see the three tools listed
% in the Commands panel. Highlight each of these tools in turn and drag it
% onto your new toolbar.

% Now you can digitize the bankfull channel for each image. Create a
% shapefile (polyline) for each image. Load the bankline shapefiles into
% ArcMAP and used the Editor Toolbar to start an editing session. Again,
% define the bankfull channel, which will not necessarily correspond to the
% edge of the water, especially if the image was acquired at low-flow
% conditions. The edge of continuous vegetation is generally a good
% indicator of bankfull stage. For each image date, create separate left
% and right banklines. Always digitize all banklines in the same direction,
% from upstream to downstream. Also, terminate your two banklines at the
% same position along the channel (i.e., don't extend one bankline further
% downstream on one side of the channel than on the other side). If your
% channel splits into multiple channels, interpret which is the main active
% channel and define your banklines for that channel alone.
% NOTE: the digitizing can also be performed in other software packages
% (e.g., ENVI); just export your vectors as shapefiles and load them into
% ArcMAP when you are finished digitizing.

% When you have digitized both banklines along your reach of interest, you
% can use the Centerline Interpolation tool in the Planform Statistics
% tools to create a channel centerline based on the banklines. See the
% associated PowerPoint for more details on the tool. To use the tool,
% click on the icon with two parallel lines and a series of dots between
% the lines. You will be prompted to select the left bankline (left side of
% the channel when facing downstream) - click OK then on the appropriate

% bankline, which should be highlighted in blue. Repeat this process for
% the right bankline. Next, you will be asked to specify a distance between
% centerline points; a value of ~20% of the mean bankfull width is
% recommended. Enter the maximum number of points to find - set this to a
% very large value, like 10,000. After the tool runs, you will be prompted
% to enter a new output shapefile name. You can now load the centerline
% into ArcMap and compare it to the position of your two banklines. Repeat
% this process for each image and its pair of right and left digitized
% bankfull lines to acquire a bankfull centerline. Along with each channel
% centerline shapefile, the Centerline Interpolation tool also produces a
% spearate text file. Refer to the PowerPoint for information on the
% contents of the shapefile and text file.

% After you have created an interpolated centerline for your images you can
% move on to measuring lateral channel migration. To do so, use the Lateral
% Distance Measurement tool from the Planform Statistics toolbox. First,
% you will be prompted to select the 'to' centerline to which distances
% will be measured to determine how far the channel has moved - this is the
% earlier (in time) centerline. Next select the 'from' or reference
% centerline (the latter dated image) that is used to store the migration
% distance data. You will then be asked whether you want to consider apex
% lines that connect bends that move by downstream translation; you usually
% will not need this tool (but consult the PowerPoint for more information)
% and you can just click OK. After the tool runs you will be asked to
% specify an ouput file name and a lateral distance from the centerline for
% drawing polygons created by this tool. A value about 1.5 times the mean
% channel width when the images were acquired should be sufficient. The
% tool will run some more and a number of lines will appear on your map,
% representing the inferred migration trajectory of the channel centerline
% between your two image dates.

% The lines indicating inferred migration trajectories are actually just
% graphics that are not included in a shapefile. The migration distance
% algorithm described in the PowerPoint file also creates a set of three
% imtermediate centerlines, which you can delete by selecting them with the
% black arrow tool and pressing delete; be careful to select the
% intermediate centerlines and not the perpendicular lines, which represent
% inferred migration trajectories. Once you have isolated the trajectory
% lines, convert them into a separate shapefile by right clicking on the
% name of the data frame (i.e., Layers) in the table of contents, and the
% choosing Convert Graphics to Features. In the resulting dialog, make sure
% Line graphics is selected, specify an output shapefile name, and click
% OK. You can then add the new migration trajectory line shapefile directly
% to your ArcMap document. To add the migration distance information to

% these lines, open the attribute table, select Add Field from the drop
% down list in the upper left, and provide a field name (e.g., MigrDist),
% change the Data Type to Float, and set Precision to 10 and Scale to 4.
% Next, right click on the name of the new field and select Calculate
% Geometry, click Yes to continue if prompted, and then OK to calculate the
% length of each of these lines.

%% Calculate statistical significance of migration vectors
% Create a new variable in MATLAB called MigVecChng, which will be an n x 5
% matrix, where n is the number of migration vector endpoint verticies
% (the number of migration vectors multiplied by two). The five columns
% will be copied in from the migration vectors shapefile attribute table
% in ArcMap and will contain the following values:
% column 1 = ID
% column 2 = Pair ID
% column 3 = Migration Dist calculated with Planform Statistics
% column 4 = X coordinate (real-world coordinate; e.g., UTM)
% column 5 = Y coordinate (real-world coordinate; e.g., UTM)
% An example of how your data should look when copied into MATLAB (you
% might want to paste from ArcMap to Excel, clean up the variables in
% Excel, then copy from Excel to MATLAB) is provided in TestData.xlsx.

% Assess the significance of lateral migration vectors against spatially
% variable error.
% First, create a series of interpolants that can evaluate the value of E_y
% and E_x at any query point (i.e., this will be the endpoints of the
% migration vectors) based on the E_y and E_x values supplied at the
% location of each GCP in the base image. The current selected
% interpolation is linear, but see MATLAB's documentation for
% scatteredInterpolant for other possible interpolation methods.
% Fx2 and Fy2 stand for the function being calculated for the second image
% in the time series (assuming the first image is the base image). If more
% than one warped image will be used, a sequential numbering can be
% continued, as in the example below.
Xresid = Xresid';
Yresid = Yresid';
Fx2 = scatteredInterpolant(b_GCPs(:,1),b_GCPs(:,2),Xresid,'linear');
Fy2 = scatteredInterpolant(b_GCPs(:,1),b_GCPs(:,2),Yresid,'linear');
%Fx3 = scatteredInterpolant(btiepnts_2011(:,1),btiepnts_2011(:,2),resid_X,'linear');
%Fy3 = scatteredInterpolant(btiepnts_2011(:,1),btiepnts_2011(:,2),resid_Y,'linear');

% Create an empty list to populate with 0's (not significant change) and
% 1's (significant change) for each migration vector.
sigList_SVE = [];

```matlab
% Start loop for length of the matrix
for ii = 1:length(MigVecChng)
    % If the row number is odd, create a 2 x 2 matrix that contains the x
    % and y coordinates for the two vertexes defining the end points of a
    % single migration vector
    if mod(ii,2) ~= 0
        chng = [MigVecChng(ii,4) MigVecChng(ii,5); MigVecChng(ii+1,4)
MigVecChng(ii+1,5)];
        % Use the endpoint of the migration vector that was on the channel
        % centerline in time 1 to calculate error for E_y and E_x at that
        % location in space using scatteredinterpolant
        Ey_time2 = Fy2(chng(1,1),chng(1,2));
        Ex_time2 = Fx2(chng(1,1),chng(1,2));
        %Ey_time3 = Fy3(chng(1,1)-300310,4562610-chng(1,2));
        %Ex_time3 = Fx3(chng(1,1)-300310,4562610-chng(1,2));
        % Calculate \epsilon
        Exy_time2 = sqrt(((Ey_time2)^2)+((Ex_time2)^2));
        %Exy_time3 = sqrt(((Ey_time3)^2)+((Ex_time3)^2));
        % Define the error ellipse
        % Assume ellipse center coordinates are at (0,0)
        x0 = 0;
        y0 = 0;
        % Define points in a vector used to create the ellipse
        t = -pi:0.01:pi;
        % If the channel centerline from the base image was used to infer
        % migration vector distances being assessed for statistical
        % significance, use the first set of x and y equations provided
        % Example: You have 3 images in a time series. The three images
        % were acquired in 2009, 2011, and 2012, and 2012 was the base
        % image to which 2009 and 2011 were registered. Use the following
        % equations if you are assessing the statistical significance of
        % the migration vector distances between 2011 and 2012 channel
        % centerlines, because we are assuming the base image (2012) has
        % E_y and E_y values of 0 meters. Digitizing error should be
        % provided in the manual inputs section.
        x=(x0+(sqrt(((Ex_time2)^2)+((digError)^2))))*cos(t);
        y=(y0+(sqrt(((Ey_time2)^2)+((digError)^2))))*sin(t);
        % If the channel centerline from the base image was not used to
        % infer migration vector distances being assessed for statistical
        % significance, use the second set of x and y equations provided.
        % Said another way, use the second set if both images used to infer
        % migration vector distances were warped to a separate base image
        % Example: You have 3 images in a time series. The three images
        % were acquired in 2009, 2011, and 2012, and 2012 was the base
```

```
% image to which 2009 and 2011 were registered. Use the following
% equations if you are assessing the statistical significance of
% the migration vector distances between 2009 and 2011 channel
% centerlines, because neither image was the base image during
% image registration. Digitizing error should be provided in the
% manual inputs section.
%x=(x0+(sqrt(((Ex_time2)^2)+((Ex_time3)^2)+((digError)^2))))*cos(t);
%y=(y0+(sqrt(((Ey_time2)^2)+((Ey_time3)^2)+((digError)^2))))*sin(t);
% Calculate angle \theta and use to rotate all points (x, y) in
% in vector t to new locations (xr, yr)
% NOTE: x' and y' from eqns. 7 and 8 in the Lea and Legleiter
% manuscript are equivalent to xr and yr
thet = atand((abs(Ey_time2)/(abs(Ex_time2))));
xr = x*cos(thet)-y*sin(thet);
yr = x*sin(thet)+y*cos(thet);
% Translate the rotated ellipse to its actual location in space
% along the time 1 channel centerline, defined as xt, yt.
xt = xr + chng(1,1);
yt = yr + chng(1,2);
% Determine if the endpoint of the migration vector located on the
% time 2 channel centerline is inside or outside the rotated error
% ellipse positioned with its center at the endpoint vertex for the
% selected migration vector along the time 1 channel centerline.
in = inpolygon(chng(2,1),chng(2,2),xt,yt);
% If the vertex along the time 2 channel centerline is not inside
% the error ellipse (i.e., migration vector distance > error
% ellipse), the change is statistically significant. Elseif the
% vertex along the time 2 channel centerline is inside the error
% ellipse (i.e., migration vector distance < error ellipse), the
% change is not statistically significant
if in == 0
    sig = 1;
elseif in == 1
    sig = 0;
end
% Add either a 1 (significant change) or 0 (not significant change)
% to a list, denoting the chosen migration vector either
% significant or not significant.
sigList_SVE = [sigList_SVE sig];
    end
end
% Transpose sigList
sigList_SVE = sigList_SVE';
```

```matlab
% If desired, assess the significance of lateral migration vectors against
% RMSE
% Create an empty list to populate with 0's (not significant change) and
% 1's (significant change) for each migration vector.
sigList_RMSE = [];
% Manually set RMSE
RMSE_time2 = .82;
RMSE_time3 = .82;
% Start loop for length of the matrix
for ii = 1:length(MigVecChng)
    % If the row number is odd, create a 2 x 2 matrix that contains the x
    % and y coordinates for the two vertexes defining the end points of a
    % single migration vector
    if mod(ii,2) ~= 0
        chng = [MigVecChng(ii,4) MigVecChng(ii,5); MigVecChng(ii+1,4)
MigVecChng(ii+1,5)];
        % Calculate migration vector length
        Mag_xy = pdist(chng);
        % Use this eqn if base image is one of the images being used
        % e.g. 2011 and 2012, where 2012 is base
        %RMSE_total = sqrt((((RMSE_time2)^2)+((digError)^2)));
        % Use this eqn if both images were warped to a separate base year
        % e.g. 2009 and 2011, where 2012 is base
        RMSE_total = sqrt((((RMSE_time2)^2)+((RMSE_time3)^2)+((digError)^2)));
        % Assess if migration vector length exceeds RMSE value
        if Mag_xy > RMSE_total
            sig = 1;
        elseif Mag_xy <= RMSE_total
            sig = 0;
        end
        sigList_RMSE = [sigList_RMSE sig];
    end
end
% Transpose sigList
sigList_RMSE = sigList_RMSE';

% If desired, assess the significance of lateral migration vectors against
% 90th percentile error
% Calculate 90th percentile for 2nd order polynomial error vectors
Perc90_time2 = prctile(XYresid,90);
%Perc90_time3 = prctile(resid_XY,90);
% Create an empty list to populate with 0's (not significant change) and
% 1's (significant change) for each migration vector.
sigList_90 = [];
```

```matlab
% Start loop for length of the matrix
for ii = 1:length(MigVecChng)
    % If the row number is odd, create a 2 x 2 matrix that contains the x
    % and y coordinates for the two vertexes defining the end points of a
    % single migration vector
    if mod(ii,2) ~= 0
        chng = [MigVecChng(ii,4) MigVecChng(ii,5); MigVecChng(ii+1,4)
MigVecChng(ii+1,5)];
        % Calculate migration vector length
        Mag_xy = pdist(chng);
        % Use this eqn if base image is one of the images being used
        % e.g. 2011 and 2012, where 2012 is base
        Perc90E_total = sqrt(((((Perc90_time2)^2)+((digError)^2)));
        % Use this eqn if both images were warped to a separate base year
        % e.g. 2009 and 2011, where 2012 is base
        %Perc90E_total = sqrt((((((Perc90_time2)^2)+((Perc90_time3)^2)+((digError)^2)));
        % Assess if migration vector length exceeds 90 percentile error
        if Mag_xy > Perc90E_total
            sig = 1;
        elseif Mag_xy <= Perc90E_total
            sig = 0;
        end
        sigList_90 = [sigList_90 sig];
    end
end
sigList_90 = sigList_90';

% Devon Libby's additions to simplify and automate the process of creating a
% csv file containing the information of significant and nonsignificant
% migration.

% Creating the header names in an array
ColumnNames = {'FID','Sig_SVE','Sig_RMSE','Sig90'};
% Creating the ID field which will serve as the foreign key in
% to join the significant/insignificant table with the migration
% measurement table in ArcMap. This is accomplished by selecting every
% other entry from column two in the MigVecChng variable and moving it
% into a standalone matrix
ID = MigVecChng(1:2:end,2:2);
% This concantenates the ID field, SVE, RMSE, and 90th percentile
% significant/insignificant tables into one.
sigList_All = [ID sigList_SVE sigList_RMSE sigList_90];
% This function was downloaded from
```

```
%  https://www.mathworks.com/matlabcentral/fileexchange/29933-csv-with-column-
headers
%  (credit: Keith Brady)and allows a csv file to be written from the newly
%  concatenated list and given the header from "ColumnNames".
csvwrite_with_headers('MATLABoutput.csv',sigList_All,ColumnNames)


% Devon Note: This next paragraph is no longer necessary to do since the previous block
of script was written to accomplish this automatically.
%% Displaying statistical significance in ArcMAP

% After creating SigList for SVE, RMSE, and 90th percentile, you can copy
% and paste the results into a Microsoft Excel file, save as a .csv file,
% and join the data to your lateral migration vectors in ArcGIS to visually
% inspect where channel change was and was not statistically significant.
% First, open a new Microsoft Excel sheet and copy the sigList_SVE n x 1
% vector into column B and starting with the first value in row 2.
% Similarly, copy the sigList_RMSE and SigList_90 n x 1 vectors into
% columns C and D, respectively, and also starting in row 2. For each of
% these three columns, provide an appropriate name label in row 1. For
% column A, give the name 'FID' to match to the attribute table of the
% channel migration vectors in ArcGIS. Starting in row 2, enter the value
% 0, in row 3 enter a value of 1, and then extend the values to match the
% number of migration vector endpoint verticies. When ready, save the file
% as a .csv file. Keep saving through any warnings - note you can only have
% a single sheet as part of the .csv file format (no multiple tabs at the
% bottom).

% Devon Note: Again most of this is unnecessary to manually do if the "Post MATLAB
Processing" script is run which again automates the process.  The symbology will still
need to be changed to fit the users graphical display purposes.

% Now in ArcMap with your migration vector shapefile (the ones you
% saved from the line graphics), open the attribute table and add three new
% fields for spatially variable error, RMSE, and 90th percentile error.
% Suggested names are 'Sig_SVE', 'Sig_RMSE' and 'Sig90'. Then right click
% on the layer in the Table of Contents and go to Joins and Relates -> Join.
% In the Join Data menu that appears, choose the field the join will be
% based on as 'FID'. Then load the .csv file from disk, and choose the
% field in the table to base the join on as 'FID'. Now if you open the
% attribute table you can see the joined columns to the attribute table. To
% save the joined columns to their respective columns you added to the
% attribute table, right click one of the column headings and select Field
% Calculator. Ignore any warnings, and in the Field Calculator window set
```

% the variable equal to the equivalent variable from the joined .csv file.
% The list should change then from a list of all 0's to a list of mixed 0's
% and 1's, assuming any change occurred. Repeat this for all three error
% metrics, then remove the join to the .csv file. You can display the 1's
% and 0's as different colors under Properties -> Symbology.

Appendix E
"Pre MATLAB Processing" script created by Devon Libby.

Pre MATLAB Processing Script.py
Created 11/9/16
Author Devon Libby
Description: The purpose of this script is to take the existing trajectory polyline
shapefile and give it correct measurements that identify migration rates to the
left with positive values and migration to the right with negative values. This script
also retrieves a point shapefile that identifies the two ends of each migration
line and assigns them x and y coordinates so it can be ran in the MATLAB script
"ChannelChangeSignif" produced by Lea and Legleiter (2016). This code can be
retrieved
from http://www.fluvialremotesensing.org/tools.html

Set the necessary product code
import arcinfo

# Import modules
import arcpy
import shutil

#Set Workspace
arcpy.env.workspace = arcpy.GetParameterAsText (0)
arcpy.env.overwriteOutput = True

Local variables:
#Mandatory Changes
    #This is the trajectory polyline file
TRJLF = arcpy.GetParameterAsText (1)
TRJLF_LYR = "TRJLF_lyr" #This is the temporary layer file needed to be able to
"Select Layer by Location" and make calculations
    #This needs to be the centerline of the earlier of the two years (T1)
T1_CL = arcpy.GetParameterAsText (2)

```python
#Other Variables
TFPath = arcpy.env.workspace #Path to store intermediate files produced during
geoprocessing
TF = "Temp_Folder" #Folder the intermediate files are stored in
Buffer = r"\Temp_Folder\Buffer.shp" #Buffer needed to select migration downstream
right
XY = "XYpoints.shp" #The point file that will contain the the columns needed for
"ChannelChangeSignif" Matlab Code
ExTable = "MigVecChng.xls"

#Create a place to house temporary/intermediate files to avoid cluttering primary folder
arcpy.CreateFolder_management(TFPath, TF)

# Add Field - This adds the field where migration measures will be stored
arcpy.AddField_management(TRJLF, "Mig_Dist", "DOUBLE", "7", "2", "", "",
"NULLABLE", "NON_REQUIRED", "")

# Calculate Field- Calculates and populates "Mig_Dist" field in meters
arcpy.CalculateField_management(TRJLF, "Mig_Dist", "\"!shape.length@meters!\"",
"PYTHON_9.3", "")

# Buffer- Buffer created on the downstream right side of the river to differentiate left and
right migration
arcpy.Buffer_analysis(T1_CL, Buffer, "1000 Meters", "RIGHT", "ROUND", "NONE",
"", "PLANAR")

# TRJLF first needs to have a layer file associated with it so it can then be used to "Select
Layer by Location"
arcpy.MakeFeatureLayer_management(TRJLF, TRJLF_LYR)

#Select Layer By Location - uses the layer file and buffer to select only the migration
trajectories that are downstream right
arcpy.SelectLayerByLocation_management(TRJLF_LYR,
"HAVE_THEIR_CENTER_IN", Buffer, "", "NEW_SELECTION", "NOT_INVERT")

# Calculate Field - Assigns a negative value to all downstream right migration
arcpy.CalculateField_management(TRJLF_LYR, "Mig_Dist", "!Mig_Dist! *-1",
"PYTHON_9.3", "")

# Select Layer By Attribute - Clears selected features so all attributes are able to be
geoprocessed
arcpy.SelectLayerByAttribute_management(TRJLF_LYR, "CLEAR_SELECTION", "")

# Feature Vertices To Points - Every trajectory line has a point created for each end
```

```
arcpy.FeatureVerticesToPoints_management(TRJLF, XY, "BOTH_ENDS")

# Add XY Coordinates - The point file created from the trajectory file is assigned XY
coordinates
arcpy.AddXY_management(XY)

#Table to Excel - Allows easy access to variables that need to be entered into the
"ChannelChangeSignif" code in Matlab
arcpy.TableToExcel_conversion(XY, ExTable, "NAME", "CODE")

#Deletes the Temporary Folder that was used to store intermediate data. Comment the
following line out to preserve intermediate file.
shutil.rmtree(arcpy.env.workspace + r"\Temp_Folder")

print "Alright Alright Alright"
```

Appendix F
The script for the function "csvwrite_with_headers" written by Keith Brady and retrieved
from http://www.mathworks.com/matlabcentral/fileexchange/29933-csv-with-column-
headers?focused=5176300&tab=function on 4/19/2017

```
% This function functions like the build in MATLAB function csvwrite but
% allows a row of headers to be easily inserted
%
% known limitations
%   The same limitation that apply to the data structure that exist with
%   csvwrite apply in this function, notably:
%       m must not be a cell array
```

```
%
% Inputs
%
%   filename    - Output filename
%   m           - array of data
%   headers     - a cell array of strings containing the column headers.
%                 The length must be the same as the number of columns in m.
%   r           - row offset of the data (optional parameter)
%   c           - column offset of the data (optional parameter)
%
%
% Outputs
%   None
function csvwrite_with_headers(filename,m,headers,r,c)

%%% initial checks on the inputs
if ~ischar(filename)
    error('FILENAME must be a string');
end

% the r and c inputs are optional and need to be filled in if they are
% missing
if nargin < 4
    r = 0;
end
if nargin < 5
    c = 0;
end

if ~iscellstr(headers)
    error('Header must be cell array of strings')
end


if length(headers) ~= size(m,2)
    error('number of header entries must match the number of columns in the data')
end

%%% write the header string to the file

%turn the headers into a single comma seperated string if it is a cell
%array,
header_string = headers(Aadland);
for i = 2:length(headers)
```

```matlab
    header_string = [header_string,',',headers(Aadland)];
end
%if the data has an offset shifting it right then blank commas must
%be inserted to match
if r>0
    for i=1:r
        header_string = [',',header_string];
    end
end

%write the string to a file
fid = fopen(filename,'w');
fprintf(fid,'%s\r\n',header_string);
fclose(fid);

%% write the append the data to the file

%
% Call dlmwrite with a comma as the delimiter
%
dlmwrite(filename, m,'-append','delimiter',',','roffset', r,'coffset',c);
```

Appendix G
"Post MATLAB Processing" script created by Devon Libby.

```python
# ----------------------------------------------------------------------------
# Post MATLAB Processing Script.py
# Created 11/7/16 Modified 4/24/17
# Author Devon Libby
# Description: The purpose of this script is to take the existing trajectory polyline
shapefile and populate fields that show if the lateral
# migration is statistically significant or insignificant according to Spatial Variable Error
(SVE), Root-Mean-Square-Error (RMSE), and 90th
# percentile. In addition, each trajectory line is assigned a downstream distance giving it a
spatial location. A field is also populated on
```

```
# every file with annual migration rates. Final outputs include a shapefile and excel table
with all measures of error, as well as, standalone
# shapefiles and excel files that replace statistically insignificantmigration distances with
a value of zero. Finally, a point shapefile named
# "Color_Mig" is created that can be used in combination with a desired symbology (e.g.
hot and cold color scheme) and data
# classification to create maps that visually represent channel mobility.
# --------------------------------------------------------------------------


# Import modules
import arcpy
import shutil

#Set Workspace: This workspace must contain both 1)the polyline file that stores the
trajectories and 2) the output CSV from Matlab
#with column 1 being "FID" column 2 being "SVE" column 3 being "RMSE", and
column 4 being "Nintey" Note: These must be exact spellings
#and capitalizations
arcpy.env.workspace = arcpy.GetParameterAsText (0)
arcpy.env.overwriteOutput = True

# Local variables:
#User Changes
    #This is the trajectory polyline file
TrjLF = arcpy.GetParameterAsText (1)
    #This is output CSV storing "FID", "SVE", "RMSE", and "Nintey" columns that were
copied from Matlab output variables
SigCSV = arcpy.GetParameterAsText (2)
    #The number of years between the two centerlines
NumYears = arcpy.GetParameterAsText (3)
    #Depending on the River direction flow, the Coordinate Priority along which the river
(route.shp) accumulates measure may need to be changed
CoorPriority = arcpy.GetParameterAsText (4)
    #Centerline for T1/Earlier year in the interval
T1 = arcpy.GetParameterAsText (5)

#Other Variables
TFPath = arcpy.env.workspace #Path to store intermediate files produced during
geoprocessing
TF = "Temp_Folder" #Folder the intermediate files are stored in
TempTable = "\\Temp_Folder\\Temp.dbf" #csv converted to dbf for quicker indexing
PKey = "FID" #Join Primary Key
FKey = "OID" #Join Foreign Key
```

##F2Point = "\\Temp_Folder\\F2Point_temp.shp" #Feature to Point output generated from the centroid of the trajectory polyline files
##P2Line = "\\Temp_Folder\\P2L_temp.shp" #Point to Line output using F2Point as the input
IntPoint = "\\Color_Mig.shp"
Route = "\\Temp_Folder\\Route_Temp.shp" #Turning P2Line into a route in order to get downstream distances
LFAR = "\\Temp_Folder\\LFAR" #Event table created during the Locate Feature Along Route (LFAR) tool in order to get attributes with correct distances
OETP = "RID POINT MEAS" #Out Event Table Properties which consists of route location fields and the events that will be written to the output table
SVE = "SVE.shp" #StandAlone .shp file for statistically significant measurements according to SVE
SVEFields = ["SVE","Mig_Dist","An_Mig"] #fields used with update cursor
RMSE = "RMSE.shp" #StandAlone .shp file for statistically significant measurements according to RMSE
RMSEFields = ["RMSE","Mig_Dist","An_Mig"] #fields used with update cursor
Ninety = "Ninety.shp" #StandAlone .shp file for statistically significant measurements according to 90th percentile errror
NinetyFields = ["Ninety","Mig_Dist","An_Mig"] #fields used with update cursor
ExTableAll = "Excel_Table_All.xls" #Final table is with all information exported to an excel document in the working directory
ExTableSVE = "Excel_Table_SVE.xls" #Final table is with SVE information exported to an excel document in the working directory
ExTableRMSE = "Excel_Table_RMSE.xls"#Final table is with RMSE information exported to an excel document in the working directory
ExTableNinety = "Excel_Table_Ninety.xls"#Final table is with 90th percentile error information exported to an excel document in the working directory

#Create a place to house temporary/intermediate files to avoid cluttering primary folder
arcpy.CreateFolder_management(TFPath, TF)

# Delete Field - Drop unnecessary field "Name"
arcpy.DeleteField_management(TrjLF, "Name")

# Table to Table- Takes the csv file and converts it into a dbf for quicker indexing
arcpy.TableToTable_conversion(SigCSV, TF, "Temp.dbf", "", "", "")

# Join Field - This takes the statistically significant (1) and insignificant(0) measurement information generated in Matlab
# and permanetly joins it to the appropriate trajectory measurements in the polyline shapefile. Note: Spelling and Capitalization must
# exact to the last parameter below
arcpy.JoinField_management(TrjLF, PKey, TempTable, FKey, "SVE;RMSE;Ninety")

```
#The following 4 lines have been commented out since they only work when TRJ lines
are unedited without additionals lines being added for corrections
## Feature To Point - This take the center of ever line in the trajectory file and creates a
point
##arcpy.FeatureToPoint_management(TrjLF, F2Point, "CENTROID")
## Points To Line - This takes the points generated in the last tool and creates a line from
them
##arcpy.PointsToLine_management(F2Point, P2Line, "", "", "NO_CLOSE")

# Intersect Analysis - This creates points at the intersection of the TRJ polyline file and
the T1 centerline
arcpy.Intersect_analysis([T1, TrjLF], IntPoint, "ALL", "0.1 Meters", "POINT")

# Create Routes - This takes the line created in the last tool and converts it to a route in
order to give it measure
arcpy.CreateRoutes_lr(T1, "Id", Route, "LENGTH", "", "", CoorPriority, "1", "0",
"NO_IGNORE", "INDEX")

# Locate Features Along Routes - This takes the points that were created and assigns
them downstream measure which will inturn give the
# trajectory lines measure in the next step
arcpy.LocateFeaturesAlongRoutes_lr(IntPoint, Route, "Id", "1 Meters", LFAR, OETP,
"FIRST", "NO_DISTANCE", "ZERO", "FIELDS", "M_DIRECTON")

# Wildcard is needed in order to automate selection of the foreign key since it inserts the
shapefiles name and could vary among users
fid_year = arcpy.ListFields(LFAR, "FID_*_*")[0].name
# Join Field - This steps permanently joins the downstream measurements from the point
file to the corresponding trajectory line
arcpy.JoinField_management(TrjLF, PKey, LFAR, fid_year, "MEAS")

#Add Field for annual migration rates
arcpy.AddField_management(TrjLF, "An_Mig", "DOUBLE", "7", "2", "", "",
"NULLABLE", "REQUIRED", "")
arcpy.AddField_management(IntPoint, "An_Mig", "DOUBLE", "7", "2", "", "",
"NULLABLE", "REQUIRED", "")

#Calculate Field to populate annual migration rates
arcpy.CalculateField_management(TrjLF, "An_Mig", "!Mig_Dist! /(Aadland 2015)"
.format(NumYears), "PYTHON_9.3", "")
arcpy.CalculateField_management(IntPoint, "An_Mig", "!Mig_Dist! /(Aadland 2015)"
.format(NumYears), "PYTHON_9.3", "")
```

```
# Copy Feature: Allows for new files that look at specific methods of source error
arcpy.CopyFeatures_management (TrjLF, SVE)
arcpy.CopyFeatures_management (TrjLF, RMSE)
arcpy.CopyFeatures_management (TrjLF, Ninety)

#This uses the Update Cursor to update the Migration Distances (Mig_Dist) for each of
the newly created files so if the distance is not
#statistically significant based on its individual error method then the the Migration
Distance will equal zero. Delete field is also used
#in order to cleanup the final output tables

#Update SVE
with arcpy.da.UpdateCursor(SVE, SVEFields) as cursor:
    for row in cursor:
        if row[0]==0:
            row[1]="0"
            row[2]="0"
            cursor.updateRow(row)
del row
del cursor

#delete excess fields
arcpy.DeleteField_management(SVE, ["RMSE","Ninety"])

#Update RMSE
with arcpy.da.UpdateCursor(RMSE, RMSEFields) as cursor:
    for row in cursor:
        if row[0]==0:
            row[1]="0"
            row[2]="0"
            cursor.updateRow(row)
del row
del cursor

#delete excess fields
arcpy.DeleteField_management(RMSE, ["SVE","Ninety"])

#Update Ninety
with arcpy.da.UpdateCursor(Ninety, NinetyFields) as cursor:
    for row in cursor:
        if row[0]==0:
            row[1]="0"
            row[2]="0"
            cursor.updateRow(row)
```

```
del row
del cursor

#delete excess fields
arcpy.DeleteField_management(Ninety, ["SVE","RMSE"])


#Conversion of the final trajectory files to an excel table
arcpy.TableToExcel_conversion(TrjLF, ExTableAll)
arcpy.TableToExcel_conversion(SVE, ExTableSVE)
arcpy.TableToExcel_conversion(RMSE, ExTableRMSE)
arcpy.TableToExcel_conversion(Ninety, ExTableNinety)

#Deletes the Temporary Folder that was used to store intermediate data. Comment the
following line out to preserve intermediate file.
#shutil.rmtree(arcpy.env.workspace + "\\Temp_Folder")

print "Alright Alright Alright"
```

Appendix H
Reach Break Down

Reach 1
Anthropogenically controlled stretch (city of Mankato)
Little evidence of sandbar presence
Beginning of the overall study reach (Minnesota/Blue Earth Confluence
Is almost immediately met by rip-rap/earthen levee which transitions into a cement flood
control structure

3 Bridges (HWY 169, Veterans Memorial/Belgrade, and HWY 14 – Respectively Downstream)
After HWY 14, 3 wing-dams followed by a slight bend in the river
This bend is at a bedrock outcrop
Historic Meander Bend (prior to 1937)
Noticeable decrease in channel width at this point
End of Reach 1

Reach 2
Outside the city of Mankato
Large amount and size of bars/depositional areas
5 Cutoffs from 1937-2013
1 from 1951-1964
1 from 1964-1980
1 from 1980-1991
2 from 1991-2013
reducing stream length significantly
End of Reach 2 and the HWY 22 Bridge (City of St. Peter)
Width appears to bottle-neck at this bridge

Reach 3
Beginning at HYW 22 Bridge
Passes under the 99 bridge
Valley width gets significantly bigger
Significant appearance of bars again
Contains 3 Cutoffs from 1937-2013
1 from 1937-1951
1 from 1964-1980
1 from 1991-2013
Fairly sinuous stretch
Ends at Geomorphic break (see Reach 4)

Reach 4
Almost completely straight
Very few bars – small in size
Reach is pressed up against east side of the valley (DS right)
Evidence of historic meanders in this section, but little migration in the past 76 years
Ends at Geomorphic Break (See Reach 5)

Reach 5
Very sinuous
Dominated with large point bars
Small reach but contains two cutoffs from 1937-2013
1 from 1937-1951

1 from 1964-1980
Ends at 336th Street Bridge/Bridge Street (Le Sueur)

Reach 6
Begins at 336th Street Bridge/Bridge Street (Le Sueur)
Only a few small depositional features
Short reach yet it contain a 1 meander with a wavelength extending from the east river
valley wall (City of Le Sueur) to the west valley wall (HWY 169).
Amplitude of the meander very large comparted to Reach 6.
End at HWY 169 Bridge

Reach 7
Begins at the HWY 169 Bridge
Significantly more depositional features than the prior reach
Low sinuosity
Majority pressed up against the east valley wall
Contains 3 Cutoffs from 1937-2013
1 from 1951-1964
2 from 1991-2013
Rush River flows in near the beginning and appears to have a high amount of sediment
End at a Geomorphic Break
Reduced width
Press up against east valley wall
Beginning of few depositional features

Reach 8
Increase in sinuosity
Contains 3 Cutoffs from 1937-2013
1 from 1964-1980
2 from 1991-2013cc
Ends at geomorphic break

Reach 9
Small section characterized by lack of depositional features and completely straight

Reach 10
High sinuosity
Meanders through out the entire river valley
Significant increase in depositional features

Reach 11
Low sinuosity – Multiple long straight sections of river
Very little evidence of in channel depositional features outside one point bar
Ends just upstream of Beaven's Creek

Reach 12
Beginning at Beaven's Creek
Increased sinuosity, in channel depositional features, and width
Including mid-channel point
Meander Translation dominates this stretch

Reach 13
This has a distinct pattern change from the previous reach with much larger meanders
The river swings back and forth between the valley walls multiple times
This stretch is also on the edge of the Metro with agricultural land use still being
dominate especially on the east side.
Ends at the HWY 41 Bridge (Chaska)

Reach 14
This stretch is starts the HWY 41 Bridge
This stretch also is the beginning of dominate urban land use
The sinuosity is lower than the prior reach
This reach also occupied the entire river valley but doesn't bounce around as much as the
prior reach
Ends at the beginning of where the channel is actively dredged

Reach 15
Begins at the beginning of the channel that is actively managed for barge traffic
Has meanders that start to straighten towards the end of the reach
Contains the beginning of barge traffic and dredged channel
Two of the Four dredging locations are contained in this reach
Heavy industrial encroachment on the river within the river valley
Ends at 35W bridge

Reach 16
Begins at the 35W Bridge
This stretch is very straight with many wetlands and lakes present of both sides of the
river within the valley
The stretch has been modified for barge traffic
The other two of four dredging locations are in this stretch
3 Cutoffs are present from 1964-1980 and are most likely engineered
Ends at the confluence of the Mississippi River

Appendix I

With Cutoffs

1964-1980 Annual Migration (Meters/Year)

Kilometers
(Blue Earth River Confluence to the Mississippi River Confluence)

★ Cutoff

1980-1991 Annual Migration (Meters/Year)

Kilometers
(Blue Earth River Confluence to the Mississippi River Confluence)

★ Cutoff

224

1991-2013 Annual Migration (Meters/Year)

Meter per Year

(-) migration downstream right (+) migration downstream left

Kilometers
(Blue Earth River Confluence to the Mississippi River Confluence)

★ Cutoff   ★ Cutoff characteristics, but not included in the total cutoffs count

1937-1951 Annual Migration (Meters/Year)

Meter per Year

(-) migration downstream right (+) migration downstream left

Kilometers
(Blue Earth River Confluence to the Mississippi River Confluence)

★ Cutoff

1951-1964 Annual Migration (Meters/Year)

(Blue Earth River Confluence to the Mississippi River Confluence)

★ Cutoff

Without Cutoffs

1937-1951 Annual Migration without Cutoffs (Meters/Year)

(Blue Earth River Confluence to the Mississippi River Confluence)

1951-1964 Annual Migration without Cutoffs (Meters/Year)

Meter per Year

(-) migration downstream right (+) migration downstream left

Kilometers

(Blue Earth River Confluence to the Mississippi River Confluence)

1964-1980 Annual Migration without Cutoffs (Meters/Year)

Meter per Year

(-) migration downstream right (+) migration downstream left

Kilometers

(Blue Earth River Confluence to the Mississippi River Confluence)

1991-2013 Annual Migration without Cutoffs (Meters/Year)

Meter per Year
(-) migration downstream right (+) migration downstream left

Kilometers
(Blue Earth River Confluence to the Mississippi River Confluence)

1991-2013 Annual Migration without Cutoffs (Meters/Year)

Meter per Year
(-) migration downstream right (+) migration downstream left

Kilometers
(Blue Earth River Confluence to the Mississippi River Confluence)

228

Appendix J

1937 Width

Kilometers
(Blue Earth River Confluence to the Mississippi River Confluence)

1951 Width

Kilometers
(Blue Earth River Confluence to the Mississippi River Confluence)

1964 Width

Kilometers
(Blue Earth River Confluence to the Mississippi River Confluence)

1980 Width

Kilometers
(Blue Earth River Confluence to the Mississippi River Confluence)

1991 Width

2013 Width

Appendix K
Reach 1
   River Reach 1 closely mirrors the analysis from section 3.4.2.1 which focused on the city of Mankato's heavily engineered river stretch containing riprap, earthen levees,

and cement flood walls. This characteristic is what was used to define this first river reach. The biggest anomaly seen in this stretch is the decrease in channel migration starting in the 1964-1980 interval and extending to the present. The timing of this decrease correlates to the flood control structure being built in the city in the mid-1960's. Despite the river migration decreasing, width in this reach still increased while sinuosity saw very little variability of the time of record.
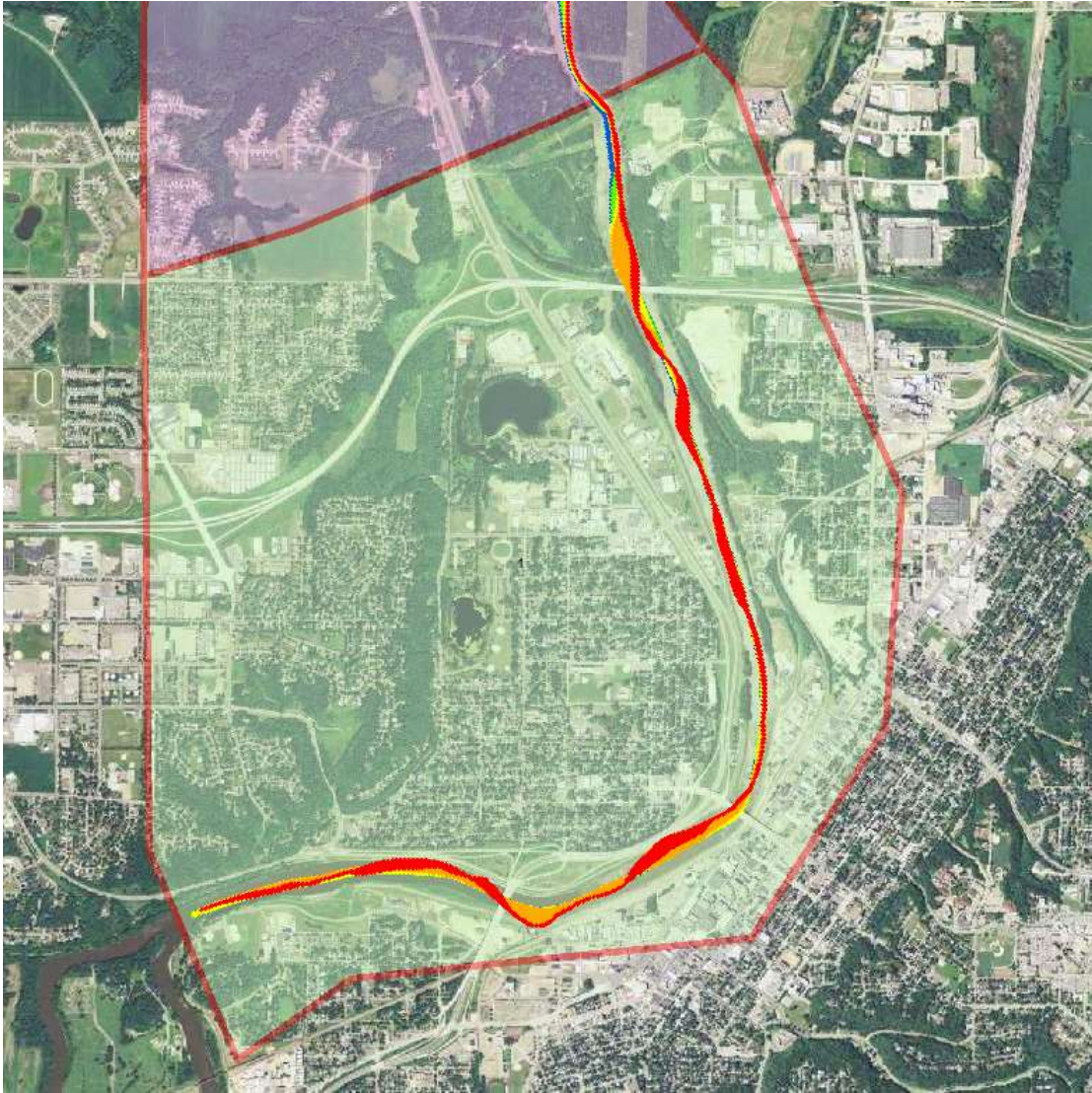
Reach 1 with migration displayed (Red = 1937-1951, Orange = 1951-1964, Yellow = 1964-1980, Green = 1980-1991, Blue = 1991-2013)
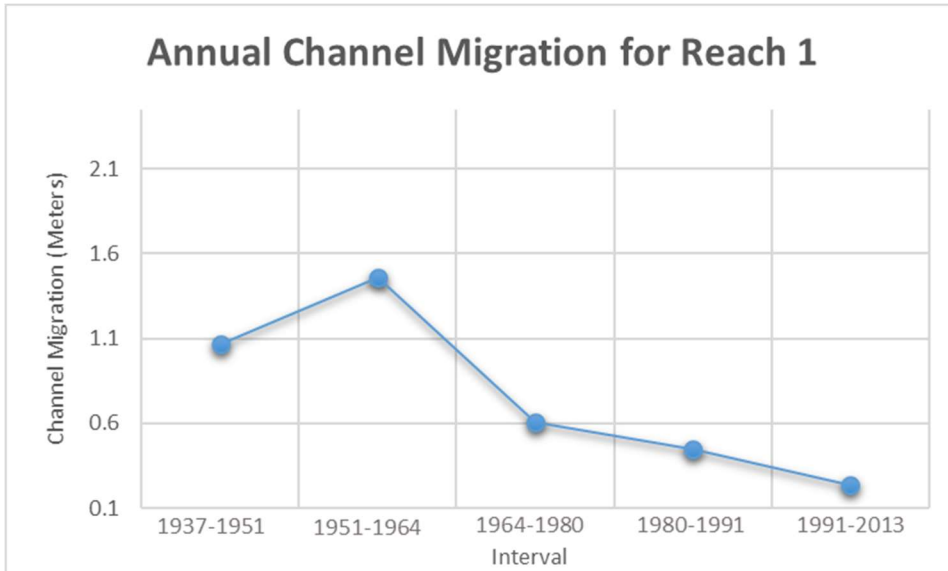
Reach 1 annual channel migration from 1937-2013
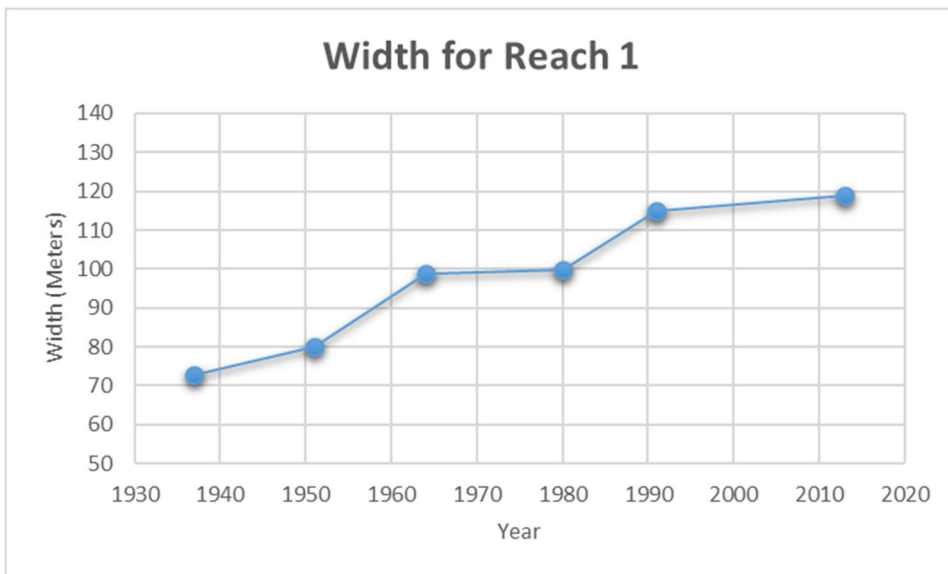
Reach 1 width change from 1937-2013
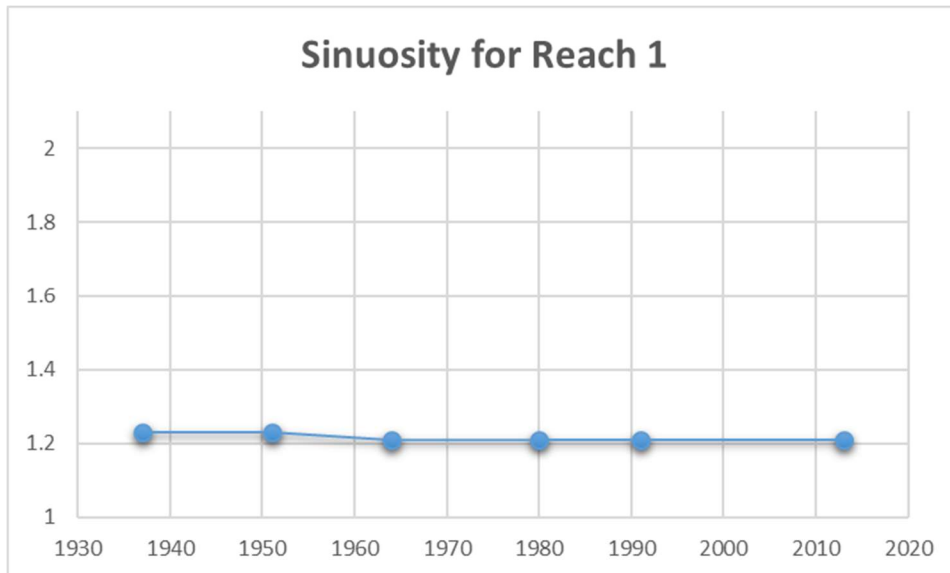
Reach 1 sinuosity from 1937-2013

Reach 2

Reach 2 extends from the city of Mankato to St. Peter. This stretch contains a much higher annual migration than the prior reach that is temporally increasing. The width in this stretch has more than doubled in size from 1937-2013. This reach has also seen a significant decrease in sinuosity due to the five cutoffs of record. This reach has experienced the most cutoffs of any of the reaches in this study. This stretch has been highly dynamic in all planform metrics. This is likely due to being the first unconfined stretch downstream from the Blue Earth River confluence which doubles the flow on the Minnesota River and contributes a large amount of sediment to the system. Since Mankato is largely confined is can pass the flow and sediment comparatively effectively making Reach 2 the first unconfined stretch able to adjust to the change in hydrology and sediment load.
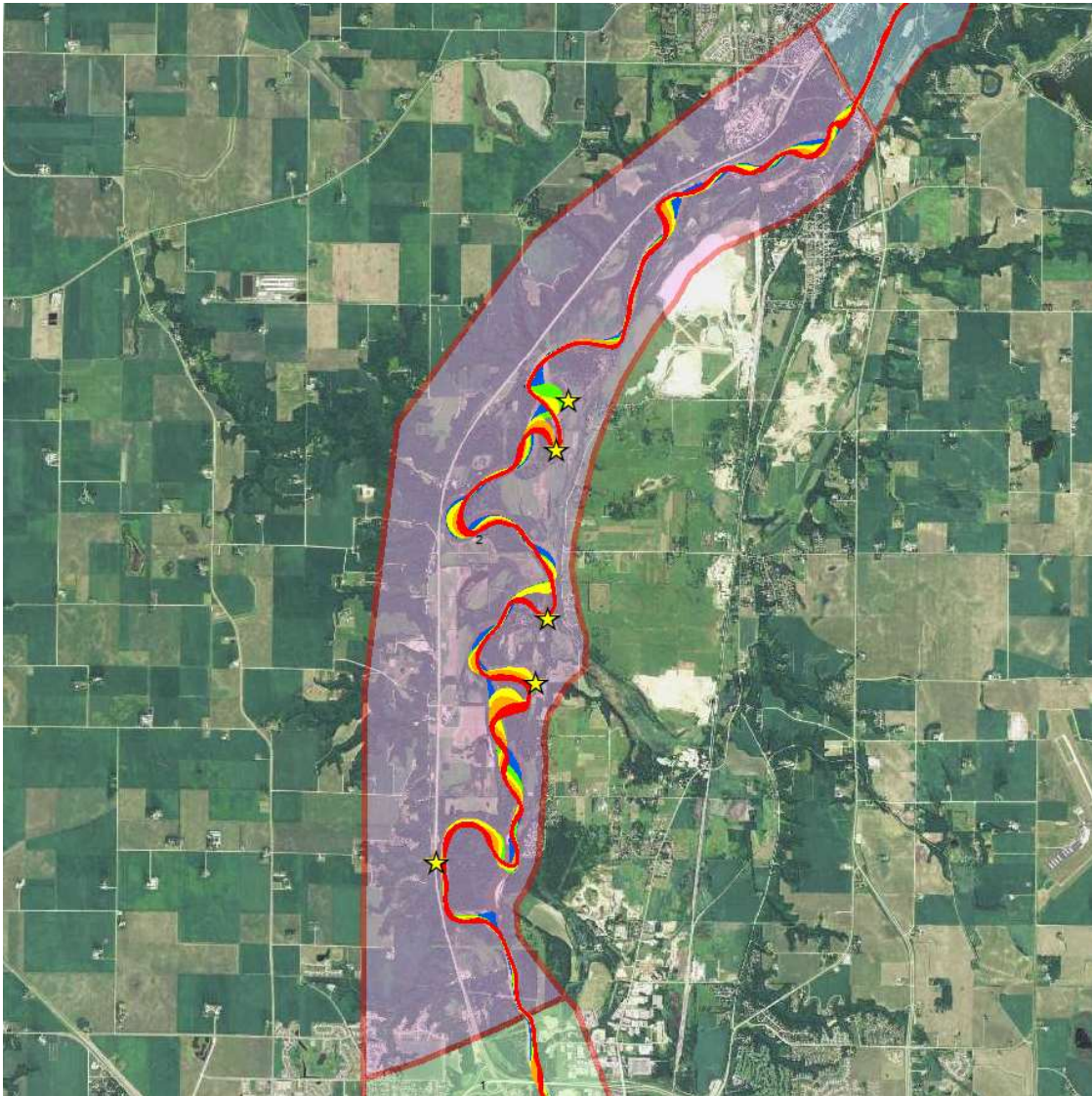
Reach 2 with migration displayed (Red = 1937-1951, Orange = 1951-1964, Yellow = 1964-1980, Green = 1980-1991, Blue = 1991-2013)
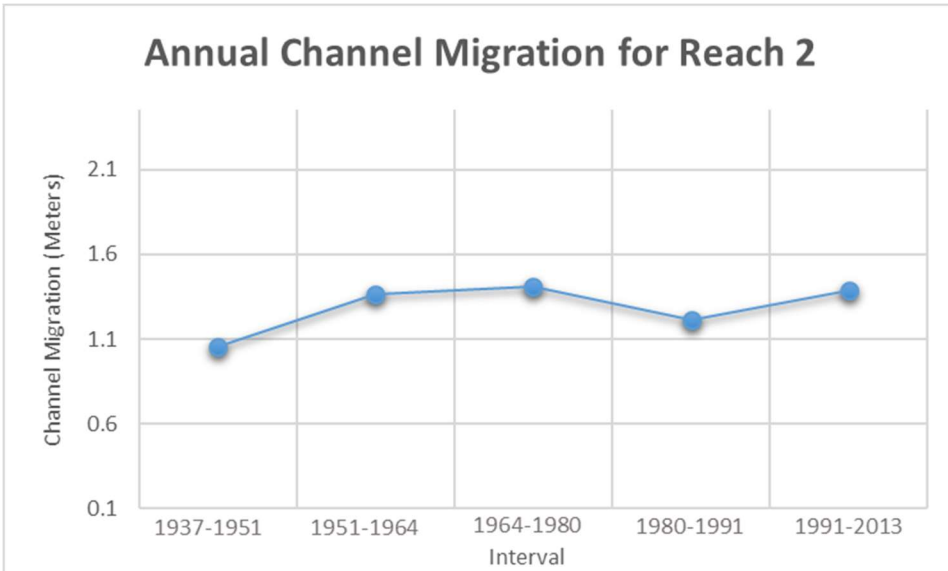
Reach 2 annual channel migration from 1937-2013
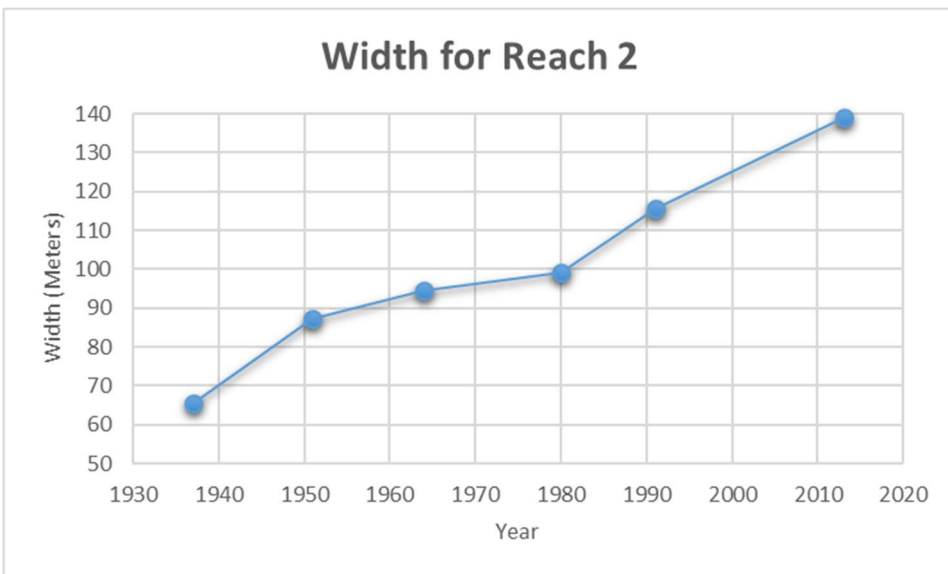
Reach 2 width change from 1937-2013
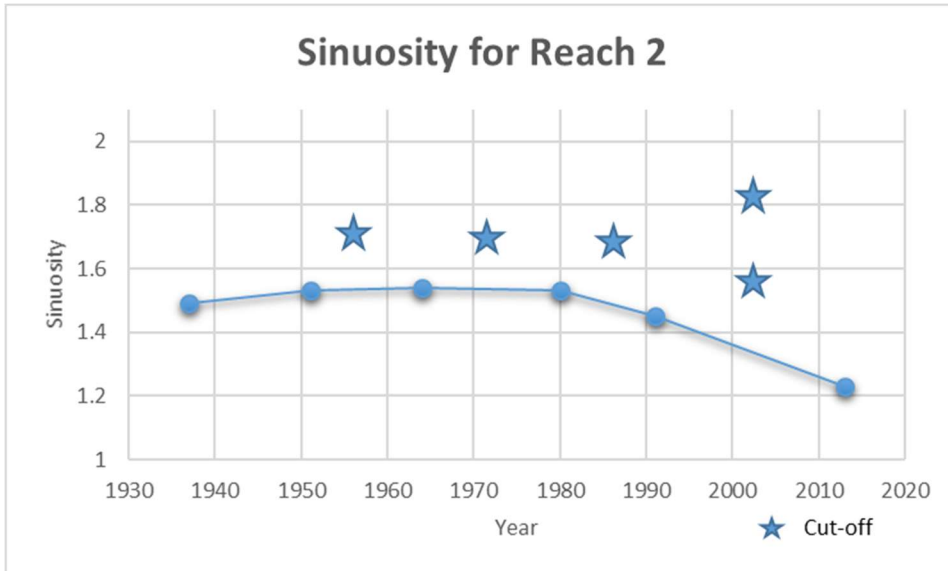
Reach 2 sinuosity from 1937-2013

Reach 3

Reach 3 begins at Highway 22 Bridge on the south end of St. Peter and extends into a rural landscape with Highway 169 bordering the west side. The migration in this reach is less dynamic and overall temporally stable. Width has shown a normal increase, but not as dynamic as Reach 2, and sinuosity has seen a decrease due to three cutoffs of record, but remains relatively sinuous overall.
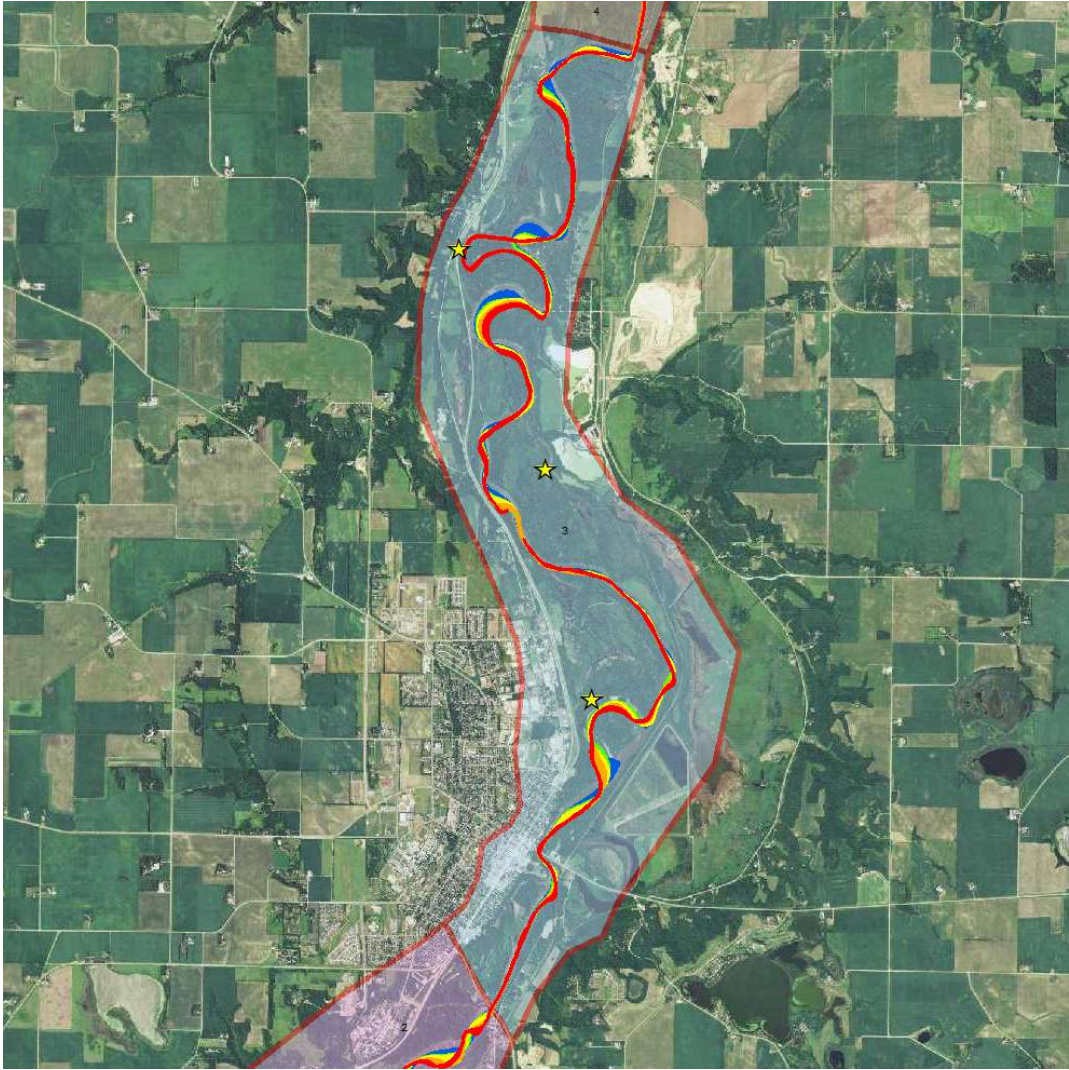
Reach 3 with migration displayed (Red = 1937-1951, Orange = 1951-1964, Yellow = 1964-1980, Green = 1980-1991, Blue = 1991-2013)
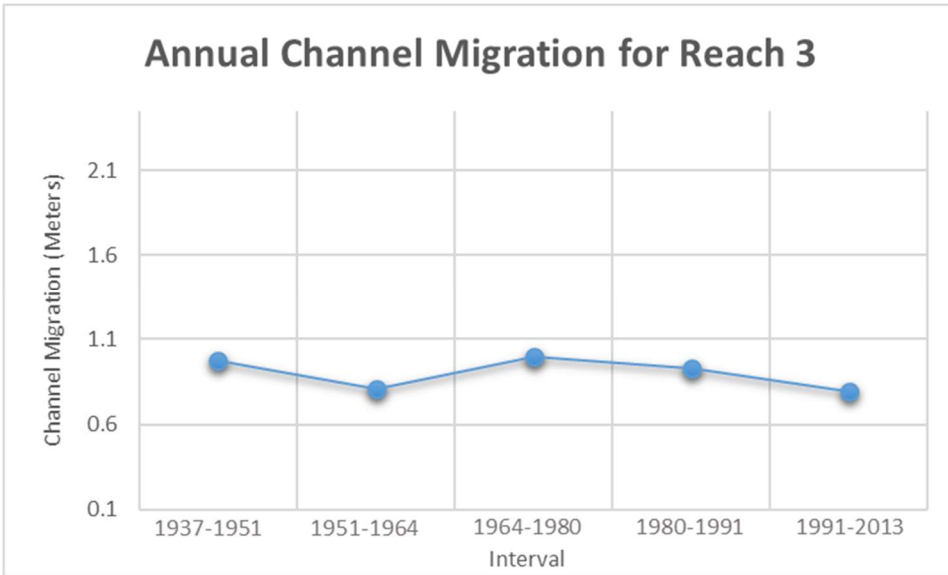
Reach 3 annual channel migration from 1937-2013
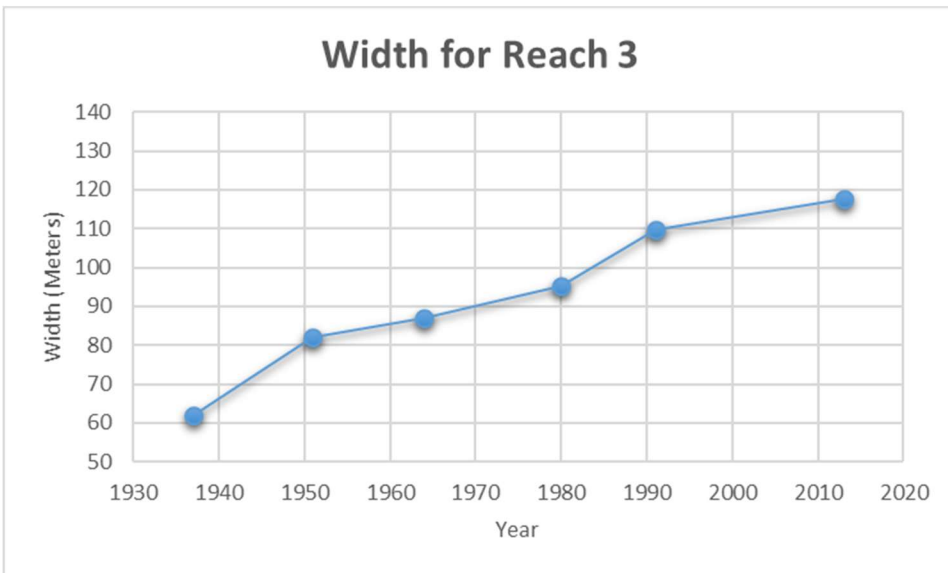
Reach 3 width change from 1937-2013
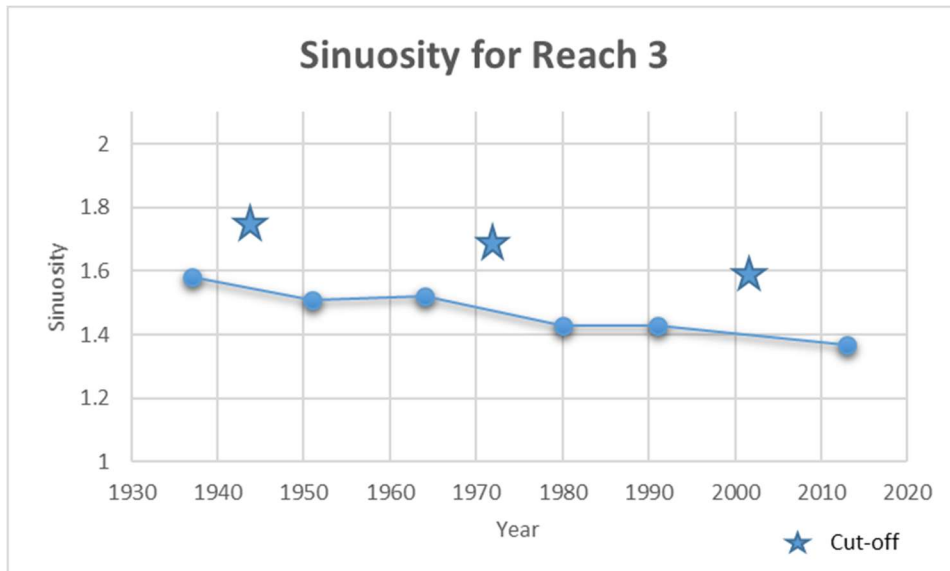
Reach 3 sinuosity from 1937-2013

Reach 4

Reach 4 is ~3.6 km rural stretch of river that is abnormally straight in terms of the reach upstream and downstream of it, the study area overall, and naturally meandering rivers in general. There has been some migration observed in this reach but has been contained to the east side of the valley. Width has increased in this reach but not as dramatically as other reaches. Since the channel is so straight in this reach, a sinuosity just above one has been observed over the record of time. Despite the river being so straight over a 76 year period of time, the oxbow lake observed in the south-west portion of the reach shows this straight channel has not always been characteristic. Based on the LiDAR an initial hypothesis that this stretch of river is being pressed up against the east valley wall by a large alluvial fan from a large sediment laden tributary (Barney Fry Creek) entering from the west side of the valley.
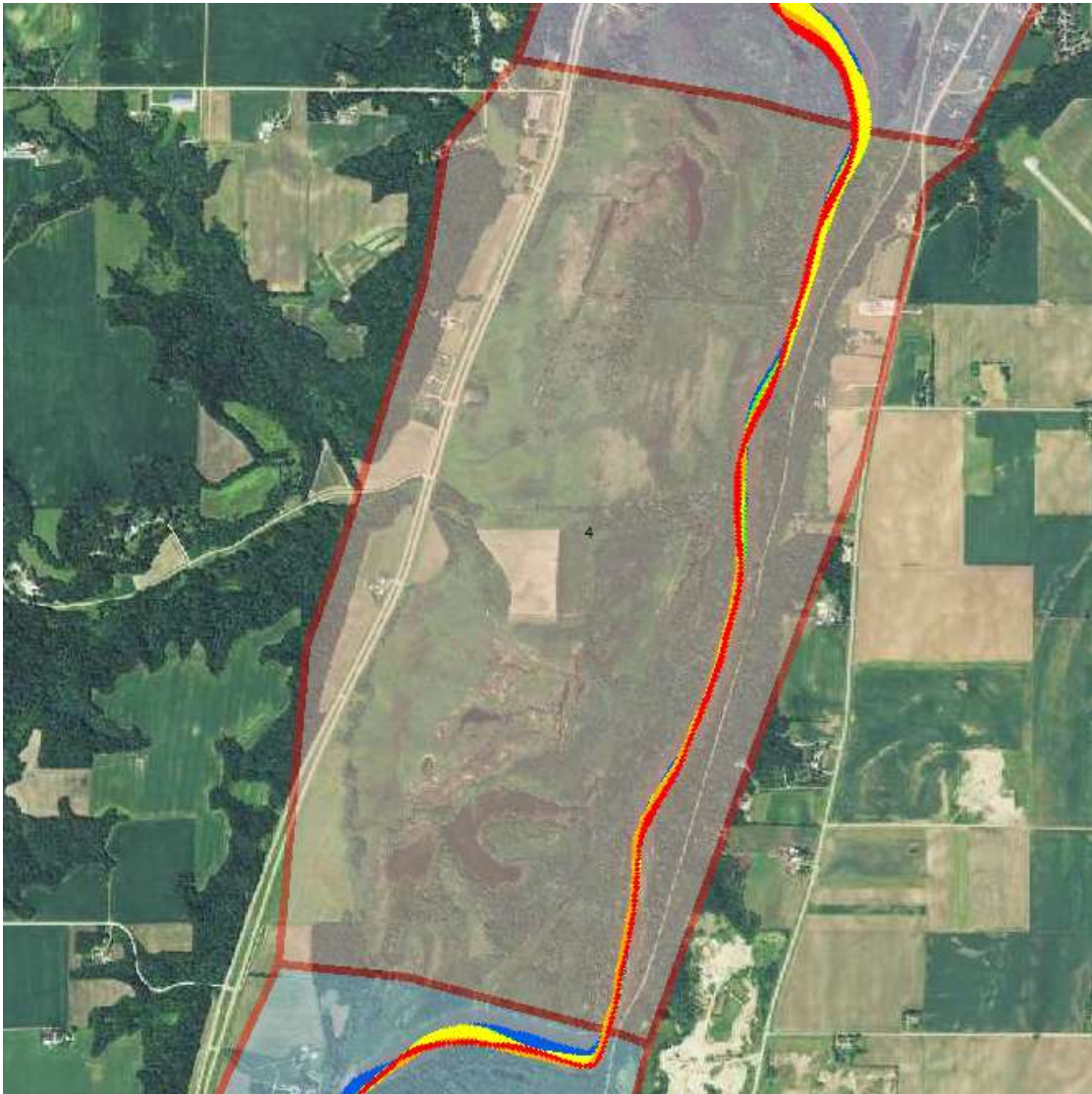
Reach 4 with migration displayed (Red = 1937-1951, Orange = 1951-1964, Yellow = 1964-1980, Green = 1980-1991, Blue = 1991-2013)
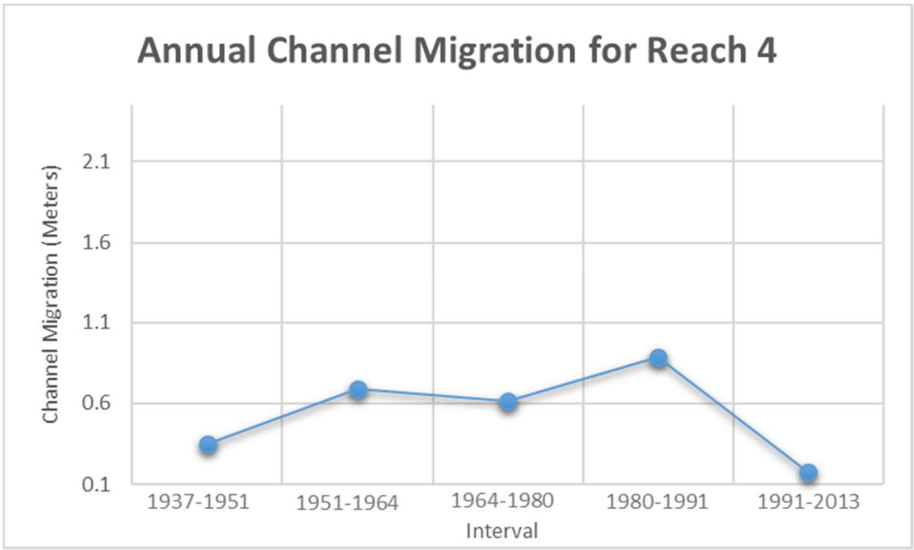
Reach 4 annual channel migration from 1937-2013
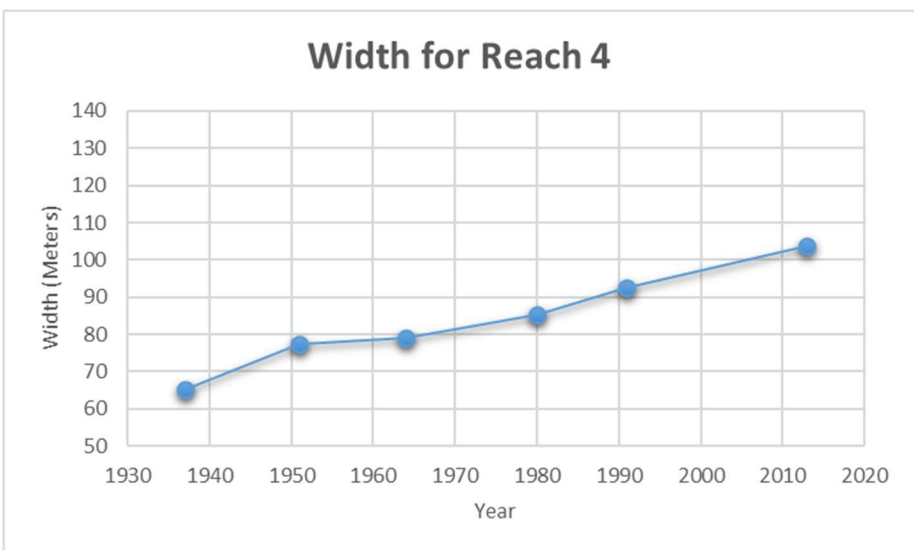
Reach 4 width change from 1937-2013
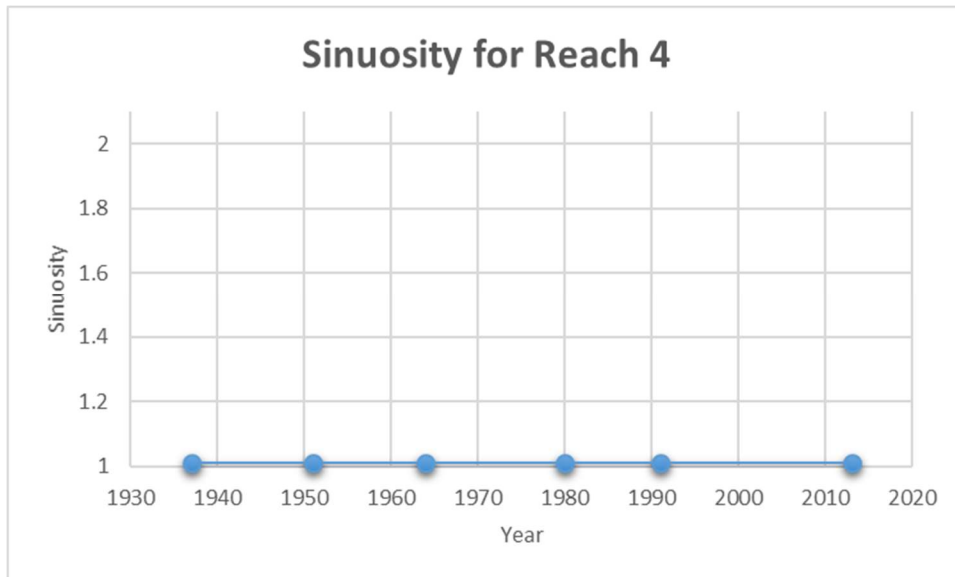
Reach 4 sinuosity from 1937-2013

Reach 5

Reach 5 is approximately the same stream length as Reach 4 but juxtaposes the former reach in planform characteristics. This reach is highly active in terms of channel migration, with significant width increase, and a sinuosity between 1.5-1.7 and two cutoffs over the record of time. If the prior zone in being controlled by an alluvial fan this area could mark the transition away from that control allowing the river to react in a highly dynamic way much like Reach 2 from Reach 1.
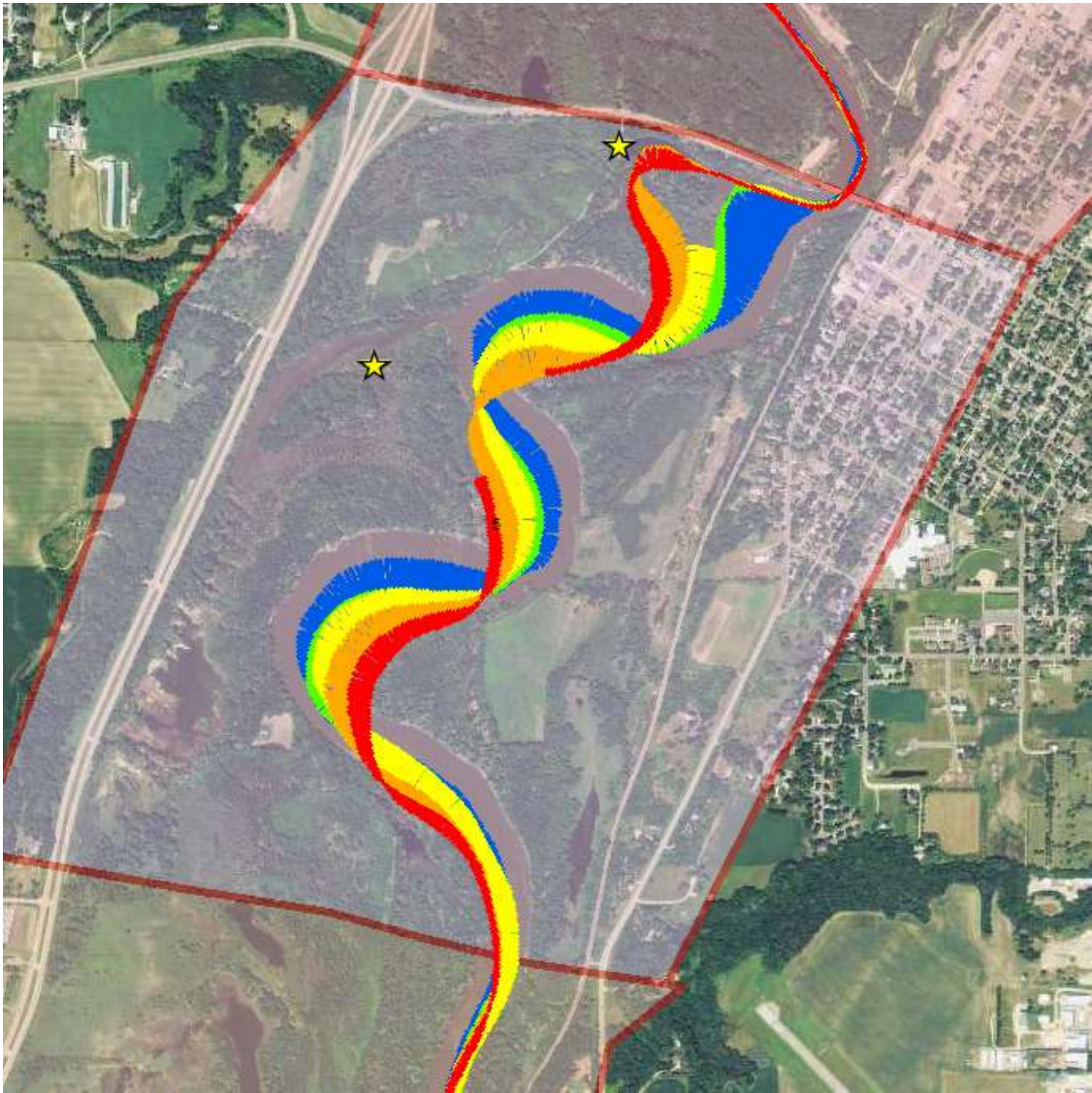
Reach 5 with migration displayed (Red = 1937-1951, Orange = 1951-1964, Yellow = 1964-1980, Green = 1980-1991, Blue = 1991-2013)
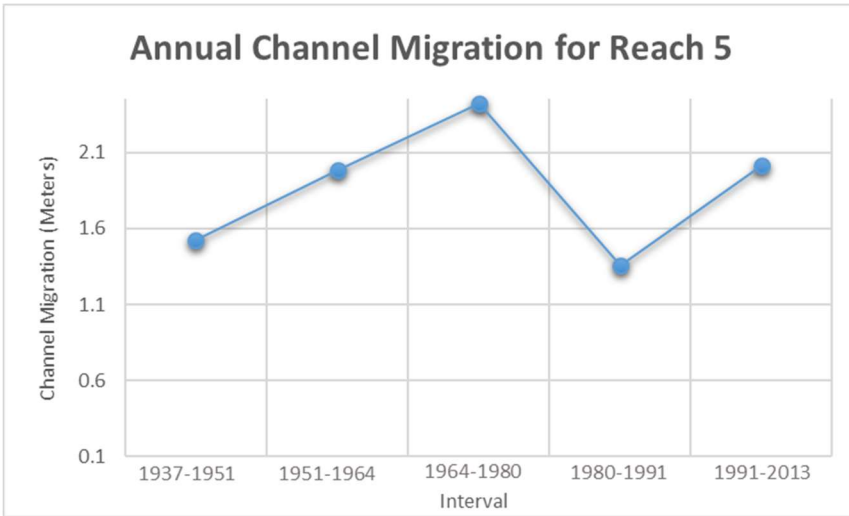
Reach 5 annual channel migration from 1937-2013

Reach 5 width change from 1937-2013
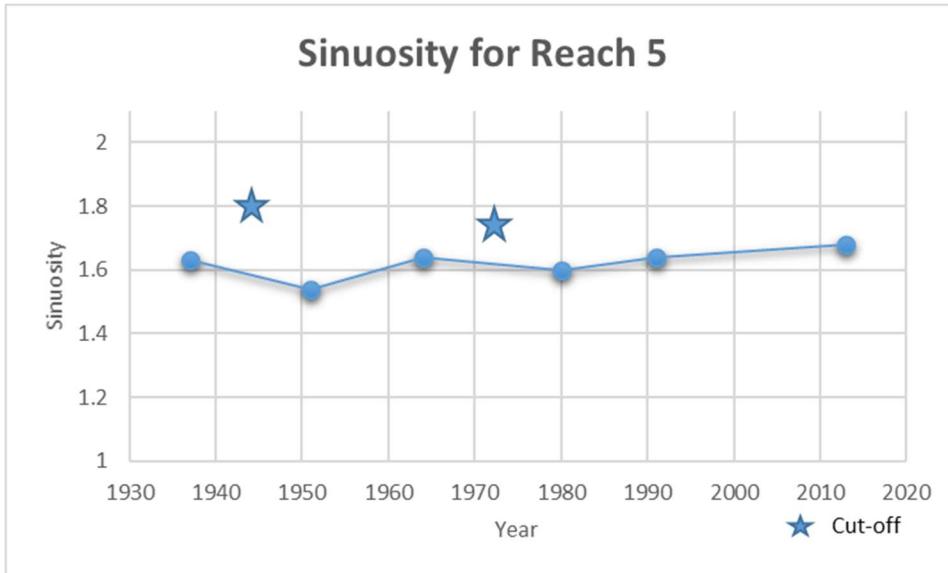
Reach 5 sinuosity from 1937-2013

Reach 6

     Reach 6 is approximately the length of prior two reaches, but again displays a differing planform. This reach is between the at 336th Street Bridge and Highway 169 Bridge with the city of Le Sueur on the east side and Highway 169 running along the west and north west side. The annual migration is rather steady temporally hovering right around 0.6 meter/year. The width in this reach saw an increase over time, but not as great as most other reaches. The sinuosity has remained very high in this stretch with the channel traveling between the valley walls twice in a short span. The geometry of this stretch of channel is likely influenced greatly by the encroachment and confinement of anthropogenic structures.
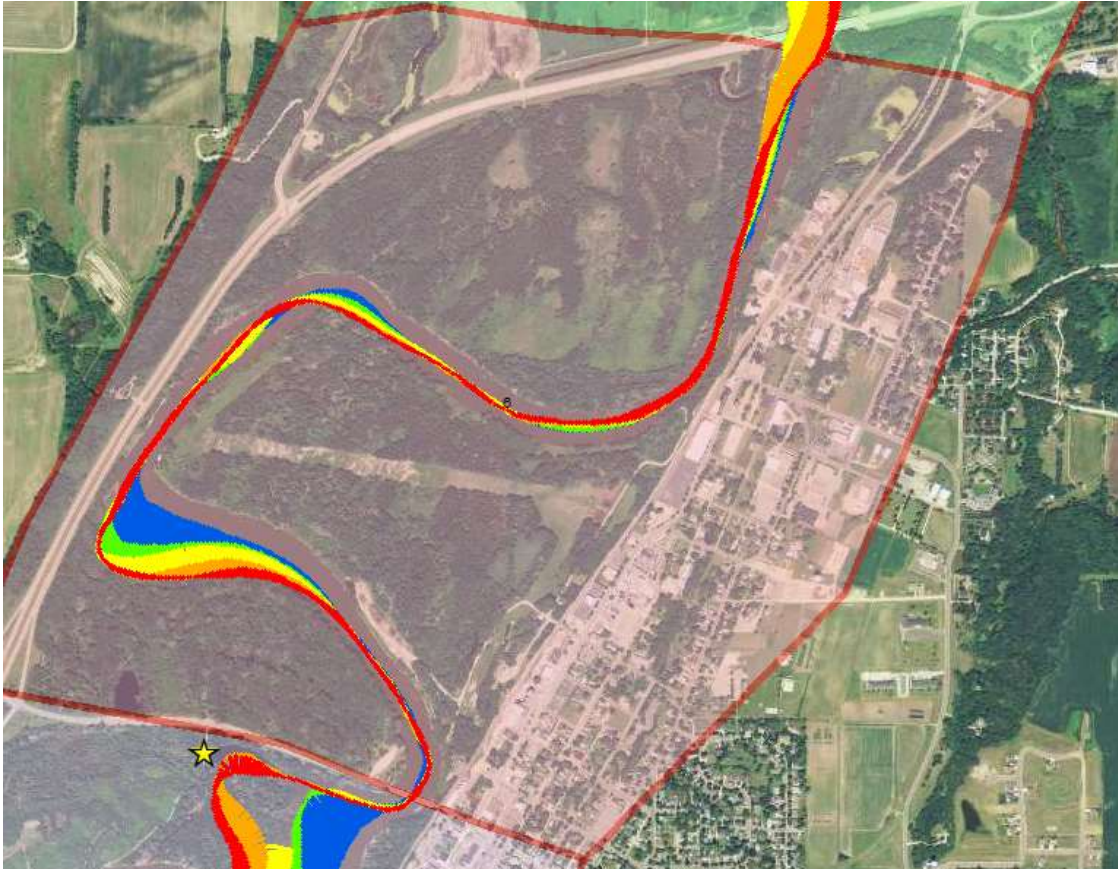
Reach 6 with migration displayed (Red = 1937-1951, Orange = 1951-1964, Yellow = 1964-1980, Green = 1980-1991, Blue = 1991-2013)
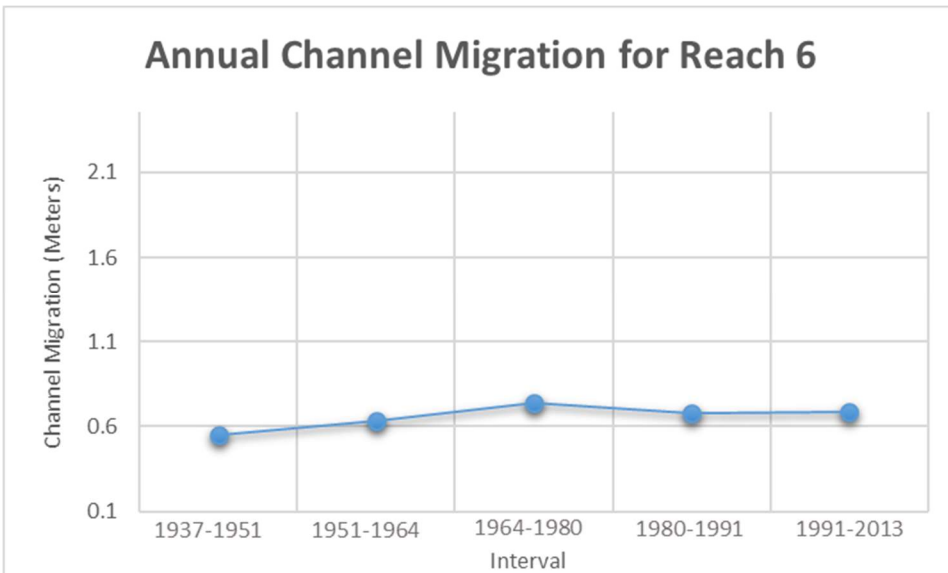
Reach 6 annual channel migration from 1937-2013
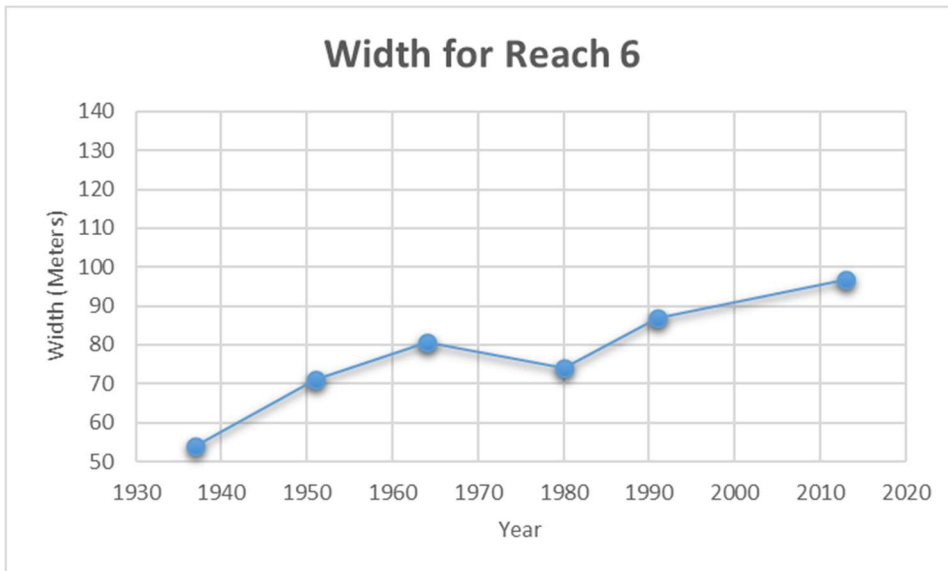
Reach 6 width change from 1937-2013
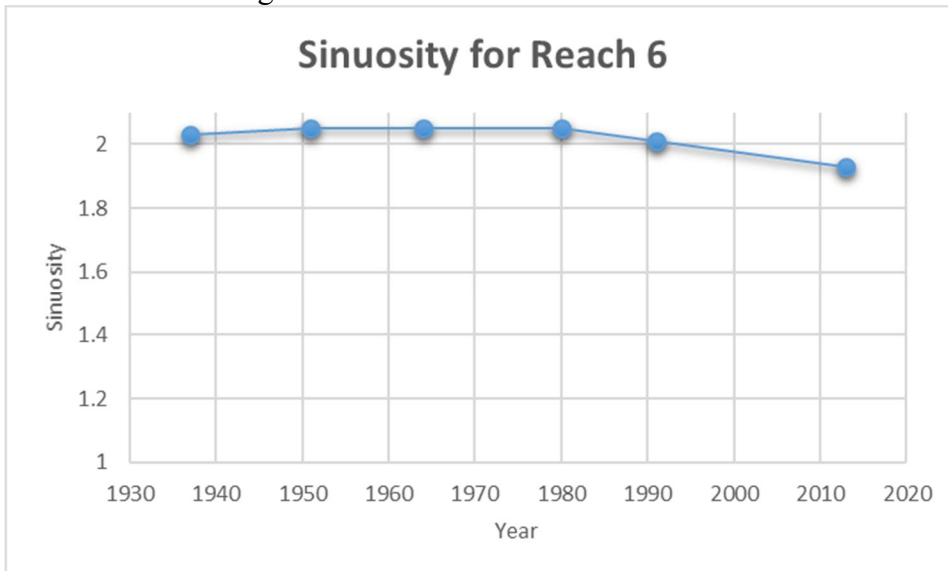
Reach 6 sinuosity from 1937-2013

Reach 7

Reach 7 extends from the Highway169 Bridge in Le Sueur into a rural area past the town of Henderson. This reach has seen a fairly significant increase in migration and width temporally. This stretch was very sinuous compared to other reaches but has experienced three cutoffs of record with one in the 1991-2013 interval which reduced the stream length by 4 km decreasing sinuosity by 0.5. The reach also has another very sediment laden tributary (Rush River) entering from the west. Two of the three cutoff occurred right at the confluence of the Rush River. It is also interesting to note that a section of this reach is rather straight and in close proximity to the east wall much in the same way Reach 4 is. This furthers the hypothesis of high sediment tributaries ability to

248

constrain and straighten the channel against a valley wall. Also like Reach 4, there are old oxbow lakes present indicating this has not always been characteristic. This leads to furthering the hypothesis to increases in hydrology and bank erosion altering the characteristics of the modern channel.
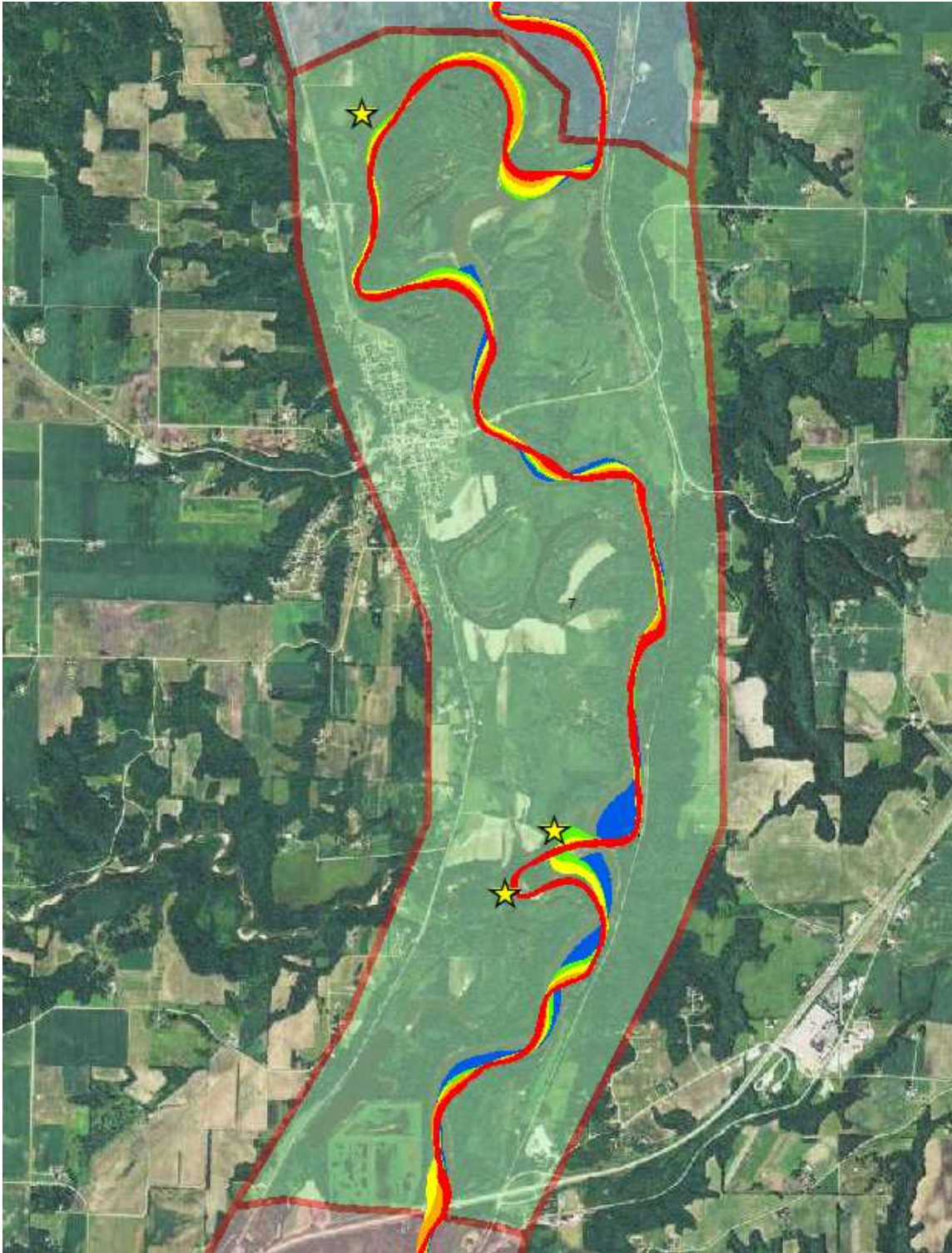
Reach 7 with migration displayed (Red = 1937-1951, Orange = 1951-1964, Yellow = 1964-1980, Green = 1980-1991, Blue = 1991-2013)
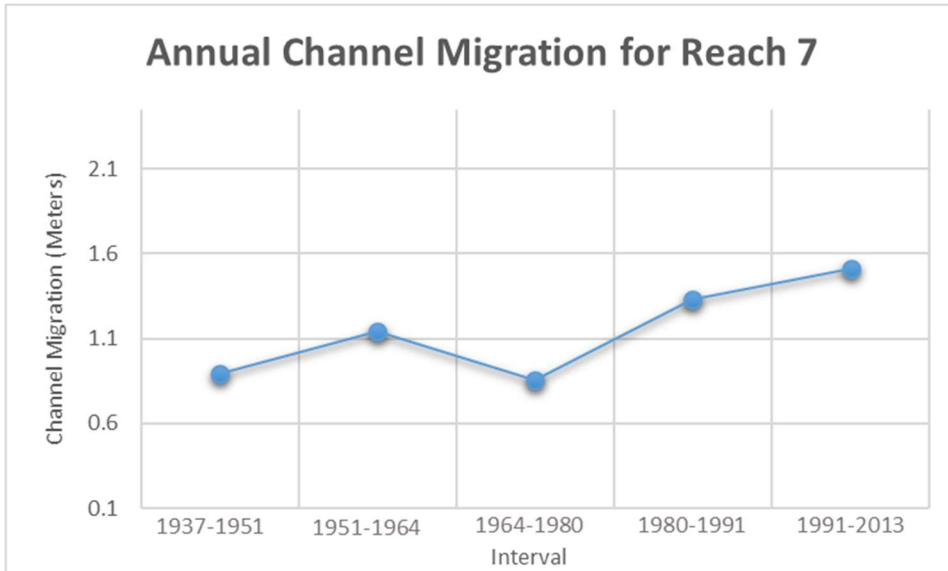
Reach 7 annual channel migration from 1937-2013
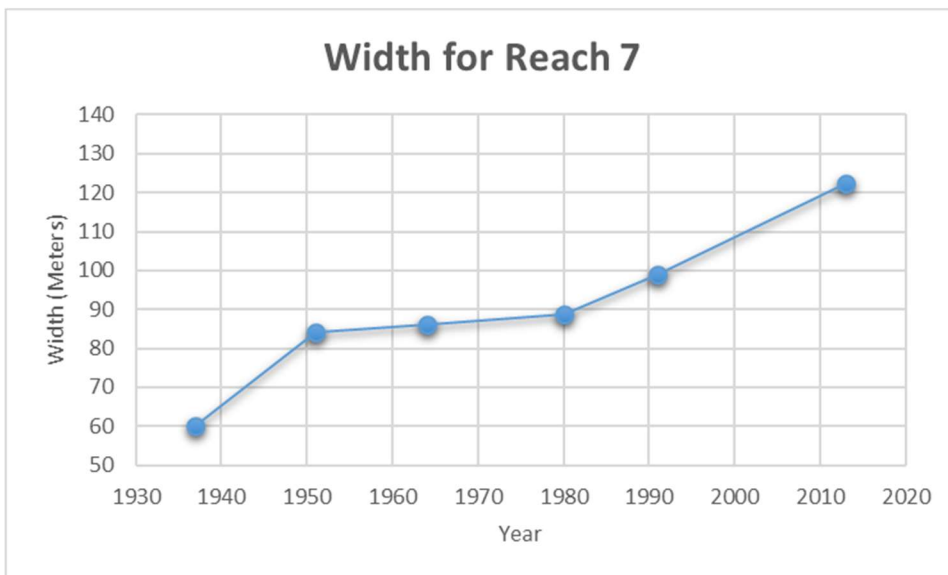
Reach 7 width change from 1937-2013
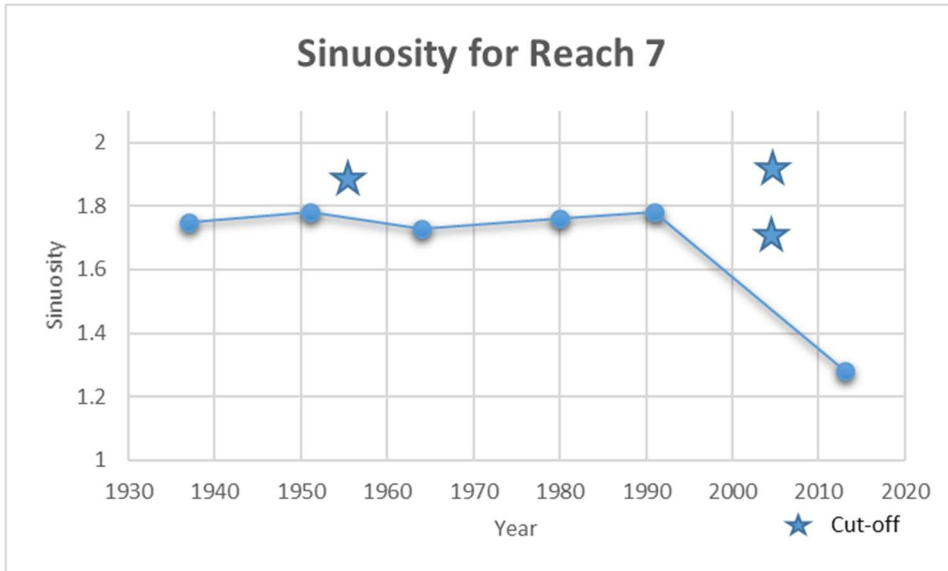
Reach 7 sinuosity from 1937-2013

Reach 8
Reach 8 is another stretch of river that is highly active in terms of channel migration and increasing temporally along with width increasing steadily temporally as well. This reach has seen a decline in sinuosity due to the present of three cutoffs, two of which occurred between 1991-2013. These are the last cutoffs seen in the lower portion of the study area.
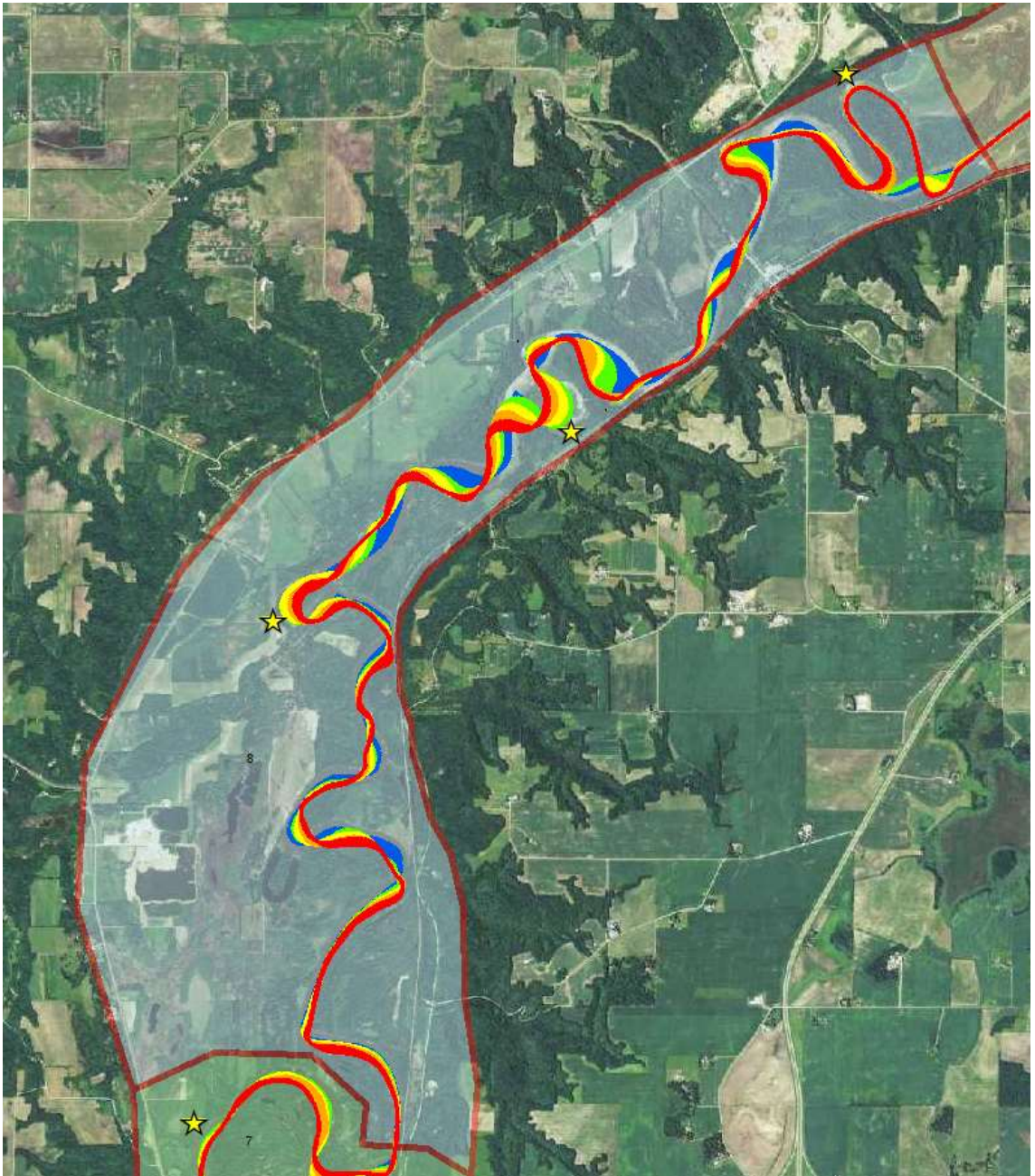
Reach 8 with migration displayed (Red = 1937-1951, Orange = 1951-1964, Yellow =
1964-1980, Green = 1980-1991, Blue = 1991-2013)
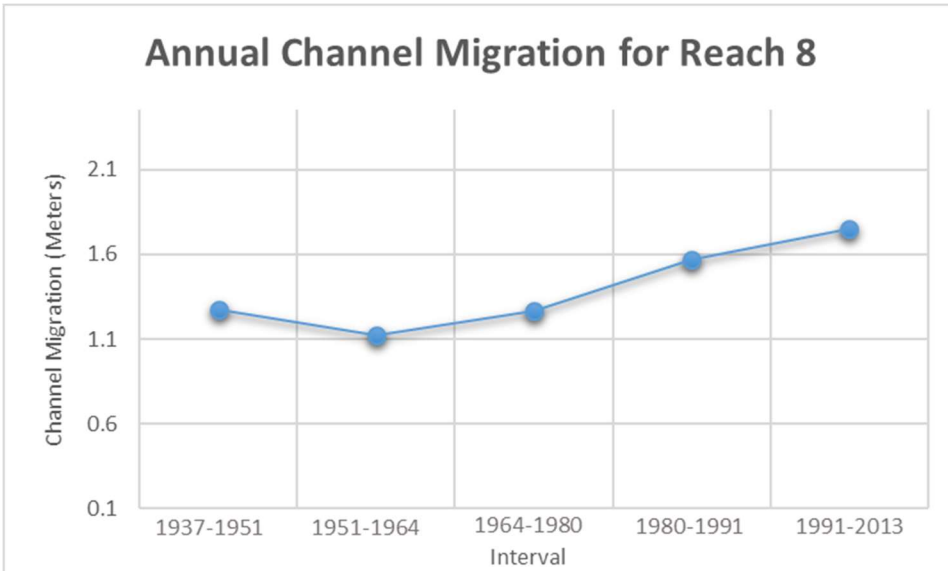
Reach 8 annual channel migration from 1937-2013
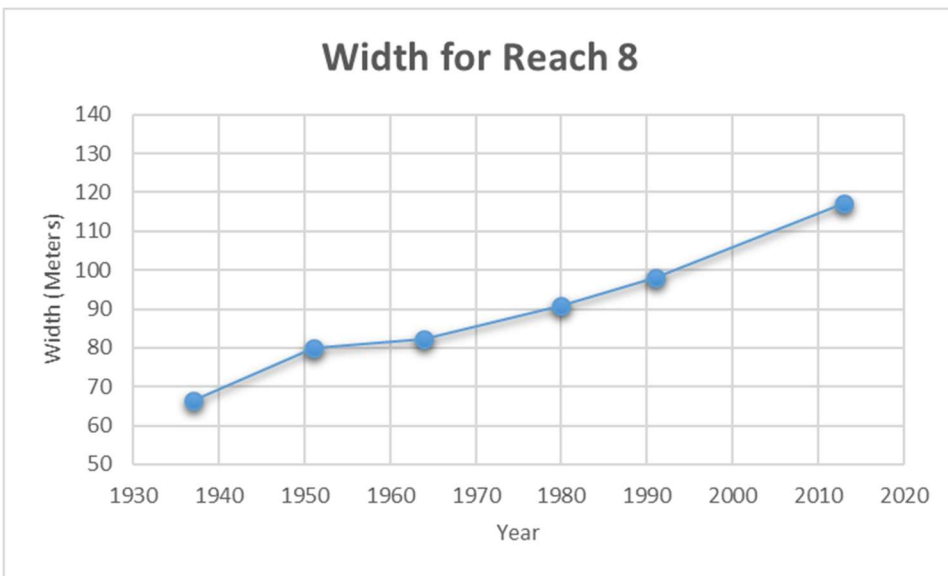
Reach 8 width change from 1937-2013
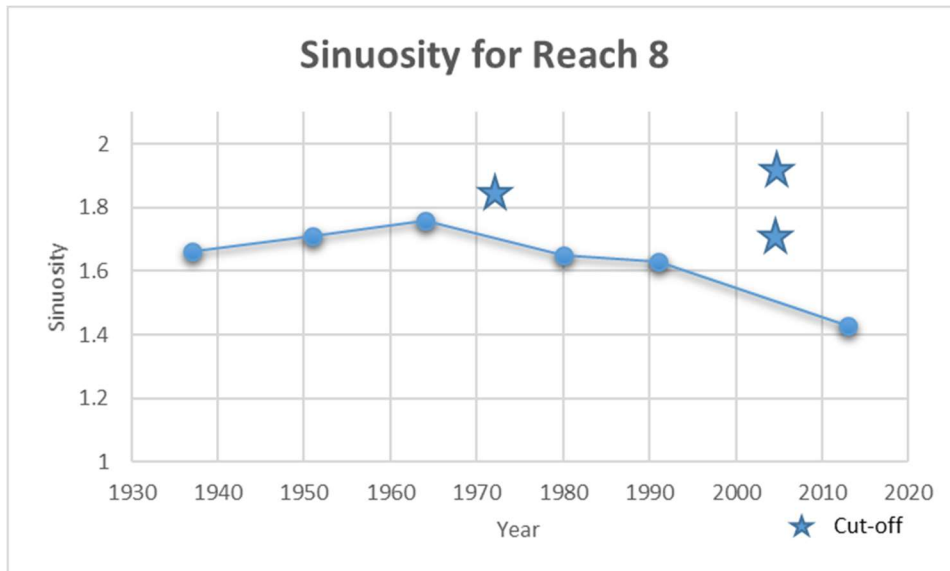
Reach 8 sinuosity from 1937-2013

Reach 9

Reach 9 is another very straight stretch of river. Little channel migration has occurred in this area and has experienced channel widening but less than that of other reaches. Sinuosity has steadily stayed just above over the past 76 years. Although it was hypothesized that other straight stretches were being constrained by high amounts of sediment contributed from tributaries pressing the channel up against the valley wall, this is not the case in this stretch. This reach is not against the valley wall and no major tributaries are present. However, this stretch does contain various wetland areas surrounding it which could have a stabilizing effect.
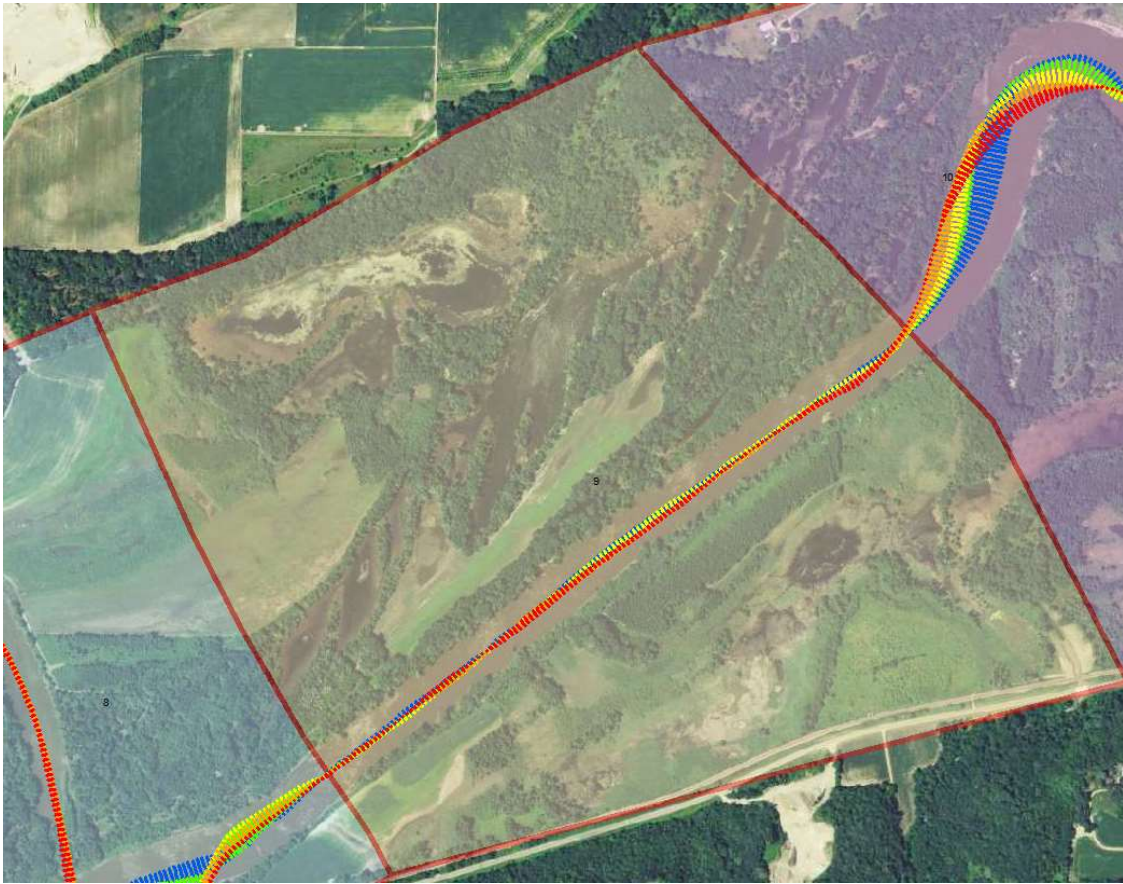
Reach 9 with migration displayed (Red = 1937-1951, Orange = 1951-1964, Yellow = 1964-1980, Green = 1980-1991, Blue = 1991-2013)
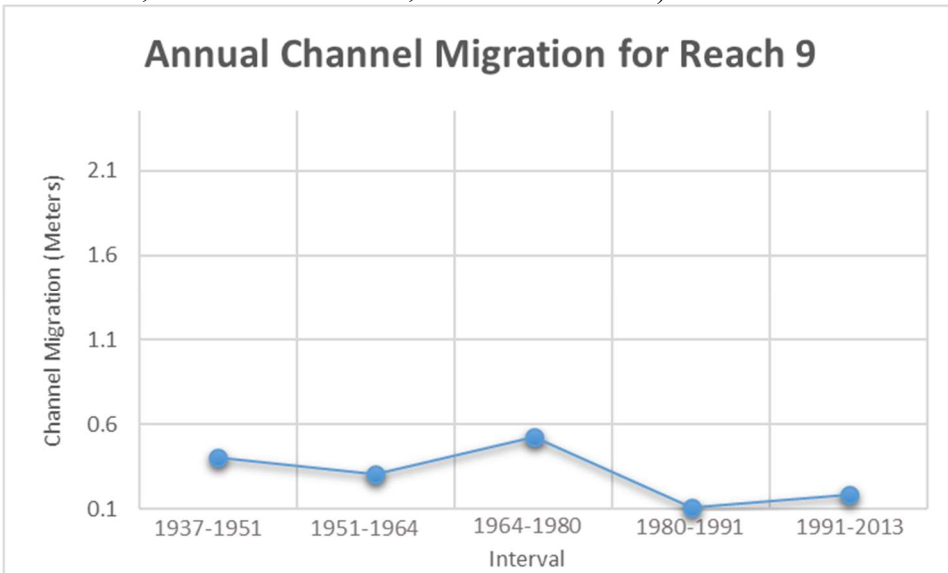
Reach 9 annual channel migration from 1937-2013

Width for Reach 9
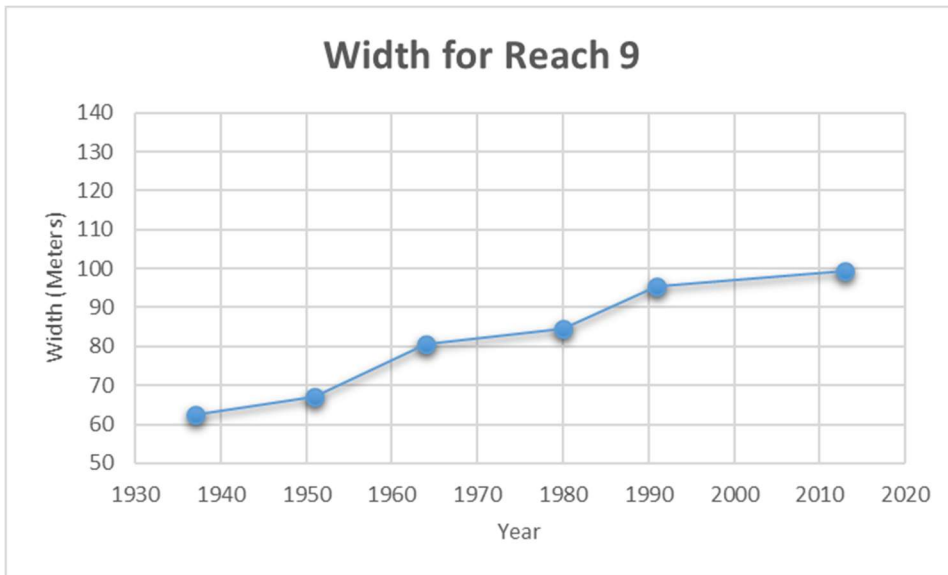
Reach 9 width change from 1937-2013

Sinuosity for Reach 9
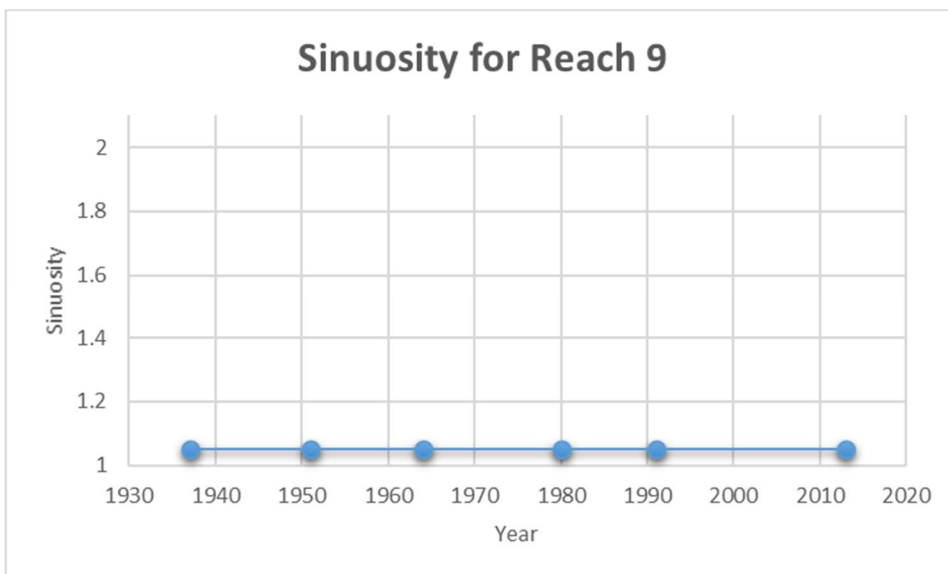
Reach 9 sinuosity from 1937-2013

Reach 10

Reach 10 is has a moderate but increasing channel migration and a common increasing channel width. This reach however differs from its upstream and downstream reaches in having a significantly greater sinuosity. It also occupying the entire river valley and has historic fluvial features (oxbows, scroll bars) throughout the valley.
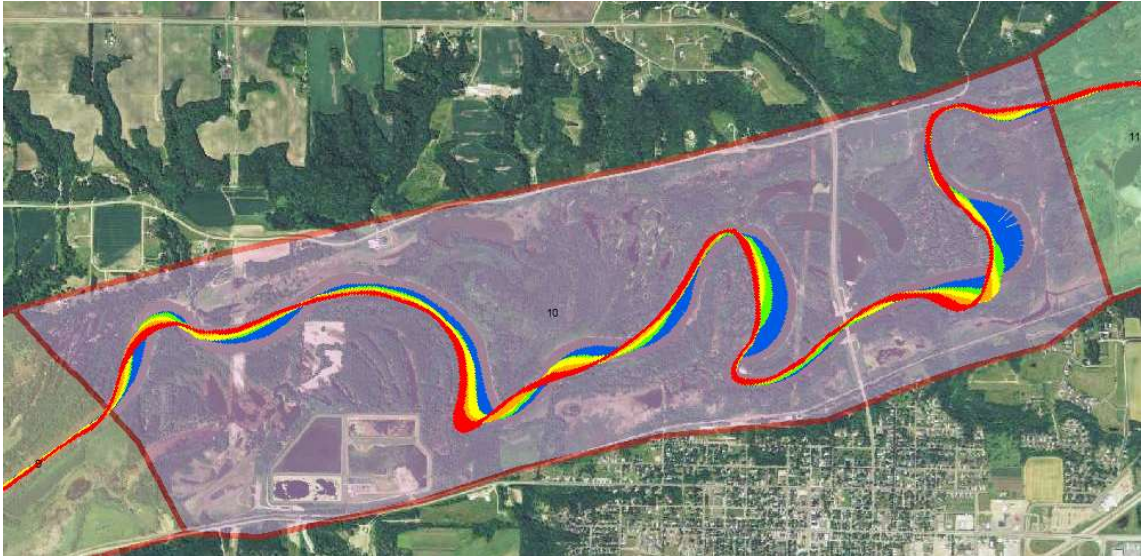
Reach 10 with migration displayed (Red = 1937-1951, Orange = 1951-1964, Yellow = 1964-1980, Green = 1980-1991, Blue = 1991-2013)
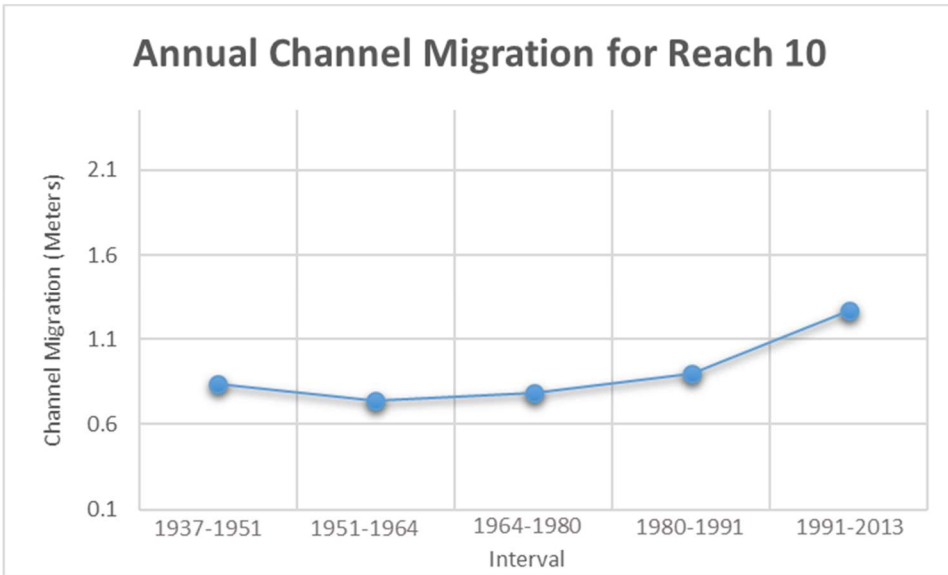
Reach 10 annual channel migration from 1937-2013

Width for Reach 10
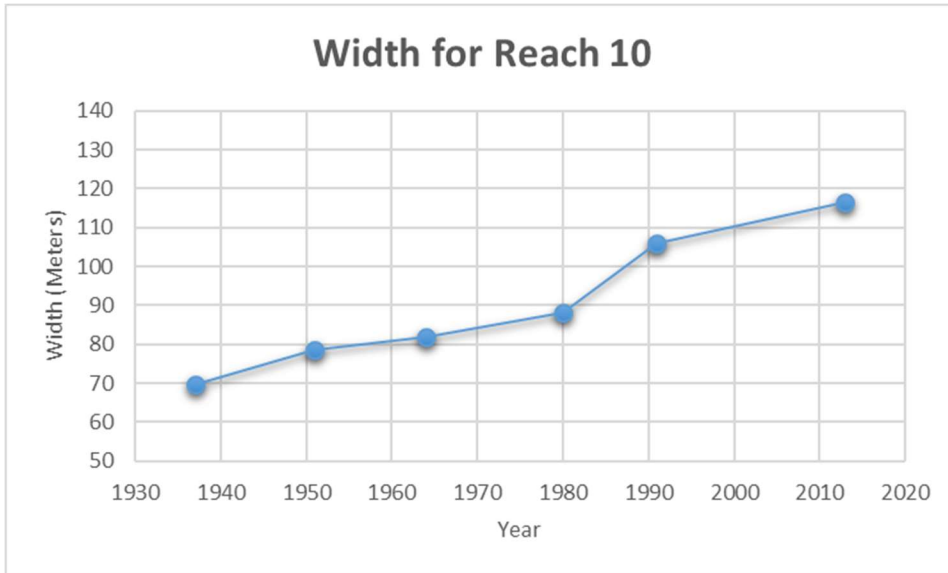
Reach 10 width change from 1937-2013

Sinuosity for Reach 10
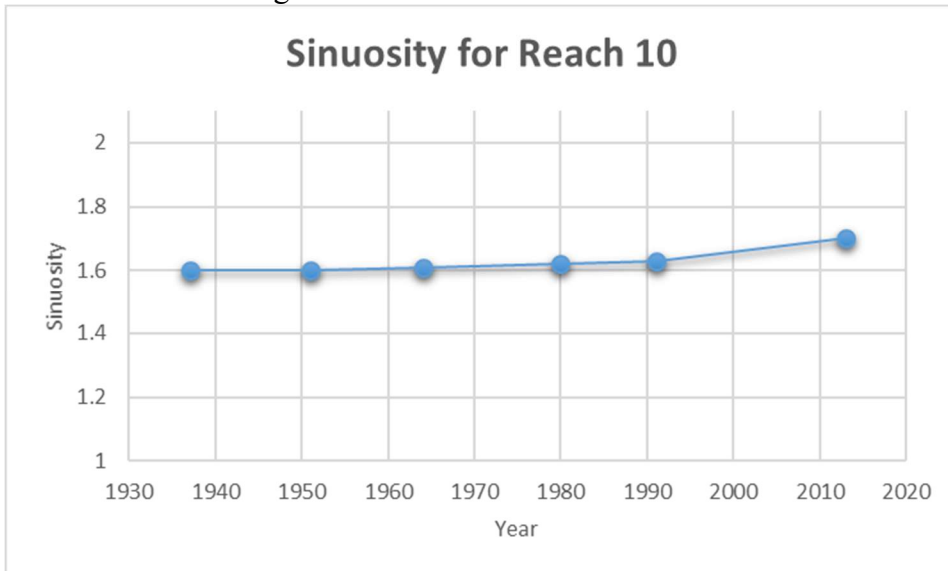
Reach 10 sinuosity from 1937-2013

Reach 11

     Reach 11 is a relatively static compared to its upstream and downstream reaches. Except for two meanders very little migration has been seen in this reach with a significant decline in the 1991-2013 interval. Channel width has also seen a relatively gradual increase compared to other reaches which is typical of other reaches that experience less migration. Sinuosity has also remained static and low through the record of time.
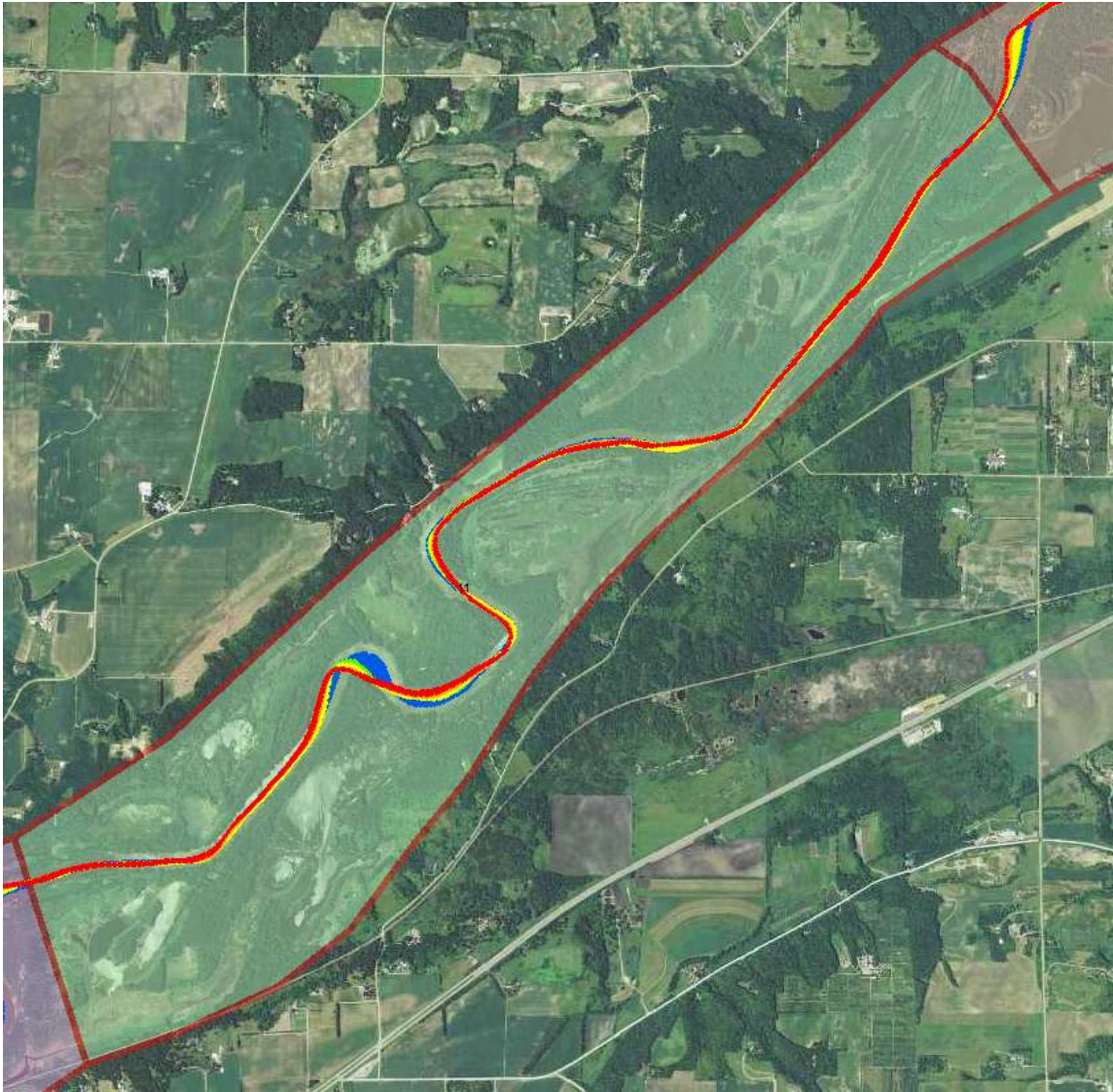
Reach 11 with migration displayed (Red = 1937-1951, Orange = 1951-1964, Yellow = 1964-1980, Green = 1980-1991, Blue = 1991-2013)
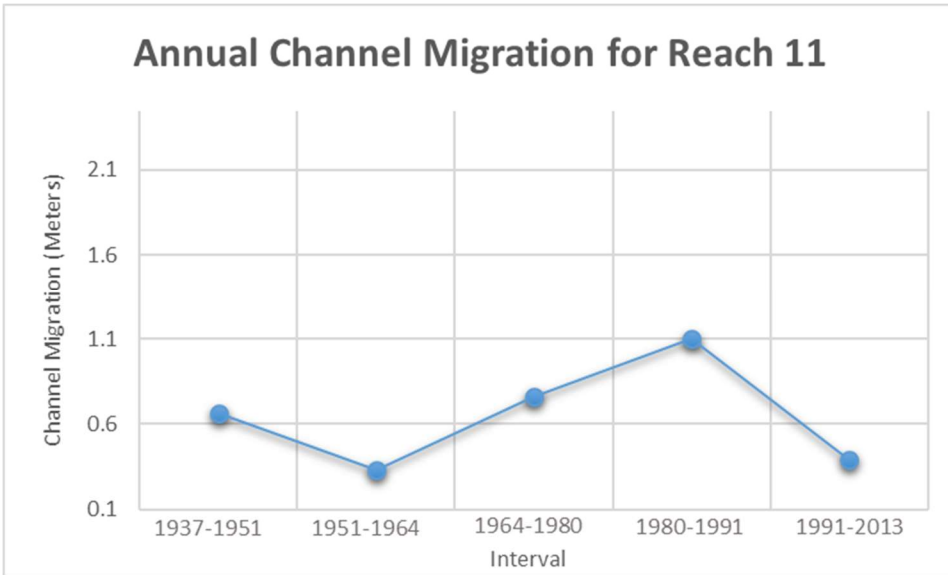
Reach 11 annual channel migration from 1937-2013
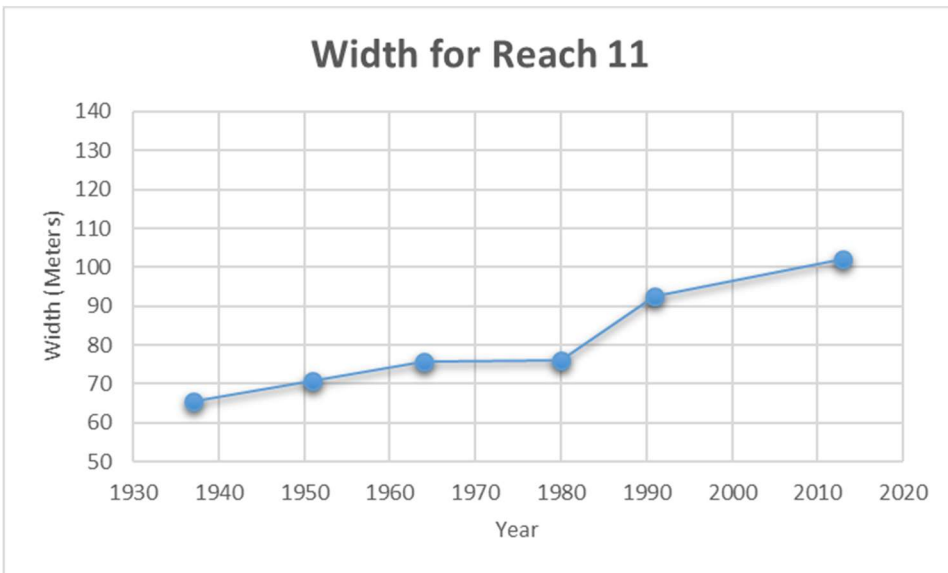
Reach 11 width change from 1937-2013
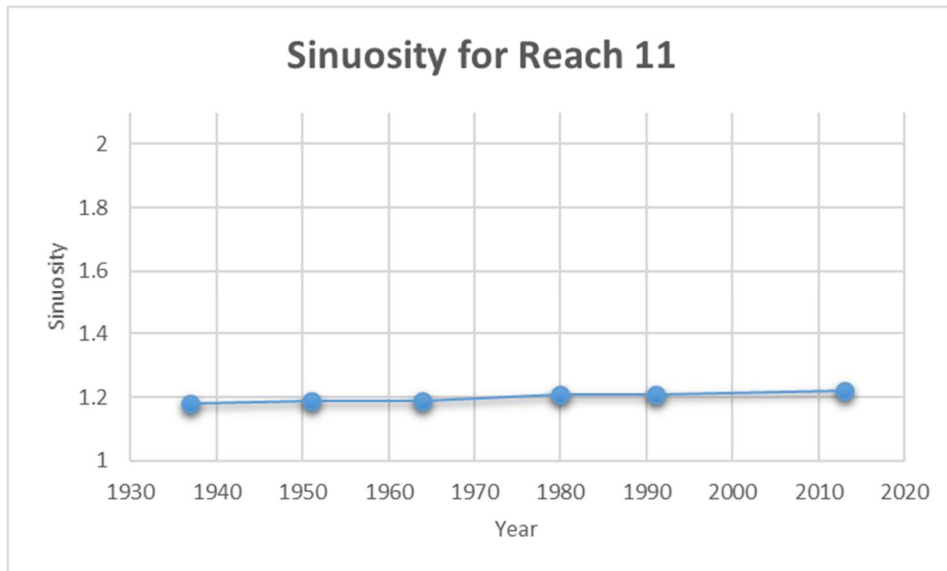
Reach 11 sinuosity from 1937-2013

Reach 12

      Reach 12 marks a significant reach for several interrelated reasons. The middle of this reach is the city of Jordan which is where Groten, Ellison, and Hendrickson 2016 noted the sediment yield is two and half times greater than at Mankato with a sharp decline following this area indicating this reach is a significant sediment sink. Due to this, this is the last highly dynamic region in planform channel change, especially channel migration. Channel width is increasing and relatively high in this reach and in sinuosity has remained stable and high. This reach is also downstream another high sediment contributing tributary, Beavens Creek. This area is dominated by translation.
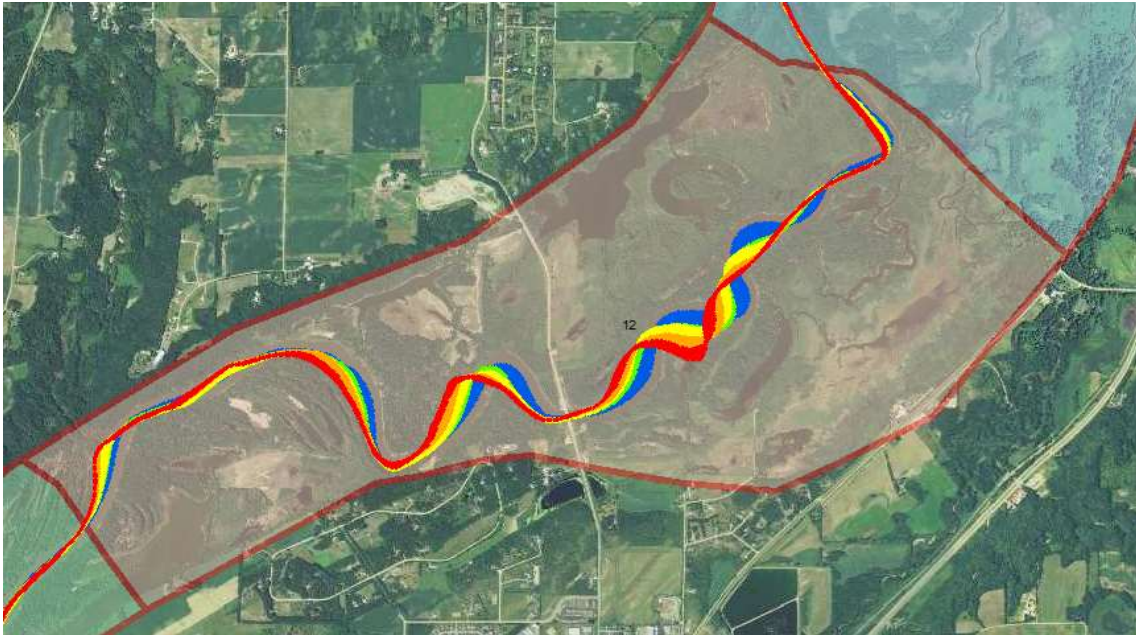
Reach 12 with migration displayed (Red = 1937-1951, Orange = 1951-1964, Yellow = 1964-1980, Green = 1980-1991, Blue = 1991-2013)
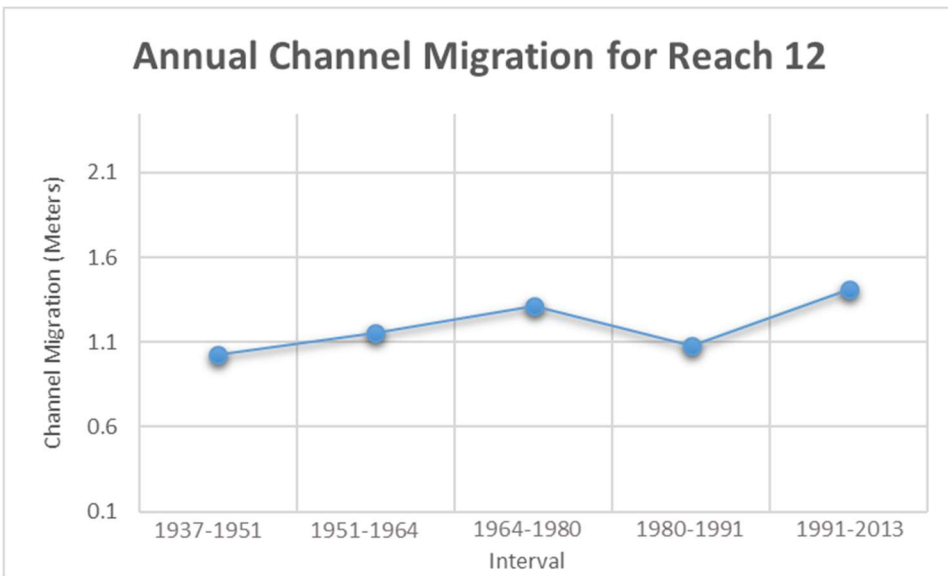
Reach 12 annual channel migration from 1937-2013
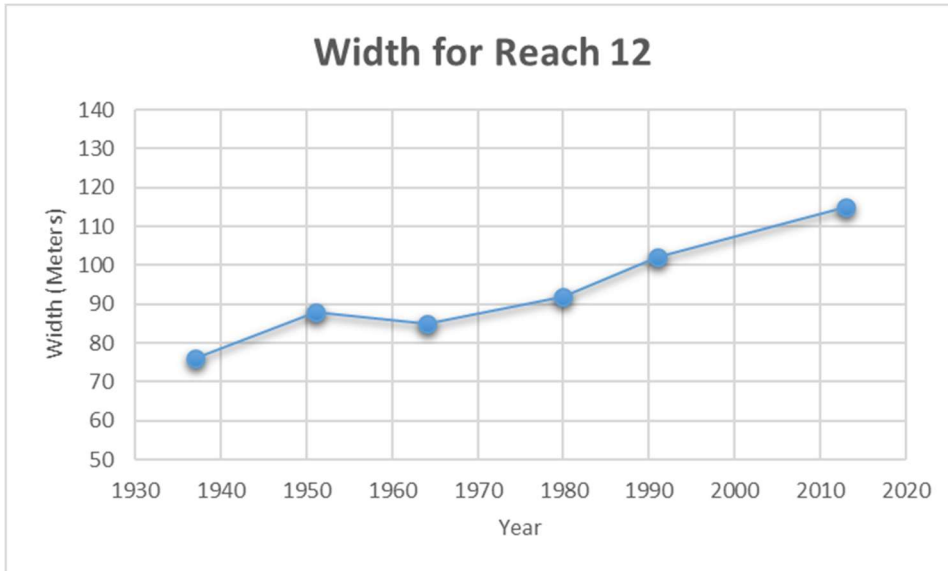
Reach 12 width change from 1937-2013
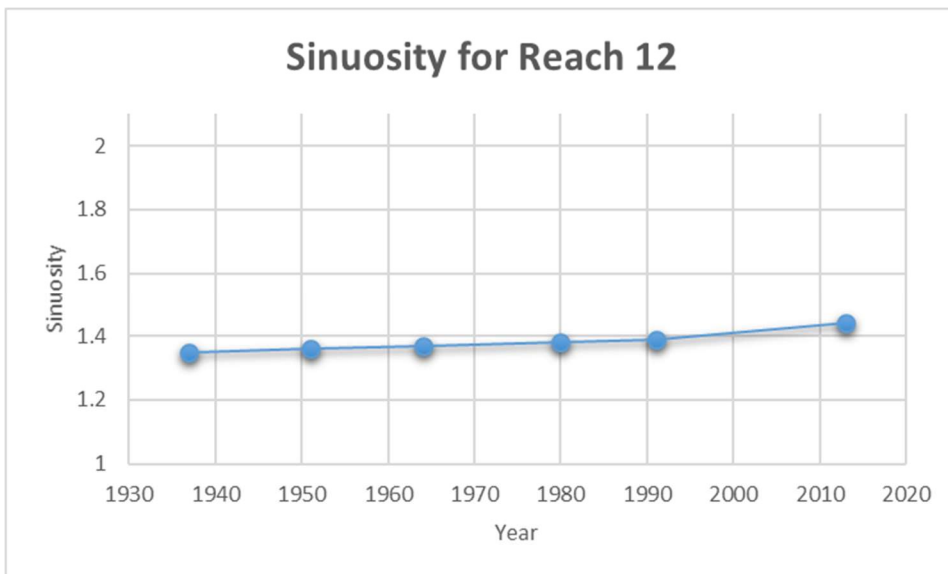
Reach 12 sinuosity from 1937-2013

Reach 13

     Reach 13 marks the beginning of the reaches with relatively little channel migration. It is also right on the edge of entering the metro area with agricultural land use still dominating outside of the river valley. This reach has had an increase in channel width but has remained the same since 1980. Despite the stability it is a highly sinuous stretch. This channel has a distinct pattern of large meanders that swing across the valley multiple times.
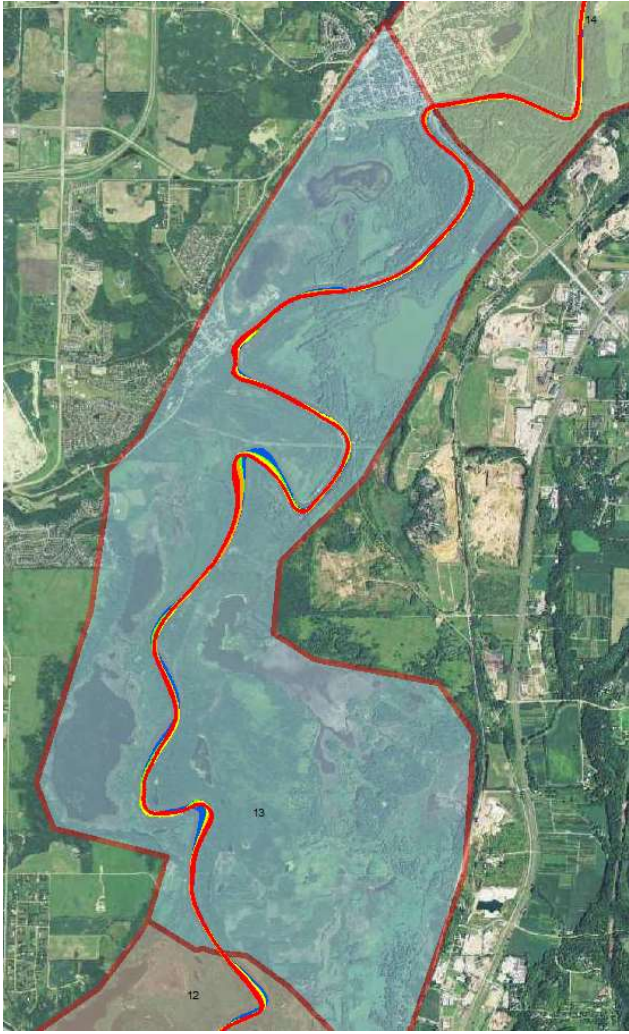
Reach 13 with migration displayed (Red = 1937-1951, Orange = 1951-1964, Yellow = 1964-1980, Green = 1980-1991, Blue = 1991-2013)
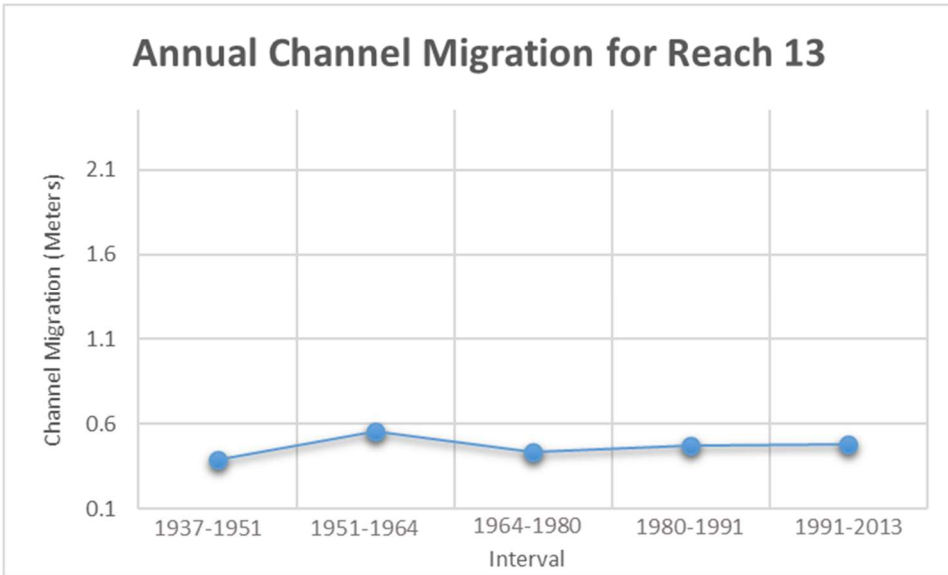
Reach 13 annual channel migration from 1937-2013
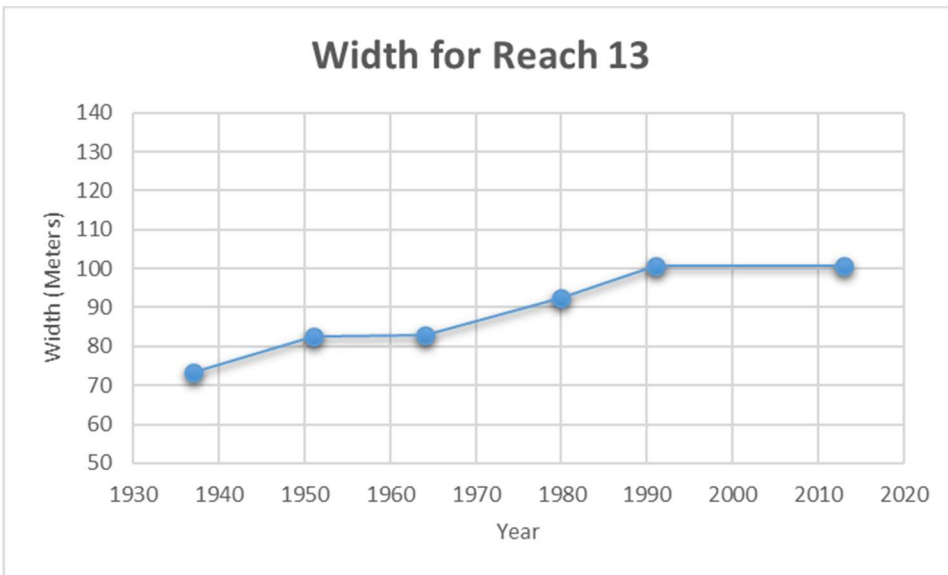
Reach 13 width change from 1937-2013
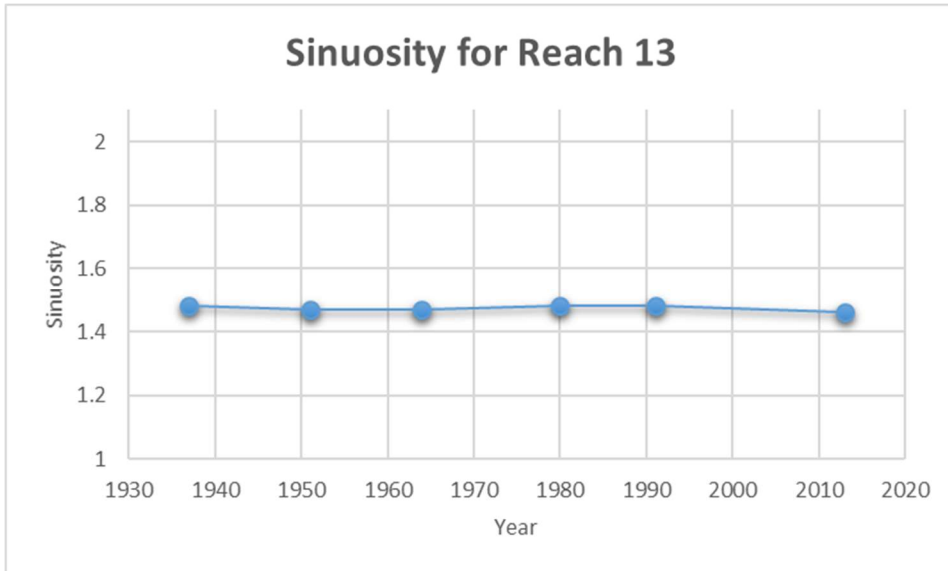
Reach 13 sinuosity from 1937-2013

Reach 14

     Reach 14 marks the first stretch that is in dominate urban land use, yet ends before where the channel is actively dredged for barge traffic. Very little channel migration has historically been seen in this reach with highest rate being ~0.6 meters per year in the 1964-1980 interval. Channel width in this stretch has only increase from an average of ~75 meters to ~95 meters, and sinuosity has remained static at ~1.2 which is lower than the prior reach.

Reach 14 with migration displayed (Red = 1937-1951, Orange = 1951-1964, Yellow = 1964-1980, Green = 1980-1991, Blue = 1991-2013)
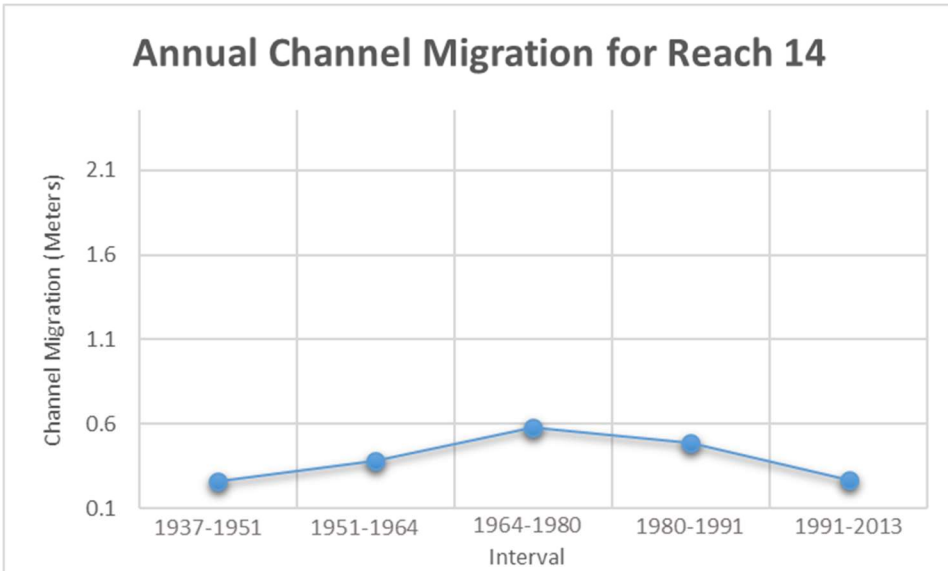
Reach 14 annual channel migration from 1937-2013
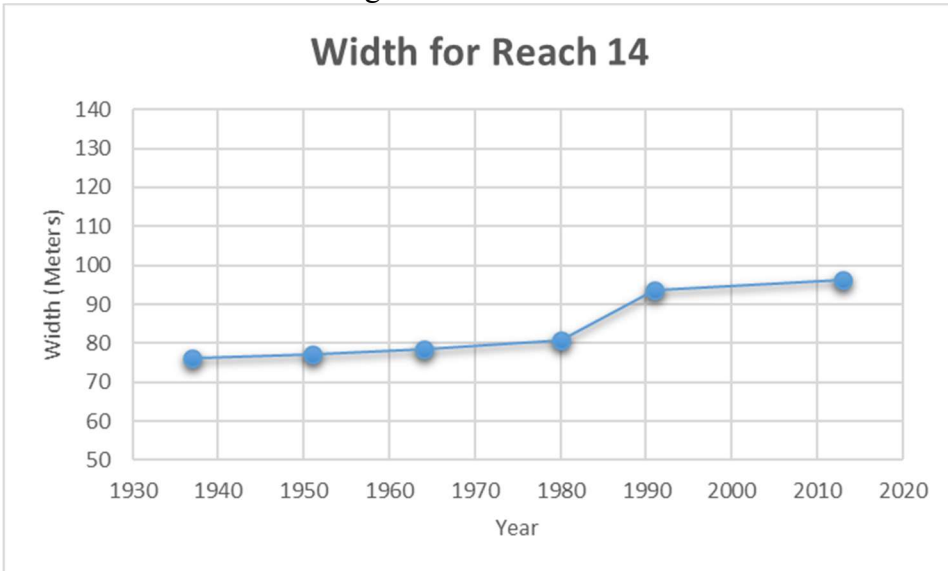
Reach 14 width change from 1937-2013
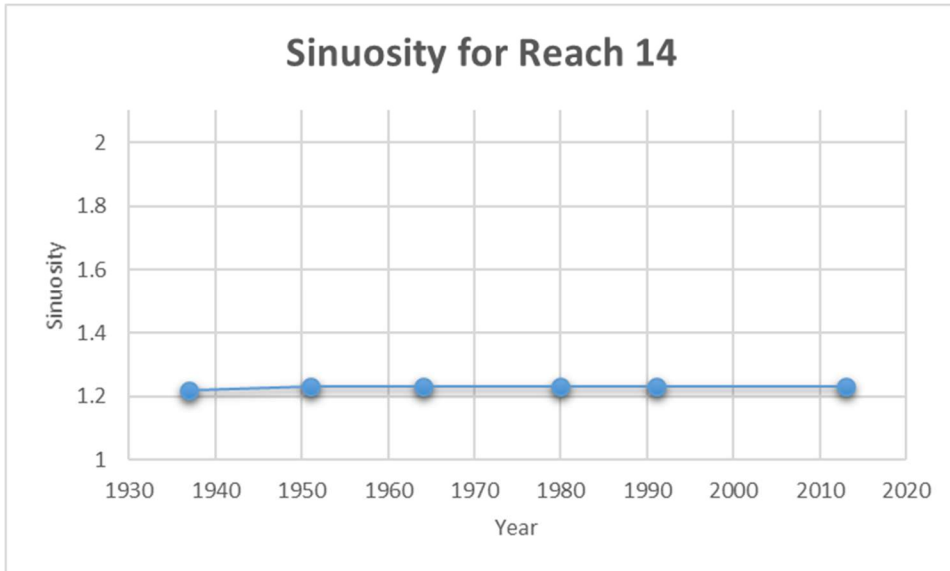
Reach 14 sinuosity from 1937-2013

Reach 15

     Reach 15 begins the channel that is actively dredging for barge traffic with two of the four dredging locations contained in it. This stretch also has heavy industrial encroachment in the river valley from barge loading areas. Migration has been low in this area with very little in the past 22 years, and width has increased more so than the prior reach. However, sinuosity decreased even more than the prior reach.
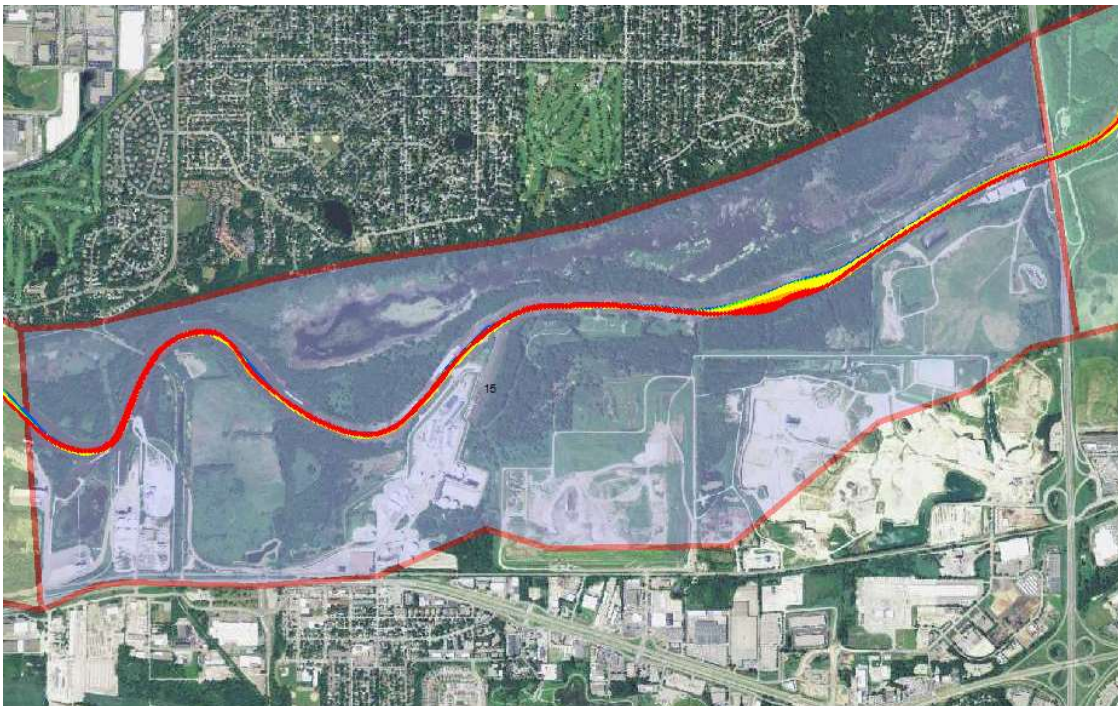
Reach 15 with migration displayed (Red = 1937-1951, Orange = 1951-1964, Yellow = 1964-1980, Green = 1980-1991, Blue = 1991-2013)
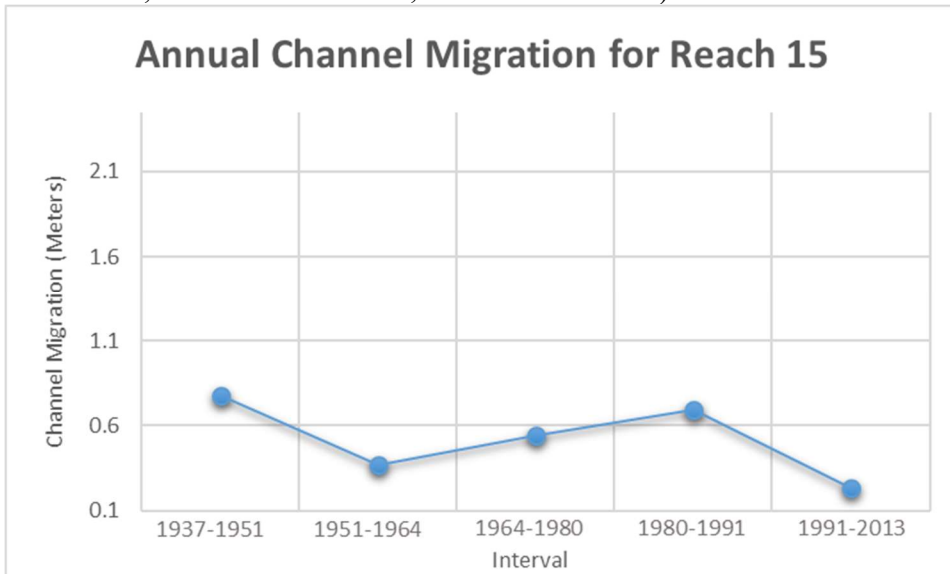
Reach 15 annual channel migration from 1937-2013
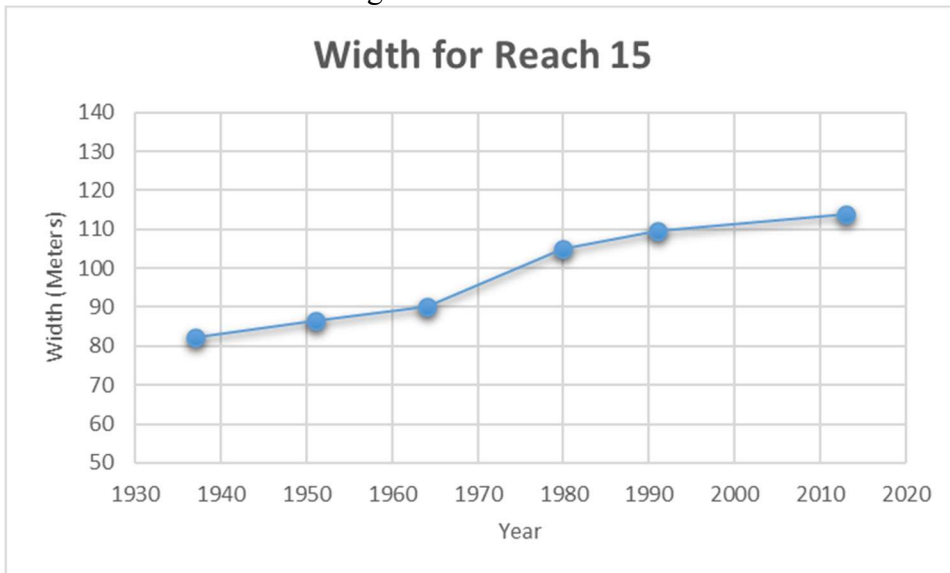
Reach 15 width change from 1937-2013
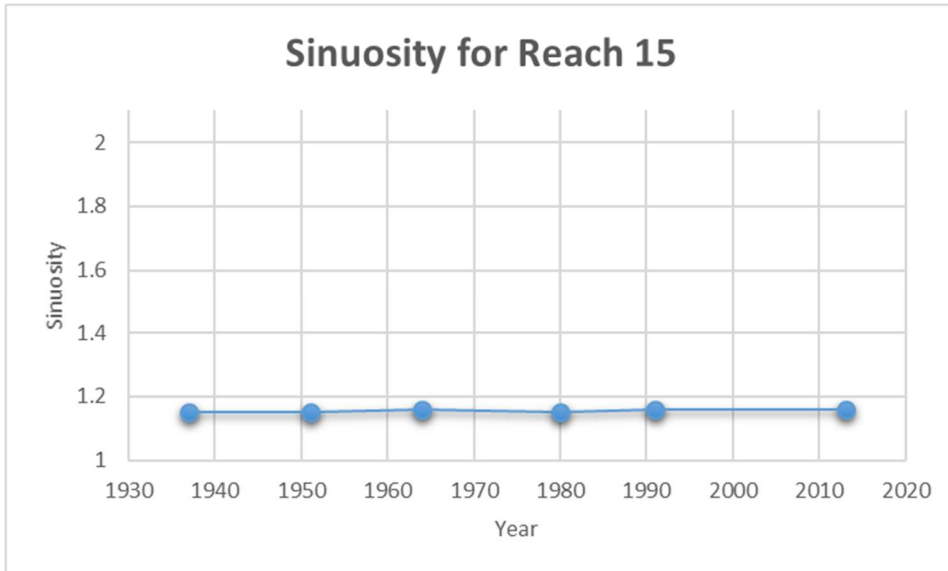
Reach 15 sinuosity from 1937-2013

Reach 16

      Reach 16 marks the last stretch ending at the confluence with the Mississippi. This reach has multiple characteristics that make it unique. The channel migration was significantly increasing over time until almost becoming completely stable in 1991-2013 interval. This could likely be due to the channel being managed for barge traffic. Width change has steadily increased. This reach also had very low sinuosity, yet still experienced three cutoffs in the 1964-1980 reducing it even further. These cutoffs are of interest since they are spatially out of place compared to the other cutoffs in the study area. No evidence could be found that these were created to increase the ease of barge traffic, yet further investigation would be required to make the formation of these fully intelligible.
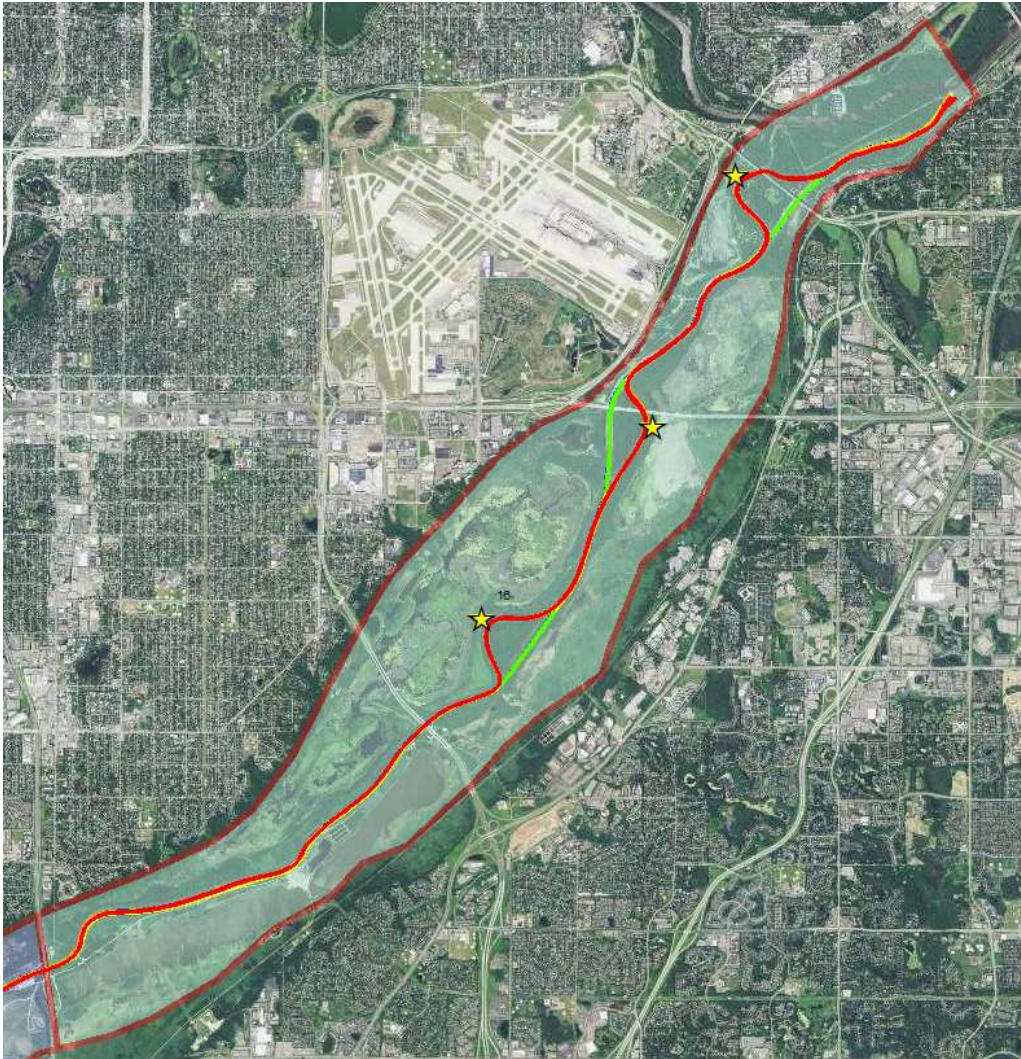
Reach 16 with migration displayed (Red = 1937-1951, Orange = 1951-1964, Yellow = 1964-1980, Green = 1980-1991, Blue = 1991-2013)
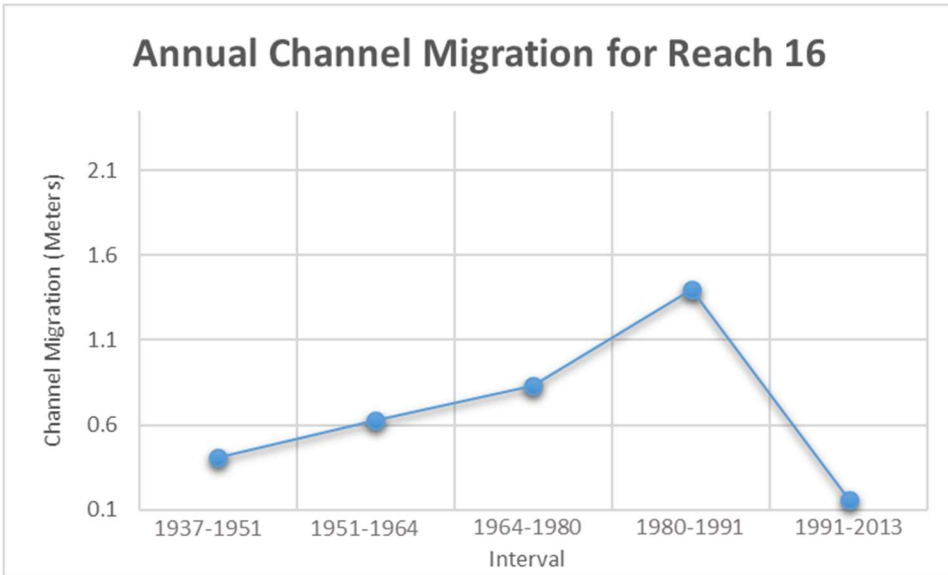
Reach 16 annual channel migration from 1937-2013
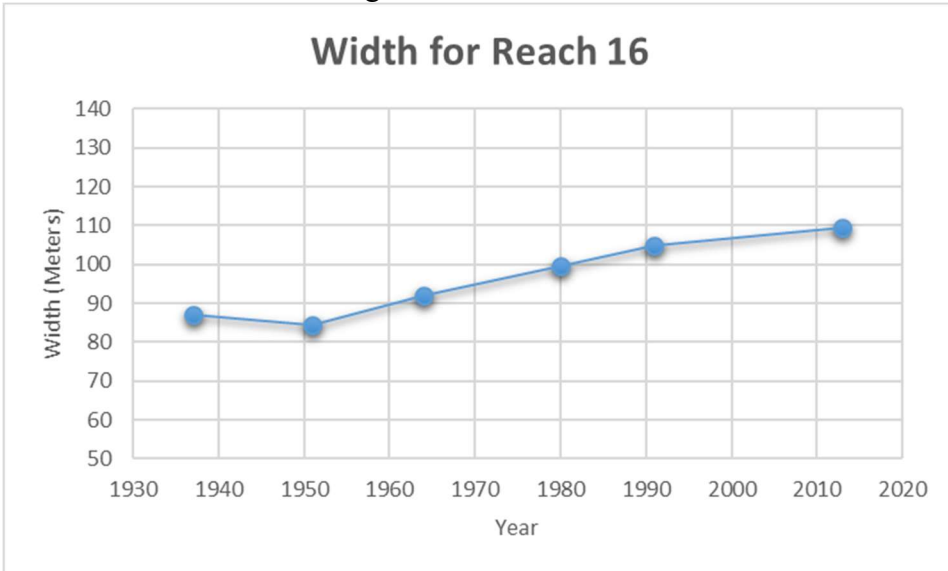
Reach 16 width change from 1937-2013
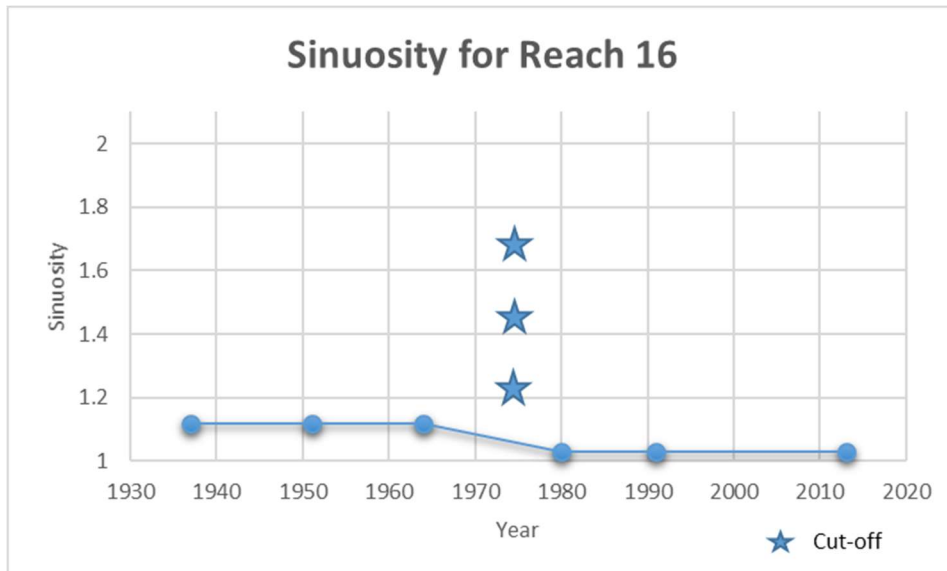
Reach 16 sinuosity from 1937-2013

Task 2: Carp Behavior

Invasive aquatic species are increasingly threatening waters in Minnesota and round the globe. Discovery of Invasive carp DNA in the Mississippi River in the Twin Cities metropolitan area has triggered renewed concern, not just for the Invasive carp and the threat they pose to Minnesota habitats, but the general issue of aquatic invasive species. Research is underway on technologies that might work to stop the carp, or divert them from one river into another. But there's no off-the-shelf gadget that would fit Minnesota's wide and fast-flowing rivers. Currently, many of the proposals under consideration don't have clear price tags.

Eradication of any established population of Invasive carp might be difficult and expensive, if possible at all. Ability to eradicate depends partly on the area that has been invaded. Invasive carp are thought to have exacting spawning requirements, requiring long rivers for the development of the eggs and larvae. If the invaded water is a reservoir or lake with no such river tributary, then Invasive carp would probably eventually die out (although this may take more than 20 years). It may also be possible to deny carp access to those rivers by erecting barriers to prohibit upstream movement to spawning habitat. Understanding the habits, lifecycle and breeding of Invasive Carp will be important to the analysis of the floodplain and connective among the main stem river and the backwaters. The behavior of invasive carp has been well researched. This component of the project will review and synthesize existing literature and integrate this research into the analysis

from this project and how it relates to the Minnesota River. This information will be researched and made available to the other phases and tasks in this project.

Deliverables:
Report on the connection between the floodplain analysis and the Carp behavior in the Minnesota River Basin. Quantify the areas of the river best suited for adults, juveniles, and spawning.

Timeline:
January 2015 - June 2017

RESULTS: *Predicting Invasive Carp Habitat Suitability in the Minnesota River, Minnesota, USA.*

Author(s): Melissa Oubre[1], Luis Escobar[2], Phillip Larson[3]
[1] Department of Biology/AGES Laboratory – Minnesota State University, Mankato
[2] Department of Fish and Wildlife Conservation – Virginia Tech
[3] Earth Science Programs/AGES Laboratory - Minnesota State University, Mankato

Corresponding Author:
Melissa Oubre – Email: mjoubre23@gmail.com Phone: 6025052639

Data Available (links require username/password: landforms/rock):
Raw Data: https://geo.mnsu.edu/geo/DNR-InvasiveCarp/Melissa-CarpModeling/Data/
Native Range Data: https://geo.mnsu.edu/geo/DNR-InvasiveCarp/Melissa-CarpModeling/Native_Range_Maps/
Model Results: https://geo.mnsu.edu/geo/DNR-InvasiveCarp/Melissa-CarpModeling/Data/ModelResults/

1. Introduction: Aquatic Invasive Species: Invasive Carp

Invasive species, as broadly defined by Executive Order 13112 during the Clinton administration, are "non-native to the ecosystem…whose introduction causes or is likely to cause economic or environmental harm or harm to human health". Invasive species typically possess characteristics that make them an immense ecological and monetary concern (e.g. high number of offspring, fast growth rate, high dispersal rate) (Lodge 1993; McMahon 2002). Successful invasive species have: 1) high abundance in their native range, 2) utilize a broad food source, 3) rapid population turn-over facilitated by quick sexual maturation, 4) the ability for fertilized females to colonize alone, 5) high genetic variability, 6) beneficial use to humans, and 7) are tolerant of a wide variety of habitats (Ehrlich 1984). These traits may be necessary for a species to survive in their native range, or the area a species historically originated from (McMahon 2002).   In new environments, invasive species lack many controls to their population (e.g. predators,

competition for food or space, and diseases) that would otherwise limit their populations (Simberloff 1989). The traits of a successful invasive species are not limited to terrestrial species.

Aquatic invasive species have multiple vectors of introduction which can be grouped into two major categories: natural and anthropogenically assisted (Lovell, Stone, and Fernandez 2006). Natural vectors conduce the movement of invasive species to new areas without anthropogenic forcing (e.g. natural dispersal, parasitism on waterfowl, and movement to new waterways during high flood stages) (Rasmussen 2002; Hermann and Sorensen 2009). Anthropogenically assisted vectors require human assistance through intentional or accidental behavior. Many invasive species are unintentionally released along trade routes or through recreational activities (e.g. zebra mussel (Dreissena polymorpha), Eurasian water milfoil (Myriophyllum spicatum), and hydrilla (Hydrilla verticillata)) (Coetzee, Hill, and Schlange 2009; Rasmussen 2002; Horsch and Lewis 2009) A well-known example of this are zebra mussels, Dreissena polymorpha. Introduced to the Great Lakes system through the release of infested ballast water, zebra mussels quickly spread through movement of water and recreational equipment between waterbodies (Rasmussen 2002). Not all species introductions are accidental however, some species are brought intentionally through the pet trade (e.g. lionfish (Pterois volitans)), as ornamental vegetation (e.g. purple loose strife (Lythrum salicaria)), to enhance recreation or trade (e.g. Northern pike (Esox lucius) in California), or as a biological controlling agent (e.g. black carp (Mycophatgynodon piceus)) (Blossey, Skinner, and Taylor 2001; Ferber 2001; Lee 2001; Semmens et al 2004).

Anthropogenic alterations (e.g. dams, river channelization, river straightening) can alter an ecosystem so that native species are no longer adapted to the modified conditions, leaving an open niche for invasive species to exploit (Aguiar, Ferreira, and Moreira 2001; Byers 2002; Johnson et al. 2008). For example, invasive parrot feather watermilfoil (Myriophyllum aquaticum) encroached on the Mondego River's riparian zone after river straightening and bank reinforcement (Aguiar, Ferreira, and Moreira 2001). Human-caused disturbances promote the spread of invasive species by creating new microhabitats and possibly opening new niches, reducing predator or competing populations making it less possible for them to control invading populations, and increasing the area of accessible habitat to invaders (Byers 2002).

Once established, invasive species can disrupt an ecosystem (Carlton 2001). Invasive species are the second leading cause of reduction in biodiversity, or variety of species, an indicator of a healthy ecosystem (Vitousek et al. 1997). For example, after the introduction of Nile perch (Lates spp.), Lake Victoria experienced the extirpation of approximately 200 vertebrate species in less than a decade (Goldschmidt, Witte, and Wanink 1993). In addition to altering the community, invasive species can alter the structure and quality of habitat available. Common carp (Cyprinus carpio), a common invasive species within the United States, can decrease water quality by increasing turbidity, or the amount of sediment within the water, and mobilizing nutrients (e.g.

phosphorous) that contribute to toxic algal blooms (Weber and Brown 2009). The effects of invasive species are not limited to environmental factors. Environmental effects often manifest as devastating economic costs, with national estimates suggesting upwards of $128 billion spent annually to mitigate the effects of invasive species (Pimentel et al. 2000; Lovell, Stone, and Fernandez 2016).

Invasive carp are one group of aquatic invasive species that are of major concern throughout the United States (Ferber 2001; Herborg et al. 2006; Kolar et al. 2007; Sass et al. 2014; Zhang et al. 2016). There are four species of invasive carp: grass carp (Ctenophaygodon idella), silver carp (Hypophthalmichthys molitrix), bighead carp (Hypophthalmichthys nobilis), and black carp (Mylopharyngodon piceus) (Figure 1.1).

Figure 1.1. Invasive carp. From top to bottom: Grass carp (C.idella), Silver carp (H. molitrix), Bighead carp (H. nobilis), and Black carp (M. piceus). © Joseph R. Tomelleri.

Invasive carp share evolutionary roots in the Yangtze River on the Asian continent, but were intentionally brought to the United States for use in aquaculture (Kolar et al. 2007). By the 1990s, invasive carp had escaped captivity and were reproducing in the Mississippi River. Invasive carp have quickly expanded their range upstream and through tributaries of the Mississippi River Basin (Kolar et al. 2007; Figure 1.2.)
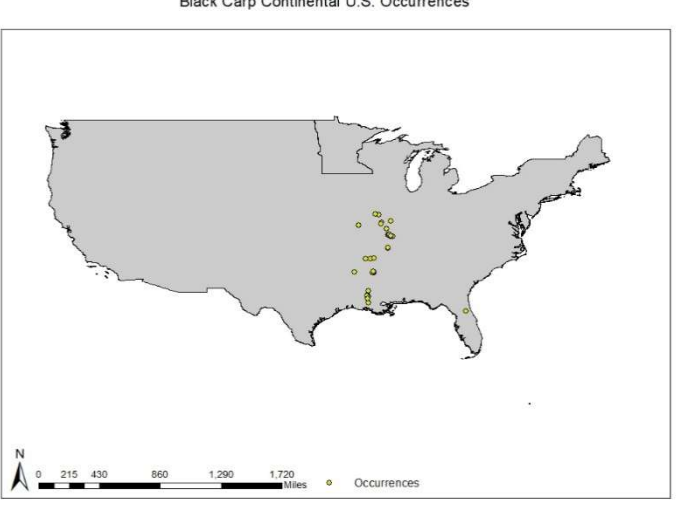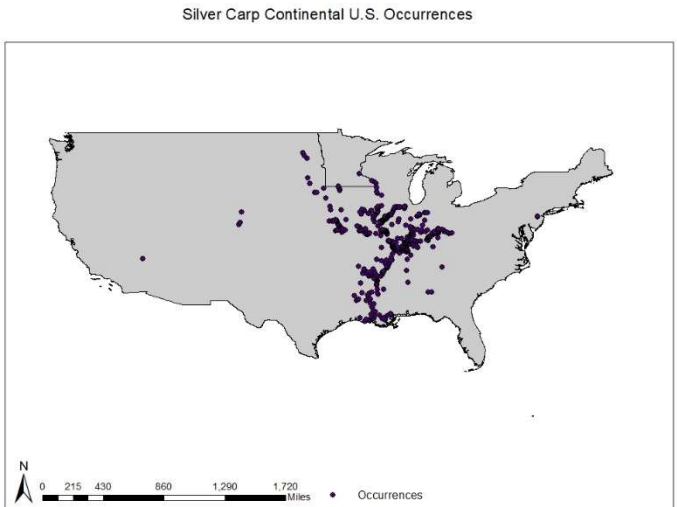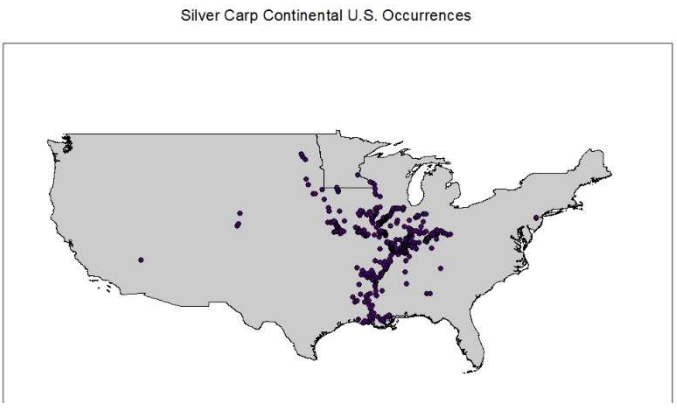
Figure 1.2. Invasive carp distributions in the United States. From upper left to lower right: Grass carp, Silver carp, Bighead carp, Black carp

Grass carp are native to waters stretching from southern Russia into northern Vietnam (Cudmore and Mandrak 2004; Figure 1.3). This area experiences average air temperatures between -6° C and 25° C (Cudmore and Mandrak 2004). Commercial fishing records provide the little information available on the abundance of wild grass carp within their native range (Cudmore and Mandrak 2004). Catch rates suggest localized population decline in parts of the native range due to overfishing during the 1950s and 60s (Shireman and Smith 1983). Despite limited population declines, grass carp are populations are on the rise in many locations outside of their native range (Raibley, Blodgett, and Sparks 1995; Pflieger 2011; Chapman et al. 2013). This is in part to grass carp being exposed to a variety of environmental conditions in its native range.
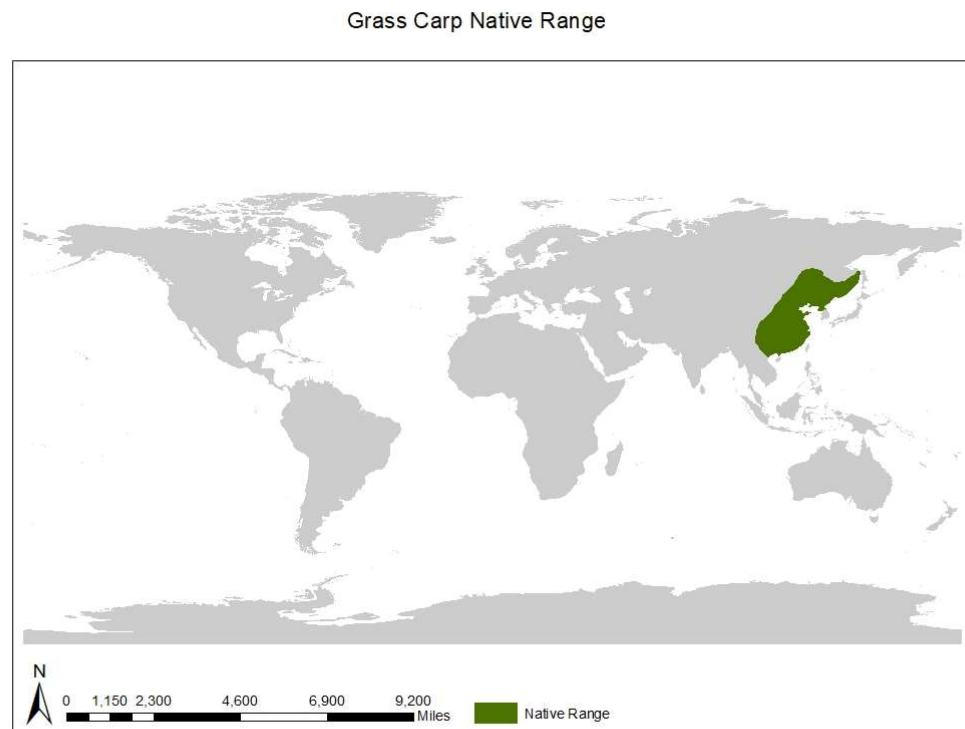
Figure 1.3. Grass carp's (C. idella) native range, adapted from Cudmore and Mandrak (2004).

Grass carp are highly adaptable and can survive in diverse environmental conditions. For example, adult grass carp can survive in water temperatures as high as 35°C, but can overwinter in temperatures as low as 1°C (Opuszynski 1972). Despite the large range, grass carp show preference for water around 25°C (Bettoli et al. 1985). Grass carp are also tolerant to low water quality, with yearlings surviving dissolved oxygen concentrations as low as 0.22 mg/L (Opuszynski 1967). Grass carp fry are more

susceptible to low dissolved oxygen levels than older carp (Opuszynski 1967). Additionally, adult grass carp can utilize brackish waters, surviving in salinity concentrations up to 19 parts per trillion for brief periods (PPT) (Shireman and Smith 1983).

Adult grass carp are capable of growing up to one meter in length and weighing 36 kg in their native range (Shireman and Smith 1983; Chilton and Muoneke 1992; Cudmore and Mandrak 2004). Wild grass carp, within their native range, typically live 5-11 years, becoming sexually mature between year 2-10 depending on food availability, temperature, and dissolved oxygen levels (Shireman and Smith 1983; Cudmore and Mandrak 2004). In the United States however, grass carp as old as 33 years have been caught and records indicate sexual maturation between years 4-5 (Chilton and Muoneke 1992; Cudmore and Mandrak 2004). Adult grass carp favor densely vegetated habitat in backwaters, ponds, and lakes and usually remain in the littoral zone (Shireman and Smith 1983; Page and Burr 1991). Adult grass carp do utilize rivers, particularly when it is time to spawn.

Sexually mature grass carp will migrate to the main river channel, particularly areas with rapids or sand bars, to spawn once triggered by river conditions. Spawning triggers include a rise in water level of at least 122 cm in 12 hours, an optimum water temperature of 20°C to 22°C, and a river velocity between 0.6-1.5 m/sec (Stanley, Miley and Sutton 1978; Shireman and Smith 1983; Chilton and Muoneke 1992). In their native range, grass carp begin migrating to their spawning grounds when water temperatures are around 15-17°C and will begin spawning once water temperatures surpass 18°C. Grass carp spawns peak at different temperatures, between 20°-22°C in Russia and 26°-30°C in China (Cudmore and Mandrak 2004). Areas with temperate climate tend to have spawns that are well defined and short lived. In contrast, spawns can be much more ambiguous in tropical regions (Cudmore and Mandrak 2004). In rare years, if conditions are met often enough, multiple spawnings have been documented (Shireman and Smith 1983). Successful spawns have been known to occur outside of the idealized ranges (Shireman and Smith 1983; Crossman, Nepszy, and Krause 1987; Cudmore and Mandrak 2004). However, if the optimum conditions are not met female carp will reabsorb their eggs (Gorbach 1970).

Even if environmental conditions for a spawn to be successful are met, grass carp eggs must stay afloat within well oxygenated water for 50-180 km (Niklosky 1963; Stanley, Miley and Sutton 1978; Chilton and Muoneke 1992). If the eggs sink and settle on the river bottom during the incubation period, the embryo will suffocate. Research suggests an optimal velocity of 0.8 m/s for incubation, although a velocity as low as 0.23 m/sec has shown to keep grass carp eggs afloat long enough to hatch (Cudmore and Mandrak 2004). For this reason, preferred spawning sites are turbid, turbulent reaches near large river confluences as the water in these areas are typically well oxygenated and provide a large enough area for incubation (Stanley, Miley and Sutton 1978). During the incubation period, the ideal water temperature is between 21-26°C, with marked

increased in deformities and death below 20°C (Shireman and Smith 1983). Once hatched, in order to survive, larval grass carp must move into calmer water, which typically occurs in habitat adjacent to the river, such as floodplain lakes.

Larval grass carp consume zooplankton and insect larvae until their growth exceeds 30 mm when they become almost exclusively herbivores (Opuszynski and Shireman 1995). As adults, 95% of a grass carp's diet is made up of macrophytes, or aquatic plants (Fedorenko and Fraser 1978). These "selective generalists" are known to eat more than 50 genera of food items, but show a preference for soft-leafed plants over firm-leafed plants or filamentous algae (Van Dyke, Leslie, and Nall 1984; Bain et al. 1990; Opuszynski and Shireman 1995; Dibble and Kovalenko 2009). In areas where there is little to no aquatic vegetation, grass have a more variable diet. Although grass carp do show plasticity in diet, when consuming non-preferred items (e.g., crayfish or emergent vegetation) individuals tend to be in poorer condition (Cudmore and Mandrak 2004). The preference for macrophytes makes grass carp appealing for use in aquaculture.

Grass carp have established self-sustaining populations in 50% of the 115 countries they were introduced in globally despite occurring in low densities in their native range (Cudmore and Mandrak 2004). The large bodied omnivores are used to control aquatic vegetation in aquaculture (Cudmore and Mandrak 2004). Grass carp were imported into the United States for use in aquaculture in 1963 and escaped into open water shortly after. The presence of grass carp has been recorded in 45 states since their introduction. Grass carp are capable removing all the aquatic vegetation from an area which can have drastic impact on an ecosystem (Dibble and Kolvalenko 2009; Van Dyke, Leslie, and Nall 1984; Wiley, Tazik, and Sobaski 1987). After the introduction of grass carp, modifications in plant communities towards invasive plants or non-palatable species has been documented, disrupting the food web and in some cases causing trophic cascade (Van Dyke, Leslie, and Nall 1984; McKnight and Hepp 1995; Dibble and Kolvalenko 2009). A decrease in water quality has also been reported due to sediment resuspension during grass carp feeding and the collapse of nutrient cycling mechanisms responsible for vegetated growth leading to algal blooms (Shireman and Smith 1983; Kirkagac and Demir 2004; Dibble and Kolvalenko 2009).   Despite the risk, triploid, or sterile, grass carp are still used in aquaculture, although the efficiency of these genetic modification to prevent spawns are still in question (Wiley, Tazik, and Sobaski 1987; Cudmore and Mandrak 2004; Dibble and Kovalenko 2009).

Silver Carp (H. molitrix)

Silver carp are native to Asia between the latitudes of 22°N and 54°N (e.g. China, northern Vietnam, and Siberia) (Xie and Chen 2001; Figure 1.4). The historical limits of silver carp's range is not known due to wide introductions in eastern Asia (Kolar et al. 2007). A large natural range has allowed the silver carp to evolve a tolerance to many environmental conditions (Xie and Chen 2001). Larval silver carp are capable of surviving in water temperatures ranging from 0°C to 46°C, although the optimal range is

between 26°C and 39°C (Opuszynski et al. 1989; Kolar et al. 2007). Silver carp can survive in brackish waters. For example, larval and fingerlings have been reported migrating to the Caspian Sea, with 6-12% salinity, to grow until sexual maturity (Abdusamadov 1987). Little information exists on adult silver carp use of brackish water, but there are recorded captures in estuarine areas in Brazil (Garcia et al. 2004). Normally, silver carp are found in slow flowing rivers and backwaters. Favoring favor open and eutrophic water, silver carp show preference for the upper and middle levels of the water column (Kolar et al. 2007).

Silver Carp Native Range
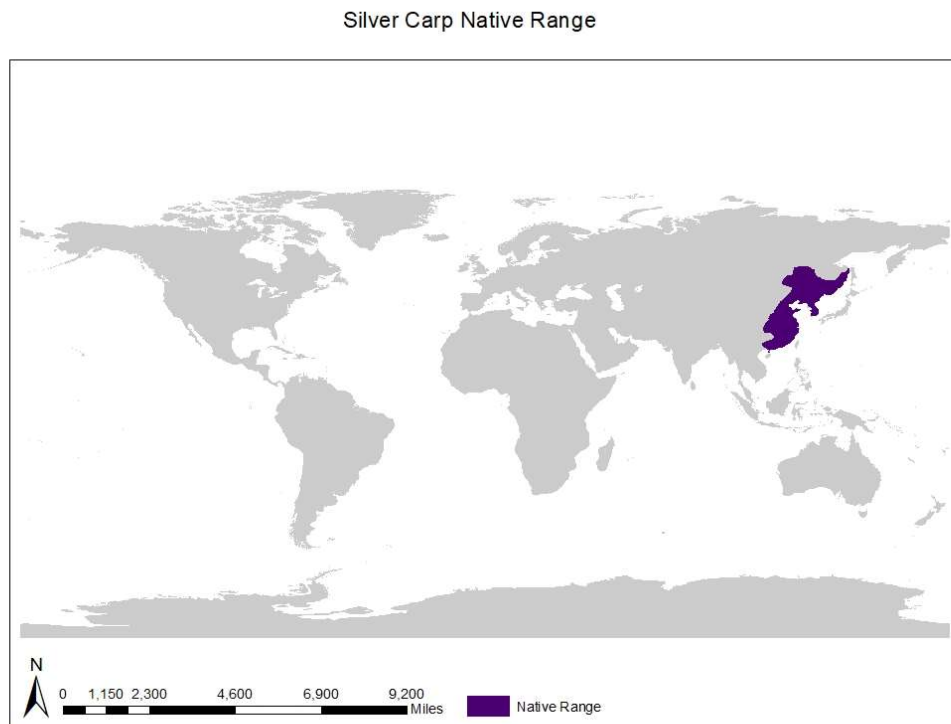
Figure 1.4. Silver carp's (H. molitrix) native range, adapted from Cudmore and Mandrak 2004

Adult silver carp are often found in large schools (Kolar et al. 2007). Large adults can reach up to 40 kg and over one meter in length (Kamilov and Salikhov 1996; Kolar et al. 2007). Silver carp grow quickly and live upwards of 20 years, becoming sexually mature between year three and six (Berg 1964; Konradt 1965; Abdusamadov 1987; Kolar et al.2007). A highly fecund species, female silver carp produce an average of 171 eggs per gram of body weight, with records showing up to 1.3 million eggs (Jhingran and Pullin 1985; Abdusamadov 1987).

Sexually mature silver carp, triggered by environmental conditions, migrate to swift waters, usually near the mouths or confluences of rivers, to spawn (Konradt 1965). Spawning conditions are not universally agreed upon, but research suggests that an increase in water level, a minimum velocity of 0.7 m/s, water temperature of at least 17°C, and flooded backwaters are indicators for spawning events (Verigin et al. 1978; Krykhtin and Gorbach 1981; Schrank et al. 2001; DeGrandchamp et al. 2007; Lohmeyer and Garvey 2009). It is argued the increase in flow may not initiate the spawn, but instead causes an increase in turbidity which triggers the silver carp to start spawning (Stanley et al. 1978). This hypothesis is supported by evidence in the highly turbid Kara Kum Canal, which is controlled for water level, but meets the flow and temperature criteria during part of the year. This canal has had occurrences of silver carp spawning events despite consistent water level, supporting that the spawning criteria may be flexible (Aliyev 1976). Silver carp are known to spawn up to 3 times in a year (Ruebush 2011), but if environmental conditions are not ideal, female carp will reabsorb some or all their eggs, conserving energy (Gorbach 1970). Eggs released in a spawning event will continue downstream until hatched.

Flow velocity is important in maintaining egg buoyance, as the eggs must stay afloat until they are hatched (Niklosky 1963; Murphy and Jackson 2013). It was believed that at least 100 km of river is needed for the eggs to hatch (Krykhtin and Gorbach 1981), but more recent research suggests incubation time is site specific and dependent on water temperature and velocity (Murphy and Jackson 2013). In some cases, the eggs floated as little as 25 km before hatching (Murphy and Jackson 2013). Once hatched, larval silver carp migrate to slower water in flooded backwaters where they consume zooplankton and grow (Krykhtin and Gorbach 1981; Williamson and Garvey 2005). At around 18 days old the primary diet of silver carp switches to phytoplankton, which remains their preferred food choice for the remainder of their life (Sobolev 1970; Cremer and Smitherman 1980; Spataru, Wohlfarth, and Hulata 1983; Williamson and Garvey 2005).

Highly modified gill rakers allow silver carp filter plankton and other particles out of the water (Kolar et al. 2004). The gill rakers are capable of filtering particles as small as 3.2 μm (Chorella spp. Algae) (Kolar et al. 2007). Research has found no difference in the proportion of taxa or particle size in the gut of silver carp in comparision to water samples, suggesting they are not selective (Cremer and Smitheran 1980). When phytoplankton densities are low, silver carp will also consume algae, zooplankton, bacteria, and detritus in large quantities (Schroeder 1978; Opuszynski 1981; Spataru and Gophen 1985). The ability of silver carp to filter large quantities of plankton made the fish appealing for biocontrol.

Silver carp have been imported or spread to 88 countries globally (Kolar et al. 2007). Of those 88, 23 countries have reproducing populations and 32 countries are unsure if silver carp are established. There are multiple accounts of silver carp being imported to the United States for aquaculture or biofiltration of sewage ponds (Cremer and Smitheran 1980; Shelton and Smitherman 1984). It is believed silver carp initially

escaped from Arkansas into tributaries of the Mississippi River (Kolar et al. 2004). As of 2018, there are occurrences of silver carp in 21 states. Silver carp's ability to indiscriminately filter out small particles in the water was useful in biofiltration and aquaculture, but now makes the species a danger to native populations. For example phytoplankton communities experience a species composition shift towards smaller species in the presence of silver carp (Kucklentz 2017). Similar shifts can be seen in zooplankton communities, but this may be due to competition for food, not predation (Fukushima et al. 1999; Radke and Kahl 2002). In addition to altering species communities, silver carp also effect human recreational activities. Adult silver have a physical reaction to noise disturbances in the water. When startled by noise, like a boat motor, the fish jump out of the water (Nikolsky 1963). Jumping may be a defense mechanism in response to a perceived predator (Perea 2002). This reaction does pose a serious danger to boaters, as jumping silver carp capable of breaking bones or causing concussions as they fly through the air and come into contact with people (Kolar et al. 2007).

Bighead carp are native to eastern China, Siberia, and far northern portions of North Korea, between latitudes of 24°N and 47°N (Figure 1.5). Similar to silver carp, bighead carp's natural native range may never be known because of wide introductions throughout eastern Asia (Kolar et al. 2007). Chinese commercial fisheries catch records suggest that bighead carp populations are abundant in their native range. In 1998, silver carp and bighead carp combined made up more than 60% of the 1,294,000 metric ton commercial fishing haul from Chinese reservoirs (Kolar et al. 2007). The native distribution for bighead carp has a large air temperature range of -30°C to 40°C (Kolar et al. 2007).

Bighead Carp Native Range
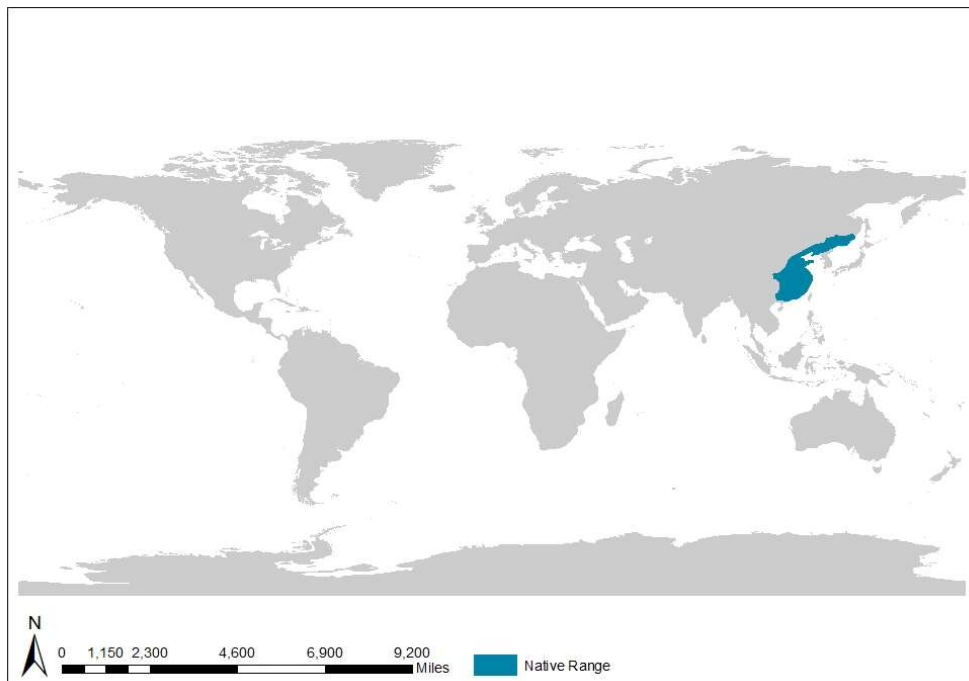
Figure 1.5. Bighead carp's (*H. nobilis*) native range, adapted from Cudmore and Mandrak 2004

A large historical range allowed bighead carp to evolve tolerance to range of environmental conditions. In a laboratory study, bighead carp preferred water temperatures of 25.0-26.9°C (Bettoli et al. 1985). The same study concluded bighead carp's thermal maximum as 38°C (Bettoli et al. 1985). The lower thermal limit has not been researched, but bighead carp survive in the Manchurian Plain, which remains frozen for 4 to 6 months of the year, so it is assumed they are cold tolerant (Kolar et al. 2007). Similar to the previous species of invasive carp, bighead carp are able to survive in brackish water with low salinity. A study conducted on bighead carp fry in Laguna Lake in the Philippines, which experiences saltwater intrusion, concluded that bighead carp must have some osmoregulation abilities that allowed them to continue to grow after facing exposure to saline water (Garcia et al. 1999). Habitat use by bighead carp is also very similar to silver carp. Most adult bighead carp remain in waters that are slower than 0.3 m/s within the river channel or neighboring backwaters. Staying below 3 meters, bighead carp are not seen at the surface unless spawning or feeding (Kolar et al. 2007). Bighead carp tend to be rather stationary moving less than 15 km daily, except during a spawn (Peters, Pegg, and Reinhardt 2006).

Bighead carp are capable of growing to lengths over 1.5 meters long and 40 kg (Kolar et al. 2007). Not much is known about the longevity of the species in the native range. The oldest bighead carp caught in the United States was 8-10 years old and showed evidence of recent growth (Morrison et al. 2004). Generally, bighead carp become sexually mature during their third to fourth year of life, although environmental factors will influence this (Jennings 1988). Female bighead carp are highly fecund, usually producing 126 eggs per gram of body weight (Jhingran and Pullin 1985).

The bighead carp spawn typically occurs between April and June in Asia, peaking in late May (Kolar et al. 2007). Akin to the other invasive carp species, bighead carp are triggered to migrate upstream to spawning grounds by a rise in water level (Jennings 1988). Characteristic bighead carp spawning grounds are found where the mixing of waters in occurring (e.g. confluences, rapids, behind sandbars). Native spawning sites typically have rapidly flowing turbid water with a velocity of 0.6-2.3 m/s and visibility of 10-15 cm (Verigin et al. 1978). Ideal water temperature ranges from 18°C to 30°C (Verigin et al. 1978; Kolar et al. 2007). Evidence of successful spawns have occurred outside these conditions (e.g. Kara Kum Canal), suggesting plasticity in spawning requirements (Aliev 1976; Opuszynski and Shireman 1995). Once laid, the drifting eggs must stay afloat in an oxygenated current until mature enough to migrate into nursery habitat (e.g. backwaters) where they feed on zooplankton (Kolar et al. 2007; Deters, Chapman, and McElroy 2013).

Bighead carp remain zooplanktonivorous throughout their lives (Cremer and Smitherman 1980; Jhingran and Pullin 1985). Bighead carp have two feeding methods,

pump feeding and ram suspension feeding (Kolar et al. 2004). When pump feeding, bighead push water through their gill rakers, filtering out particles (Kolar et al. 2007). Ram suspension feeding occurs at the surface, where bighead swim through the water with their mouth open, pushing water through their gill rakers in intermittent gulps (Kolar et al. 2007). Unlike silver carp, bighead carp will selectively feed when food densities are high (Jennings 2988). However, bighead carp are known to be opportunistic when zooplankton densities are low, switching to phytoplankton or detritus.

Bighead carp have records in 73 countries and have established populations in 19 countries (Kolar et al. 2007). Introduced to the United States in 1972, bighead carp were used in aquaculture farm in Arkansas to improve water quality (Jennings 1988). It is unknown when bighead carp escaped containment, but the first captures in open waters occurred during the early 1980s (Jennings 1988). Once in a system, bighead carp are a great risk to native planktivores that have overlapping diets, like the gizzard shad (Dorosoma cepedianum) and bigmouth buffalo (Ictiobus cyprinellus) (Irons et al. 2007; Sampson, Chick, and Pegg 2009). Studies done on the Illinois River showed a decline in population and condition of gizzard shad and bigmouth buffalo post silver and bighead carp invasion (Irons et al. 2007).

Black Carp (M. piceus)

Black carp have a native range from southern Russia to southern China, but are absent from the Korean peninsula (Nico, Jelks, and Williams 2005; Figure 1.6). This includes most Pacific Ocean draining watershed in east Asia from 22°N and 51°N (Nico, Jelks, and Williams 2005). Unfortunately, due to incomplete records and introductions into non-native waters the true historical range may never be known. Similar to grass carp, wild native black carp populations may also be in decline in some areas due to overfishing (Berg 1945; Nico, Jelks, and Williams 2005). Black carp are so rare in Russia, they were listed as a species threatened with extinction in the early 2000s (Nico, Jelks, and Williams 2005). However, black carp are thriving in other parts of their native range, including the Chang River basin (Berg 1949; Nico, Jelks, and Williams 2005).

Black Carp Native Range
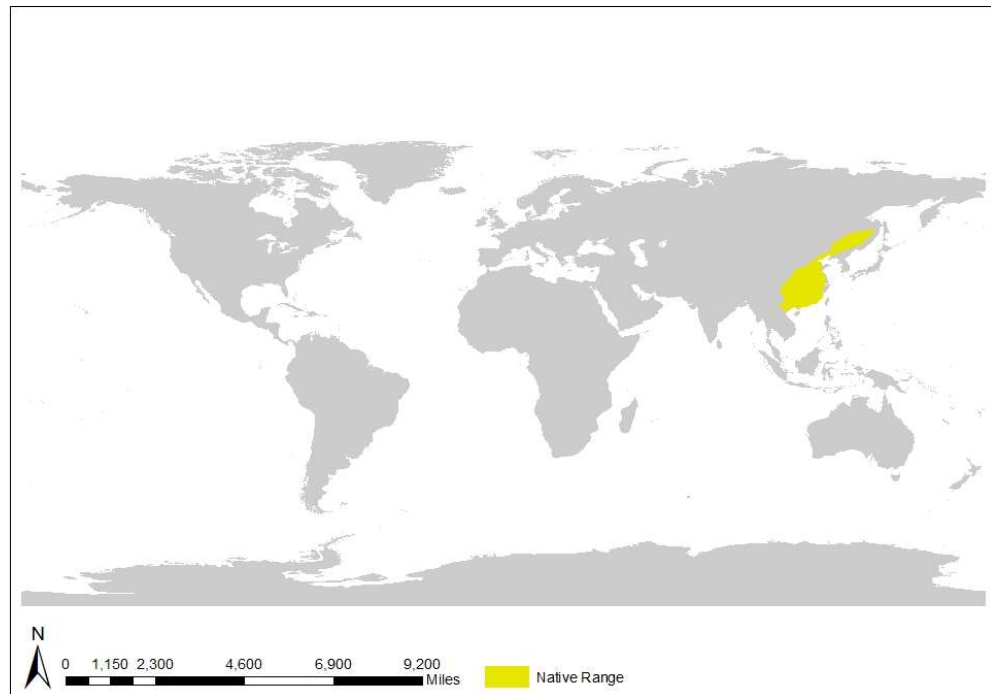
Figure 1.6. Black carp's (M. piceus) native range, adapted from Cudmore and Mandrak 2004

Little research exists on black carp outside their use in aquaculture but these benthic fish are hypothesized to have all the same life requirements as the other invasive carp species (Nico and Jelks 2011). Black carp are native to a variety of climates, ranging from subtropical to cold (Nico, Jelks and Williams 2005). Thermal limits for wild black carp are not known, but research shows the fish do best between 4°C and 30°C (Nico, Jelks and Williams 2005). Their large native range suggests black carp are cold tolerant, as portions of the Amur River are frozen for part of the year (Nico, Jelks and Williams 2005). There is also no data on the salinity limits of black carp, but they have been captured in brackish water before (Gorbach 1961; Nico, Jelks and Williams 2005). Black carp prefer clear water, with dissolved oxygen levels around 5mg/L, but can survive dissolved oxygen levels as low as 2 mg/L (Nico, Jelks and Williams 2005). Similar to the other invasive carp species, black carp can be found in rivers, backwaters, and lakes depending on their life stage (Nico, Jelks and Williams 2005).

Black carp are large-bodied with records showing growth up to 1.5m in length and over 70kg (Nico, Jelks, and Williams 2005). Growth rates and age of maturity are related to latitude, with carp at lower latitudes becoming to sexual mature at a younger age (Nico, Jelks, and Williams 2005). Male black carp reach maturity anywhere from six to eleven years of age, although there have been instances of sexually mature males as young as three in China (Nico, Jelks, and Williams 2005). Female black carp are highly fecund, producing 82 ova per gram of body weight, with research showing occurrence of up to a million eggs (Jhingran and Pullin 1985). Adult black carp inhabit slow moving water within the middle and lower portions except during spawning events where they move to large rivers (Nico and Jelks 2011).

In their native range, black carp spawn in late spring into summer, depending on seasonal flooding (Nico, Jelks, and Williams 2005). Surges in water level, increased velocity, and water temperatures between 26°-30°C are cues for black carp to move to large rivers to spawn (Soklov 2002; Nico, Jelks, and Williams 2005). In aquaculture, black carp spawn later than silver carp or bighead carp despite similar spawning requirements (Atkinson 1977). Multiple black carp spawns have been suggested in the literature, but the occurrence of multiple spawns has never been recorded (Nico, Jelks, and Williams 2005). Similar to other invasive carp, black carp eggs need to remain buoyant until hatched (Nico, Jelks, and Williams 2005). Once hatched, larval black carp migrate to nursery habitat in backwaters and attached lakes to feed (Chang 1966).

Larval black carp consume zooplankton until their pharyngeal teeth grow, at which point they become full time molluscivores, consuming mostly bivalves and snails (Nico, Jelks, and Williams 2005). Pharyngeal teeth are a distinguishing feature of black carp in comparison to other invasive carp species. The structure allows black carp to crack the hard outer shells of their prey (Nico, Jelks, and Williams 2005). Information on wild black carp diet, particularly selectivity of taxa, is lacking. Most information available about black carp diet is from aquaculture, where mollusks are supplemented (Nico, Jelks, and Williams 2005). This lack of data makes interpreting the trophic ecology of black carp difficult. Despite the unknown trophic risk, black carp were widely introduced to control mollusk populations (Nico, Jelks, and Williams 2005).
Black carp have been introduced in 30 countries globally (Nico, Jelks, and Williams 2005). Initially, black carp was imported into the United States as a "contaminant" in grass carp stocks in 1973 (Nico, Jelks, and Williams 2005). Beginning in the 1980s, black carp were used as a biocontrol for parasites hosted in snails and reared for food (Nico, Jelks, and Williams 2005). It was also believed black carp could be used as a biocontrol for zebra mussels, but further research did not support this (Nico, Jelks, and Williams 2005). In 1994, there was a documented escape of black carp into open waters, but a wild invasive black carp was not captured in the wild until 2003 (Chick et al. 2003; Nico, Jelks, and Williams 2005). Eleven states are now listed as having black carp occurrences, much less than other invasive carp species (Nico, Jelks, and Williams 2005). Black carp are rarely detected and typically only captured in hoops nets, indicating low abundances or an aversion to current sampling methods (Nico and Jelks 2011). Listed as injurious in

2007 under the Lacey Act, black carp are still used in Arkansas and Mississippi for aquaculture in their fertile diploid form, but can no longer be imported or transported across state lines (Nico and Jelks 2011). Due to lack of data, it is difficult to predict the impact this species will have, black carp's diet could negatively effect native mollusk populations (Nico, Jelks, and Williams 2005).

1.1. Efforts to Control Invasive Carp

Aquatic invasive species are nearly impossible to eradicate once in a non-native aquatic system (Chen et al. 2007). Therefore, the most effective way to manage aquatic invasive species is to prevent their arrival and establishment (Lovell et al. 2006). In systems where invasive carp are established, managers work to control their distribution and population size in attempts to prevent them from causing further harm to native ecosystems. Strategies for controlling invasive fish post invasion include mechanical removal (e.g. electrofishing or gill netting), piscicides such as Rotenone or other chemicals, or habitat modifications through barriers (Moy et al. 2011). Mechanical removal, particularly electrofishing, allows the selective removal of species, but is more labor intensive. Piscicides are less labor intensive, but can cause more non-target species mortality. Neither mechanical removal nor piscicides is a long-term solution if the waterbody is connected to other infested waters. Many times, they are used in conjunction with environmental modifications (e.g. gates, barriers).

Anthropogenically created barriers are one of the most commonly used methods for preventing the spread of invasive fish. Some types of barriers include: strobe lights, acoustic deterrents, bubble curtains, velocity barriers, hypoxic zones, magnetic fields, or electric barriers (Ruebush 2011; Noatch and Suski 2012). The effectiveness of barriers like these was studied be in in the Chicago Sanitary and Shipping Canal, Illinois.

Completed in 1858, the Chicago Sanitary Shipping canal was created to manage sewage away from Chicago's water source, Lake Michigan, and to increase trade productivity (Rasmussen 2002; Moy et al. 2011). Reversing the flow hydrologically connected the watershed of the Great Lakes to that of the Mississippi River, allowing for species exchange between the two watersheds, which had previously been disconnected towards the end of the last ice age (Rasmussen 2002; Moy et al. 2011). However historically, the Chicago Sanitary Ship Canal was so highly polluted that it could not support aquatic life (Rasmussen 2002). Following the enactment of the Clean Water Act in 1972, water quality was improved and the system is now capable of supporting life and facilitating the flow of species between systems (Rasmussen 2002; Moy et al. 2011). For example, zebra mussels and round gobies (Neogobius melanostomus) utilized the channel to invade and establish in the Mississippi River basin (Ray and Corkum 1997; Rasmussen 2002). Electric barriers were first installed in 2002 to prevent invasive carp from moving into the Great Lakes (Rasmussen 2002; Moy et al. 2011). Radio-telemetry research on the effectiveness of the electric barrier was conducted using common carp (Sparks et al. 2010). Of the 130 tagged common carp released, only one fish was tracked as having

passed through the barrier (Sparks et al. 2010). Further telemetry research conducted by the Illinois Department of Natural Resources (IL DNR) corroborates that the electric barrier is effective, with zero live fish, out of 215, moving upstream of the barrier (IL DNR 2016). However, electric barriers are not entirely effective and have associated issues (e.g. maintenance costs, malfunctions, required time offline for maintenance, reduced effectiveness for smaller fish, and reduced efficiency during high water stages) (Rasmussen 2002; Sparks et al. 2010; Noatch and Suski 2012). The barriers in the Chicago Sanitary Ship Canal cost approximately $1.5 million to build and continues to cost tax payers over $22,000 annually to maintain (Rasmussen 2002). Regardless, barriers only assist in preventing the spread of invasive carp, they do not control population sizes (Rasmussen 2002; Sparks et al. 2010).

The electric barriers on the Chicago Sanitary Shipping canal are not the only course of action being taken in Illinois to prevent the spread of invasive carp into the Great Lakes. IL DNR is also being proactive about lowering the density of invasive carp in the Illinois River, a tributary of the Mississippi River infested with grass carp, silver carp, and bighead carp (IL DNR 2017). Contracting commercial fisherman to deploy 2,901.6km of gill nets, IL DNR harvested a total of 2,504 tons of invasive carp from the Illinois River between 2010-2016 (IL DNR 2016). This equates to 3,226 grass carp, 474,264 silver carp, and 85,710 bighead carp, a total of 563,200 fish, removed from the system in the last six years (IL DNR 2016). Sampling conducted detected a 62% decrease in invasive carp density between 2015 and 2016 in portions of the Illinois River (IL DNR 2016). Despite efforts in Illinois, the range of invasive carp is still expanding in other previously uninfested areas of the Mississippi River Basin (MN DNR 2017). Preventative strategies are best the practice to mitigate the threat posed by invasive carp to remaining uninfested waters (Lovell et al. 2006).

1.2.   Predicting Invasive Carp Habitat with Ecological Niche Modeling

Ecological niche models provide useful and efficient tools to forecast the spatial location of potentially suitable habitat for an invasive species (Elith et al. 2006; Chen et al. 2007; Herborg et al. 2007; Kulhanek, Leung, and Ricciardi 2011; Escobar et al. 2017 Romero-Alvarez et al. 2017). An ecological niche model estimates the possible "niche," or the ecological conditions that a species requires to have a sustainable population (Peterson et al. 2011). Environmental factors (e.g. temperature, precipitation, pH) can limit the distribution of an invasive species. Ecological niche models identify tolerable environmental conditions for a target species based previous occurrences and creates thresholds to compare other spatial locations to (Peterson et al. 2011). The product of ecological niche models will indicate where a species' distribution may be limited by abiotic factors, as well as, where suitable habitat may be located. Previous ecological niche modelling for invasive carp successfully predicted 93.7% of the known silver carp occurrences and 71.8% of the bighead carp occurrences within the United States (Chen et al. 2007). This research suggests that ecological niche models would be at able to predict the potential for invasive carp expansion into new aquatic systems.

1.3.   Study Site: Minnesota River Basin, Minnesota, United States

The modern Minnesota River valley, of southern Minnesota, USA, developed following Late Wisconsinan glaciation, carved by episodic outburst floods from glacial Lake Agassiz (Matsch and Wright 1967; Fisher 2004; Gran et al. 2013). Preceded by glacial River Warren, the modern day Minnesota River flows from Big Stone Lake on the Minnesota and South Dakota border to the confluence with the Mississippi River in Saint Paul, Minnesota, a total of 515 km (MN DNR 2018d; Figure 1.7). A 7th-8th order stream, the Minnesota River drains an area of 44,030 km2 across Minnesota, South Dakota, and Iowa (MN DNR 2018d). The Minnesota River is highly altered for agricultural and urban development, including five dams located in the upper reaches. Despite the dams, the Minnesota River still flows freely for 386km and houses large migratory fish species such as the paddlefish (Polyodon spathula) (MN DNR 2018d).Unfortunately, the Minnesota River is affected by large inputs of sediment and nutrients, lowering water quality (Gran et al. 2009; Belmont et al. 2011; MN DNR 2018d). In spite of undesirable changes in water quality, the Minnesota River ecosystem is diverse with over 80 species of fish utilizing the main channel (MN DNR 2018d). This diverse fish community could be altered by the introduction of invasive carp (Feber 2001; Schrank, Guy and Fairchild 2003; Sampson, Chick, and Pegg 2009; Sass et al. 2014; Zhang et al. 2016).
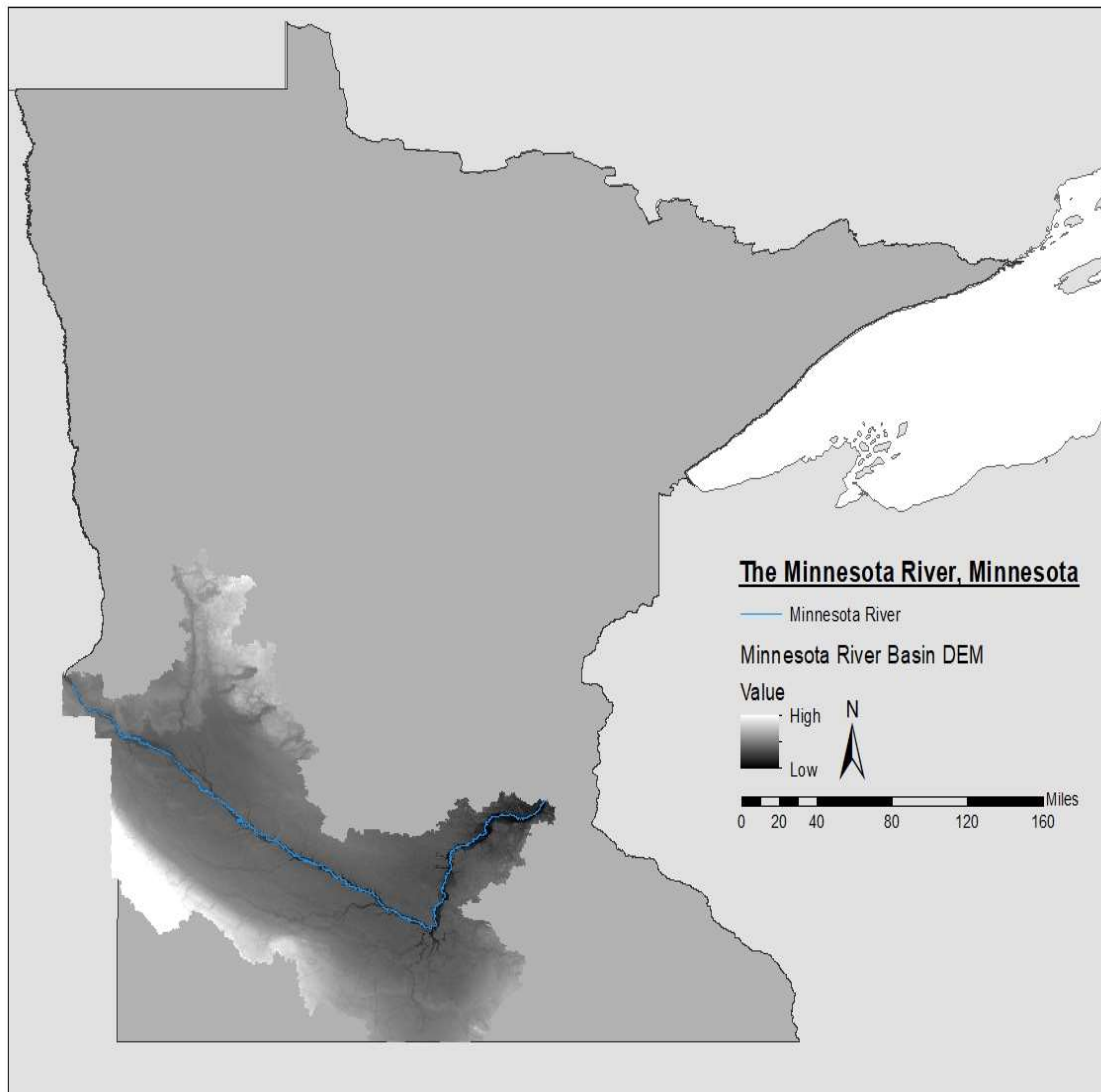
Figure 1.7. Study site: Minnesota River valley, Minnesota, U.S.A.

There is growing concern about invasive carp reaching the Minnesota River and sustaining an established, reproducing, population in the system (MN DNR 2018). As of 2017, all four species of invasive carp had occurrences in the connected Upper Mississippi River watershed. Bighead carp and grass carp, specifically, have been caught in the Minnesota River prompting the Minnesota Department of Natural Resources to list the river as infested for those species (MNDNR 2017). While rare occurrences of invasive carp have happened, researchers do not believe there are breeding, or naturalized, populations in Minnesota (MPR News 2017).

If invasive carp were to naturalize within the Minnesota River, it could put many native species population under increased pressure due to increased food competition, loss of habitat, or predation (Ferber 2001; Schrank, Guy, and Fairchild 2003; Sampson, Chick, and Pegg 2009; Sass et al. 2014; Zhang et al. 2016). External to damaged ecosystems, changes in the aquatic community from these effects could affect the quality of recreational activities (e.g. fishing, boating, water sports) having powerful economic impacts. For example, recreational fishing creates 43,000 jobs and $2.8 billion in retail spending in Minnesota annually (MN DNR 2011). The consequences of invasive carp infesting the Minnesota River are not limited to Minnesota, as the river connects to the Red River of the North during high flood stages (Levine 2017). Invasive carp spreading to the Red River would provide a thruway to North Dakota and Canada. To prevent this, Minnesota is being proactive in implementing plans to assist in early detection and quick, calculated, response if invasive carp are found (MN DNR 2014).

1.4.   Research Questions

The Minnesota Invasive Carp Prevention Workplan began in 2014 with the aim to collect geomorphic, hydrologic, and biologic data to inform decisions being made regarding invasive carp prevention and management in the Minnesota River. All three types of data are crucial to fully understanding fish habitat. Fluvial geomorphology, or the physical characteristics of a river and the river's interactions with the landscape, is the template for habitat and controls the physical structure (e.g. river type, length, water depth, substrate type), whereas hydrology impacts how species interact with their habitat (Schramm 2017). As the final stage of the project, this evaluation connects geomorphic and hydrologic data on the Minnesota River to the environmental requirements of invasive carp to better inform managers of habitat suitability within the region.

1.5. The goals of this evaluation are as follows:

- Evaluate the success of using an ecological niche model to predict invasive carp occurrences
- Employ ecological niche modeling to predict habitat suitability for invasive carp in Minnesota
- Employ high resolution ecological niche modeling to predict and quantify habitat suitability for invasive carp in the Minnesota River

2. Ecological Niche Modeling: Predicting Invasive Carp Habitat in Minnesota

The U.S. Fish and Wildlife Service listed invasive species as a top contributing factor in endangerment and extinction of freshwater fishes (USFWS 2012). Establishment of invasive carp could be especially detrimental to Minnesota's 162 species of fish (MN DNR 2018a; MN DNR 2018b). For example, silver carp and bighead carp could place direct competition for food resources on imperiled planktivorous native species like the black buffalo (Ictiobus niger) and paddlefish (Polyodon spathula) (Schrank, Guy and Fairchild 2003; Sampson, Chick, and Pegg 2009; MN DNR 2018e).

When researching the risk aquatic invasive species pose to a system, it is beneficial to forecast areas of greatest concern (Kulhankek, Leung, and Ricciardi 2011). Using species occurrence data and environmental variables, ecological niche models can predict habitats that are environmentally suitable for a target species (Peterson 2003; Peterson and Robins 2003; Peterson and Nakazawa 2008; Pyron, Burbink, and Guiher 2008; Jimenez-Valverde et al. 2011; Kulhankek, Leung, and Ricciardi 2011; Escobar et al. 2017; Romero-Alvarez et al. 2017). The objectives of this chapter are to 1) evaluate the success of ecological niche models in predicting invasive carp occurrences and 2) employ ecological niche models to predict habitat suitability for invasive carp in Minnesota.

2.1. Methodology

2.1.1. Algorithm Selection

Many ecological niche modeling algorithms exist, but the most appropriate algorithm for a study is data and system dependent (Qiao, Soberon, and Peterson 2015). Algorithms vary in complexity, data requirement, and computing power necessary. To evaluate abilities of a model to predict previous invasive carp occurrences an algorithm requiring small data quantities with quick computing time was desired. NicheA is an open source algorithm that allows multiple environmental variables to be incorporated, utilizes presence-only occurrence data, and produces simple results that can be evaluated statistically (Qiao et al. 2016) and thus was selected.

2.1.2. Occurrence Data

Scientific name search phrases were used to compile occurrence data from https://nas.er.usgs.gov/, http://www.fishnet2.net/, https://www.gbif.org/, https://bison.usgs.gov/, http://splink.cria.org.br/. The search terms included current names: Hypophthalmichtys moilitrix, Hypophthalmichtys nobilis, Ctenopharyngodon idella, and Mylopharyngodon piceus, as well as historic names: Mylopharyngodon aethiops, Myloleuciscus atripinnis, and Aristhichtys nobilis. Current and historic names were both used to increase the likelihood obtaining a dataset with true global distribution of all targeted species.

Occurrence data from each source was compiled into a single database for each species. All data older than 1900 were deemed too old to be relevant climactically and removed. Occurrences were also deleted if they had the terms preserved specimen, aquaculture, fish market, or aquarium associated with them because the point was considered an artificial occurrences, or somewhere the fish might not survive without human interference. Data missing coordinate information were georeferenced using details about locality in google earth. Occurrence records that could not be georeferenced they were deleted. Due to potential duplication in occurrence data, as multiple sources were used, replicated occurrence points were deleted. Occurrence data were then plotted in ArcMap using the display X, Y data tool and compared to a base map to verify the country listed matched the spatial location (Figures 2.1.A-D).
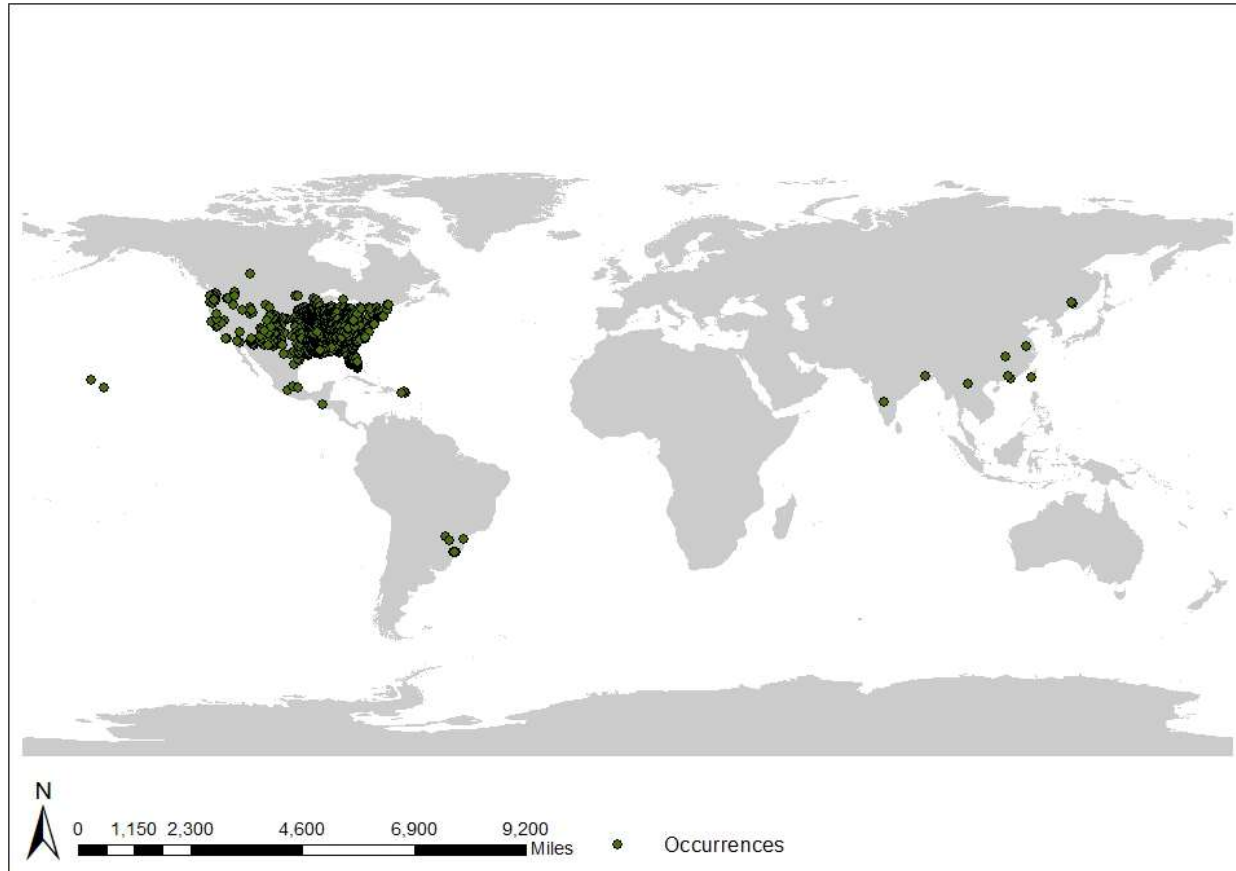
Figure 2.1.A. Grass carp (C. idella) global occurrence data

Silver Carp Occurrence Records
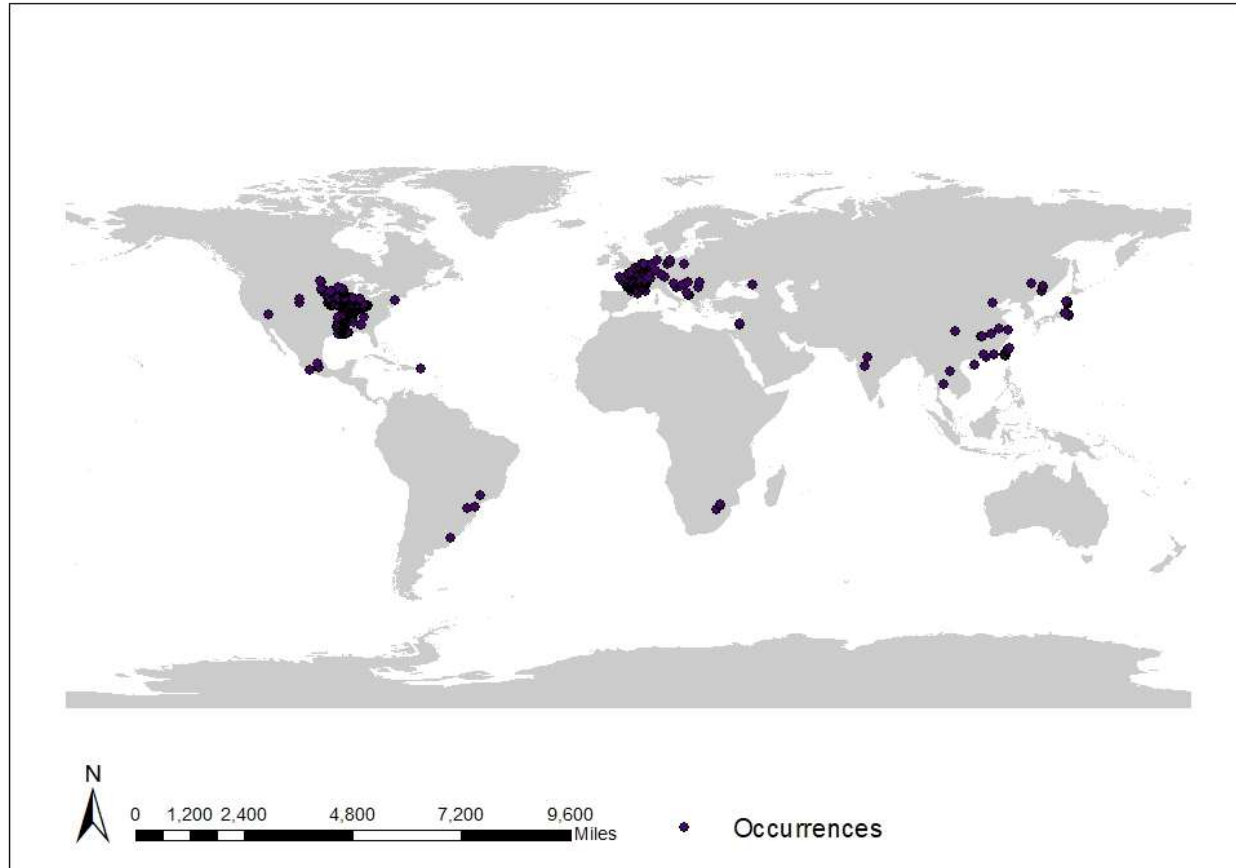
Figure 2.1.B. Silver carp (H. molitrix) global occurrence data.

Bighead Carp Occurrence Records
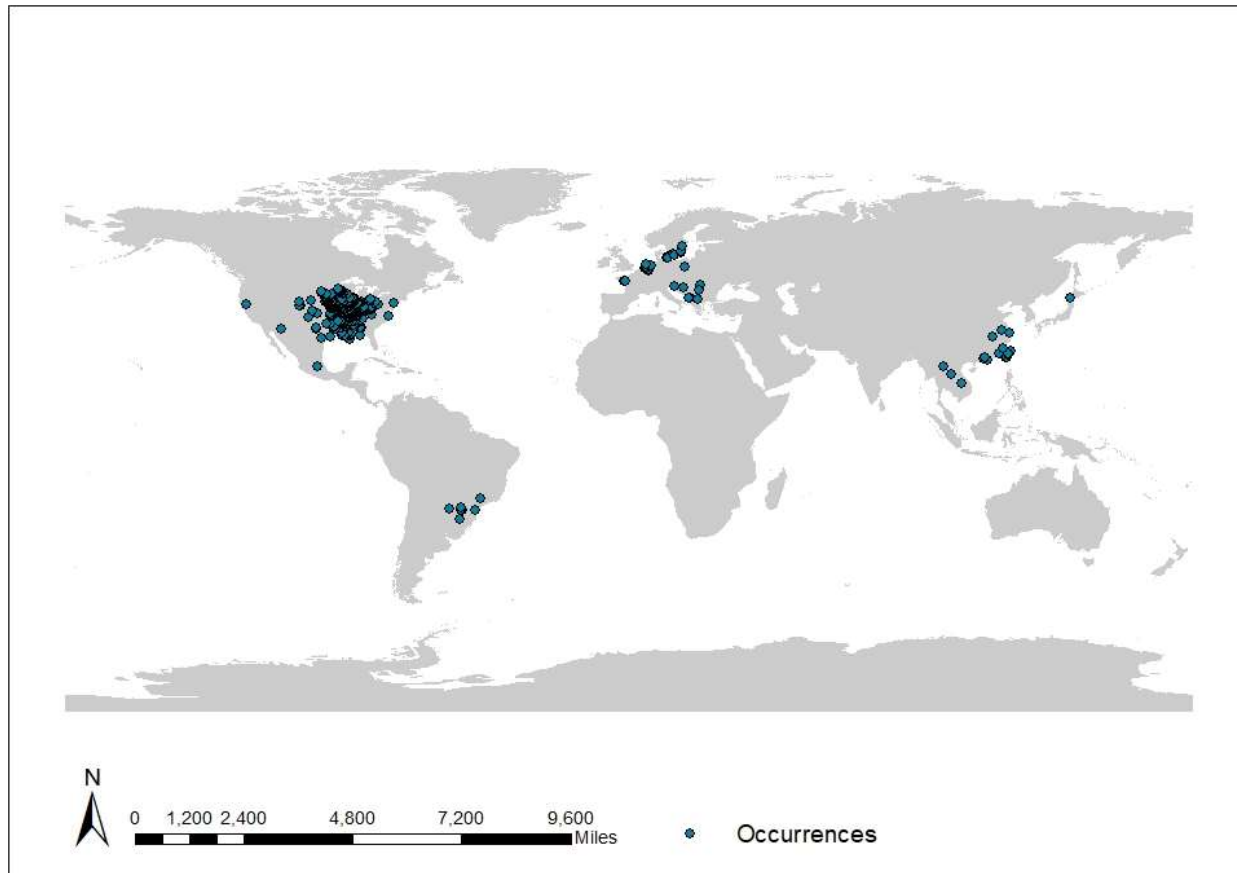
Figure 2.1.C. Bighead carp (H. nobilis) global occurrence data

Black Carp Occurrences
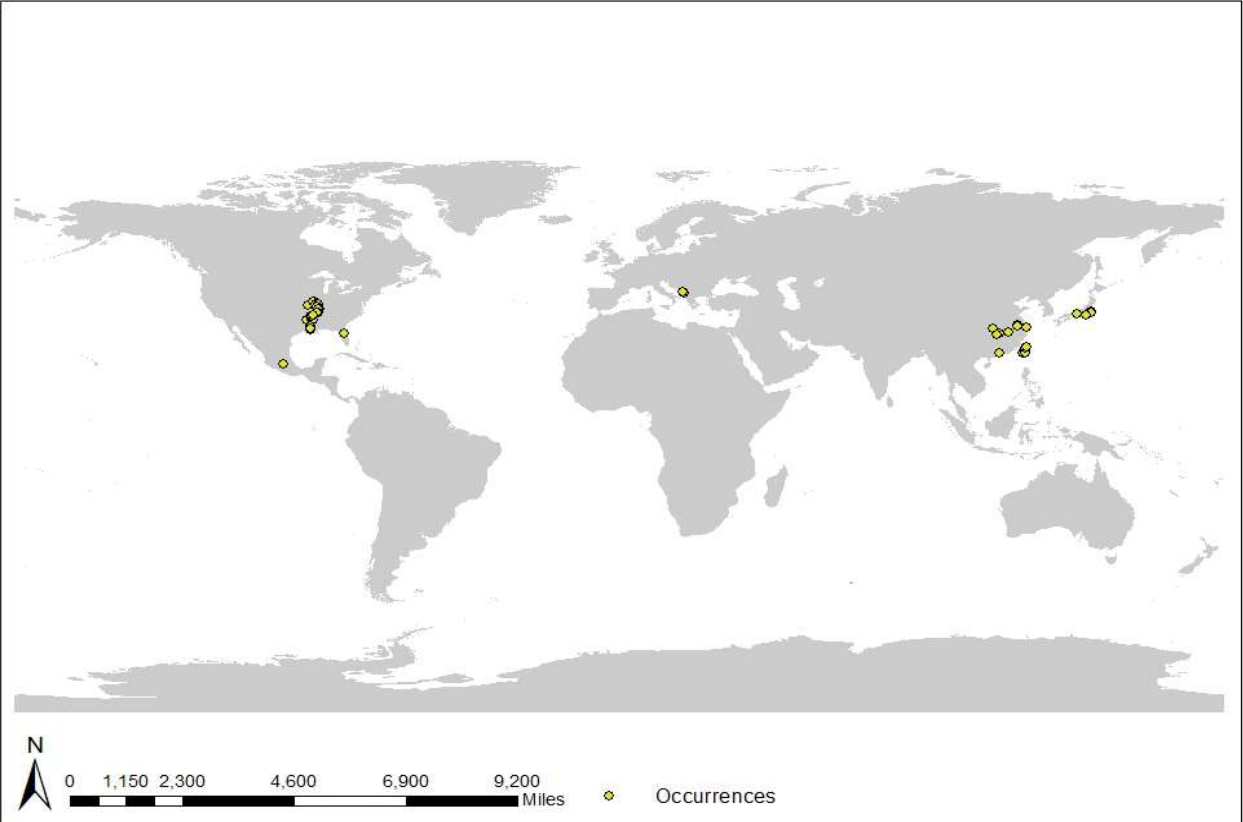
Figure 2.1.D. Black carp (M. piceus) global occurrence data.

2.1.3. Environmental Data

In selecting environmental variables, river level variables (e.g. water temperature, dissolved oxygen, pH) were not a viable option because they are not globally standardize in collection method or available in all countries. Thus, climate variables were used as an indicator for river data because they are consistent and globally available. Environmental data were downloaded from http://ecoclimate.org/downloads/ by selecting present raster file under the modern category. The downloaded file included 19 variables related to temperature and precipitation at a spatial resolution of 0.5° (Table 2.1). A principle component analysis was run utilizing the spatial analysis toolbox in ArcMap to determine variable correlation between the 19 ecoclimate variables (Peterson et al. 2011; Merow et al. 2013). The top three principal components contained over 80% of the variance and would be used as the environmental input to best capture the benefit of a multivariate approach without the redundancy of highly correlated variables.

2.1.4. Limiting Environmental Variables

When using environmental variables to train ecological niche models it is important to limit the spatial area to only areas that are relevant to the species (Barve et al. 2011). The data in these files should be limited to spatial locations that would be accessible to the species of interest (Barve et al. 2011; Merow et al. 2013). Studies have shown that altering environmental training extents may cause shifts in the location and amount of suitable habitat (Phillips and Dudik 2008; Anderson and Raza 2010; Barve et al. 2011). In the validation stages of modeling, larger than necessary extents can result in the models being less ecologically relevant than they appear when using evaluation metrics (Lobo, Jimenez-Valverde, and Real 2007; Barve et al. 2011; Merow et al. 2013).

Zone specific environmental files were created for each species. To create a species file specific to the United States, occurrence data for one species were sorted by country code and US records were copied into a new .csv file. A shapefile was then created from the zone specific occurrence data file using the display X, Y data function in ArcMap. Using the new occurrence point shapefile, a polygon was created that contained all the occurrence points using the minimum bounding geometry tool in the data management tool box. A centroid for the polygon was calculated using the feature to point tool in the data management toolbox . Mean average distance between occurrence points and centroid points was then calculated using the point distance tool in the analysis toolbox. This distance is representative of the average movement or mobility of the species in that region. The mean average distance was used to limit the environmental area used to inform the models. To do this, the global occurrence file for the species was then uploaded in ArcMap and the points plotted using the display X, Y data tool. Using that mean average distance, a fixed distance buffer was created around each of the global occurrence points using the buffer tool in the analysis toolbox. The dissolve tool from the data management toolbox was then used to merge the buffers into a single polygon. This polygon represents an estimate of the area that would be accessible to the species,

quantified by the average distance from each occurrence point to the centroid in a specified region. The same process was replicated for the Europe-limited environmental files, using a .csv of European occurrences to calculate average distance.

The procedure used to limit the United States and Europe files was not possible for the native range due to low occurrence records in the region. To take into account the entirety of the native range, a figure of each native range from Mandrak and Cudmore 2004 was digitized and georeferenced in ArcMap to create a shapefile. A centroid was then calculated using the feature to point tool in the data management toolbox. Lines were drawn from the centroid to the most distance parts of the native range and their total length was measured using the add geometry attributes tool in the data management toolbox. The average distance was manually calculated using the values found above. A fixed distance buffer was then created and dissolved to create a single polygon representative of the area accessible to a species using the procedures previously described.

The environmental data were then clipped by the resulting polygons by utilizing the extract by mask tool in the spatial analyst toolbox. Silver carp and bighead carp had three zones: the United States, Europe, and the species' native range. Grass carp and black carp had two zones: the United States and the species' native range. The process was repeated for each species individually in each zone. In total, ten files were created.

2.1.5. Model Evaluation

In order for a model to be successful, it should be able to predict occurrences better than at random. The NicheA modeling algorithm produces binary results that classify a cell as suitable or unsuitable. For these results to be better than at random, the probability of successfully predicting an occurrence needs to be higher than 50%. Occurrence data were divided into two groups, cal and evl, in R (Appendix A). These groups were then used within the NicheA algorithm to predict the fundamental niche, or environmentally suitable habitat, of each species in multiple trials. The goal of this process was to see how many of the evl occurrence, or occurrences not used to train the model, were correctly predicted by the cal trial results, and vice versa.

First, the environmentally limited files for the region were uploaded into the model using create a background cloud (BC) function. This function plots the environmental data in three dimensional space. The niche for the trial was then created using the Generate N(s) from occurrences function utilizing the cal occurrence group previously created in R as the input. This function creates a convex hull that contains the occurrences points plotted onto of the environmental data and a minimum-volume ellipsoid (MVE) that is representative of the fundamental niche. The Generate N(s) from occurrence function creates a file named present.tif that contains this information and can be used in ArcMap to geographically visualize the predicted niche. This procedure was repeated using the same environmental file, but inputting the evl occurrence instead.

To collect the data for calculating the probability of success, the present.tif file from the cal trial and the cal and evl occurrence files were uploaded in ArcMap. The occurrence data was plotted using the display X,Y data tool and the symbology changed so they were easily distinguishable. The raster present.tif file automatically produces stretched symbology, this is not useful however because there is only one value. To correct this, the file was reclassified using the reclassify tool in the spatial analyst toolbox to create one class. The reclassified present.tif file was then used as raster input with the evl point data in the extract values to points tool in the spatial analyst toolbox. The resulting attribute table for the evl occurrences lists the value of the reclassified present.tif file as a field and can be more easily counted. The data in this attribute table was used in Excel to calculate the probability of an occurrence point being correctly predicted in suitable habitat. To calculate the probability of success, the amount of points correctly predicted as suitable was divided by the total amount of occurrence points. The p-value was also was calculated using a binomial distribution function and the totals calculated above. This process was repeated for every species and limited environmental file combination and resulted in 20 files.

3.   Results

NicheA model trials for silver carp had the highest probabilities of an occurrence point being correctly predicted as suitable, with an average probability of 70.12%. Grass carp had the second highest probabilities, with an average of 62.03% of the occurrences being forecasted correctly. All of the bighead carp or black carp model trials had a probability of correctly identifying occurrences under 50%. Bighead carp had an average probability of 29.25%, while black carp was even lower with an average probability of 23.64%. The average probability of correctly predicting occurrences in all of the model trials combined was 46.94%. All of the models had a p-value of < 0.0001 except two black carp models. Only one of the black carp models was not statistically significant, with a p-value of 0.6595 (Table 2.2).

According to the NicheA model, grass carp had the greatest amount of suitable habitat in Minnesota, with only a small area in the northern Minnesota being unsuitable (Figure 3.1). Silver carp also had high amount of suitable habitat, especially in central and southern Minnesota (Figure 3.2.). Bighead carp had less suitable habitat than grass and silver carp, all of which is located in southern Minnesota (Figure 3.3). The NicheA models for black carp did not predict any suitable habitat within the state of Minnesota (Figure 3.4.).

Grass Carp NicheA Habitat Suitability
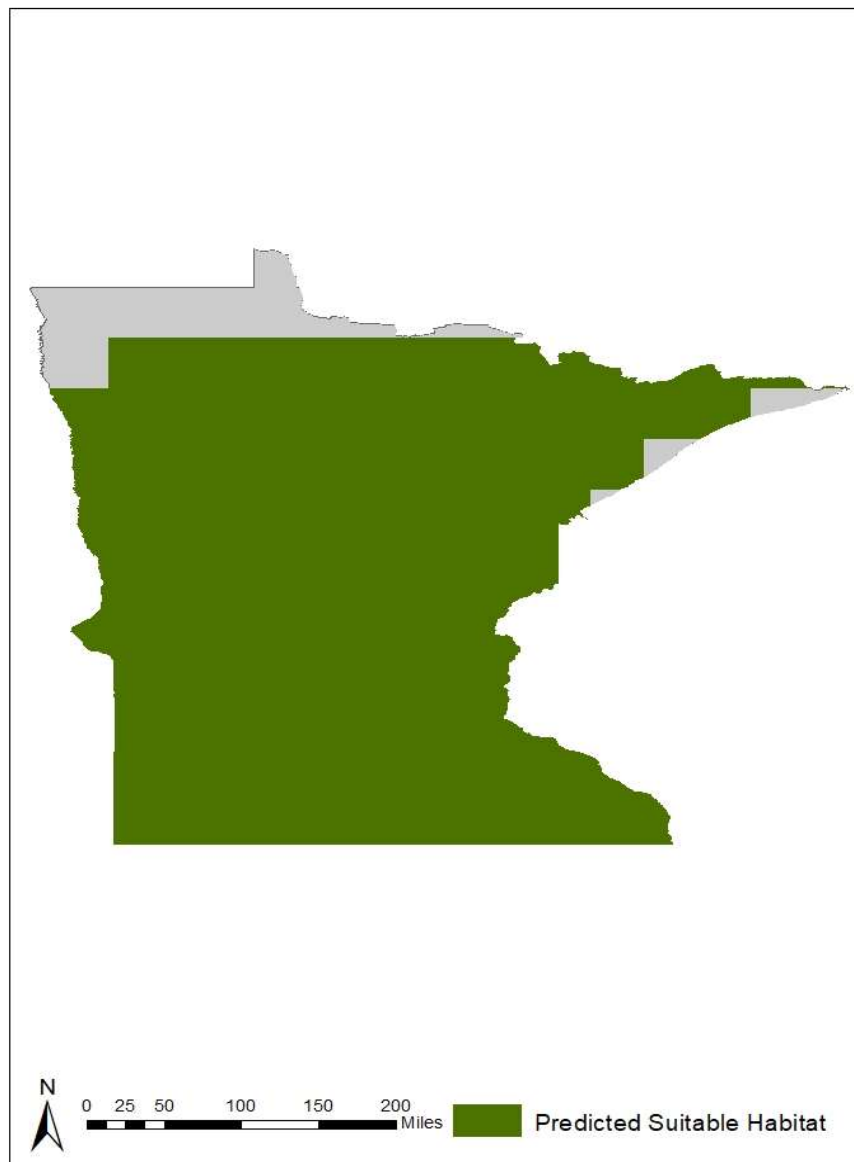
Figure 3.1. Grass carp (C. idella) NicheA model results when calibrated with coarse climatic data. The green area represents climatically suitable habitat.

Silver Carp NicheA Habitat Suitability

0 25 50   100   150   200 Miles

Predicted Suitable Habitat
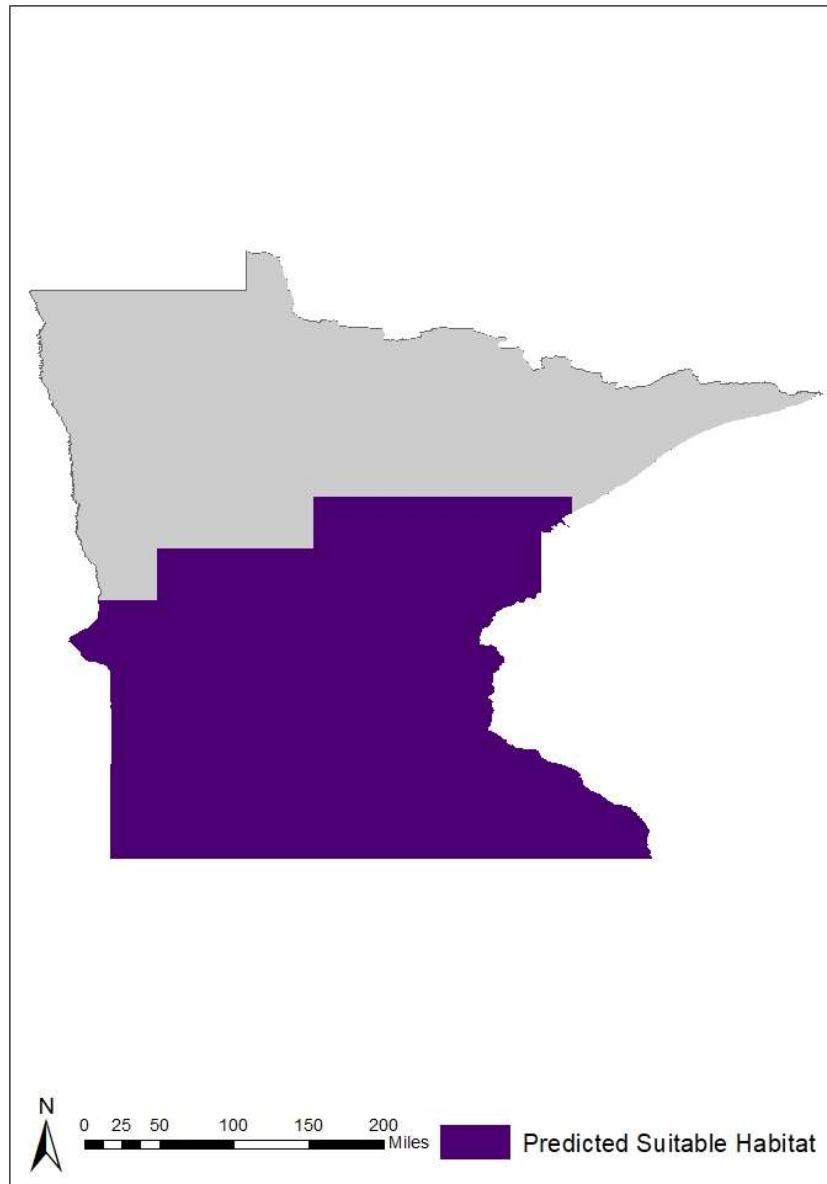
Figure 3.2. Silver carp (H. molitrix) NicheA model results

Bighead Carp NicheA Habitat Suitability
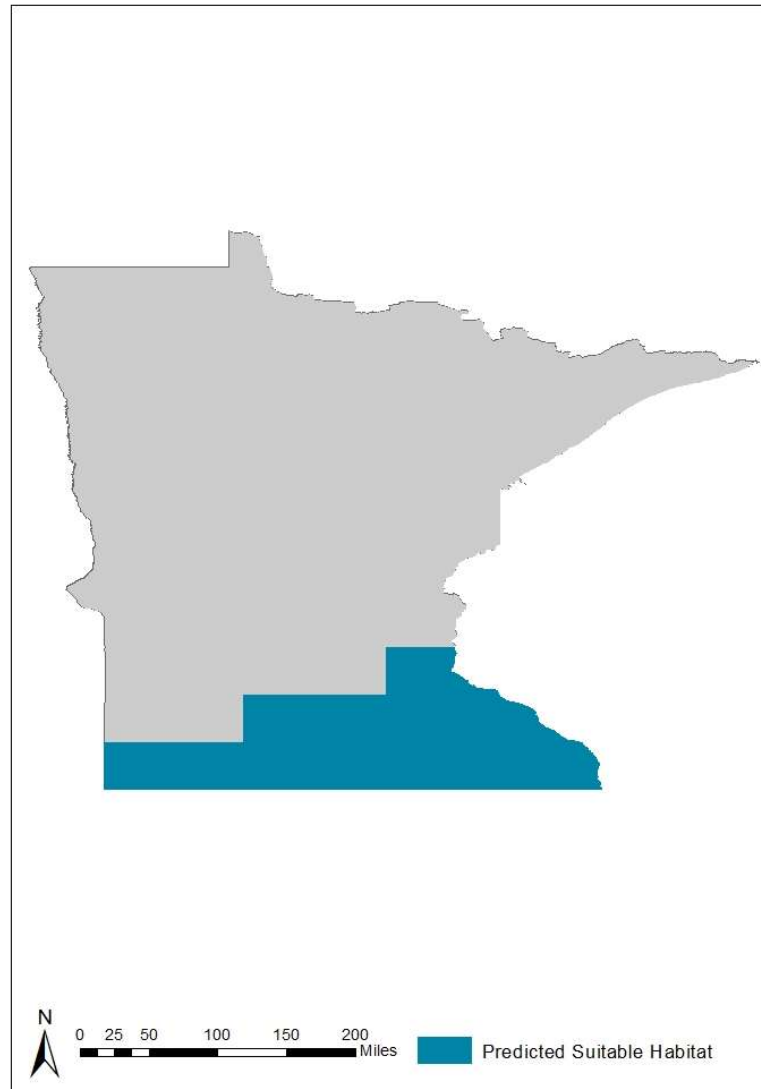
Figure 3.3. Bighead carp (H. nobilis) NicheA model results when calibrated with coarse climatic data. The blue area represents climatically suitable habitat.

Black Carp NicheA Habitat Suitability
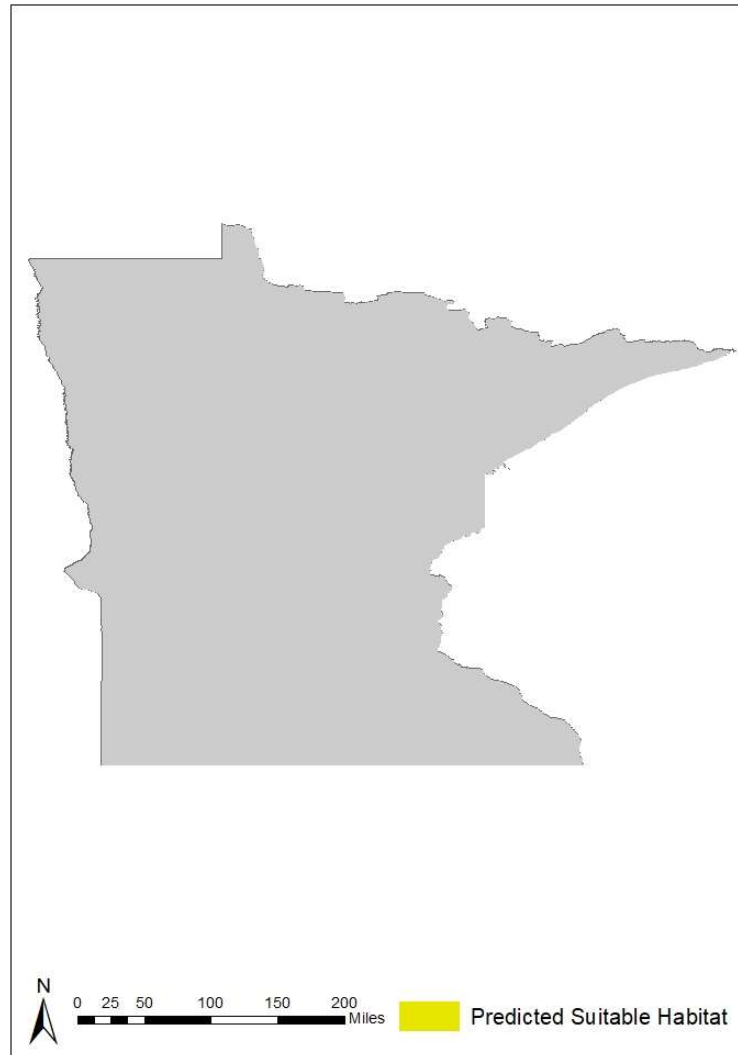
Figure 3.4. Black carp (M. piceus) NicheA model results when calibrated with coarse climatic data. The model predicted no climatically suitable habitat in Minnesota.

4.   Discussion

The NicheA modeling algorithm, using coarse climactic data, predicted suitable habitat within Minnesota for three of the four invasive carp species. While alarming, only 50% of model trials were successful in predicting suitable habitat for invasive carp better than at random. This low success rate could be linked to a variety of sources of error within the modeling process.

Prediction results may have been influenced by the differing amounts of occurrence records for each species. Models trials for silver and grass carp were successfully better than random, but were also informed over 2,400 occurrence records each. Contrastingly, bighead carp model trials were informed by 1,632 occurrences and black carp trials only a meager 72 total records and neither species had a trial with a probability better than at random. NicheA may overfit the data, or restrict predicted suitability to only areas spatially near an occurrence record. This could be part of the reason black carp did not have any suitable habitat in Minnesota, as it is the only species without an occurrence record in the state (Figure 4). To better grasp the risk invasive carp, particularly black carp, pose to Minnesota, a modeling algorithm that is sensitive to low occurrence data quantities may provide better results.

Invasive Carp Occurrences in Minnesota, U.S.A (1900-2016)
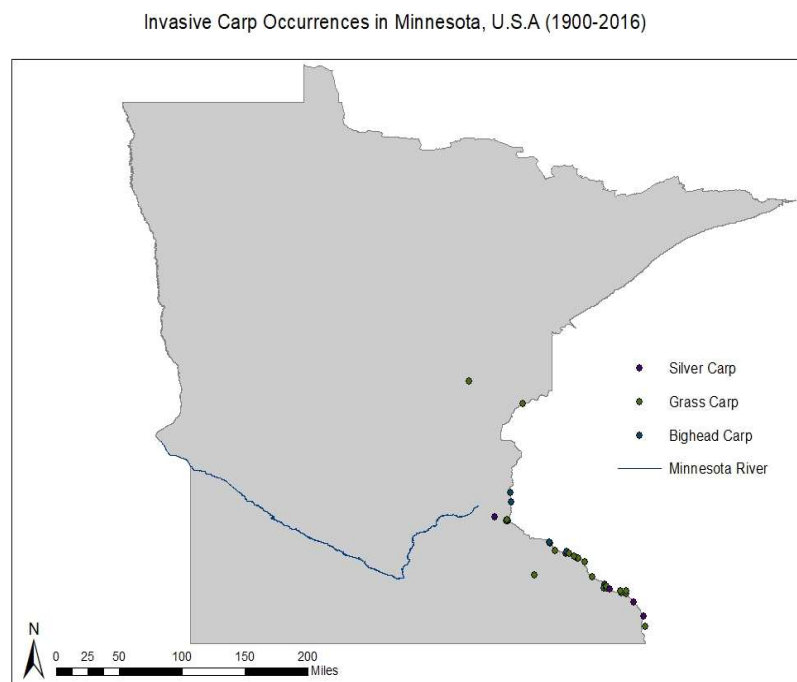
Figure 4. Invasive carp occurrences in Minnesota.

307

The quantity of occurrence points is not the only source of error within the data; spatial distribution of occurrence records may have also impacted model results. High concentration of occurrence points clumped in highly sampled areas, particularly near the Mississippi River, may have spatially biased the models towards areas with higher record counts. Unfortunately, some of this spatial bias is due to low amounts of recorded data in regions where invasive carp are common. This was evident in the need to supplement the methods when limiting the environmental file to the native ranges. Unequal sampling efforts, or data availability, may lead to a region appearing unsuitable even though invasive carp are present. The effect of clumped occurrence points is compounded by using coarse resolution environmental data.

The climactic variables used to inform the NicheA models had a spatial resolution of 0.5° x 0.5°. This equates to a pixel covering around a 3,080 km2 area. To place this in perspective, the state of Minnesota has an area of 225,180 km2 and the Minnesota River is 515 km long. At this pixel size, the clumped distribution of the occurrence data is going to result in many of the data points having the same climactic value. A resolution this coarse may not be biologically relevant because it assumes habitat homogeneity, or continuous similar habitat, over such a large area. It also does not produce results that are a significant within a single water body. At this scale, it is not possible to differentiate habitat suitability within areas of a river, instead only in large reaches. A small area that would be highly suitable and act as a refuge for the species could be masked by surrounding unsuitable environments, and therefore be classified as unsuitable. In order for model results to be relevant on the scale of a river, high resolution data that captures the variability in available environments is needed.

The simplistic binary results of the NicheA algorithm could also play a role in the success of the model. In the NicheA modeling process each cell is classified as suitable or unsuitable, there is no gradient. This is not ideal when trying to inform management decisions because areas of low suitability will be classified the same as areas of very high suitability. A more useful model would produce continuous or categorical results allowing managers to target their efforts on areas at highest risk.

4.1.   Conclusion

Ecological niche modeling using the NicheA algorithm successfully predicted suitable habitat better than at random in 50% of the trials conducted for four species of invasive carp. Model success rate may have been influenced by limited amounts of occurrences or the spatial clustering of occurrence data used in the trials. The coarse resolution of the environmental data used also contributed to results that may not have been biologically relevant. Nonetheless, the NicheA models predicted suitable habitat in Minnesota for three of the four invasive carp species. This suggests further, more complex, modeling at a finer scale is warranted.

5.   Predicting Invasive Carp Habitat in the Minnesota River Valley

Grass carp (Ctenophaygodon idella), silver carp (Hypophthalmichthys molitrix), bighead carp (Hypophthalmichthys nobilis), and black carp (Mylopharyngodon piceus) (collectively referred to as invasive carp hereafter) were transported to the United States for their use in aquaculture (Kolar et al. 2007). After escaping into the Mississippi River and spreading to many of its tributaries (e.g. Illinois River, Missouri River and Ohio River), the qualities that were beneficial in aquaculture are now detrimental to native ecosystems (Feber 2001; Schrank, Guy and Fairchild 2003; Sampson, Chick, and Pegg 2009; Sass et al. 2014; Zhang et al. 2016). Invasive carp are capable of destroying aquatic habitat and reducing food availability (Schrank, Guy and Fairchild 2003; Dibble and Kovalenko 2009; Sampson, Chick, and Pegg 2009; Sass et al. 2014; Zhang et al. 2016; USFWS 2017). Currently, a lack of high resolution data on the suitability of habitat within Minnesota for invasive carp exists, making it difficult to manage risks associated with their invasion.

Ecological niche models are commonly used in invasive species research because they forecast habitat suitability in areas without occurrences by utilizing environmental variables and available occurrences from other locations (Peterson 2003; Peterson and Robins 2003; Peterson and Nakazawa 2008; Pyron, Burbink, and Guiher 2008; Jimenez-Valverde et al. 2011; Kulhankek, Leung, and Ricciardi 2011; Escobar et al. 2017; Romero-Alvarez et al. 2017). The ecological niche models completed in chapter two were low resolution and simplistic. The spatial resolution used, 0.5°, was unable to show variability in small reaches of the Minnesota River and broadly classified large areas as either suitable or unsuitable. This made it difficult to identify which portions of the Minnesota River were most at risk. The objective for this chapter was to employ high resolution ecological niche modeling to predict and quantify habitat suitability for invasive carp in the Minnesota River.

6.   Methodology

6.1.   Algorithm Selection

The ecological niche models produced in chapter two used the modeling algorithm NicheA. These models produced simple, binary, results that classified an area as suitable or unsuitable, making it impossible to narrow results to reaches of the Minnesota River that were the most vulnerable to invasion. There was also concern that the algorithm may have underestimated suitability for black carp due to low occurrence record quantities. To overcome these issues, the MaxEnt modeling algorithm was selected (Phillips et al. 2005; Phillips et al. 2006). MaxEnt is the "gold standard" in ecological niche modeling and works by contrasting environmental conditions in the area of interest against the conditions where occurrences are located (Merow et al. 2013; Qiao, Soberón and Peterson 2015). In a comparison study, MaxEnt ranked amongst the most effective presence-only ecological niche models (Elith et al. 2006). Research comparing

the effect of sample size on ecological niche models showed that MaxEnt had the best extrapolative power across a range of sample sizes, including inputs as low as ten occurrence records (Wisz et al. 2008). This complex algorithm produces a gradient of suitability, which can be transformed for analysis using geographic information systems (GIS). The MaxEnt software is open source (https://biodiversityinformatics.amnh.org/open_source/maxent/). The most updated version of MaxEnt, 3.4.1, was used for this study.

6.2. Occurrence Data

The occurrence record datasets created in section 2 were used as the species input for the MaxEnt models.

6.3. Environmental Data

Many types of variables were considered for the environmental input into the MaxEnt models. River level variables (e.g. water temperature, dissolved oxygen, pH) collection methods are not globally standardized nor were they available in all countries so they were not selected. The models created in the previous chapter were informed by coarse climactic data and did not produce results that would be biologically relevant due to the large cell size. To improve upon this work, Moderate Resolution Imaging Spectroradiometer (MODIS) data was used. The MODIS/Terra Vegetation Indices 16-day L3 global 250m product (MOD13Q1) were downloaded for the years 2000, 2008, and 2016. This product measures canopy greenness by utilizing the surface reflectance values of three spectral bands, blue red, and near infrared(NIR), at a spatial resolution of 250m/pixel. The greenness of vegetation is related to environmental conditions such as temperature and precipitation. The MOD13Q1 corresponds to the enhanced vegetation index (EVI) equation and is more sensitive to variation in areas that have dense vegetation.

MOD13Q1 data are available for download from the Land Processes Distributed Active Archive Center (LP DAAC). The data are classified into different tiles based on spatial location. A kml file indicating the extent and name of each tile was downloaded from http://spatial-analyst.net/KML/MODIS_tiles.kmz. This kml file was opened in google earth, as well as all four species occurrence records. Tiles containing occurrence records for the desired years were downloaded using R (Appendix B). Downloaded files were then converted from .hdf to .tif using the MODIS reprojection tool (LP DAAC). Tiles for the same 16-day group (e.g. all tiles created on 02/18/2000) were mosaic together in ArcMap using the mosaic tool in the data management toolbox. In order to minimize computing time, the average and standard deviation of each season was found using the cell statistics tool in the spatial analyst toolbox in ArcMap. Seasons were defined by the 2016 solstices and equinoxes: winter December 21- March 18, spring March 19- June 19, summer June 20- September 21, and fall September 22- December

20. The season files were then converted into .asc files using the raster to ASCII tool in the conversion toolbox.

6.3.   Executing and Evaluating a Model

Each species of invasive carp was modelled individually using MaxEnt's default settings. Once models were completed, the resulting .asc files were converted to rasters using the ASCII to raster tool in the conversion toolbox within ArcMap.

A receiver operating characteristic (ROC) approach was utilized to evaluate if the MaxEnt model predictions were better than at random. The MaxEnt program automatically creates an area under the curve (AUC) plot for each model. AUC summarizes a model's ability to predict an occurrence record using a nonparametric measure (Peterson et al. 2011). AUC can range from 0-1and are plotted two-dimensionally with predicted area on the x-axis and sensitivity, or 1- the amount of cells that have occurrences within them, but are predicted as not suitable (omission rate). A random prediction expected to have an average slope, or AUC, of 0.5. A model that is better than random will have an AUC closer to 1.

6.4.   Limiting Results to Accessible Areas

To better predict the risk of invasive carp establishment, the model results needed to be clipped to areas that would be accessible to the carp. The raw results did not provide any indication of the spatial location where the habitat transitions from aquatic to terrestrial. Instead, previously modeled floodplain inundation for 5 year, 10 year, 25 year, 50 year, and 100 year floods (Smith 2016) limited the model results to only aquatic areas accessible to invasive carp within the Minnesota River. This was completed using the extract by mask tool in the spatial analyst toolbox.

6.5.   Analysis

The visual representation provided by ecological niche modeling results is useful when looking for general areas of concern but does not provide quantitative amounts of area that are highly suitable. To provide this kind of data, all of the clipped result data were converted to integer using the raster calculator tool in the spatial analyst toolbox using int([FILE] *1000000) as the equation. Now integers, attribute tables were created for the raster files using the build raster attribute table tool in the data management toolbox. The files were then reprojected to NAD 1983 UTM Zone 15 using the project raster tool in the data management toolbox ensuring the output cell size was set to 250, 250. The files needed to be reprojected to convert cell size units from degrees to meters. Lastly the extract by attribute tool in the spatial analyst toolbox was used to extract cells that fit within a threshold. Threshold to rank suitability have not been evaluated for invasive carp in the literature, so quartiles were used. The following equations were used in the extract by attribute tool:

- Poor Suitability "VALUE" < 250000
- Low Suitability "VALUE" ≥ 250000 AND "VALUE" < 500000
- Moderate Suitability "VALUE" ≥ 500000 AND "VALUE" < 750000
- High Suitability "VALUE" ≥ 750000

Area was found to quantify the amount of habitat in each suitability category. Area was calculated by multiplying cell size by cell count (e.g. cell count * 2502). Percent of total area for each suitability class was also calculated to make general comparisons easier. Percent area was found by dividing the suitability class area by total area and then multiplying the subtotal by 100.

7.   Results

The MaxEnt modeling algorithm, when informed by vegetation indices, predicted suitable habitat in the Minnesota River for all species of invasive carp. The amount of each class of suitable habitat was dependent on the species. (Table 5.A-B). Across all species, most of the highly suitable habitat in the Minnesota River can be found near the headwaters. However, there are localized pockets of highly suitable habitat throughout the river. All four species of invasive carp had AUC values better than at random (Figures 5)
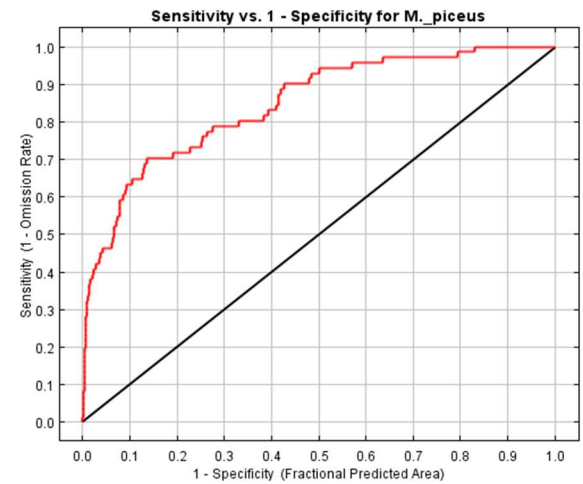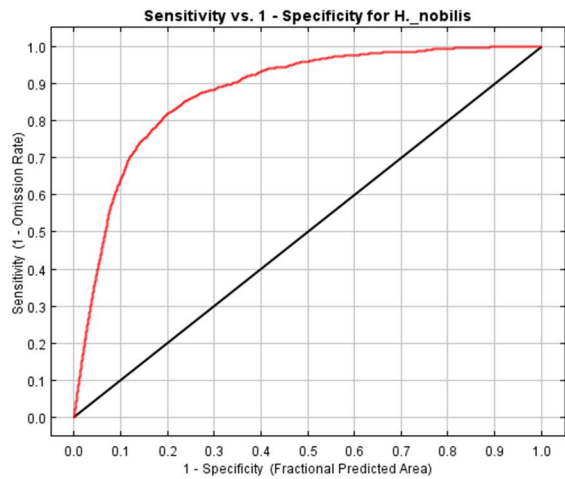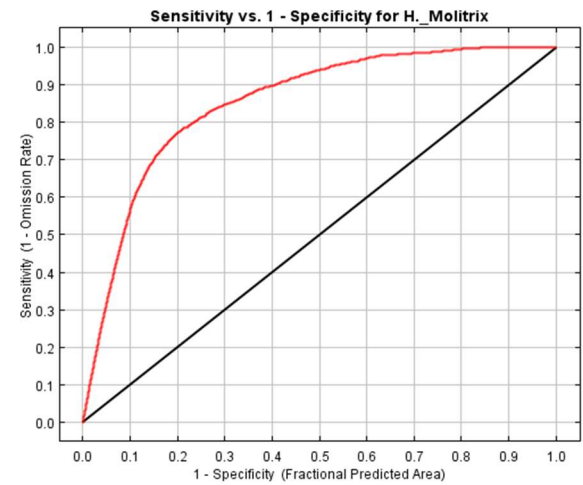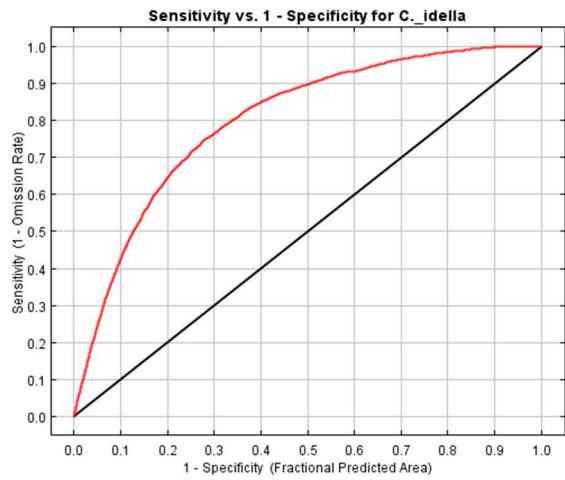
Figure 5. Maxent model results' AUC

7.1. Grass Carp (C. idella)

Grass carp had the highest percentage of moderately suitable habitat with an average of 62.3% of the accessible area (Figures 5.2.A-E). However, a majority of the remaining habitat, 34.8%, had low suitability. An average of 2.3% of the predicted grass carp habitat was highly suitable. This left only 1.3% of habitat as poorly suited, the lowest predicted average in the study. Grass carp experienced a decline in highly and moderately suitable habitat as flooded area increased while simultaneously experiencing an increase in low suitability. The percent of poorly suited habitat had a small decline, 0.1%. The grass carp model predicted occurrences better than at random with an AUC of 0.800.
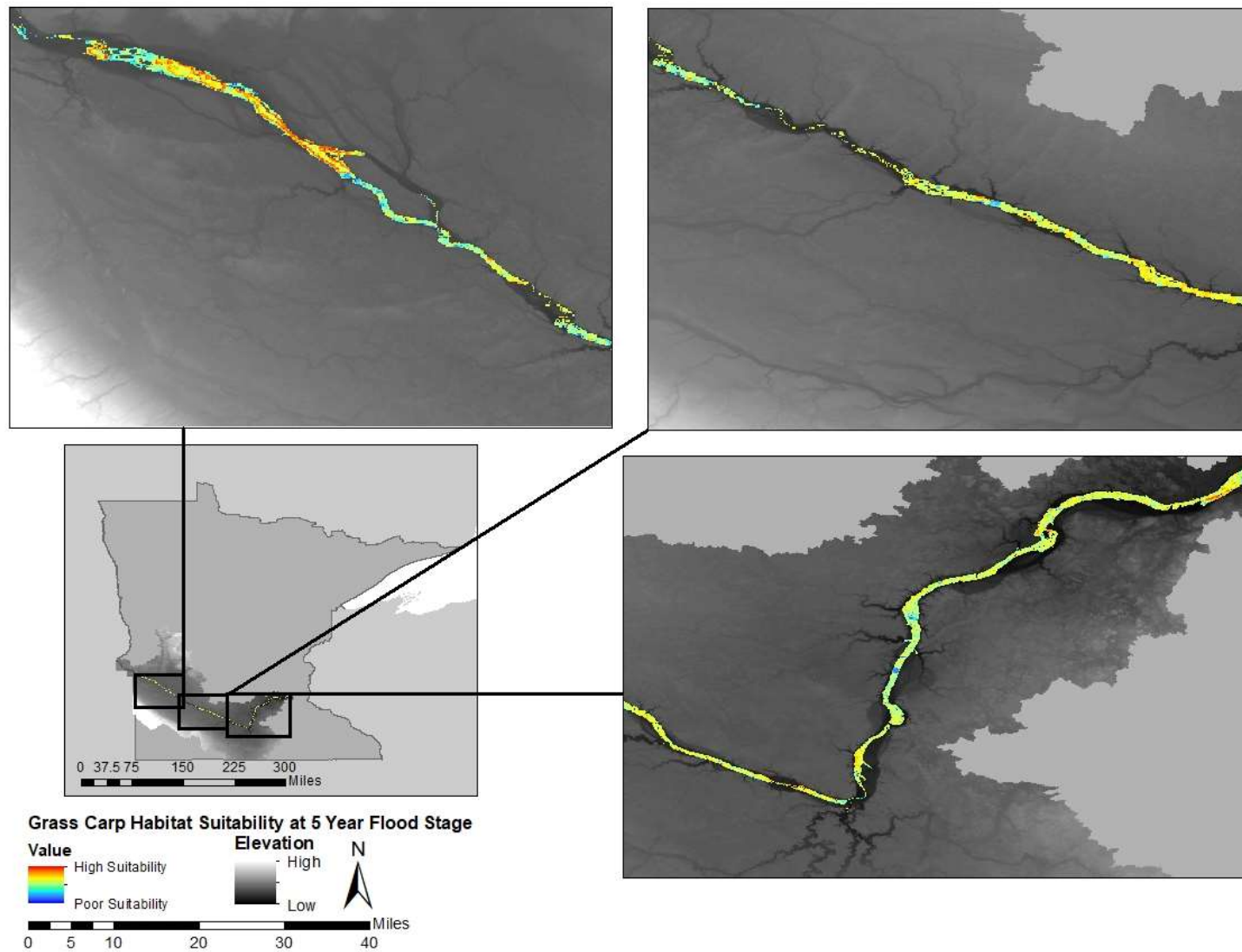
Figure 5.2.A. Predicted suitable habitat for grass carp (C. idella) in the Minnesota River during a 5-year flood.
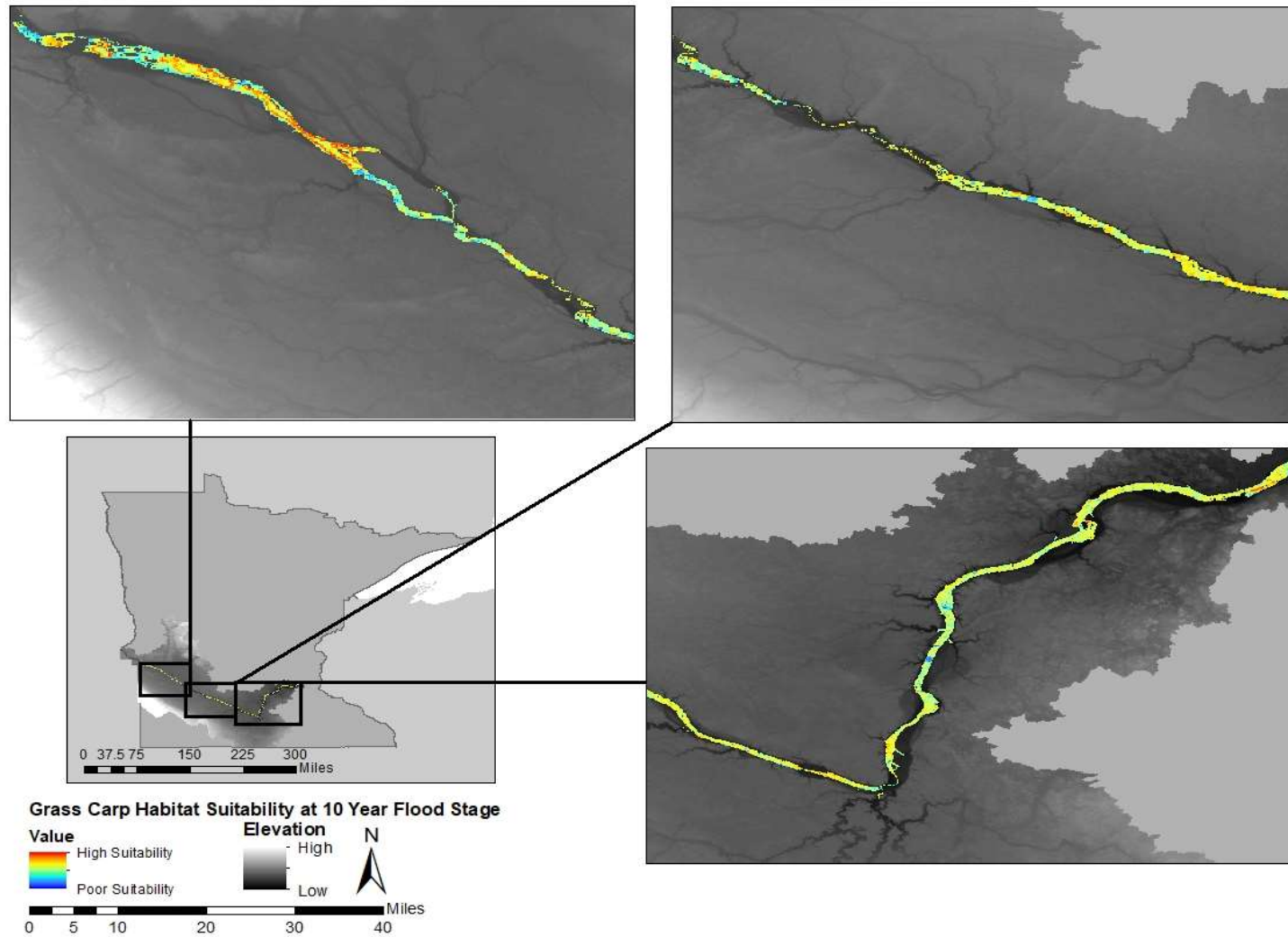
Figure 5.2.B. Predicted suitable habitat for grass carp (C. idella) in the Minnesota River during a 10-year flood.

316

Grass Carp Habitat Suitability at 25 Year Flood Stage
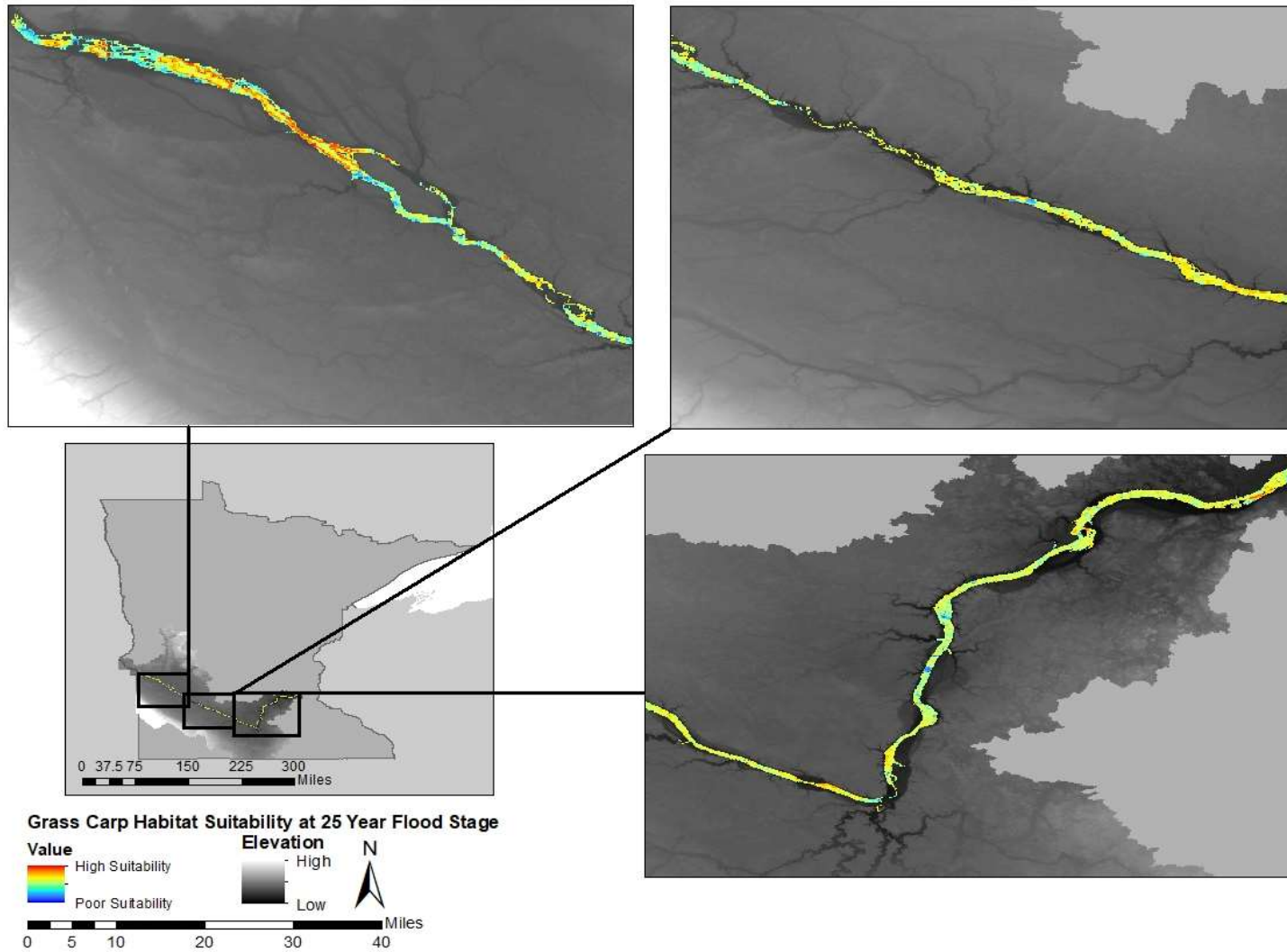
Figure 5.2.C. Predicted suitable habitat for grass carp (C. idella) in the Minnesota River during a 25-year flood.
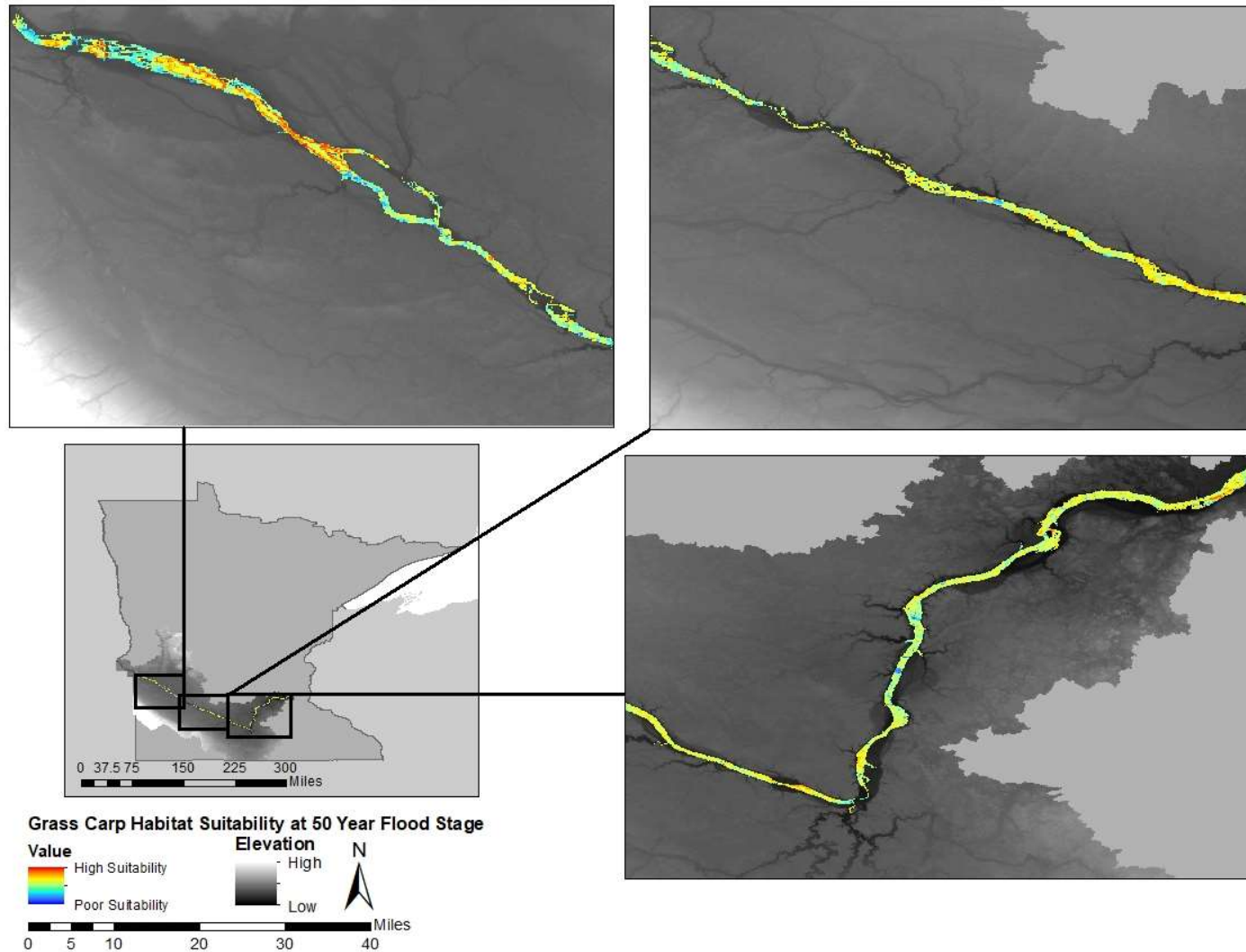
Figure 5.2.D. Predicted suitable habitat for grass carp (C. idella) in the Minnesota River during a 50-year flood.
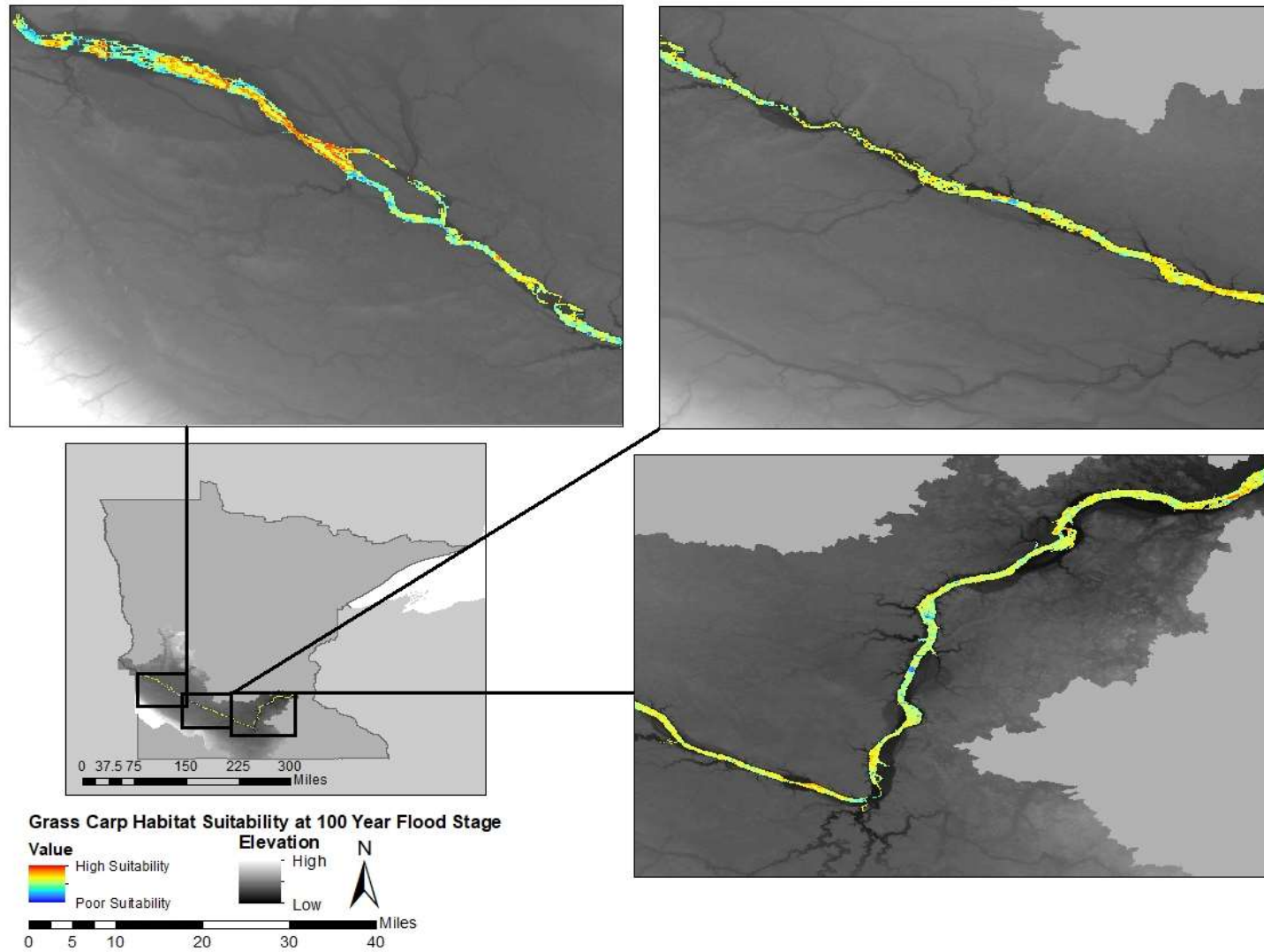
Figure 5.2.E. Predicted suitable habitat for grass carp (C. idella) in the Minnesota River during a 100-year flood.

7.2.   Silver Carp (H. molitrix)

A majority of potential habitat for silver carp had moderate or low suitability. On average across flood years, 5.2% of the area had poor suitability, 52.8% had low suitability, 41.3% had moderate suitability, and 1.3% had high suitability (Figures 5.3A-E). There was not a large difference in the suitability of habitat available between the 5 year flood stage and the 100 year flood stage for silver carp. However, as the inundated area increased, the percent of highly and moderately suitable habitat decreased less than 2%, while low and poor suitability increased by less than 2%. The model for silver carp had an AUC of 0.851.
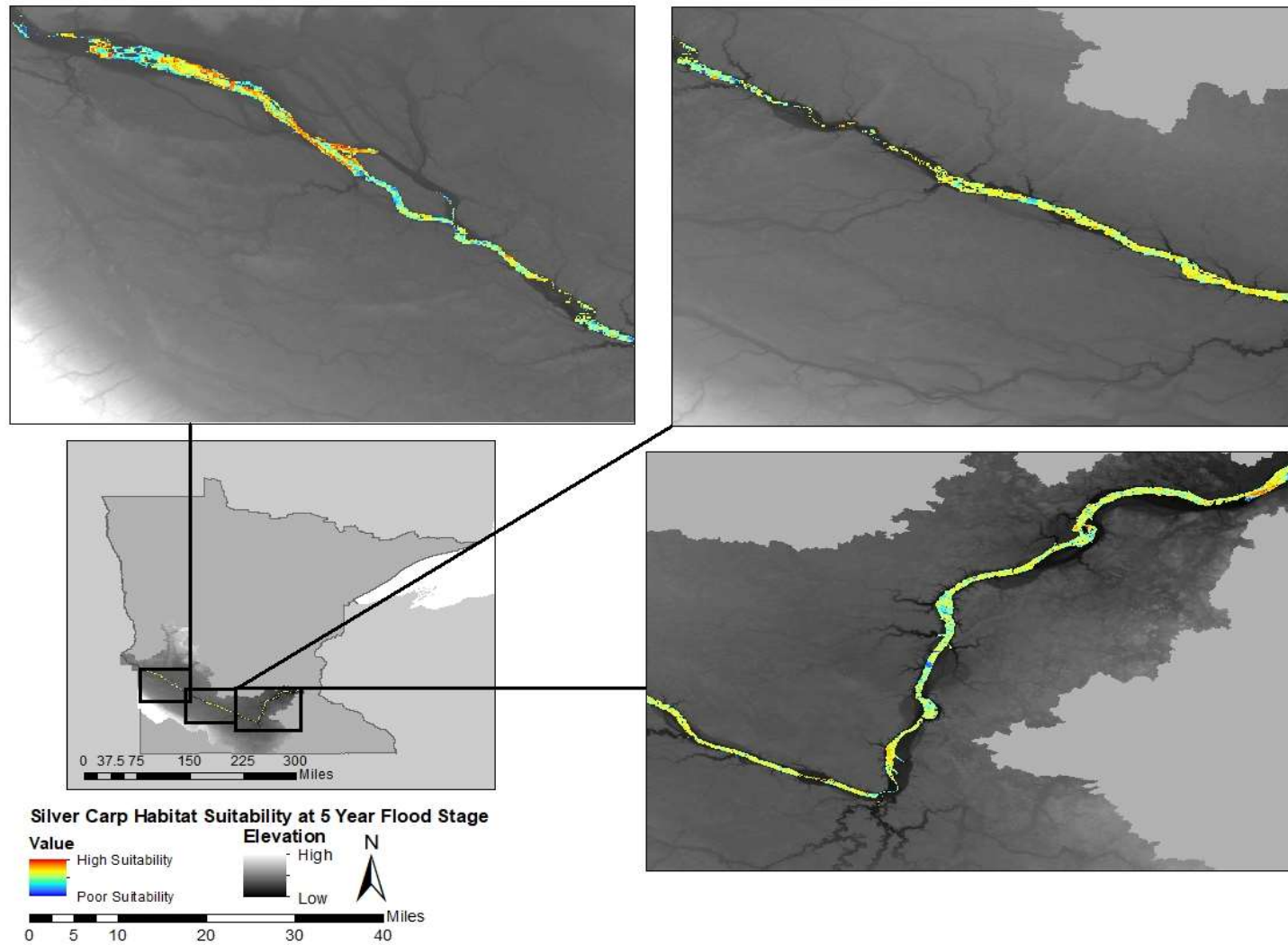
Figure 5.3.A. Predicted suitable habitat for silver carp (H. molitrix) in the Minnesota River during a 5-year flood.
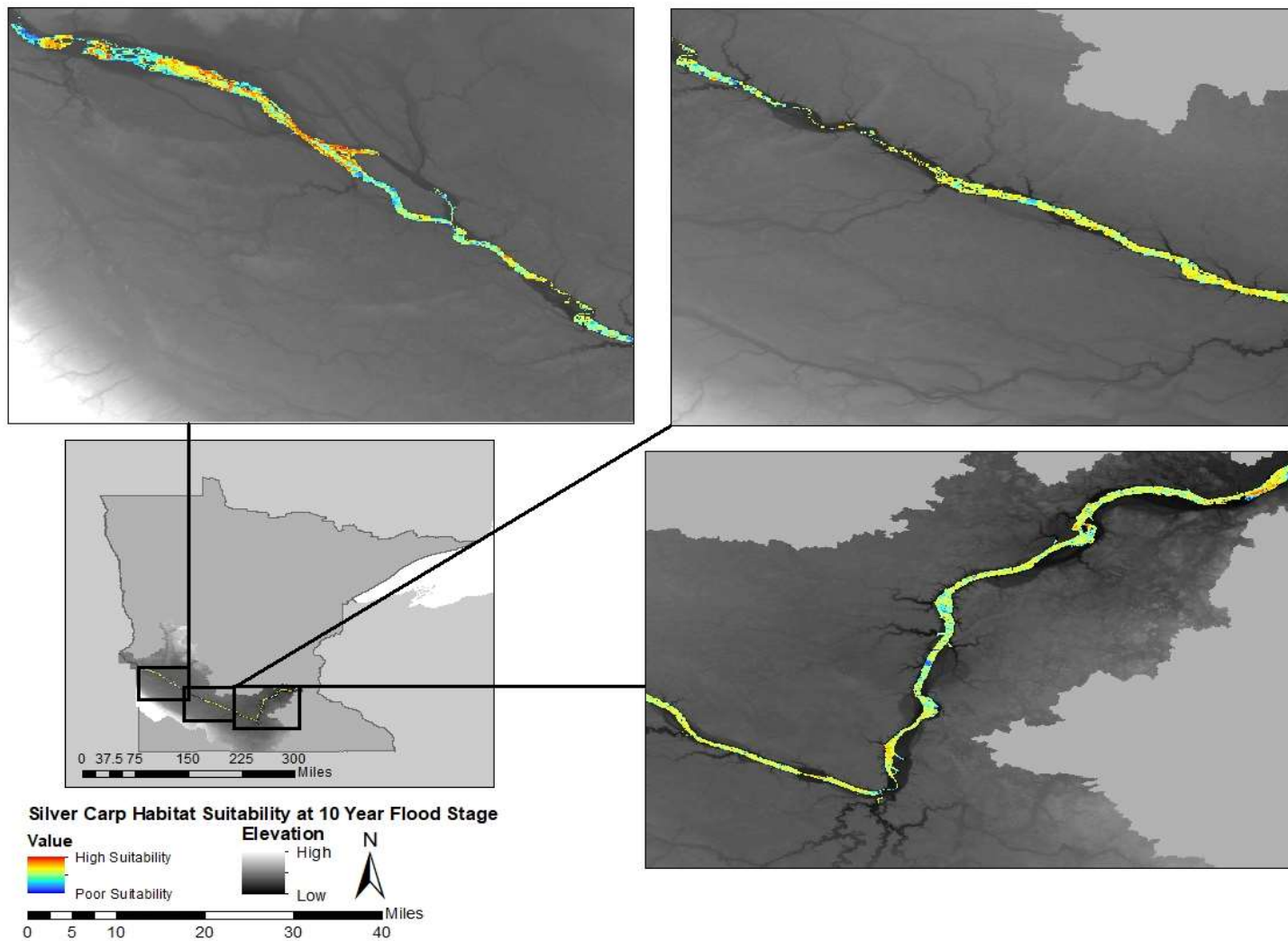
Figure 5.3.B. Predicted suitable habitat for silver carp (H. molitrix) in the Minnesota River during a 10-year flood.

322
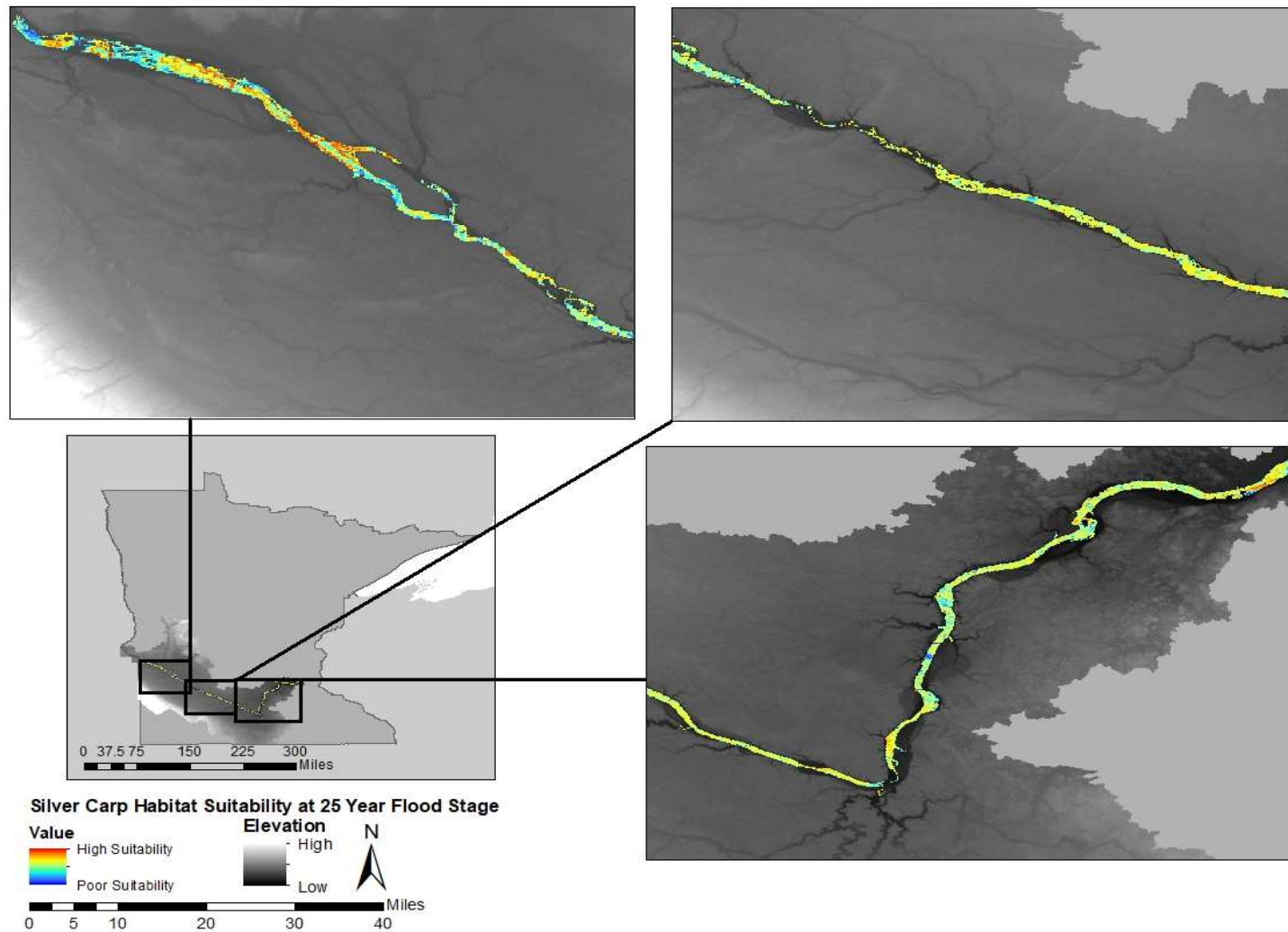
Figure 5.3.C. Predicted suitable habitat for silver carp (H. molitrix) in the Minnesota River during a 25-year flood.
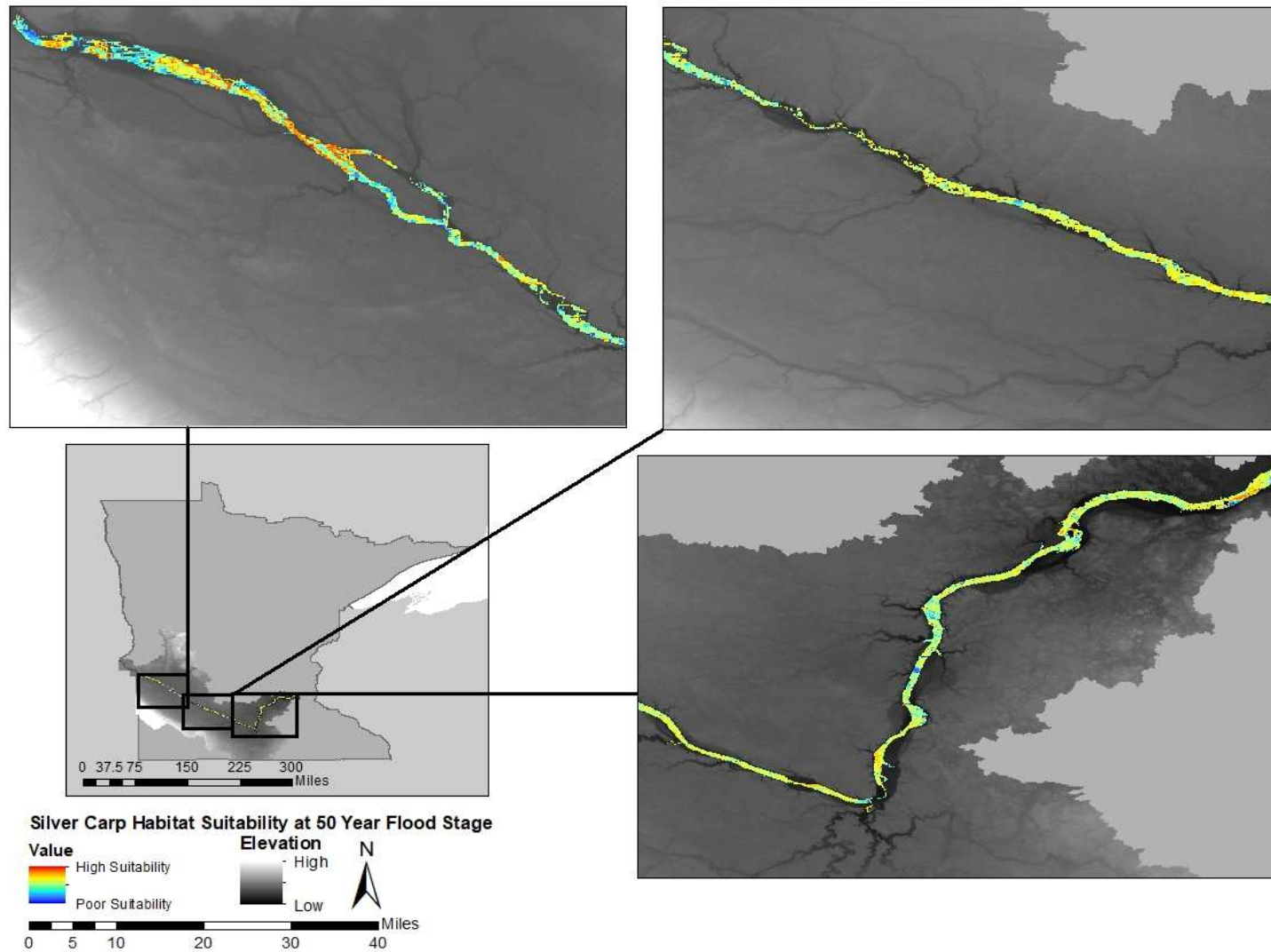
Figure 5.3.D. Predicted suitable habitat for silver carp (H. molitrix) in the Minnesota River during a 50-year flood.

324
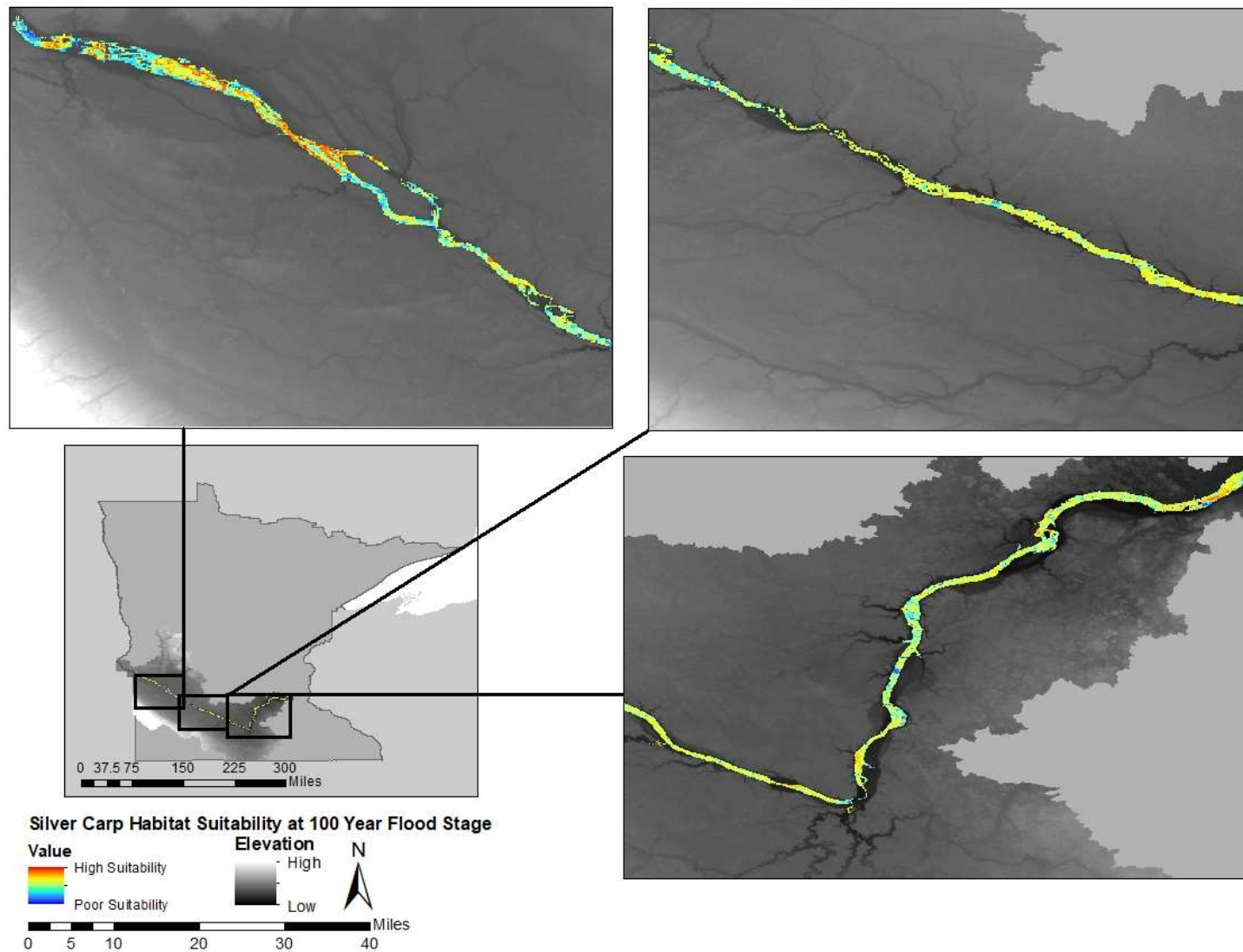
Figure 5.3.E. Predicted suitable habitat for silver carp (H. molitrix) in the Minnesota River during a 100-year flood.

7.3. Bighead Carp (H. nobilis)

Bighead carp had the highest average percentage of highly suitable habitat at 15.9% (Figures 5.4.A-E). When averaging the flood years, the majority of area, 53.9%, was moderately suitable. Despite that, there was still a large percentage, 31.0%, of area that was classified as having low suitability or poor suitability. Similar to silver carp, as inundated area increased, the percent of highly suitable habitat decreased. Concurrently, the percentage of habitat with low or poor suitability increased. The bighead carp model had an AUC of 0.876
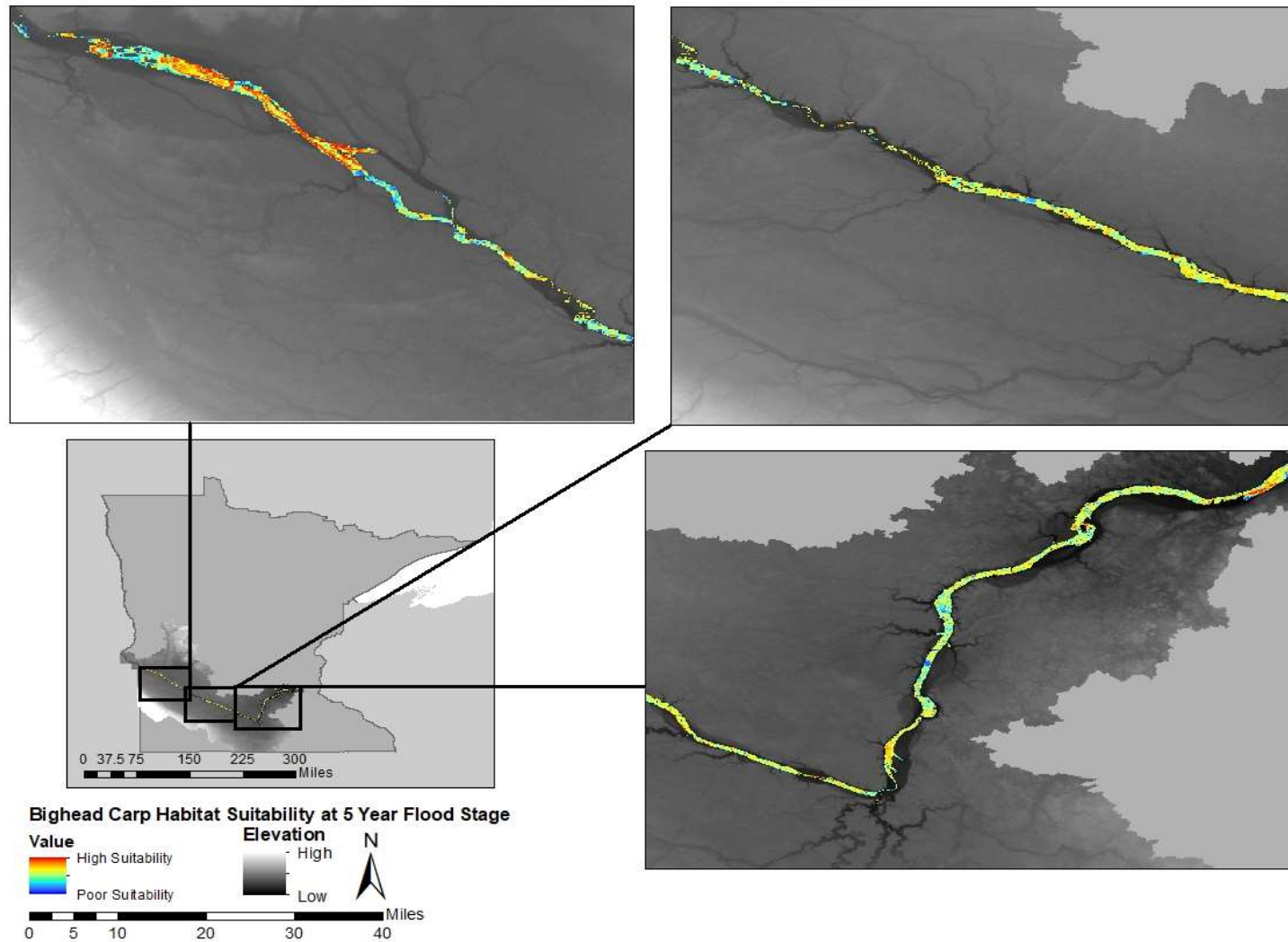
Figure 5.4.A. Predicted suitable habitat for bighead carp (H. nobilis) in the Minnesota River during a 5 year flood.

327
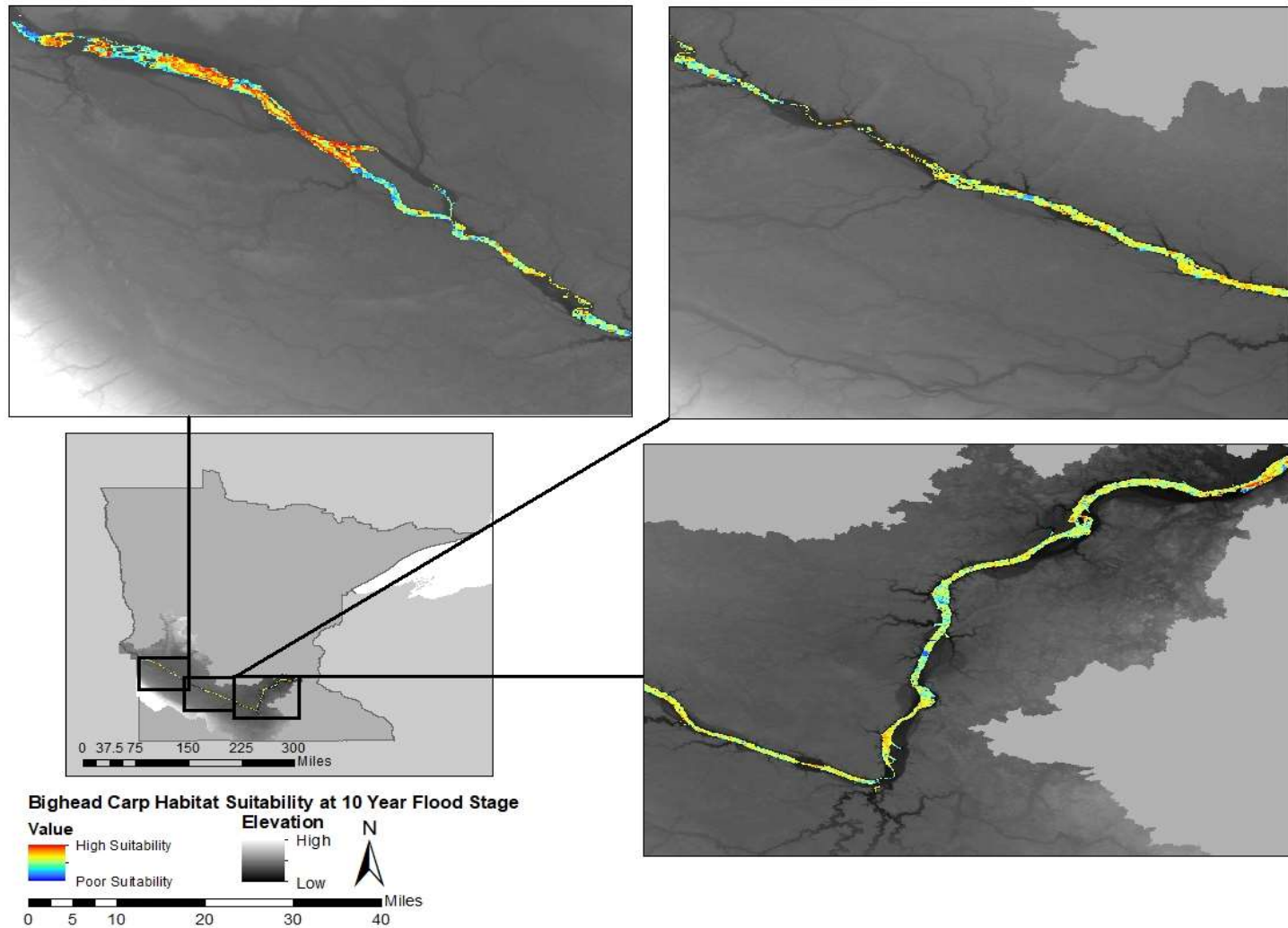
Figure 5.4.B. Predicted suitable habitat for bighead carp (H. nobilis) in the Minnesota River during a 10-year flood.
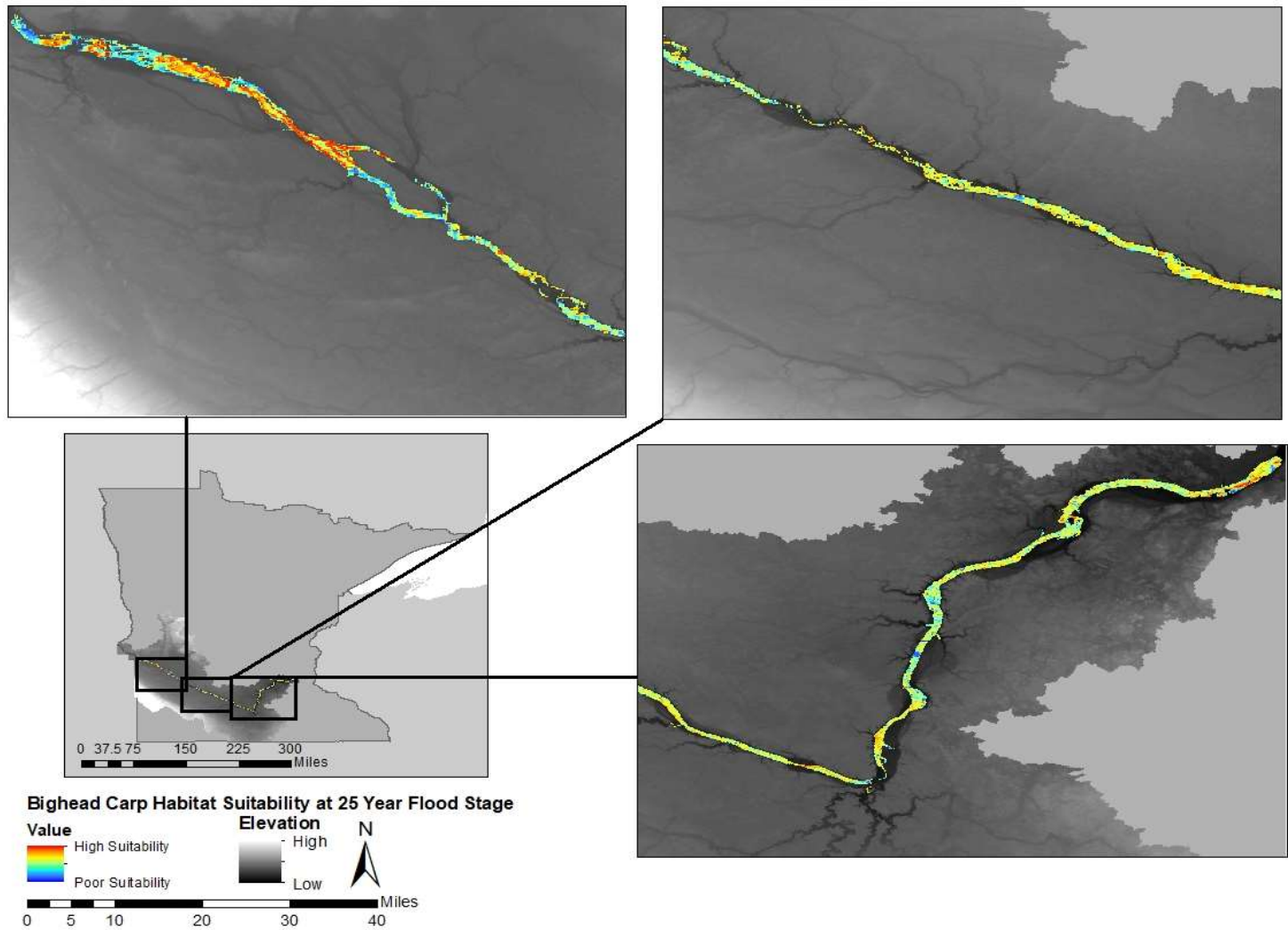
Figure 5.4.C. Predicted suitable habitat for bighead carp (H. nobilis) in the Minnesota River during a 25-year flood.
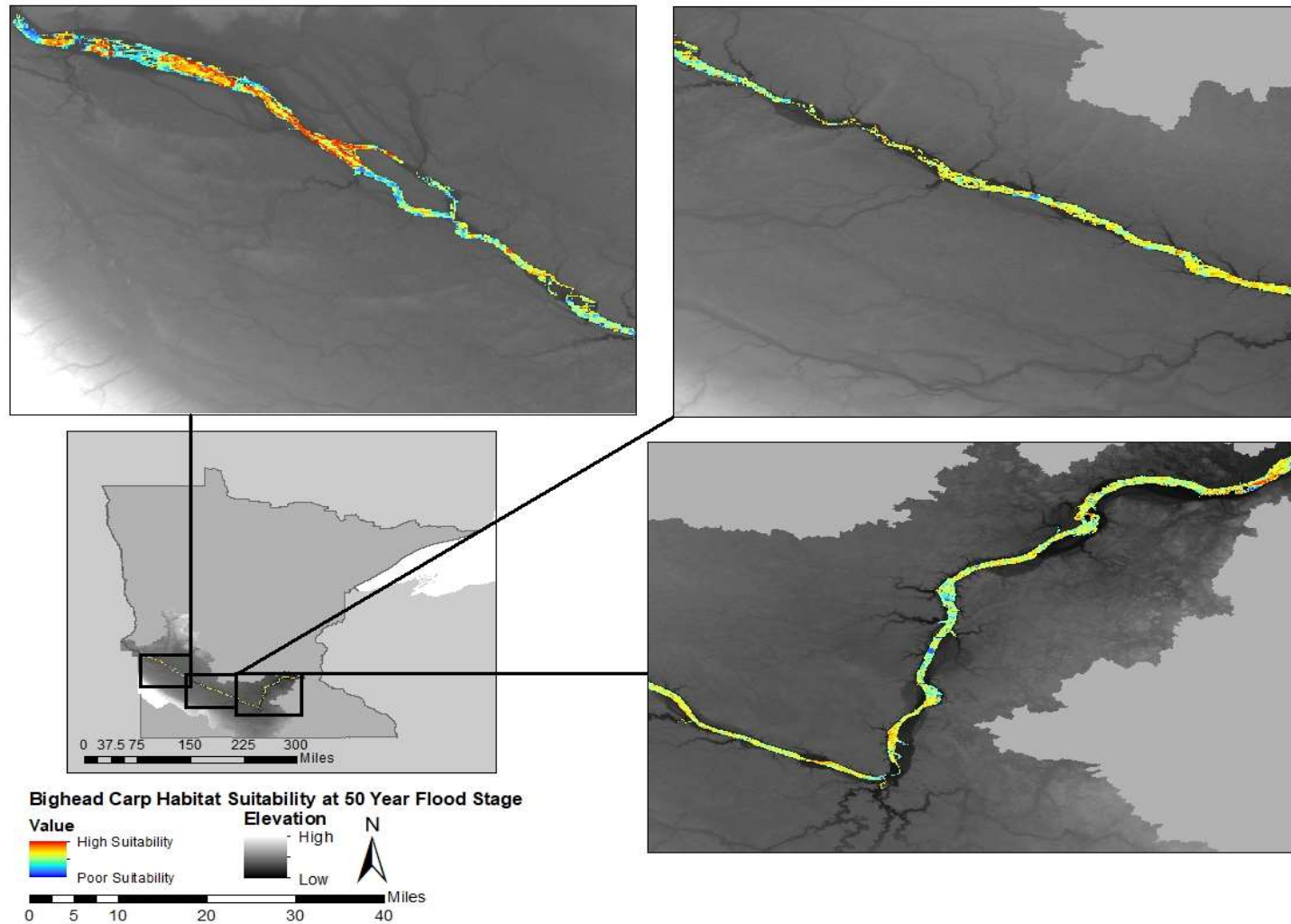
Figure 5.4.D. Predicted suitable habitat for bighead carp (H. nobilis) in the Minnesota River during a 50-year flood.
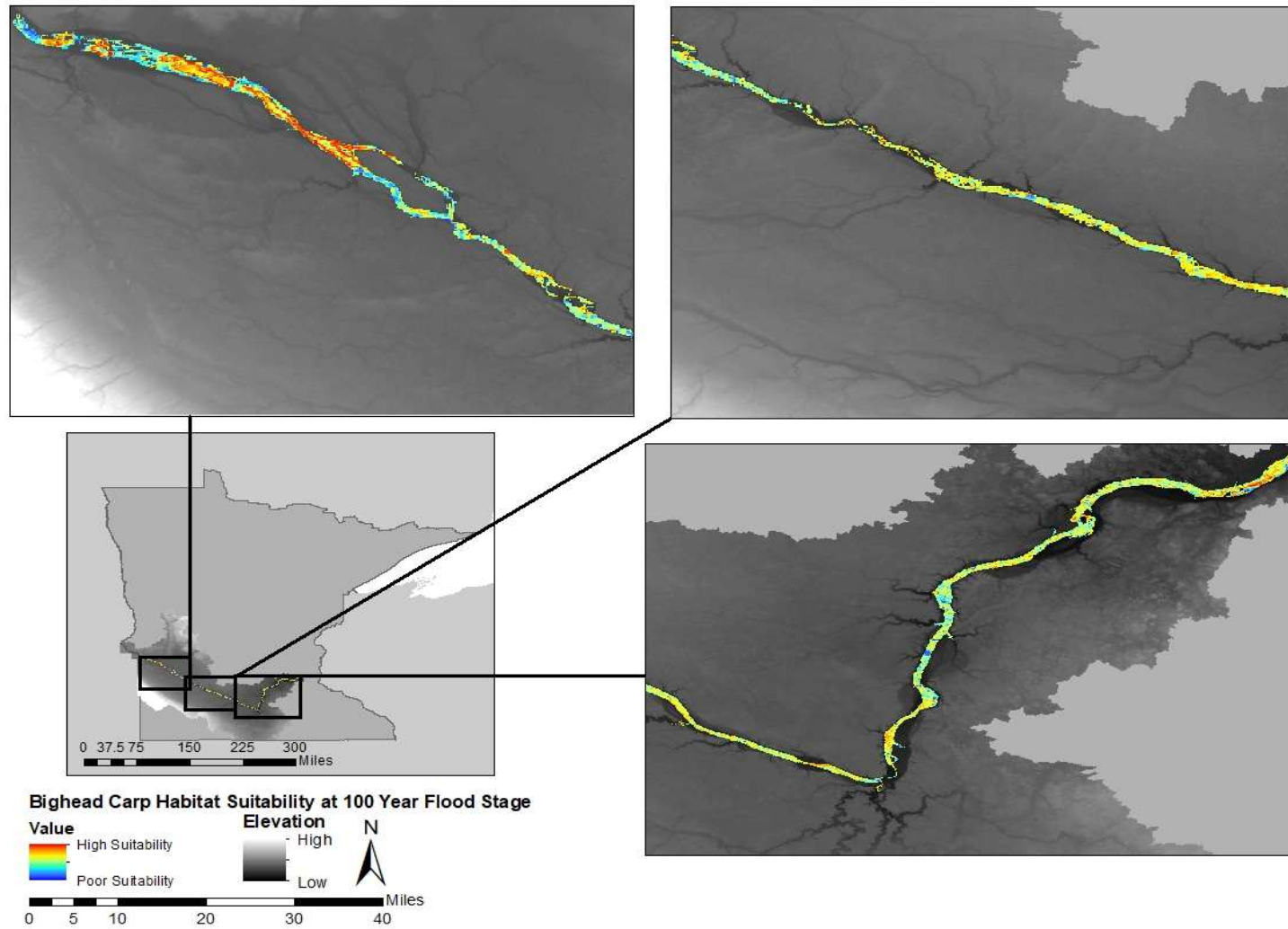
Figure 5.4.E. Predicted suitable habitat for bighead carp (H. nobilis) in the Minnesota River during a 100 year flood.

331

7.4.   Black Carp (M. piceus)

Black carp had the lowest overall suitability in comparison with other invasive carp species, with an average of only 7.3% of the area being highly suitable and 9.1% being moderately suitable (Figures 5.5A-E). Most of the area, an average of 47.6%, was classified as having low suitability. Black carp had the highest percentage, 36.9%, of poorly suited habitat. Black carp did not experience the same trend as the other invasive carp species. Instead, the percent of poorly suited habitat increased, while high, moderate, and low suitability decreased by less than 1.0%. The black carp model had an AUC of 0.847.
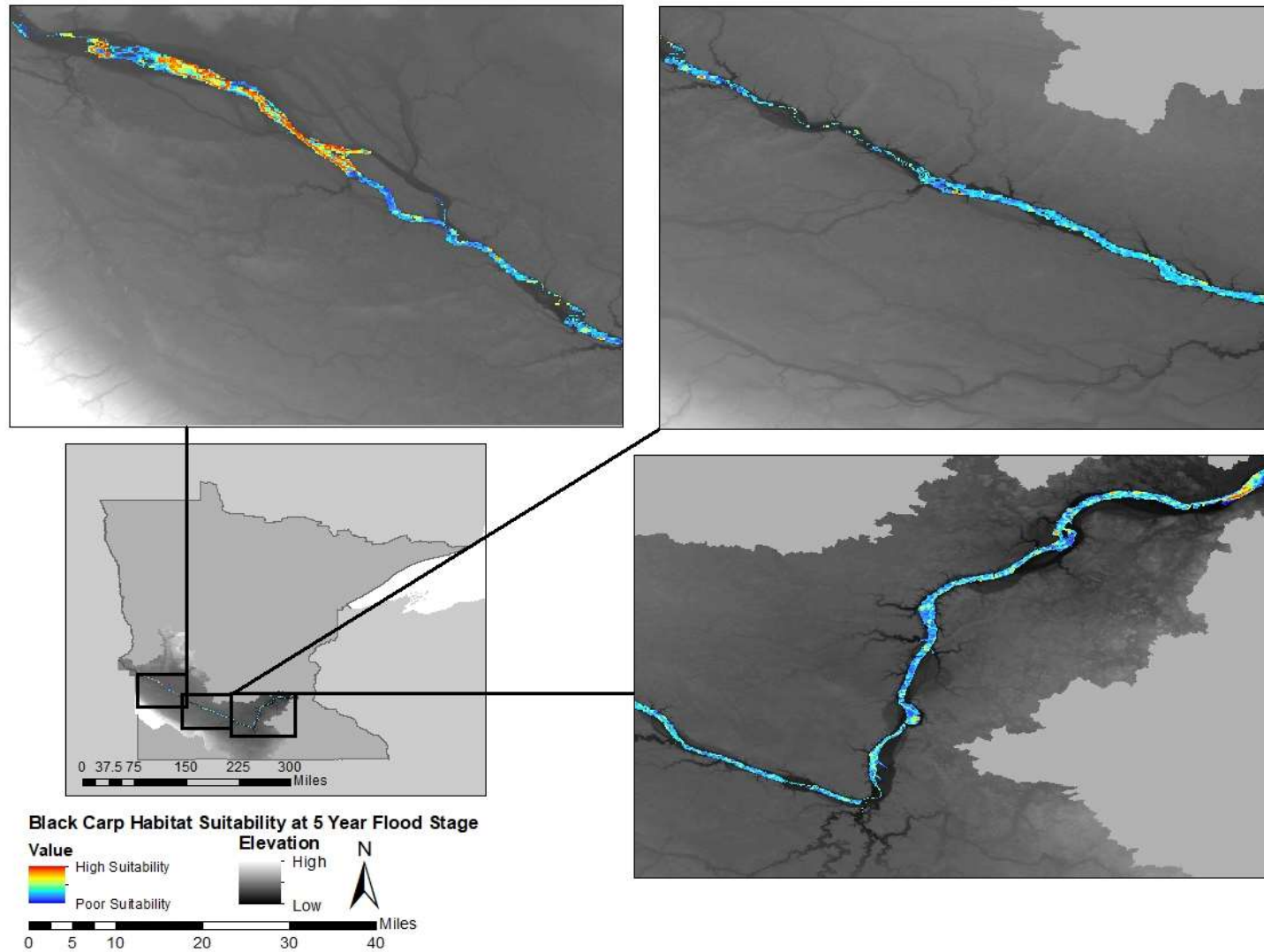
Figure 5.5.A. Predicted suitable habitat for black carp (M. piceus) in the Minnesota River during a 5 year flood.
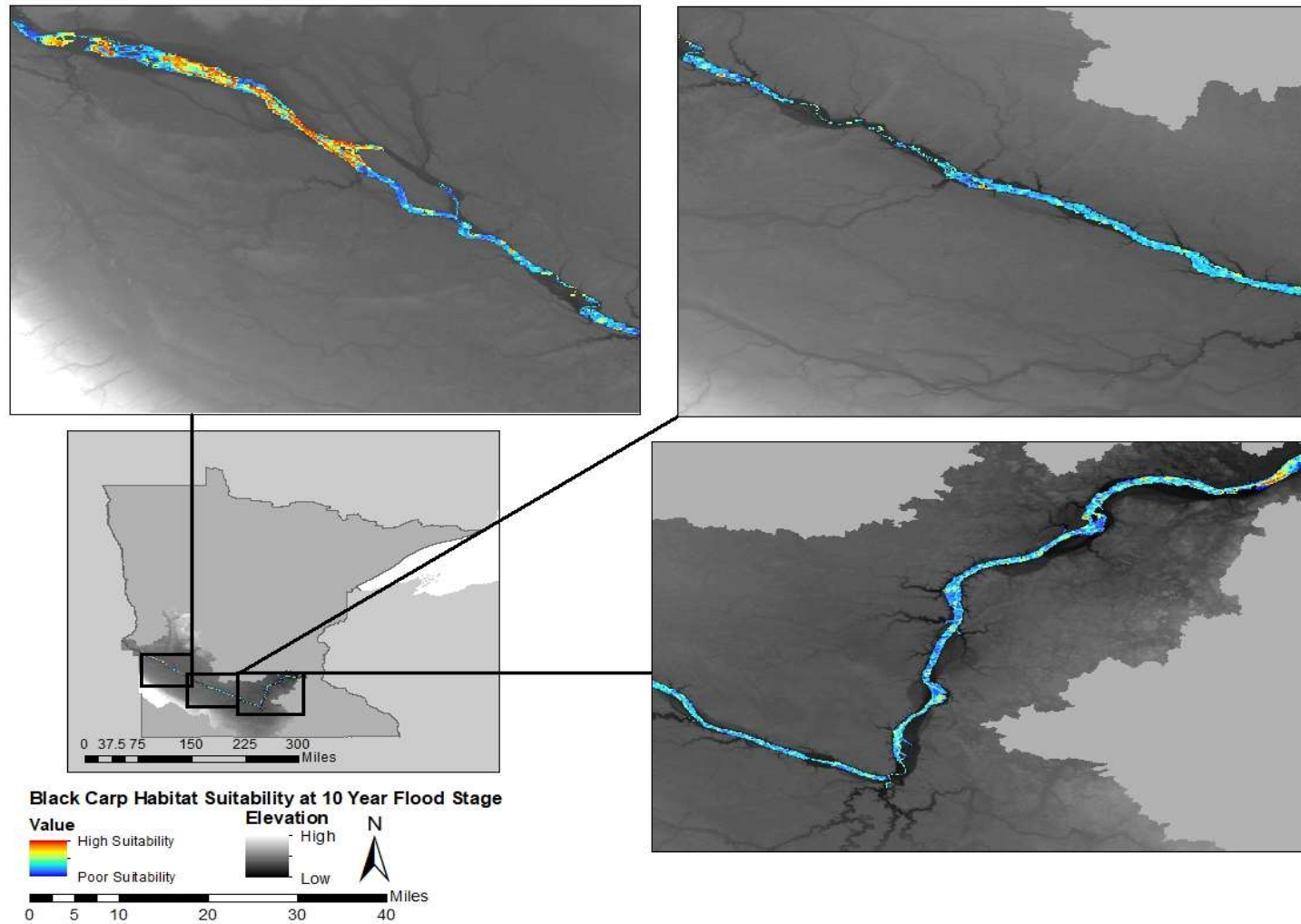
Figure 5.5.B. Predicted suitable habitat for black carp (M. piceus) in the Minnesota River during a 10-year flood.

334
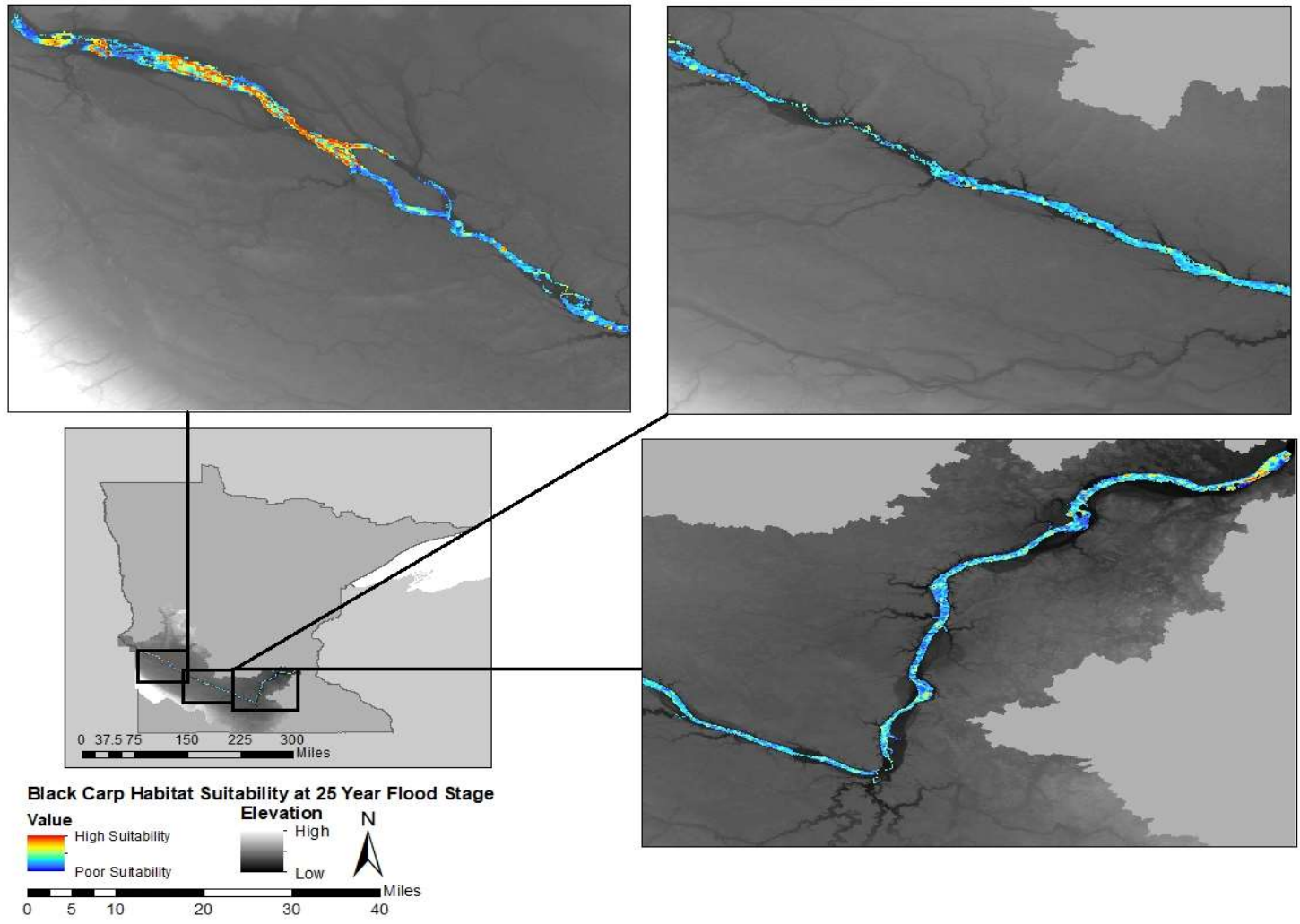
Figure 5.5.C. Predicted suitable habitat for black carp (M. piceus) in the Minnesota River during a 25-year flood.

335
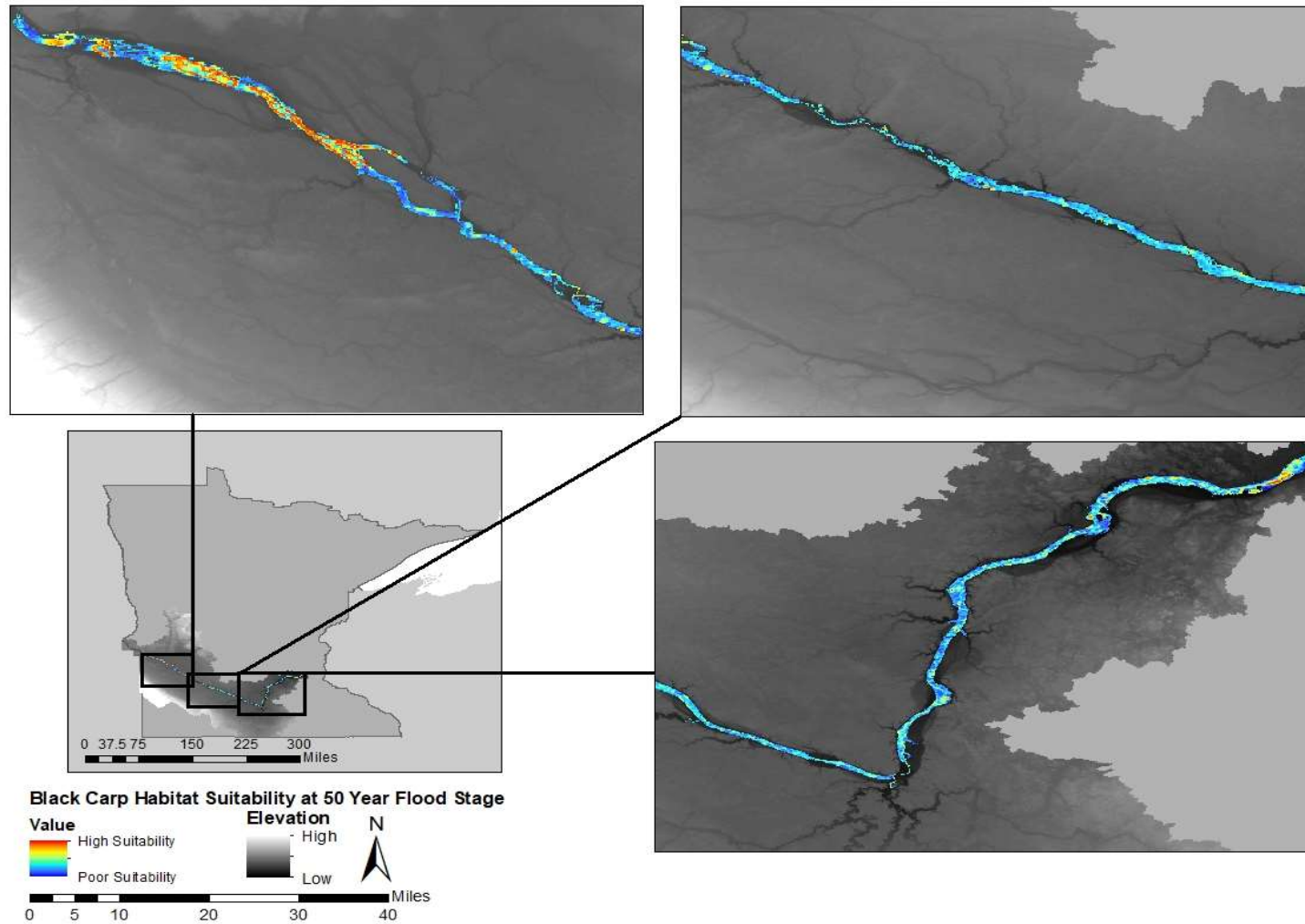
Figure 5.5.D. Predicted suitable habitat for black carp (M. piceus) in the Minnesota River during a 50-year flood.
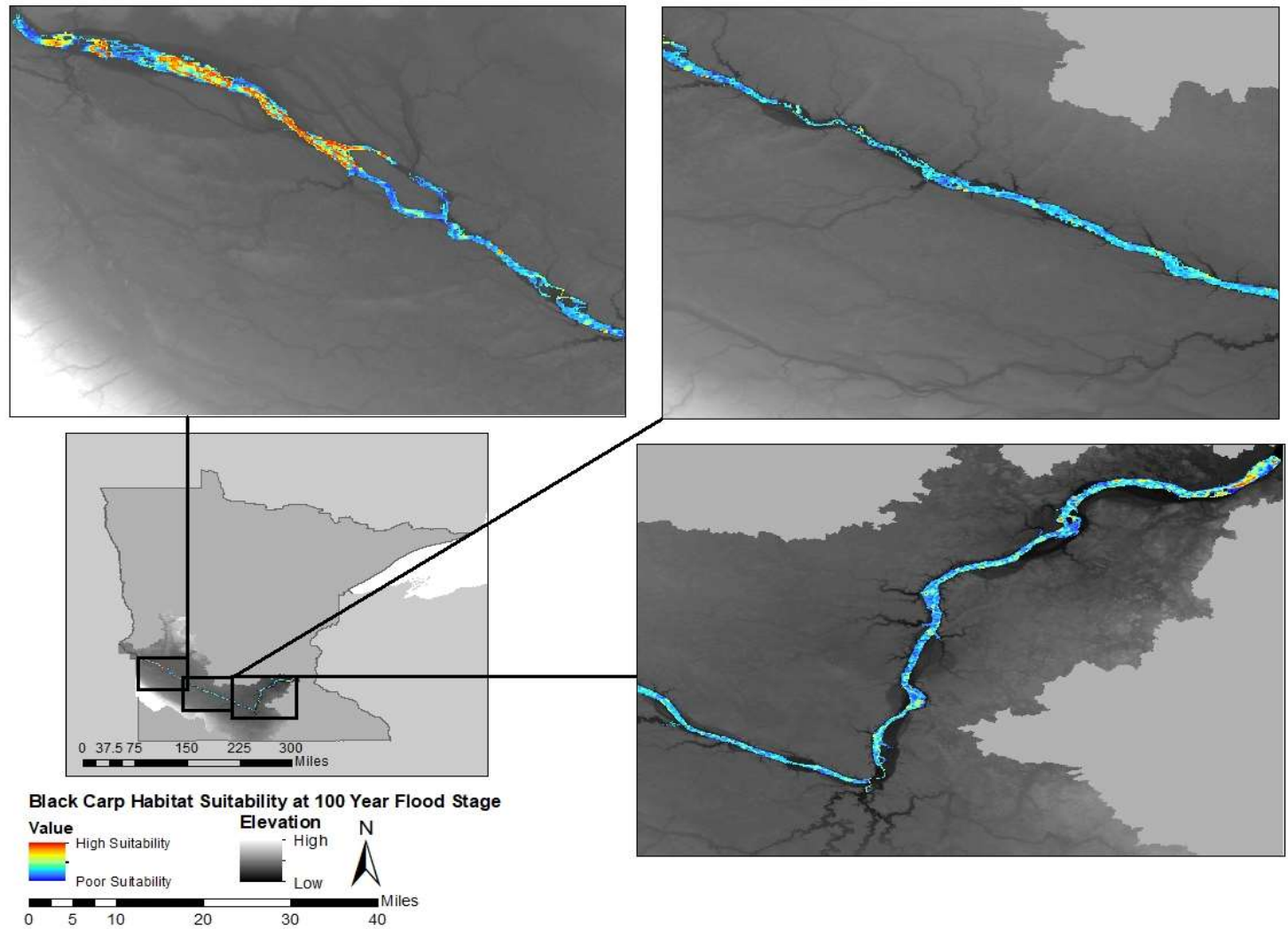
Figure 5.5.E. Predicted suitable habitat for black carp (M. piceus) in the Minnesota River during a 100-year flood.

8. Discussion

The MaxEnt results show that the Minnesota River is not equally suitable for all species (Figure 5.2.-5.5.). According to the model, the Minnesota River was most highly suited for the bighead head carp, with 70% of the area being moderately suitable or higher. Grass carp also had large amounts of suitable area within the river, with 64% of the area being classified as moderately suitable or above. Silver carp had 43% of area moderately suitable or above on average. These results do not support NicheA models that suggested the risk may be highest for grass and silver carp and lower for bighead carp. The model results for black carp did, however, support NicheA models showing low suitability within the Minnesota River. On average, MaxEnt showed only 17% of area was classified as moderately suitable or higher. This means while highly suitable areas existed within the river, they were less common and more localized. The variability between MaxEnt and NicheA models is likely a result of the environmental calibration and resolution of the data utilized to create said models. Uncertainty exists inherent in using the MODIS vegetation index used to calibrate the MaxEnt models. This index may have resulted in underpredicted suitability within the Minnesota River for invasive carp. The areas predicted as highly suitable often correlated with areas of open water, away from vegetation. It is possible that this resulted in calibration of the model to predict areas of the river enclosed in terrestrial vegetation as less suitable, despite suitable river conditions. Further field verification and testing of the MaxEnt results should be conducted to verify the high-resolution variability displayed in the model results. NicheA models, on the other hand, have a high degree of uncertainty given the coarseness of the data utilized in the model.

Despite the variability in results between the two models and uncertainty in utilization of the MODIS vegetation index in MaxEnt, both models do reveal, based on the climatological proxy parameters used, that it is highly probable that the Minnesota River would be a suitable habitat for invasive carp. Further field investigation is necessary to verify and test the robustness of models. MaxEnt indicates "Moderately suitable habitat" was most abundant throughout the river for all species, with the exception of black carp. "High suitability" did not have the greatest percentage of area for any of the species, but was present in localized hot spots that require field verification. A majority of the highly suitable areas for invasive carp were near the headwaters where the river is impounded, or near backwaters along the river. Areas of highest suitability closely resemble conditions on the Mississippi River (e.g. slow-moving water, wide channel, pools). This is not unexpected however, as a majority of occurrences used to calibrate the models were in the Mississippi River Basin. The similarities are relevant to the life histories of invasive carp. Adult invasive carp often remain in slow-moving waters or pools when not spawning. Areas of highly suitable habitat could be places to increase sampling efforts to detect adult founder population. Backwaters that were predicted as highly suitable, on the other hand, could be used to target invasive carp in early life stages (e.g. larval, juvenile). However, the abundance of moderately suitable habitat suggests monitoring throughout the river is likely needed.

In order to create a more robust risk assessment, conditions in the Minnesota River need to be considered (e.g. water temperature, pH, turbidity, flow velocity). Understanding fine scale patterns could help identify reaches of the river that are more vulnerable to invasive carp. The Minnesota River can be very dynamic in the short term. For example, after a rain storm in June of 2016 the amount of total suspended solids (TSS), or the amount of sediment and other materials in the water, spiked from 244 mg/L to 628 mg/L in five days. Research on invasive carp has suggested spikes in turbidity, a metric related to TSS, could trigger spawning activities. Tracking spikes in TSS in the Minnesota River could help managers isolate portions of the river that would be more prone to invasive carp spawning, but additional research on flow, temperature, and discharge patterns would also be needed. Unfortunately, available long-term Minnesota River data currently does not capture the full variability of water conditions because there are only a few sampling locations. Success of any of the invasive carp species would also be dependent on interspecies interactions (e.g. food availability, predation on young carp, pathogens). Further research on the Minnesota River's ecosystem is warranted to provide the data needed to assess these interactions. Examples of studies that would benefit invasive carp risk include topics such as plankton densities and native mussel populations.

The modeling framework used to complete the study also has room for improvement. Default settings in MaxEnt were utilized due to computing limitations. In future studies, customized settings for each species should be used. Moreover, multiple algorithms should have been tested for each species prior to selection. MaxEnt may have not been the best option for all species. The addition of multiple algorithms and trials would have allowed a stronger evaluation metric like akaike information criterion (AIC). Research conducted examining the effectiveness of evaluation metrics suggests the AUC may not be ideal in studies using presence only data and highlights the importance of multiple evaluation metrics (Lobo, Jimenez-Valverde, and Real 2007; Escobar et al. 2018).

8.1.   Conclusion

The MaxEnt modeling algorithm trained with high resolution vegetation indices produced results suggesting the Minnesota River is suitable for invasive carp. Bighead, silver, and grass carp had the greatest area of well suited habitat and may be at greatest risk for establishment, but habitat may not be ideal for black carp, with results showing a majority of area having low suitability. The data produced in this study can be used to preliminarily predict risk of invasion for invasive carp. However, continued ecological niche modeling is merited to further analyze risk.

Table 2.1. Variables obtained from Ecoclimate.org

Variable	Units
Annual mean temperature	°C
Mean diurnal range	°C
Isothermality	%
Temperature seasonality	%
Max temperature of warmest month	°C
Min temperature of coldest month	°C
Temperature annual range	°C
Temperature annual range	°C
Mean temperature of wettest quarter	°C
Mean temperature of driest quarter	°C
Mean temperature of warmest quarter	°C
Mean temperature of coldest quarter	°C
Annual precipitation	mm/ m2
Precipitation of driest quarter	mm/ m2
Precipitation of driest month	mm/ m2
Precipitation seasonality	%
Precipitation of wettest quarter	mm/ m2
Precipitation of driest quarter	mm/ m2
Precipitation of warmest quarter	mm/ m2
Precipitation of coldest quarter	mm/ m2

Table 2.2. Results of NicheA model evaluations

Species Name	Environmental Range	Trial	Probability of Prediction	P-Value
Silver Carp	Native Range	CAL	54.65%	< 0.0001
Silver Carp	Native Range	EVL	64.24%	< 0.0001
Silver Carp	United States	CAL	71.55%	< 0.0001
Silver Carp	United States	EVL	81.85%	< 0.0001
Silver Carp	Europe	CAL	67.85%	< 0.0001
Silver Carp	Europe	EVL	80.56%	< 0.0001
Silver Carp Average			70.12%	< 0.0001
Bighead Carp	Native Range	CAL	22.14%	< 0.0001

Bighead Carp	Native Range	EVL	22.14%	< 0.0001
Bighead Carp	United States	CAL	35.15%	< 0.0001
Bighead Carp	United States	EVL	22.26%	< 0.0001
Bighead Carp	Europe	CAL	33.38%	< 0.0001
Bighead Carp	Europe	EVL	40.42%	< 0.0001
Bighead Carp Average			29.25%	< 0.0001
Grass Carp	Native Range	CAL	50.71%	< 0.0001
Grass Carp	Native Range	EVL	62.28%	< 0.0001
Grass Carp	United States	CAL	61.51%	< 0.0001
Grass Carp	United States	EVL	73.60%	< 0.0001
Grass Carp Average			62.03%	< 0.0001
Black Carp	Native Range	CAL	14.76%	0.0122
Black Carp	Native Range	EVL	14.76%	< 0.0001
Black Carp	United States	CAL	32.52%	0.6595
Black Carp	United States	EVL	32.52%	< 0.0001
Black Carp Average			23.64%	0.1680
Total Average			46.94%	

Table 3.1A. Invasive carp MaxEnt model results quantified

Species	Flood Stage	Area of High Suitability (m2)	% Area of High Suitability	Area of Moderate Suitability (m2)	% Area of Moderate Suitability	Area of Low Suitability (m2)	% Area of Low Suitability	Area of Poor Suitability (m2)	% Area of Poor Suitability
Silver Carp	5	5,687,500	1.3%	182,437,500	42.0%	226,312,500	52.1%	20,750,000	4.8%
Silver Carp	10	6,125,000	1.3%	196,562,500	41.9%	248,750,000	53.0%	24,000,000	5.1%
Silver Carp	25	6,375,000	1.3%	209,250,000	41.3%	265,562,500	52.5%	27,562,500	5.5%
Silver Carp	50	6,375,000	1.2%	213,437,500	41.9%	277,750,000	53.2%	28,187,500	5.4%
Silver Carp	100	6,437,500	1.2%	219,437,500	40.5%	289,437,500	53.4%	29,500,000	5.4%
Average Silver Carp			1.3%		41.3%		52.8%		5.2%
Bighead Carp	5	70,375,000	16.2%	236,187,500	54.4%	112,812,500	26.0%	18,125,000	4.2%
Bighead Carp	10	76,875,000	16.4%	252,187,500	53.7%	119,687,500	25.5%	20,937,500	4.5%
Bighead Carp	25	79,937,500	15.8%	272,187,500	53.8%	134,875,000	27.0%	23,375,000	4.6%
Bighead Carp	50	81,062,500	15.5%	281,187,500	53.9%	141,062,500	27.0%	23,750,000	4.6%
Bighead Carp	100	83,187,500	15.3%	290,562,500	53.6%	147,937,500	27.3%	24,937,500	4.6%
Average Bighead Carp			15.9%		53.9%		26.5%		4.5%

Table 3.1B. Invasive carp MaxEnt model results quantified

Species	Flood Stage	Area of High Suitability (m2)	% Area of High Suitability	Area of Moderate Suitability (m2)	% Area of Moderate Suitability	Area of Low Suitability (m2)	% Area of Low Suitability	Area of Poor Suitability (m2)	% Area of Poor Suitability
Grass Carp	5	10,500,000	2.4%	272,375,000	62.7%	147,750,000	34.0%	6,000,000	1.4%
Grass Carp	10	11,125,000	2.4%	292,000,000	62.2%	162,312,500	34.6%	6,500,000	1.4%
Grass Carp	25	11,500,000	2.3%	315,187,500	62.3%	176,312,500	34.8%	6,5625,00	1.3%
Grass Carp	50	11,500,000	2.2%	324,812,500	62.2%	183,312,500	35.1%	6,625,000	1.3%
Grass Carp	100	11,500,000	2.1%	336,312,500	62.0%	191,812,500	35.4%	6,875,000	1.3%
Average Grass Carp			2.3%		62.3%		34.8%		1.3%
Black Carp	5	33,312,500	7.7%	39,875,000	9.2%	208,937,500	48.1%	157,250,000	36.2%
Black Carp	10	35,250,000	7.5%	44,250,000	9.4%	224,000,000	47.7%	171,687,500	36.6%
Black Carp	25	36,687,500	7.3%	46,500,000	9.2%	240,000,000	47.4%	186,562,500	36.9%
Black Carp	50	36,875,000	7.1%	47,250,000	9.1%	248,125,000	47.5%	194,875,000	37.3%
Black Carp	100	37,125,000	6.9%	48,937,500	9.0%	257,187,500	47.4%	203,437,500	37.5%
Average Black Carp			7.3%		9.1%		47.6%		36.9%

Appendices

Appendix

A. R script to divide data into cal and evl groups

```
library(ENMeval)#dismo, raster, rgdal

occ<-read.table("BHC_Combined.csv", head=T, sep=",")
occ<-occ[,c(2,3)]
env<-raster("Bio1b.tif")
plot(env)

#calibration
bg<-as.data.frame(env, xy=T)
block_df<-get.block (occ, bg)
occ$group<-block_df$occ.grp

cal<-occ[which(occ$group %in% c(1,4)),]
evl<-occ[which(occ$group %in% c(2,3)),]
write.table(cal, "cal.csv", row.names = F, sep=",")
write.table(evl, "evl.csv", row.names = F, sep=",")

plot(occ$DecimalLongitude, occ$DecimalLatitude, pch=".", col=rainbow(7)[occ$group])
```

Appendix B. R script to download MODIS data

```
# MODIS auto-time series download
install.packages("gWidgetsRGtk2")
library(gWidgetsRGtk2)
install.packages("MODIStsp")
library(MODIStsp)
MODIStsp()
```

9.   References

Abdusamadov, A.S. 1987. Biology of the white amur (Ctenopharyngodon idella), silver carp (Hypophthalmichthys molitix), and bighead (Aristichthysnobilis), acclimatized in the Terek region of the Caspian Basin. Journal of Ichthyology 26(4):41-49.

Aguiar, F.C., M.T. Ferreira, and I. Moreira. 2001 Exotic and native vegetation establishment following channelization of a western Iberian river. Regulated Rivers: Resource Managament 17: 509-526.

Aliyev, D.S. 1976. The role of phytophagous fishes in the reconstruction of commercial fish fauna and the biological improvement of water. Journal Ichthyology 16(2): 216-29.

Anderson, R.P. and A. Raza. 2010. The effect of the extent of the study region on GIS models of species geographic distributions and estimates of niche evolution: preliminary tests with montane rodents (genus Nephelomys) in Venezuela. Journal of Biogeography 37(7):1378-1393.

Barve, N., V. Barve, A. Jiménez-Valverde, A. Lira-Noriega, S.P. Maher, A.T. Peterson, J. Soberón, and F. Villalobos. 2011. The crucial role of the accessible area in ecological niche modeling and species distribution modeling. Ecological Modelling 222(11):1810-1819.

Bain, M.B., D.H. Webb, M.D. Tangedal, and L.N. Mangum. 1990. Movement and habitat use by grass carp in a large mainstream reservoir. Transactions of the American Fisheries Society 119(3):553-561.

Belmont, P., K.B. Gran, S.P. Schottler, P.R. Wilcock, S.S. Day, C. Jennings, J.W. Lauer, E. Viparelli, J.K. Willenbring, D.R. Engstrom, and G. Parker. 2011. Large Shift in Source of Fine Sediment in the Upper Mississippi River. Environmental science & technology 45(2):8804-8810.

Berg, L.S. 1964. Freshwater Fishes of the USSR and Adjacent Countries 2(4). Washington D.C.: The Smithsonian Institution and the National Science Foundation.

Bettoli, P.W., W.H. Neill, S.W. Kelsch. 1985. Temperature preference and heat resistance of grass carp, Ctenopharyngodon idella (Valenciennes), bighead carp, Hypophthalmichthys nobilis (Gray), and their F1 hybrid. Journal of Fish Biology 27(3):239-247.

Blossey, B., L.C. Skinner, and J. Taylor. 2001. Impact and management of purple loosestrife (Lythrum salicaria) in North America. Biodiversity and Conservation 10(10):1787-1807.

Byers, J. E. 2002. Impact of non-indigenous species on natives enhanced by anthropogenic alteration of selection regimes. Oikos 97(3):449-458.

Carlton, J.T. 2001. Introduced Species in U.S. Coastal Waters: Environmental Impacts and Management Priorities. Arlington, VA: Pew Oceans Commission.

Carpenter, S.R. and D.M. Lodge. 1986. Effects of submersed macrophytes on ecosystem processes. Aquatic Botany 26:341-370.

Chapman, D.C., J.J. Davis, J.A. Jenkins, P.M. Kocovsky, J.G. Miner, J. Farver, and P.R. Jackson. 2013. First evidence of grass carp recruitment in the Great Lakes Basin. Journal of Great Lakes Research 39(4):547-554.

Chen, P., E.O. Wiley, and K.M. Mcnyset. 2007. Ecological niche modeling as a predictive tool: silver and bighead carps in North America. Biological Invasions 9:43-51.

Chick, J.H., R.J. Maher, B.M. Burr, and M.R. Thomas. 2003. First black carp captured in U.S.. Science 300(5627):1876-1877.

Chilton III, E.W. and M.I. Muoneke. 1992. Biology and management of grass carp

(Ctenopharyngodon idella, Cyprinidae) for vegetation control: a North American perspective. Reviews in Fish Biology and Fisheries 2(4):283-320.

Coetzee, J. A., M. P. Hill, and D. Schlange. 2008. Potential spread of the invasive plant Hydrilla verticillata in South Africa based on anthropogenic spread and climate suitability. Biological Invasions 11(4):801-812.

Cremer, M.O. and R.O. Smitherman. 1980. Food habits and growth of silver and bighead carp in cages and ponds. Aquaculture 20(1):57-64.

Crossman, E.J., S.J. Nepszy, and P. Krause. 1987. The first record of grass carp, Ctenopharyngodon idella, in Canadian waters. Canadian Field-Naturalist 101(4):584-586.

Cudmore, B. and N.E. Mandrak. 2004. Biological synopsis of grass carp (Ctenopharyngodon idella). Canadian Manuscript Report of Fisheries and Aquatic Sciences.

DeGrandchamp, K.L., J.E. Garvey, and L.A. Csoboth. 2007. Linking adult reproduction and larval density of invasive carp in a large river. Transactions of the American Fisheries Society 136(5):1327-1334.

Deters, J.E., D.C. Chapman, and B. Mcelroy. 2013. Location and timing of Asian carp spawning in the Lower Missouri River. Environmental Biology of Fishes 96(5):617-629.

Dibble, E.D. and K. Kovalenko. 2009. Ecological impact of grass carp: a review of the available data. Journal of Aquatic Plant Management 47:1-15.

Ehrlich, P.R. 1984. Which animal will invade?. Ecology of Biological Invasions of North America and Hawaii: 79-95. New York, NY: Springer.

Elith, J., C. Graham, R. Anderson, M. Dudík, S. Ferrir, A. Guisan, R. Hijmans, F. Huettmann, J.R. Leathwick, A. Lehmann, J. Li, L.G. Lohmann, B.A. Loiselle, G. Manion, C. Moritz, M. Nakamura, Y. Nakazawa, J. McOverton, A.T. Peterson, S.J. Phillips, K. Richardson, R. Scachetti-Pereira, R.E. Schapire, J. Soberón, S. Williams, M.S. Wisz, N.E. Zimmermann and M. Araujo. 2006. Novel methods improve prediction of species' distributions from occurrence data. Ecography 29(2):129-151.

Escobar, L.E. and M.E. Craft. 2016. Advance and limitations of disease biogeography using ecological niche modeling. Frontiers in Biogeography 7:1174.

Escobar, L.E., H. Qiao, C. Lee, and N.B. Phelps. 2017. Novel methods in disease biogeography: A case Study with heterosporosis. Frontiers in Veterinary Science 4(105).

Executive Order No. 13112. 1999. Federal Register 64(25).

Fedorenko, A.Y., and F.J. Fraser.1978. A review of the biology of grass carp (Ctenopharyngodon idella, Val.) and its evaluation as a potential weed control agent in British Columbia. Technical Report. Fisheries and Marine Service of Canada 786.

Ferber, D. 2001. Will black carp be the next zebra mussel?. Science Magazine, 13 April: 292.

Fischenich, M. Invasive carp found in river. The Free Press, February 25, 2016.

Fisher, T.G. 2004. River Warren boulders, Minnesota, USA: Catastrophic paleoflow indicators in the southern spillway of glacial Lake Agassiz. Boreas 33:349-358.

Fukushima, M., N. Takamura, L. Sun, M. Nakagawa, K. Matsushige, and P. Xie. 1999. Changes in the plankton community following introduction of filter-feeding planktivorous fish. Freshwater Biology 42(4):719-735.

Garcia, A.M., D. Loebmann, J.P. Vieira, and M.A. Bemvenuti. 2004. First records of introduced carps (Teleostei, Cyprinidae) in the natural habitats of Mirim and Patos Lagoon estuary, Rio Grande do Sul, Brazil. Revista Brasileira de Zoologia 21(1).

Garcia, L.M., C.M. Garcia, A.F. Pinedam E,A, Gammad, J. Canta, S.P. Simon, G.V. Hilomen-

Garcia, A.C. Gonzal, and C.B. Santiago. 1999. Survival and growth of bighead carp fry exposed to low salinities. Aquaculture International 7(4):241-250.

Goldschmidt, Y., F. Witte, and J. Wanink. 1993. Cascading effects of the introduced nile perch and the detritivorous/phytoplanktivorous species in the sublittoral areas of Lake Victoria. Conservation Biology 7(3):696-700.

Gorbach, E.J. 1961. Age composition, growth and age of onset of sexual maturity of white Ctenopharyhgodon idella (Val) and bleck Mylopharyngodon pisceus (Rich amur) in the Amur river basin. Voprosy Ikhtiologii 1(18):119-126.

Gorbach, E.I. 1970. Condition and fatness of the grass carp [Ctenopharyngodon idella (Val.)] in the Amur basin. Journal of Ichthyology 1(1):880-890.

Gran, K.B., P. Belmont, S.S. Day, C. Jennings, A. Johnson, L. Perg, and P.R. Wilcock. 2009. Geomorphic evolution of the Le Sueur River, Minnesota, USA, and implications for current sediment loading. Management and restoration of fluvial systems with broad historical changes and human impacts: Geological Society of America Special Paper 451:119-130.

Gran, K.B., N. Finnegan, A.L. Johnson, P. Belmont, C. Wittkop, and T. Rittenour. 2013. Landscape evolution, valley excavation, and terrace development following abrupt postglacial base-level fall. Bulletin of the Geological Society of America 125:1821-1894.

Herborg, L., C.L. Jerde, D.M. Lodge, G.M. Ruiz, and H.J. MacIssac. 2007. Predicting invasion risk using measures of introduction effort and environmental niche models. Ecological Applications 17(3):663-674.

Hermann, K.K. and R.E. Sorensen. 2009. Seasonal dynamics of two mortality-related trematodes using an introduced snail. Journal of Parasitology 95(4):823-828.

Horsch, E.J. and D.J. Lewis. 2009. The effects of aquatic invasive species on property values: evidence from a quasi-experiment. Land Economics 85(3):391-409.

Illinois Department of Natural Resources. 2016. 2016 Interim Summary Report: Asian Carp Monitoring and Response Plan.

Illinois Department of Natural Resources. 2017. 2017 Asian Carp Monitoring and Response Plan.

Irons, K.S., G.G. Sass, M.A. McClelland, and J.D. Stafford. 2007. Reduced condition factor of two native fish species coincident with invasion of non-native Asian carps in the Illinois River, U.S.A. Is this evidence for competition and reduced fitness?. Journal of Fish Biology 71:258-273.

Jennings, C.E. 2007. Overview of the quaternary geological history of the Minnesota River watershed. Native Plant Communities and Rare Species of the Minnesota River Valley Counties: Minnesota County Biological Survey Biological Report 89.

Jennings, D.P. 1988. Bighead carp (Hypophthalmichthys nobilis): A Biological Synopsis FWS-88 (29). Gainesville, FL: National Fisheries Research Center.

Jhingran, V.G., and R.S.V. Pullin. 1985. A Hatchery Manual for the Common, Chinese, and Indian Major Carps 252. WorldFish.

Jiménez-Valverde, A., A.T. Peterson, J. Soberón, J.M. Overton, P. Aragón, and J.M. Lobo. 2011. Use of niche models in invasive species risk assessments. Biological invasions 13(12):2785-2797.

Johnson, P.T.J., J.D. Olden, and M.J. Vander Zanden. 2008. Dam invaders: impoundments facilitate biological invasions into freshwaters. Frontier in Ecology and the Environment 6(7):357-363.

Kamilov, B.G. and T.V. Salikhov. 1996. Spawning and reproductive potential of the silver carp Hypophthalmichthys molitrix from Syr Darya River. Journal of Ichthyology 36(8):600-606.

Kirkagac, M. and N. Demir. 2004. The effects of grass carp on aquatic plants, plankton and benthos in ponds. Journal of Aquatic Plant Management (42):32-39.

Kokotovich, A. and D. Andow. Potential adverse effects and management of Silver and Bighead carp in Minnesota: Findings from focus groups (Working paper).

Kolar, C.S., D.C. Chapman, W.R. Courtenay Jr., C.M. Housel, J.D. Williams, and D.P. Jennings. 2007. Bigheaded carps: A Biological Synopsis and Environmental Risk Assessment. Bethesda, MD: American Fisheries Society.

Konradt, A.G. 1965. Methods of breeding the grass carp, Ctenopharyngodon idella and the silver carp, Hypophthalmichthys molitrix. FAO Fisheries Report 4(9):195-204.

Krykhtin, M.L. and E.I. Gorbach. 1981. Reproductive ecology of the grass carp, Ctenopharyngodon idella, and the silver carp, Hypophthalmichthys molitrixi, in the Amur. Basin Journal of Ichthyology 21(2):109-123.

Kucklentz, V. 2017. Rstoration of a small lake by combined mechanical and biological methods. SIL Proceedings 22(4):2314-2317

Kulhanek, S.A., A. Ricciardi, and B. Leung. 2011. Is invasion history a useful tool for predicting the impacts of the world's worst aquatic invasive species?. Ecological Applications 21(1):189-202.

Lager, W. 2015. Upper St. Anthony lock closing after half a century; blame the carp. MPR News, June 08.

Lee, D.P. 2001. Northern Pike Control at Lake Davis, California. Rotenone in fisheries: Are the rewards worth the risk: 55-61.

Levine, S. 2017. Possible connectivity of the Little Minnesota River and Lake Traverse. Unpublished manuscript.

Lobo, J. M., A. Jiménez-Valverde, and R. Real.2008. AUC: a misleading measure of the performance of predictive distribution models. Global ecology and Biogeography 17(2):145-151.

Lodge, D.M. 1993. Biological invasions: lessons for ecology. Treands in ecology & evolution 8(4):133-137.

Lohmeyer, A.M. and J.E. Garvey. 2009. Placing the North American invasion of Asian Carp in a spatially explicit context. Biological Invasions 11(4):905-916.

Lovell, S.J., S.F. Stone, and L. Fernandez. 2006. The economic impacts of aquatic invasive species: a review of the literature. Agricultural and Resource Economics Review 35(1):195-208.

Matsch C.L. and H.E. Wright. 1967. The southern outlet of Glacial Lake Agassiz. Glacial Lake Agassiz: 231-244.

McKnight, S.K. and G.R. Hepp. 1995. Potential effect of grass carp herbivory on waterfowl foods. The Journal of Wildlife Management: 720-727.

McMahon, R.F. 2002. Evolutionary and physiological adaptations of aquatic invasive animals: r selection versus resistance. Canadian Journal of Fisheries and Aquatic Sciences 59 (7):1235-1244.

Minnesota Department of Natural Resources (MN DNR). 2011. Fishing creates 43,000 Minnesota jobs, $2.8 billion in retail spending. Available at

http://news.dnr.state.mn.us/2011/05/05/fishing-creates-43000-minnesota-jobs-28-billion-in-retail-spending/ (last accessed 21 April 2018).

Minnesota Department of Natural Resources (MN DNR). 2014. Minnesota Invasive Carp Action Plan.

Minnesota Department of Natural Resources (MN DNR). 2017. Minnesota River listed for zebra mussels, invasive carp. Available at https://www.dnr.state.mn.us/invasive-carp/index.html (last accessed 21 April 2018).

Minnesota Department of Natural Resources (MN DNR). 2018a. Fish and fishing. Available at https://www.dnr.state.mn.us/faq/mnfacts/fishing.html. (last accessed March 18, 2018).

Minnesota Department of Natural Resources (MN DNR). 2018b. Fishes of Minnesota. Available at https://www.dnr.state.mn.us/fish/index.html. (last accessed March 18, 2018).

Minnesota Department of Natural Resources (MN DNR). 2018c. Invasive carp. Available at https://www.dnr.state.mn.us/invasive-carp/index.html. (last accessed March 20, 2018).

Minnesota Department of Natural Resources (MN DNR). 2018e. Rare Species Guide. Available at https://www.dnr.state.mn.us/rsg/filter_search.html. (last accessed April 4, 2018).

Morrison, B.J., J.C. Casselman, I.B. Johnson, and D.L. Noakes. 2004. New Asian carp genus (Hypopthalmichthys) in Lake Erie. Fisheries 29(8):6-7.

Moy, P.B., I. Polls, J.M. Dettmers, D. Chapman, and M. Hoff. 2011. The Chicago sanitary and ship canal aquatic nuisance species dispersal barrier. American Fisheries Society Symposium 74:121-137.

MPR News. 2017. DNR: Minnesota's largest invasive carp captured near Redwood Falls. MPR News.

Mukhamedova, A.F. 1977. The level of standard metabolism of young silver carp, Hypophthalmichthys molitrix. Journal of Ichthyology 17:292-298.

Murphy, E.A. and P.R. Jackson. 2013. Hydraulic and Water-quality Data Collection for the Investigation of Great Lakes Tributaries for Asian Carp Spawning and Egg-transport Suitability. Reston, VA: U.S. Geological Survey.

Musser, K., S. Kudelka, and R. Moore. 2009. Minnesota River Basin trends. Minnesota State University, Mankato, Water Resources Center.

Nagaraju, S.K., R. Gudasalamani, N. Barve, J. Ghazoul, G.K. Narayanagowda, and U.S. Ramanan. 2013. Do ecological niche model predictions reflect the adaptive landscape of species?: a test using Myristica malabarica Lam., an endemic tree in the Western Ghats, India. PLoS One 8(11):e82066.

Nico, L.G., J.D. Williams, and H.L. Jelks. 2005. Black carp: Biological Synopsis and Risk Assessment of an Introduced Fish. Bethesda, MD: American Fisheries Society.

Nico, L.G., and H.L. Jelks. 2011. The black carp in North America: an update. American Fisheries Society Symposium 74. Bethesda, MD: American Fisheries Society.

Nikolsky, G.V. 1963. The ecology of fishes. New York, NY: Academic press.

Noatch, M.R. and C.D. Suski. 2012. Non-physical barriers to deter fish movements. Environmental Reviews 20(1):71-82.

Opuzynski, K. 1967. Comparision of temperature and oxygen tolerance in grass carp (Ctenopharyngodon idella Val.), silver carp (Hypophthalmichthys molitrix Val.) and mirror carp (Cyprinus carpio L.). Państwowe Wydawnictwo Naukowe. Oddział

Opuszynski, K. 1981. Comparison of the usefulness of the silver carp and the bighead carp as additional fish in carp ponds. Aquaculture 25(2):223-233.

Opuszynski, K., A. Lirski, L. Myszkowski, and J. Wolnicki. 1989. Upper lethal and rearing

temperatures for juvenile common carp, Cyprinus carpio L., and silver carp, Hypophthalmichthys molitrix (Valenciennes). Aquaculture Research 20(3):287-294.

Opuszynski, K. and J.V. Shireman. 1995. Herbivorous Fishes: Culture and Use for Weed Management. Boca Raton, FL: CRC Press.

Page, L.M. and B.M. Burr. 1991. A Field Guide to Freshwater Fishes. Boston, MA: Mifflin Company.

Perea, J. P. 2002. Asian carp invasion: fish farm escapees threaten native river fish communities and boaters as well. Outdoor Illinois 10(5):8.

Peters, Lindsay M., Mark A. Pegg, and Ulrich G. Reinhardt. 2006. Movements of adult radio-tagged bighead carp in the Illinois River. Transactions of the American Fisheries Society 135(5): 1205-1212.

Peterson, A.T. 2003. Predicting the geography of species' invasions via ecological niche modeling. The quarterly review of biology 78(4):419-433.

Peterson, A.T., and C.R. Robins. 2003. Using ecological-niche modeling to predict barred owl invasions with implications for spotted owl conservation. Conservation Biology 17(4):1161-1165.

Peterson, A.T., and Y. Nakazawa. 2008. Environmental data sets matter in ecological niche modelling: an example with Solenopsis invicta and Solenopsis richteri. Global ecology and Biogeography 17(1):135-144.

Peterson, A.T., J. Soberón, R.G. Pearson, R.P. Anderson, E. Martínez-Meyer, M. Nakamura, and M.B. Araújo. 2011. Ecological Niches and Geographic Distributions. Princeton, NJ: Princeton University Press.

Pflieger, W.L. 1978. Distribution and Status of the Grass Carp (Ctenopharyngodon idella) in Missouri Streams. Transactions of the American Fisheries Society 107(1):113-118.

Phillips, S.J. 2005. A brief tutorial on MaxEnt. AT&T Research.

Phillips, S.J. and M. Dudík. 2006. Modeling species distributions with MaxEnt: New extension and a comprehensive evaluation. Ecography 31(2):161-175.

Pimentel, D., L. Lach, R. Zuniga, D. Morrizon. 2000. Environmental and economic costs of nonindigenous species in the United States. Bioscience 50(1):53-56.

Pyron, R.A., F.T. Burbrink, and T.J. Guiher. 2008. Claims of potential expansion throughout the US by invasive python species are contradicted by ecological niche models. PloS one 3(8):e2931.

Qiao, H., A.T. Peterson, L.P. Campbell, J. Soberón, L. Ji, and L.E. Escobar. 2016. NicheA: creating virtual species and ecological niches in multivariate environmental scenarios. Ecography 39(8):805-813.

Qiao, H., J. Soberón, and A.T. Peterson. 2015. No silver bullets in correlative ecological niche modelling: insights from testing among many potential algorithms for niche estimation. Methods in Ecology and Evolution 6(10):1126-1136.

Radke, R.J. and U. Kahl. 2002. Effects of a filter-feeding fish [silver carp, Hypophthalmichthys molitrix (Val.)] on phyto- and zooplankton in a mesotrophic reservoir: results from an enclosure experiment. Freshwater Biology 47:2337-2344.

Raibley, P.T., D. Blodgett, and R.E. Sparks. 1995. Evidence of Grass Carp (Ctenopharyngodon idella) Reproduction in the Illinois and Upper Mississippi Rivers. Journal of Freshwater Ecology 10(1):65-74.

Rasmussen, J.L. 2002. The Cal-Sag and Chicago Sanitary and Ship Canal: A Perspective on the

Spread and Control of Selected Aquatic Nuisance Fish Species. Rock Island, IL: U.S. Fish and Wildlife Service, Region 3 White Paper, Fisheries Resources Office.

Ray, W.J. and L.D. Corkum, 1997. Predation of zebra mussels by round gobies, Neogobius melanostomus. Environmental Biology of Fishes 50(3):267-273.

Robison, H.W. and T.M. Buchanan. 1988. Fishes of Arkansas. Fayetteville, AR: University of Arkansas Press.

Romero-Alvarez, D., L.E. Escobar, S. Varela, D.J. Larkin, and N.B. Phelps. 2017. Forecasting distributions of an aquatic invasive species (Nitellopsis obtusa) under future climate scenarios. PloS one 12(7):e0180930.

Ruebush, B.C. 2011. In-situ tests of sound-bubble-strobe light barrier technologies to prevent the range expansions of Asian carp. PhD diss., University of Illinois at Urbana-Champaign.

Sampson, S.J., J.H. Chick, and M.A. Pegg. 2009. Diet overlap among two Asian carp and three native fishes in backwater lakes on the Illinois and Mississippi rivers. Biological Invasions 11(3):483-496.

Sass, G.G, C. Hinz, A.C. Erickson, N.N. McClelland, M.A. McClelland, and J.M. Epifanio. 2014. Invasive bighead and silver carp effects on zooplankton communities in the Illinois River, Illinois, USA. Journal of Great Lakes Research 40(4):911-921.

Schramm Jr, H.L. 2017. The fishery resources of the Mississippi River: A model for conservation and management. Fisheries 42(11):574-585.

Schrank, S.J. and C.S. Guy. 2003. Competitive interactions between age-0 bighead carp and paddlefish. Transactions of the American Fisheries Society 132:1222-1228.

Schrank, S.J., P.J. Braaten, and C.S. Guy. 2001. Spatiotemporal variation in density of larval bighead carp in the lower Missouri River. Transactions of the American Fisheries Society 130(5):809-814.

Schroeder, G.L. 1978. Autotrophic and heterotrophic production of micro-organisms in intensely-manured fish ponds, and related fish yields. Aquaculture 14(4):303-325.

Semmens, B.X., E. R. Buhle, A. K. Salomon, and C.V. Pattengill-Semmens. 2004. A hotspot of non-native marine dishes: evidence for the aquarium trade as invasion pathway. Marine Ecology Progress Series 266:239-244.

Shelton, W.L. and R.O. Smitherman. 1984. Exotic fishes in warmwater aquaculture. Distribution, biology, and management of exotic fishes. The Johns Hopkins University Press, Baltimore, Maryland.

Shireman, J.G. and C.R. Smith. 1983. Synopsis of biological data on the grass carp, Ctenopharyngodon idella (Cuvier and Valenciennes, 1844). Food and Aquaculture Organization Synopsis 135.

Simberloff, D. 1989. Which insect introductions succeed and which fail. Biological invasions: a global perspective: 61-75.

Singh, W. 1989. Fecundity of silver carp, Hypophthalmichthys molitrix (Val.). Indian Journal of Animal Sciences.

Smith, C. 2016. Testing a semi-automated geospatial methodology for floodplain inundation mapping: Case study of the Minnesota River valley. M.S. app, Department of Geography, Minnesota State University, Mankato.

Sobolev, Y.A. 1970. Food interrelationships of young grass carp, silver carp and carp reared jointly in ponds in Belorussia. Journal of Ichthyology 10(4): 528-533.

Sparks, R.E., T.L. Barkley, S.M. Creque, J.M. Dettmers, and K.M. Stainbrook. 2010. Evaluation

of electric fish dispersal barrier in the Chicago Sanitary and Ship Canal. American Fisheries Society Symposium 74:139-161.

Spataru, P., G.W. Wohlfarth, and G. Hulata. 1983. Studies on the natural food of different fish species in intensively manured polyculture ponds. Aquaculture 35:283-98.

Spataru, P. and M. Gophen. 1985. Feeding behaviour of silver carp Hypophthalmichthys molitrix Val. and its impact on the food web in Lake Kinneret, Israel. Hydrobiologia 120(1):53-61.

Stanley, J.G., W.W. Miley II, and D.L. Sutton. 1978. Reproductive requirements and likelihood for naturalization of escaped grass carp in the United States. Transactions of the American Fisheries Society 107(1):119-128.

U.S. Fish and Wildlife Service (USFWS). 2012. The Cost of Invasive Species.

U.S. Fish & Wildlife Service (USFWS). 2018. Minnesota: County distribution of federally-listed threatened, endangered, proposed, and candidate species. Available at https://www.fws.gov/midwest/endangered/lists/minnesot-spp.html (last accessed 21 April 2018).

USGS. 2016. NAS-Nonindigenous Aquatic Species. Available at https://nas.er.usgs.gov/viewer/omap.aspx (last accessed 6 December 2016).

Van Dyke, J.M., A.J. Leslie Jr., and J.E. Nall. 1984. The effects of the grass carp on the aquatic macrophytes of four Florida lakes. Journal of Aquatic Plant Management 22:87-95.

Verigin, B.V., A.P. Makeyeva, and M.Z. Mokhamed. 1978. Natural spawning of the silver carp Hypophthalmichthys molitrix, the bighead carp Aristichthys nobilis, and the grass carp Ctenopharyngodon idella, in the Syr-Dar'ya River. Journal of Ichthyology 18(1):143-146.

Vitousek, P.M., HA. Mooney, J. Lubchenco, and J. M. Melillo. 1997. Human domination of Earth's ecosystems. Science 277(5325):494-499.

Weber, M.J. and M.L. Brown. 2009. Effects of common carp on aquatic ecosystems 80 years after "carp as a dominant": Ecological insights for fisheries management. Reviews in Fisheries Science 17(4):524-537.

Wiley, M.J., P.P. Tazik, and S.T. Sobaski. 1987. Controlling aquatic vegetation with triploid grass carp. Illinois Natural History Survey Circular 57.

Williamson, C.J. and J.E. Garvey. 2005. Growth, fecundity, and diets of newly established silver carp in the middle Mississippi River. Transactions of the American Fisheries Society 134(6):1423-1430.

Wisz, M.S., R.J. Hijmans, J. Li, A.T. Peterson, C.H. Graham, A. Guisan, and NCEAS Predicting Species Distributions Working Group. 2008. Effects of sample size on the performance of species distribution models. Diversity and distributions 14(5):763-773.

Xie, P. and Y. Chen. 2001 Invasive carp in China's plateau lakes. Science 224(5544):999-1000.

Yi, Y., Z. Wang., and Z. Yang. 2010. Impact of the Gezhouba and Three Gorges Dams on habitat suitability of carps in the Yangtze River. Journal of Hydrology 387(3):283-291.

Zhang, H., E.S. Rutherford, D.M. Mason, J.T. Breck, M.E. Wittmann, R.M. Cooke, D.M. Lodge, J.D. Rothlisberger, X. Zhu, and T.B. Johnson. 2016. Forecasting the impacts of silver and bighead carp on the Lake Erie food web. Transactions of the American Fisheries Society 145(1):136-162.

Zielinski, D.P. and P.W. Sorensen. 2016. Bubble curtain deflection screen diverts the movement of both Asian and common carp. North American Journal of Fisheries Management 36(2):267-276.

Zielinski, D.P. and P.W. Sorensen. 2017. Silver, bighead, and common carp orient to acoustic

particle motion when avoiding a complex sound. PloS one 12(6).

Phase 2:

Task 1: Bathymetry

Besides knowing the extent of the floodplain above the water line, the bathymetry of the river needs to be surveyed and mapped to determine the feasibility of the carp barrier. Barrier construction and cost estimation requires data on the channel cross-sectional profile. In order to understand the hydraulic characteristics of the river at a given location channel geometry data is also necessary, as discussed above. Thus, there is a vital need for bathymetric data collection along key reaches of interest and potentially the entirety of the river to both locate possible barrier sites and determine the feasibility at such sites.

The project proposes to create a bathymetric map for key reaches of the mainstem of the river. Approximately 42 km (of the ~600 km total) of the river bathymetry has been mapped during the summers of 2013 and 2014 by Utah State University utilizing a highly efficient suite of instruments. The mapping of the bathymetry is fairly time sensitive as we need the right flows; 2014 was an ideal year. Mapping bathymetry for cutoffs is more challenging, but could be important for Invasive carp habitat. If flows do not get high enough to map cutoffs with our Acoustic Doppler Current Profiler (ADCP), the project could map them with rtkGPS (real time kinematic GPS) surveys.
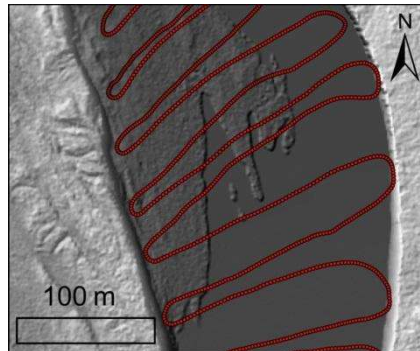
Deliverables:
Bathymetry maps for key reaches of the mainstem of the river.

Timeline:
January 2015 - December 2016

RESULTS: *Bathymetry Mapping*

Author(s): Patrick Belmont[1], Sara A. Kelly[1], Bruce Call[1], Shayler Levine[1], Adam Fisher[1]

[1]Watershed Sciences - Utah State University

Corresponding Author:
Patrick Belmont – Email: patrick.belmont@usu.edu; Phone: 4357973794

GIS Data Available (links require username/password: landforms/rock):
https://geo.mnsu.edu/geo/DNR-InvasiveCarp/Patrick-Sara-Bathymetry/MinnesotaRiverBathymetry_Hydroshare/

1. Introduction

River bathymetry is essential for mapping aquatic habitat, simulating hydraulics, and monitoring change in river morphology over time. River channels are highly variable spatially and can be highly dynamic over time, often representing the most dynamic 1% of any given landscape. High resolution topography data from aerial lidar is dramatically enhancing our abilities to identify critical features and measure geomorphic change over vast areas. However, most lidar datasets do not contain topography data within the channel itself because the wavelengths utilized are fully attenuated, even in shallow water. Bathymetric maps of rivers remain somewhat rare, largely due to logistical challenges. A spatially extensive bathymetry dataset provides the foundation for understanding habitat characteristics for Invasive carp as well as key information for planning mitigation strategies, including water depth, spatial variability in water depths and velocities, and temporal changes in bed elevation.

A variety of techniques are available for measuring river bathymetry (Brasington et al., 2000; Legleiter and Kyriakidis, 2008; McKean et al., 2008, 2009; Kinzel et al., 2012; Passalacqua et al., 2015). The standard historical practice has been to measure individual cross-sectional surveys. However, such manual surveys are time intensive and the spacing between surveys is often inadequate for representing the critical three-dimensional morphology of the channel bed. Additionally, the limited temporal and spatial coverage of cross sectional surveys is often inadequate for assessing three-dimensional change over time. Manual surveys using real-time-kinematic (rtk) GPS are useful for relatively shallow streams and for relatively short reaches, but are impractical for large rivers and spatially extensive surveys. Optical techniques, such as terrestrial lidar, green-wavelength aerial lidar and photogrammetry and spectral depth modeling from aerial photos or satellite images are commonly used in relatively shallow and highly transparent streams and rivers (Brasington et al., 2000; Legleiter et al., 2009, 2011; McKean et al., 2009). However, use of these approaches is not feasible in relatively deep and highly turbid rivers such as the Minnesota. Thus, hydroacoustic techniques are the preferred option for collecting the data required in this study. While a range of hydroacoustic techniques are available we chose to utilize an Acoustic Doppler Current Profiler, coupled with a rtkGPS

system to rapidly map bathymetry of the mainstem Minnesota River (Mueller and Wagner, 2008).

2. Methods

2.1. Site Selection

We selected sites along the upper, middle and lower Minnesota River mainstem to map bathymetry. In selecting sites, we aimed to obtain bathymetry data across a wide range of environments, with an emphasis on locations that could serve as effective Invasive carp management sites. Other limitations included accessibility (functional boat ramps within a reasonable distance), flow depths at the time of surveying, and safety.

In total we surveyed 10 reaches of the mainstem Minnesota River, most of which were surveyed multiple times so that we could monitor changes in bed morphology. In total, we surveyed 234.2 km of the mainstem Minnesota River. Where possible we leveraged bathymetry data that we had collected prior to the start of this project. Survey site A, Granite Falls, was surveyed in 2015, covering 12.6 km. Site B, New Ulm, was surveyed in 2015 and 2016, covering 15.5 and 12.8 km respectively. Site C, Judson to Mankato, was surveyed in 2013, 2014, and 2016, covering 14.3, 16.1, and 2.9 km respectively. Site D, Mankato, was surveyed every year between 2013-2016, with each year covering 6.5, 6.4, 4.8, and 5.7 km. Site E, Seven Mile Creek, was surveyed in 2013, 2014, and 2016, with each year covering 11, 10.8, and 10.6 km respectively. Site F, St. Peter, was surveyed in 2015 and 2016, covering 8.4 and 8.3 km respectively. Site G, Belle Plaine, was surveyed in 2014, 2015, and 2016, each covering 9.5, 7.9, and 7.6 km. Site H, Jordan, was surveyed in 2015 and 2016, covering 8.9 and 5.6 km respectively. Site I, Chaska, was surveyed in 2015 and 2016, covering 10.2 and 9.7 km respectively. Site J, Shakopee, was surveyed in 2015 and 2016, covering 16 and 12.2 km respectively. In total, 234.2 km were surveyed along the Minnesota River between 2013 and 2016.

Figure 1. Bathymetry survey coverage colored by the number of years with available bathymetry, and labeled by survey site.
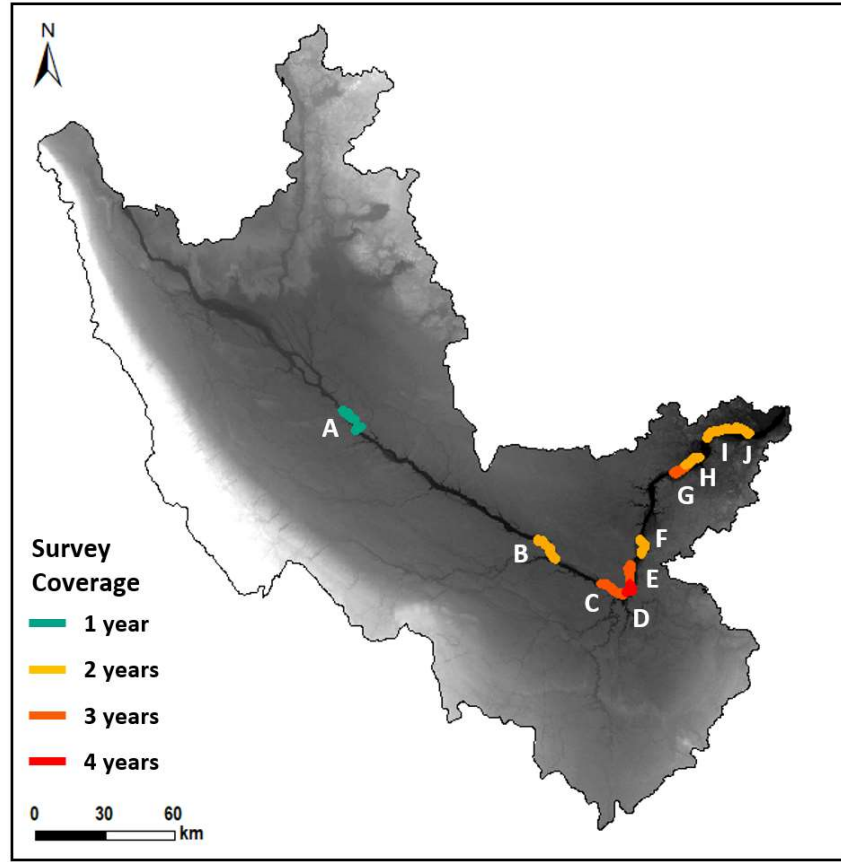
Table 1. Distance for each of the bathymetric surveys

		Reach lengths in kilometers by year			
Reach	**Name**	**2013**	**2014**	**2015**	**2016**
A	Granite Falls			12.6	
B	New Ulm			15.5	12.8
C	Judson to Mankato	14.3	16.1		2.9
D	Mankato	6.5	6.4	4.8	5.7
E	Mankato to 7 Mile Creek	11.0	10.8		10.6
F	St. Peter			8.4	8.3
G	Belle Plaine		9.5	7.9	7.6
H	Jordan			8.9	5.6
I	Chaska			10.2	9.7
J	Shakopee			16.0	12.2

356

2.2. Instrumentation and data processing

Bathymetric surveys were conducted using a Teledyne RD Instruments River Ray Acoustic Doppler Current Profiler coupled with a real-time-kinematic GPS system that was linked to the Minnesota Continuous Operating Reference System (MN CORS, MN Department of Transportation, 2018). The River Ray has four phased-array beams pulsing an acoustic signal at 600 kHz with a profiling range of 0.4 to 60 m. Standard technical specifications of the River Ray include velocity profiling accuracy of approximately ± 0.002 m/s and depth measurement accuracy of ± 1% (Teledyne RDI, 2014). Over the course of the project, we used two different rtkGPS units. Surveys for 2013, 2014 and 2015 utilized a Leica Viva GS15 Smart Antenna. In 2016 we used an rtk-enabled Hemisphere A325. Both systems were linked to the MN CORS network to achieve 2-5 cm location accuracy. Any data points collected when rtk precision was not available were deleted in post-processing steps. Data were transmitted continuously to a laptop via Bluetooth (from ADCP) and wired connection (from GPS) and assimilated using WinRiver II software (Teledyne RDI, 2006). All of this instrumentation was rigged on a 16' cataraft with an outboard motor (Figure 2). Surveys were conducted by sweeping the boat perpendicular across the channel from bank to bank and advancing upstream on each sweep. Approximately 10 to 50 m spacing was used between sweeps, depending on the variability of the bed topography, which could be seen in real time on the on-board laptop computer.

Figure 2. Equipment and instrumentation used for bathymetry mapping.

The Python scripts take ASCII outputs from WinRiver II and extract the necessary information from ADCP measurement files to calculate bed elevations and save the results as a shapefile. The first script reads in the data and exports temporary files formatted for geoid corrections that can be performed between running the first and second script. The second script uses the formatted data files and calculated geoid corrections to perform the necessary

calculations to extract bed elevations from the four beams of the ADCP. To run the scripts, the user must have their Python environment configured to use the ArcGIS Python API arcpy as well as the open source numpy and pandas Python libraries. For further questions regarding the scripts, and please contact Bruce Call at brucecall@gmail.com

3. Results

3.1. Overview of surveys

All of the raw data files have been posted to the MNSU server and have also been backed up on the Belmont Lab server for long term archiving. In addition, we have posted to both servers the processed data as point and polygon feature data, raster grids, and TINs for each of the surveys. With permission from Minnesota DNR we have also published these data as publicly available on the data server Hydroshare (https://www.hydroshare.org/, Kelly et al., 2018). Table 2 shows all of the dates that we collected bathymetry data for this project as well as previous projects with data in the same reaches of the Minnesota River. Table 3 shows the average discharge at the nearest USGS gage for the survey dates.

Table 2. Bathymetry Survey Dates (mm/dd)

Site	Name	2013	2014	2015	2016
A	Granite Falls			6/28, 6/29	
B	New Ulm			6/23, 6/24	6/13, 6/15, 6/16, 6/17
C	Judson to Mankato	6/15, 6/16	6/9, 6/10, 6/11, 6/12, 6/13 6/17, 6/18, 6/20 6/21, 6/22		6/6, 6/9
D	Mankato	6/22	6/9, 6/10, 6/11, 6/12	6/10, 6/20	5/18, 5/19, 5/26, 5/27, 5/29
E	Mankato to 7 Mile Creek	6/10, 6/11, 6/13, 6/22	6/6, 6/8, 6/9, 6/10, 6/12		5/26, 5/27, 5/29
F	St. Peter			6/17	5/30, 6/8
G	Belle Plaine		7/1, 7/2	6/18, 6/19	6/24, 6/26
H	Jordan			6/18	6/21, 6/23, 6/24
I	Chaska			6/12, 6/13, 6/14	5/31, 6/1
J	Shakopee			6/14, 6/15, 6/16	6/1, 6/2, 6/3

Table 3. Mean Discharge (cfs) over Survey Dates

Site	Name	USGS Gage	2013	2014	2015	2016

A	Granite Falls	05311150			3,351	
B	New Ulm	05316580			4,961	1,944
C	Judson to Mankato	05325000 minus 05320000	10,742	23,753		6,338
D	Mankato	05325000	11,832	12,816	8,066	10,505
E	Mankato to 7 Mile Creek	05325000	9,726	13,639		9,658
F	St. Peter	05325000			7,608	10,940
G	Belle Plaine	05330000		41,847	7,614	17,997
H	Jordan	05330000			7,701	20,348
I	Chaska	05330000			8,181	14,843
J	Shakopee	05330000			8,052	14,725

Bathymetry varies considerably across the range of sites surveyed. We highlight several reaches below to illustrate key differences, but considerably more information can be extracted from the data themselves for targeted questions that emerge during the planning phase for the Invasive carp management plan.

3.2. Static bathymetry maps of key reaches

The Granite Falls reach (site A in Figure 1) exhibits considerable variability in bed topography, with recurring sequences of deeper pools and shallower zones (Figure 3). The topography tends to be more complex near meander bends, often with large scour pools found towards the beginning and outside bend of the meanders. In general, variability in bed topography tends to be on the order of 1-2 meters, but approached 5 meters in the vicinity of meander bends. The largest scour pool that can be observed in the bottom part of Figure 3 (immediately downstream from the 90 degree left turn in the river and approximately 1.5 km upstream from the downstream terminus of the survey, is associated with a structural feature that focuses flow into the middle of the channel. The structure may be a natural bedrock outcrop, piers from an old bridge or a structure to reduce bank erosion. However, most of this structure was not visible at the time of surveying so it was not possible to determine its extent or purpose. Similarly, a large pool occurs just above the downstream terminus of the survey. This feature appears to be forced by a natural bedrock outcrop on river left.

Figure 4 shows water depth at the time of surveying for the reach through downtown Mankato. This survey occurred in summer 2014, when flows were moderately high, which allowed us to survey the entire width of the channel. The bathymetry data show relatively deep pools along the outside edge of each bend in the channel, especially downstream from the highway 169 bridge, which crosses the Minnesota River toward the bottom left of the image. The inside portion of each of the bends tends to be relatively shallow water, consistent with the generally expected trend of hydraulics, scour and deposition of meander bends. While this would

theoretically suggest that the meander bends in this reach are unstable and have established the bed topography and hydraulics necessary for active meander migration, the channel through this reach has been heavily engineered and stabilized. Notably, however, there are no large scour pools associated with the bridge crossings, as we see at numerous other locations.
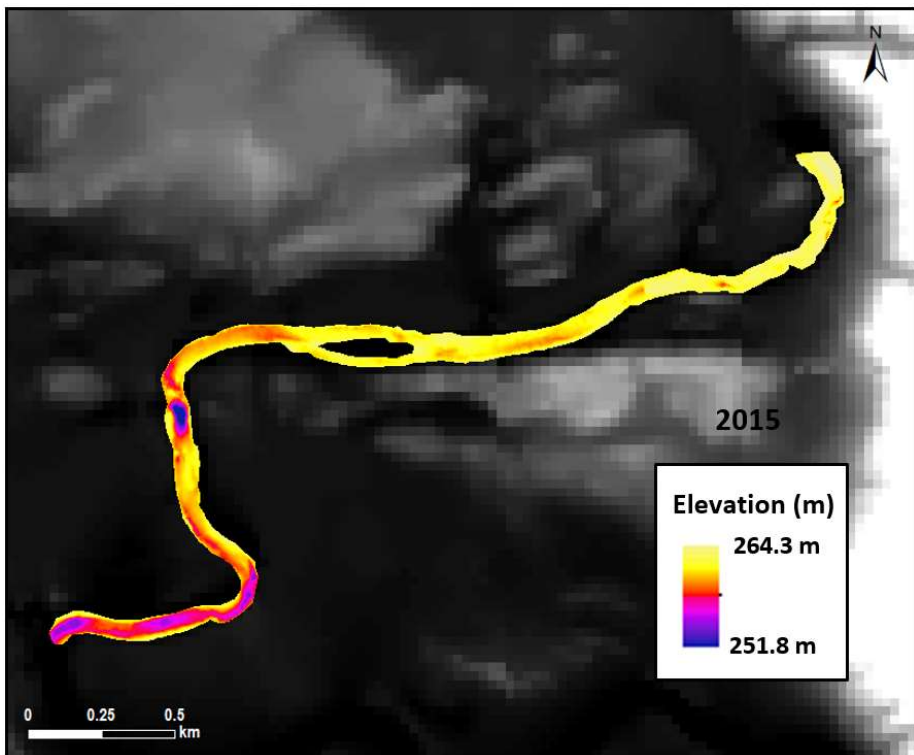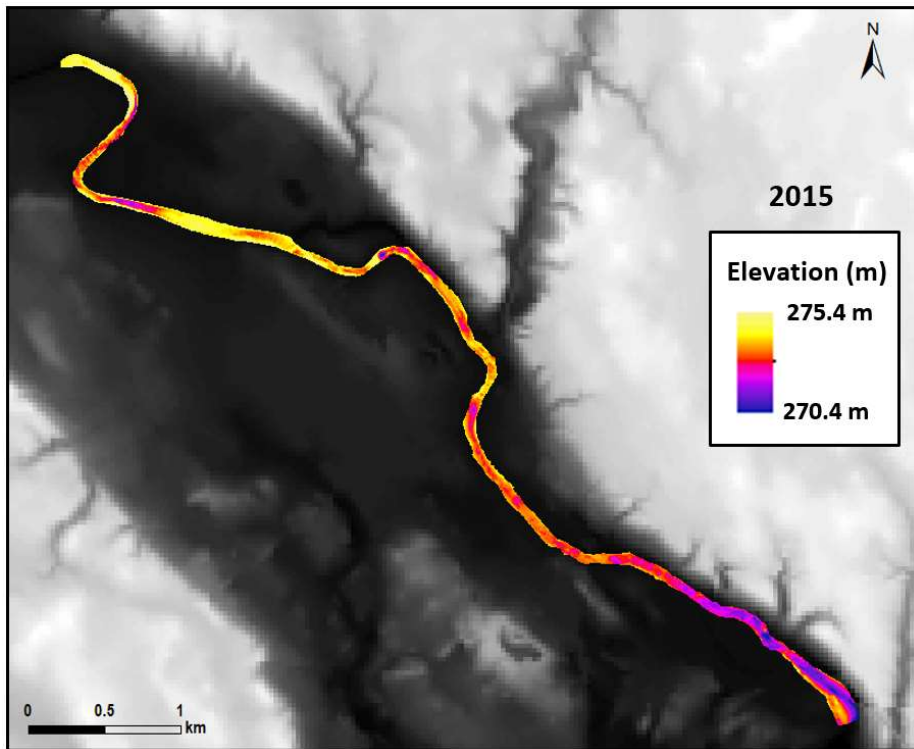
Figure 3. Channel bathymetry from 2015 at Granite Falls, Minnesota (site A in Figure 1 above). Top figure is upstream of the Granite Falls Dam. Bottom figure is downstream of the dam. Flow is from top left to bottom right in the top figure and top right to bottom left in the bottom figure.
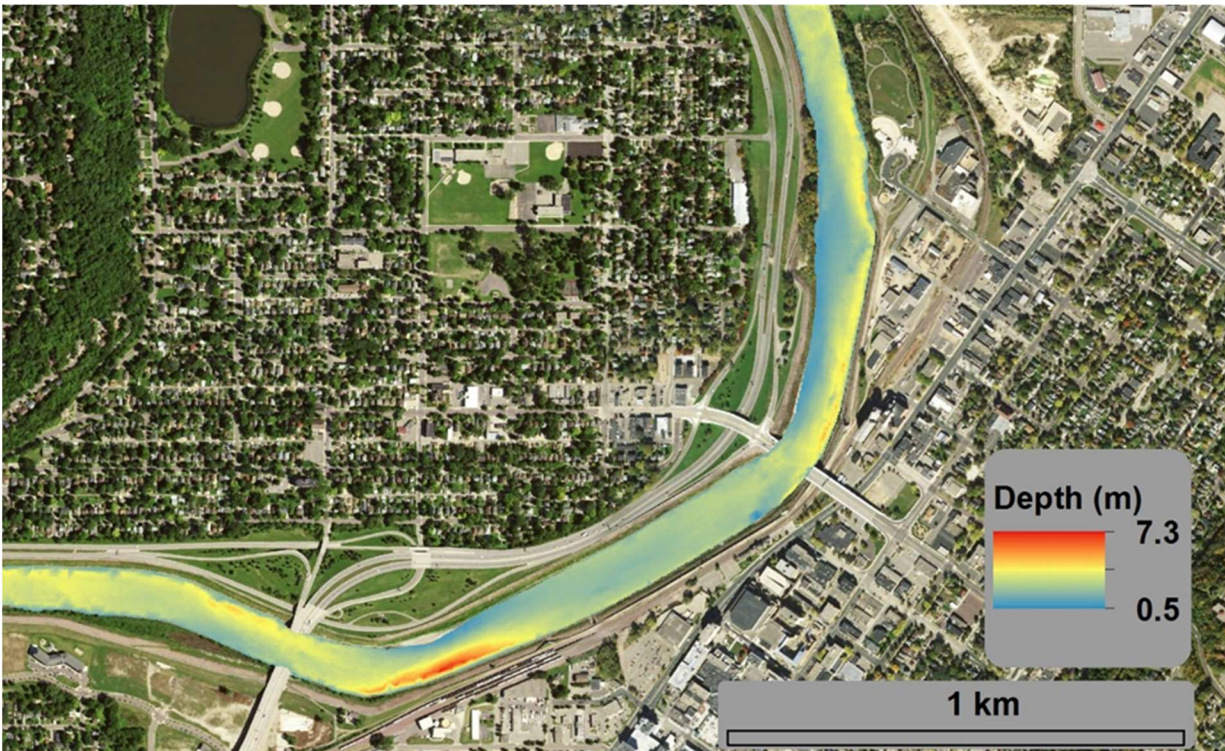
Figure 4. Water depth (meters) model from our bathymetric survey of the reach through downtown Mankato (site D in Figure 1) in 2014. Flow is from bottom left to top right.

Figure 5 shows bathymetry in the reach through St. Peter. The most striking feature in the reach is the long and deep scour pool that has formed in association with the highway 99 bridge, approximately 2 km from the upstream boundary of the survey (towards the bottom of the image). Water depth in this scour pool exceed 11.5 meters (nearly 38 feet). The scour is caused by the engineered constriction in the river, which inhibits the channel from widening, despite the substantial increase in flows that have occurred in the Minnesota River (Kelly et al., 2017; Call et al., 2017). The rest of the surveyed reach is characterized by relatively high variability in bed topography, with differences in bed elevation of 5 to 6 m across the channel. The deeper portion of the channel tends to shift around from left to right and is more narrowly focused in some parts of the channel than others. As observed in other locations, the variability in bed topography is highest in association with meander mends or engineered features, such as the bank stabilization features that are protecting highway 169 at the uppermost end of the survey reach, where the channel is adjacent to the road and stark differences in water depth can be observed.
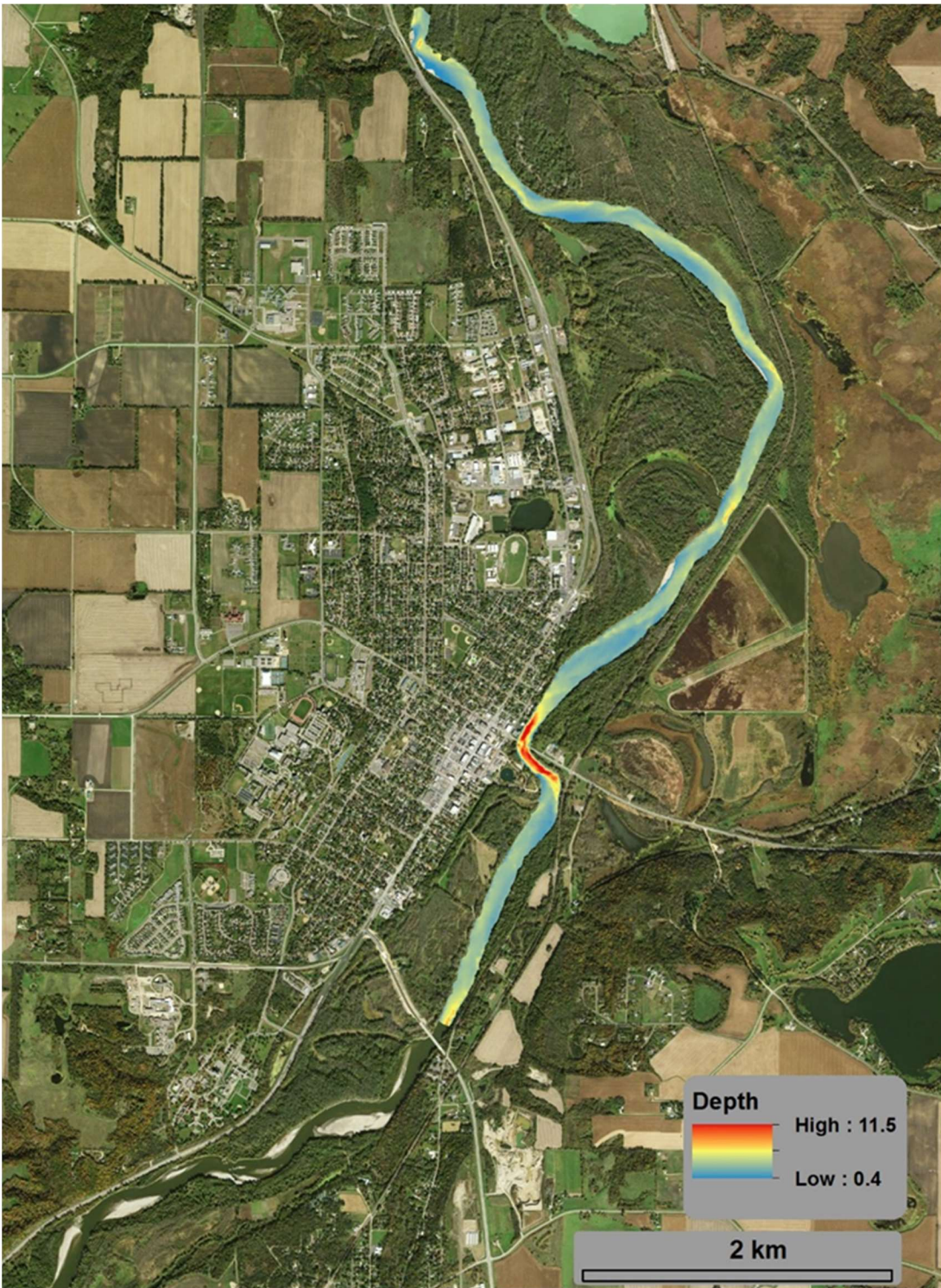
Figure 5. Water depth (meters) model from our bathymetric survey of the reach through downtown St. Peter (site F in Figure 1) in 2015. Flow is from bottom to top.

We surveyed the entire reach from Belle Plaine to Jordan, Minnsota twice and the lower half of that same reach a third time. This reach was of particular interest because it appears to be a critical transition from the highly dynamic, coarser grained, actively meandering reach with

relatively high sediment transport rates (Mankato to Jordan) to the relatively passive, finer grained, lower Minnesota River mainstem (Jordan to Fort Snelling). The bathymetry reflects this transition. Near Belle Plaine (lower left corner of lower image in Figure 6) the highway 25 bridge causes a considerable constriction on the river, causing a scour pool that is approximately 6 meters (20 feet) deeper than the average of the channel in this reach. Downsteam from that point most scour pools occur on the outside of meander bends, with many reaching similar depths of 10 to 12 meters (4 to 6 meters deeper than the reach average). A moderate amount of channel complexity is observed throughout out the reach, but again, mostly associated with meander bends. Another large scour pool is observed in the half kilometer upstream from highway 11, near Jordan.
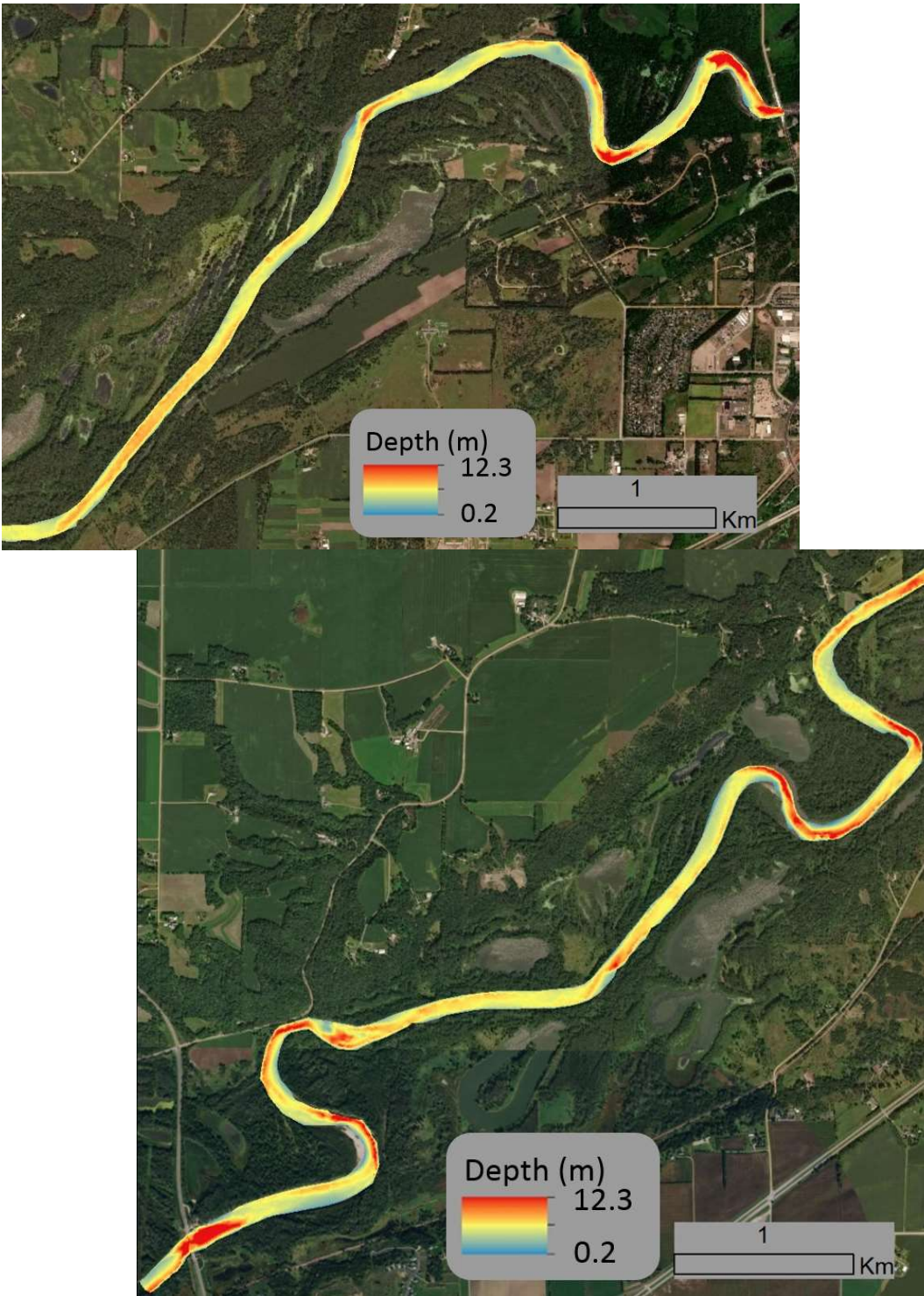
Figure 6. Water depth (meters) model from our 2015 bathymetric survey of the reach that runs from Belle Plaine (bottom left of bottom figure, site G in Figure 1) to Jordan (top right of top figure, site H in Figure 1). Flow is from left to right.

The behavior of the Minnesota River in the downstream most reaches, near Chaska and Shakopee, differs significantly from reaches upstream from Jordan, as discussed in earlier

sections of this report. In particular, the reaches between Mankato and Jordan have relatively higher meander migration rates, compared with the downstream reaches. Additionally, the reaches between Mankato and Jordan have increased considerably more in channel width over the past few decades compared to the downstream reaches, despite the fact that both have experienced a considerable increase in flow magnitude and duration. Following these trends, the character of the bathymetry also differs considerably (Figure 7). Specifically, the lowermost reaches of the river tend to have less topography in the channel bathymetry. Nearly all of the scour pools are associated with the outside of meander bends. Deeper pools tend to be on the bends with a smaller radius of curvature. Interestingly, there is considerably less variability in bed topography along the long, straight reaches.

Figure 7. Water depth (meters) model from our bathymetric survey of the reach through downtown Chaska and Shakopee (sites I and J in Figure 1) in 2015. Flow is from left to right.

3.2. Comparison of repeat bathymetry surveys to determine scour and deposition patterns

We surveyed most reaches multiple times in an effort to determine which portions of the river exhibit changes in channel bathymetry due to scour or deposition from year to year. This information is intended to provide a general sense for the magnitude, style, and locations of channel bathymetry change. Net erosion appears as incrementally darker shades of red, net deposition appears as incrementally darker shades of blue. While a complete uncertainty budget was not performed for these analyses (Wheaton et al., 2008; Passalacqua et al., 2015), uncertainty has been estimated as 25 cm, based on GPS quality during the surveys (typically < 5 cm vertical precision) and potential errors introduced in interpolation of the bed between survey transects. Any calculated change that falls within 25 cm of 0 is represented as white in the DEMs of difference (DoD).

The reach from Judson to Mankato (site C in Figure 1) exhibits moderate amounts of erosion and deposition in relatively predictable locations (Figure 8). The entire reach was surveyed in 2013 and 2014 and a portion of the reach was resurveyed in 2016, allowing for us to

make DoDs for two different time periods. The reach that was resurveyed in 2016 (top panel in Figure 8) is the meander bend approximately 2 km upstream from Land of Memories Park near Mankato, where highway 71 impinges on the Minnesota River. The greatest amounts of erosion occurred on the outside of meander bends between 2014 and 2016. Along the entire survey reach (bottom panel of Figure 8, considerable scour is observed near the apex of most meander bends, typically on the order of 1-2 meters. Deposition is observed elsewhere throughout the reach.

The reach through downtown Mankato (site D on Figure 1) exhibited primarily deposition between 2013 to 2016 (Figure 9). While there are patches of erosion observed on the outside of the bends immediately up and downstream from the highway 169 bridge (near the upstream terminus of the survey that spans 2014-2016), deposition pervades both sets of geomorphic change detection. Eliminating all areas that fall below the 25 cm minimum level of detection, we computed the spatially averaged net change in elevation of the bathymetry. We estimate 0.22 m of deposition between 2013 and 2014 and 0.07 m of deposition between 2014 and 2016. While these are both relatively small numbers, we have some confidence that they represent real aggradation of the channel. First and foremost, deposition is more likely to be underestimated in calculations of geomorphic change because deposition tends to occur as relatively thin, spatially extensive areas that are more likely to fall below the level of detection. In contrast, scour tends to occur as relatively deep (well above the minimum level of detection), but spatially limited patterns. Second, we know that large floods in 2010-2016 caused anomalously high sediment loads from the Greater Blue Earth River Basin (Schaffrath et al., 2015; Kelly and Belmont, 2018), just upstream from this reach on the Minnesota River. Coarse sand and gravel contributed from rapid and pervasive bluff erosion during those events would likely take years to decades to make its way through the tributary system and down through the reach of the mainstem Minnesota River in Mankato (Czuba and Foufoula, 2015; Gran and Czuba, 2017). It is unknown whether this reach will continue to aggrade in coming years or transport the pulse of sediment and degrade back to the elevation observed in 2013 or possibly lower. However, for the purpose of installing equipment for Invasive carp management, it would be important to continue to monitor this reach with high precision surveys in future years.
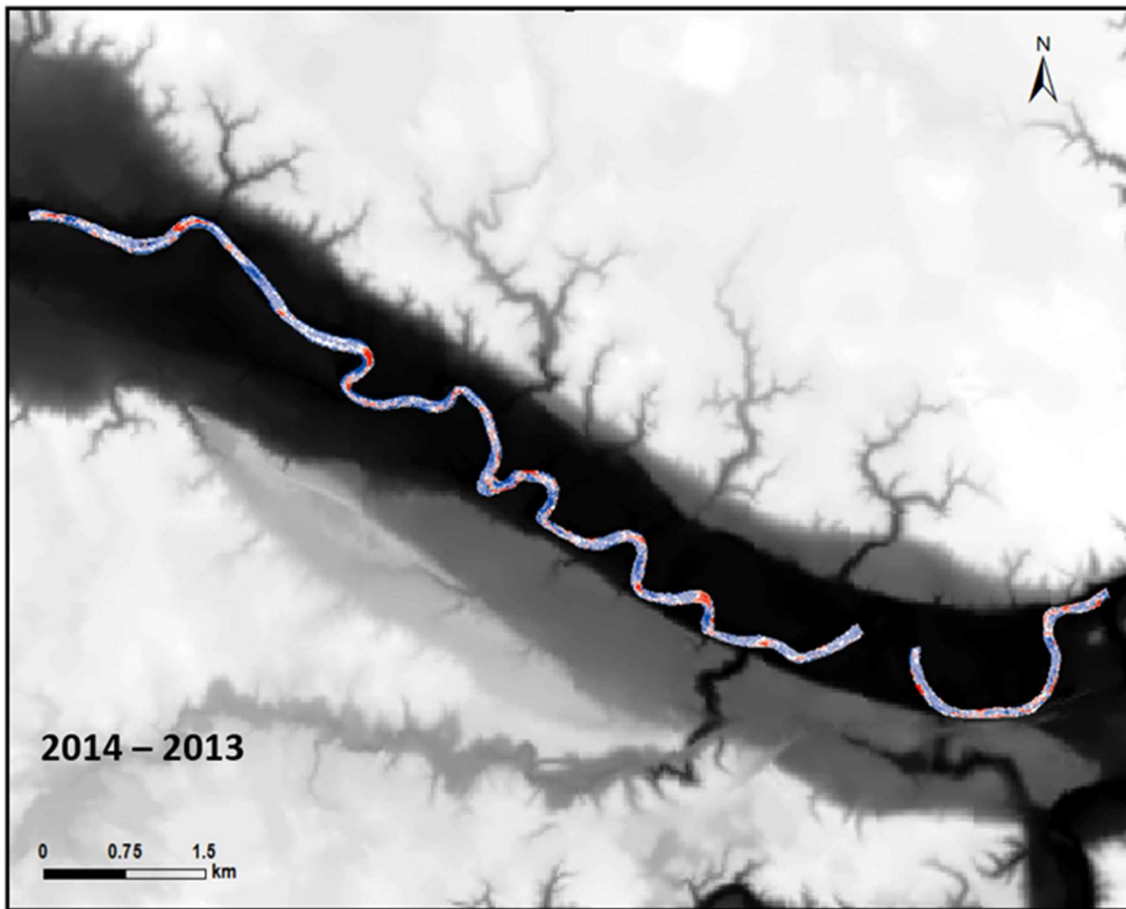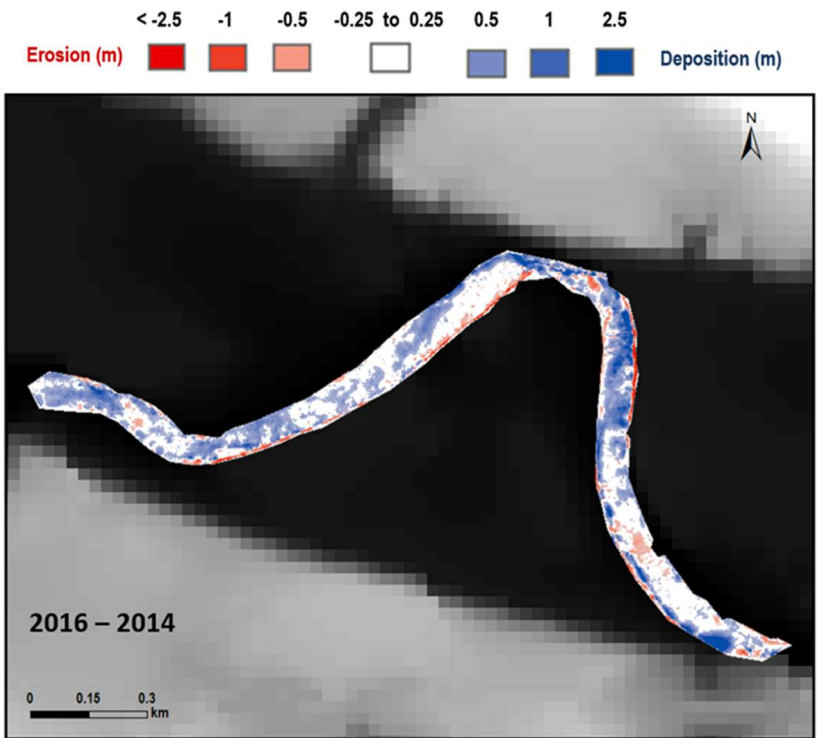
Figure 8. DEMs of difference (DoD) at site C, from Judson to Mankato. Top figure shows the DoD for the reach that was repeat surveyed in 2014 and 2016. Bottom figure shows the reach that was repeat surveyed in 2013 and 2014. Erosion between the surveys is indicated as red, deposition is blue, and change below a 25 cm minimum level of change is white. Flow is from left to right in both figures.
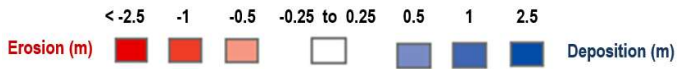
Figure 9. DEMs of difference at site D, Mankato, between 2013 and 2014 (top) and 2014 and 2016 (bottom). Erosion is red, deposition is blue, and change below a 25 cm minimum level of change is white.

The reach between Mankato and St. Peter (site E on Figure 1) also predominately shows deposition, but exhibits a highly variable pattern of erosion and deposition throughout the reach (Figure 10). Erosion primarily occurs along the channel margins and is more apparent in the 2014-2016 comparison (right panel of Figure 10) than in the 2013-2014 survey. But overall the net signal is aggradational as our calculations of spatially averaged net change in bed elevation indicates 0.21 m of deposition between 2013 and 2014 and 0.31 m of deposition between 2014 and 2016. These numbers are consistent with the amount of aggradation observed in the reach through downtown Mankato. The highly localized pattern of erosion and deposition translates to rather complex hydraulic structures in this reach, which is consistent with the rapid rates of meander migration and channel width adjustment.
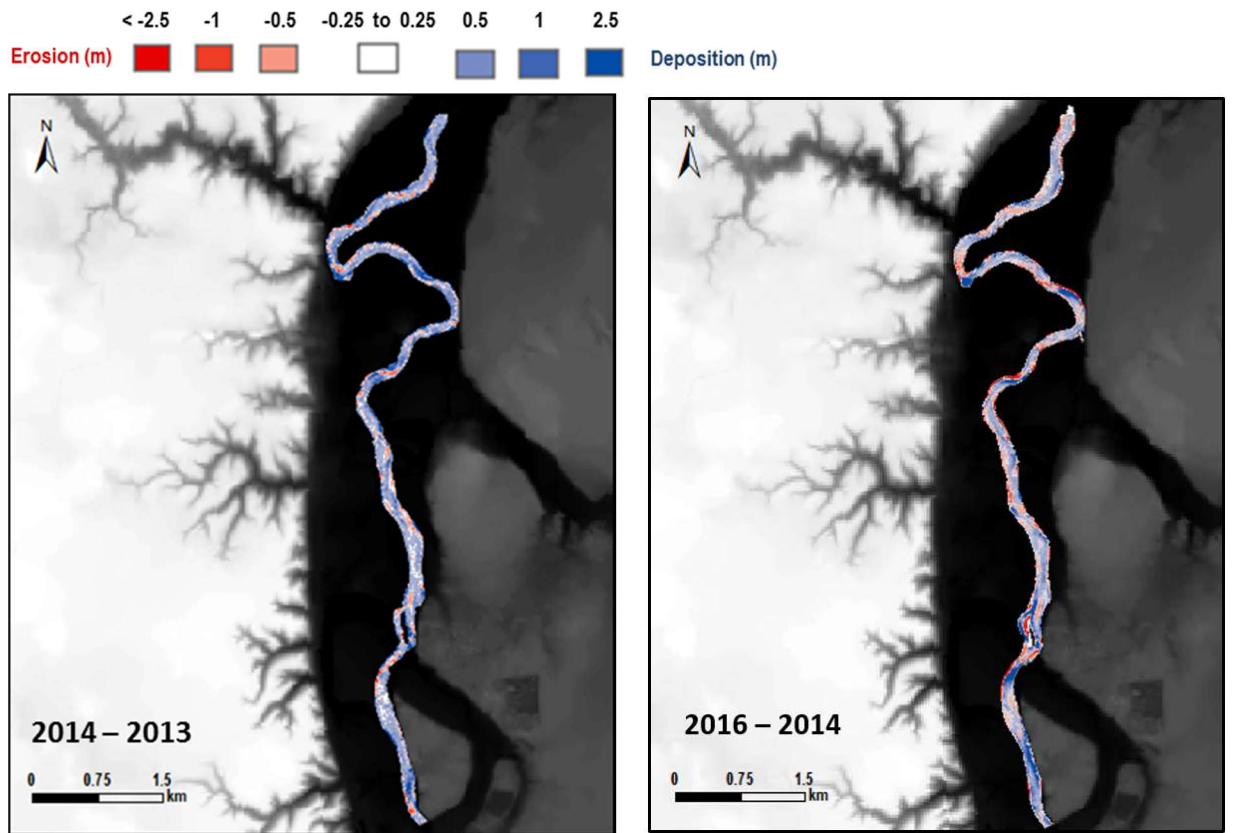
Figure 10. DEMs of difference at site E, Mankato to Seven Mile creek, between 2013 and 2014 (left) and 2014 and 2016 (right). Erosion is red, deposition is blue, and change below a 25 cm minimum level of change is white.

The reach near Belle Plain also exhibits rather stark patterns of erosion and deposition. We surveyed a deep scour pool (> 12 m deep) associated with the highway 25 bridge near Belle Plaine in 2014 (Figure 11). The DoDs from the two subsequent years show considerable infilling of that scour pool, with nearly 2.5 m of deposition between 2014-2015 and at least another 2.5 m of deposition from 2015-2016. This exemplifies the large shifts in bed elevation that can occur in areas with flow constrictions, which may pose challenges for maintaining Invasive carp management structures. Considerable scour is observed through the tight meander bends just downstream from highway 25 in 2014 and 2015, with additional erosion occurring on the outside of those meander bends between 2015-2016. However, the net signal from 2014-2016 is depositional. Our spatially averaged calculations of net bed elevation change indicate 0.01 m of erosion (essentially negligible net change) between 2014 and 2015 and 0.61 m of deposition between 2015 and 2016. We only conducted repeat bathymetry surveys on a limited extent of the reach near Jordan in 2015 and 2016. The DoD for the reach near Jordan indicates erosion on the outside of meander bends with spatially averaged net bed elevation change of 0.33 m of deposition between 2015 and 2016 (Figure 12).
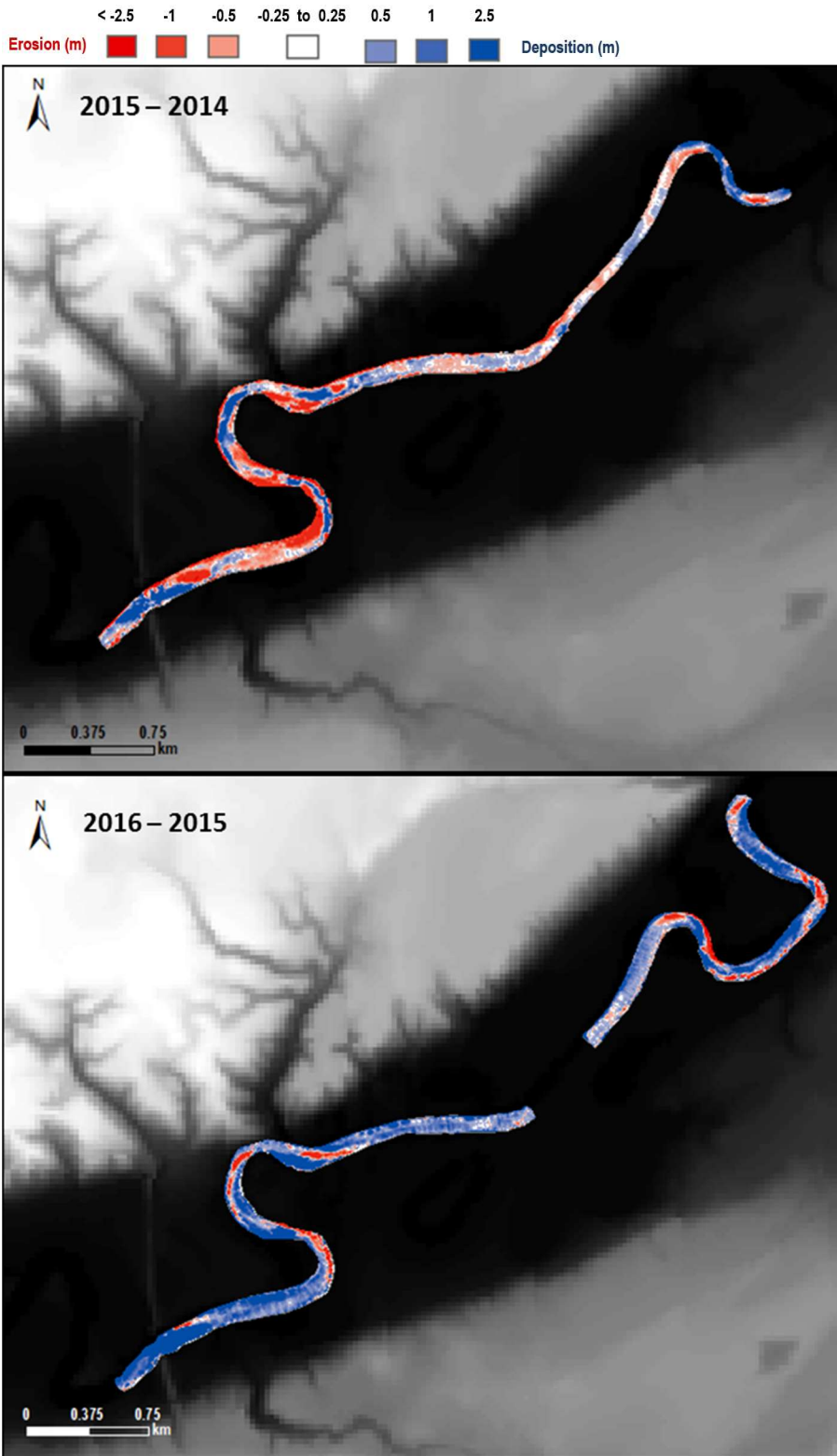
Figure 11. DEMs of difference at site G, Belle Plaine, between 2014 and 2015 (left) and 2015 and 2016 (right). Erosion is red, deposition is blue, and change below a 25 cm minimum level of change is white.
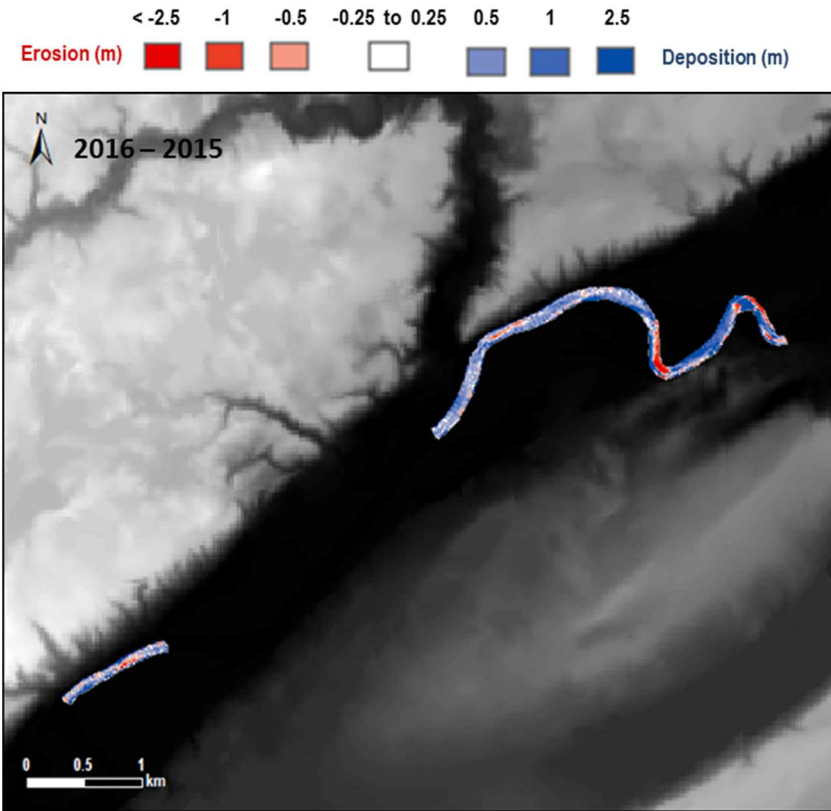
Figure 12. DEM of difference at site H, Jordan, between 2015 and 2016. Erosion is red, deposition is blue, and change below a 25 cm minimum level of change is white.

The reach between Chaska and Shakopee (site I in Figure 1) shows extensive erosion between 2015-2016, in contrast to all other upstream reaches (Figure 13). Notably, this reach has limited capacity for meander migration and has exhibited less capacity for channel width adjustment in response to the large increases in flows that have been observed on the mainstem Minnesota River. It is because of this limited capacity for width adjustment that the channel must instead adjust its depth to accommodate the increases in flow. Our calculations of spatially averaged net bed elevation change indicate 0.20 m of erosion between 2015 and 2016 for the reach between Chaska and Shakopee.
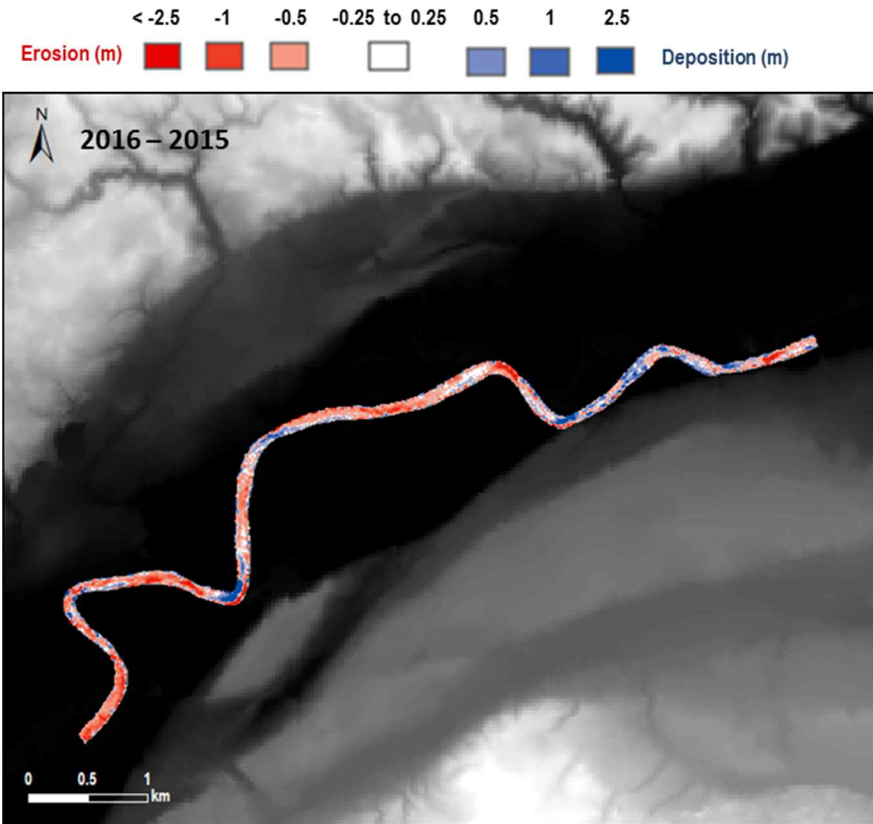
Figure 13. DEM of difference at site I, Chaska, between 2015 and 2016. Erosion is red, deposition is blue, and change below a 25 cm minimum level of change is white.

4. Conclusions

Variability in bed topography is caused by, and in turn causes, complex hydraulic structures in the river. Significant variability in bed topography, as is observed in the reaches from Mankato through Belle Plaine indicates strong topographic steering of flows, which results in transverse and helical flow patterns that scour banks and cause lateral migration of the channel. In contrast, the relatively modest amount of bed topography observed in the lower reaches through Chaska and Shakopee suggest that the channel is less dynamic in terms of meander migration and channel width adjustment, consistent with our observations in these lower reaches. The reaches from Mankato through Belle Plaine have a strong tendency to be depositional between 2014-2016, though limited areas of scour occurred, often associated with meander bends. Areas with flow constrictions are consistently highly dynamic across the wide range of environments surveyed for bathymetry, and especially at key locations in Granite Falls, St. Peter, and Belle Plaine. While more targeted questions can be explored with the vast data repository that was generated by this project, the results highlighted in this report demonstrate that the mainstem Minnesota River is a highly variable and dynamic river, with hotspots of change associated with flow constrictions and locations with large inputs of coarse sediment. Such locations pose considerable challenges to maintaining equipment for Invasive carp management.

5. References

Brasington, J., B.T. Rumsby, and R.A. McVey, 2000. Monitoring and Modelling Morphological Change in a Braided Gravel-Bed River Using High Resolution GPS-Based Survey. Earth Surface Processes and Landforms. 25:973-990.

Czuba, J.A. and Foufoula-Georgiou, E., 2015. Dynamic connectivity in a fluvial network for identifying hotspots of geomorphic change. Water Resources Research, 51(3), pp.1401-1421.

Gran, K.B. and Czuba, J.A., 2017. Sediment pulse evolution and the role of network structure. Geomorphology, 277, pp.17-30.

Kelly, S.A. and Belmont, P., 2018. High Resolution Monitoring of River Bluff Erosion Reveals Failure Mechanisms and Geomorphically Effective Flows. Water, 10(4), p.394.

Kelly, S., B. Call, S. Levine, P. Belmont, P. Larson, 2018. Minnesota River Bathymetry: 2013 – 2016 , HydroShare, http://dx.doi.org/10.4211/hs.6cd3728f69cb4cb39c6f11baac1734ec,

Kinzel, Paul J., Carl J. Legleiter, and Jonathan M. Nelson, 2012. Mapping River Bathymetry with a Small Footprint Green LiDAR: Applications and Challenges. Journal of the American Water Resources Association. 49(1): 183-204. DOI: 10.1111 ⁄jawr.12008

Legleiter, C.J., P.J. Kinzel, and B.T. Overstreet, 2011. Evaluating the Potential for Remote Bathymetric Mapping of a Turbid, Sand-Bedded River 1. Field Spectroscopy and Radiative Transfer Modeling. Water Resources Research. 47:W09531, doi:10.1029/2011WR010591.cd.

Legleiter, C.J. and P.C. Kyriakidis, 2008. Spatial Prediction of River Channel Topography by Kriging. Earth Surface Processes and Landforms. 33(6):841-867.

Legleiter, C.J., D.A. Roberts, and R.L. Lawrence, 2009. Spectrally Based Remote Sensing of River Bathymetry. Earth Surface Processes and Landforms. 34(8):1039-1059.

Leica Geosystems, 2015. Leica Viva GS 15 data sheet. Leica Geosystems 774100en - 04.17, 2 p. https://leica-geosystems.com//media/files/leicageosystems/products/datasheets/leica%20viva%20gs15%20ds%20en.ashx?la=en-us (Accessed June 15, 2018)

McKean, J.A., D. Nagel, D. Tonina, P. Bailey, C.W. Wright, C. Bohn, and A. Nayegandhi, 2009. Remote Sensing of Channels and Riparian Zones With a Narrow-Beam Aquatic-Terrestrial LIDAR. Remote Sensing 1(4):1065-1096.

Minnesota Department of Transportation, 2018. Minnesota Continuously Operating Reference Station Network. http://www.dot.state.mn.us/surveying/cors/ (Accessed June 15, 2018)

Mueller, D.S., and Wagner, C.R., 2009. Measuring discharge with acoustic Doppler current profilers from a moving boat: U.S. Geological Survey Techniques and Methods 3A–22, 72 p., available at http://pubs.water.usgs.gov/tm3a22 (Accessed June 15, 2018)

Passalacqua, P., Belmont, P., Staley, D.M., Simley, J.D., Arrowsmith, J.R., Bode, C.A., Crosby, C., DeLong, S.B., Glenn, N.F., Kelly, S.A. and Lague, D., 2015. Analyzing high resolution topography for advancing the understanding of mass and energy transfer through landscapes: A review. Earth-Science Reviews, 148, pp.174-193.

Schaffrath, K.R., Belmont, P. and Wheaton, J.M., 2015. Landscape-scale geomorphic change detection: Quantifying spatially variable uncertainty and circumventing legacy data issues. Geomorphology, 250, pp.334-348.

Teledyne RD Instruments, 2006. WinRiver II quick start guide: San Diego, Calif., Teledyne RD Instruments, P/N 957–6230–00, 3 p.

Teledyne RD Instruments, 2014. RiverRay ADCP Technical Specifications Data Sheet, Teledyne RD Instruments WR-1029, 2 p. http://www.teledynemarine.com/Lists/Downloads/riverray_datasheet_hr.pdf (Accessed June 15, 2018)

Wheaton, J.M., Darby, S.E. and Sear, D.A., 2008. The scope of uncertainties in river restoration. River restoration: Managing the uncertainty in restoring physical habitat, pp.21-40.

Task 2: Depth Gradient Profile and Stream Longitudinal Profile

Utilizing the bathymetry data, a depth gradient map of the entire river will be completed. This would entail a long profile of the channel depth along the entire reach of the river and also at specific cross-sections (narrow reaches) that may be suitable for barrier construction. The locations will be determined under the advisement of the DNR. In addition, a water surface longitudinal profile will be created for comparison.

Deliverables:
Depth gradient map of the Minnesota River.

Timeline:
January 2015 - December 2016

Results:

We extracted spatially averaged water depths from the four-beam point returns of each bathymetry survey. Figure 1 shows reach-average water depths (bars) for each of the surveys 2013-2016. The values at the top of each bar represent the average discharge value at the nearest USGS stream gage, averaged over the time period of the bathymetric survey (typically 1-3 days). The water depth data are also summarized in Table 1.

The rate of change in water depth as a function of discharge varies somewhat for the reaches surveyed. Figure 2 shows a scatter plot of discharge versus spatially averaged water depth (i.e., the same data shown in Figure 1), but re-organized by site. For Figure 2 we only included sites where we had at least 3 years of repeat surveys across a range of discharges. All four sites show increasing and non-linear trends in water depth as discharge increases. The non-linearity in these relations is primarily caused by two factors. First, the relationship between water velocity and friction at any given site is non-linear. Second, as discharge rises above bankfull, water spills out onto the floodplain, at which point water depth increases at a slower rate as a function of discharge. The reaches near Judson, Mankato and 7 Mile Creek exhibit a relatively similar pattern. But the reach near Belle Plaine exhibits a much steeper relationship between discharge and water depth.
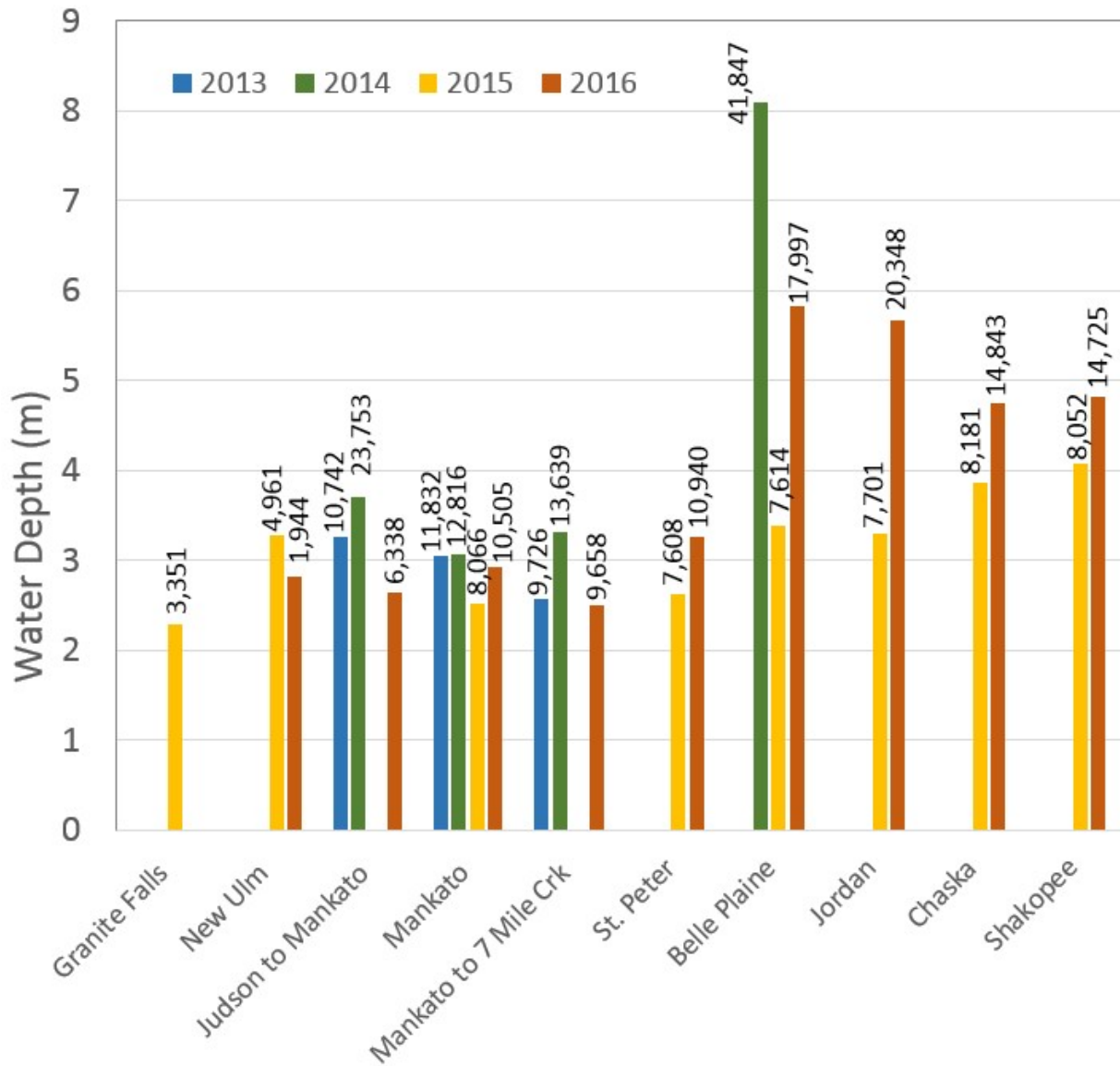
Figure 1. Illustration of spatially averaged water depths (bars) for each of the surveys conducted from 2013 to 2016. Numbers at the top of bars indicate discharge from the nearest stream gage, averaged over the survey.

Table 1. Spatially averaged water depth (meters) for each bathymetry survey conducted

Site	Name	2013	2014	2015	2016
A	Granite Falls			2.29	
B	New Ulm			3.29	2.83
C	Judson to Mankato	3.27	3.70		2.64
D	Mankato	3.06	3.07	2.53	2.93
E	Mankato to 7 Mile Crk	2.57	3.31		2.50
F	St. Peter			2.63	3.27
G	Belle Plaine		8.09	3.39	5.83
H	Jordan			3.30	5.67
I	Chaska			3.86	4.76
J	Shakopee			4.08	4.82
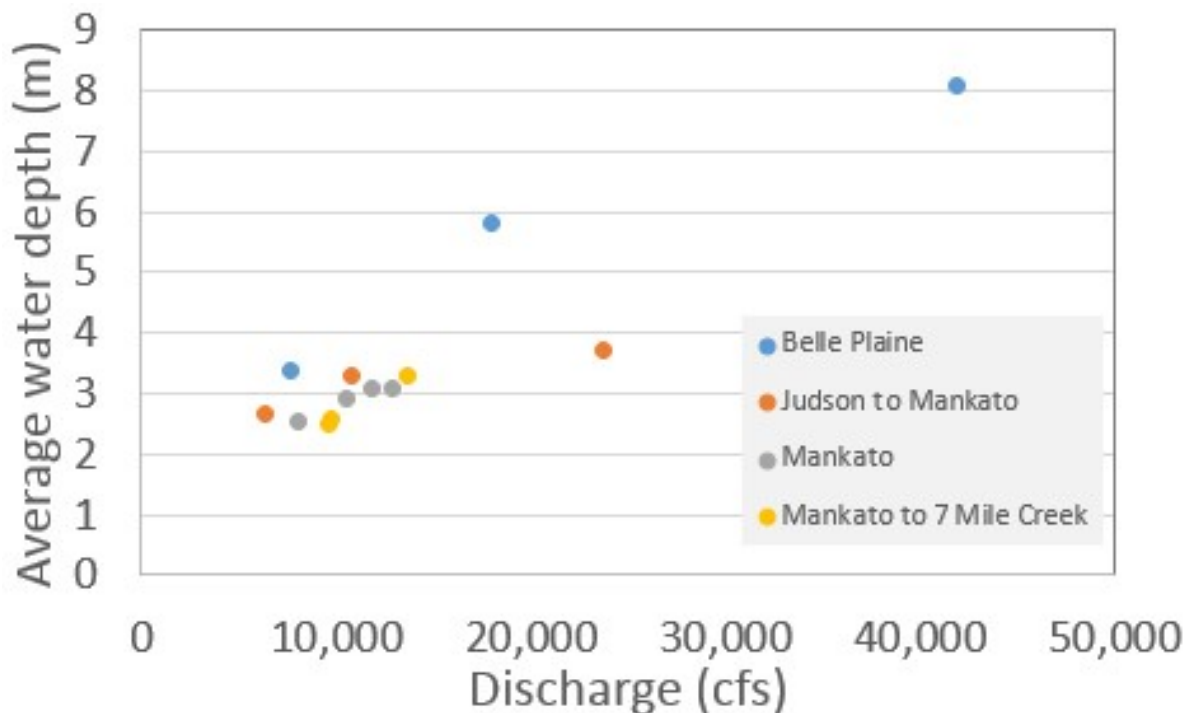
Figure 2. Relationship between discharge and spatially averaged water depth for the four reaches for which we have at least three bathymetric surveys between 2013-2016.

Task 3: Substrate Map

A substrate map would be created so we have detailed descriptions of the underlying materials at places that may possibly be proposed for these barriers. These data are also needed for the hydraulic modeling to make predictions of flood inundation. There are several ways the substrate map could be done. The first technique could be done in late summer/fall when flows are low. The mapping would be a combination of field work and high resolution air photograph

interpretation (from a drone, NAIP, or high-res satellite photos). The second technique would require use of the Flying Eyeball underwater microscope developed by the USGS. The underwater microscope consists of a waterproof video camera with a magnifying lens mounted in a heavy steel ball. A ring of led lights provide illumination. A video recorder stores the images for analysis later on a computer. The USGS developed special software measures sand grain size from the images.

Deliverables:
A substrate map of the underlying materials at places that may possibly be proposed for barriers.

Timeline:
January 2015 - December 2016

RESULTS: *Substrate composition*

Author(s): Sara A. Kelly[1], Patrick Belmont[1]

[1]Watershed Sciences - Utah State University

Corresponding Author:
Patrick Belmont – Email: patrick.belmont@usu.edu; Phone: 4357973794

GIS Data Available (links require username/password: landforms/rock):
https://geo.mnsu.edu/geo/DNR-InvasiveCarp/Patrick-Sara-Bathymetry/Grainsize/

1. Introduction

Fluvial sediments span a wide range of grain sizes, which tend to be well-sorted into discrete deposits within the river channel and floodplain system. The range of grain sizes spans clays on the order of 1 µm (0.001 mm) up to very large boulders that are several meters in diameter. Each of these grain sizes plays a role in forming ecological habitat. The ability, or inability, of the river to transport the amount and range of grain sizes delivered from upstream ultimately determines whether the channel aggrades or degrades, which governs the overall morphology and dynamics of the river channel. Bedrock substrate, rather than alluvial sediments, dominates the benthic environment of some rivers, which has entirely other implications for fluvial habitat conditions and dynamics.

We performed a targeted analysis of river substrate along the mainstem Minnesota River. Data collected as part of this analysis provides useful information regarding the grain sizes present in different portions of the river. This information can in turn be used to inform our understanding of habitat conditions, delivery, transport and storage of different grain sizes throughout the system, and factors influencing channel change in different parts of the river network. In addition, knowing the composition of the substrate would be useful for any engineering solutions that need to be installed in the river for management of Invasive carp.

2. Methods

We selected sampling locations to cover the range of fluvial environments encountered along the mid- to lower mainstem Minnesota River (Figure 1). River systems have a tendency to sort different sediments into different landforms, including the channel bed, alluvial bars, and floodplain. Thus, we sampled the channel bed (as close to the thalweg as possible) and bars separately. We took multiple samples from the bars when multiple distinct facies were present.
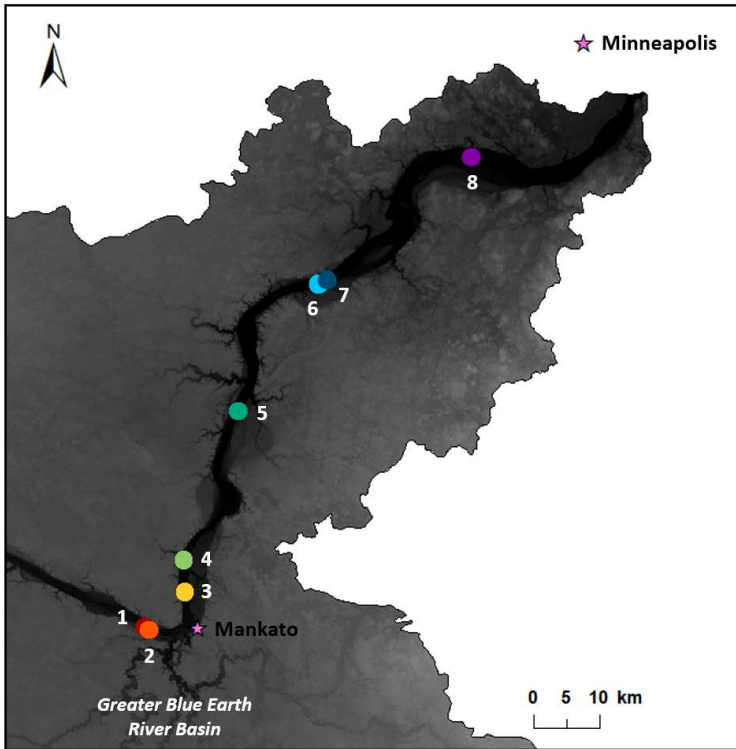
Figure 1. Grain size sampling sites along the lower Minnesota River, numbered from upstream to downstream. Sites 1 and 2 are located upstream of the Blue Earth River confluence, near Minneopa State Park. Sites 3 and 4 are located near Lime Township and Seven Mile Creek respectively. Sites 5 – 8 were sampled near the towns of Le Sueur, Belle Plaine, and Shakopee.

Fluvial systems often become 'armored', meaning that the layer at the surface becomes depleted in smaller grain sizes, due to selective transport, and is therefore coarser grained than undisturbed deposits (which underlay the armored layer) and the sediment load in transport during large events (which is generally consistent with the underlaying deposits (Dietrich et al., 1989). We collected armor and subsurface samples where appropriate. We used a shovel to collect the sample and a gallon ziplock bag for each sample. The quantity of each sample was determined such that the largest grain comprised no more than 2% of the total sample (Church et al.,1987).

We oven dried the samples, then we sieved the samples using a rotap device and weighed them in the following size classes (in millimeters): 0.025, 0.063, 0.09, 0.125, 0.18, 0.25, 0.351, 0.5, 0.71, 1, 1.4, 2, 2.8, 4, 5.6, 8, 12.5, 19, 25, 38.1, 50, 63, 75, 90, 128. We followed standard USGS protocols for sieving samples (Guy, 1969). Samples were sieved in their entirety, to avoid biases that may be introduced in the process of reducing or splitting the samples into smaller quantities. Samples were sieved on the rotap for a minimum of 45 minutes each to ensure thorough sorting.

Data are presented in linear units representing the sieve diameter, or the diameter opening of the sieve through which the given particle will just pass. Generally, grain size data are presented in base-2 log units (i.e., a geometric scale) in recognition of the fact that it spans many orders of magnitude. For example, grains that are 1 mm versus 2 mm in diameter (an entire base-2 log cycle) are much more different from one another than two grains that are 64 mm vs 65 mm, despite the fact that both only differ in diameter by 1 mm. Thus, we present the data on base-2 log scale axes.

3. Results and Discussion

The Minnesota River is predominately a sand bed river, with sand defined as grain sizes between 0.0625 mm to 2 mm. Only a very small fraction of the grain size distributions collected at any of our sample sites fall outside this range (Figure 2). The general trend in cumulative grain size distributions of the channel bed samples (solid lines) is a considerable increase in grain size from the sites near Minneopa State Park (sites 1 and 2) to sites that are immediately downstream from the confluence with the Greater Blue Earth River (sites 3, 4 and 5). This increase in the caliber of grains is most apparent immediately downstream from Mankato at our sampling site near Lime Township and progressively diminishes in the downstream direction at sites near Seven Mile Creek and the city of Le Sueur. The grain size distributions continue to diminish further in the downstream direction in Belle Plaine (sites 6 and 7) and Shakopee (site 8). The sample from Lime Township is the only sample that is dominated by anything other than sand, with a median grain size of approximately 3 mm (technically referred to as very fine gravel) and approximately 20% of the distribution comprised of medium gravel (8 to 16 mm).
Samples from bars (dashed lines) are generally finer-grained than samples from the channel thalweg (solid lines) as indicated by the dashed lines typically falling to the left of the solid lines for most samples, at any given percentile in the cumulative grain size distribution. A notable exception to this trend is Site 4, on the Minnesota River near the confluence with Seven Mile Creek. In this case, bars are considerably coarser than the thalweg samples.
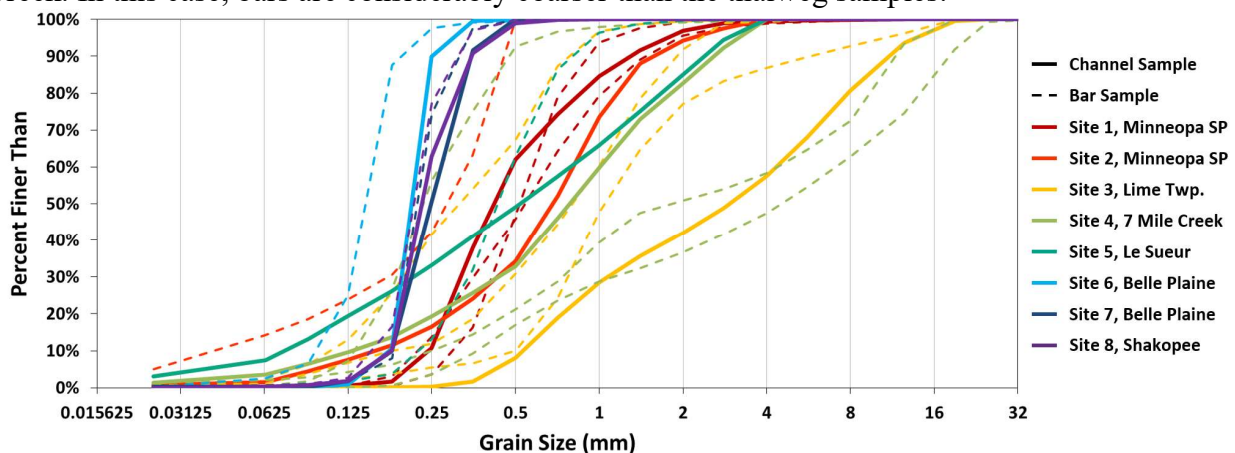
Figure 2. Cumulative percent finer than grain size distributions for 8 sites along the lower Minnesota River. All samples were collected from the subsurface (below the armor layer) during low flow conditions. Channel samples were collected from as close to the thalweg as was wadeable. Bar samples were collected from distinct facies, where available. In most cases, upstream of the Greater Blue Earth River confluence and downstream of 7 Mile Creek, bars contained only one or two facies.

Due to the complexity in working computationally with entire distributions of grain sizes, the distributions are often represented by particular characteristic percentiles of the distribution. While many different percentiles are used in the literature, the 16th, 50th (median) and 84th percentiles (D16, D50 and D84, respectively) are most commonly used to represent the distribution. Figure 3 displays those three characteristic percentiles for each of the channel bed samples presented in Figure 2. This representation of the data confirms the significant increase in the median (D50) and upper end of the grain size distribution (D84) and an overall increase in variance of the distributions as the three characteristic grain sizes are more spread apart for all three of those samples. Sites in Belle Plain and Shakopee exhibit a very narrow range of grain sizes both within and among samples.
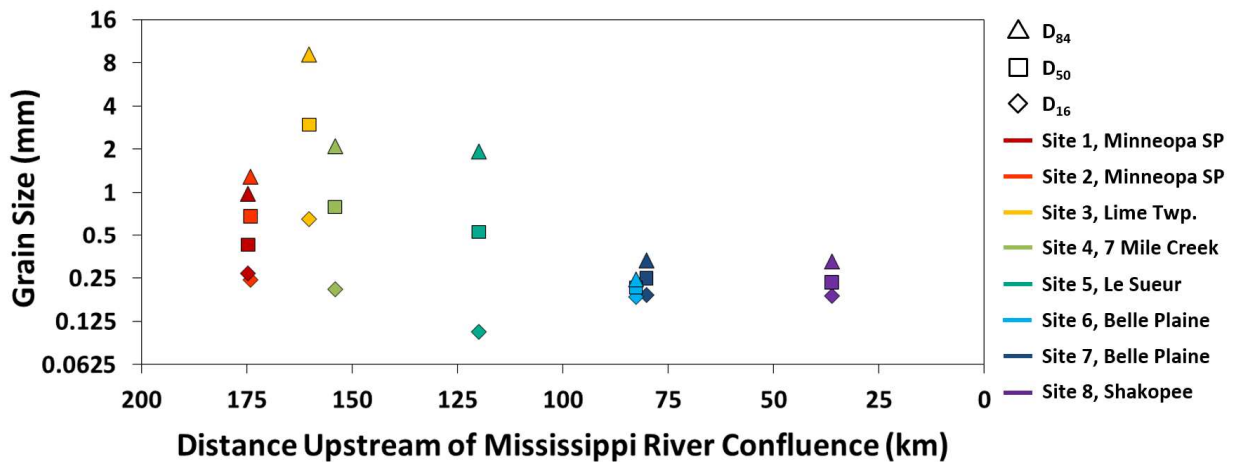
Figure 3. Channel subsurface D16, D50, and D84 grain sizes for 8 sites along the lower Minnesota River. Bed grain size variability increases between Minneopa State Park (SP) and Lime Township, where the Greater Blue Earth River joins the Minnesota River. Grain size variability is lowest between Belle Plaine and Shakopee.

4. Conclusion

Grain size data analyzed in this report illustrate several key points for managing Invasive carp. First and foremost, the data confirm that the Minnesota River is predominately a sand-bed river. The low gradient, aggradational setting of the mainstem Minnesota River ensures that this characteristic is unlikely to change in any substantive way for the foreseeable future, regardless of what changes in flow, sediment supply, and engineering along the channel and floodplain occur. The exception to this general observation is the reach immediately downstream from Mankato, after the confluence of the Greater Blue Earth River, which contributes a significant gravel load to the mainstem Minnesota River. The gravel is not transported far downstream in the Minnesota River. We see very little gravel or even coarse sand downstream from the city of Le Sueur and no gravel whatsoever as far downstream as Belle Plaine. The inference that coarser material is stored within the mainstem Minnesota River channel is consistent with the observations of Wilcock (2009) and our conclusion that the reach between Mankato and Jordan is highly dynamic due to the fact that sediment loading from major tributaries greatly exceeds transport capacity. The fine-grained substrate that dominates the mainstem Minnesota River

presents a challenge for implementing Invasive carp management engineering solutions because the sediments are mobile under a wide range of flows and therefore the bed is highly dynamic, as documented in our river bathymetry geomorphic change detection.

5. References

Church, M., McLean, D.G., and Wolcott, J.F. (1987) River bed gravels: sampling and analysis. In Sediment Transport in Gravel Bed Rivers (Eds C.R. Thorne, J.C. Bathurst and R.D. Hey), John Wiley & Sons Ltd, Chichester.

Dietrich, W.E., Kirchner, J.W., Ikeda, H. and Iseya, F., 1989. Sediment supply and the development of the coarse surface layer in gravel-bedded rivers. Nature, 340(6230), p.21Guy, H., 1969. Laboratory theory and methods for sediment analysis. Techniques of Water-Resources Investigations of the United States Geological Survey. Chapter C1 Laboratory Theory and Methods for Sediment Analysis. 64 pp.

Wilcock, P. R., 2009. Identifying sediment sources in the Minnesota River Basin, in Minnesota River Sediment Colloquium Report, Minnesota Pollution Control Agency, pp. 1–18, St. Paul, Minn. [Available at https://www.pca.state.mn.us/sites/default/files/wq-b3-43.pdf, accessed online June 15, 2018]

Task 4: Case-site Velocity Profile

Under the advisement of DNR officials, determining certain locations that would be potential site locations for fish barriers will then allow for case-site specific channel velocity cross sections. The project would create case-site specific channel velocities. Utilizing HEC-RAS or some similar model, we would create a channel velocity profile of the sites. Knowing the bathymetry and profile of the river, we can determine the velocity profiles and this will aid in determining the effectiveness of "bubble-barriers."

Deliverables:

Gradient Map of the velocity profile at case site specific locations in the Minnesota River

Timeline:
January 2015 - December 2016

RESULTS: Case-site Velocity Mapping

Author(s): Patrick Belmont[1], Adam Fisher[1], Eden Furtak-Cole[2], Bruce Call[1], Shayler Levine[1],

[1]Watershed Sciences - Utah State University
[2]Mathematics and Statistics - Utah State University

Corresponding Author:
Patrick Belmont – Email: patrick.belmont@usu.edu; Phone: 4357973794

Data Available (links require username/password: landforms/rock):

Raw migration data: https://geo.mnsu.edu/geo/DNR-InvasiveCarp/Devon-PlanformChange/ForDNR/All_raw_migration_data/

1. Introduction

We measured velocity profiles of the Minnesota River in three reaches to demonstrate the variability in water velocities within and among sites. Additional water velocity transects could be extracted from the raw bathymetry data posted on the server. We selected a meander bend near Belle Plaine for our first set of velocity profiles to demonstrate the variability in velocities associated with the asymmetry in bed topography through a meander bend and associated helical flow patterns (Figure 1). A total of 23 velocity transects were measured over the course of two days in this meander bend. The second set of six velocity profiles were measured in the reach between Mankato and St. Peter, Minnesota (Figure 2). And the third set of eight velocity profiles was measured in the reach through downtown Mankato (Figure 3).
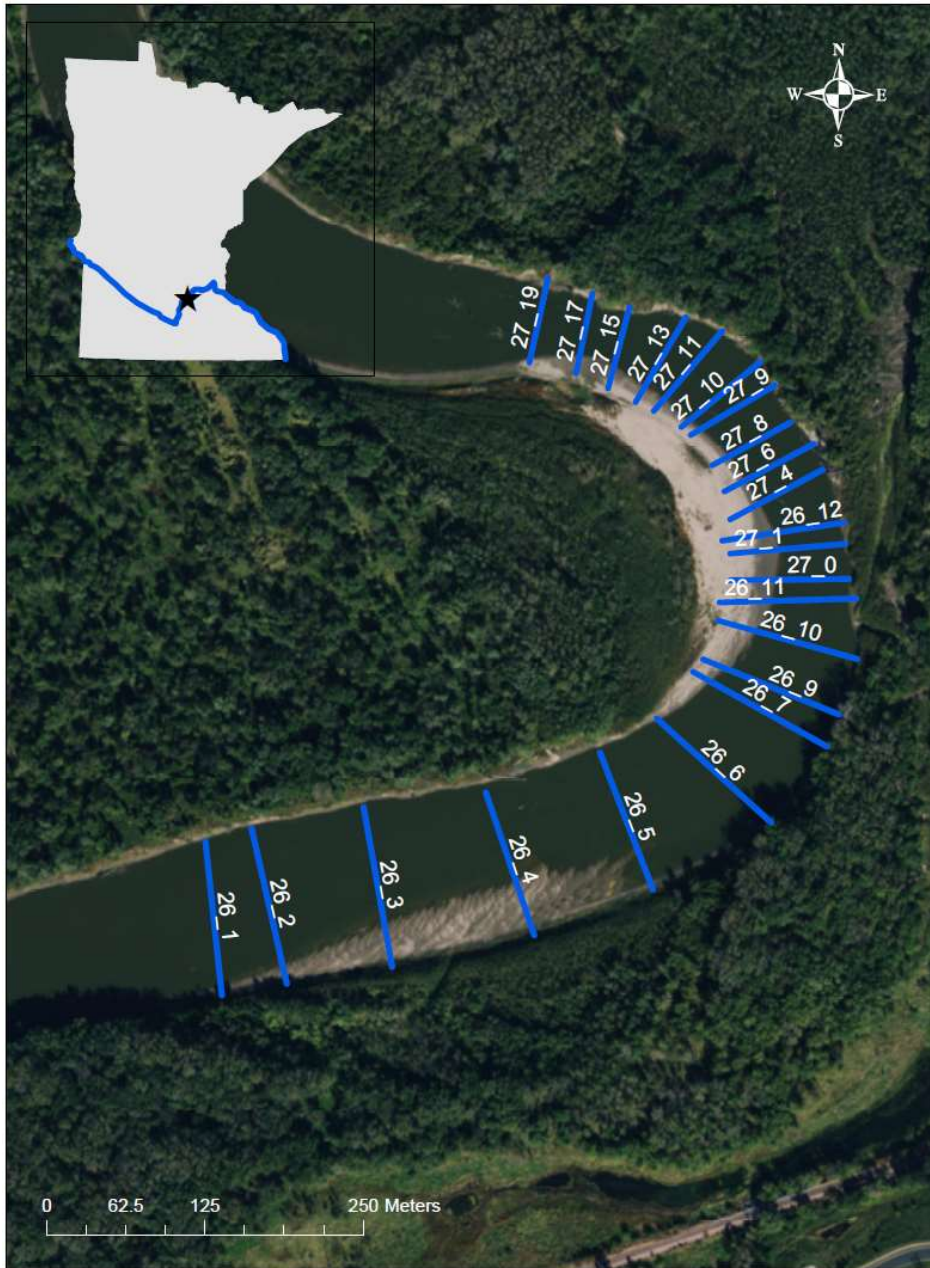
Figure 1. Blue lines show transects that were surveyed for velocity profiles, near Belle Plaine, Minnesota. Numbers on transects are referenced in the captions for velocity profile figures below.

385

Figure 2. Orange lines show transects that were surveyed for velocity profiles for the reach between Mankato and St. Peter, Minnesota. Numbers on transects are referenced in the captions for velocity profile figures below.

Figure 3. Orange lines show transects that were surveyed for velocity profiles for the reach through downtown Mankato, Minnesota. Numbers on transects are referenced in the captions for velocity profile figures below.

2. Methods

Water velocity profiles were measured using the same equipment and instrumentation described in the bathymetry mapping section of this report. Briefly, we used a Teledyne RD Instruments River Ray Acoustic Doppler Current Profiler coupled with a real-time-kinematic GPS system that was linked to the Minnesota Continuous Operating Reference System (MN CORS, MN Department of Transportation, 2018). The River Ray has four phased-array beams pulsing an acoustic signal at 600 kHz with velocity profiling accuracy of approximately ± 0.002 m/s and depth measurement accuracy of ± 1% (Teledyne RDI, 2014). Data were transmitted continuously to a laptop via Bluetooth (from ADCP) and wired connection (from GPS) and assimilated using WinRiver II software (Teledyne RDI, 2006). All of this instrumentation was rigged on a 16' cataraft with an outboard motor.

The primary difference between methods for bathymetry mapping and velocity transect profiling is that we deliberately controlled start and end points of each survey and as a result, the data can be processed as a coherent transect using WinRiver II software. We surveyed the velocity transects from bank to bank where possible, but were limited in some cases by the water depth, or in a few cases, by woody debris near the bank. All post-processing was completed using WinRiver II software.

3. Results and Discussion

All transects are available on the data link listed at the beginning of this section. We review only a select number of transects to demonstrate trends in downstream and cross-channel water velocities.

3.1. Velocity Transects near Belle Plaine

Discharge at the gage nearest the Belle Plain transects (Jordan Minnesota, USGS gage 05330000) averaged approximately 9,700 cfs during the survey on May 26 and 10,600 cfs during the survey on May 27. Transects for this reach are named with respect to the survey date (May 26 or 27) followed by the transect number.

Transect 26_01 (Figure 4) is relatively symmetrical box-shape with the flow depth only varying from approximately 4 to 4.5 meters deep. Water velocities are most rapid and are fairly uniform, averaging approximately 1.1 m/s throughout the transect, with somewhat slower velocities near either bank, averaging closer to 0.6 m/s. Approximately 200 m downstream at transect 26_04 (Figure 5), there is a pronounced sand bar on river right. The asymmetry of the cross section and shallower water depths on the right side of the transect cause considerably slower flow (0.2 to 0.3 m/s) on the right margin of the channel. Water velocities are approximately 1.0 m/s on the left side of the channel, which is deeper than upstream cross sections (up to 5 m) in order to compensate for the shallower, slower flow on river right. Just another 200 m downstream at transect 26_6 (Figure 6) the fast flowing thalweg remains on the left side of the channel, just as the channel enters the leftward turning meander bend. Slower water velocities on the right side of the channel at transect 26_6 indicated the presence of a slow

flow eddy that formed behind the sand bar on river right, the tail end of which can be seen as the small topographic bump between 10-30 m from the right edge of the transect. At transect 26_11 (Figure 7) the sand bar on river left (i.e., the inside of the meander bend) causes a stark asymmetry of the channel. As a result, high flow velocities shift to the right side of the channel and the channel has deepened to nearly 10 m on the outside bend due to the helical flow patterns that force the fast flowing water coming into the bend downward, causing bed scour. The asymmetry persists through transect 27_4 (Figure 8), located just past the apex of the bend. But the thalweg has shifted slightly towards the center of the channel with velocities exceeding 1.5 m/s in places. By transect 27_9 (Figure 9) the thalweg remains in the middle of the channel, with a narrow band of water exceeding 1.5 m/s. A relatively low velocity zone occurs on river left, associated with the sand bar and an eddy has formed on river right, where velocities less than 0.2 m/s are observed. The channel expands abruptly by transect 27_10 (Figure 10) and as a result a much more developed eddy forms on the right side of the channel with velocities approaching zero. These low velocity zones have a tendency to cause deposition, or channel narrowing. The average thalweg velocity remains approximately 1.0 m/s. By transect 27_15 (Figure 11) the channel narrows again and water velocities on the outside bend again exceed 1.5 m/s in places, which ultimately causes scour of the bank, or channel widening. The stark differences in water velocities along the right side of the channel illustrate the physical mechanisms that maintain a relatively consistent channel width over short length-scales in river channels and serve as an example of how the hydraulics respond to constrictions and expansions in the channel, which could be imposed by natural or engineered structures. By transect 27_17 (Figure 12), the channel has become more symmetrical as it comes out of the meander bend, but maintains a V-shape with a maximum depth of nearly 10 m. The thalweg remains on the right half of the channel, but has moved away from the bank.

3.2. Velocity Transects between Mankato and Seven Mile Creek

We collected 6 velocity transects in the reach between Mankato and 7 Mile Creek on July 4, 2014. Discharge at the USGS gage in Mankato (USGS gage 05325000) averaged approximately 26,500 cfs, allowing us to observe water velocities at a relatively high flow. The most downstream transect (2014_1, Figure 13) is relatively asymmetrical with a large bar on river right. Water depths reach nearly 8 m in the thalweg on river left with an average velocity of approximately 1.8 m/s and exceeding 2.0 m/s in localized areas. On the shallow right side of the channel water velocities remain around 0.9 to 1.2 m/s. Just slightly upstream at transect 2014_2 (Figure 14) a constriction immediately upstream on river left causes a pronounced eddy, observed as a low velocity zone near the left edge of the channel. Several other smaller eddy features can be observed in the channel cross section as the channel oscillates from very fast (1.8 to 2.0 m/s) to moderately fast (1.0 to 1.3 m/s) flowing water through much of the rest of the transect. At transect 2014_3 the effects of the constriction can be observed with uniformly rapid water velocities across the left three-quarters of the transect, with velocity averaging 1.9 m/s and exceeding 2.4 m/s in localized areas. A large eddy is observed on river right, which is just past the apex of the right hand meander bend. Moving upstream to transects 2014_4 (Figure 16), 2014_5 (Figure 17) and 2014_6 (Figure 18), again the effects of channel expansion and contraction are observed with water velocities most rapid in the most constricted of the three transects (2014_4). Water velocities are relatively lower in the widest of the set of three transects (2014_5) and a very low velocity eddy has formed on river right.

3.3. Velocity Transects in downtown Mankato

We measured water velocity transects in the reach through downtown Mankato on June 10, 2015 and June 20, 2015. Discharge at the USGS gage in Mankato (USGS gage 05325000) averaged approximately 8400 cfs on June 10, 2015 and 7650 cfs on June 20, 2015. Transects 2015_1 through 2015_7 (Figures 19-25, were all measured within a half kilometer upstream from the highway 14 bridge just north of Mankato. Average water velocities for each of the transects was approximately 1.0 m/s with very little systematic variability across channel. Transects 2015_8 and 2015_9 (Figures 26 and 27) were measured just upstream from the Belgrade Avenue bridge. These cross sections have a similar average water velocity of approximately 1.0 m/s, but exhibit a large eddy on river left, the inside of the bend in the engineered channel.
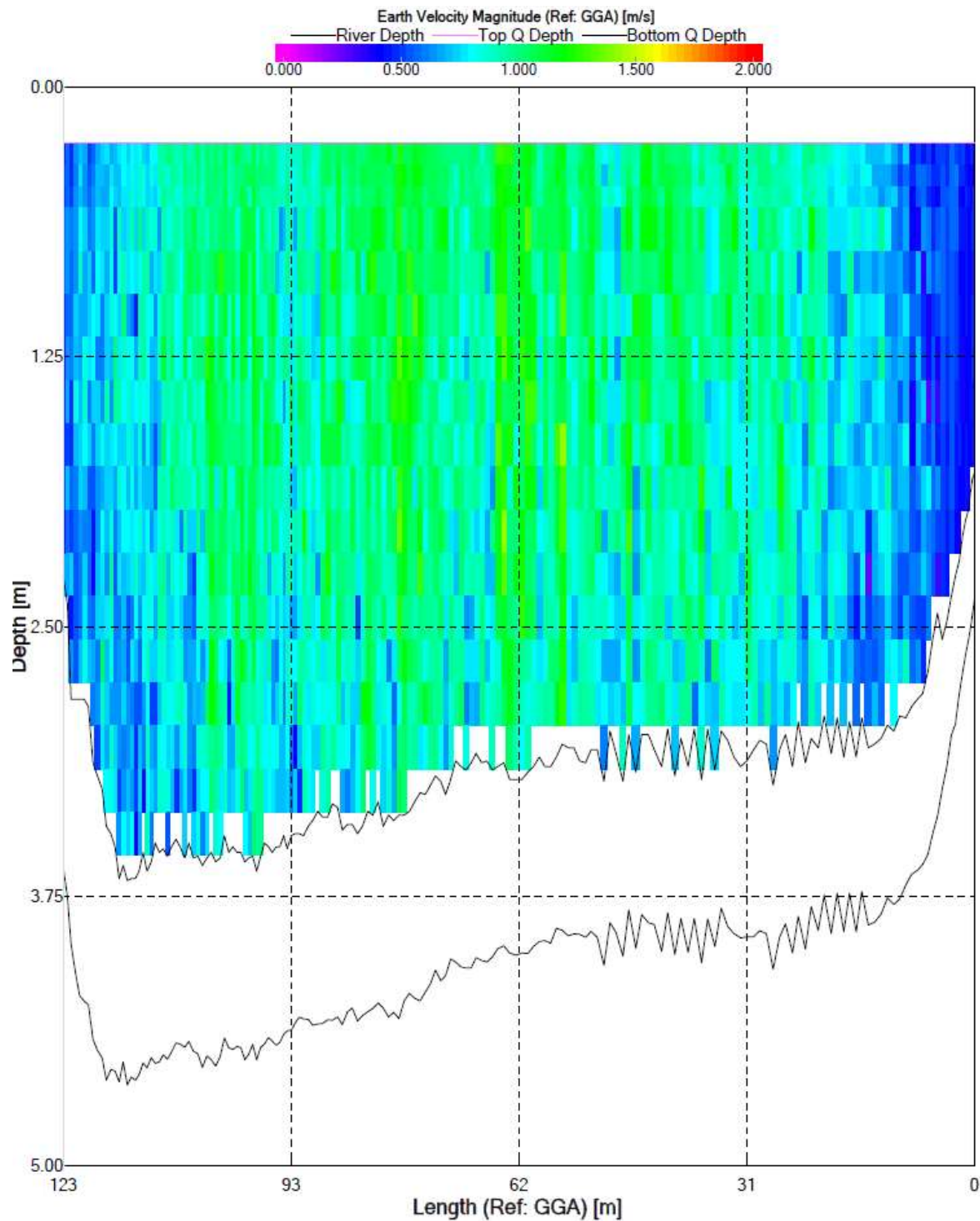
Figure 4. Velocity profile for transect 26_01. Colors indicate water velocity according to legend at the top of the figure. Lowest black line plotted indicates the channel bed. Next higher black line plotted indicates the lowest extent of reliable water velocity measurements. Transect is oriented looking downstream, such that the left of the plot corresponds to river left.
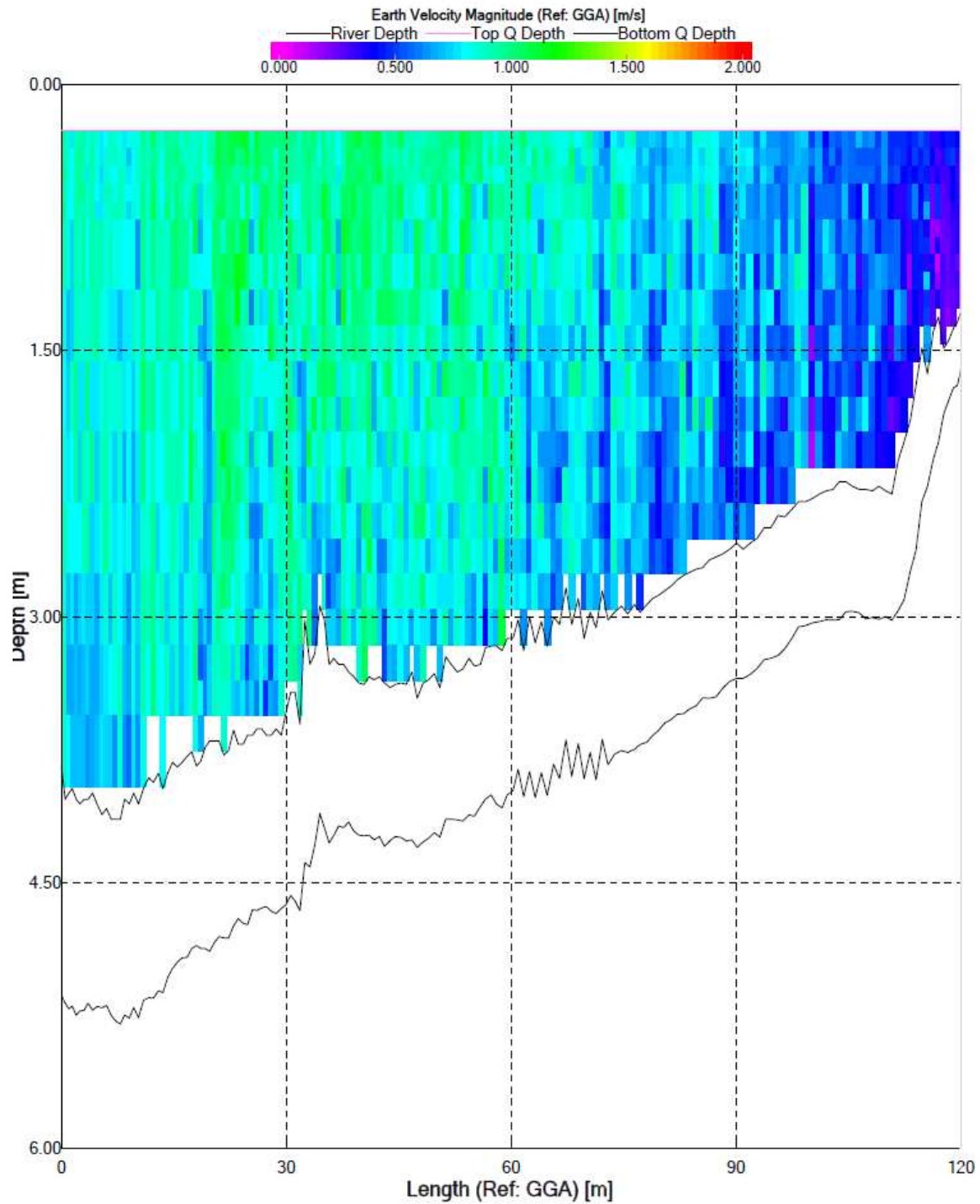
Figure 5. Velocity profile for transect 26_04. Colors indicate water velocity according to legend at the top of the figure. Lowest black line plotted indicates the channel bed. Next higher black line plotted indicates the lowest extent of reliable water velocity measurements. Transect is oriented looking downstream, such that the left of the plot corresponds to river left.
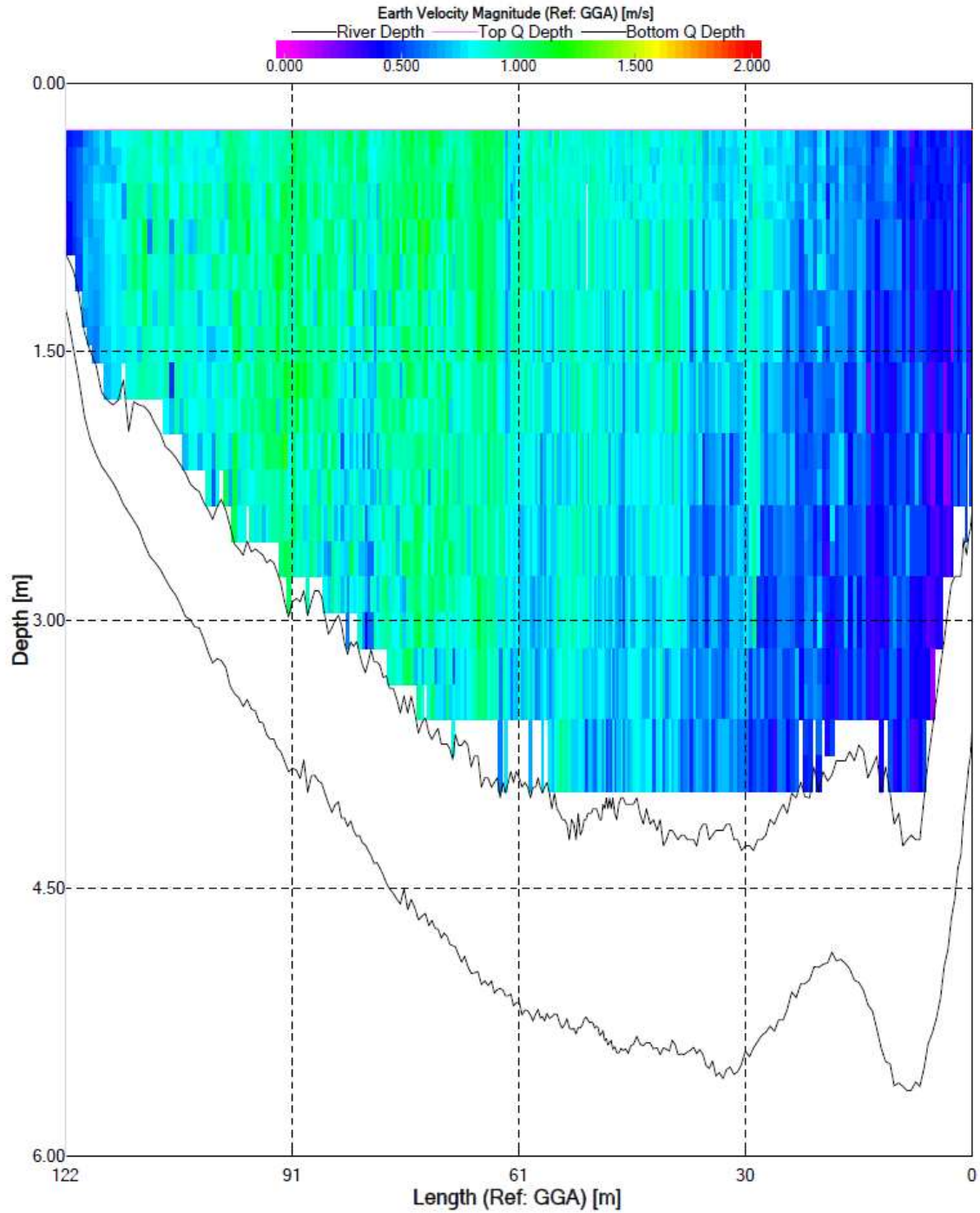
Figure 6. Velocity profile for transect 26_06. Colors indicate water velocity according to legend at the top of the figure. Lowest black line plotted indicates the channel bed. Next higher black line plotted indicates the lowest extent of reliable water velocity measurements. Transect is oriented looking downstream, such that the left of the plot corresponds to river left.
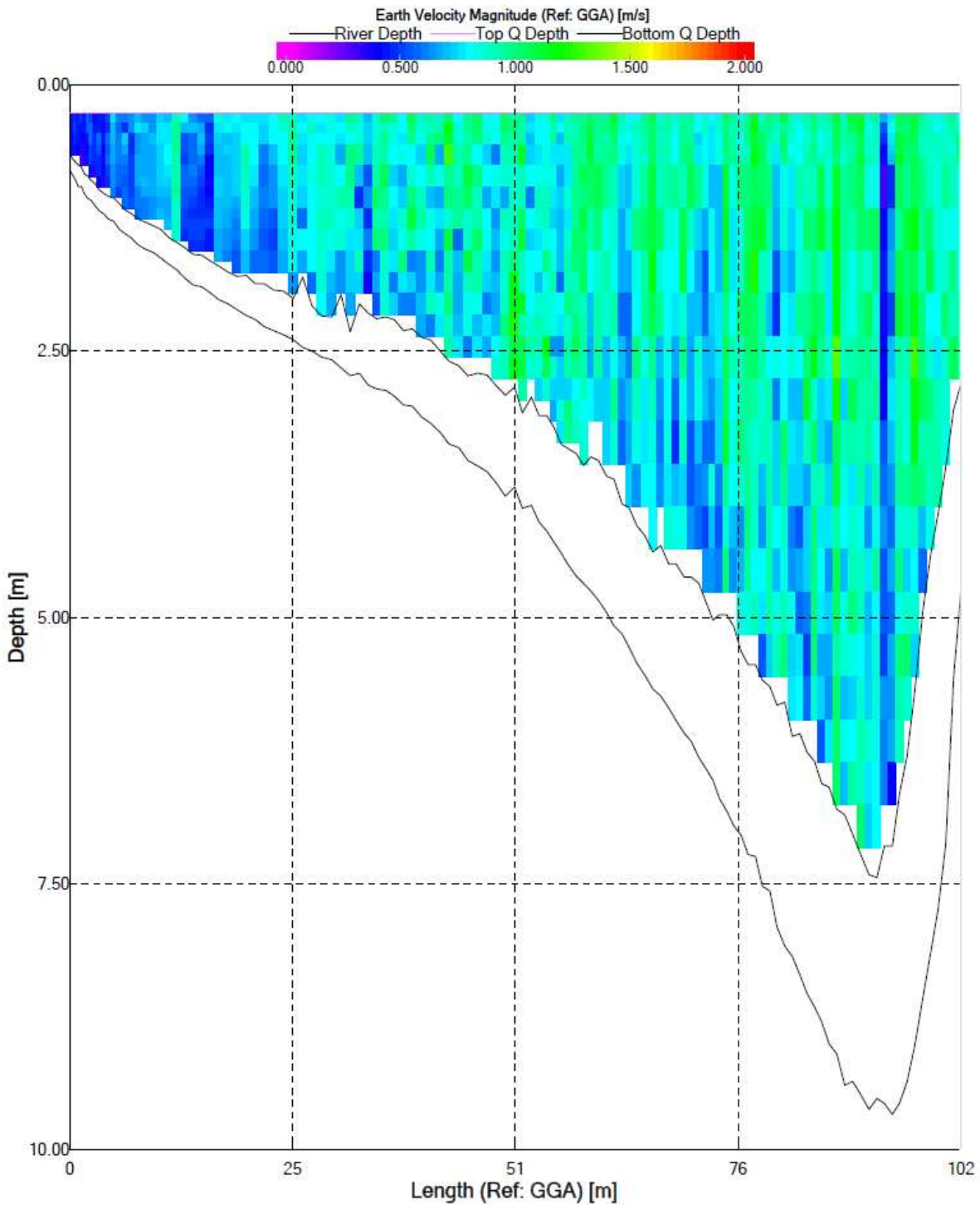
Figure 7. Velocity profile for transect 26_11. Colors indicate water velocity according to legend at the top of the figure. Lowest black line plotted indicates the channel bed. Next higher black line plotted indicates the lowest extent of reliable water velocity measurements. Transect is oriented looking downstream, such that the left of the plot corresponds to river left.
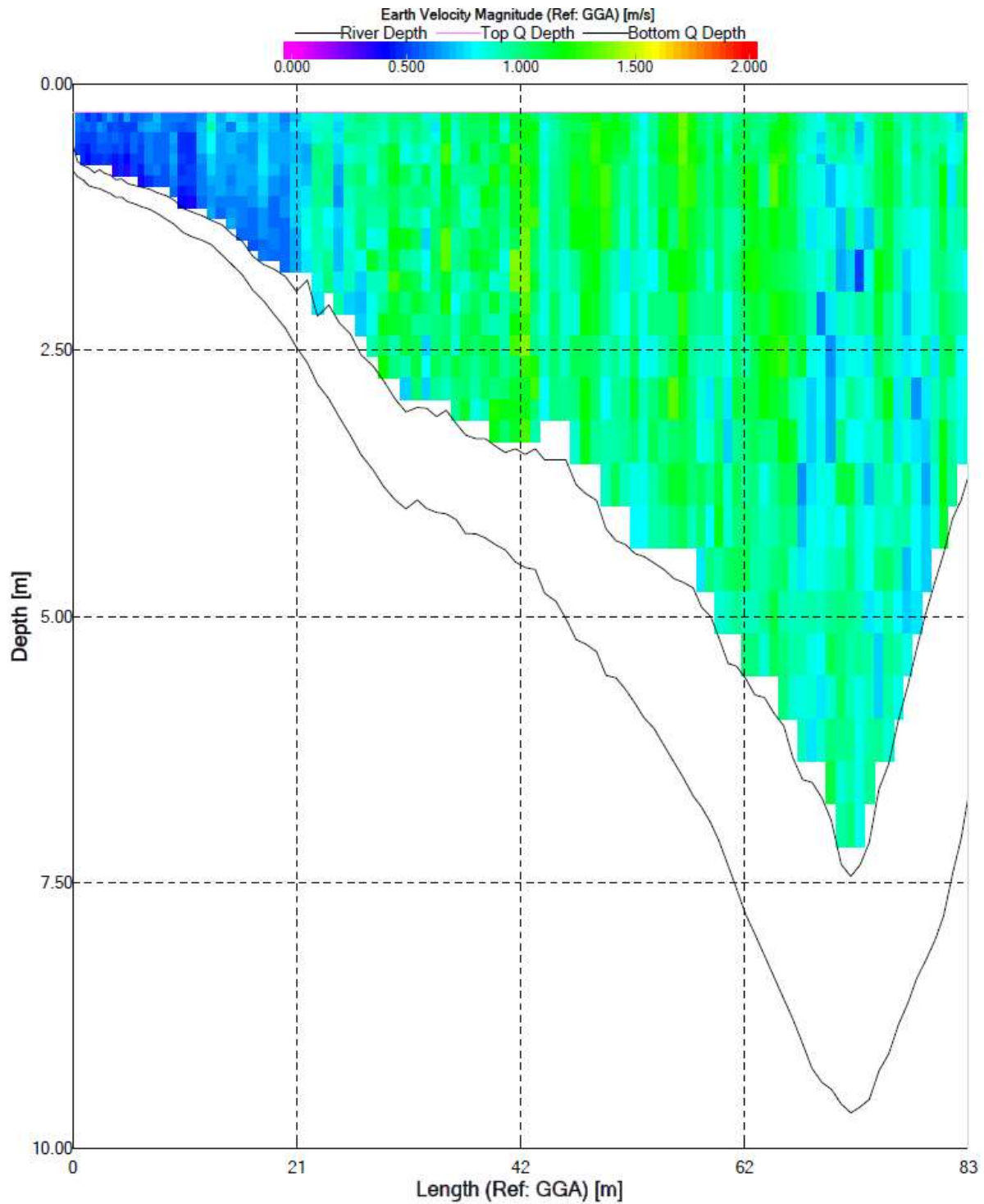
Figure 8. Velocity profile for transect 27_4. Colors indicate water velocity according to legend at the top of the figure. Lowest black line plotted indicates the channel bed. Next higher black line plotted indicates the lowest extent of reliable water velocity measurements. Transect is oriented looking downstream, such that the left of the plot corresponds to river left.
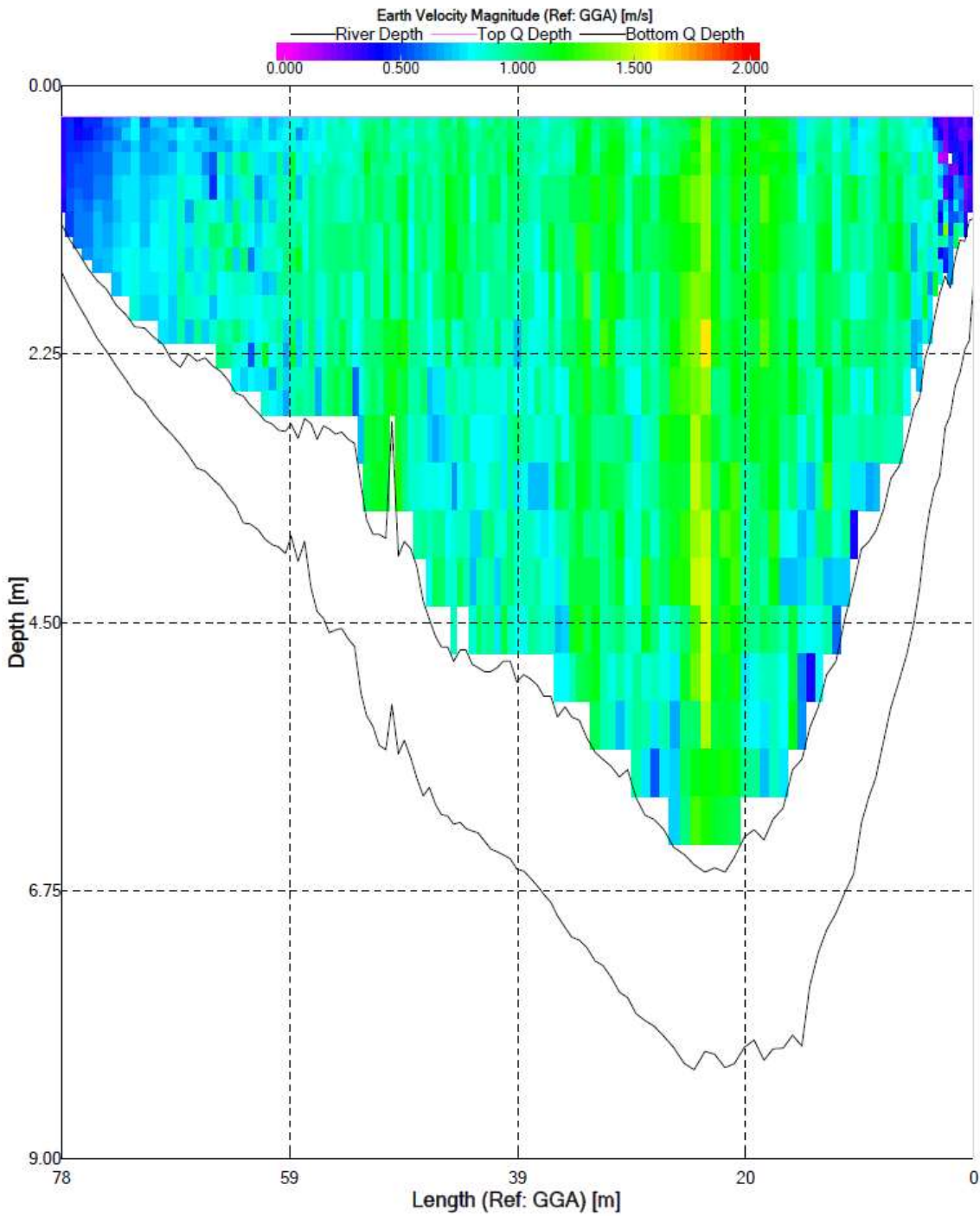
Figure 9. Velocity profile for transect 27_9. Colors indicate water velocity according to legend at the top of the figure. Lowest black line plotted indicates the channel bed. Next higher black line plotted indicates the lowest extent of reliable water velocity measurements. Transect is oriented looking downstream, such that the left of the plot corresponds to river left.
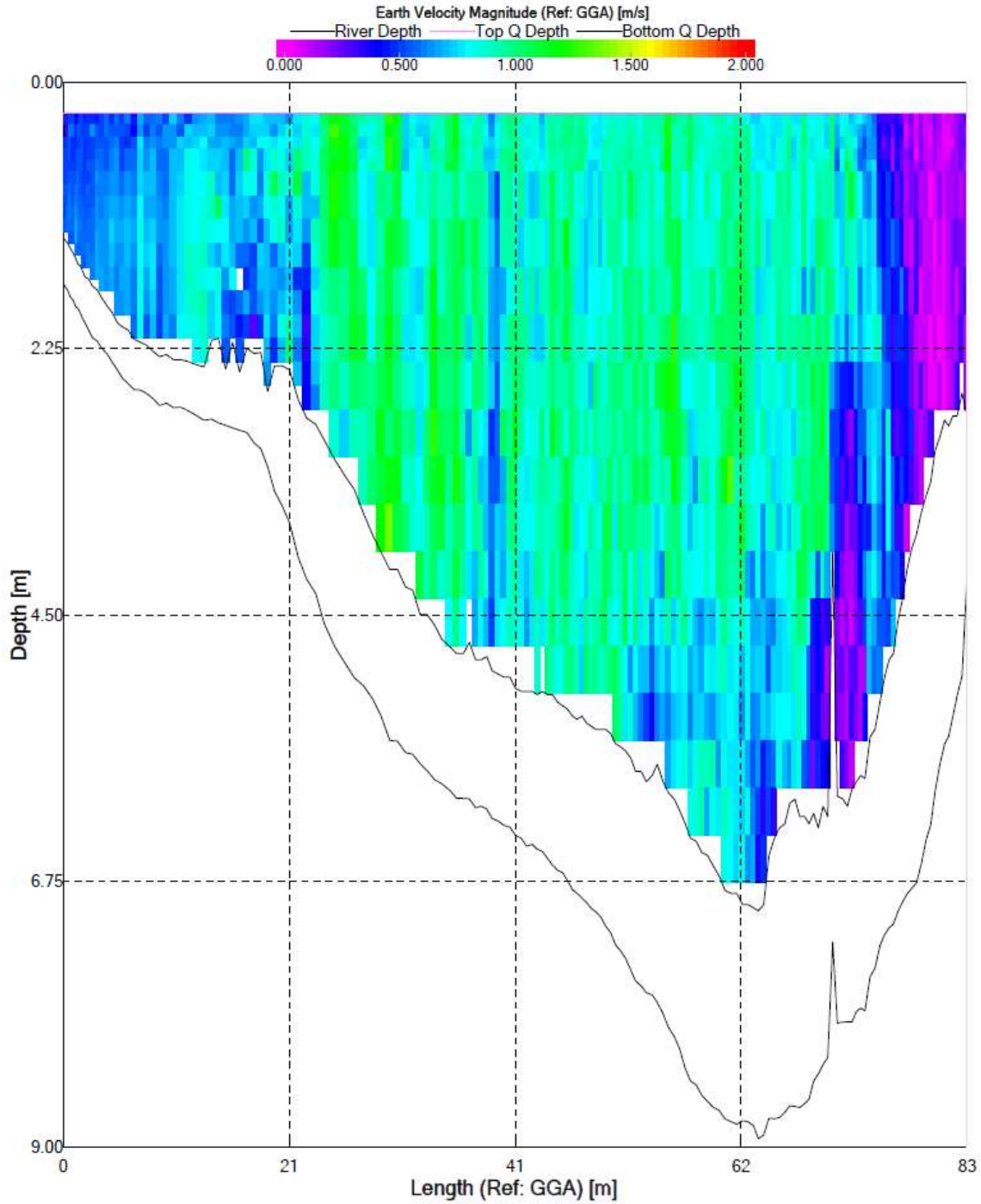
Figure 10. Velocity profile for transect 27_10. Colors indicate water velocity according to legend at the top of the figure. Lowest black line plotted indicates the channel bed. Next higher black line plotted indicates the lowest extent of reliable water velocity measurements. Transect is oriented looking downstream, such that the left of the plot corresponds to river left.
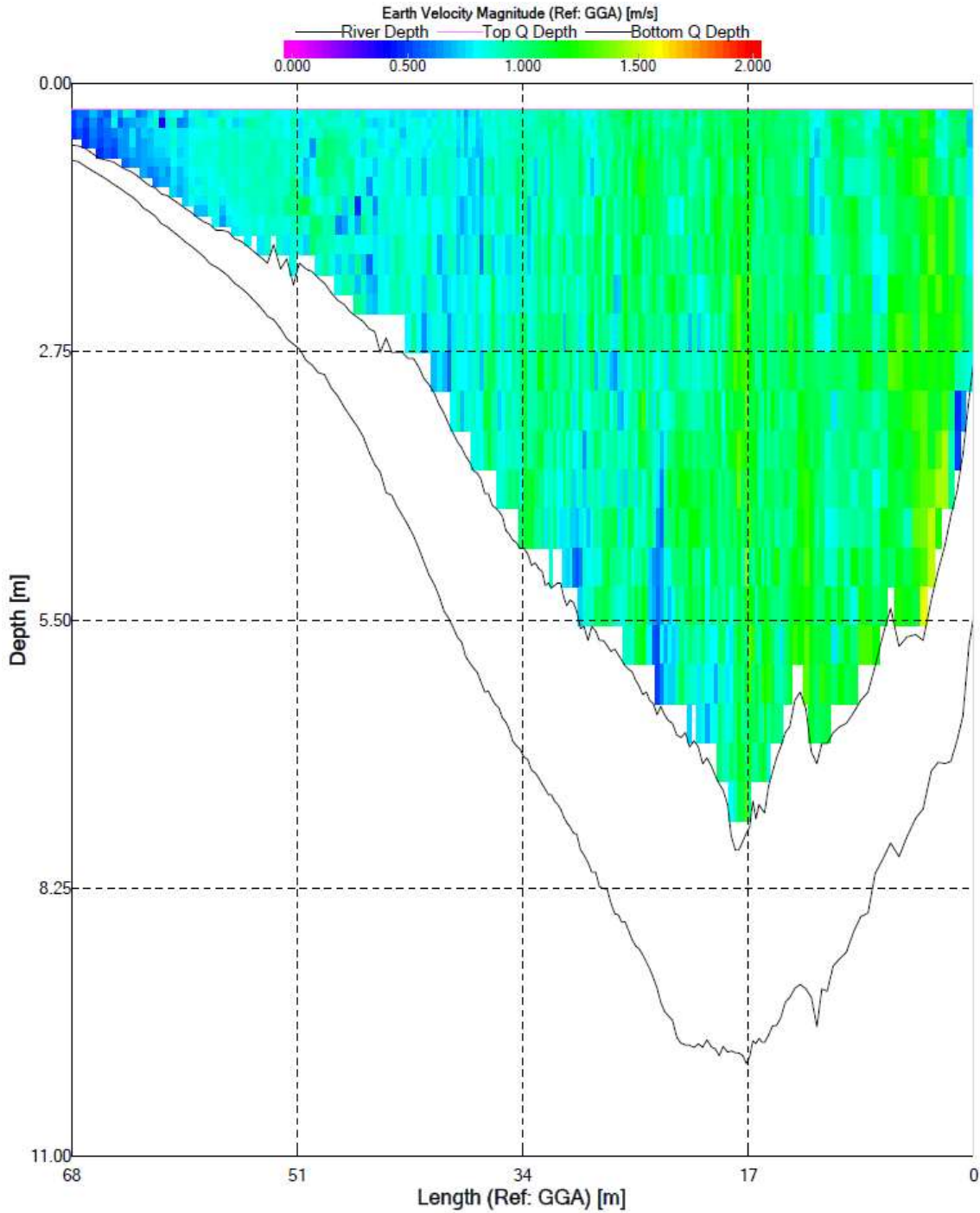
Figure 11. Velocity profile for transect 27_15. Colors indicate water velocity according to legend at the top of the figure. Lowest black line plotted indicates the channel bed. Next higher black line plotted indicates the lowest extent of reliable water velocity measurements. Transect is oriented looking downstream, such that the left of the plot corresponds to river left.
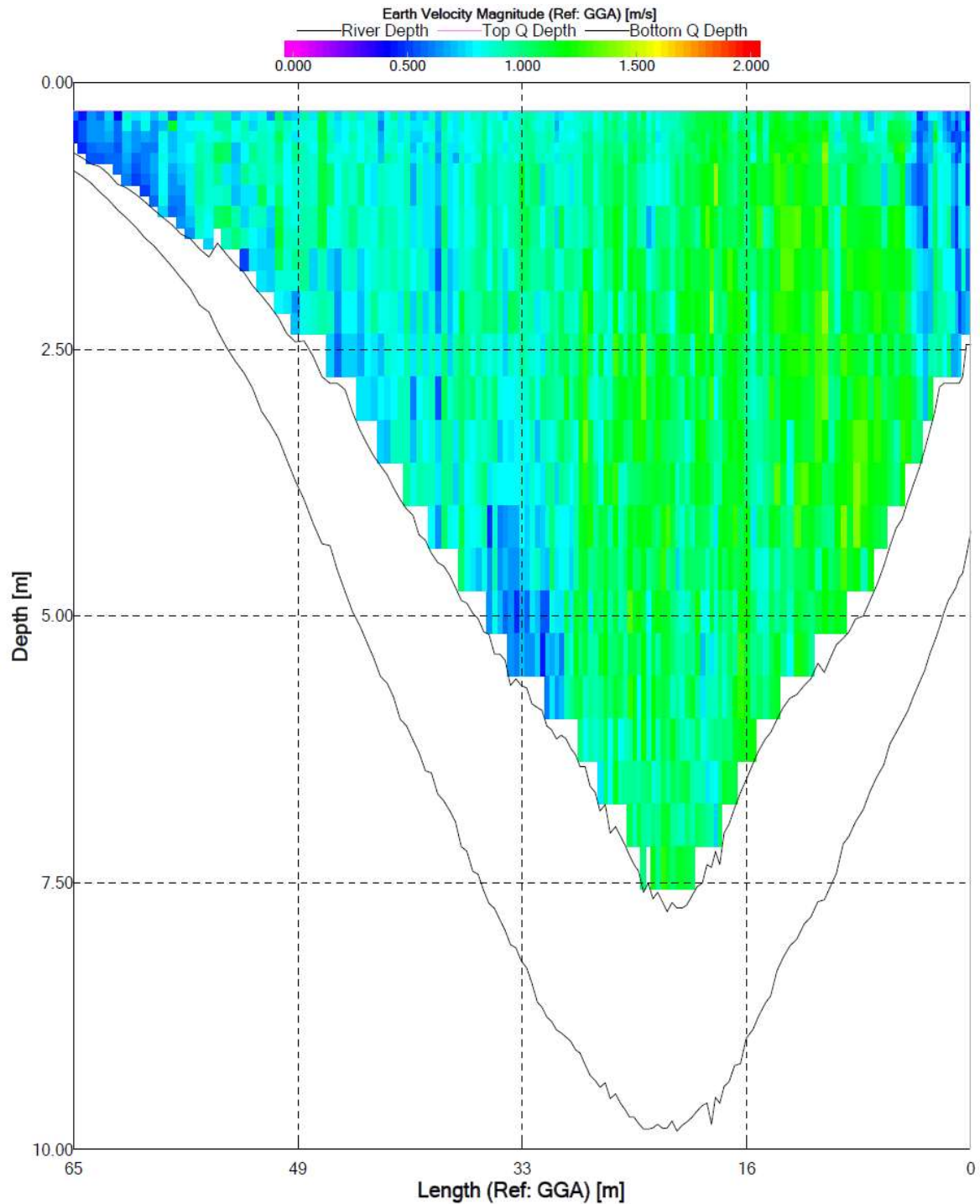
Figure 12. Velocity profile for transect 27_17. Colors indicate water velocity according to legend at the top of the figure. Lowest black line plotted indicates the channel bed. Next higher black line plotted indicates the lowest extent of reliable water velocity measurements. Transect is oriented looking downstream, such that the left of the plot corresponds to river left.
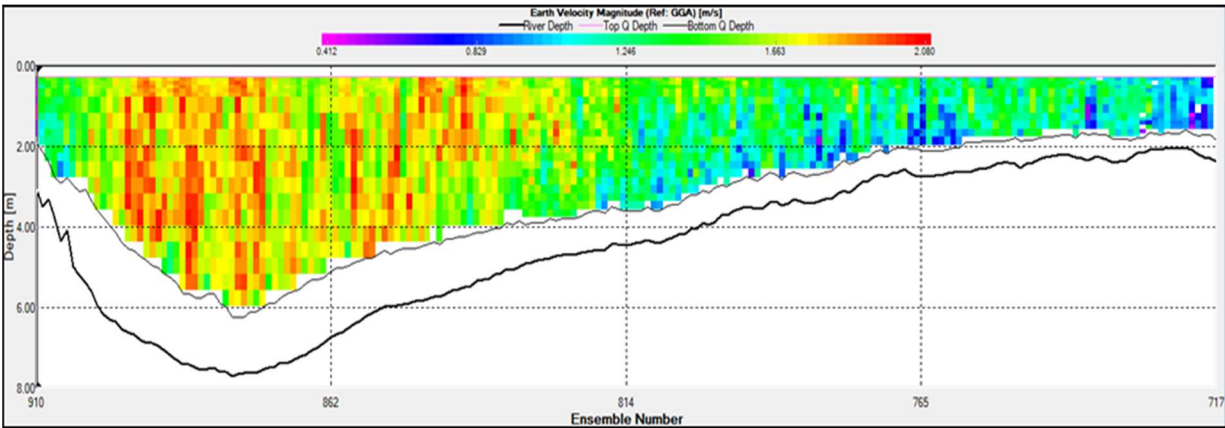
Figure 13. Velocity profile for transect 2014_1. Colors indicate water velocity according to legend at the top of the figure. Lowest black line plotted indicates the channel bed. Next higher black line plotted indicates the lowest extent of reliable water velocity measurements. Transect is oriented looking downstream, such that the left of the plot corresponds to river left.
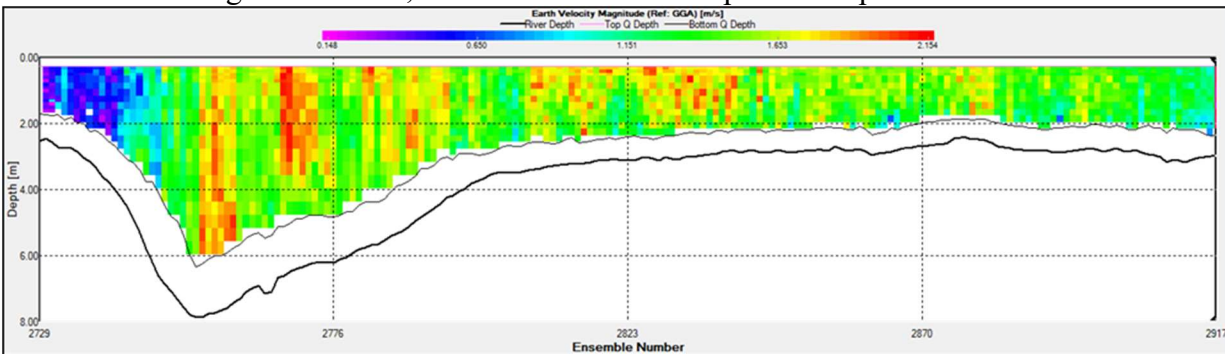
Figure 14. Velocity profile for transect 2014_2. Colors indicate water velocity according to legend at the top of the figure. Lowest black line plotted indicates the channel bed. Next higher black line plotted indicates the lowest extent of reliable water velocity measurements. Transect is oriented looking downstream, such that the left of the plot corresponds to river left.
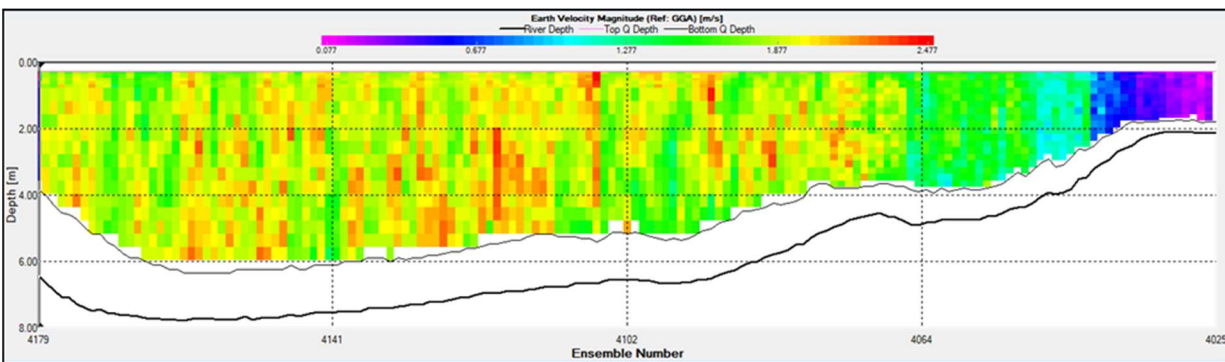
Figure 15. Velocity profile for transect 2014_3. Colors indicate water velocity according to legend at the top of the figure. Lowest black line plotted indicates the channel bed. Next higher black line plotted indicates the lowest extent of reliable water velocity measurements. Transect is oriented looking downstream, such that the left of the plot corresponds to river left.
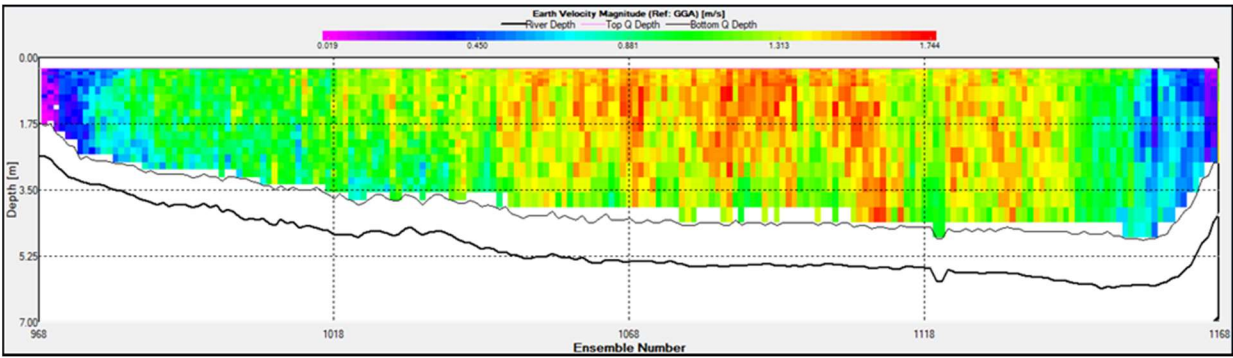
Figure 16. Velocity profile for transect 2014_4. Colors indicate water velocity according to legend at the top of the figure. Lowest black line plotted indicates the channel bed. Next higher black line plotted indicates the lowest extent of reliable water velocity measurements. Transect is oriented looking downstream, such that the left of the plot corresponds to river left.
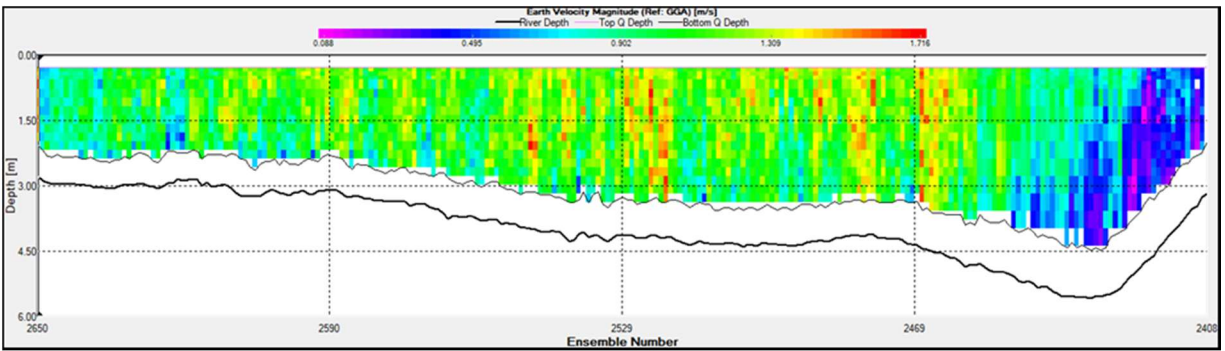
Figure 17. Velocity profile for transect 2014_5. Colors indicate water velocity according to legend at the top of the figure. Lowest black line plotted indicates the channel bed. Next higher black line plotted indicates the lowest extent of reliable water velocity measurements. Transect is oriented looking downstream, such that the left of the plot corresponds to river left.
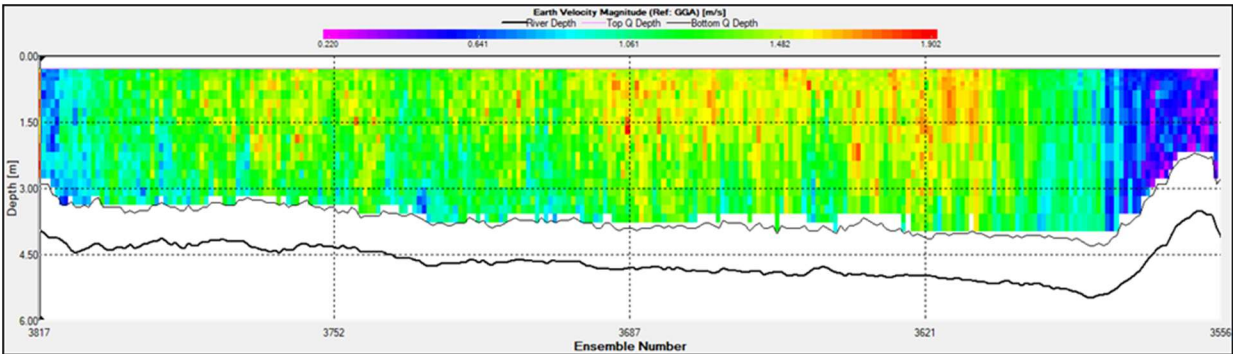
Figure 18. Velocity profile for transect 2014_6. Colors indicate water velocity according to legend at the top of the figure. Lowest black line plotted indicates the channel bed. Next higher black line plotted indicates the lowest extent of reliable water velocity measurements. Transect is oriented looking downstream, such that the left of the plot corresponds to river left.

Below are transects within downtown Mankato.
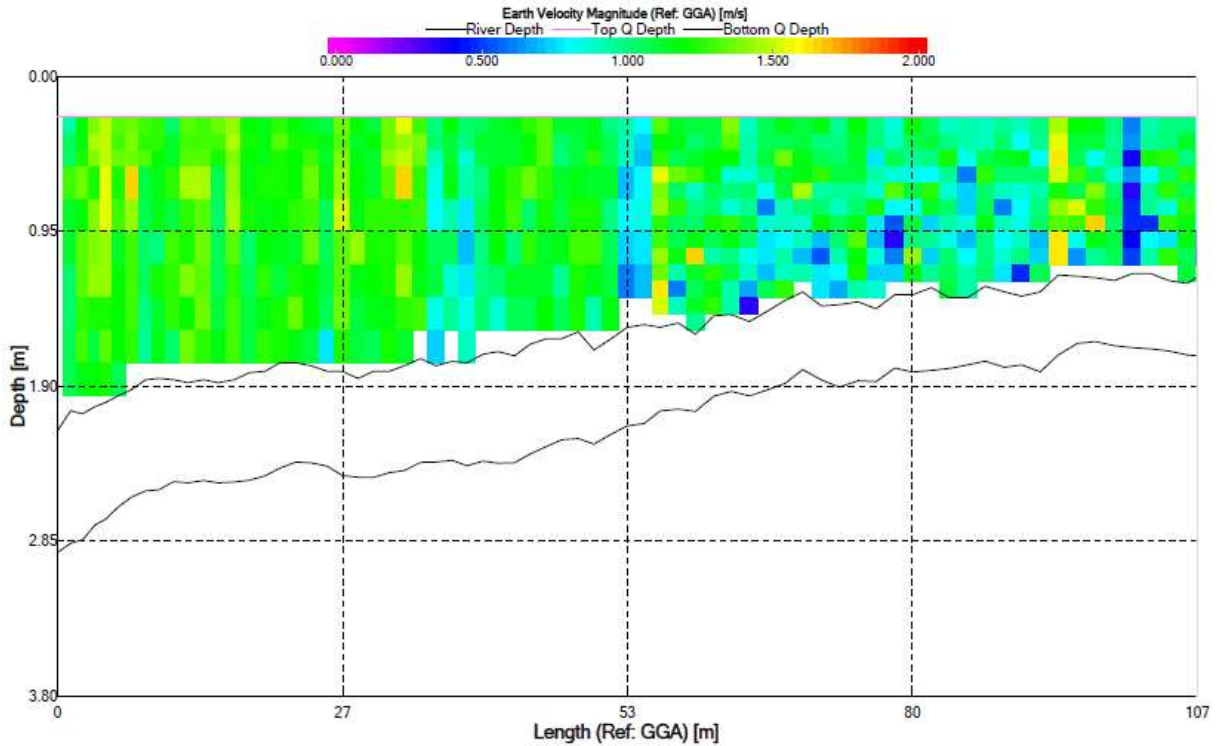
Figure 19. Velocity profile for transect 2015_1. Colors indicate water velocity according to legend at the top of the figure. Lowest black line plotted indicates the channel bed. Next higher black line plotted indicates the lowest extent of reliable water velocity measurements. Transect is oriented looking downstream, such that the left of the plot corresponds to river left.
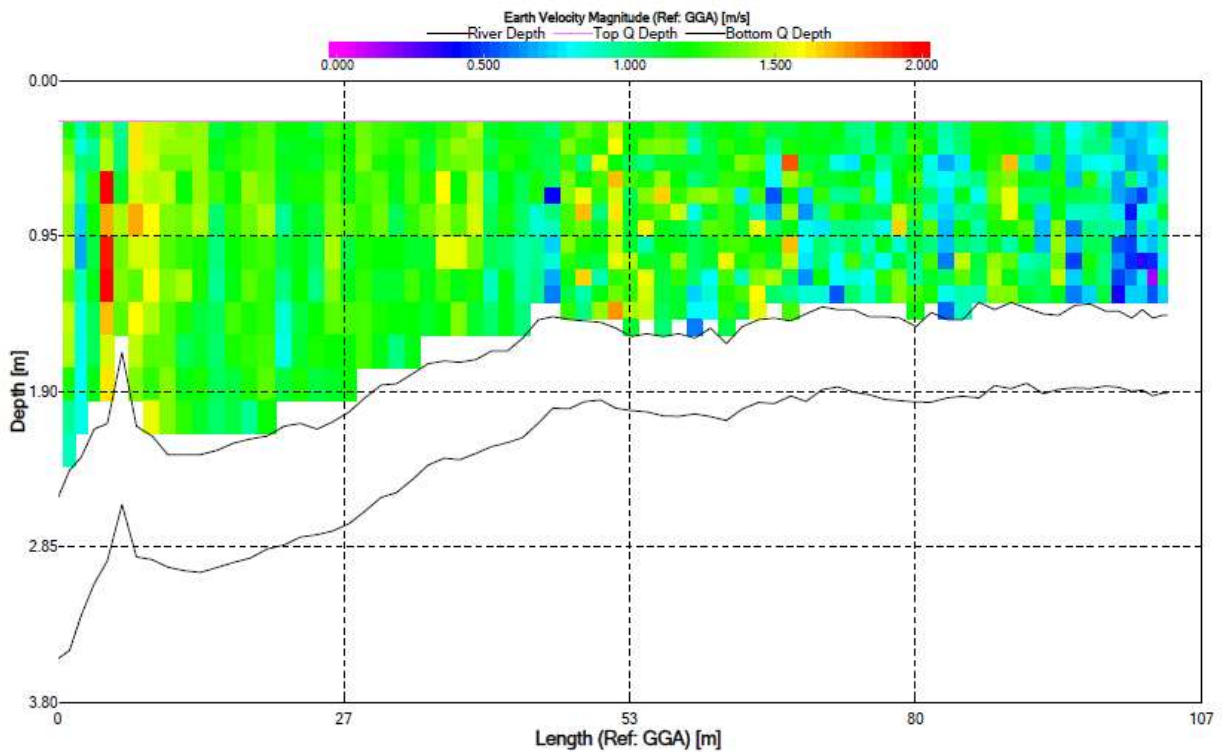
Figure 20. Velocity profile for transect 2015_2. Colors indicate water velocity according to legend at the top of the figure. Lowest black line plotted indicates the channel bed. Next higher black line plotted indicates the lowest extent of reliable water velocity measurements. Transect is oriented looking downstream, such that the left of the plot corresponds to river left.
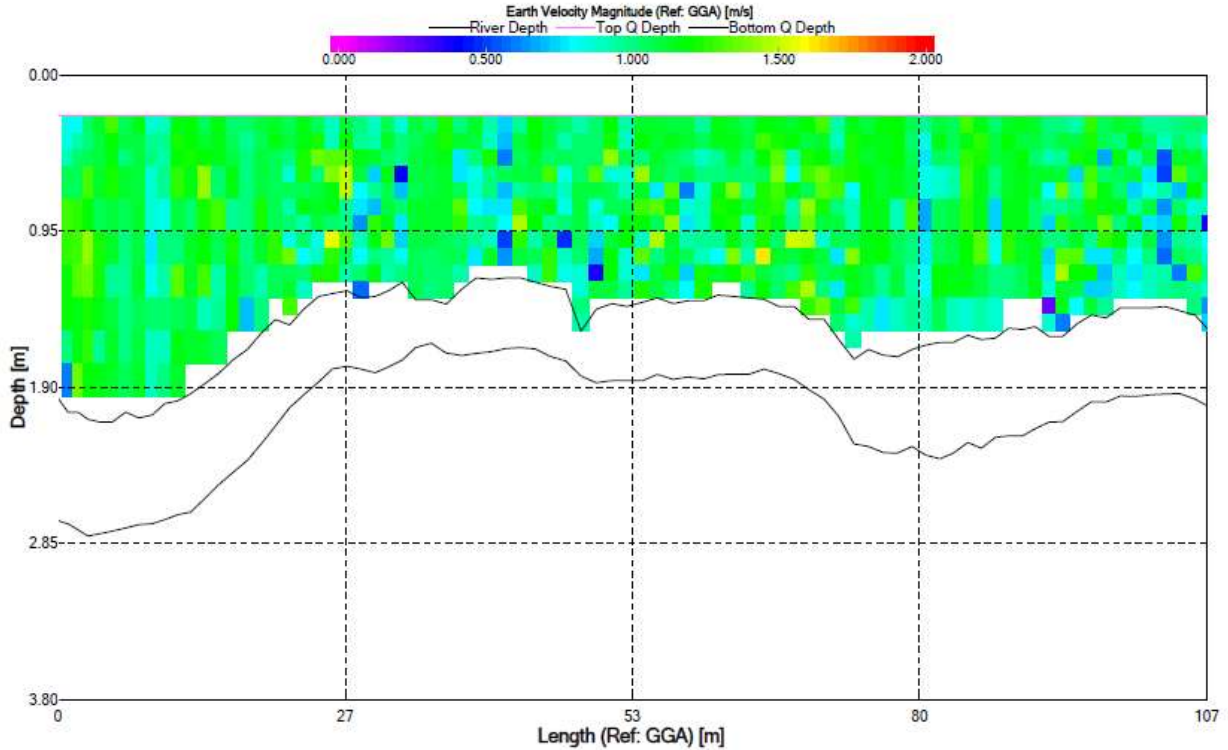
Figure 21. Velocity profile for transect 2015_3. Colors indicate water velocity according to legend at the top of the figure. Lowest black line plotted indicates the channel bed. Next higher black line plotted indicates the lowest extent of reliable water velocity measurements. Transect is oriented looking downstream, such that the left of the plot corresponds to river left.
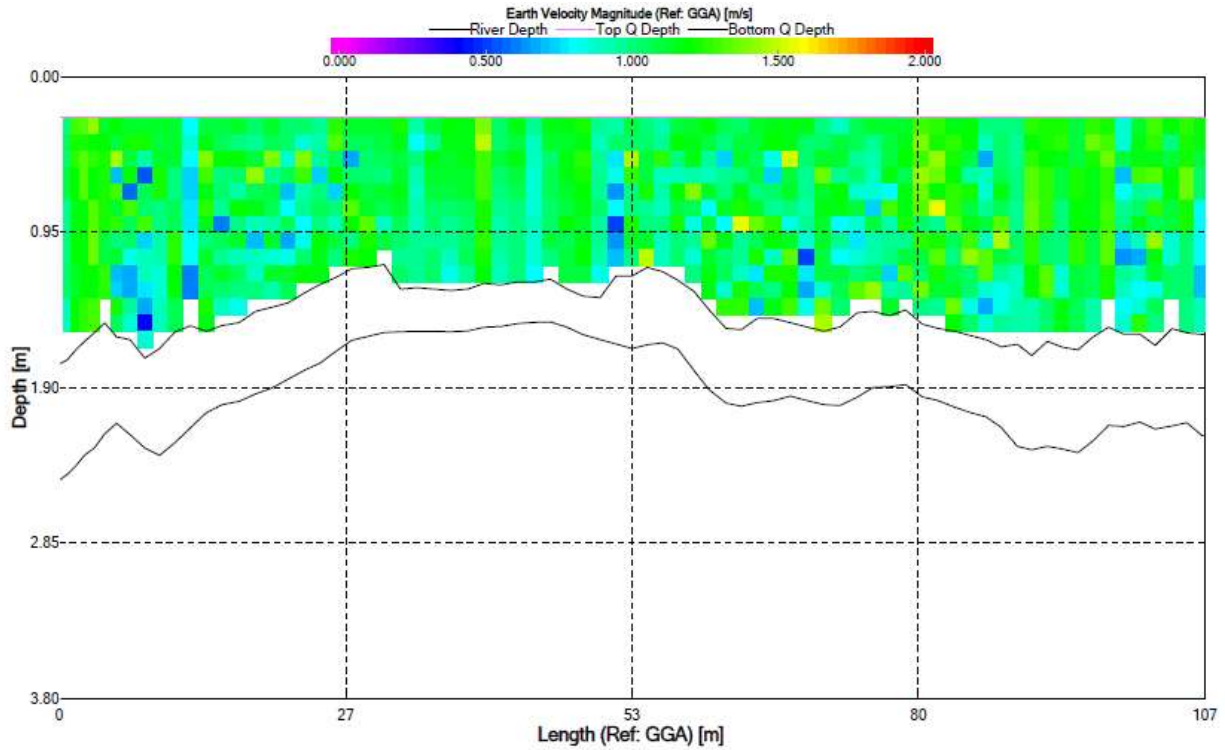
Figure 22. Velocity profile for transect 2015_4. Colors indicate water velocity according to legend at the top of the figure. Lowest black line plotted indicates the channel bed. Next higher black line plotted indicates the lowest extent of reliable water velocity measurements. Transect is oriented looking downstream, such that the left of the plot corresponds to river left.
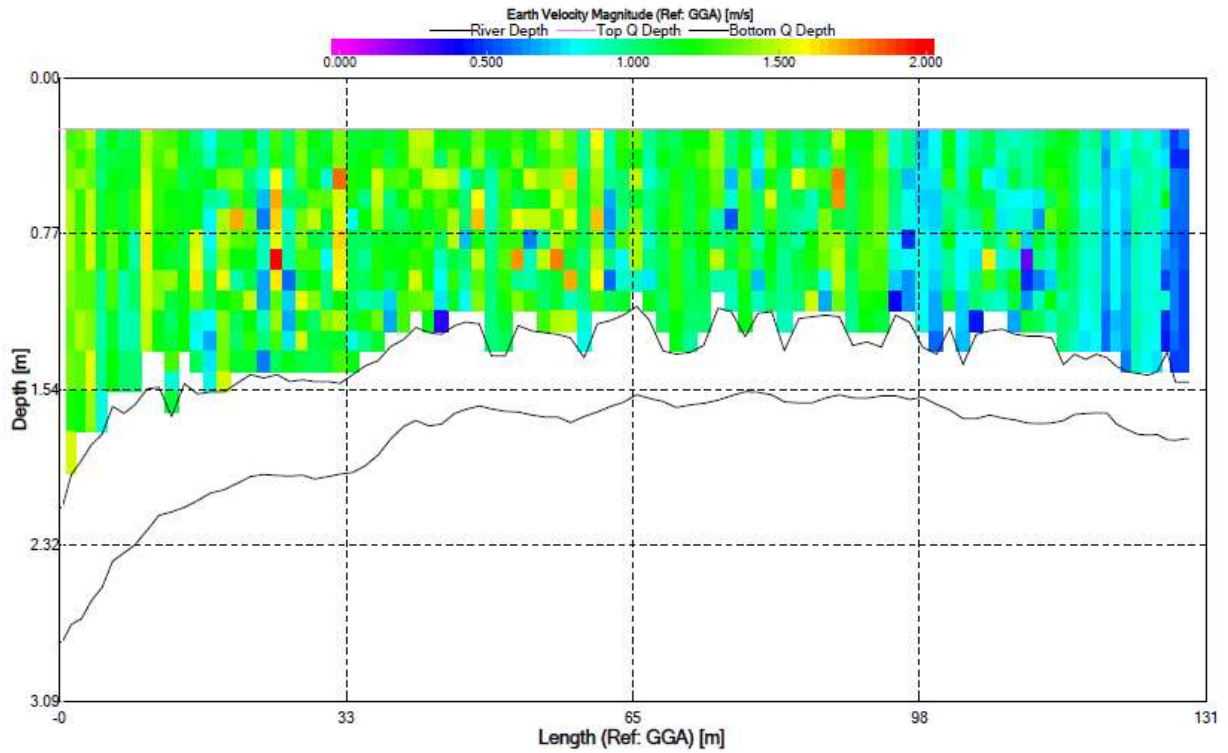
Figure 23. Velocity profile for transect 2015_5. Colors indicate water velocity according to legend at the top of the figure. Lowest black line plotted indicates the channel bed. Next higher black line plotted indicates the lowest extent of reliable water velocity measurements. Transect is oriented looking downstream, such that the left of the plot corresponds to river left.
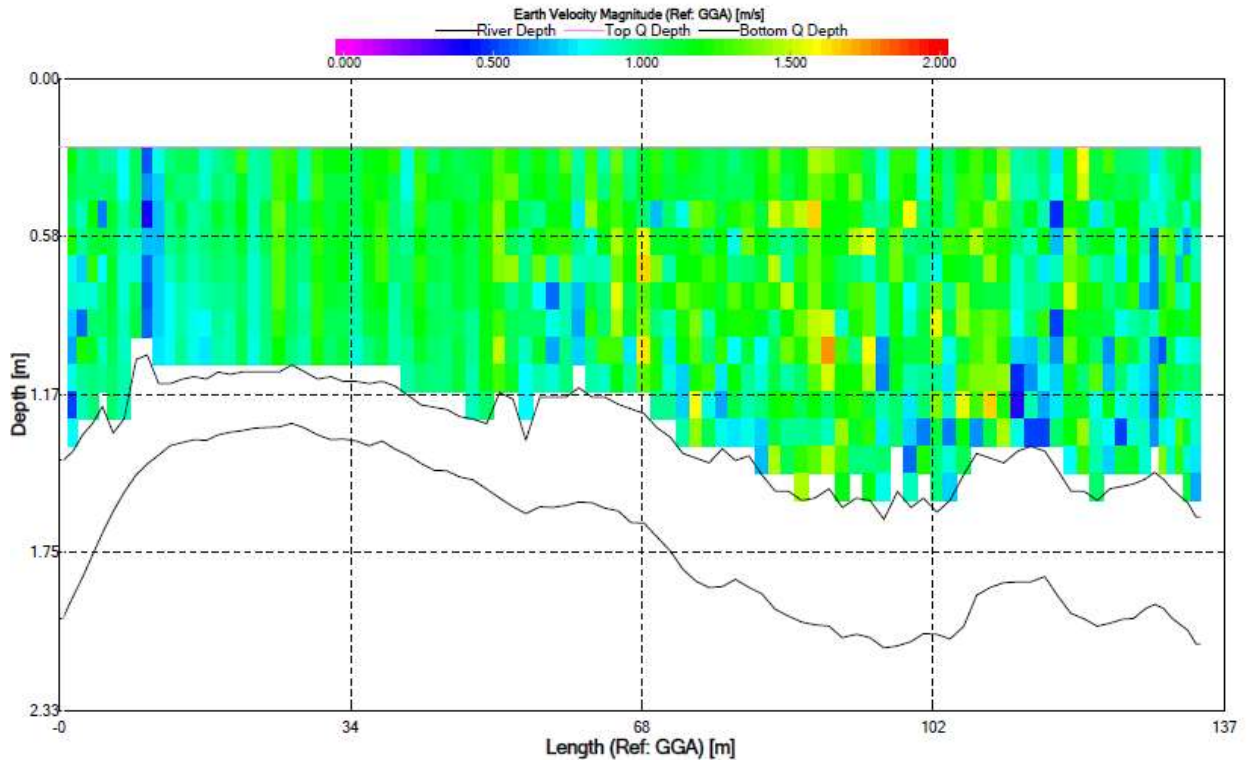
Figure 24. Velocity profile for transect 2015_6. Colors indicate water velocity according to legend at the top of the figure. Lowest black line plotted indicates the channel bed. Next higher black line plotted indicates the lowest extent of reliable water velocity measurements. Transect is oriented looking downstream, such that the left of the plot corresponds to river left.

406
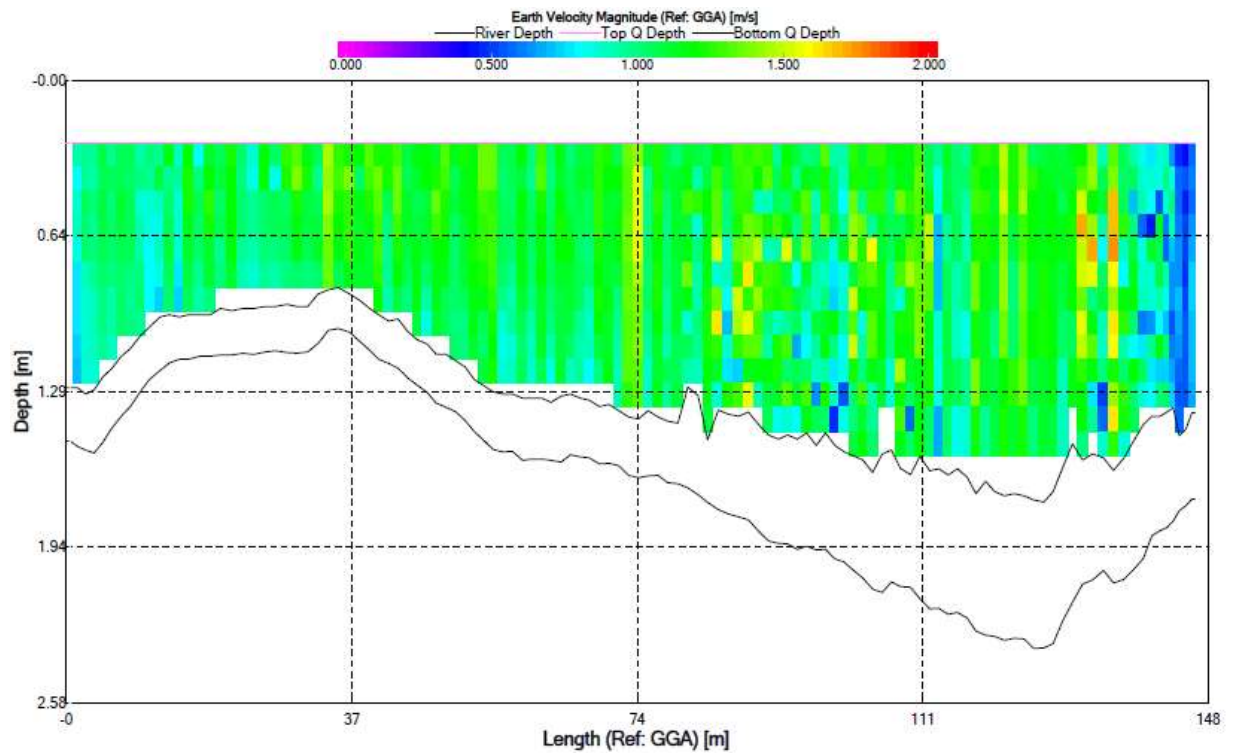
Figure 25. Velocity profile for transect 2015_7. Colors indicate water velocity according to legend at the top of the figure. Lowest black line plotted indicates the channel bed. Next higher black line plotted indicates the lowest extent of reliable water velocity measurements. Transect is oriented looking downstream, such that the left of the plot corresponds to river left.
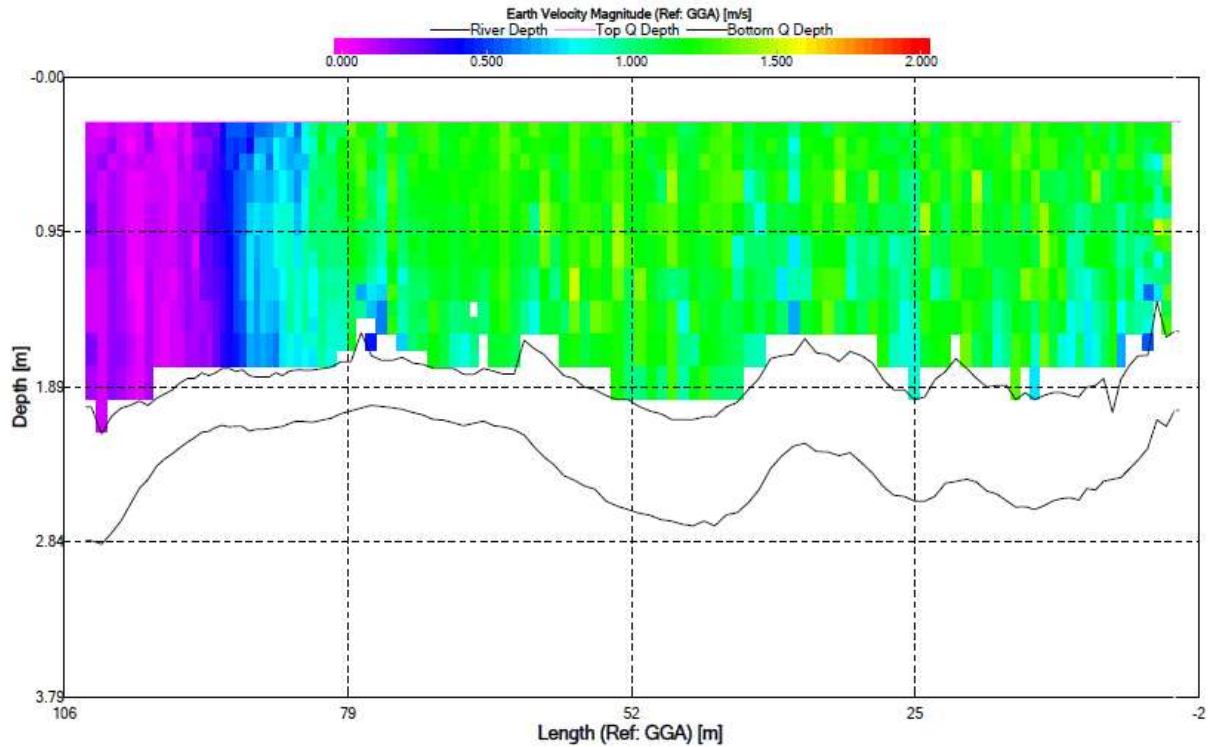
Figure 26. Velocity profile for transect 2015_8. Colors indicate water velocity according to legend at the top of the figure. Lowest black line plotted indicates the channel bed. Next higher black line plotted indicates the lowest extent of reliable water velocity measurements. Transect is oriented looking downstream, such that the left of the plot corresponds to river left.
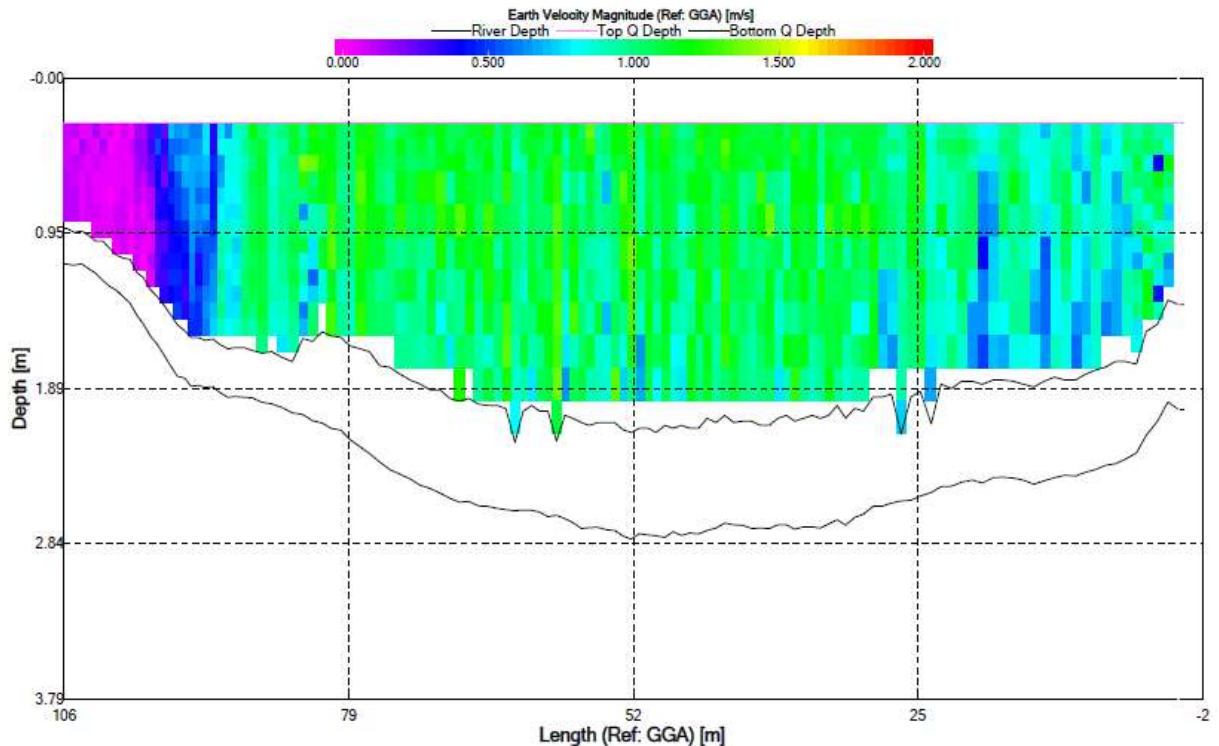
Figure 27. Velocity profile for transect 2015_9. Colors indicate water velocity according to legend at the top of the figure. Lowest black line plotted indicates the channel bed. Next higher black line plotted indicates the lowest extent of reliable water velocity measurements. Transect is oriented looking downstream, such that the left of the plot corresponds to river left.

Task 5: Temperature and Conductivity ranges

Under the advisement of DNR officials, determining certain locations that would be potential site locations for fish barriers will then allow for case-site specific parameters. Depending on the type of barrier being considered, environmental factors may impact the design of the barrier. Two potentially important factors are temperature and conductivity. The average, range, and variability will be determined using continuously recording meters.

Deliverables:
Temperature and conductivity graphs at case site specific locations in the Minnesota River

RESULTS: *Final Database*
(click on link below – username/password = landforms/rock):
https://geo.mnsu.edu/geo/DNR-InvasiveCarp/For_Phil/Final_Database.xlsx

Author: Ben Von Korff[1]

[1]Water Resources Center, Minnesota State University, Mankato

Corresponding Author:
Ben Von Korff – Email: benjamin.von-korff@mnsu.edu; Phone: 5073892355/5073895493;
Website: http://cset.mnsu.edu/wrc/dir/

Notes on Data:
Data Sources
Minnesota Pollution Control Agency (MPCA) Watershed Pollutant Load Monitoring Network
(WPLMN)
https://www.pca.state.mn.us/quick-links/environmental-quality-information-system-equis
Data was obtained via the EQUIS Database for the MN River at Judson and MN River at St.
Peter. It is also stored on Water Resources Center servers in an EQUIS Template.
2 sites: MN River at Judson (S001-759) and MN River at St. Peter (S000-041) were monitored
by the Water Resources Center since 2004 (prior to this, Metropolitan Council carried out the
monitoring).
Data type – YSI sonde data (YSI Pro Plus or YSI series 6 sonde)
USGS
https://nwis.waterdata.usgs.gov/mn/nwis/qwdata/
Parameters with slight method variation were combined into a single column (such as cases
where USGS separates field and laboratory measurements as different parameters)
The 1/23/2018 version of the database combined NTU and NTRU but the 5/24/18 version on the
flash drive I separated these values (A 2008 paper by Greg Johnson shows NTU and NTRU are
correlated but not interchangeable as I thought).
Data type – grab samples.
Metropolitan Council
This data was sent to us directly from Emily Ressenger via email upon request.
MN River at Fort Snelling data (measured by a continuous sensor) – this data is uncorrected for
drift, so Emily suggested using with caution.
I adjusted the times for this continuous data so that it was in CST time, because Met Council said
that the data they sent me was in local time (watch time). Some gaps in the time existed at the
time change each year (2 AM on Sundays) that suggested their raw data was indeed in local time,
however these gaps were not present every year, which made me wonder if the time was not
consistent. I assumed all their data was in local time still despite this inconsistency.
Met Council would like to be contacted before this Fort Snelling data is used in a publication,
because they have not performed QA/QC on much of the data.
MN St Peter data (continuous data)
Data was provided to us in CST time according to Met. Council, so no adjustment of time was
performed.
MN Judson (continuous data)

Data only exists through 2000

Data was provided to us in CST time according to Met Council, so no adjustment of time was performed.

All Met Council data was sent to us as specific conductivity. To obtain raw conductivity, I used a linear compensation conversion equation (Equation from YSI Series 6 sonde manual).

MNSU

A HOBO U-24 conductivity sensor was installed in the MN River at Mankato, housed in PVC pipe. Holes were drilled in the PVC pipe to ensure that water flowed in and out. The sensor was installed on the downstream side of the bridge pillar to avoid getting destroyed during high flow events. The sensor was submerged at all times during both high and low flow. Data was off-loaded from the sensor using a HOBO water-proof shuttle (U-dtw-1).

The data collected from HOBO logger from 11/2015 through November 2017. Two data gaps are present (3/20/2017-4/6/2017, and 8/7/2017-9/15/2017). The reason for the gaps is unclear, but it appears likely that the sensors memory filled up and stopped logging, and restarted when the data was off-loaded again.

The Conductivity Assistant (part of Hoboware software program) was used to convert raw conductivity data measured by the HOBO logger to calibrated (drift corrected) specific conductance, using monthly YSI (series 6 sonde) readings to calibrate the data (except for the winter when reaching the logger was not possible at times). The calibrated specific conductance was converted back to raw conductivity to obtain calibrated (drift corrected) raw conductivity data using the formula: Specific Conductance (at 25 degrees C) = Raw conductivity / (1 + TC x (T – 25)), where TC = 0.0191, and T is temperature in degrees celcius [source – YSI series 6 sonde manual]. Note – the raw conductivity values in the final database are these calibrated (drift corrected) values.

During May, 2016, data was downloaded from the logger, but the calibration reading was not obtained until a couple days later. Ideally, we should combine the data prior to the calibration point into the previous month's file, however, Hoboware does not currently support using an edited text file in the conductivity assistant, so if the data file is edited, it will not run in the conductivity assistant. Onset tech support says this feature is something they would like to add but it is currently not available. Until then, they suggested taking the calibrated data from June, and using the first data point to calibrate the previous month's data, since it is known to be accurate.

Called onset in May 2017, and they still don't have plans to add the ability to run edited files in the conductivity assistant. They said some of their customers analyze data manually with excel. I considered doing the drift correction manually using conversion factors from ISO 7888, but this would be extremely time consuming, and Onset tech support thought it was not necessary.

Field methods (calibration readings):

Series 6 YSI sonde was calibrated the day of measurement for conductivity, pH, and dissolved oxygen. The conductivity probe on the YSI sonde was brushed and cleaned weekly.

The sonde was placed as close to the HOBO conductivity sensor as possible to obtain a calibration reading. After the first calibration reading, data was downloaded from the logger, and the sensor was cleaned with a cue-tip and dilute detergent, and rinsed with distilled water. A second calibration reading was taken after re-deployment.

Calibration readings were tied to measurements in the downloaded data and the data was calibrated using HOBOware software. In some cases, the calibration reading was tied to the

second data point from the top or bottom of the data set to avoid selecting a data point when the logger was on the boat prior to data download or re-deployment.

Phase 3: Determine if the Minnesota River and Red River are connected

Task 1: Identify of potential watershed breaches up to a 500-year flood event through GIS and local knowledge

As identified by local fisheries offices, potential watershed breaches have been identified. Through local fisheries offices and DNR representatives' knowledge, floods have integrated the Minnesota and Red River watersheds in the past. Little is understood, however, about the nature of such events.

We will utilize the plug-in for ArcGIS to map floodplain inundation for any specified river stage above the bank (see Belmont, 2011). This will be useful for exploring connectivity between the MN River and Red River systems and determining how high the river must get for integration to occur. Analysis of LiDAR and aerial photography will also aid in determination of possibly integration sites.

Deliverable:
Identify potential breaches between HUC4 and HUC8 watersheds.

Timeline:
January 2016 - December 2017

Task 2: Ground truth each potential breach

After Identification of potential breaches, through local fisheries knowledge and the GIS analysis of the landscape, field work to ground truth the potential breach sites would need to be completed. This field work would entail detailed surveying and geomorphic analysis to identify the nature of the integration and if any field evidence exists to suggest what water level that breach would occur.

Deliverables:
Investigate potential locations where a breach may occur using detailed surveying and geomorphic analysis.

Timeline:
January 2016 - December 2017

Task3: Quantify each breach

After completing the GIS analysis and ground truthing, we would attempt to quantitatively describe the nature of possible breach sites. This would include stage height necessary for

integration and evidence (or lack thereof) of previous integration events to possibly aid in a frequency analysis.

Deliverables:
Quantify the potential for a breach to occur using detailed surveying and geomorphic analysis.

Timeline:
January 2016 - December 2017

RESULTS: *Determining if the Red River and Minnesota River Are Connected*
Possible Connectivity of the Little Minnesota River and Lake Traverse

Author(s): Shayler Levine[1], Patrick Belmont[1]
[1]Watershed Sciences - Utah State University

Corresponding Author:
Patrick Belmont – Email: Patrick.belmont@usu.edu; Phone: 4357973794

1. Introduction

The Upper Minnesota River watershed is 1308 km2, northwest of Browns Valley, Minnesota (Figure 1). This area includes the subtle drainage divide between the Little Minnesota River (flows south) and the headwaters of the Red River of the North (Lake Traverse) which flows north and eventually drains into Hudson Bay. This study aims determine conditions under which the two river systems (Little Minnesota and Red River) may become hydrologically connected. Connectivity is important to understand because of the potential for invasive carp to spread from the Little Minnesota River to the Red River of the North. Ground reconnaissance and geospatial mapping of flood inundation levels reveal no other likely area of connection. Importantly, this is the only location we discovered where historical records indicate that these two bodies of water have connected, infrequently, in the past (Minnesota Department of Natural Resources Waters Division 2007).

In spring of 1820 the area between the Little Minnesota River and Lake Traverse was described as a marsh by explorers Graham and Laidlaw, who used the marsh to drag and float a boat full of grain from the Red River to the Minnesota River (The Red River Trails). The dike that now constitutes the southern boundary of Lake Traverse was constructed in 1941 to stop a pathway between watersheds where exotic biota could spread during floods (Spading 2000).
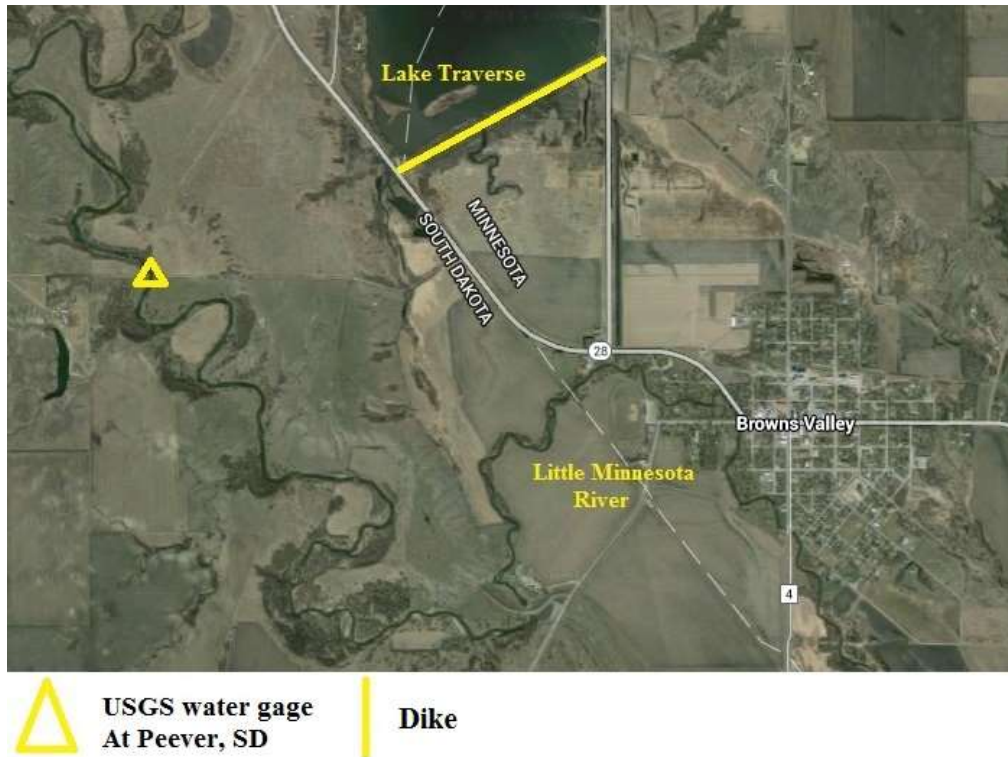
Figure 1. Browns Valley, Minnesota, Lake Traverse is the headwaters for the Red River of the North. The Little Minnesota River flows south

The marsh that was noted by Graham and Laidlaw now appears to be an open field covered in perennial vegetation and/or crops. This field and highway separate the Little Minnesota River and Lake Traverse. Aerial photography suggests that there is little or no activity taking place on field in recent years. Figure 2 depicts topography from the Little Minnesota River to the levee bordering Lake Traverse.
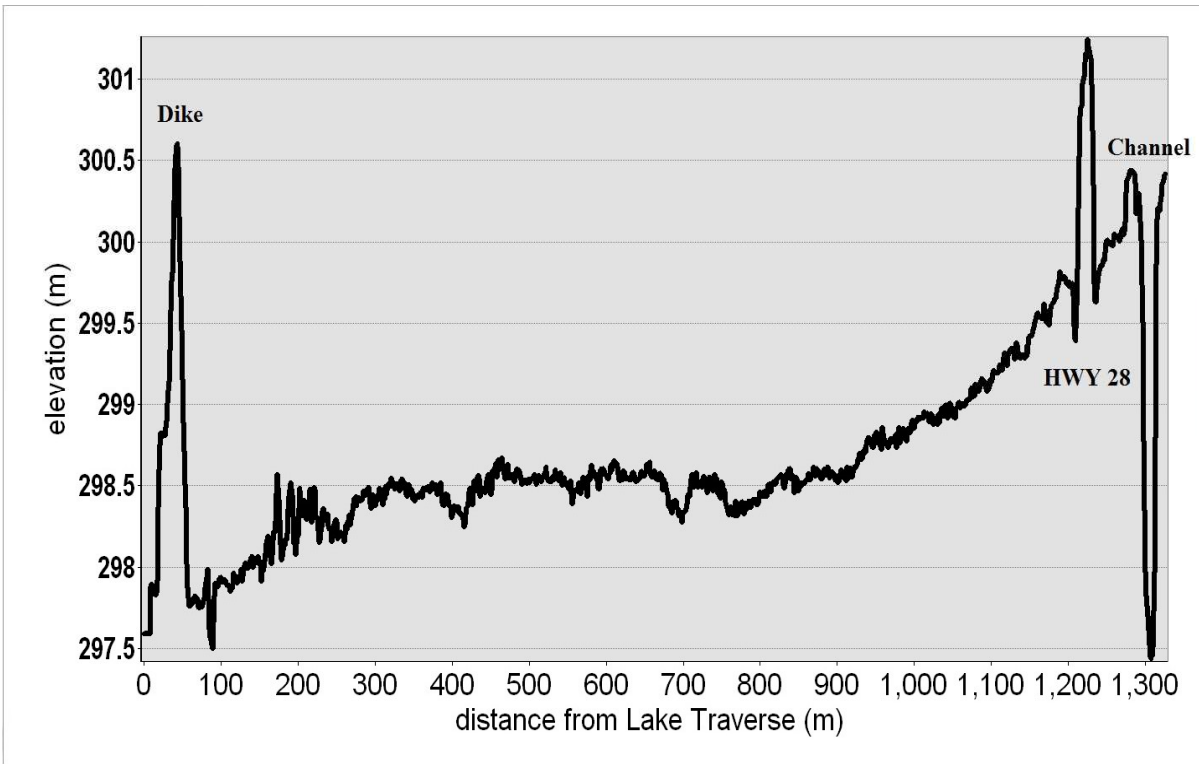
Figure 2. Topographic profile extracted from 1 m resolution LIDAR data to show the terrain from the right bank of the Little Minnesota River to Lake Traverse dike.

2. Historical Flooding

The U.S. Army Corps of Engineers (USACE) has complied data on the historical flooding of the Little Minnesota River. Flood events that caused hydrologic connectivity between Little Minnesota and Lake Traverse (headwaters of the Red River) are provided in Table 1.

Table 1. Historical flooding events that connected of Little Minnesota and Lake Traverse (headwaters of the Red River of the North) near Browns Valley, MN. Table created by USACE (Spading 2000)

Date	Peak Flow, cfs	Mean Daily Peak, cfs	Was the Peak River Stage affected by ice? (1)	Notes
July 25, 1993	8,900	5,400	No	Breakout Flow to Lake Traverse
April 8, 1952	4,730	4,400	No	
March 25, 1943	4,320	------	Yes	Breakout Flow, Brown's Valley Dike Breached
Spring 1916	See Note No. 2	------	NA	Breakout flow probably occurred
March 28, 1997	3,590	3,420	Yes	Breakout flow probably occurred
April 6, 1969	3,270	2,100	No	
May 23, 1962	3,140	2,440	No	
June 22, 1919	NA	2,970	No	Estimated Peak Mean Daily Flow, see Note No. 3
March 21, 1976	2,960	2,260	No	
June 7, 1942	2,960	1,810	No	Peak Discharge Equal to 1976
June 2, 1965	2,920	1,740	Yes	
April 11, 1947	2,780	2,550	No	
March 13, 1995	2,700	1,500	No	
May 27, 1954	2,300	201	No	
March 16, 1972	2,180	1,910	No	
March 28, 1978	2,140	1,920	Yes	

1. Peak stages in 22 of the 59 years of record (1940-1998) were affected by ice. This is not necessarily indicative of ice effects downstream at the breakout reach (at Browns Valley, MN). Also, peak flows are not affected by ice jams (only stages).
2. Reference No. 4, Page 47 suggests the 1916 flood approximated the 1943 flood in regards to the volume of breakout flow into Lake Traverse.
3. Estimate from Reference No. 4, Page 19.

We have further synthesized information regarding the flood events of 1943, 1993, and 1997. We chose these particular years because they had the most information about what occurred during the event. The US Army Corps of Engineers (USACE) defines 'breakout flows' as flows in which water levels exceed the elevation of specifically the left bank because that can lead to connectivity with the Red River (Lake Traverse). Some of these breakout flows were affected by ice jams, which leads to elevated water stage but has no effect on the maximum peak flow, whereas others are simply the result of extreme rainfall events (Spading 2000).

March-April 1943: Ice jams near Browns Valley, Minnesota caused the river to overflow its banks on March 31, 1943. River stage during this event was elevated (up to 5 meters). The flood waters pooled south of the recently completed Browns Valley Dike (shown at the northern end of Lake Traverse in Figure 1). The dike was circumvented by highway 28 causing water to flow into Lake Traverse. This is the first time the levee failed to stop the water from flowing north (Spading 2000).

July 1993: Precipitation as high as 10 inches in a 24 hour period was reported in the Little Minnesota River basin prior to this flood, and a peak flow of 8,900 cfs at the U.S.G.S. gage at Peever, SD occurred on July 25th. The USACE personnel from the Lake Traverse Project observed water flowing northward from the Little Minnesota River into Lake Traverse. On August 6, 1993 water was observed to be flowing southward from Lake Traverse to Little Minnesota River. They were connected for 6 days (Spading 2000).

April 1997: Peak flow measure at the Peever, SD gage on March 28, 1997 was 3,590 cfs. During this time, flooding associated with ice jams occurred in the City of Browns Valley (Spading 2000).

These three events were in the top 5 floods for this area. Of the 16 events listed in Table 1, these three were the only events that were directly observed and thoroughly documented by U.S. Army Corps of Engineer personnel. Ice jams have affected the peak flow 22 years of out the last 59 years, but not all ice-affected peak flows result in water elevations that connect the two water bodies (Spading 2000). Recently, around 2009-2010 an overflow channel was constructed to bypass Browns Valley when Little Minnesota River floods. We believe the channel was built to mitigate the effects of ice jams in response to the 2007 flood (Minnesota Department of Natural Resources Waters Division, 2007), but we were unable to find specific information that guided the design and construction of the channel. A diagram illustrating flood flow paths and the locations of culverts is shown in Figure 3.
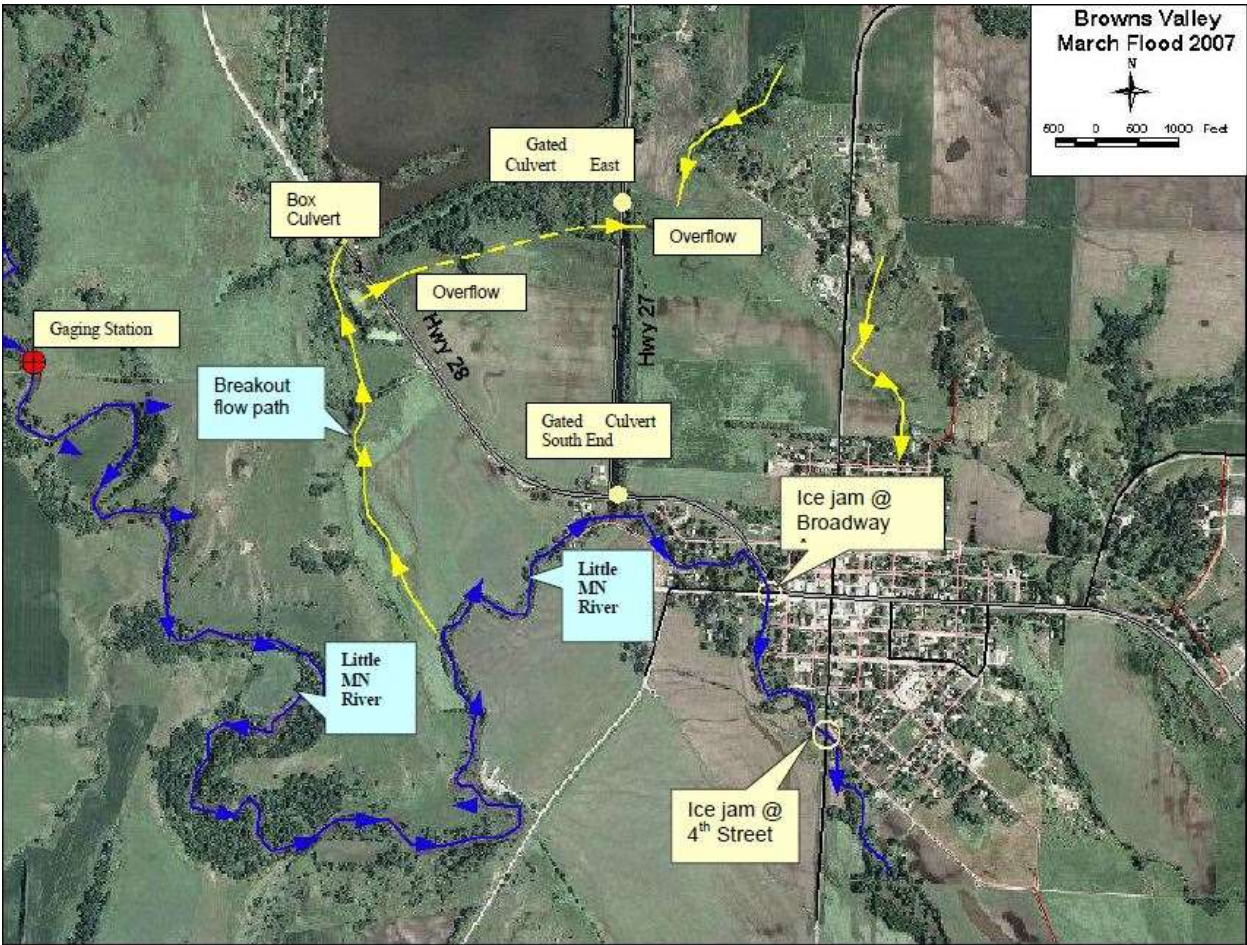
Figure 3. Flow paths and the locations of culverts and ice jams included in the USACE model of the 2007 flood. Figure copied from Minnesota Department of Natural Resources Waters Division, 2007.

2. Methods - Flood Frequency

We used the Log-Pearson Type III method to characterize the flood frequency and magnitude for the gage at Peever, SD. The period of record for the Peever, SD water gage is from 1941 to 1981, 1990 to 2002, and 2009 to 2014. Peak flow data were available for three time periods, 1940-1981, 1990-2002, and 2009-2013, but data were not available for the two intervening time periods, presumably because the gage was out of commission. Peak flows were sorted from largest to smallest and ranked from 1 to 60. Data were log transformed and the mean, standard deviation and skew were computed from the log transformed data. Skewness was used to find the frequency factor (KT) appropriate for the 1.5, 2, 5, 10, 25, 50, 100, and 200 year flood (http://streamflow.engr.oregonstate.edu/analysis/floodfreq/meandaily_tutorial.htm). Flood magnitude was computed for each of those return periods according to equation 1:

$$eq. \, log(Q_T) = \overline{log(Q)} + K_T \times \sigma_{log(Q)}$$

where QT is the magnitude of the flood of interest (with recurrence interval T), $\overline{\log(Q)}$ is the average of log-transformed values, KT is the frequency factor, and $\sigma_{\log(Q)}$ is the standard deviation of log-transformed values.

Table 2. Flood magnitudes computed using LP III method using data from 1940-1981, 1990-2002, 2009-2013

Return Period (years)	Flood magnitude (cfs)
1.5	321
2	935
5	2,369
10	3,651
25	5,568
50	7,167
100	8,876
200	10,669

The U.S. Army Corps of Engineers (USACE) used the HEC-2 model to model the left bank breakout flows to determine which magnitude/recurrence interval floods would connect Little Minnesota and Lake Traverse. Their method did not account for any overland flow from the right bank. Results indicated that a 10 year flood connects the two bodies of water, therefore having a 10 % chance to occur every year (see Table 3.).

Table 3. Discharge-frequency estimates computed by USACE, copied from Table 6-1 in Spading, 2000

Table 6-1
Discharge-Frequency, Little Minnesota River, In the Vicinity of Browns Valley, MN
Source: Browns Valley, Minnesota Flood Insurance Study, Reference No. 19.

Location	Drainage Area Sq. Mi.	Recurrence Interval and Peak Discharge (cfs) (1)			
		10-Yr	50-Yr	100-Yr	500-Yr
Little MN River Nr Peever, SD U.S.G.S. Gage No. 05290000	447				
Little MN River at MN-SD State Boundary (at the breakout point) See **Plate Nos. 1-2 and 2-2**	452	2,970	5,870 (2)	6,970(3)	9,260 (4)

1. Stage-Frequency should be considered because of ice jams. Due to ice jams, breakout flows will occur more frequently than indicated by discharge-frequency.
2. This flow (50-yr) has been reduced by a breakout flow to Lake Traverse of 350 cfs.
3. This flow (100-yr) has been reduced by a breakout flow to Lake Traverse of 1,020 cfs.
4. This flow (500-yr) has been reduced by a breakout flow of 3,830 cfs of which 1,600 enters Lake Traverse. The remainder flows north around the city and reenters the Little MN River.

July 1999, Revised January 2000

13

Our peak flood magnitudes range from 700- 1,900 cfs greater than the USACE estimated values. Differences may be explained by the fact that the USACE model used maximum annual flow values from Oct. 1939 to Sept. 1981 and Oct. 1989 to 1999. Higher peak flows in the most recent time period used in my dataset (1990-2002 and 2009-2013) appear to have significantly influenced the peak flow estimates. It appears that flood magnitudes may be non-stationary in Browns Valley, as we have observed to be the case in many other locations in the Minnesota River Basin (Belmont, personal communication). As a result, care must be used in extrapolating from this historical flood record to future flood risk. Further study is needed to adequately characterize the future flood regime of Browns Valley.

2.1. Methods - Floodplain Mapper Tool

Floodplain Mapper tool was created by Barr Engineering and Patrick Belmont and was described, tested and applied by Belmont (2011) to study the floodplain topography in Browns Valley. The tool is an open-code (Python) plug-in to ArcGIS and is available for free download from the Belmont Hydrology and Fine Sediment Laboratory webpage: http://www.cnr.usu.edu/htm/facstaff/belmont-hydrology-and-fine-sediment-lab/belmont-lab-resources.

3. Results – Floodplain Mapper Tool

The Floodplain Mapper tool was developed to delineate areas that are inundated at user-specified heights above the top of a river channel bank. In our specific case, we were interested in determining the water surface elevation that would result in a hydrologic connection between the Little Minnesota River and Lake Traverse. The colored area in Figure 4 indicates water depth for a water height that is 5 meters taller than the bank of the Little Minnesota River. Water depths range from 0.01 m (red) to 9.6 m in dark blue. The Little Minnesota River is able to flood and connect the two bodies of water at a discharge of around 3,000 cfs, according to Spading, 2000. The area between the Little Minnesota and Lake Traverse is sloped towards Lake Traverse, so any over-bank flows on the Little Minnesota River have the potential to connect. The culvert is not gated so therefore always open and it will have the potential to connect if over-bank flow occurs. If the culvert were gated, the water would need to rise another 2 meters to able to flow on the highway and allowing the water to flow into Lake Traverse.
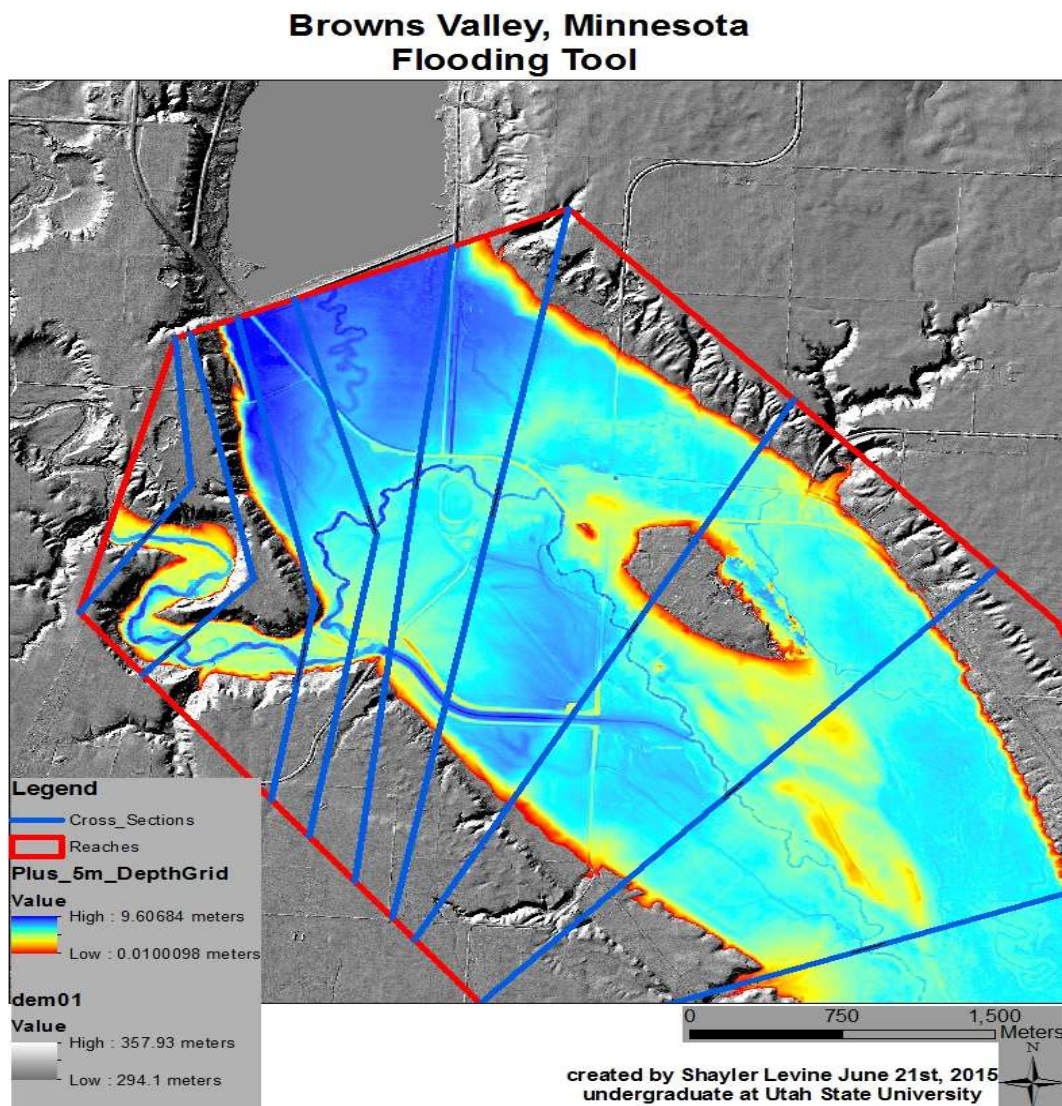
Figure 4. Floodplain mapper model of the area and depth that is inundated by a water stage elevation that exceeds the top of the left bank of the Little Minnesota River by 5 meters.

Lidar topography data shows a distinct paleo-channel meandering across the field between the Little Minnesota River and Lake Traverse. The slope of the paleo-channel indicates that, at one time, water from the Little Minnesota River flowed directly to the lake. The size of the paleo-channel appears to be similar to the modern Little Minnesota River, but ground-surveying would be helpful to verify the width and depth. From analyzing old aerial photographs we can see that the channel was present as early as 1951. It may be possible to date sediments in that paleo-channel using Optically Stimulated Luminescence or Carbon-14 dating to determine the time at which the channel was abandoned and therefore when the Little Minnesota River began to flow south from Browns Valley and became integrated into the Minnesota River Basin. However, that is beyond the fiscal limitations in this study. We are unable to find any information suggesting whether the alteration of course of the Little Minnesota River was caused by human or natural events.

Figure 5. 1951 aerial photograph from the University of Minnesota. This shows Lake Traverse, the Little Minnesota River, and Browns Valley. The mostly dry channel that runs from the Little Minnesota River to Lake Traverse is subtly visible.

3.1. Results – Field Analysis/Verification

Generally speaking, it is much more likely that water from the Little Minnesota River would spill into Lake Traverse than vice versa simply because the water surface elevation of Lake Traverse is 6-8' lower than the Little Minnesota River floodplain, as can be seen in Figures 2 and 4 above. Thus, it would require a substantial, and likely unrealistic, increase in elevation for Lake Traverse to flood into the Little Minnesota. At the same time, moderate floods, caused by high flows or ice jams, could cause the Little Minnesota to flood into Lake Traverse. The

main point of connection between the two water bodies is the (open, ungated) box culvert at the southwest corner of Lake Traverse, shown in Figure 3.

We conducted additional field work during summer 2016 to document the points of connectivity between the two water bodies and determine if/how the area between the Little Minnesota River and Lake Traverse has been altered to mitigate flooding in the area. We found that the area had been substantially altered to mitigate flooding. The link below provides general information regarding modifications, which were completed by Houston Engineering. Briefly, in response to extensive flood damage in 2007, Houston Engineering constructed a floodway channel and outlet, diversion dam and floodway inlet structure, concrete slab span bridges, and restored a 50-acre wetland and a Toelle Coulee drainage system. The system was constructed to preferentially flood in the case of ice jams or other high flow events and was designed to protect Browns Valley from a 100 year flood, though no information is provided regarding how the 100 year flood was estimated. We contacted Houston Engineering in an attempt to ascertain more information about the design and functionality of the side channel, but they would not release any other information due to a possible lawsuit with one of the designers in another project. A local resident from Browns Valley who has lived there 25 years claimed that flooding and connectivity between the Little Minnesota and Lake Traverse has not occurred since the structure was installed.

Link to online article about the engineering project:
http://finance-commerce.com/2011/05/feats-of-engineering-browns-valley-flood-mitigation-project/

During our field visit in June 2016 we took numerous photos, the locations of which are shown in Figure 6. Each of the photos are provided below with brief descriptions.
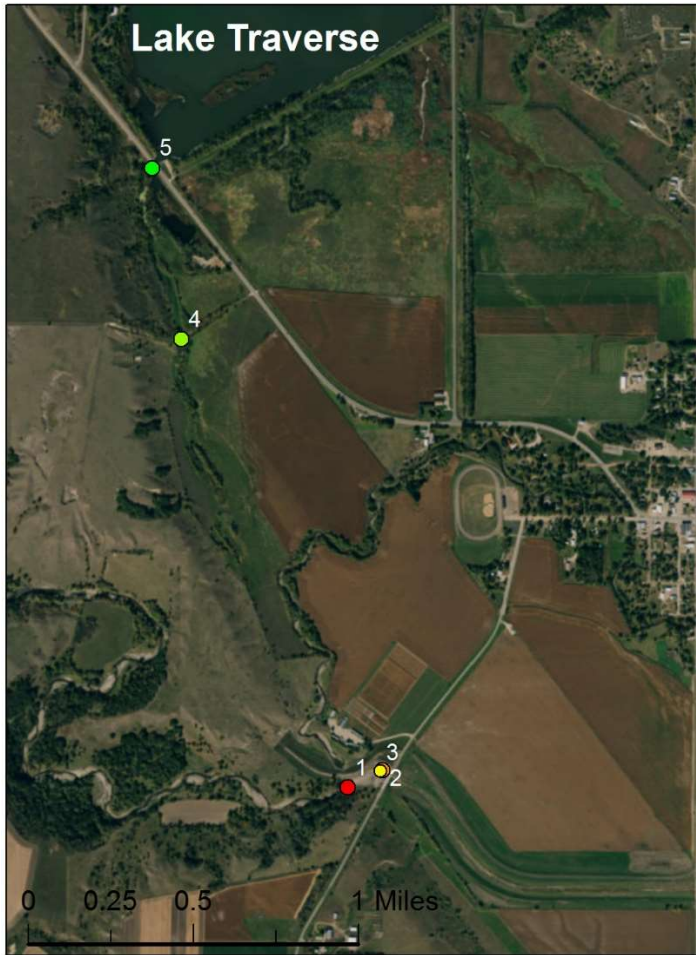
Figure 6. Shows locations of the following 5 photos, taken during field work in summer 2016.

Picture 1. shows the Little Minnesota River continuing towards the city of Browns Valley, MN.

This culvert was installed to help move the Little River Minnesota water towards the structure in an event of an ice jam.

Picture 2. looking towards the Little Minnesota River from the structure that Houston Engineering installed; the rocks are the start of the structure put in to help relieve flooding.

Picture 3. The structure Houston Engineering built to relieve flooding. This allows water to flow to a downstream part of the Little Minnesota River (below Browns Valley). The rocks are put there to stop scour around the bridge and elevate the side channel to allow it to be only used when an ice jam occurs.

Picture 4. Top photo is looking south towards the Little Minnesota River, the bottom is looking north towards Lake Traverse. This area is the gateway to the Lake Traverse and is the pathway that can connect the two watersheds.

The natural side channel shown in pictures 4a and b has been flooded when the Little Minnesota River floods and connects to Lake Traverse. There were many downed trees in the channel that are oriented in a way that suggests they were moved during a flooding event.

There is a box culvert that allows water from Lake Traverse to cross onto the west/south side of the highway, where the Little Minnesota River could connect when it floods, shown in picture 5. Under typical conditions, the lake water does not extend far south enough to connect to the Little Minnesota River, and it appears unlikely that the Lake Traverse water surface elevation

would rise enough to connect to the Little Minnesota River. However, this culvert allows any flood water from the Little Minnesota to enter Lake Traverse.

Picture 5. This is the box culvert leading from the Lake Traverse to the south side of the highway. The box culvert is always open and does not have a gate to stop flow, so when the Little Minnesota River floods into Lake Traverse the water does not have any restrictions to prevent connecting the two watersheds.

4. Conclusion/ Future Work

In conclusion we can see that flood events from major storms or related to ice jams readily connect the two watersheds. Analyses with the Floodplain Mapper confirmed that topography slants downwards consistently from the Little Minnesota River to Lake Traverse. Information from the USACE and Minnesota DNR concluded that a 10-year flood which can occur 10% of the time in any given year, will connect the River and Lake. Our hydrologic analysis indicates that flood magnitudes have increased recently and therefore this 10% prediction may be an underestimate for the risk of connectivity in the future.
Future research questions and needs:

Date sediments in that paleo-channel using Optically Stimulated Luminescence or Carbon-14 dating to determine the time at which the channel was abandoned and therefore when

the Little Minnesota River began to flow south from Browns Valley and became integrated into the Minnesota River basin.

Are flood magnitudes in the Browns Valley area systematically increasing (i.e., non-stationary) like they are in the rest of the Minnesota River basin? If so, will that mean connections are going to become more frequent?

5. References

Background on the March 13-14, 2007 Flooding in Browns Valley (Traverse County), Minnesota. Rep. Minnesota Department of Natural Resources Waters Division, 20 Apr. 2007. Web. 25 Mar. 2015.
<files.dnr.state.mn.us/waters/publications/brownsvalley042007.pdf>.
Belmont, P. 2011. Floodplain width adjustments in response to rapid base level fall and knickpoint migration. Geomorphology 128(1-2): 92-102.
"LiDAR Elevation Data for Minnesota." Minnesota Geospatial Information Office. N.p., n.d. Web. 25 Mar. 2015. <http://www.mngeo.state.mn.us/chouse/elevation/lidar.html>.
Spading, Kenton. Browns Valley Dike History and Potential For Interbasin Flow. Rep. St. Paul:U.S. Army Corps of Engineering, 2000. Web. 21 June 2015.
The Red River Trails, Oxcart Routes Between St. Paul and the Selkirk Settlement, 1820-1870, Rhoda R. Gilman, Carolyn Gilman, and Deborah M. Stultz, Minnesota Historical Society, St. Paul, Minnesota, 1979.